Novel *N*-heterocyclic carbene ligands for use in asymmetric catalysis

---

A thesis submitted in partial fulfilment of the requirements for the degree of Doctor of Philosophy in Chemistry at the University of Canterbury.

Will Kerr

January 2017

Comes a time when your driftin'
Comes a time when you settle down

Neil Young

Contents

Acknowledgements

This thesis was made possible by my supervisor Dr. Chris Fitchett and his research team. Chris, my respect and admiration for your mentorship as a supervisor and knowledge of chemistry has grown throughout my time working with you and continues to do so. Thank you for your profound patience, motivation and practical help, particularly with crystallography. To the rag-tag bunch that are the past and present members the Fitchett group, including Jayne, Paul, Robbie, Nic, Sam and Joe; you have made this experience worthwhile. In this regard, I wish to extend my thanks to members of the Steel and Kruger groups, and friends and colleagues in the wider department. Your friendship and inclusive attitude is the heart of this department. I would especially like to thank Dr. Dave Young who, in addition to being an excellent chemistry role-model, remains one of my oldest and dearest friends.

This story could not have been told without the contribution of some central characters. The sagely technical advice and guidance of Dr. Matt Polson has been essential to me throughout my PhD. Dr. Marie Squire and Dr. Amelia Albrett have also contributed immeasurably to this work. The time you have all spent performing mass spectrometry and assisting me with challenging aspects of NMR spectroscopy and GC-FID analysis made this work possible. Chemical synthesis can only be performed once the glassware and reagents have been hunted down so thankyou Gill Ellis and Laurie Anderson for your helpful service in the storeroom. Furthermore, I am grateful to our glassblowing maestro Rob McGregor and the workshop wizardry of Wayne Mackay and the boys downstairs. You have never failed to lend assistance when needed, and importantly, with a positivity that has been hugely appreciated.

I would like to thank the University of Canterbury for providing a doctoral scholarship and the Department of Chemistry for financial aid whilst concluding my research.

PhD research follows you home at the end of every day and my experience with this was two-sided. It provided personal value through purpose; satisfying a desire for invention and discovery, but at times, it overshadowed the things that provide meaning outside

of the office. For me, finding this balance has been one of the most challenging aspects of research and, as such, I am genuinely indebted to my friends for regularly providing an outlet through basketball, good beer and great company. I am likewise fortunate to have an extremely supportive family and know that Mum, Dad and my brothers, Lewis and Cam, are always there for me. Finally, I wish to acknowledge my Grandparents; Grandma and Granddad Kerr, and Oma, for their unwavering love and generosity. Grandma and Granddad, I know how excited you both were for me to finish this and I deeply regret not completing it sooner. This work is dedicated to you.

Abstract

This investigation sought to establish new and adaptable methods for incorporating an enantiomeric component into NHC ligands and to develop novel precatalyst prototypes capable of asymmetric induction for use in transition metal mediated catalysis. This thesis details the fulfilment of these objectives through the design, synthesis and characterisation of forty-eight previously unreported compounds including twenty-six new NHC proligands and fourteen NHC complexes.

NHC derivatives of the chiral mono-terpene camphor are explored in Chapter 2, primarily through the synthesis of a series of bornyl-acetamide linked NHC proligands, demonstrating expedient incorporation of an enantiomeric moiety by acetamide linkage. Bornyl-acetamide NHC complexes of Ag(I), Pd(II), Pt(II) and Ru(II) are studied and structural elucidation supported by comparison with the Pd(II) and Pt(II) complexes of an achiral cyclohexyl-acetamide analogue (Chapter 3). Chapter 4 introduces metallo-NHC proligands derived from imidazo[4,5-*f*][1,10]phenanthroline, capable of backbone coordination of a ruthenium-polypyridine component. Alternatively, use of an acetamide-tether provides metallo-NHC proligands of 5-acetamido-1,10-phenanthroline and 4-acetamido,2,2'-bipyridine (Chapter 5). Also outlined is the synthesis of several remarkable hetero-dinuclear NHC complexes in addition to the effective enantiomeric resolution of a metallo-NHC proligand.

The performance of selected systems in an asymmetric Suzuki coupling is examined in Chapter 6. Several of the organic-NHC ligands elicit comparable activity to reported systems, however, product formation is not observed when using an acetamide-linked metallo-NHC ligand. This is most likely related to amide-group coordination which occurs readily for the metallo-NHC ligands compared with the bornyl and cyclohexyl analogues. Such conclusions are supported by the comprehensive structural elucidation of all NHC complexes prepared in this thesis, providing evidence for the behaviour of catalytic intermediates involving these ligands.

Abbreviations

NHC: *N*-Heterocyclic Carbene

Bipy: 2,2'-Bipyridine

Phen: 1,10-Phenanthroline

Acac: Acetylacetonate

Ar^{iPr}: Diisopropyl-phenyl substituent

Ppy: Polypyridine

MeCN: Acetonitrile

MeOH: Methanol

EtOH: Ethanol

DCM: Dichloromethane

DMF: Dimethylformamide

DMSO: Dimethylsufoxide

TLC: Thin Layer Chromatography

HPLC: High Performance Liquid Chromatography

NMR: Nuclear Magnetic Resonance

COSY: Correlation Spectroscopy

HSQC: Heteronuclear Single Quantum Coherence

HMBC: Heteronuclear Multiple Bond Correlation

TOCSY: Total Correlation Spectroscopy

NOESY: Nuclear Overhauser Effect Spectroscopy

MP: Melting Point

FT-IR: Fourier Transform Infrared Spectroscopy

UV/vis: Ultraviolet/visible

ESI-MS: Electrospray Ionisation Mass Spectrometry

GC-FID: Gas Chromatography with Flame Induction Detection

XRD: X-ray Diffraction

Chapter 1

introduction

1.1. Stereochemistry and Chirality

Isomers are compounds that have the same atomic composition, that is, the same molecular formula, but a different molecular arrangement.[1] Constitutional isomers differ in the connectivity of molecular components. For example, a compound with the molecular formula C_6H_7N can be constructed in numerous ways (Figure 1.1).

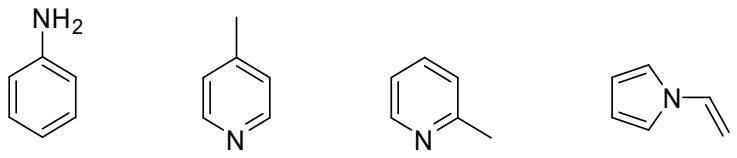

Figure 1.1: *Constitutional isomers with the molecular formula C_6H_7N.*

Isomers that have the same connectivity but a different spatial arrangement are referred to as stereoisomers and are classified as either diastereomers or enantiomers. Diastereomers of a compound have distinct chemical energies, usually related to a difference in the distance between structural components. They are therefore distinguishable spectroscopically and can be chemically separable. Diastereomers include *E/Z*- and *cis/trans*- geometric isomers as well as conformational isomers (Figure 1.2).

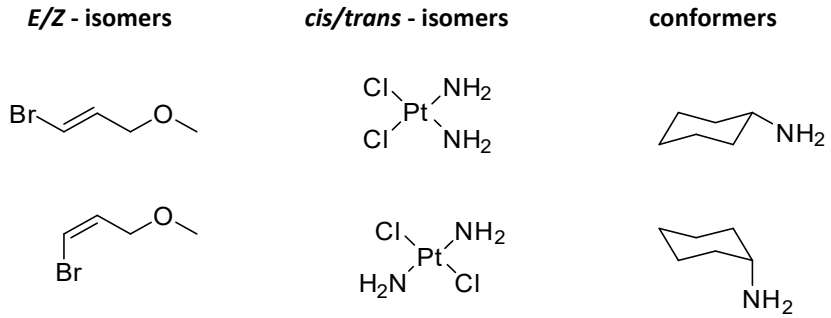

Figure 1.2: *Examples of* E/Z- *and* cis/trans-*, and conformational diastereoisomers.*

Enantiomers are compounds that are non-superimposable mirror images of one another. As such, the internuclear distance between any two atoms in one enantiomer is identical for the equivalent pair of atoms in the other enantiomer (Figure 1.3). As a result, they have the same chemical energy and are spectroscopically indistinguishable (with the exception of polarimetry). The two enantiomers of a compound will rotate the plane of monochromatic-linearly polarised light in opposite directions and hence are often referred to as optical isomers and given the descriptor + or – depending on whether the light is rotated clockwise, (+), or counterclockwise, (–). The designations *D* (dextrorotary, clockwise) and *L* (levorotary, anticlockwise) are applied similarly.

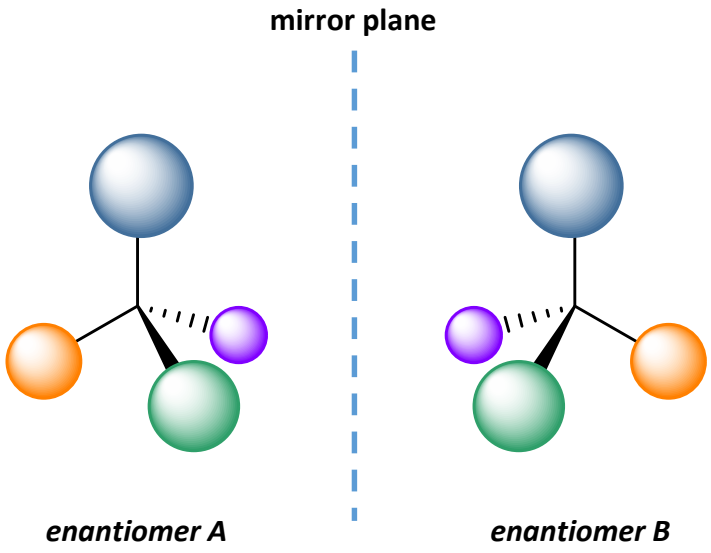

Figure 1.3: *Enantiomers shown as their non-superimposable mirror images.*

Molecules that exist as pairs of enantiomers are chiral compounds. Chiral, from the Greek "cheiro" meaning "hand,"[2] is in reference to our left and right hands which, like enantiomers, are non-superimposable mirror images. Enantiomers can arise due to the presence of a stereogenic centre; a tetrahedral node, commonly carbon, bearing four different substituents as represented in Figure 1.3. Molecules with more than one stereocentre can give rise to enantiomers and diastereomers (Figure 1.4). It is important to emphasise here that it is possible for any molecule with more than one enantiomeric

component it to exist as diastereomers. This is also true for chiral molecules engaged in non-bonding interactions. Therefore, when a pair of chemically indistinguishable enantiomers associate with another singularly enantiomeric species, a pair of diastereomeric adducts is generated. Because diastereomers are chemically distinct, this provides a mechanism by which to differentiate between the original enantiomers. Every stereochemical application relies on this concept in some way and it is central to much of the following discourse.

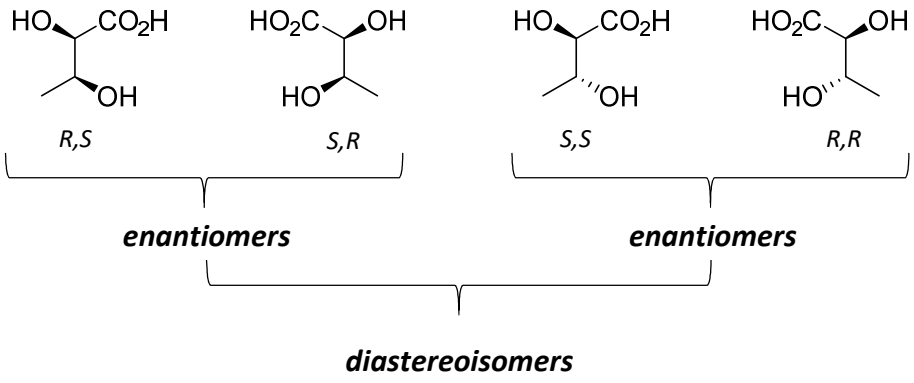

Figure 1.4: *Stereoisomers of 2,3-dihydroxybutyric acid.*

The absolute configuration of the stereocentre can be assigned on the basis of its three-dimensional structure using the Cahn-Ingold-Prelog (CIP) rules which provide an *R* or *S* designation.[3] Other three-dimensional configurations can give rise to enantiomers even in the absence of an asymmetric centre; examples of this are shown in Figure 1.5. A molecule such as 1,1'-binaphthalene-2,2'-diol (BINOL) contains a chiral axis due to the mutually axial orientation of its aromatic rings.[4] Stereoisomers of this type are known as atropisomers. Planar chirality, such as that exhibited by mono substituted ferrocenes, is another source of enantiomerism.[5] Molecules including helicene provide an example of a helically chiral structure which is analogous to a left or right handed screw-thread.[6] This concept is also relevant to macro-molecular helices like DNA and the tertiary structure of many proteins. Again, these enantiomers are designated in accordance with the CIP rules using *M* (minus) or *P* (plus) descriptors, although, *R/S* can also be used for cases of axial and planar chirality.

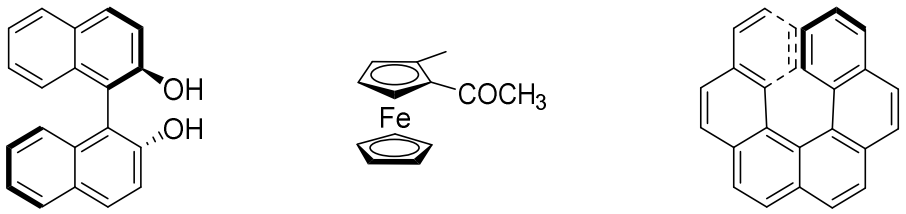

(*M*)-BINOL (*R*)-1-acetyl-2-methyl ferocene (*P*)-hexahelicene

Figure 1.5: *Molecules with axial, planar and helical chirality.*

Another manifestation of helical chirality is the Δ/Λ stereochemistry of octahedral metal complexes bearing two or more chelating ligands. Tris-bidentate octahedral complexes such as $[Ru(phen)_3]^{2+}$ exist as one of two enantiomers that are determined by the helical sense of the coordination sphere generated by the ligands. Figure 1.6 shows how the Λ-enantiomer has a sense of anti-clockwise rotation, resembling a left handed screw when viewed along the three-fold axis. The Λ-enantiomer has a clockwise helical sense.

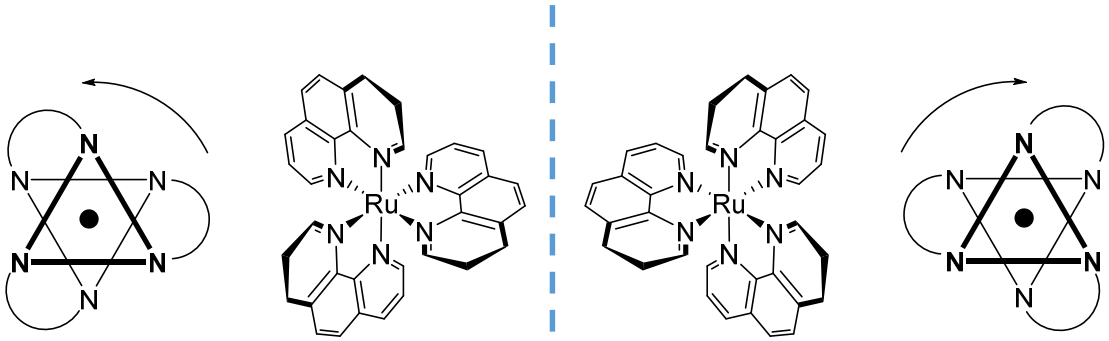

left-handed screw Λ-$[Ru(phen)_3]^{2+}$ Δ-$[Ru(phen)_3]^{2+}$ right-handed screw

Figure 1.6: *Enantiomeric octahedral metal complexes assigned as having Λ or Δ absolute configurations.*

1.1.1. Chirality in biochemical systems

Chirality is ubiquitous in nature with many of the biomolecules essential to the processes of life occurring as only one enantiomer. L-amino acids and D-carbohydrates predominate in natural systems as do stereochemical preferences for the helical arrangement of polymers, including DNA and proteins. Because natural systems are stereochemically enriched, it follows that the different enantiomers of chiral bioactive molecules including pharmaceuticals can elicit different biochemical responses. Despite the two enantiomers of a compound being chemically indistinct, their association with the inherently chiral receptor of, for example, an enzyme, results in diastereomeric transient states that are energetically differentiable. Hence organisms can recognise and respond differently to the two enantiomers of a chiral compound.

Often, only one enantiomer of a pharmacologically active chiral compound (called the eutomer) has the desired therapeutic effect while the other enantiomer (the distomer) has no impact or, at worst, an adverse effect.[7] For example, the *R*-enantiomer of the notorious class-A drug methamphetamine is actually a decongestant. It is the *S*-enantiomer that makes methamphetamine highly addictive and affords it its stimulant effect (Figure 1.7).[8]

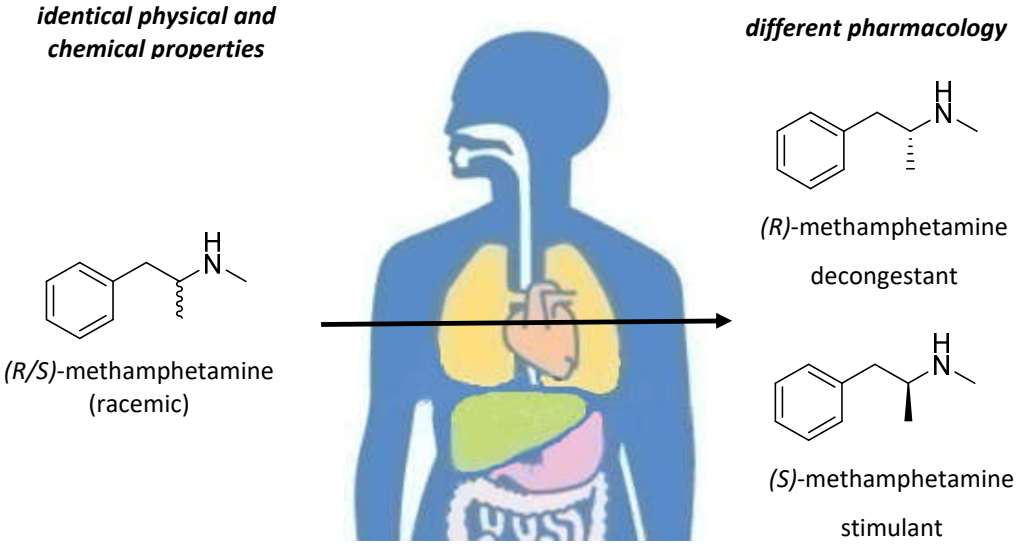

Figure 1.7: *The different pharmacology of methamphetamine enantiomers.*

By convention the ratio of enantiomers in a sample of chiral compounds is expressed as the enantiomeric excess (*ee*). This is calculated as the percentage excess of the major enantiomer (say *S*), over the other (*R*) as per the formula:

$$ee = \frac{(S) - (R)}{(S) + (R)} \times 100$$

A sample with an equal ratio of the two enantiomers has an *ee* of 0% and is known as a racemic mixture or a racemate.

Chiral compounds are the active component in over 50% of today's pharmaceuticals, and drug regulation agencies increasingly favour single enantiomer therapeutics above racemates.[9] This is a justified measure against potential side effects caused by the distomer.

1.1.2. Enantiomeric enrichment of compounds by resolution

In the realm of drug design and isolation there is demand for pharmaceutical preparations to deliver enantiomeric and diastereomeric purity of products.[10] In some convenient cases the starting material is derived from a naturally occurring chiral compound (such as enzymatically expressed amino-acids), however, more often than not, chirality is introduced during synthesis from achiral starting materials. Synthesis of enantiomers in this way, without any external stereochemical influence, will always result in a racemic mixture because each enantiomer forms via degenerate transition-states and are themselves, chemically identical.

Separation of enantiomers can be achieved in the presence of some other enantiomerically enriched chiral component. This relies on the two enantiomers of a racemate interacting differently with an external chiral species through the formation of intermediary diastereomers. These, by virtue of their different chemical properties, are separable.[11] Separation of enantiomers in this way is called enantiomeric resolution

and is applied in a number of ways. Enantiomers can be synthetically converted into diastereomeric pairs and separated by traditional means such as crystallisation of diastereomeric salts often referred to as "classical resolution". The popular anti-inflammatory drug *S*-(+)-ibupropen is isolated in this way by crystallisation with (*S*)-lysine (Scheme 1.1).[12]

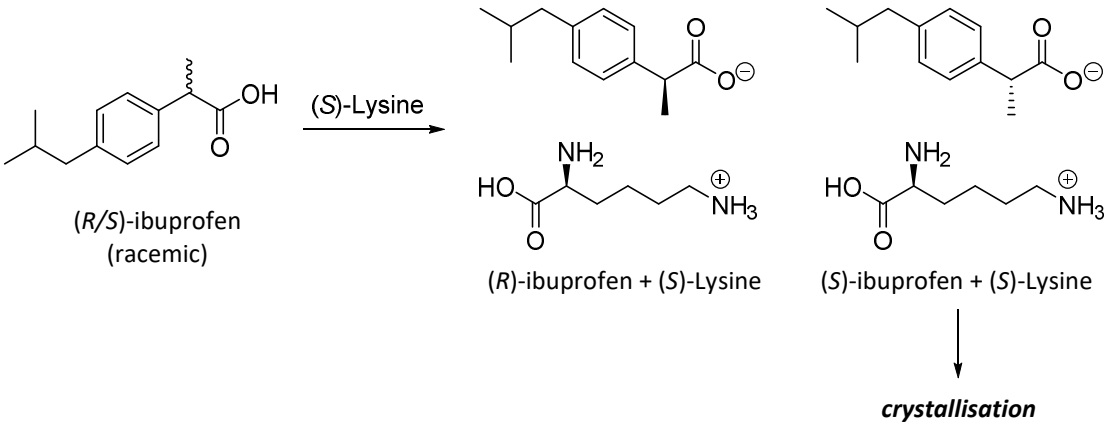

Scheme 1.1: *Resolution of (*R/S*)-ibuprofen by crystallisation with (*S*)-lysine.*

Another approach is kinetic resolution which relies on one enantiomer being consumed faster than the other in a reaction. For example, the hydrolytic kinetic resolution of many epoxide substrates is achieved using Jacobsen's catalyst (Scheme 1.2).[13]

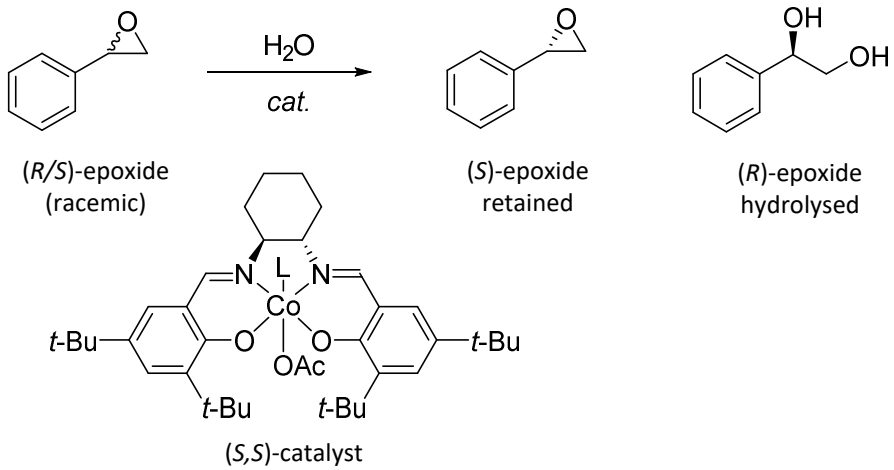

Scheme 1.2: *Kinetic resolution of epoxides by stereoselective hydrolysis using a chiral catalyst.*

Chiral chromatography can also be performed to resolve the enantiomeric components of a racemic mixture.[14] Non-bonding interactions between the enantiomeric species and a chiral stationary phase result in transient diastereomers, one of which is more stable than the other. The more stable transient species has a stronger association to the column hence is retained longer, providing the basis for separation.

Several techniques are used to evaluate the enantiomeric composition of a material. Foremost is optical rotation spectroscopy which provides the angle of optical rotation (α).[15] Polarimetry measures α for a specific wavelength, conventionally the D-line emission of a sodium vapour lamp at 589 nm (α_D) whereas optical rotatory dispersion (ORD) provides a spectrum of α over a range of wavelengths. The absolute optical rotation [α] is the angle of rotation for a given concentration and is always quoted with the temperature and wavelength at which it was recorded, for example $[\alpha]_D^{25}$. Racemates have zero optical rotation ($\alpha = 0^o$). To calculate the ratio of enantiomers in a sample, [α] must be known for one of the enantiomers thus limiting this technique to known resolved compounds. X-ray crystallography has become an invaluable tool for characterising the absolute configuration of a crystallised enantiomer,[16, 17] but it is not suited to the screening of enantiomeric mixtures. Other techniques that are better suited to this include chiral HPLC[11, 18] and chiral shift reagents for NMR detection.[19-21] Reacting the analyte with a chiral auxiliary to produce diastereomeric products for analysis is another approach.[21]

Even in light of the above resolution methods, separating the enantiomeric constituents of a racemic mixture is often difficult and expensive. Furthermore, the undesired enantiomer is inevitably wasted unless it can be easily racemised and subjected to sequential separations. It is therefore preferable when the yield of the target enantiomer is enriched through stereoselective synthesis.

1.1.3. Asymmetric Synthesis

Asymmetric synthesis refers generally to a synthesis in which enantiomers or diastereomers are generated under some form of stereochemical control. This is achieved by introducing a substrate or catalyst with a predefined chirality into the reaction.

A substrate controlled asymmetric synthesis employs an enantiomerically pure auxiliary species which is incorporated into the starting material to provide a chiral precursor. The reaction to form a new enantiomer now proceeds diastereoselectively because of the influence of the chiral fragment. The auxiliary species can be cleaved at the conclusion of the reaction to provide the enantiomerically enriched product.[22] Numerous auxiliaries have been applied to asymmetric synthesis and are often derived from compounds that occur naturally as a single enantiomer. These are broadly classed as "chiral pool" molecules and include amino-acids, carbohydrates and various terpenes.[23] Scheme 1.3 illustrates a diastereoselective aldol condensation performed using an auxiliary derived from the chiral pool mono-terpene camphor.[24]

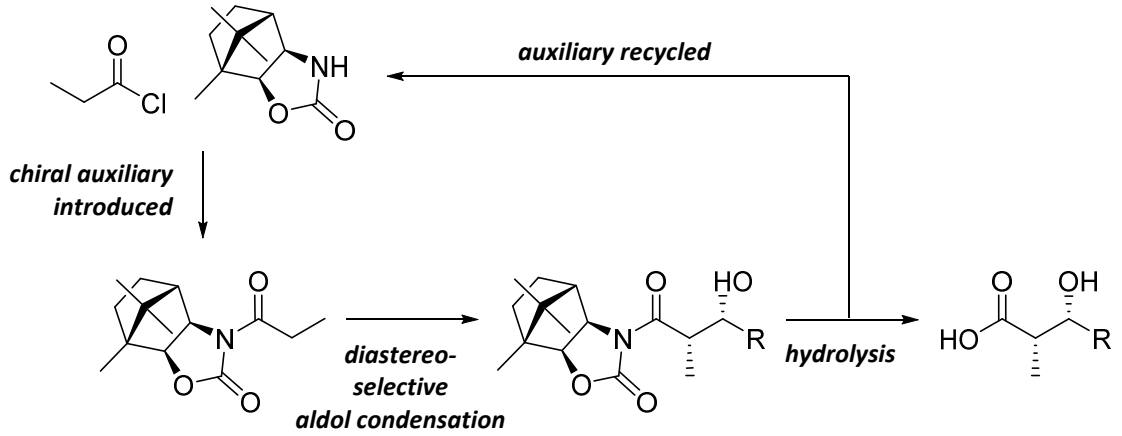

Scheme 1.3: *Diastereoselective aldol condensation using a camphor-derived chiral auxiliary.*

A more convenient way of achieving stereochemical control is through chiral induction by an enantiomerically pure catalyst. Efficient asymmetric catalysis is a powerful method by which a single enantiomer can be generated from achiral synthons as dictated by a chiral-moiety on the catalyst.[25] This principle will be explored independently in section 1.2.3.

1.2. Catalysis

A catalyst is an additive that acts to accelerate a chemical process without being consumed itself. Catalysis is a kinetic effect in which the catalyst brings together and mediates the combination of substrates, thereby decreasing in the activation barrier of a reaction and speeding up the process (Figure 1.8). However, it is a falsehood to assume that all catalysts simply lower the transition state energy of the un-catalysed pathway. In many cases a catalyst can facilitate the formation of an entirely different product than what would be formed in its absence. In fact, many reactions do not proceed un-catalysed. As will be addressed, coupling reactions such as the Suzuki coupling of aryl-halides and aryl-boronic acids relies on catalysis as these substrates will not react independently.

When the catalyst is in a different phase to the reactant media it is termed heterogeneous catalysis. Palladium on activated charcoal is an example of a heterogeneous catalyst used to facilitate hydrogenation reactions. Homogeneous catalysts function in the same phase as the reacting species and are typically dissolved in solution with the substrates. The following discussion and examples will focus on homogeneous systems as these are the subject of this thesis.

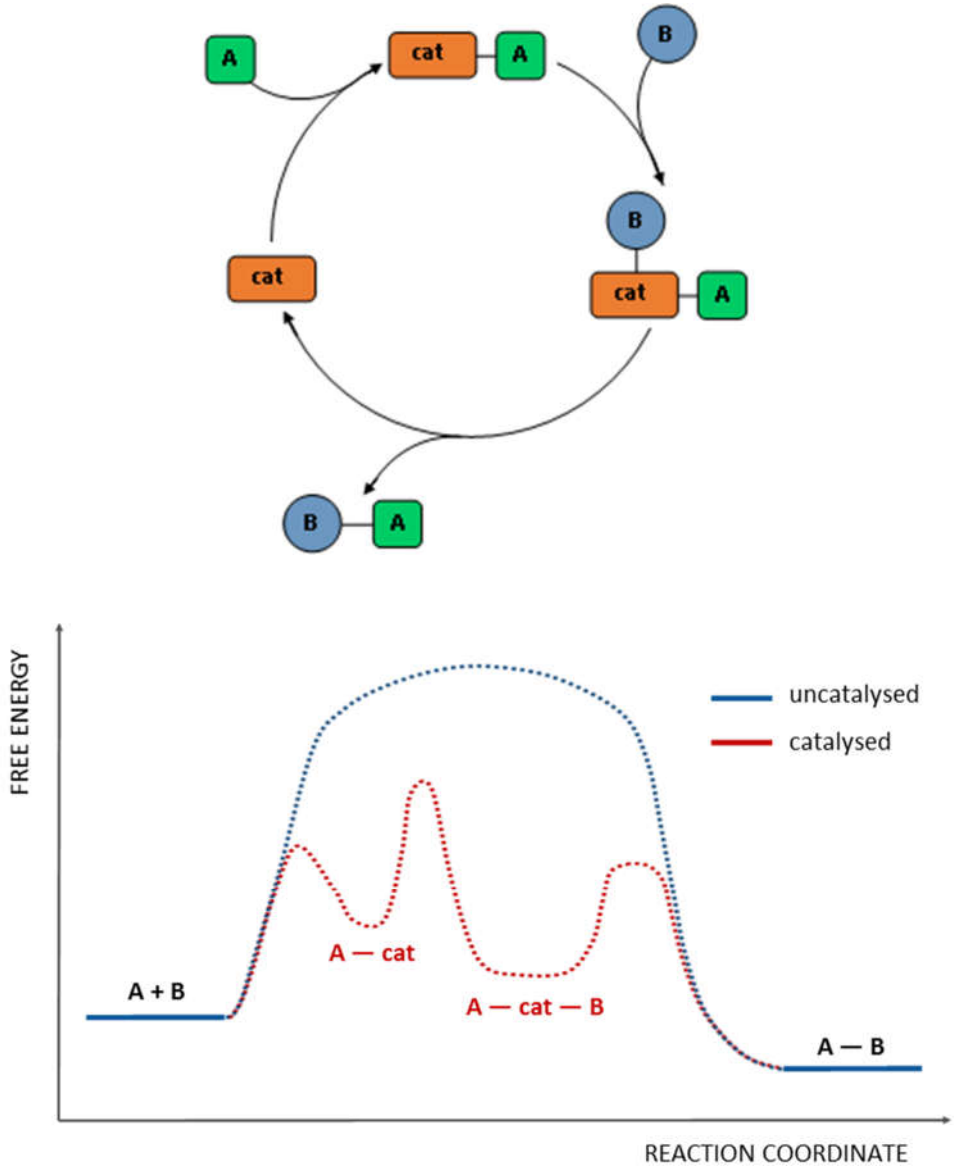

Figure 1.8: *A representative catalyst cycle and reaction coordinate diagram showing the different energetic pathways for a catalysed and uncatalysed process.*

1.2.1. Transition metal mediated synthesis

Transition metals have been used to catalyse numerous chemical transformations with myriad substrates.[26] Their catalytic activity is reliant on the coordination and dissociation of ligands from the electropositive metal centre which is notionally equivalent to substrate binding and release. Ligand exchange is a fundamental aspect of transition metal chemistry that is enabled by the ability of an individual centre to

undergo changes in its valence electron count. This can be rationalised in the context of the 18-electron rule which dictates that the most stable ligand field is one in which the transition metal centre has a valence configuration of 18 electrons. Although, stable transition metals complexes with 12 – 22 valence electrons are known, it is generally true that low oxidation state organometallic complexes tend to obey the 18-electron rule.[27] However, the catalytic capability of a transition metal centre is often dependent on its ability to support an active 16-electron configuration. This is the basis of catalysis by "platinum group" metals, a historical term that encompasses platinum, palladium, iridium, rhodium, ruthenium and osmium. These are prone to forming coordinatively unsaturated 16-electron complexes in addition to more "traditional" coordinatively saturated 18-electron species. It is the 16-electron species that is responsible for catalytic induction and may be introduced as a stable, pre-formed complex or generated in situ (see section 1.2.2.1).[28]

Being coordinatively unsaturated and capable of supporting a valence electron count below 18-electrons enables these centres to engage in oxidative addition, the crucial first step in most catalytic pathways. Reductive elimination is the reverse process by which the product is released and the active species regenerated. These concepts will be elaborated in the context of palladium catalysed coupling reactions in the following section.

1.2.2. Palladium catalysed coupling reactions

Palladium catalysed coupling reactions have become a foundational method in modern organic synthesis due to their widespread applicability and appreciable substrate tolerance. Palladium facilitates bond formation between coupling partners as per a generally accepted cyclic mechanism, an example of which is provided for the Suzuki coupling in Scheme 1.5. In principle, the pathway is similar for most palladium mediated couplings. All reactions of this type begin with oxidative addition of an aryl halide (or pseudo-halide such as OTf or OAc) to the active $L_nPd(0)$ species.[29] Besides this initiation step, these reactions are classified differently based upon the coupling partners used.

In Mizoroki-Heck type reactions, oxidative addition is followed by coordination of a terminal alkene which is coupled with the initial substrate to give a disubstituted alkene product.[30] Alternatively, the second coupling partner can be introduced by transmetalation of an organometallic species to generate a 16-electron Pd(II) intermediate bearing two organic coupling partner fragments. Reductive elimination releases the coupled product and regenerates the active $L_nPd(0)$ species. Main group metals are commonly used in the organometallic coupling partner and are associated with named reactions, these include tin (Stille), zinc (Negishi), boron (Suzuki) and for alkynes, copper (Sonogoshira). Lithium, magnesium, aluminium, zirconium and silicon (Hiyama) have also been used.[28] This methodology can also be applied to formation of carbon to heteroatom bonds, notably carbon-nitrogen bond formation by the Buchwald-Hartwig amination reaction.[31]

This thesis is concerned with the synthesis and structural elucidation of novel palladium complexes with an eye towards applying them in catalysis. The abundance of systems and coupling partners with which palladium functions provides ample opportunity to find an operational system. Limited time and resources meant that only the catalytic performance of these new complexes in an asymmetric Suzuki coupling was assessed as part of this work. Suzuki couplings are explored further in the following section, although, the principles apply generally to all palladium catalysed cross-couplings with organometallic partners.

1.2.2.1. Aryl-Aryl Suzuki couplings

The palladium (and nickel) catalysed cross-coupling reactions of organoboron compounds is referred to as a Suzuki-Miyaura coupling, or simply Suzuki coupling. It is named for the pioneering work of Norio Miyaura and Akira Suzuki and is one of the foremost methods for coupling aryl fragments.[32] Suzuki couplings are often favoured over the tin and zinc based Stille and Negishi couplings because the organoboron reagents are comparatively stable, non-toxic and synthetically accessible.[33] Arylboronic acids are the most widely applicable organoboron reagent to aryl-aryl coupling, although, other derivatives may be preferred depending on the reaction.[34] Arylboronic

acids are readily synthesised by lithiation of the corresponding aryl-bromide, followed by reaction with a boric ester such as trimethyl borate. The resulting boronic ester is hydrolysed under acidic conditions to provide the desired boronic acid (Scheme 1.4). Numerous other syntheses of boronic acids and related organoboron substrates are available if required.[33, 34]

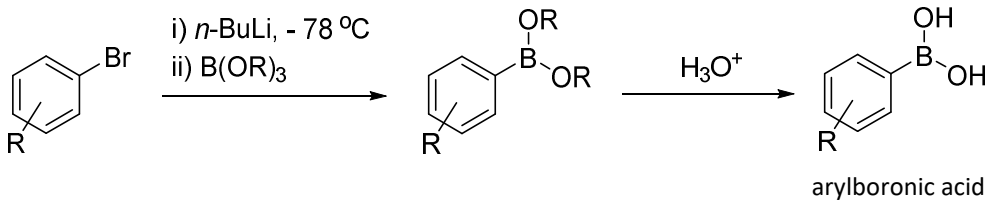

Scheme 1.4: *One route to arylboronic acids from an aryl halide.*

Scheme 1.5 depicts the generalised catalytic cycle of a Suzuki coupling. As has been established, initiation occurs with oxidative addition of a $L_nPd(0)$ adduct (**I**) into the Ar^1–X bond to produce the 16-electron intermediate $L_nXPd(II)–Ar^1$ (**II**). Typically, the most reactive Ar^1–X substrates are diazonium salts (X = N_2^+) followed by halides (I < Br < Cl) which are by far the most common substrates. Sulfonates are the least reactive substrates (OTf < OTs < OMs), however, the generalised reactivity series presented here, diazonium salts < halides < sulfonates, is dependent on the catalyst and the reaction conditions.[35]

The subsequent transmetalation step is preceeded by conversion of the borane, boronic acid or boronic ester precursor into an anionic boronate species. This requires attack by a hard anion such as hydroxide, alkoxide, carbonate, fluoride or phosphate (Y), one of which is introduced at the outset of the reaction. Transmetalation of the boronate to generate $L_2Pd(II)–Ar^1Ar^2$ (**III**) proceeds slowly and is the rate limiting step. Reductive elimination provides the coupled product $Ar^1 – Ar^2$ and the active species $L_2Pd(0)$.

The final elimination step relies on the organic fragments Ar^1 and Ar^2 being mutually *cis* to one another, however, bulky aryl-groups favour a *trans*-configuration. Judicious

choice of the auxiliary ligand L can hugely influence the geometric preference of $L_2Pd(II)–Ar^1Ar^2$ (**III**) (see section 1.2.3).

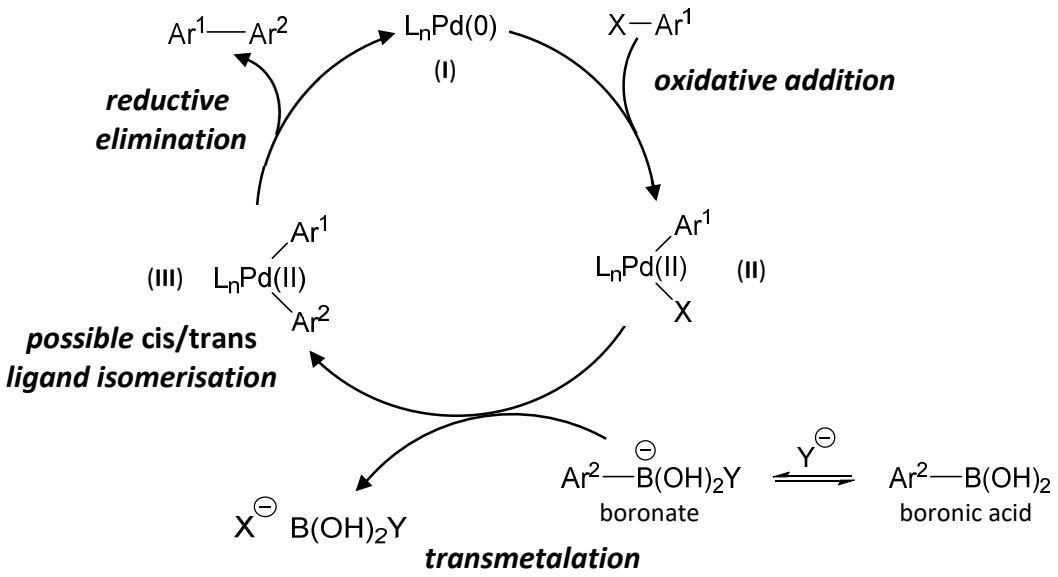

Scheme 1.5: *A generic mechanism for aryl-aryl Suzuki coupling.*

The catalyst is often introduced to the reaction in its active form. Stable, zero-valent palladium complexes such as tetrakis(triphenylphosphine)palladium(0) ($Pd(PPh_3)_4$) or tris(dibenzylideneacetone)dipalladium(0) ($Pd_2(dba)_3$) can be used for this purpose. It is also possible to generate the active species in situ from a palladium(II) precatalyst. A study by Moreno-Mañas and coworkers revealed that reduction of Pd(II) to Pd(0) can occur via homocoupling of aryl boronic acids.[36] Other researchers suggest that reductive elimination of an ancillary ligand adduct is responsible in specific cases.[37, 38] Regardless of the precise pathway, the literature abounds with examples of palladium(II) precatalyst complexes that have been successfully applied to Suzuki coupling reactions.[29, 39] Precatalyst based systems are often preferred for asymmetric synthesis as they can be prepared with well-defined stereochemical attributes.

1.2.3. Asymmetric catalysis and the "privileged ligands"

The objective of asymmetric catalysis is to generate large quantities of optically active material using a tiny amount of enantiomeric promotor. Excellent enantiomeric excesses of over 98% have been realised for an array of asymmetric reactions.[22] However, these are often specific to individual syntheses and hence researchers are perpetually required to develop new catalysts to expand the scope of asymmetric systems.[40]

Ancillary ligands play a nuanced role in homogeneous asymmetric catalysis. As in all metal mediated catalysis, the active centre behaves as a templating agent, bringing the reacting substrates together. Ancilliary ligands are required to stabilise the various catalytic intermediates and prevent deactivation through, for example, aggregation, whilst maintaining sufficient reactivity. In homogeneous catalysis the ligand is essential to maintaining solubility in the chosen media. Additionally, asymmetric catalysts require ligands that possess an enantiomeric functionality or are arranged in a stereochemical architecture that exerts steric influence over the active centre (see section 1.2.3.1). To render efficient stereoselectivity at the active site, the directing ligand must remain bound throughout repeated catalyst cycles, often to a metal that is alternating between different oxidation states.

Certain ligand types have excelled at fulfilling all of the above obligations to provide outstanding selectivity in multiple types of reactions. These are known as the privileged ligands (Figure 1.9)[41] and include the C2 symmetric ligands BINAP (related to BINOL, Figure 1.5), the metallocene forming Brintzinger's ligand, bis-oxazolines and salen complexes of the type used in used in the kinetic resolution of epoxides (Scheme 1.2). Several specialist chiral phosphines also qualify (Scheme 1.7).[22] Note that these are all bidentate ligands, which is often advantageous because it enforces *cis* relationship between substrates to better facilitate their reaction.

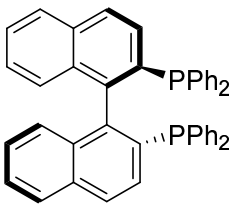

(*M*)-BINAP

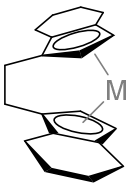

(*S,S*)-*ansa*-metallocene
(Brintzinger's ligand)

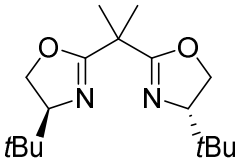

(*S,S*)-*t*Bu-bis(oxazoline)

Figure 1.9: *Some examples of "privileged ligands" used in asymmetric catalysis.*

BINAP, for example, derives its chirality from an atropisomeric 2,2-binaphthalene fragment. Having this chiral axis dictates the relative orientation of phenyl-rings around the active centre, thus imposing stereochemical requirements on the coordinating substrates. Quadrant diagrams are useful for illustrating how the phenyl rings of the BINAP ligand occupy the space around the metal centre (Figure 1.10).

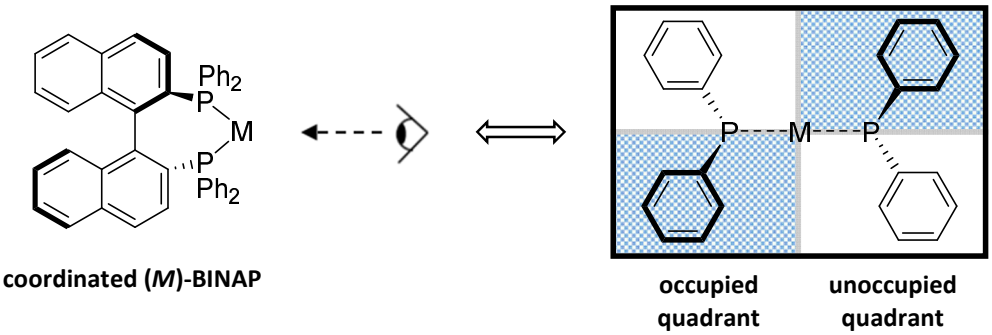

Figure 1.10: *Quadrant diagram of (*M*)-BINAP.*

Shaded quadrants indicate a forward phenyl ring is obstructing this region whereas the unshaded quadrants are relatively unoccupied. Scheme 1.6 shows how (*M*)-BINAP generates an environment that is selective for one enantiomeric product of a palladium catalysed asymmetric allylation reaction. The major product forms with its main substituents in the unoccupied quadrants such that steric clashes with the phenyl rings are minimised.

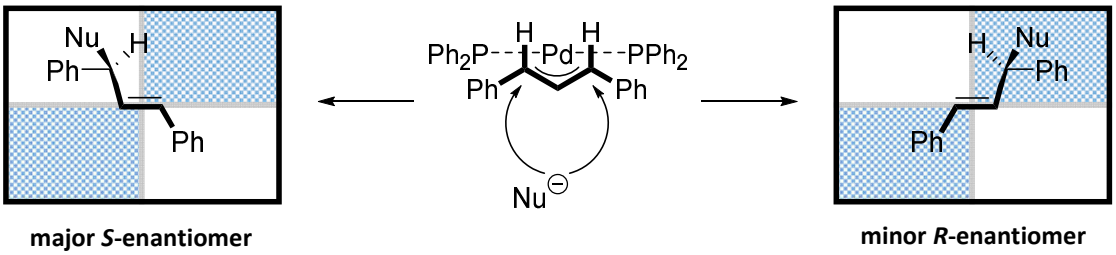

Scheme 1.6: *(*M*)-BINAP driven selectivity of an asymmetric allylation reaction illustrated using quadrant diagrams.*

A well-known example of an industrialised asymmetric synthesis is that of the precursor to (L)-DOPA, a commercially available drug used in the treatment of Parkinson's disease. Chemical manufacturing giant Monsanto successfully employs an asymmetric hydrogenation reaction[42, 43] using a rhenium catalyst with the chiral phosphine ligand (*R,R*)-DIPAMP to obtain the precursor in a 90% yield at 95% *ee* in quantities of one ton per year (Scheme 1.7).[40]

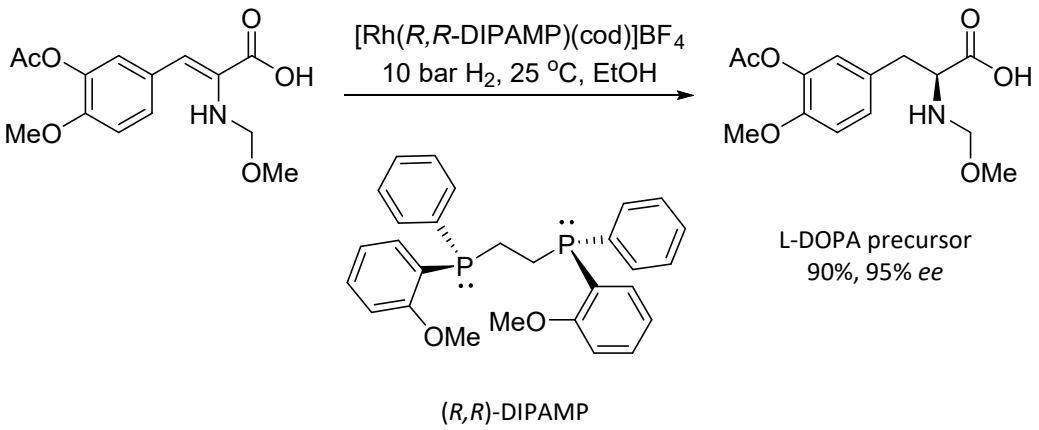

Scheme 1.7: *Synthesis of the precursor to L-DOPA using an asymmetric hydrogenation catalyst with the enantiomeric phosphine ligand (*R,R*)-DIPAMP.*

Despite a handful of celebrated cases such as the one above, asymmetric catalysis remains uncommon for industrial synthesis of enantiomerically pure materials, and

classical resolution of racemic mixtures or enzymatic resolution is still preferred. There is therefore ample incentive to further the field of asymmetric catalysis for wholescale application.

1.2.3.1. Metal-centred chirality in asymmetric catalysis

It is important to draw attention here to a niche class of asymmetric catalyst which contain metal-centred chirality as it is immediately relevant to this work. Broadly speaking, catalyst systems that utilise metal centred chirality can be divided into two categories; those in which the chiral centre is also the active centre, and those in which the chiral centre is distinct from the active centre. Numerous examples also exist where centrochiral metal complexes are used as auxiliaries[44, 45] however, these will not be discussed here.

Figure 1.11 provides two examples of catalysts in which the metal centre is bifunctional. This includes an example of the C2 symmetric Brintzinger system introduced previously. Here the achiral ligand is locked into a conformation with planar chirality by the coordinating titanium centre. Complexes such as *ansa*-bis(tetrahydroindenyl)titanium dichloride (Figure 1.11a) are useful polymerisation and lewis acid catalysts.[46] Also shown is an octahedral iridium catalyst with Δ/Λ-stereochemistry (Figure 1.11b) used for photo-assisted enantioselective alkylation.

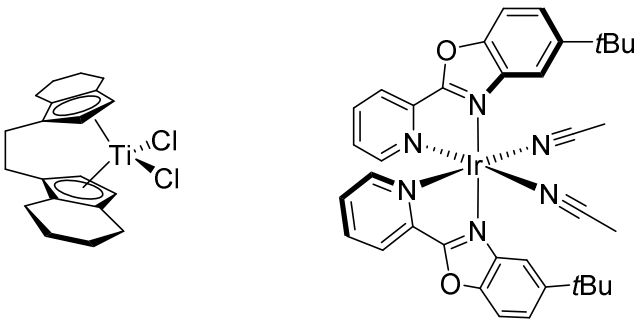

(a) (b)

Figure 1.11: *Examples of bifunctional asymmetric catalysts in which the active metal centre is also the source of stereochemistry.*

More relevant to this work are catalysts where the enantiomeric metal centre comprises part of a stereodirecting ligand as in Figure 1.12. For example, the rhodium hydrogenation catalyst in Figure 1.12a is coordinated by bridging phosphine donors to a pseudo-tetrahedral rhenium piano-stool complex providing a formal stereocentre.[47] The diastereomeric phosphine ligand in Figure 1.12b contains both an organic stereocentre and a ferrocenyl moiety with planar chirality.[48] This has been employed in asymmetric cross-couplings. Figure 1.12c presents an interesting system containing an octahedral tris-bidentate iridium complex with resolved Δ or Λ stereochemistry appended to a hydrogen bonding organocatalyst. The enantiomeric iridium moiety has shown excellent proficiency for stereodirecting transfer hydrogenation, producing enantiomeric excesses of up to 99%.[49]

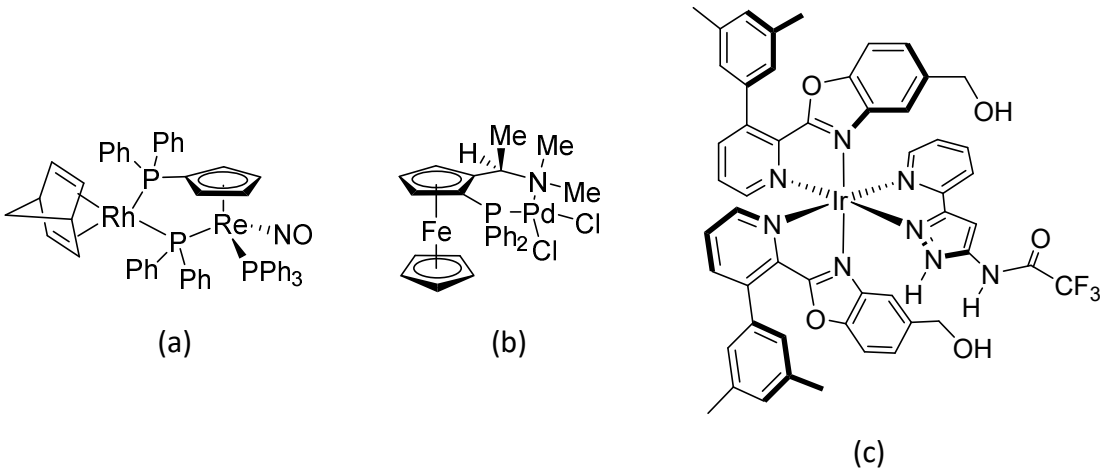

Figure 1.12: *Examples of asymmetric catalysts with metal centred chirality separate from the active site.*

Despite the above examples, there has only been stuttered development in this arena of asymmetric catalysis.[50] Curiously, enantiomerically resolved tris-bidentate octahedral complexes have not been derivatised as stereodirecting ligands for a separate active metal centre.[51] This would be conceptually similar to the system in Figure 1.12c, but for metal driven catalysis rather than organocatalysis. It is surprising given that enantiomeric resolution of complexes such as $[Ru(phen)_3]^{2+}$ and related precursors is well documented (see section 5.7). Furthermore, their excellent thermal stability means

they are resistant to racemisation which is cited as a major drawback of utilising metal centred chirality in asymmetric syntheses.[40, 50, 52] Part of this research project therefore endeavoured to establish a synthetic protocol towards plausible ligands bearing enantiomerically resolved Δ-$[Ru(phen)_3]^{2+}$ or Λ-$[Ru(phen)_3]^{2+}$ components for use in metal-mediated catalysis. This is discussed further in section 1.1.1.

1.3. *N*-heterocyclic carbenes

A carbene is defined as a compound with a neutral divalent carbon centre that has six electrons. Carbenes have long been employed as highly reactive intermediates in organic synthesis,[53] however, their status as transient species was revised in 1991 when Arduengo and co-workers isolated and crystallised the first free carbene, the *N*-heterocyclic carbene (NHC) shown in Figure 1.13.[54]

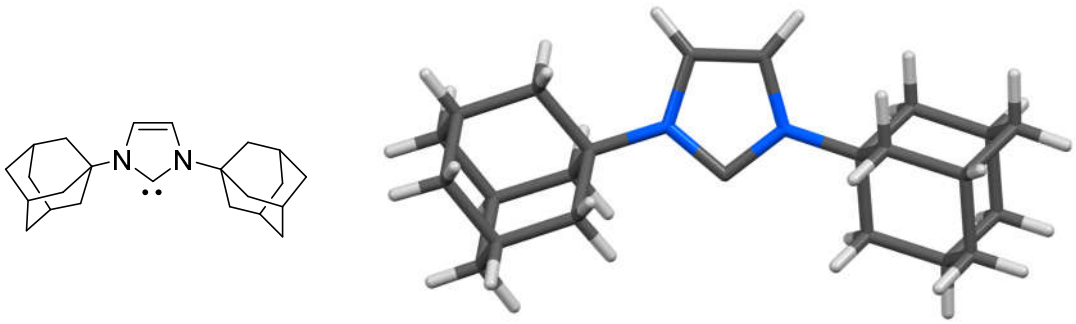

Figure 1.13: *The first isolated carbene and its crystal structure.*

This ground-breaking demonstration of NHC stability heralded an explosion of interest and in the intervening years NHCs have become ubiquitous in the literature, particularly as ligands for transition-metals.

The term *N*-heterocyclic carbene refers to a broad class cyclic carbene with a nitrogen atom adjacent to the carbene centre. There are a number of possible NHC core motifs derived from different *N*-heterocycles, some of these are shown in Figure 1.14. Imidazole based imidazolin-2-ylidene NHCs are the most frequently reported class of NHC ligand. As they are also the focus of this thesis, the following introduction will centre on NHCs of this type. Nonetheless, modulation of the NHC core provides a valuable means of diversifying a system's functionality. For example, saturated imidazolidin-2-ylidenes have different σ-basicity and π-acceptor ability when compared with imidazolin-2-ylidenes due to the lack of conjugation. This can appreciably change the reactivity of both the free carbene and its complexes.[55, 56] Different core structures are exploited for tailored applications as is the case for thiazole and triazole derived NHCs which have excelled as organocatalysts in umpolung reactions such as the benzoin condensation.[57] As the 6-membered hexahydropyrimidin-2-ylidene shows, NHCs are not restricted to 5-membered heterocycles. Carbenes of 3, 4 and 7-membered *N*-heterocycles have also been reported.[58]

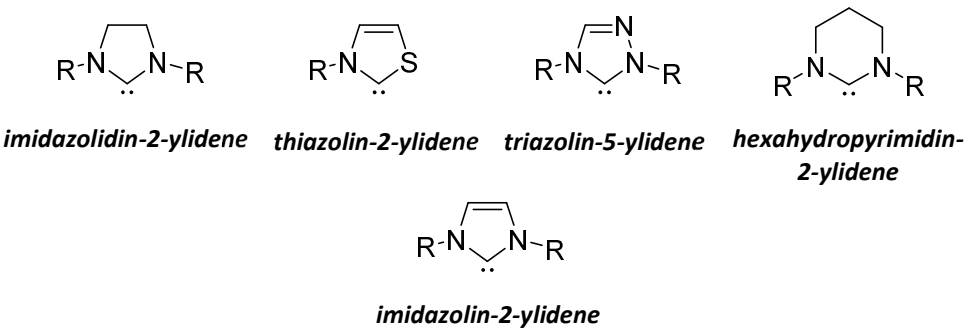

Figure 1.14: *Examples of different NHC core units.*

NHC ligands have been utilised for a variety of applications including supramolecular frameworks,[59, 60] luminescent probes[61-63] and in medicinal compounds.[64] Their most widespread application, however, continues to be as ligands in metal-mediated catalysis for which their excellent electron donating properties and steric tunability has been

exploited with tremendous success.[65] Introduction of new structural features to NHCs sees their catalytic uses continue to expand.

1.3.1. Organometallic *N*-heterocyclic carbene compounds

NHCs have been shown to form stable complexes with all of the transition metals as well as many lanthanides and main-group elements.[58] Stabilisation of carbenes by metal coordination has long been utilised in organometallic synthesis. The first ligated carbene was isolated as a tungsten carbonyl carbene complex; $(CO)_5WC(OMe)Me$ by Fischer in 1964.[66] Heteroatom substituted singlet-carbene ligands, including NHCs, are known as "Fischer carbenes" in homage to this pioneering work. Prior to this, Wanzlick had begun investigating the chemistry of NHCs,[67] however, it was not until 1968 that he and Schönherr reported the first NHC-metal complex (Scheme 1.8).[68]

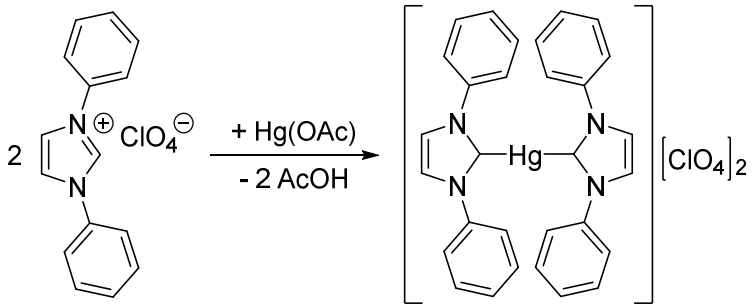

Scheme 1.8: *Synthesis of the first reported NHC-metal complex by Wanzlick et al.*

Carbenes have either a triplet or singlet electronic state depending on how the two non-bonding electrons are distributed within a σ-molecular orbital and p-atomic orbital (referred to as p_π) (Figure 1.15a). A singlet ground-state occurs when both electrons occupy the σ orbital with an anti-parallel spin orientation giving rise to an sp^2-hybridised carbon centre. Alternatively, in a triplet ground-state, the carbon centre is *sp*-hybridised and the two non-bonding electrons separately occupy the σ and p_π orbitals with parallel

spins.[58] Steric and electronic effects of the substituents at the carbene centre control the multiplicity of the ground state which, in turn, affects its reactivity.

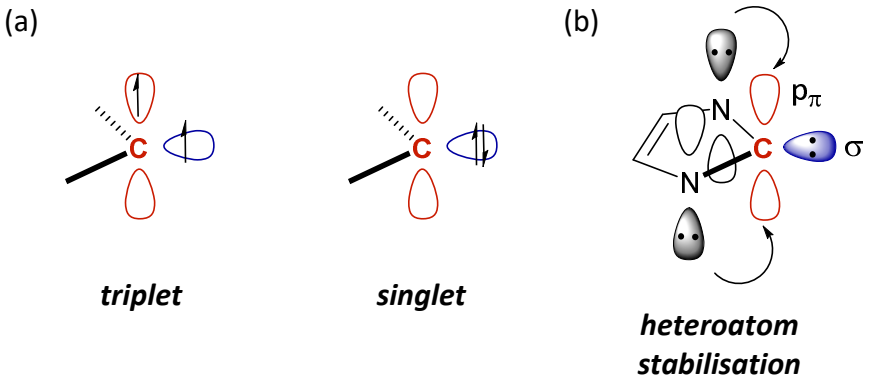

Figure 1.15 (a): *Orbital occupations of triplet and singlet carbenes and,* ***(b)*** *electronic resonance stabilisation conferred by nitrogen atoms in an NHC.*

Singlet carbenes are significantly stabilised by π donation into the empty p_π orbital, and by σ-withdrawing substituents adjacent to the carbene centre. In NHCs, heteroatom stabilisation is provided by at least one nitrogen atom neighbouring the carbene centre (Figure 1.15b). Consequently, Fischer type carbenes, including NHCs, invariably have a singlet configuration to ensure a vacant p_π orbital. Stabilisation in this way offsets the pairing energy required to overcome electron-electron repulsion in a singlet spin-state. Because NHCs possess a filled σ-orbital and empty p_π orbital they are proficient σ-donors with the capacity to accept electron density and, as such, are ambiphilic in nature.[58] Organometallic bonding of NHCs is characterised by strong σ-donation coupled with the weak π-accepting ability conferred by the vacant p_π orbital (Figure 1.16).[55]

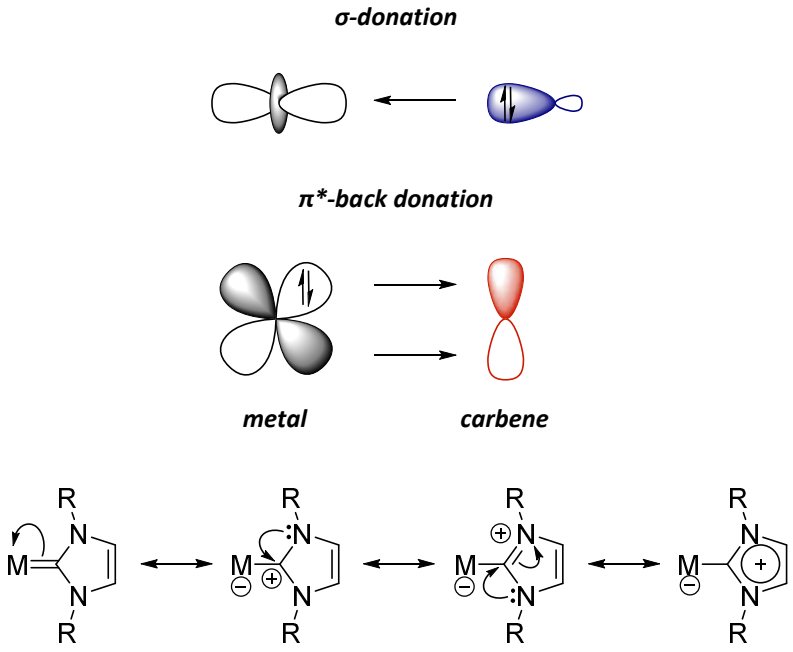

Figure 1.16: *Showing the organometallic bonding of NHC (Fischer type) complexes and highlighting the conjugation in NHC ligands.*

Alkylidene or Schrock carbene complexes have no heteroatoms adjacent to the carbenic carbon and hence are devoid of heteroatom stabilisation. These favour a triplet-configuration to minimise inter-electron repulsion and are considered to be a diradical. The metal-alkylidene bond is covalent in nature resulting from the coupling of two triplet fragments to give a nominal double bond (Figure 1.17).

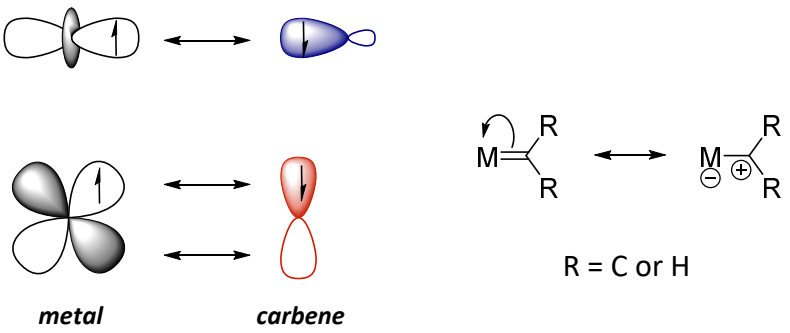

Figure 1.17: *Showing the organometallic bonding of alkylidene (Schrock type) complexes and highlighting the lack of stabilisation.*

These species are nucleophilic and much less stable than their Fischer carbene counterparts.

1.3.2. Structure and properties of NHC complexes

Early investigations of the use of NHC ligands treated them as simple tertiary phosphine mimics due to their comparable σ-donating ability. However, although NHCs and phosphines have similar electronic properties, NHCs are more tolerant to manipulation of substituents and are therefore more tuneable.[69] Figure 1.18 indicates the sites for modification of an imidazolin-2-ylidene complex. Changing *N*-atom substituents R_1 and R_3, referred to here as pendant groups, allows for manipulation of the kinetic stability of the free carbene as well as the stability of the NHC-metal complex through steric effects. Bulky *N*-bound substituents provide crucial kinetic stabilisation to free NHCs by sterically shielding the carbene centre. It is no coincidence that the first isolable NHC was functionalised with adamantyl groups as shown in Figure 1.13.

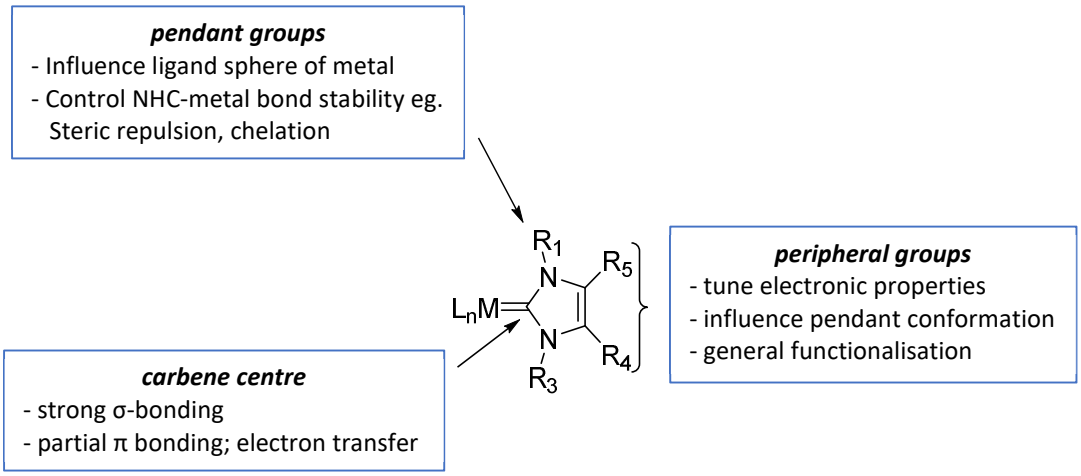

Figure 1.18: *Summarising the key features of an imidazolin-2-ylidene NHC core.*

Conversely, increased steric crowding reduces NHC – metal bond stability by enforcing a longer metal to ligand bond.[70] Pendant groups can be modified with coordinating

substituents to produce stabilising multi-dentate ligands with both traditional or NHC donors.[58] Regarding catalysis, pendant groups are used to tune the steric environment at the active metal centre and modulate precatalyst stability through, for example, chelation.[71] Appropriate choice of peripheral R_4 and R_5 substituents can be used to manipulate the solubility of catalysts in different media,[70] or for fixation of catalytically active NHCs onto a solid support.[71] Bulky backbone substituents can also influence the conformation of the pendant groups whereby geometric information is transferred from the NHC backbone to the active site of catalysis via the pendant groups (see Scheme 1.10 for an example).

NHC ligands with moderately bulky pendant groups can elicit a similar steric influence to the bulkiest of tertiary phosphine ligands. This is because NHC pendant groups are directed into the coordination sphere of the metal whereas phosphine substituents point outwards (Figure 1.19).

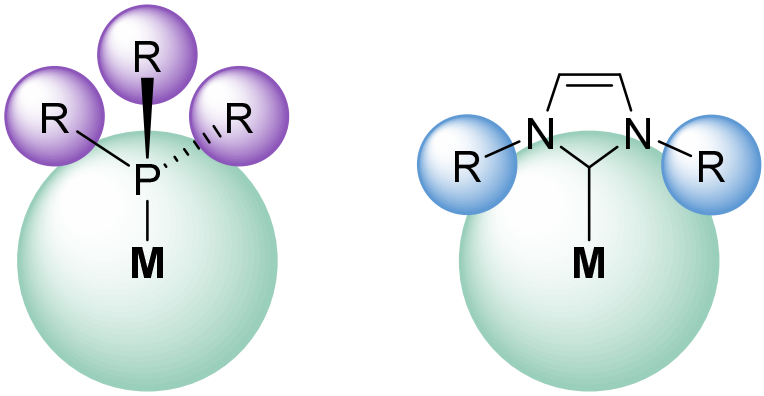

Figure 1.19: *Steric influence of a tertiary phosphine ligand vs. an NHC ligand.*

A study by Nolan and co-workers experimentally quantified this assertion by comparing crystal structures of a series of nickel-carbonyl complexes of the type $Ni(NHC)(CO)_n$ and $Ni(PR_3)(CO)_3$.[72] In an extreme case, the steric bulk of NHCs with pendant adamantyl or tertiary-butyl groups disallowed coordination of a third CO ligand resulting in trigonal planar $Ni(NHC)(CO)_2$ complexes. Nolan and Cavallo have also developed a model to

quantify NHC steric bulk as "percent buried volume" (%V_{bur}).[73] This is defined as the total volume of the metal coordination sphere occupied by the ligand and is calculated using crystallographic data.

As well as structural advantages, analysing the bond dissociation energies (BDEs) of metal to ligand bonds in a series of NHC complexes revealed them to be more stable than their phosphine analogues.[70, 72, 74] In addition to NHC to metal σ-donation, NHC to metal π-donation and metal to NHC-π^* back-donation also contribute to bond stability. The excellent electron donating ability of NHCs coupled with their steric tunability has seen them replace tertiary phosphines in many catalytic systems.[65]

1.3.3. *N*-heterocyclic carbene complexes in catalysis.

NHC ligands enjoy widespread application in metal mediated homogeneous catalysis for the reasons stated above.[39, 65, 75] Ruthenium-mediated alkene cross-metathesis catalysts are perhaps the most celebrated systems employing NHC ligands. The commercialisation of Grubb's catalysts (Figure 1.20)[76] has made alkene metathesis chemistry accessible to both academic researchers and industry alike.

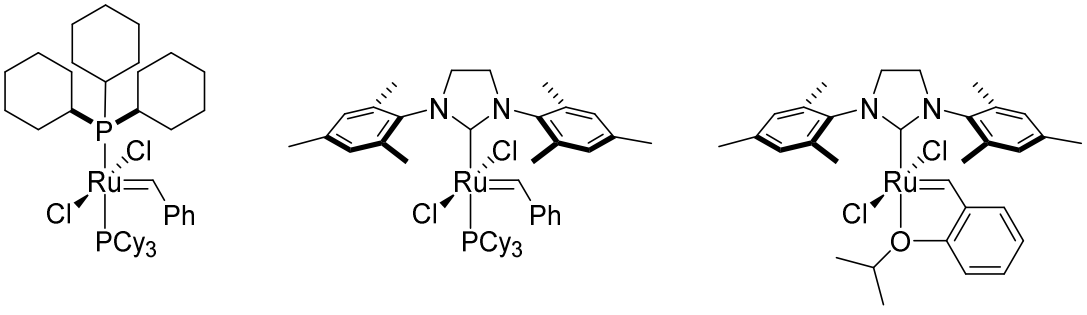

first generation ***second generation*** ***second generation (Hoveyda-Grubbs)***

Figure 1.20: *Grubb's metathesis catalyst, first and second generation.*

Recognising the significance of this, the 2005 Nobel Prize in chemistry was jointly awarded to Robert Grubbs, Yves Chauvin and Richard Schrock “for the development of the metathesis method in organic synthesis."[76-79]

Development of Grubb’s second generation catalyst provides an interesting case study exemplifying some of the merits of NHC ligands in catalysis. Scheme 1.9 depicts a generalised mechanism for ruthenium-mediated alkene metathesis.[80] The catalyst is introduced as a 16-electron ruthenium complex and initiation relies on dissociation of L_2 to produce the active 14-electron species. A low ratio of L_2 re-association is required for high activity. Replacing the phosphine ligand in the L_1 position (first generation) with a bulky NHC ligand (second generation) promotes dissociation of L_2 and inhibits re-association through steric destabilisation. Furthermore, the stronger σ-donor ability of the NHC promotes ligand exchange through the kinetic trans effect and ensures a strong NHC-Ru bond to stabilise the 14-electron catalyst intermediate and resulting alkene complex.

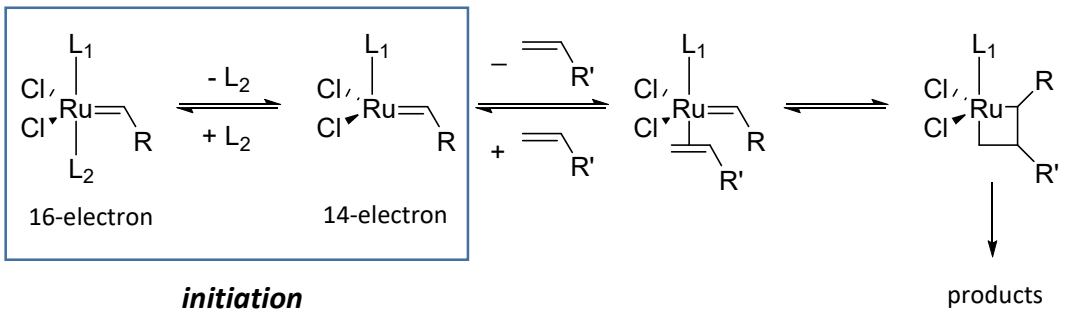

Scheme 1.9: *General metathesis mechanism with initiation step highlighted.*

This NHC-metal bond stability is central to the effectiveness of NHC ligands in catalysis as it ensures long-lived active species with preservation of the active site environment for product consistency. This is particularly important for achieving high enantiomeric excess in stereoselective reactions. Because structural alteration of the NHC core can be performed without greatly weakening its organometallic bonding, existing catalyst systems are easily adapted for asymmetric catalysis. For example, Grubb’s and co-

workers successfully developed a catalyst suited to asymmetric ring closing metathesis by replacing the achiral NHC ligand of their second generation catalyst with an enantiomeric one (Scheme 1.10).[81]

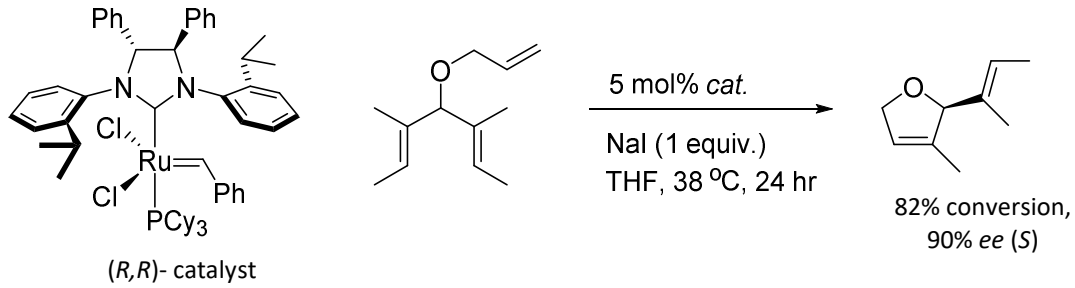

Scheme 1.10: *Enantioselective ring closing metathesis directed by a chiral NHC ligand.*

Here the NHC ligand dictates the stereochemical configuration of the metathesis product. Interestingly, this also demonstrates how chiral information from the peripheral substituents can be communicated to the active site via the pendant groups. Related systems have also been deployed in the stereoselective synthesis of some pharmaceutically relevant compounds such as (+)-erogorgiaene, an inhibitor of mycobacterium tuberculosis.[82]

More relevant to this current investigation is the application of NHC ligands for palladium mediated coupling reactions such as the Suzuki-Miyaura coupling. Again, NHCs are well suited to substitute phosphines in this role as they coordinate strongly to both Pd(II) and neutral Pd(0). As in the metathesis example above, the NHC renders electronic and kinetic stabilisation to the active Pd(0), in fact, NHC complexes of zero-valent Pd(0)[83] and Ni(0)[84] have been isolated and characterised. Strong bonding is maintained throughout the cycle of Pd(II) intermediates, preserving the active site environment. Several simple NHC ligated palladium complex motifs have proven to be effective systems for Suzuki cross coupling reactions and other palladium couplings. These include Pd(NHC)(allyl)Cl,[85] Pd(NHC)(acac)Cl,[38] Pd(NHC)(Me)Br[86] and PEPPSI systems[87] (Figure 1.21).

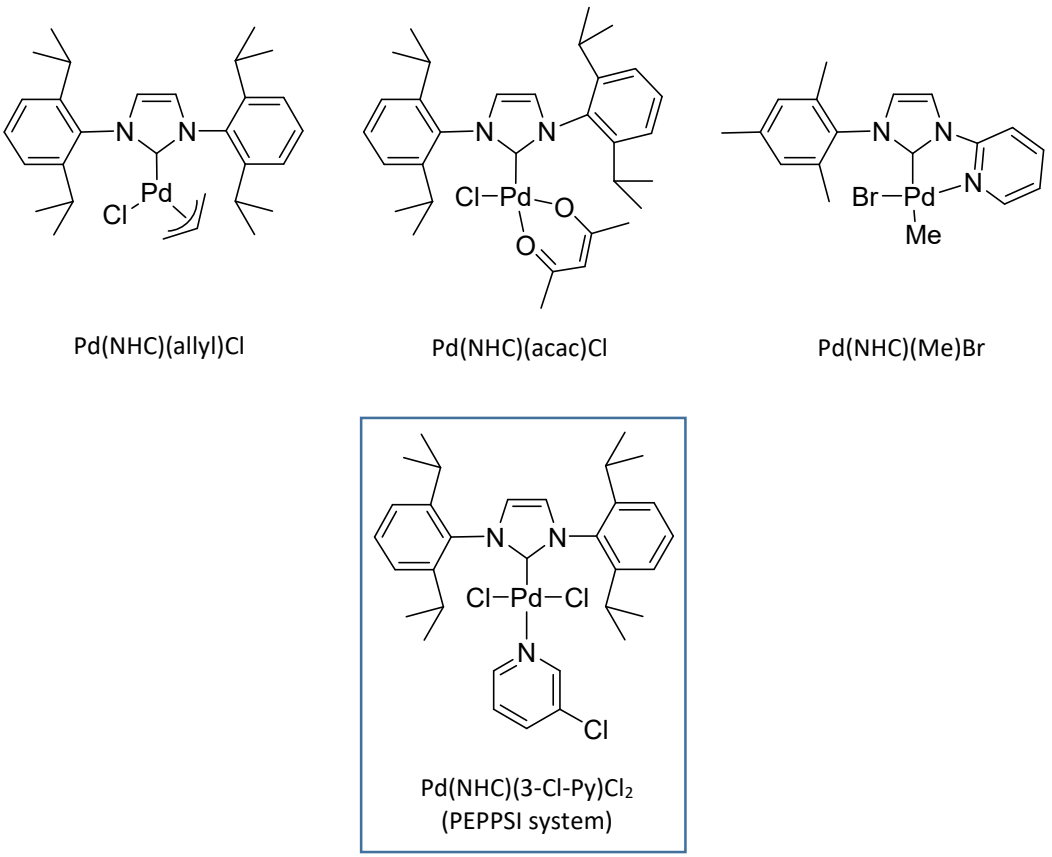

Figure 1.21: *NHC precatalysts systems for palladium catalysed reactions.*

The PEPPSI (Pyridine-Enhanced Precatalyst Preparation Stabilization and Initiation) class in particular has emerged as a highly efficient, stable precatalyst for palladium mediated couplings and can be purchased commercially on a multi-kilogram scale. PEPPSI catalysts employ a 3-chloro-pyridine "throw-away" ligand which serves to stabilise the precatalyst whilst facilitating rapid activation by dissociating readily.[88] The NHC ligand binds the metal tightly throughout the cycle and its steric bulk improves reductive elimination of the substrate which in turn increases the turnover number (TON).[89] Unlike traditional palladium phosphine catalysts, PEPPSI is robust and can be stored indefinitely outside an inert atmosphere. During reactions it is resistant to decomposition at elevated temperatures and in aqueous conditions. The active NHC-Pd(0) is generated in situ through reduction of the Pd(II) precatalyst. As such, it is considered a stabilised $Pd(PPh_3)_4$ surrogate.

Implementation of enantiomeric NHCs for asymmetric palladium couplings has been less successful than for metathesis or ruthenium, rhodium and iridium catalysed hydrogenation and transfer hydrogenation.[75, 90] Nonetheless, interest in this burgeoning field continues to simmer and many attempts have been made to exploit the power of palladium NHC complexes for asymmetric synthesis. One of the more successful examples, shown in Scheme 1.11, is a chiral adaptation of the PEPPSI system.[91] This has been applied to the synthesis of axially chiral biaryl compounds, although, only modest enantiomeric excesses could be achieved.

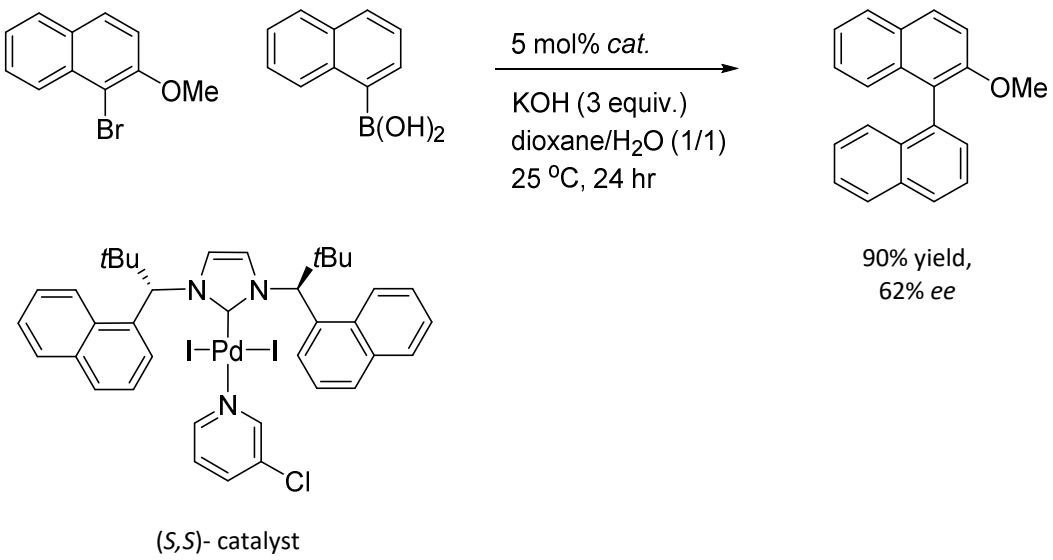

Scheme 1.11: *Enantioselective synthesis of axially chiral biaryls using an asymmetric PEPPSI catalyst.*

Employing a well-defined NHC-Pd(II) precatalyst affords control over the structure of the active entity, however, it is not necessary to use a preformed species. Often an NHC proligand is introduced to the reacting system as an imidazolium salt along with a Pd(II) source.[39] This is commonplace in Suzuki couplings which proceed under basic conditions enabling precatalyst formation in situ. It is routinely observed that withholding the NHC proligand prevents any catalysis, confirming that the NHC is essential to maintaining the activity and solubility of the palladium.

This research endeavour sought to develop novel, enantiomeric NHC ligands and incorporate them into existing catalyst systems such as those shown in Figure 1.21. The aim of doing so being to diversify NHC ligand sets and access new systems to improve enantioselectivity. This is necessary because moderate asymmetric induction and system dependence continue to hamper to the wholescale application of NHCs in synthetically relevant asymmetric palladium couplings.[92]

1.3.4. Synthesis of NHC precursors

NHCs can be generated from a variety of precursors, the syntheses of which have been detailed in an excellent review by César *et al.*[93] For imidazolin-2-ylidene NHCs, the most universally applicable precursors are imidazolium salts. All NHCs prepared in this study are derived from imidazolium salts which serves to illustrate how one approach can be manipulated to produce a myriad of different NHCs.

Methods for preparing imidazolium salts are varied and typically chosen depending on the chemistry of the appended functional groups. Scheme 1.12 summarises several common routes to imidazolium salt NHC precursors. Highly substituted symmetrical imidazolium salts are often prepared by annulation of substituted diazdienes using a C1 electrophile as in route A. The electrophile is typically formaldehyde, chloromethylethyl-ether or trimethyl-orthoformate.[94] A related one-pot synthesis using a 1,2-diketone with a primary amine and formaldehyde has been demonstrated for less hindered precursors.[95] Alternatively, pendant groups can be appended stepwise as shown in route B. This involves the nucleophilic substitution of a halogenated electrophile by a preformed *N*-substituted imidazole and is well suited to the preparation of unsymmetrical NHC precursors.[96] A less used but still efficient methodology employs the reaction of a formamidine (either symmetrical or unsymmetrical) with an α-bromoketone as in route C.[97] Oxazolines are also useful intermediates although they are rarely encountered (route D).[98]

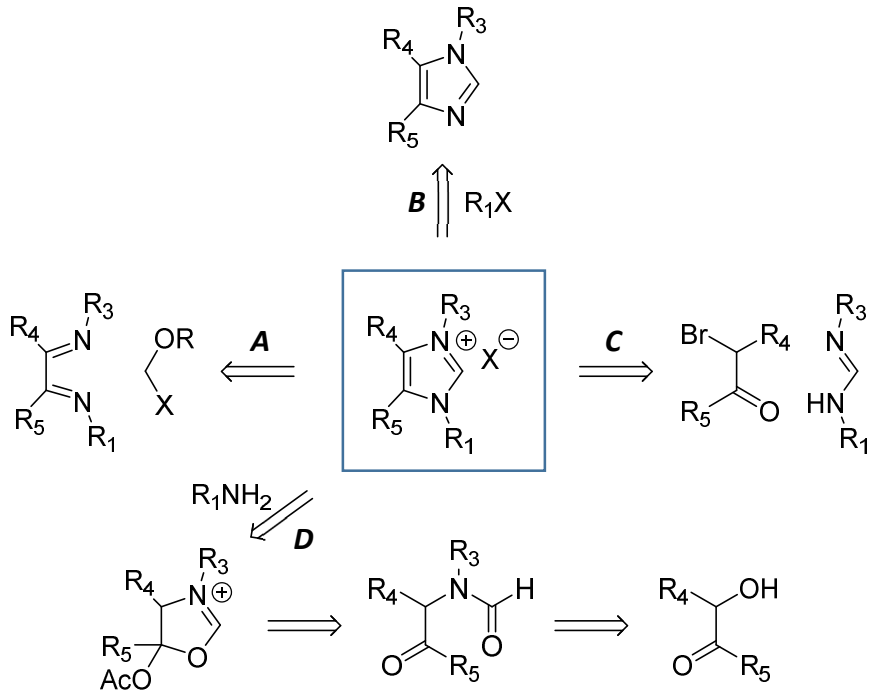

Scheme 1.12: *Retrosynthetic pathways to imidazolium salt NHC precursors.*

1.3.5. Synthesis of NHC complexes

NHC complexes can be prepared by numerous methods using various imidazolyl-adducts.[58] Imidazolium salt precursors are converted to NHCs by removal of the NC*H*N proton under basic conditions. Generally, for the synthesis of NHC complexes this is conducted in one of 3 ways; substitution of a labile ligand by a free NHC, in situ generation of the free NHC from an imidazolium salt in the presence of a metal source or, transmetalation from an NHC-silver complex.[39] The choice of approach is ultimately system dependent. These are represented in Scheme 1.13.

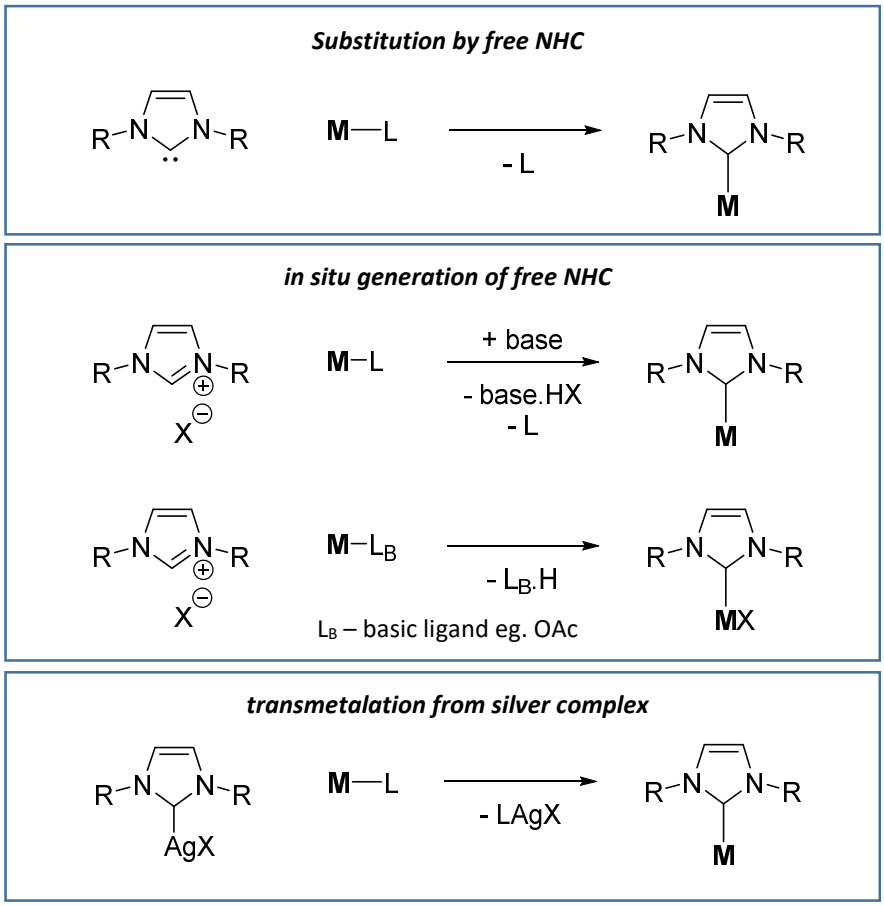

Scheme 1.13: *Common synthetic routes to NHC complexes.*

Stable NHC ligands can be prepared under anhydrous conditions by reaction with a strong base such as *t*-BuOK or NaH and isolated to be combined with a metallic fragment in a separate step.[38] It is, however, much more common to generate the NHC complex in situ by deprotonating the imidazolium salt in the presence of the metal source. NHCs generated in this way are rapidly sequestered by the metal, thus driving equilibrium towards NHC formation (Scheme 1.14).[99] This enables the use of much weaker bases including K_2CO_3, sodium acetate, or pyridine and can be applied to more functionally diverse imidazolium salts. Primary generation of a free NHC typically provides better stoichiometric control than in situ NHC-complex formation.

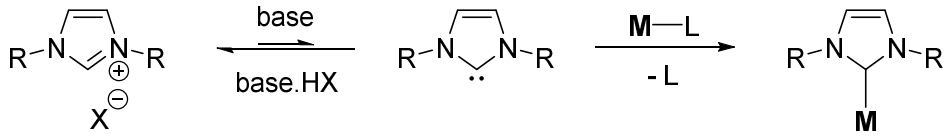

Scheme 1.14: *Mechanism proposed for NHC complex formation using a weak base or basic ligand.*

Concomitant NHC formation and coordination can also be achieved using basic metal-ion sources. These can be mildly basic salts such as metal-oxides,[100-102] hydrides[103] or acetates,[71] or complexes with basic organic ligands including alkyls[104] and acetyl-acetonate (acac).[105] Synthesis by this method is again driven by the strong metallic bonding of NHCs.

Useful late transition metal NHC complexes are regularly prepared via transmetalation of an NHC-silver complex. This has emerged as the foremost method of NHC complex preparation due to the robust and adaptable synthesis of silver-NHC complexes by reaction of an imidazolium salt with Ag_2O. It occurs in a variety of solvents at room temperature, although, elevated temperatures can be employed if necessary.[106] Silver-NHCs are often sufficiently stable to be isolated, although, are more commonly reacted onwards by in situ treatment with a transition metal precursor. The lability of the NHC – Ag(I) bond ensures efficient transmetalation that is often driven by precipitation of an insoluble silver halide.

Precursors other than imidazolium salts have also been applied to NHC generation. One example is by thermal decomposition of imidazole adducts substituted in the C2 position; these are considered “protected carbenes.” A representative example shown in Scheme 1.15 employs a pentafluorophenyl-NHC adduct.[107] This approach has also been demonstrated using NHC dimers and alkoxyl[108] or carbon-dioxide NHC adducts.[109]

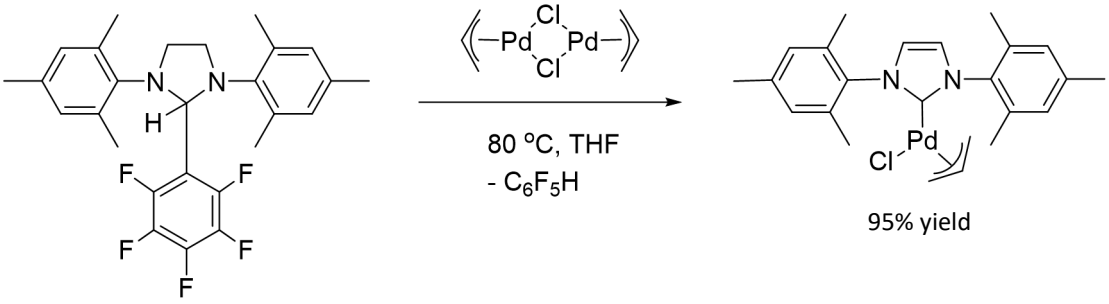

Scheme 1.15: *NHC complex formation by thermal decomposition.*

1.4. Novel system design and development

Despite a handful of notable exceptions, the application of enantioselective synthesis in industry remains in its infancy. This is due to the lack of efficient and generally applicable methodologies and, for this reason, researchers remain in pursuit of novel asymmetric catalysts. Continual development of functional enantioelective syntheses is crucial to accessing new chiral compounds of social importance such as pharmaceuticals. Improved asymmetric synthesis will also serve to streamline existing commercial preparations which rely on the expensive and wasteful resolution of racemates. This would provide an essential cost saving measure to improve consumer access to life-saving therapeutics.

NHC ligands have been used expansively in transition metal catalysis with notable examples including Grubbs metathesis catalysts and PEPPSI coupling catalysts. However, enantiomeric NHC ligands are yet to be applied widely to asymmetric palladium couplings. As such, the power of NHC ligands in palladium-mediated asymmetric synthesis has not been harnessed to its full potential.

This being the case, this research undertook to expand the library of enantiomeric NHC ligands, introducing several novel contributions with an eye to their use in asymmetric palladium couplings. The broad intention of this research was to:

1) Develop new methods for incorporating "traditional" enantiomeric functionality into active systems.
2) Introduce metal-centred helical chirality of tris-bidentate octahedral complexes as a novel stereodirecting unit for metal mediated asymmetric catalysis.

Systems have been established which fulfil this overall vision. Four of the NHC complexes targeted during this research are shown in Figure 1.22. These are broadly classed as being NHC ligands with organic chirality, model systems with no chirality or metal centred chirality.

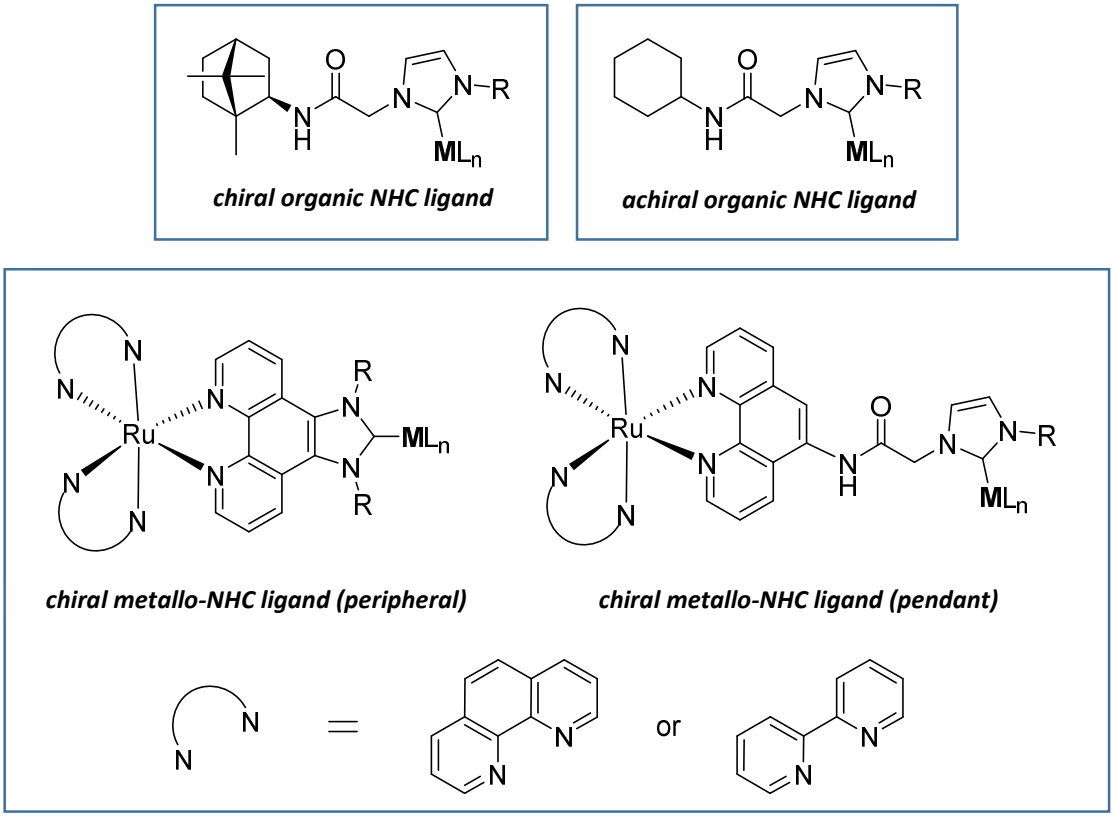

Figure 1.22: *Some of the target systems explored in this thesis.*

In three of these targets the NHC is tethered to the defining unit by an acetamide linkage. Acetamide linked NHCs are discussed in the next section. Also introduced here is the novel application of a ruthenium tris-bidentate moiety to impart stereochemical control over a catalytically active centre. Otherwise, further explanation of these targets, and others, and the reasons for their selection is provided in their respective chapters. A brief survey of their catalytic function in an asymmetric Suzuki coupling is presented in Chapter 6.

1.4.1. System functionalisation; acetamide-linked NHC derivatives

Acetamide linking units have emerged as an expedient method of NHC functionalisation but remain largely unexplored in the context of asymmetric catalysis. The acetamide-linked class of NHC derivatives encompasses many NHC proligands, NHCs and NHC complexes with at least one *N*-substitution of the azole core occurring to the *C*-terminus of an acetamide moiety (Figure 1.23). This discussion will be restricted to monoamido-functionalised NHC derivatives of imidazole (Figure 1.23a).

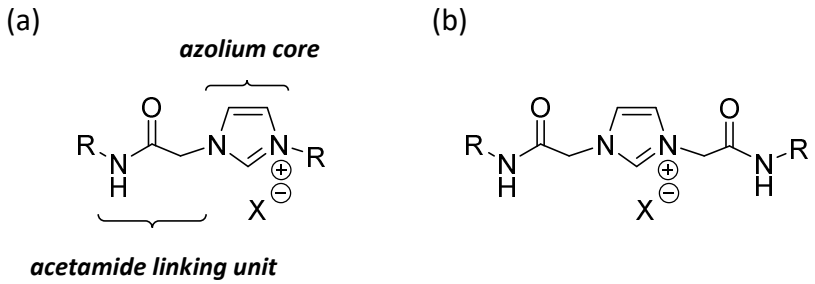

Figure 1.23 (a): *Monoamido-functionalised and,* ***(b)*** *diamido-functionalised NHC proligands derived from imidazole.*

Ligands of this type are one of the most synthetically accessible and easily modulated sources of NHC derivatives with potentially anionic functionality.[110] Incorporation of an

anionic component into an NHC ligand system may be desired for several reasons including to; improve complex stability,[111] reduce overall complex charge and to act as a hemilabile, potentially basic group, in bifunctional catalysis.[112, 113]

Complexation of monoamido-functionalised NHCs results in one of three coordination motifs; chelate, pendant or bridging (Figure 1.24). This variability is a consequence of the flexible linking unit between the NHC and a secondary amide donor that can be selectively coordinated depending on the synthetic conditions. The result is a dual functional ligand with highly dissimilar coordination sites.

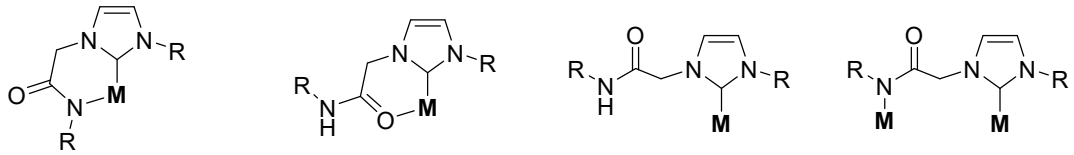

Figure 1.24: *Coordination modes exhibited by amido-functionalised NHC ligands.*

The most commonly reported coordination mode is *N*-amidate/NHC chelation between the deprotonated amide nitrogen and the NHC. Chelation between the neutral amide oxygen and the NHC is also possible, however, *O*-amido/NHC type binding has been reported exclusively for complexes with Ru(II).[114, 115] When acting as a monodentate ligand, coordination only occurs via the NHC resulting in a pendant type complex. These form preferentially with metals that favour a linear geometry such as Ag(I) and Au(I)[116, 117] or when reaction conditions are insufficiently basic to allow deprotonation of the amide.[105, 118] It has been shown in this study that pendant type complexes are also favoured by ligands with bulky *N*-amido substituents due to steric destabilisation of the corresponding chelated form. The bridging of two metal centres by amido-functionalised NHC ligands is uncommon, demonstrated once by Ghosh *et al.* through the synthesis of neutral 12-membered macrometallacycles with Ag(I) and Au(I) nuclei.[116]

The potential of these ligands as supramolecular synthons does not appear to have been explored further.

N-amido/NHCs have been successfully deployed as ligands in several palladium-mediated couplings.[119] In this context the presences of an amide chelating arm has several advantages. In addition to the robust NHC donor, the anionic acetamide chelation can impart a high electron density on the palladium centre thus improving oxidative addition and enabling the use of less reactive substrates such as aryl-chlorides.[120] Chelation also contributes to catalyst stability and facilitates the reductive elimination of products.[118]

These principles were applied by Lee *et al.* to a highly efficient NHC-Pd catalyst for Heck cross-couplings using an ionic liquid solvent tetra-*n*-butylammonium bromide (TBAB) at high temperatures (Scheme 1.16).[120, 121]

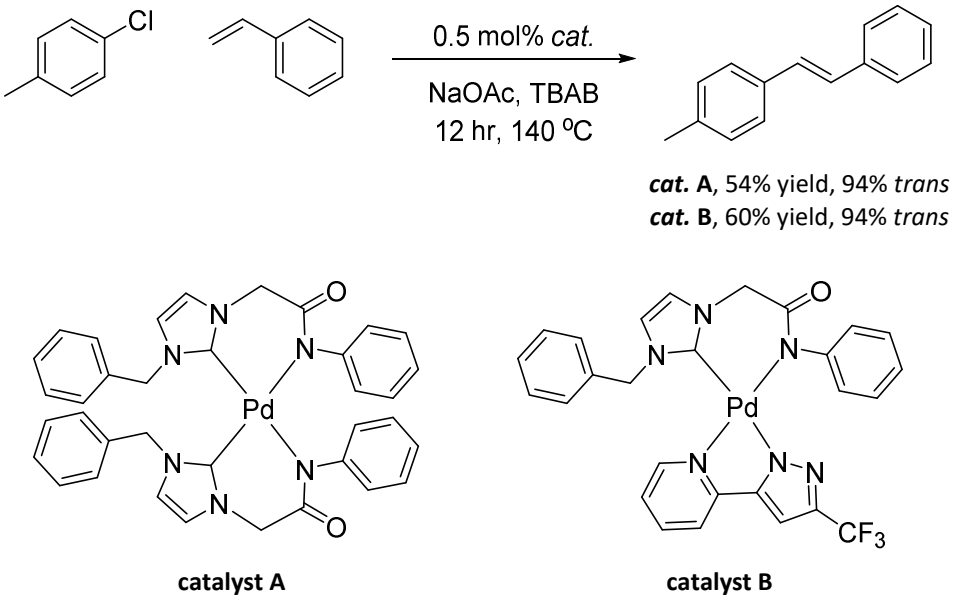

Scheme 1.16: *Heck coupling* N-*amidate/NHC palladium catalyst and a non-activated aryl chloride substrate.*

The *cis*-NHC complex (catalyst A) was found to perform adequately using aryl-chloride substrates, however, initiation times were slow due to having two tightly bound NHCs obstructing the active site. Efficiency was slightly improved by substituting one *N*-amido/NHC ligand for a similarly anionic but weaker binding 2-(trifluoromethyl)-5-(2-pyridyl)-pyrazolate (fppz) ligand (catalyst B). This system (and others) demonstrate the efficacy of using *N*-amido/NHC ligands for coupling with less reactive chloride substrates. Furthermore, it highlights the benefits of employing mono-*N*-amido/NHC precatalysts, a notion that was carried into this work.

It has also been shown that the *N*-amido/imidazolium salt can be introduced to the reaction mixture with a palladium source for the effective mediation of Suzuki couplings.[122] A range of variably functionalised *N*-amido/imidazolium salts were applied for this purpose, some of which are shown in Scheme 1.17.

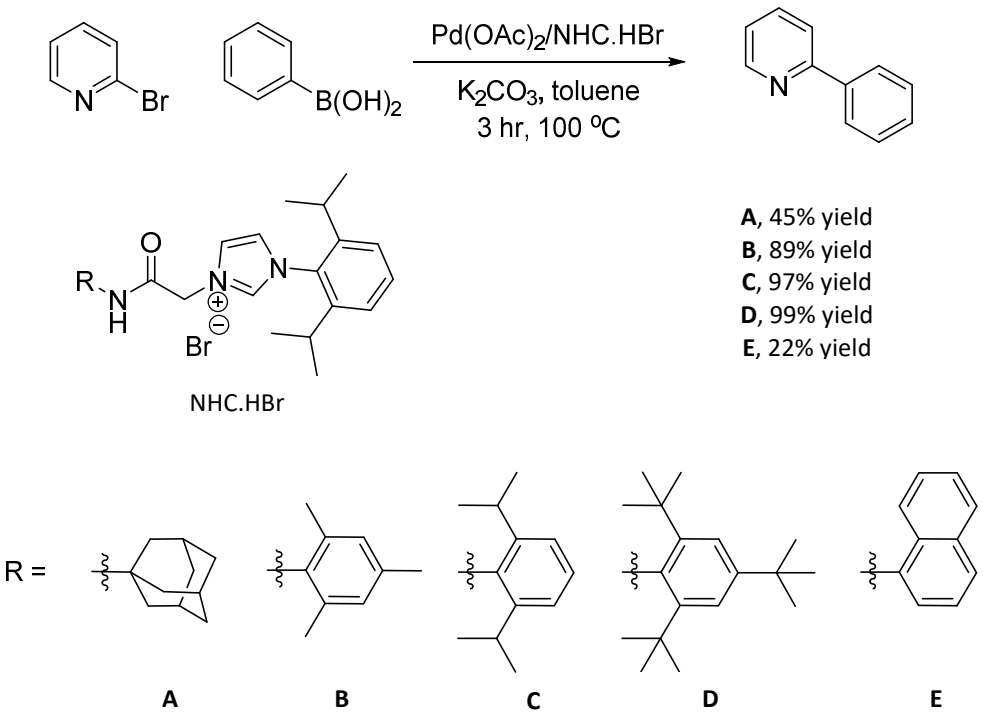

Scheme 1.17: N-*amido substituent effect of the yield of a Suzuki cross coupling using an* N-*amido/imidazolium salt NHC proligand and Pd(AcO)$_2$ catalyst.*

While these ligands displayed an excellent tolerance to a range of aryl bromides and heteroaryl bromides, they were found to be sensitive to the choice of boronic acid. Moderate efficiency was demonstrated using aryl chlorides. Most important of all, this study demonstrated that the nature of the *N*-amido functionality influences product turnover.

N-amide/NHC ligands were deemed a suitable target system based upon their ease of functionalisation and demonstrable catalytic performance. Furthermore, they remain a relatively unstudied class of NHC ligand, particularly in the context of asymmetric catalysis, with few examples of enantiomeric *N*-amide/NHC ligands known.[113, 115]

The synthesis and chemistry of acetamide-linked NHC proligands and *N*-amidate/NHC type complexes is addressed further in Chapter 1.

1.1.1. Harnessing supramolecular chirality

In section 1.2.3.1 the concept of chiral induction using metal templated enantiomers was introduced. It was noted that Δ/Λ helical chirality of tris-bidentate octahedral metal complexes has been used in organocatalytic asymmetric induction but have yet to be employed as stereodirecting groups to a separate, catalytically active metal centre.[51] One objective of this project was to develop a system that incorporates an enantiomerically resolved ruthenium-polypyridine ($[Ru(ppy)_3]^{2+}$) component into an NHC ligand which could coordinate to a catalytically active metal centre. This constitutes a novel source of chirality which, as yet, has not been applied to metal mediated asymmetric catalysis.

Octahedral ruthenium complexes with bidentate polypyridine (ppy) ligands of the type $[Ru(ppy)_3]^{2+}$ are well known as being thermally stable. Enantiomers of these are resistant to racemisation, although, this process can be induced photochemically.[123] Protocols for the resolution of racemic Δ/Λ-$[Ru(ppy)_3]^{2+}$ (and precursor complexes) into their constituent enantiomers are well established; these are introduced in section 5.7.

Because both enantiomers of a $[Ru(ppy)_3]^{2+}$ stereodirecting group can be obtained expediently, a functioning system could easily be prepared in both its Δ-$[Ru(ppy)_3]^{2+}$ and Λ-$[Ru(ppy)_3]^{2+}$ forms. Catalysts for both enantiomeric products of an asymmetric synthesis are therefore equally accessible (Scheme 1.18). This is a tremendous advantage over many "chiral pool" derived systems which may only be readily obtained as one of their enantiomers hence are only useful for the preparation of one enantiomeric product.

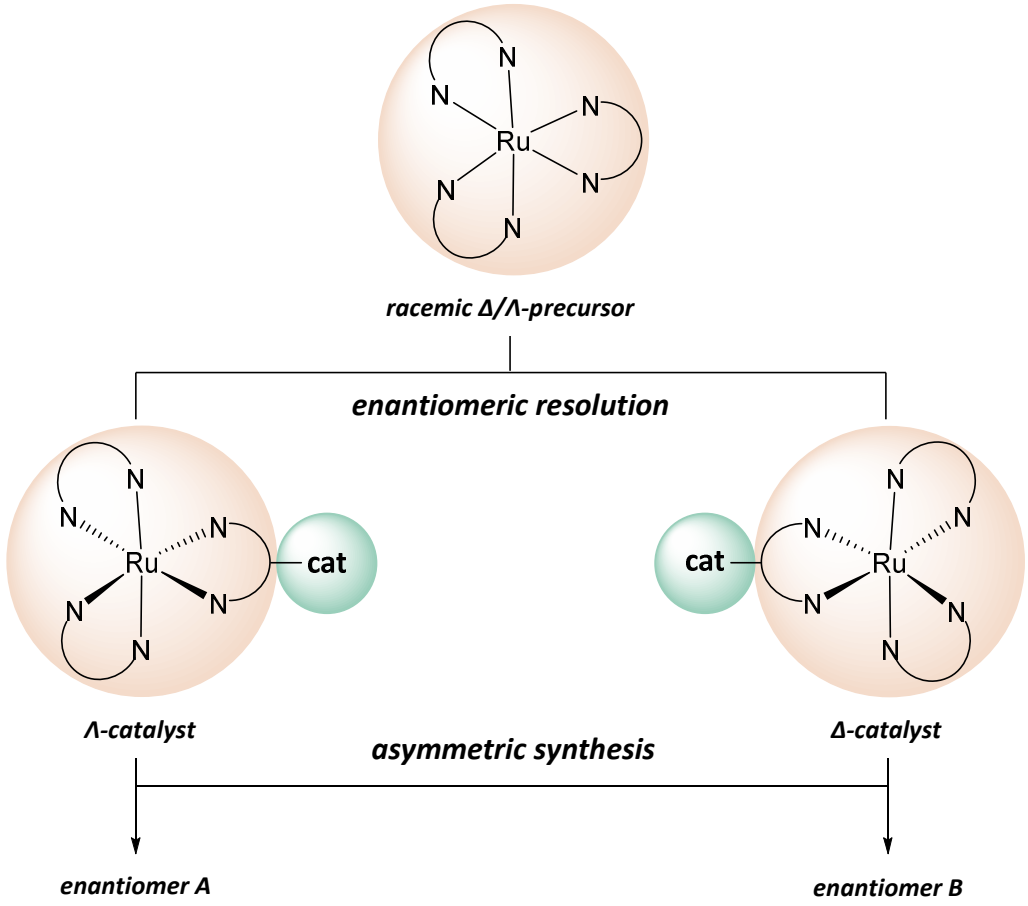

Scheme 1.18: *Illustrating how straightforward resolution of a racemic* $[Ru(ppy)_3]^{2+}$ *precursor provides both the Λ and Δ forms of a catalyst to selectively provide the two enantiomeric forms of an asymmetric product, enantiomer A and enantiomer B.*

Besides their stereochemical attributes, the metallo-NHC ligands designed and synthesised herein have other potential applications. Possessing a dominant,

hydrophilic moiety such as $[Ru(ppy)_3]^{2+}$ makes these complexes suited to catalysis in aqueous media pending selection of an appropriate counteranion such as chloride.[124] Catalysts with stereodirecting groups derived from organic fragments are less tenable to aqueous synthesis.[125] The remarkable photochemistry of $[Ru(ppy)_3]^{2+}$ provides another avenue of investigation as does potential electronic communication between metal centres in these hetero-dinuclear complexes.[126] Being bridging ligands also makes them potential supramolecular synthons. Many of these applications are beyond the scope of this thesis but serve to demonstrate the broad applicability of these systems for the benefit of future investigators.

1.1.2. Application in stereoselective synthesis.

It is hypothesised that the chiral $[Ru(ppy)_3]^{2+}$ architectures are suited to imparting stereocontrol over aromatic substrates. This is due to the, planar, aromatic surfaces of the polypyridine ancillary ligands. These systems were therefore trialled in the synthesis of axially chiral biaryl compounds by palladium catalysed asymmetric Suzuki cross-coupling. As such, the performance of several $[Ru(ppy)_3]^{2+}$ acetamide-linked NHC ligands were surveyed in this synthesis as were their organic chiral and achiral counterparts (Figure 1.22). It was hoped that the large structural differences between the *N*-amido functionality in this NHC ligand series could provide clearer insight into the effect of *N*-amido substituents on catalysis, particularly because chiral induction by these systems will be enhanced by re-association of the *N*-amidate during the catalytic cycle. It is proposed that the slow transmetalation step affords an opportunity for the catalytic intermediates to reconfigure (Figure 1.25).

Disassociation and re-association of the amidate group is expected to be heavily influenced by the steric bulk of the *N*-amido substituents as well as by resonance stabilisation of the amidate anion. Therefore, this series provides an opportunity to assess these effects on both enantiomeric excess and catalytic efficiency in general.

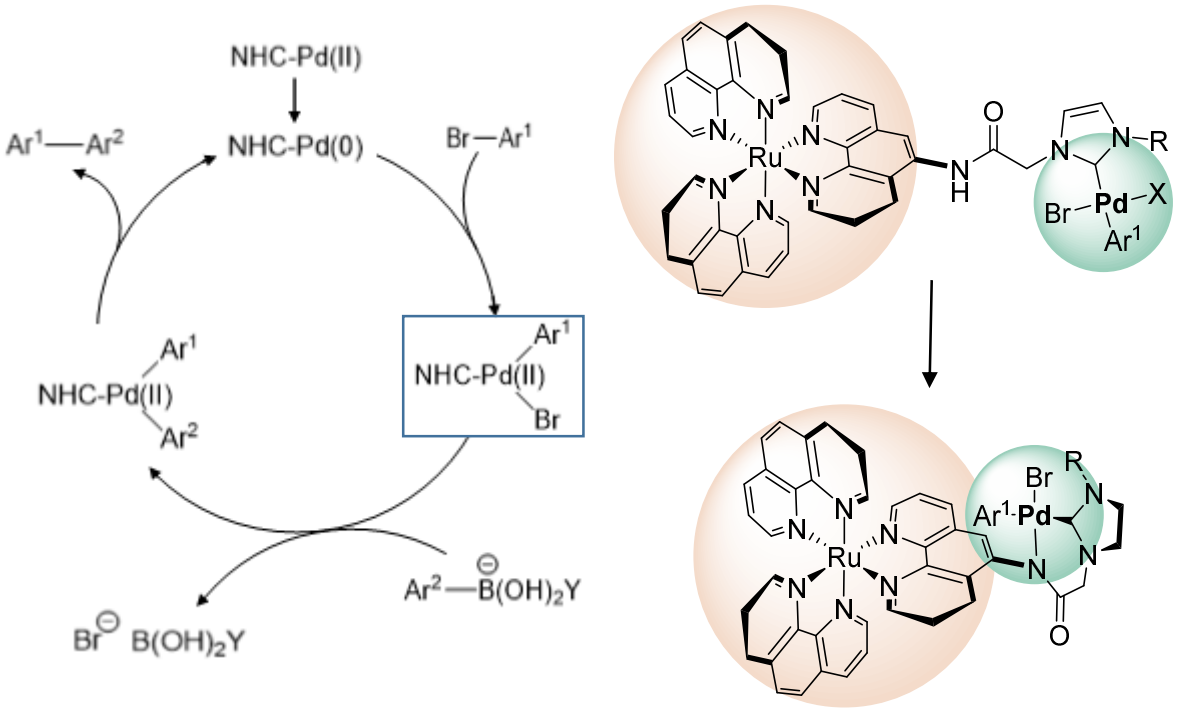

Figure 1.25: *Suzuki coupling mechanism highlighting how coordination of the amidate could occur following oxidative addition, bringing the palladium coordination sphere into the chiral environment.*

Chapter 2

organic chirality;
bornyl derivatives

2.1. Introduction

Terpenes are an extensive structurally diverse class of organic compounds produced by a variety of plants, particularly conifers, and some insects.[127] They are typically fragrant and perform a variety of biological functions from deterring herbivores to attracting pollinating insects.[128] Biosynthesis of terpenes proceeds by the assembly of isoprene units with the molecular formula C_5H_8. Monoterpenes consist of two isoprene units and hence have a ten carbon molecular core. Examples of monoterpenes include limonene which is present in citrus fruits, myrcene in hops, linalool which is responsible for the fragrance of lavender and pinene for the fragrance of pine trees (Figure 2.1).[128]

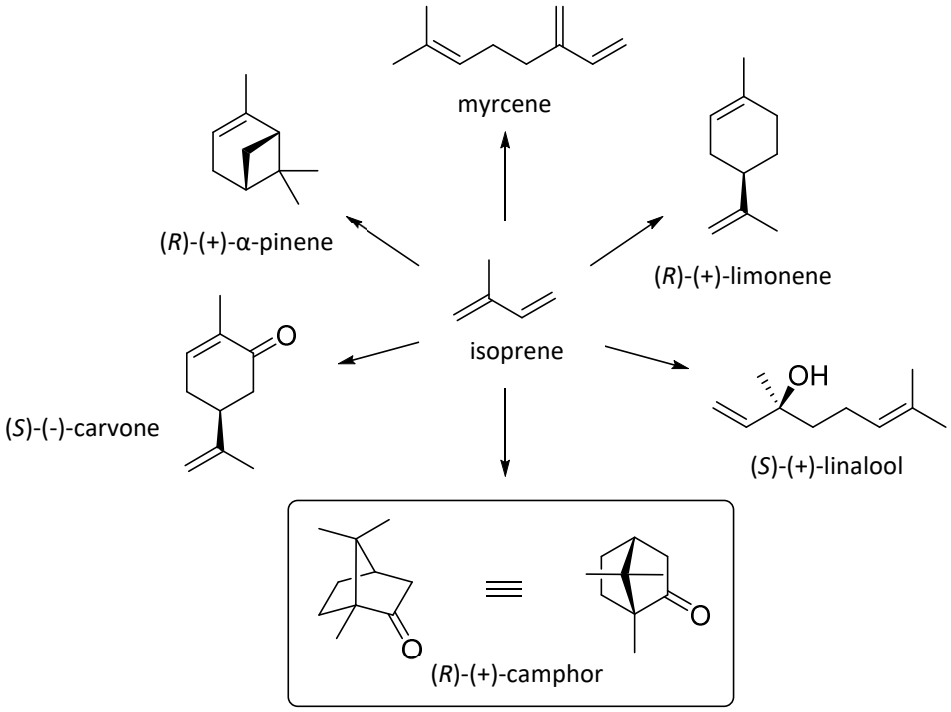

Figure 2.1: *Some examples of monoterpenes all of which are biosynthetically derived from isoprene. Camphor is an important precursor in this research.*

Most terpenes are chiral and occur naturally in a single enantiomeric form as the result of their stereospecific biosynthesis and therefore inhabit natures famed “chiral pool.” Given their known stereochemistry and assortment of structural features, they are

excellent candidates for derivatisation. Camphor is one such chiral monoterpene and is readily available in both of its enantiomeric forms, although it occurs naturally as (*R*)-(+)-camphor (Figure 2.1). Methods for the functionalisation of camphor are well established making it a particularly versatile chiral synthon.[129] For this reason, camphor derivatives have been incorporated into numerous systems, including as a chiral auxiliary,[23, 130] ligands in asymmetric catalysis,[131-135] organocatalysts,[136-138] as NMR shift reagents[20, 21] and as precursors in natural product synthesis.[129, 139]

Several works have been published in which NHC ligands bearing bornane functionality have been deployed as ligands for stereoselective catalysis.[113, 140-142] Grubb's and co-workers demonstrated that the steric attributes of a pendant bornane group could impart excellent selectivity for terminal alkene formation over self-metathesis products in an ethenolysis reaction (Scheme 2.1).[142] This represents a valuable method to convert fatty acids, as derived from renewable biomass, to synthetically useful products.

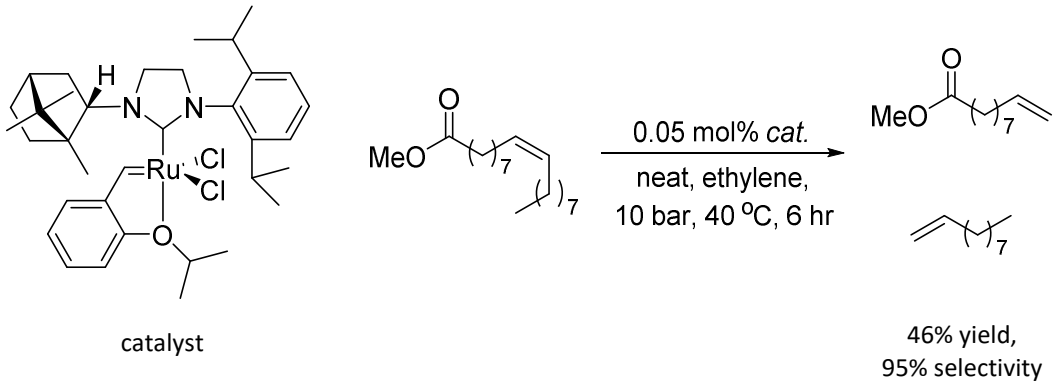

Scheme 2.1: *Ethenolysis of methyl oleate using a bornane functionalised NHC catalyst to selectively generate terminal alkenes.*

A nickel complex with bornyl derivatised NHC ligands reported by Ghosh *et al.* was used as a bifunctional catalyst in an asymmetric base-free Michael addiction (Scheme 2.2).[113] This system with its amido-chelating unit is closely related to the acetamide-linked NHCs developed in this study. The authors propose that the amidate dissociates to deprotonate the substrate and form the reactive enolate, essentially participating as a

hemi-labile group. Although an effective catalyst, it provides no stereoselectivity. This is attributed to the *cis*-relationship of the NHC ligands causing the chiral bornane auxiliaries to be remote from the site of asymmetric catalysis.

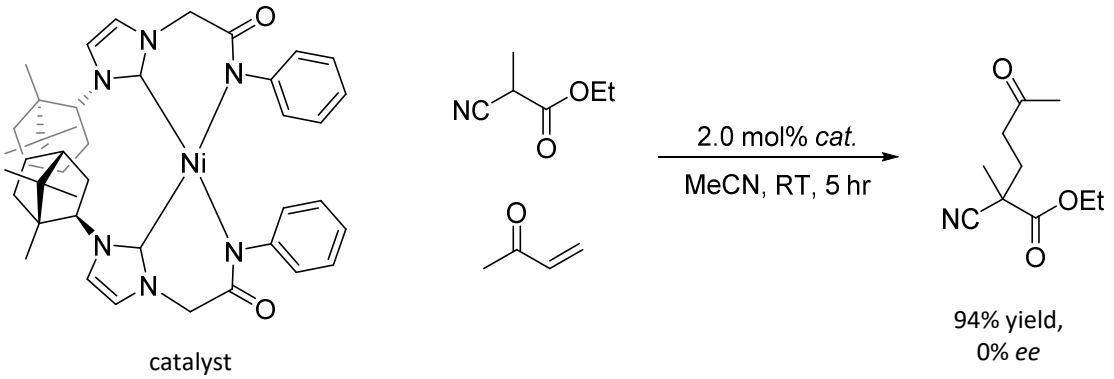

Scheme 2.2: *Base-free Michael addition using a bornane functionalised NHC-acetamide catalyst.*

The above example demonstrates that a coordinated amidate can be an active participant in catalysis. This poses the question of whether introducing a chiral component at the amide terminus could benefit asymmetric induction. Part of this research investigation therefore sought to develop a series of NHC-acetamide ligands with bornyl-amide functionality.

In all of the aforementioned applications, the rigid bicyclic bornane scaffold facilitates stereocontrol and selectivity by way of its steric bulk. This study aimed to exploit this feature to influence the metal environment in NHC complexes and elucidate new, structurally unique compounds. Platinum-group metals were targeted for NHC-complex synthesis due to their known catalytic activity. The novel complexes presented in the following work represent a new class of catalyst with potential stereodirecting capabilities. It is important to reiterate that all bornane compounds discussed in this section were derived directly from natural (*R*)-(+)-camphor. The chirality in this system therefore originates from a naturally occurring enantiomerically pure precursor.

2.2. Synthesis of bornyl-NHC proligands

2.2.1. Acetamide-linked bornyl-imidazolium salts

Following a known procedure,[135] natural (*R*)-(+)-camphor was condensed with hydroxylamine in EtOH/water giving (*R*)-camphor oxime (78% yield) which was subsequently converted into *exo*-(-)-isobornylamine (25% yield) by reduction with sodium borohydride over two equivalents of dehydrated $NiCl_2$ (Scheme 2.3).

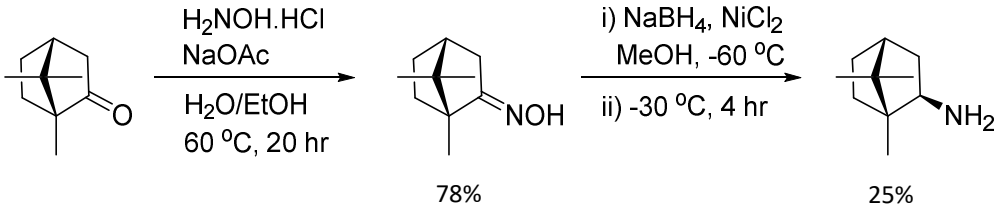

Scheme 2.3: *Synthesis of* exo-*bornylamine from (*R*)-(+)-camphor in two steps.*

Selectivity for the *exo*-bornylamine over the *endo*-bornylamine is achieved under kinetic control by slow, portion-wise addition of sodium borhydride and low reaction temperatures (-60 °C followed by 4 hours at -30 °C). Despite performing this reaction twice with careful regulation of the reaction conditions, only low yields of ≤ 25% were attained. Both times, chromatographic isolation of the product (silica, 5% MeOH/DCM) returned a considerable portion of unreacted camphor oxime. The reaction may therefore need more time to go to completion or a larger excess of sodium borohydride/$NiCl_2$, although, it is difficult to assess how this would affect stereoselectivity. Other researchers using the same method have reported yields of 50%[135] and 33%[113] suggesting that some variation is to be expected.

Reaction of the amine with chloro-acetylchloride provided 2-chloro-*N*-*exo*-bornylacetamide (**2.1**) (Scheme 2.4).

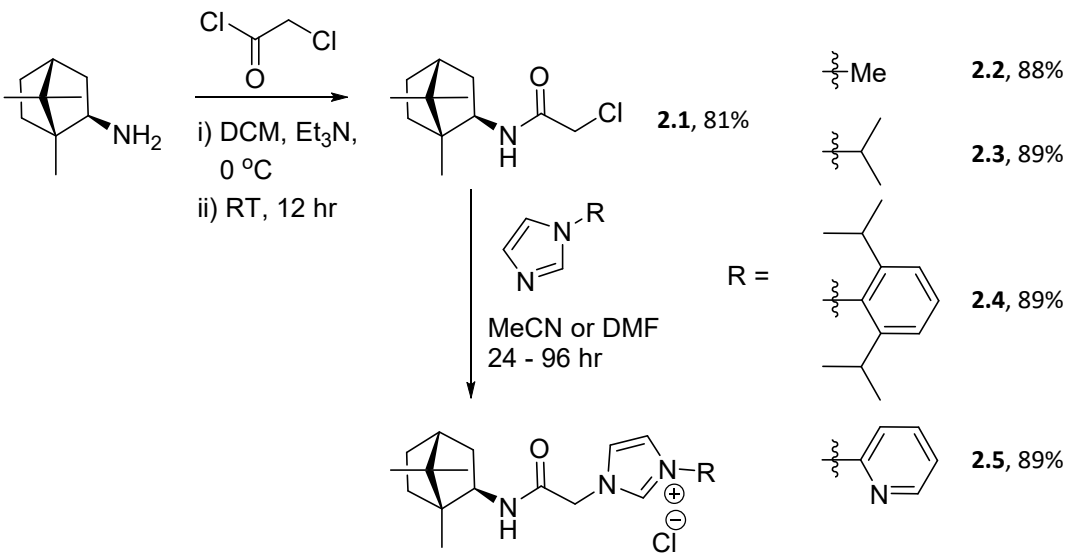

Scheme 2.4: *Synthesis and subsequent substitution of* ***2.1*** *to give 1-[2-(exo-bornylamine)-2-oxoethyl]-1H-imidazolium salts* ***2.2.HCl****,* ***2.3.HCl****,* ***2.4.HCl****, and* ***2.5.HCl****.*

Despite being a useful bornane-linked electrophile, the synthesis of **2.1** has only been attempted once in the literature using a Ritter reaction on (-)-borneol.[143] This produces racemic (±)-2-chloro-*N*-*exo*-bornylacetamide, racemising via an alleged hydride migration in the carbocation intermediate. The approach described herein using *exo*-bornylamine is the first synthesis of **2.1** in which the stereochemical configuration of the (*R*)-(+)-camphor starting material is retained. This has been confirmed by measurement of the optical rotation and designation of its absolute structure by X-ray crystallography.

A standard procedure for the chloro-acetylation of an amine performed in DCM with triethylamine as base provided **2.1** in an 81% yield after purification by flash chromatography (silica, 3:2 Et_2O/pet-ether). Optimal yields were achieved with dry DCM and freshly distilled trimethylamine. Crude **2.1** could also be purified by recrystallisation from hot MeOH/water, however, an oily brown residue occasionally deposited with the colourless needles of **2.1**.

Compound **2.1** is obtained as a single enantiomer with an absolute optical rotation $[\alpha]_D$ (MeOH, 20 °C) of - 32.68 °. Furthermore, X-ray crystallography confirms that **2.1** retains the enantiomeric configuration of natural camphor. It crystallises in the non-

centrosymmetric, orthorhombic space group $P2_12_12_1$ with two molecules of **2.1** in the asymmetric unit (Figure 2.2). The low Flack (x) and Hooft (y) values (0.007(2) and 0.030(2), respectively) confirm assignment of the correct absolute structure. The chlorine atom present in **2.1** is deemed sufficiently heavy to provide the anomalous differences required for accurate calculation of these parameters from data collected with MoKα radiation.[144]

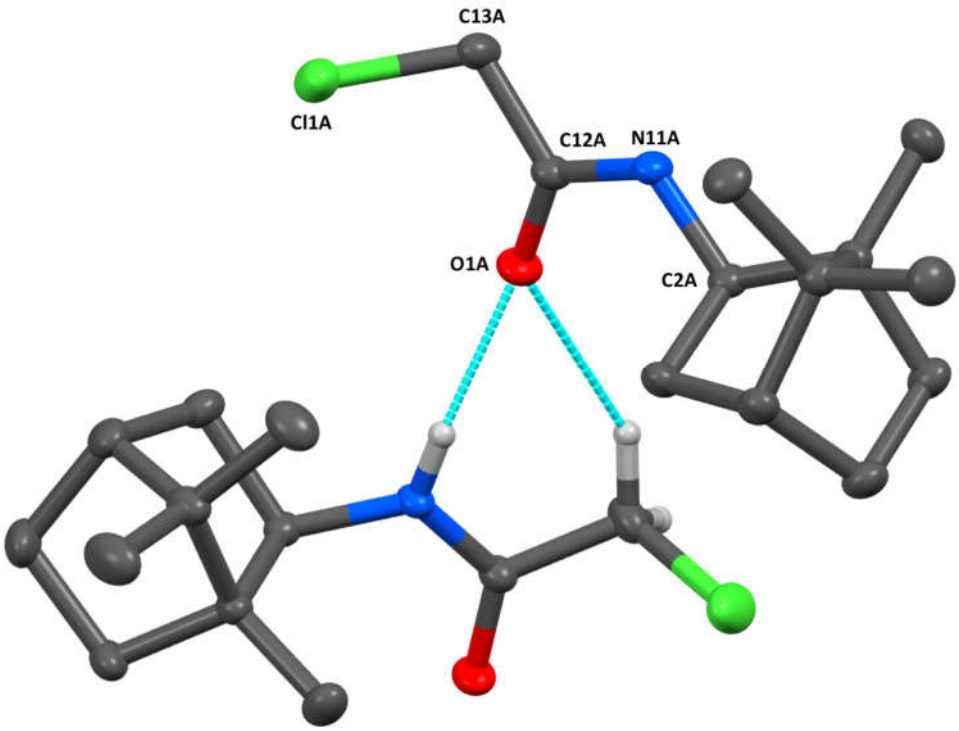

Figure 2.2: *Asymmetric unit of compound* ***2.1*** *with relevant atoms labelled and amide hydrogen bonding contacts shown. Only hydrogen atoms involved in these interactions have been included. Thermal ellipsoids are drawn at a 50% probability level.*

In the structure of **2.1** the secondary amide group is seen to adopt a *Z*-configuration which, as is generally the case,[145] has an obvious steric advantage over the *E*-amide. The dihedral angle between the N11 – H and C2 – H bonds of 131.7(2)° and 150.0(2)° (A and B) are lower than the 158 – 180° *anti*-orientation often preferred by NH – CHα containing *Z*-amides.[146] This may be a consequence of the borane's steric bulk. The *Z*-amide participates in hydrogen bonding between molecules via N*H* ··· O bonds (N11A ···

O1B = 3.086(2) Å, N11B ··· O1A = 2.901(2) Å) reinforced by a non-conventional C*H* ··· O interaction with the methylene group (C13A ··· O1B = 3.215(2) Å, C13B ··· O1A = 3.360(2) Å). The resultant *Z*-amide hydrogen bonded chain is reminiscent of that reported for the racemate (±)-**2.1**.[143]

The reaction of **2.1** with two equivalents of the *N*-substituted imidazoles in hot solvent afforded the 1-[2-(*exo*-bornylamine)-2-oxoethyl]-1*H*-imidazolium salts **2.2.HCl** – **2.5.HCl** (Scheme 2.4). These reactions were monitored by TLC and it was observed that the rate reflected the steric bulk of the imidazole-nucleophile. In refluxing MeCN, substitution by 1-(2,6-diisopropyl)phenyl-imidazole took 96 hours compared with 62 hours for the 1-(2-pyridyl)-imidazole and 24 hours for the 1-alkyl-imidazoles. If desired, the reaction could be accelerated by employing DMF as the solvent and reacting at 100 ^{o}C for 20 hours. This generated compounds **2.4.HCl** and **2.5.HCl** in yields of 70% and 86% respectively. The salts can be precipitated from the condensed reaction-liquor in a pure form by addition of Et_2O.

The synthesis and purification of all compounds from *exo*-(-)-bornylamine to imidazolium salts **2.2.HCl** – **2.5.HCl** involved TLC evaluation. Visualisation of the TLC plates was achieved using a permanganate stain prepared by a reported method.[147] This was necessary as few of the bornane-derivatives are UV-active and all respond poorly to iodine vapour.

The presence of an imidazolium moiety in compounds **2.2.HCl** – **2.5.HCl** is highlighted in their ^{1}H-NMR spectra by a downfield singlet at ~ 9.58 ppm due to the NC*H*N proton. The position of signals for N*H* and CH_2 hydrogen atoms of the acetamide linkage are conserved for salts **2.2.HCl** – **2.5.HCl** (~ 8.25 ppm and ~ 5.12 ppm respectively) but shifted significantly downfield when compared to the precursor **2.1** (7.50 ppm and 4.04 ppm) (Figure 2.3).

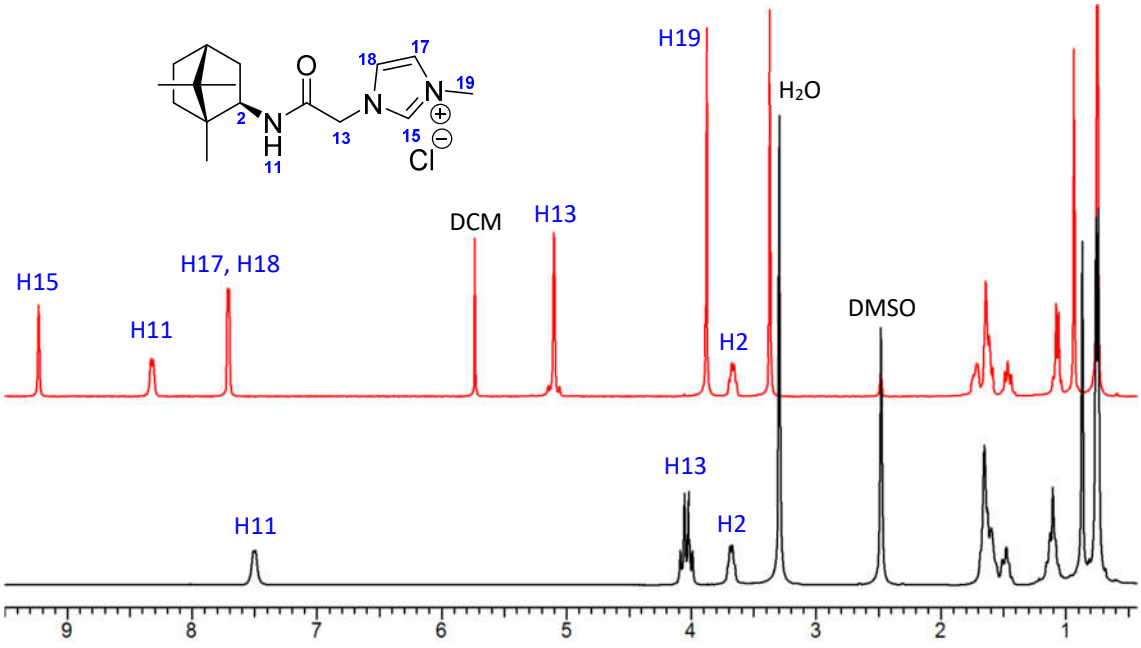

Figure 2.3: *Collated ^{1}H-NMR spectra of* ***2.1*** *(black) and* ***2.2.HCl*** *(red) in DMSO-*d6. *Note the shift in signals of the amide* NH (H11) *and methylene* CH_2 *(H13) protons.*

This is because, unlike the chlorine in compound **2.1**, the electron-deficient imidazolium ring of compounds **2.2.HCl** – **2.5.HCl** invokes both inductive and anisotropic deshielding of the adjacent methylene C*H*$_2$ proton. As the amide is more distant from the imidazolium ring it is reasoned that other interactions, such as hydrogen bonding, contribute to its large shift of $\Delta\delta \geq 0.69$ ppm. This can occur between the N*H* and chloride anion[116] and/or through intramolecular association of the amide carbonyl and the electron deficient NC*H*N proton. Interestingly, the methylene C*H*$_2$ protons are non-equivalent in the spectrum of **2.1**, producing doublets at 4.07 ppm and 4.01 ppm with a geminal coupling of 12.5 Hz. Divergence of these diastereotopic proton environments has been shown to be solvent dependent (compare the ^{1}H-NMR spectra of **2.2** in DMSO-*d6* [Figure 2.3] and **2.3** in MeCN [Figure 2.17]). They are often affected by conformational restriction of the methylene group as is observed for many of the complexes discussed in section 2.3. For **2.1**, such restrictions may occur as a result of intermolecular interactions such as hydrogen-bonding or hydrophobic association of the bornane-groups. A propensity for intermolecular association is alluded to by the mass-spectrum of **2.1**, in which a signal due to a dimeric cation ([(**2.1**)$_2$ + H]$^+$ = 459.2466)

registers at equal intensity to the expected monomolecular species ([**2.1** + H]$^+$ = 230.1263).

The application of imidazolium salts **2.2.HCl** – **2.5.HCl** as NHC proligands in the synthesis of organometallic compounds is explored in section 2.3.

2.2.2. Imidazolium salts derived from 3-amino-borneol

Certain NHC ligands derived from 3-aminoborneol are capable of tridentate coordination (Figure 2.4a). With regard to catalysis, this binding mode is expected to improve precatalyst stability and facilitate enantiomeric induction by maintaining the chiral sphere of the bornane-frame in a position proximal to the active site. It is anticipated that the bornane-group will crowd the catalytic site to a greater extent with *exo*-derivatives of 3-amino-borneol than for those of the corresponding *endo*-isomer (Figure 2.4b). This provides an interesting means of tuning the catalytic function of this system.

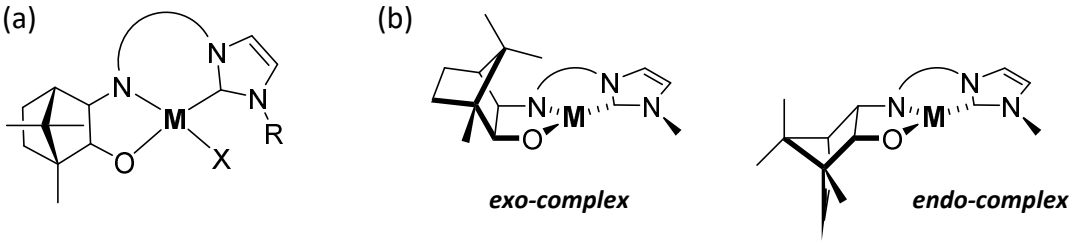

Figure 2.4 (a): *Possible tridentate coordination motif for NHC complexes based upon 3-amino-borneol and,* ***(b)*** *rendered again to highlight the stereochemical differences between the* exo- *and* endo-*complexes.*

Both isomers of 3-amino-borneol can be prepared selectively, however, *endo*-3-aminoborneol is reportedly difficult to isolate without further modification.[148] Therefore, e*xo*-3-aminoborneol was used initially with the intention to exploring *endo*-

3-aminoborneol derivatives in future. However, following difficulties in the synthesis of compounds from *exo*-3-aminoborneol, this idea was abandoned.

Exo-3-aminoborneol was prepared by a published methodology beginning with natural (*R*)-(+)-camphor (Scheme 2.5).[149] This was converted into camphorquinone-3-oxime via the camphor-enolate which reacts with *iso*-amylnitrite to give a mixture of the *syn*- and *anti*-isomers of the oxime after acidification. A reduction of the oxime using $LiAlH_4$ at 0 ^oC provides 3-aminoborneol and, although the *exo*-isomer is favoured, the *endo*-product can account for up to 10% of the total product by ^1H-NMR.

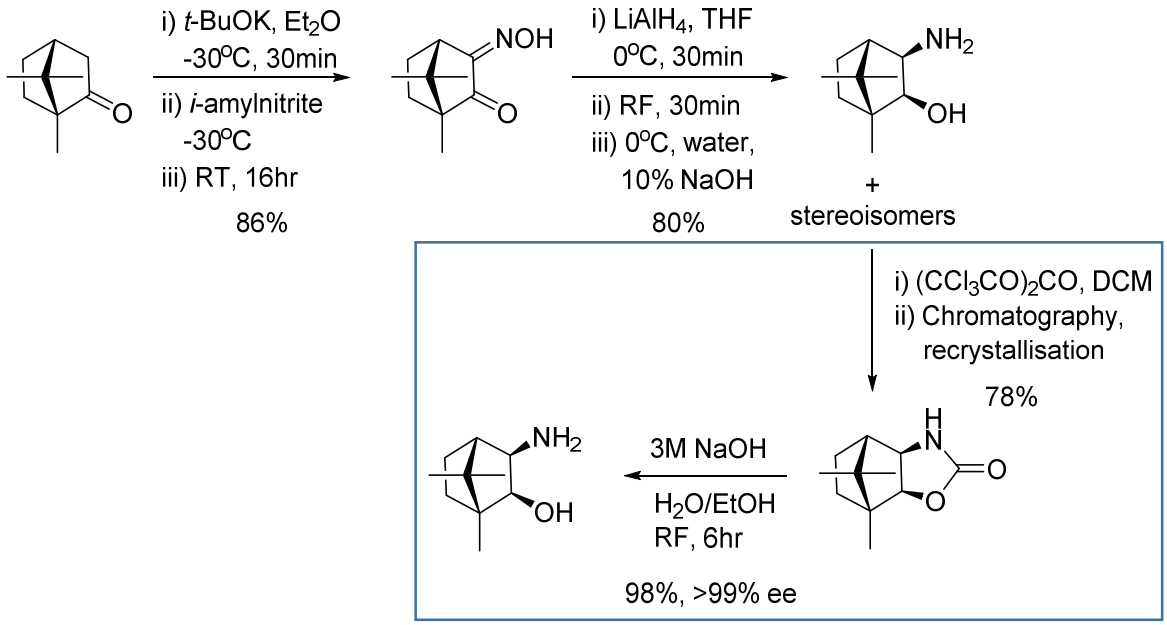

Scheme 2.5: *Synthesis of 3-amino-borneol and a possible purification route via oxazolidone formation (not attempted).*

The purification of this material is non-trivial; it does not recrystallize or sublime well and adheres tightly to any chromatographic media. The only reported purification method is to react the crude material with triphosgene and purify the resultant oxazolidone by chromatography then recrystallisation (Scheme 2.5).[150, 151] This can then be hydrolysed to regenerate pure *exo*-3-aminoborneol quantitatively. Other researchers

have demonstrated however, that proceeding with the material as is and purifying following subsequent synthetic steps can be a more agreeable approach.[24, 149]

Two strategies for appending an imidazolium moiety to 3-aminoborneol were explored (Scheme 2.6). In route A, chloro-acetylchloride is used as the coupling agent in a way that is analogous to the synthesis of the bornyl-acetamide derivatives discussed in section 2.2.1. Alternatively, route B involves reacting *exo*-3-aminoborneol directly with a pre-formed imidazolium tethered electrophile.

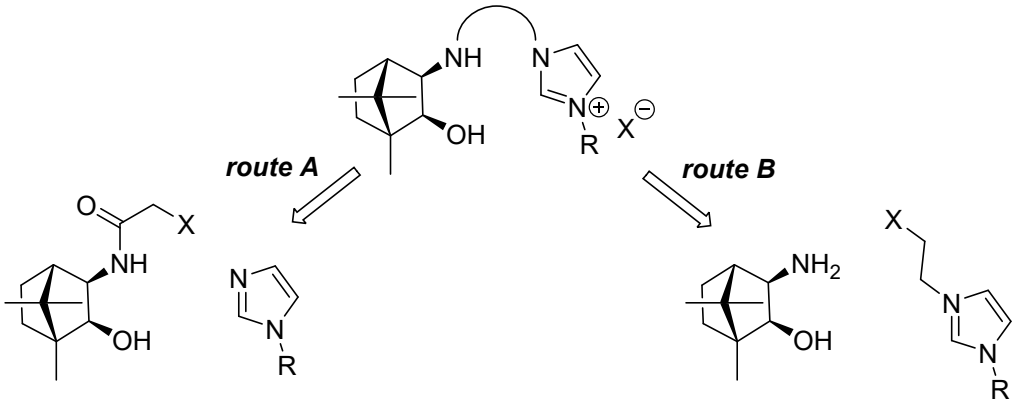

Scheme 2.6: *Synthetic routes to* exo*-3-aminoborneol appended imidazolium salts.*

Using a reactive coupling agent such as chloro-acetylchloride was considered less compatible with this system due to regioselectivity issues arising from having both an amino- and a hydroxyl- nucleophile present. However, the synthesis of compound **2.7** by Periasamy *et al.* suggests that the chloro-acetamide **2.8** is formed prior to cyclisation which is promoted by treatment with NaOH (Scheme 2.7).[152] It was hoped that conditions existed under which **2.8** could be isolated and several of the condition sets trialled are discussed.

All attempts required a stoichiometric equivalent of chloro-acetylchloride and to reduce the impact of acidic-impurities the chloro-acetylchloride was purified before use by vacuum distillation. When an aprotic solvent was used with a mild base and chloro-

acteylchloride (DCM, triethylamine, 0°C or MeCN, $NaHCO_3$, 0°C) a brown tacky residue was recovered and confirmed by ^{1}H-NMR as being a complex mixture. The mass-spectrum suggested that the desired product **2.7** had formed along with the cyclised product **2.6** and numerous others. TLC indicated that, like 3-aminoborneol, its derivatives have poor chromatographic mobility making purification nearly impossible.

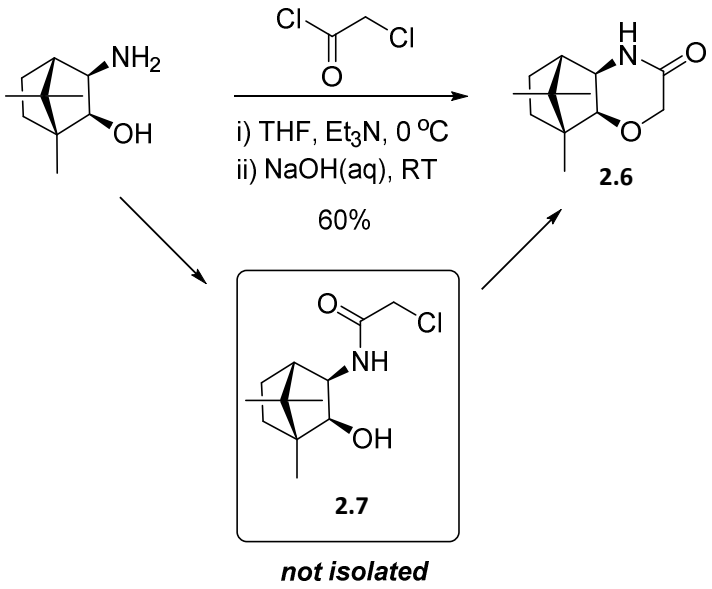

Scheme 2.7: *Synthesis of* ***2.6*** *occurring via the desired chloroacetamide* ***2.7****.*

Chloroacetamide formation using glacial acetic acid as solvent is another common approach[153] that was attempted in the hope that the acidic conditions would disfavour side reactions via substitution of the chloride (including cyclisation). This again generated an unresolvable mixture. Unwilling to invest further time in the synthesis of an acetamide-linked species, focus shifted towards the preparation of compounds via route B which was showing early promise. It is probable however, that persistent experimentation could produce **2.7**, perhaps by using chloro-acetic anhydride as a milder coupling agent. Forming then reacting **2.7** in situ to give the desired acetamide-linked imidazolium salt is also feasible.

Instead, the ethyl-linked compound **2.9.HBr** was targeted by implementing route B by the method depicted in Scheme 2.8. This novel approach in which the imidazolium-tethered electrophile **2.8.HBr** is reacted with *exo*-3-aminoborneol was devised on the basis that the amine could be selectively alkylated using reported conditions.[149] Furthermore, having pre-formed the imidazolium salt minimised the probability of cyclisation or oligomerisation reactions occurring. The bromo-ethyl imidazolium salt **2.8.HBr** has previously been utilised as a precursor to non-symmetrical bis-imidazolium salts[154] but has never been explored as a means of tethering an imidazolium moiety to other functional structures.

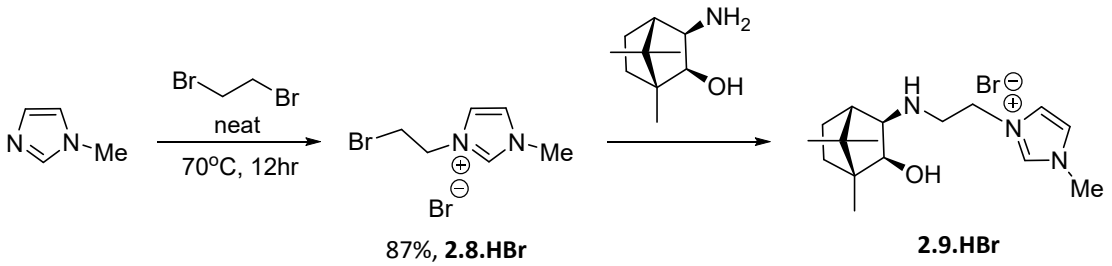

Scheme 2.8: *Synthesis of* ***2.8.HBr*** *and route to* ***2.9.HBr*** *by coupling to* exo-*3-aminoborneol.*

Compound **2.8.HBr** is prepared by stirring 1-methylimidazole in a twenty-fold excess of dibromoethane at 70 °C. Surprisingly, despite this excess, the formation of the bis-imidazolium salt **2.11.2HBr** was sometimes produced (see Scheme 2.9), on one occasion in a 1:1 mixture with **2.8.HBr**. Removing the **2.11.2HBr** contaminant from **2.8.HBr** was difficult due to their similar solubility properties and it was typically easier to repeat the synthesis. Because compound **2.8.HBr** is insoluble in dibromoethane, it begins to separate as a viscous oil after an hour of heating the reaction. The starting material 1-methylimidazole may become concentrated in this ionic liquid phase thus promoting the formation of **2.11.2HBr**. Minimising this effect through vigorous stirring and uniform heating of the reaction vessel resulted in purer **2.8.HBr**.

The conditions used to generate **2.9.HBr** are analogous to those reported for the synthesis of *exo*-3-(morpholino)isoborneol by *N*-alkylation of *exo*-3-aminoborneol.[149] Here, **2.8.HBr** and triethylamine were stirred with a slight excess of crude *exo*-3-aminoborneol in DMSO at room temperature for 48 hours (Scheme 2.9). This produced a mixture of the desired product **2.9.HBr**, its protonated salt **2.9.2HBr**, and, surprisingly the bis-imidazolium salt **2.11.2HBr**. Other compounds derived from impurities in the crude starting material were also identified including the *endo*-isomer **2.10.2HBr**, and the azepane-derivative **2.12.2HBr**.

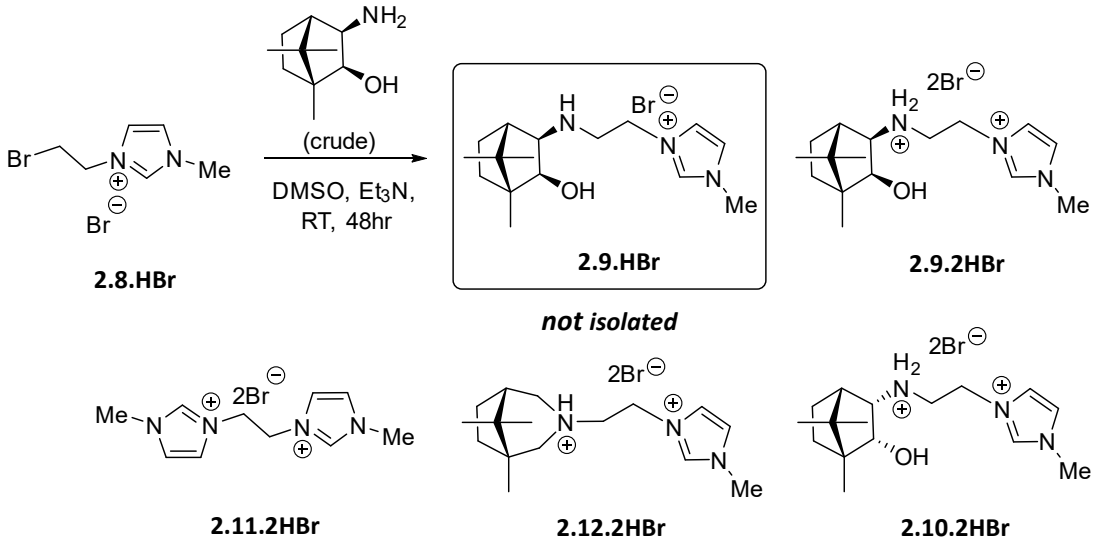

Scheme 2.9: *Synthesis of **2.9.HBr** and other identified compounds.*

Compound **2.9.HBr** was isolated as the protonated adduct **2.9.2HBr**, the protonation state of which was revealed by X-ray diffraction analysis (Figure 2.5). The crystal structure also helped confirm the presence of the minor *endo*-isomer **2.10.2HBr** which co-crystallised with **2.9.2HBr**. Although slightly convoluted, the best purification strategy was to add the DMSO reaction solution dropwise into stirring EtOAc and collect the resultant white solid by filtration. This material was a mixture of **2.9.2HBr** and **2.11.2HBr** (usually ~ 3:2, **2.9.2HBr** / **2.11.2HBr**) from which the **2.9.2HBr** was isolated by recrystallisation from MeCN. The EtOAc filtrate contained a mixture of compounds

including starting material and **2.9.HBr**. This was condensed by rotary-evaporation and the resultant oil dissolved in THF. Acidification by dropwise addition of a 0.5 M solution of HBr in THF allowed **2.9.2HBr** to be obtained as a precipitate which was collected and washed with THF. This was contaminated with compound **2.12.2HBr** which was washed from the product with DCM and obtained from the filtrate in a pure form. Compound **2.12.2HBr** comprised ~ 0.5% of the mass expected for quantitative conversion of the limiting reagent **2.8.HBr**. The structural resolution of **2.12.2HBr** and its chemical origin will be discussed shortly. A poor overall yield of 16% **2.9.2HBr** was recovered by this method.

Several attempts were made to improve this yield but to no avail. Solvent variations were limited by the poor solubility of the precursor salt **2.8.HBr,** however, MeCN and butanol were trialled as substitutes. In both cases formation of product was observed by ^{1}H-NMR but the isolated yield was negligible and, as before, **2.11.2HBr** was also produced. Substituting triethylamine with ammonium carbonate as base met with a similar outcome as did a base free set of conditions with heating (DMSO, 100 ^{o}C, 72 hours).

In using this approach, a dilemma arises from the fact that the starting material **2.8.HBr** is sensitive to deprotonation of the imidazolium moiety whereas the other starting material, *exo*-3-aminoborneol, is moderately basic. *Exo*-3-aminoborneol is a β-hydroxy amine for which the dihedral interfunctional angle is ~ 0^{o} due to the rigid bicyclic skeleton. These are known to be significantly more basic than flexible β-hydroxy amines because the protonated state is stabilised by intramolecular hydrogen-bonding between the ammonium salt and the hydroxyl-oxygen at minimal entropic cost.[155] This stabilisation is expected to increase upon substitution of the amine. Unfortunately, there is no experimental data for *exo*-3-aminoborneol and its derivatives, however, the repeated isolation of **2.9.2HBr** directly from the reaction shown in Scheme 2.9 implies that **2.9.HBr** is of a comparable basicity to triethylamine. If *exo*-3-aminoborneol is also competitively basic then it may become protonated during the reaction, diminishing its reactivity. This however, was not acknowledged as an issue in synthesis of *exo*-3-(morpholino)isoborneol under similar conditions.[149] Unfortunately, triethylamine

cannot be substituted as a stronger base would deprotonate the imidazolium salt of **2.8.HBr** or of any **2.9.HBr** formed. On the other hand, the formation of the bis-imidazolium salt **2.11.2HBr** points towards some unpredicted, adverse reactivity of the bromine-tethered imidazolium salt **2.8.HBr.** As yet, the mechanism of formation of compound **2.11.2HBr** is not understood.

As mentioned above, the identity of the protonated adduct **2.9.2HBr** was verified by X-ray diffraction analysis using crystals grown by slow vapour diffusion of Et_2O into a MeOH solution of the compound. The data was solved in the non-centrosymmetric, monoclinic space group $P2_1$ with an asymmetric unit containing one molecule of **2.9.2HBr** with full occupancy and another positionally disordered site containing 73% **2.9.2HBr** and 27% **2.10.2HBr** (Figure 2.5). The presence of two bromide anions per imidazolium compound confirms that the amine is protonated. The disordered bornane-cluster was effectively modelled as two parts by refining the free variables of each part to an overall site occupancy factor of one. For the *exo*-isomer, the distance O20 – N11 (A / B) is 2.672(6) Å / 2.678(6) Å, which is slightly longer than in the *endo*-isomer (2.577(14) Å). Likewise, the dihedral angle O20-C2-C3-N11 (A / B) is larger for the *exo*-isomer (11.8(6)^o / 11.8(8)^o) than the *endo* (1.2(2)^o). These values corroborate the previously made assessment that the hydroxyl and amino groups are spatially adjacent with low interfunctional angles. This arrangement is expected to support intramolecular hydrogen bonding, however, the anticipated N11*H* ··· O20 interaction was not detected with the hydrogen atom donor in its calculated position. No attempt to manipulate the hydrogen atom positions were made.

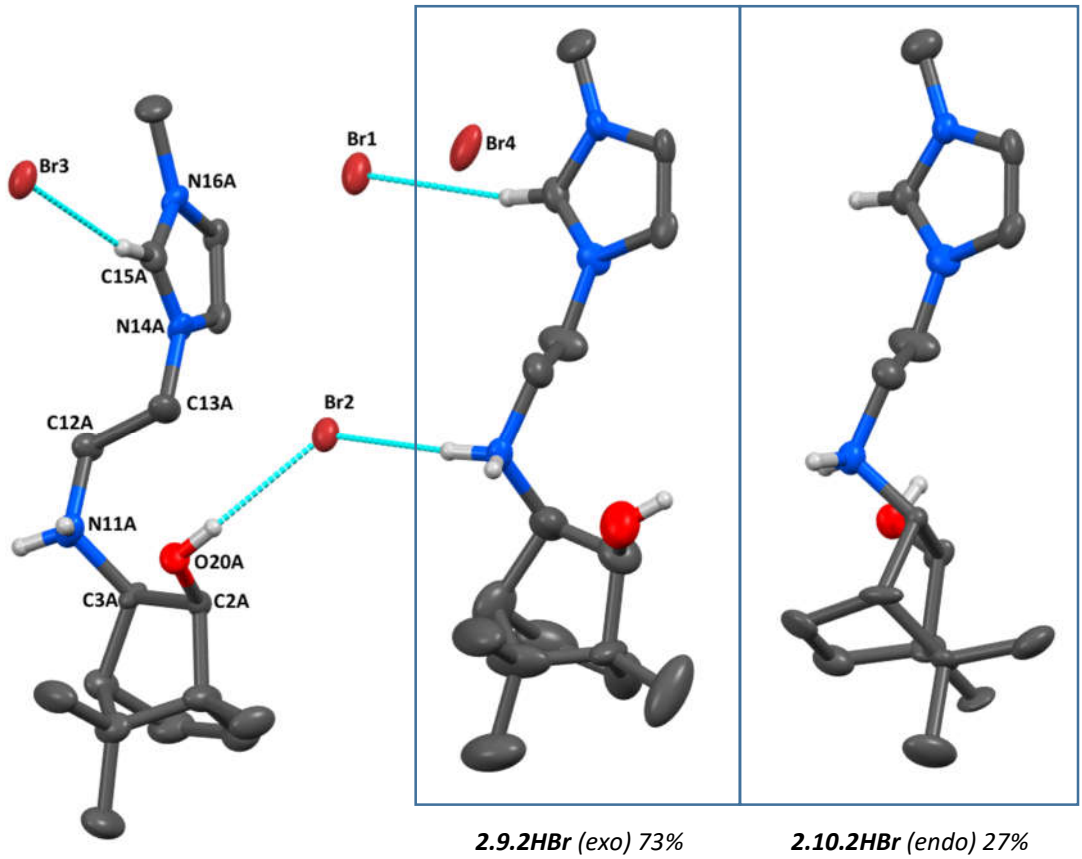

Figure 2.5: *Asymmetric unit of compound* ***2.9.2HBr*** *with relevant atoms labelled and some hydrogen bonding contacts shown. The outlined site is occupied by molecules of* ***2.9.2HBr*** *and* ***2.10.2HBr*** *in a 73 : 27 ratio. These have been rendered separately. All non-bonding hydrogen atoms have been omitted for clarity. Thermal ellipsoids are drawn at a 50% probability level.*

The structure of **2.12.2HBr** was initially deduced using NMR and mass-spectroscopy and verified by X-ray crystallography. The mass-spectrum of the then unknown compound **2.12.2HBr** displays a dominant signal at 262.2281, equivalent to the mass of [**2.9.H**]$^+$ minus an oxygen atom (calculated m/z, [**2.9.H** – O]$^+$ = 262.2278). An ^{1}H-NMR analysis revealed that the signals pertaining to the imidazolium moiety and ethyl linker are conserved when compared to the spectrum of **2.9.2HBr**, however, the "bornane" region of the spectrum was altered. Figure 2.6 shows this region of the compounds HMBC plot with the ^{1}H-NMR and ^{13}C-NMR spectra comprising the horizontal and vertical axis, respectively.

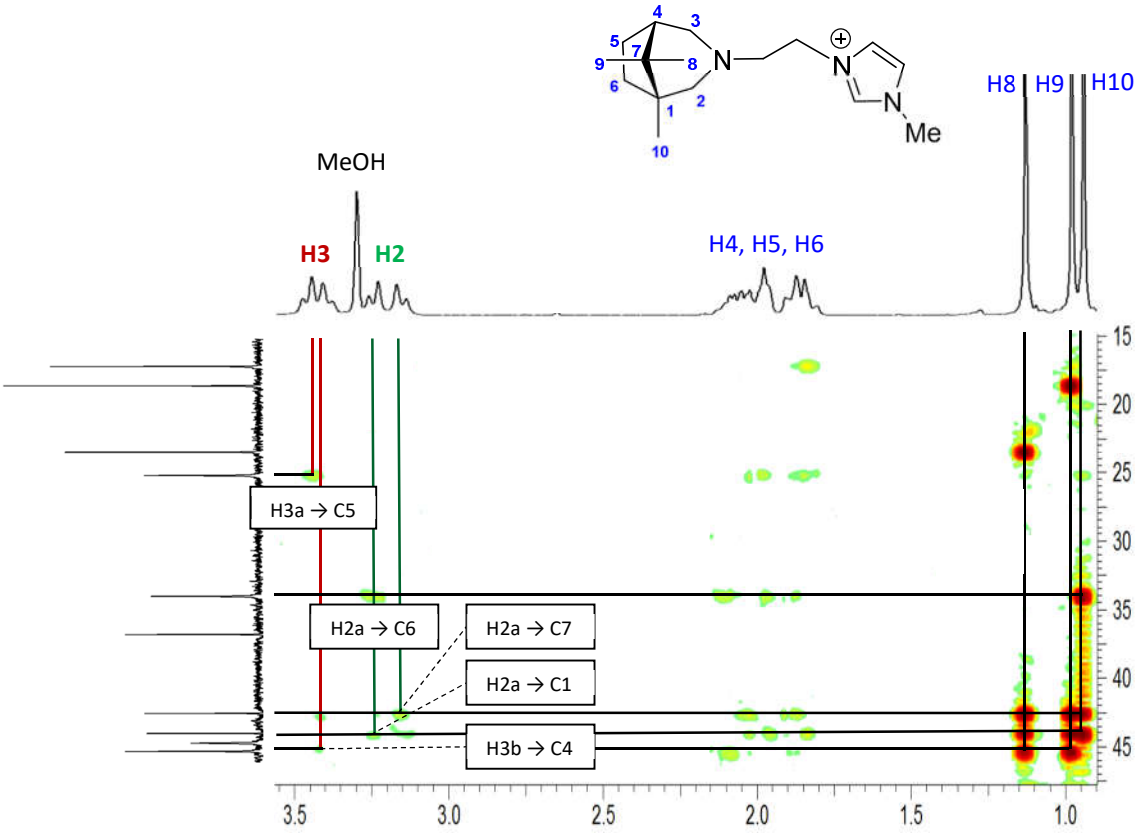

Figure 2.6: *Magnified region of the HMBC spectrum of compound* ***2.12.2HBr*** *with key correlations highlighted.*

A two proton multiplet at 3.43 ppm and a pair of doublets at 3.26 ppm and 3.16 ppm corresponding to one proton each are evidence of two "new" methylene environments. Three tell-tale methyl signals at 1.15 ppm, 1.00 ppm and 0.96 ppm allude to the retention of some bornane-character and HMBC analysis confirms that these are associated with the same structural unit as the "new" methylene protons through several two and three bond correlations to the same carbon signals. The remaining signals between 2.20 – 1.80 ppm are similarly correlated and are attributed to five proton bonded to C4, C5 and C6. In bornyl-derivatives, chemically unique *exo*- and *endo*-proton environments are observed due to the rigidity of the [2.2.1]-bicycle. The chemical shift difference between *exo*- and *endo*-proton is typically over 0.5 ppm for the C5 and C6 methylenes. Interestingly, for compound **2.12.2HBr** there is little distinction

between the *exo* and *endo* environments, probably due to the increased flexibility of the camphidine-like [3.2.1]-bicycle.

X-Ray crystallography helped verify the structural assignments made using NMR and mass-spectrometry. Diffraction data was collected using crystals grown by slow vapour diffusion of Et_2O into a MeOH/MeCN solution of **2.12.2HBr** which crystallised in the non-centrosymmetric orthorhombic space group $P2_12_12$. Two molecules of the compound are present in the asymmetric unit along with four bromine counter anions and a water molecule (Figure 2.7).

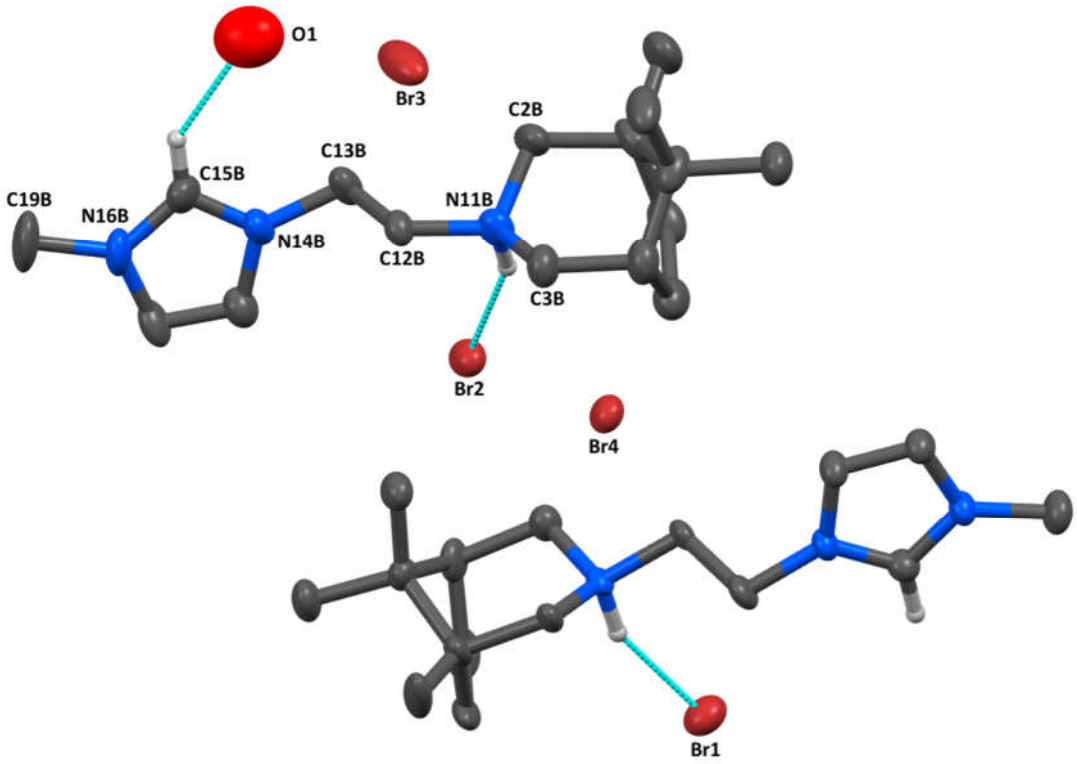

Figure 2.7: *Asymmetric unit of* ***2.12.2HBr*** *with some hydrogen-bonding interactions highlighted. All non-bonding hydrogen atoms have been omitted for clarity. Thermal ellipsoids are drawn at a 50% probability level.*

The structure clearly shows the unmistakeable seven-membered azepane ring of a camphidine-moiety. The oxygen of the water molecule occupies a site on the two-fold

axis and hydrogen atom positions could not be calculated effectively. There was insufficient residual density in the difference map to assign these hydrogen atoms manually. Regardless, it is inferred that this water molecule participates in the hydrogen bonding network that pervades the packed structure. It acts as a hydrogen bond acceptor in a C*H* ··· O interaction with the imidazolium NC*H*N hydrogen (C15B ··· O1 = 3.029(11) Å) and donor in an O*H* ··· Br interaction (O1 ··· Br3 = 2.966(8) Å). A weaker N*H* ··· Br interaction is observed between the protonated amine and bromine (N11A ··· Br1 = 3.185(6) Å and N11B ··· Br2 = 3.318(8) Å).

Compound **2.12.2HBr** probably originated with a camphidine impurity (**2.13**, Scheme 2.10) that reacted with **2.8.HBr**. A cation of mass 154.1595, equivalent to that of protonated **2.13** (calculated m/z, [**2.13** + H]$^+$ = 154.1590) is observed in the mass-spectrum of the crude *exo*-3-aminoborneol. Camphorquinone-3-oxime can undergo a Beckmann rearrangement in acidic conditions to give camphorimide[156] which in turn, could be reduced (Scheme 2.10).[157]

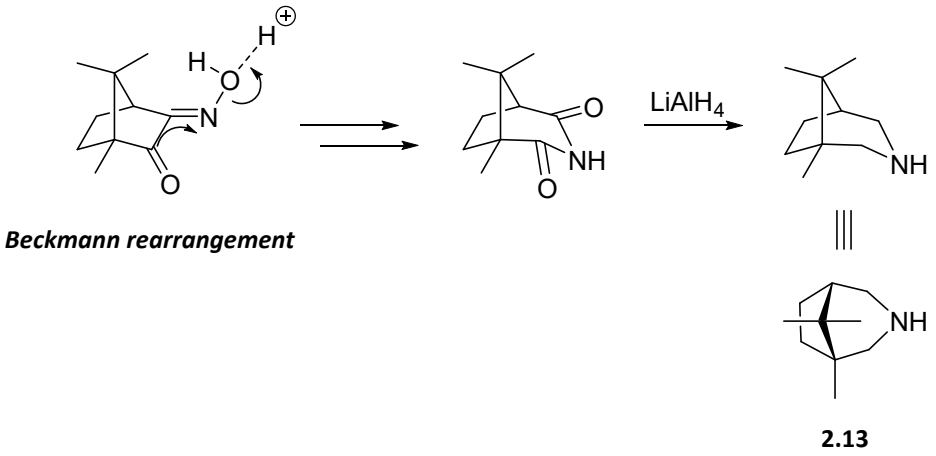

Scheme 2.10: *Possible route for the formation of camphidine* ***2.13*** *via an acid assisted Beckmann rearrangement of camphorquinone-3-oxime.*

Under the reducing conditions used (see Scheme 2.5), it may be that acidic impurities facilitate the Beckmann rearrangement. Camphidine is therefore a plausible side product of the reduction reaction used to generate *exo*-3-aminoborneol from

camphorquinone-3-oxime. Unfortunately, there was insufficient sample to analyse the optical rotation of **2.12.2HBr**

Compound **2.12.HBr** or another camphidine-tethered NHC proligand would be an interesting target compound for a future researcher. Chloro-acetylation of camphidine is achievable and would provide interesting acetamide-linked NHC ligands with the chiral, tertiary amide providing a novel hemilabile group.

2.3. Synthesis of bornyl-NHC complexes

This section will explore the synthesis of bornyl-acetamide NHC complexes from proligands **2.2.HCl** – **2.5.HCl**. In the ensuing discussion these will be generally referred to as BA ligands or BA-N when adopting NHC-amidate coordination.

Acetamide-linked NHC ligands have been used in mono-NHC complexes but are more frequently reported in square planar, ML_2 type systems with the d^8 metals nickel, palladium and platinum. Achieving the desired NHC-amidate chelation requires a moderately strong base, typically K_2CO_3, and heat input, however, resonance stabilised amidates can form and coordinate spontaneously at room temperature.[114, 158] For square planar ML_2 type complexes, the two NHC ligands will coordinate in either *cis* or *trans* geometries. Additional variants may arise depending on whether the ligand coordinates in a monodentate or bidentate fashion. Figure 2.8 depicts the three pairs of diastereomers that are anticipated when monodentate and bidentate coordination modes are combined and the ancillary ligand (X) remains unchanged.

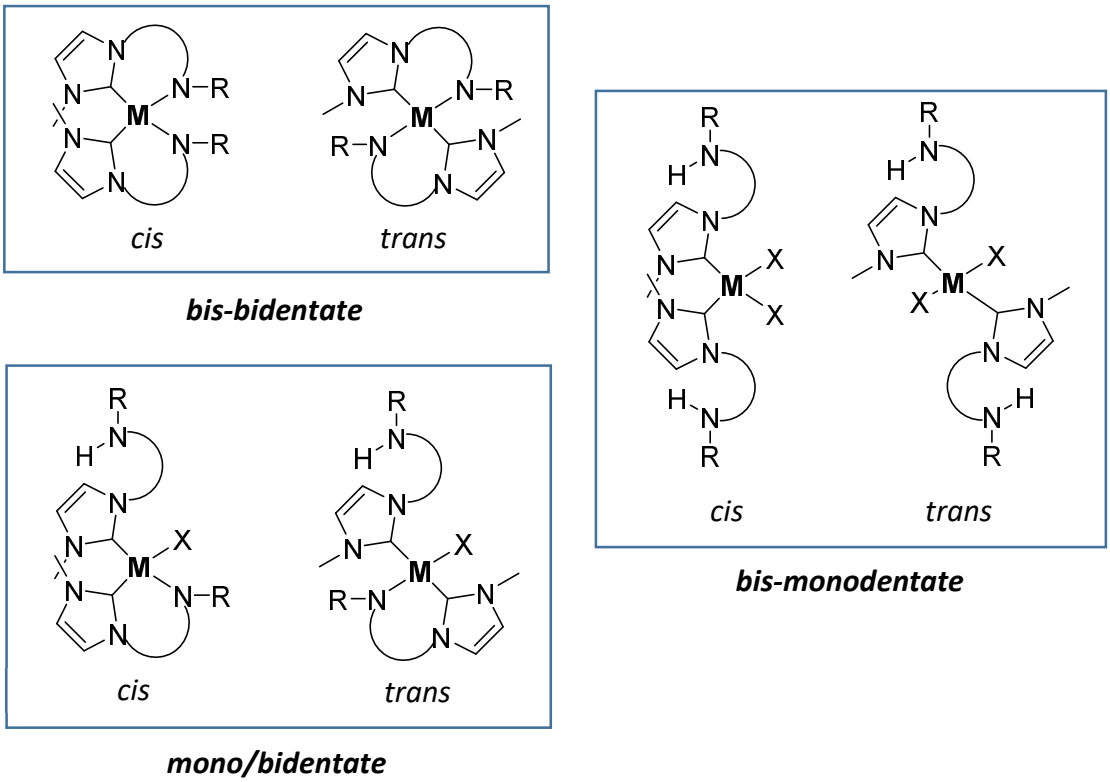

Figure 2.8: *Possible [ML_2] complexes using mono-acetamide linked NHC ligands,* cis *and* trans *refer to the relative NHC geometry.*

For unhindered NHC-acetamide ligands the synthesis of complexes with a bis-bidentate motif is conveniently achieved using an excess of ligand, K_2CO_3 and heat with straightforward separation of *cis* and *trans* isomers by crystallisation or chromatography.[112, 113, 118] For BA-N complexes however, the amidate-metal bond is destabilised both kinetically and thermodynamically by the steric bulk of the bornane-group. This statement is supported by several examples in the following text (sections 2.3.1). One consequence of this phenomenon is that when desired, coordination via the amide-nitrogen is easily avoided using mild conditions thus affording a degree of control. Unfortunately, it has proven extremely difficult to reliably prepare BA-N type complexes and complicated product mixtures are routinely observed. This otherwise simple approach of preparing bis-bidentate ML_2 complexes now becomes difficult because, despite the NHC coordinating, the amide may or may not associate. The potential for complexity is best illustrated by the attempted synthesis of the complexes

cis-[Pd(**2.2 - H**)$_2$] and *trans*-[Pd(**2.2 - H**)$_2$] (Scheme 2.11) using previously established conditions.[118]

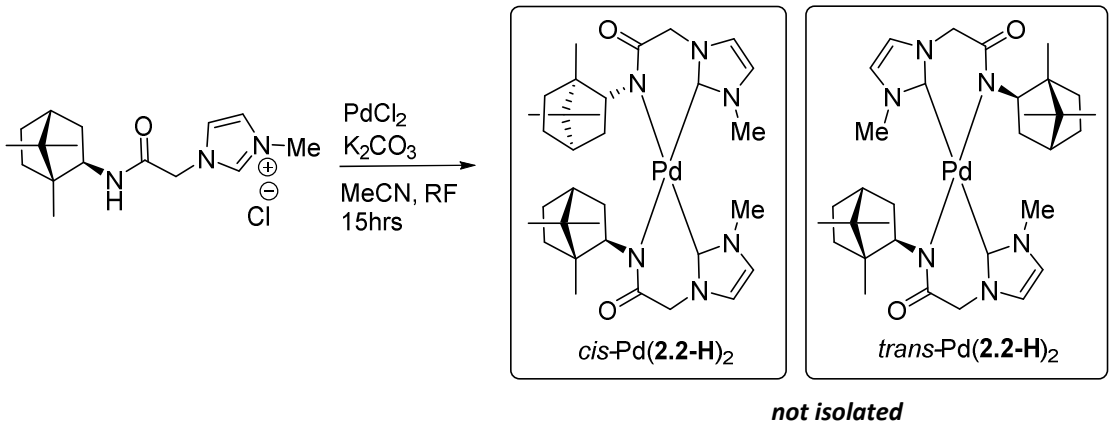

Scheme 2.11: *Attempted synthesis of* cis-*[Pd(**2.2 - H**)$_2$] and* trans-*[Pd(**2.2 - H**)$_2$].*

Proligand **2.2.HCl** was heated with $PdCl_2$ in MeCN until a homogeneous solution was obtained then K_2CO_3 was added. Over 15 hours the suspension faded in colour from a deep ochre to faint yellow/grey. The mixture was cooled and filtered through celite and the contents of the filtrate analysed by ^{1}H-NMR after removal of the solvent. This alluded to an irresolvable cocktail of products but remarkably, the low resolution mass-spectrum was dominated by a signal at 328.62 which is similar in mass to the species [Pd(**2.2**)$_2$]$^{2+}$ (calculated m/z, [Pd(**2.2**)$_2$]$^{2+}$ = 328.15).

To avoid the convolution arising from the synthesis of ML_2 type complexes, only mono-NHC complexes were explored in depth using proligands **2.2.HCl** – **2.5.HCl**. The remaining discussion will centre on the synthesis of these complexes, specifically those depicted in Figure 2.9. Unfortunately, this prevents any direct comparison between these ligands and published ML_2 systems such as the one introduced in Scheme 2.2.

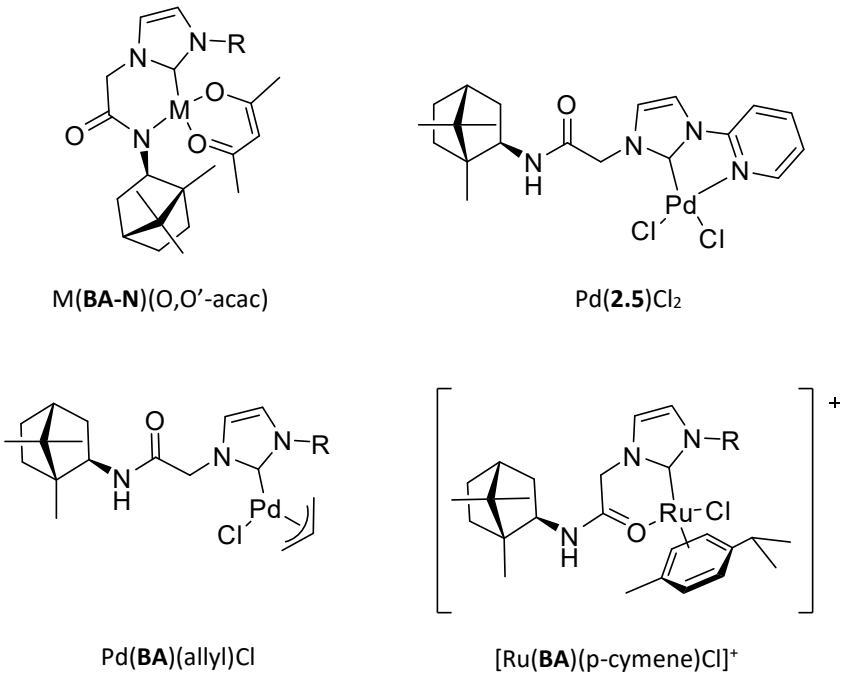

Figure 2.9: *Target compounds explored in this chapter.*

Many of the synthesised bornyl-acetamide NHC complexes possess interesting structural features and some curious conformational isomerism. Therefore, in addition to being catalytically useful compounds, considerable structural analysis was performed and some preliminary insight into their dynamic behaviour has been provided. Beyond the context of catalysis, the results presented in the following sections augment the present understanding of organometallic NHC compounds in the wider field.

2.3.1. M(NHC)(acac) type complexes

An *O,O'*-chelated acetylacetonate (acac) ancillary ligand employed with a chelated BA-N NHC could provide neutral complexes of the type Pd(**BA-N**)(*O,O'*-acac) and Pt(**BA-N**)(*O,O'*-acac) (Figure 2.9). Acac was chosen for its fairly predictable coordination properties, forming stable O-bound six-membered chelates. The rationale behind using an oxygen donor ligand was to minimise congestion around the metal centre, improving the likelihood of amidate-coordination. Examples of M(NHC)(acac) type complexes with

Pd(II)[38, 159-162] and Ni(II)[84] were first isolated some time ago but recently, the class has expanded to include an array of metal centres including Co(III),[163] Ir(II),[164] and Os(II)[165]. These have mostly been employed in catalysis, although, a Pt(II) example has been investigated for its photoluminescence.[61] Here is discussed the successful inclusion of ligand **2.4** into some highly relevant and interesting Pd(NHC)(acac) and Pt(NHC)(acac) systems.

2.3.1.1. Synthesis of Pd(2.4 - H)(*O,O'*-acac) complexes

There are several plausible approaches by which to prepare Pd(**BA-N**)(*O,O'*-acac) type complexes, however, a one-pot, three component synthesis was deemed the most appropriate. This is because chelation by the sterically hindered amidate is promoted by the use of excess base and elevated temperatures. As discussed in the opening to this section, reaction conditions employing MeCN as solvent with K_2CO_3 are complementary to preparing similar organometallic chelates. Under these same conditions in situ NHC generation can coincide with the generation of anionic ancillary ligands by deprotonation of a precursor. Kantchev and Ying outlined this methodology in their one-pot, multi-component synthesis of Pd(NHC)(dmba)Cl complexes in which both the NHC and ancillary ligand were formed by in situ deprotonation.[166] Because these conditions support both formation of the desired NHC-amidate chelate and coordination of acac, they were applied to the synthesis of Pd(**BA-N**)(*O,O'*-acac) type complexes (Scheme 2.12).

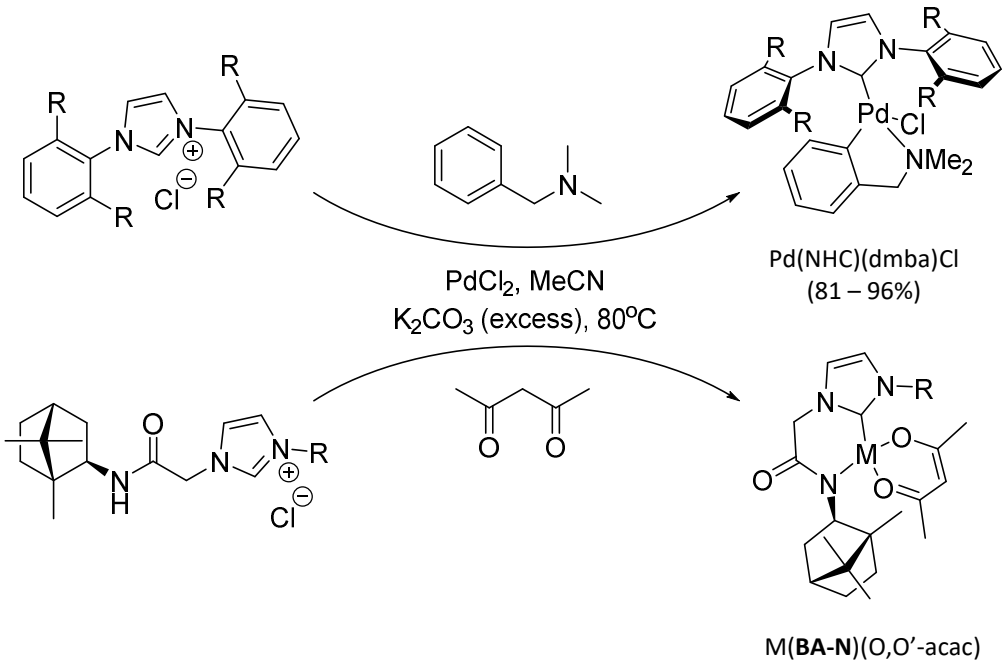

Scheme 2.12: *Previously reported Pd(NHC)(dmba)Cl type complexes as plausible synthetic analogues to Pd(**BA-N**)*(O,O'*-acac) type complexes.*

This was attempted for the synthesis of Pd(**2.4 - H**)(*O,O'*-acac) and although the complex was prepared and characterised, the yields were routinely low (≤ 14%). Various aspects of the procedure were tweaked in an effort to improve this but with little success. Typically the reaction was performed as follows; the precursor salt **2.4.HCl** and an equivalent of $PdCl_2$ were heated at 80 °C in MeCN under an inert atmosphere until all the $PdCl_2$ was dissolved. Finely divided K_2CO_3 (7.5 equivalents) was then added and heating continued. The duration of this step was varied between 10 and 90 minutes, however, the effect on yield was difficult to evaluate. After 60 minutes neither the imidazolium NC*H*N or amide N*H* proton signals are observed in the ^{1}H-NMR spectrum of the reaction mixture suggesting that this is sufficient time to form an intermediary Pd(**2.4 - H**)$(X)_n$ complex. A bleaching of the dark ochre colour of the $Pd(MeCN)Cl_2$ solution during this period also supports NHC coordination. An equivalent of acetylacetone or sodium acetylacetonate (Na(acac)) was then added and heating continued, usually for around four hours. The reaction with a representative set of conditions is shown in Scheme 2.13.

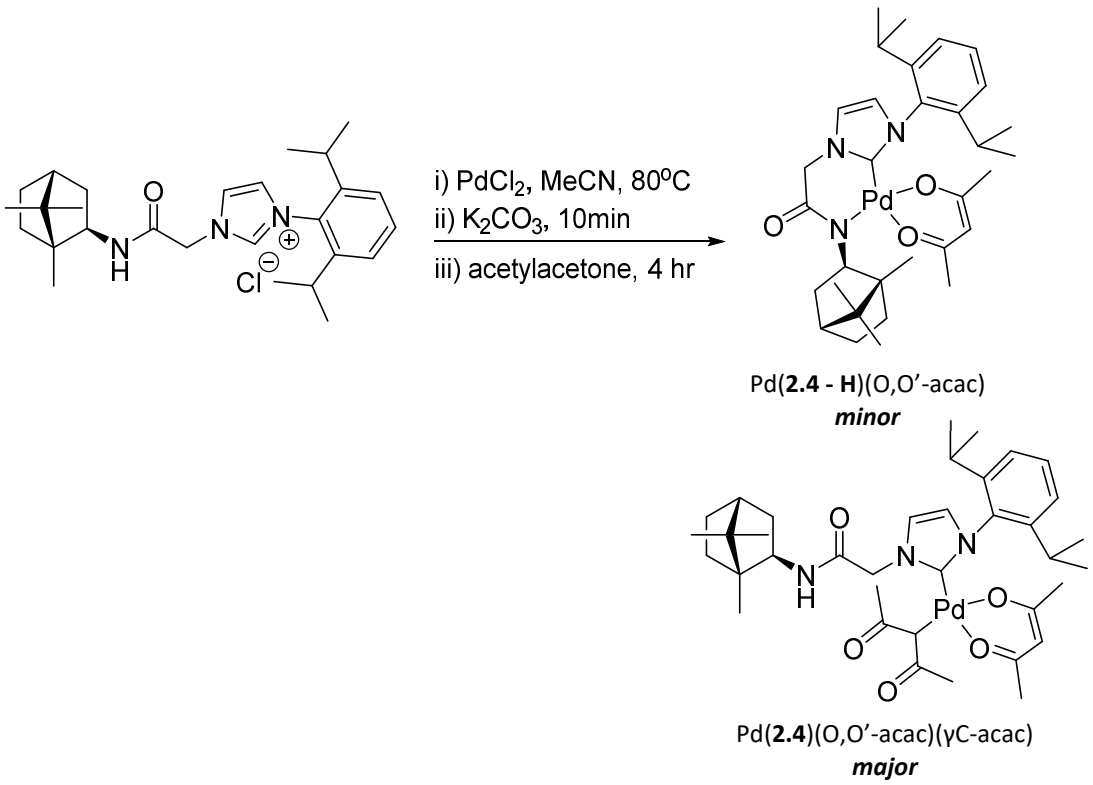

Scheme 2.13: *Synthetic protocol producing both Pd(**2.4 - H**)(O,O'-acac) and Pd(**2.4**)(O,O'-acac)(γC-acac).*

The cooled reaction mixture was filtered through celite then condensed by rotary evaporation. The residue could then be taken up in Et_2O and again filtered through celite to remove any ionic impurities including starting material, although, there was rarely any present at this stage. After removal of the solvent the material was triturated in pentane for several hours which provided acceptably pure Pd(**2.4 - H**)(*O,O'*-acac) as an off white solid. Slow evaporation of the pentane filtrate occasionally yielded an additional crystalline deposit of product. In its crystalline form, Pd(**2.4 - H**)(*O,O'*-acac) could be washed with cold Et_2O and MeCN to give very pure material. Unfortunately, these reactions proved to be extremely temperamental. Often no Pd(**2.4 - H**)(*O,O'*-acac) formation was observed when replicating a condition set which had produced it in a previous instance. Another complex was invariably isolated as the major product of this reaction (yield ≤ 30%), the identity of which was not immediately obvious. After a rigorous NMR analysis and comparison with the platinum complex of **2.4** (see section 2.3.1.2), it was determined to be Pd(**2.4**)(*O,O'*-acac)(γC-acac). The structural elucidation

of compounds Pd(**2.4 - H**)(*O,O'*-acac) and Pd(**2.4**)(*O,O'*-acac)(γC-acac) will be discussed in section 2.3.1.4. The reaction progress could be monitored by ^{1}H-NMR spectroscopy through which the presence of Pd(**2.4 - H**)(*O,O'*-acac) and Pd(**2.4**)(*O,O'*-acac)(γC-acac) were clearly indicated by signals in the region between 4 ppm and 7 ppm. Signals due to several other minor products were also observed and may be attributed to ML_2 type complexes. Such species were identified by low-resolution mass spectroscopy owing to spectral signals at 1047.57 and 474.26 corresponding to a calculated m/z of $[Pd(\mathbf{2.4})_2(O,O'\text{-acac})]^+$ = 1047.57 and $[Pd(\mathbf{2.4})_2]^{2+}$ = 474.26. Surprisingly, Pd(*O,O'*-acac)$_2$ was also detected in a small amount despite only using one equivalent of acetylacetone.

As will be discussed, Pd(*O,O'*-acac)$_2$ is implicated in the formation of complex Pd(**2.4**)(*O,O'*-acac)(γC-acac). The presence of Pd(*O,O'*-acac)$_2$ and its derivatives strongly insinuate that under the conditions described above, ligand exchange is occuring. Various aspects of the procedure were tweaked in an effort to manipulate these system dynamics and these are discussed in section 2.3.1.5. In this section, the condition sets that were trialled for the reaction shown in Scheme 2.16 are summarised in Table 2.1.

2.3.1.2. Synthesis of Pt(2.4 - H)(*O,O'*-acac) complexes

The complex Pt(**2.4 - H**)(*O,O'*-acac) was prepared as a structural analogue to Pd(**2.4 - H**)(*O,O'*-acac). This was synthesised under the conditions displayed in Scheme 2.14. DMSO was used as the solvent to accommodate the slightly higher reaction temperature (110 ^{o}C) deemed necessary to promote ligation at the more kinetically inert Pt(II) centre. Work-up of the reaction required dissolution of the reaction mixture in DCM followed by filtration to remove any inorganic matter including K_2CO_3 before washing with water and brine to remove the DMSO. The organic phase was dried over $MgSO_4$ and the solvent removed to provide a crude mixture of Pt(**2.4 - H**)(*O,O'*-acac), Pt(**2.4**)(*O,O'*-acac)(γC-acac) and a trace amount of Pt(*O,O'*-acac)$_2$.

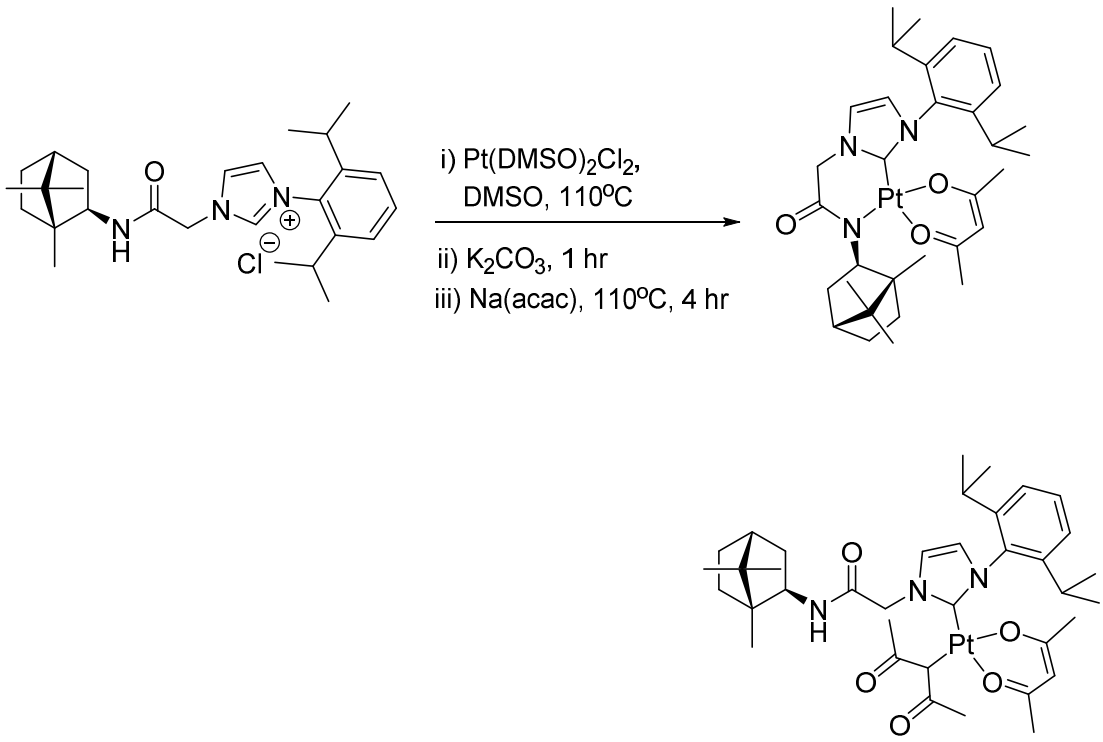

Scheme 2.14: *Synthesis of Pt(**2.4 - H**)(*O,O'*-acac) and Pt(**2.4**)(*O,O'*-acac)(γC-acac).*

The chelated complex Pt(**2.4 - H**)(*O,O'*-acac) was collected as an off-white solid after trituration in pentane and, as with its palladium analogue, crystals of Pt(**2.4 - H**)(*O,O'*-acac) formed upon slow evaporation of the pentane filtrate which could be collected and washed with Et_2O and MeCN. The combined crops of Pt(**2.4 - H**)(*O,O'*-acac) equated to an overall yield of 22%. The remaining material was adequately pure Pt(**2.4**)(*O,O'*-acac)(γC-acac) which was obtained in a 59% yield due to a slight excess of Na(acac) being used. This was purified for analysis by dissolving in MeCN and extracting into pentane. Rotary-evaporation of the pentane extract provided pure Pt(**2.4**)(*O,O'*-acac)(γC-acac) as a white solid.

The reaction proceeds slightly better with Pt(II), producing Pt(**2.4 - H**)(*O,O'*-acac) in a 22% yield compared with a best yield of 14% for Pd(**2.4 - H**)(*O,O'*-acac). This may be because complexes of Pt(II) are more kinetically inert when compared with Pd(II).[27] Additionally, the NHC – Pt(II) bond is stronger than the NHC – Pd(II) bond. The softer

Pt(II) centre accommodates greater σ-orbital overlap with the carbene ligand as well as contributing more electron-density to π* back-donation.[55, 167] The enhanced interaction of carbon-donors with Pt(II) proved important to the structural determination of complex Pt(**2.4**)(*O,O'*-acac)(γC-acac) by enabling the C-bound acac ligand to remain associated for detection of the complete complex by mass-spectrometry (see section 2.3.1.4). As the NHC – Pt(II) complex is more thermodynamically stable and kinetically inert than the NHC – Pd(II) congener, issues associated with ligand exchange are reduced. It is also surmised that using a larger metal centre such as Pt(II) decreases the kinetic barrier to coordination of the hindered amidate. That is, having a less congested coordination sphere than the isostructural Pd(II) complex should facilitate coordination of the bornyl-amidate moiety. However, because this reaction was only performed once it is difficult to assess the true extent to which chelated complex formation improves with the employment of Pt(II). As addressed in section 2.3.1.5, it is equally likely that the elevated temperature of the reaction promotes formation of the desired product. In the cyclohexyl-acetamide series there is no significant difference in the yields recorded for Pd(CyA-N)(*O,O'*-acac) (46%) and Pt(CyA-N)(*O,O'*-acac) (47%) however, as noted in section 3.3.1, the less cumbersome cyclohexyl-group could make these ligands less discerning between Pt(II) and Pd(II).

2.3.1.3. Characterisation of Pd(2.4 - H)(*O,O'*-acac) and Pt(2.4 - H)(*O,O'*-acac)

The complexes Pd(**2.4 - H**)(*O,O'*-acac) and Pt(**2.4 - H**)(*O,O'*-acac) were fully characterised using NMR spectroscopy, mass spectrometry, IR spectroscopy and X-ray crystallography. In the mass-spectrum, these complexes are detected as an $[MH]^+$ cation which produce a signal at 626.2592 for the Pd(II) complex and at 715.3175 for the Pt(II) complex (calculated m/z, [Pd(**2.4 - H**)(*O,O'*-acac) + H]$^+$ = 626.2574, [Pt(**2.4 - H**)(*O,O'*-acac) + H]$^+$ = 715.3184). Definitive structural insight was provided by X-ray crystallography which compliments the NMR and IR spectra. This discussion will begin by addressing the crystal structures of Pd(**2.4 - H**)(*O,O'*-acac) and Pt(**2.4 - H**)(*O,O'*-acac).

Crystals of Pd(**2.4 - H**)(*O,O'*-acac) suitable for single crystal diffraction analysis were grown by slow evaporation of an Et_2O solution of the compound. These crystallised in

the monoclinic space group $P2_1$ with two molecules of Pd(**2.4 - H**)(*O,O'*-acac) in the asymmetric unit (Figure 2.10), these are distinguished by the suffix A or B.

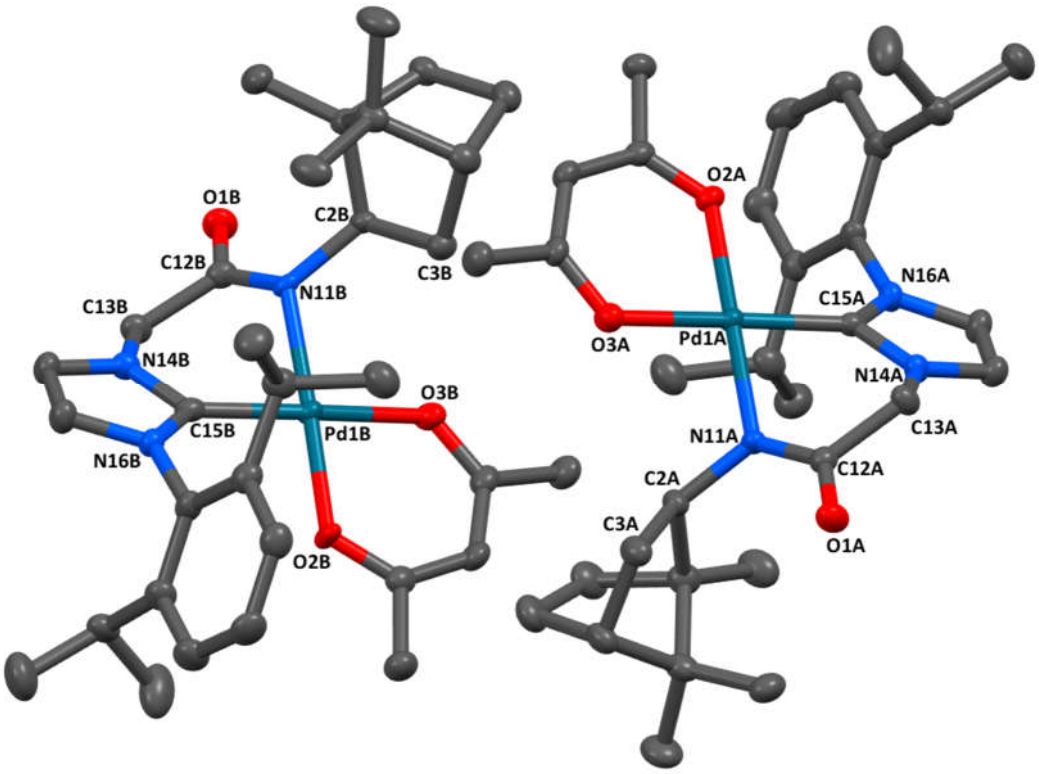

Figure 2.10: *Contents of the asymmetric unit of Pd(**2.4 - H**)*(O,O'*-acac) with relevant atoms labelled. Hydrogen atoms have been omitted for clarity. Thermal ellipsoids are drawn at a 50% probability level.*

Having an enantiopure bornane component renders the structure non-centrosymmetric with Flack(x) and Hooft(y) parameters of -0.001(8) and -0.0059(6) respectively. These verify that the correct stereochemical solution was obtained. The ligand **2.4 - H** is coordinated in a bidentate fashion, chelating between the carbenic carbon C15 and deprotonated amide nitrogen N11. That the N11 is coordinated as an amidate is implicit in the neutrality of the complex and the relatively trigonal planar configuration of bonds around the amidate nitrogen N11 as defined by their tetrahedron volumes of 0.090 $Å^3$ (A) and 0.316 $Å^3$ (B).

Relevant amide bond lengths in Pd(**2.4 - H**)(*O,O'*-acac) (A / B) are C12 – O1 = 1.236(7) Å / 1.242 Å and N11 – C12 = 1.321(6) Å / 1.333 (7) Å which fall within the range of values reported for similar NHC-amidate chelated complexes and are unchanged from the bond-lengths found in a neutral, uncoordinated amide.[118, 120, 168] The resultant 6-membered chelate ring is seen to adopt a shallow boat configuration with the apical methylene carbon C13 projected away from plane defined by the square-planar Pd(II) centre as defined by θ_{CH2} (see later). In order to reduce steric interactions with the acac ligand, the bornane and diisopropyl-phenyl groups occupy the other side of this hypothetical plane thus inducing the observed puckering of the 6-membered chelate.

This divergence from planarity gives rise to atropisomerism, with the bonds Pd1 – C15 and Pd1 – N11 each representing a chiral axis. The enantiomeric designation for each axis depends on which side of the bisecting molecular plane the major substituents reside. Because of the conserved chirality of the bornane moiety these two conformations are diastereomeric and for this reason, molecules A and B of the asymmetric unit are diastereomers (Figure 2.11). In the diastereomer of Pd(**2.4 - H**)(*O,O'*-acac) labelled "A", the bond Pd1 – C15 is a helically chiral *P*-axis and Pd1 – C15 is an *M*-axis. Both axes convert to their opposite enantiomer when the chelate ring conformation is flipped to produce diastereomer "B". The extent to which this chelate ring distorts away from a planar geometry is quantifiable by the torsion angles along the chiral axis, C15-Pd1-N14-C12 and N11-Pd1-C15-N14. For diastereomers A / B these are 52.1(6)° / 63.6(5)° and 32.0(4)° / 35.8(4)° respectively. Despite the difference in these torsions, the relative position of the methylene group remains fairly conserved. This can be represented by the angle between the line intersecting Pd1 and C13 and the plane defined by N11, C15 and Pd1, referred to as θ_{CH2}. For Pd(**2.4 - H**)(*O,O'*-acac), θ_{CH2} (A / B) is 28.4(2)° / 30.7(2)°. These values are consistent with those observed for Pt(**2.4 - H**)(*O,O'*-acac) and the M(**3.3 - H**)(*O,O'*-acac) complexes (see section 3.3.1).

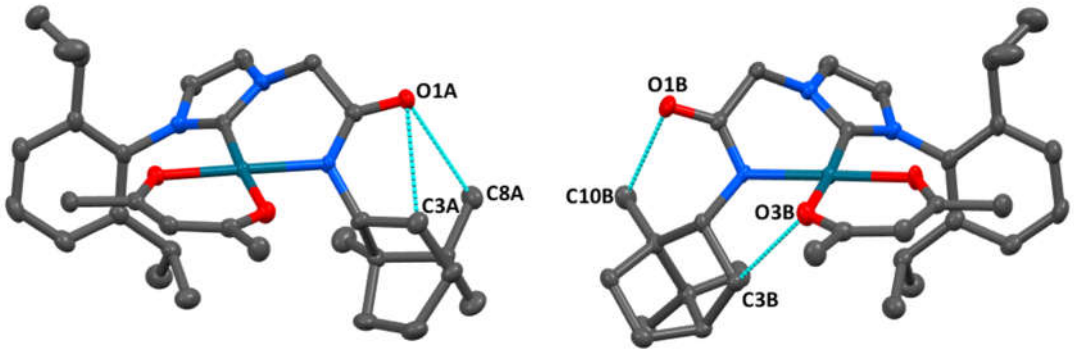

Figure 2.11: *The contents of the asymmetric unit arranged as to better illustrate the diastereoisomerism of the two conformations A and B. Also shown are several non-bonding contacts highlighting the sterically congested nature of the complex.*

Bonding to the Pd(II) centre is characterised by the following bond lengths Pd1 – C15 = 1.949(5) Å / 1.945(6) Å, Pd1 – N11 = 2.030(4) Å / 2.046(4) Å, Pd1 – O2 = 2.015(3) Å / 2.011(3) Å and Pd1 – O3 = 2.056(4) Å / 2.058(4) Å. Strong bonding by the NHC to Pd(II) is implied by the comparatively contracted Pd1 – C15 bond length. A relatively elongated Pd1 – O3 bond is evidence of the renowned trans-influence of NHC ligands in their capacity as strong σ-donors.[167] The angles between these bonds are C15 – Pd1 – N11 = 87.6(2)° / 86.1(2)°, C15 – Pd1 – O2 = 89.7(2)° / 92.5(2)°, N11 – Pd1 – O3 = 89.7(2)° / 92.5(2)°, O2 – Pd1 – O3 = 90.6(2)° / 91.3(2)°. This bonding information highlights the moderate variation between the two diastereomers of Pd(**2.4 - H**)(*O,O'*-acac) (A and B) in the solid state. Visual inspection indicates that these isomers differ significantly in the relative orientations of the bornane moiety. This difference is best expressed by the torsion angle C13-N11-C2-C3 which is 43.2(8)° for A and 172.0(5)° for B. The geometry of the amidate nitrogen N11 is also affected with N11 being trigonal planar in A with a tetrahedron volume of 0.090 $Å^3$ but slightly pyramidal in B with a larger tetrahedron volume of 0.316 $Å^3$ as noted previously.

The sterically congested nature of Pd(**2.4 - H**)(*O,O'*-acac) is exemplified by several short, intramolecular non-bonding contacts between the bornane frame and other parts of the complex at a distance greater than three bonds away (Figure 2.11). Diastereomer B

contains the shortest such non-bonding inter-nuclear distances between C10B ··· O1B at 2.884(8) Å and C3B ··· O3B at 2.839(7) Å. The closest interactions greater than three bonds apart in diastereomer A occur between C8A ··· O1A at 3.031(7) Å and C3A ··· O1A at 3.049(7) Å. It is tentatively inferred from this that, on a steric basis, diastereomer B is the less stable of the pair. This may help explain why diastereomer B also has more extreme torsions across the metal-ligand bonds (torsion angles C15-Pd1-N14-C12 and N11-Pd1-C15-N14, see above) and a non-trigonal planar amidate nitrogen. However, the crystallisation of both diastereomers in the asymmetric unit implies that crystal packing effects override any steric preferences. Interchange between these two diastereomeric conformations is observed by NMR as will be discussed. There are no stabilising intermolecular interactions of note.

A crystal structure of Pt(**2.4 - H**)(*O,O'*-acac) was obtained using a crystal grown by slow vapour diffusion of pentane into a toluene solution of the compound. This crystallised in the non-centrosymmetric monoclinic space group $P2_1$ with two molecules of Pt(**2.4 - H**)(*O,O'*-acac) in the asymmetric unit (Figure 2.12). The complex Pt(**2.4 - H**)(*O,O'*-acac) is an isostructural, crystallographic isomorph of its Pd(II) congener and has Flack(x) and Hooft(y) parameters of -0.011(3) and 0.006(2) respectively. Two A-level alerts occur in the checkcif report due to two large residual density peaks of 9.040 eÅ^{-3} and 3.920 eÅ^{-3}, each of which is adjacent to one of the Pt(II) centres (within ~ 0.90 Å). Inspection of the reciprocal lattice hinted at the presence of a very minor twin component, however, refinement of the solution with resolved twin lattices did not reduce the peak intensity. Strong absorption by the heavy platinum atoms may give rise to the observed residual density. Absorptions were corrected using the SCALE3 ABSPACK multi-scan method in CrysAlisPro, however, more rigorous absorption corrections may be necessary. Alternatively, due to the intense scattering of platinum, a minor degree of disorder may result in Q-peaks being observed for partially occupied Pt atom sites and not for the lighter atoms. Regardless, these unassigned density peaks do not prevent this model of Pt(**2.4 - H**)(*O,O'*-acac) being used as a structural characterisation tool.

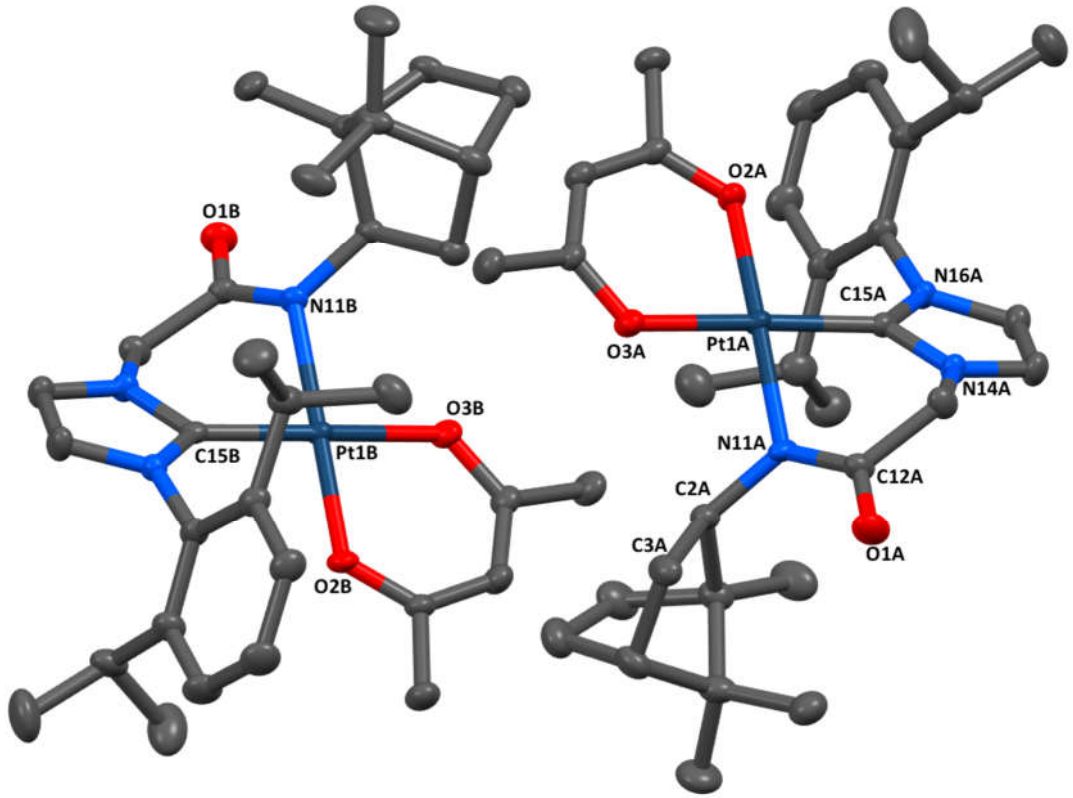

Figure 2.12: *Contents of the asymmetric unit of Pt(**2.4 - H**)(O,O'-acac) with relevant atoms labelled. Hydrogen atoms have been omitted for clarity. Thermal ellipsoids are drawn at a 50% probability level.*

Although it is anticipated that the larger Pt(II) centre can better accommodate chelation of the bornyl-amidate, no major indication of this is observed in the solid state. The M – $C_{carbene}$ bond length Pt1 – C15 of 1.931(5) Å / 1.937(5) Å is notably shorter than Pd1 – C15 (1.949(5) Å / 1.945(6) Å) owing to the stronger Pt – NHC interaction identified in section 2.3.1.2. Otherwise, bonding and torsional measurements related to the coordination conformation of ligand **2.4 - H** are comparable with the Pd(II) analogue. Data related to bonding at the Pt(II) centre is summarised in table 3.1, section 3.3.1.3. A complete structural analysis comparing data for the M(**2.4 - H**)(*O,O'*-acac) and M(**3.3 - H**)(*O,O'*-acac) complexes is also undertaken in that section. There are no mentionable features of Pt(**2.4 - H**)(*O,O'*-acac) that have not been addressed regarding Pd(**2.4 - H**)(*O,O'*-acac).

NMR and IR spectroscopy support the structures elucidated by X-ray crystallography. The presence of bornane and diisopropyl-phenyl substituents in the complexes was readily confirmed by the ^{1}H-NMR and ^{13}C-NMR spectra. That the complex bore a coordinated NHC moiety was evidenced in each ^{1}H-NMR spectrum (Figure 2.13) by the conspicuous absence of a downfield singlet due to the NC*H*N proton (H15) of the imidazolium proligand. A signal due to the carbenic carbon (C15) is found in the ^{13}C-NMR spectrum of Pd(**2.4 - H**)(*O,O'*-acac) at 153.55 ppm. This is consistent with a reported Pd(II) bonded carbene resonance when trans to O-bound acac.[38] The equivalent signal in the ^{13}C-NMR spectrum of the Pt(II) congener resonates at a lower frequency of 139.25 ppm due to the greater electronic shielding of the carbon nucleus afforded by the more π-donating, electron rich Pt(II) centre. This effect is noted to a lesser extent for the carbonyl carbon signals due to the acac ligand which are detected in the spectra of Pd(**2.4 - H**)(*O,O'*-acac) at 185.98 ppm and 184.44 ppm and slightly upfield at 183.56 ppm and 182.64 ppm for Pt(**2.4 - H**)(*O,O'*-acac). The chemical shift of the amidate carbonyl carbon is 170.29 ppm and 171.56 ppm for each complex.

Signals attributed to the O-bound acac ligand are found in the ^{1}H-NMR spectrum of the Pd(II) complex at 5.05 ppm ($(CH_3CO)_2CH$, H33), 1.89 ppm (CH_3, H31) and 0.98 ppm (CH_3, H35) and for the Pt(II) complex at 5.13 ppm ($(CH_3CO)_2CH$, H33), 1.77 ppm (CH_3, H31) and 0.93 ppm (CH_3, H35). In both spectra it was noted that one of the H35 methyl-proton resonances was unusually low field given that, in $CDCl_3$ the methyl proton of O-bond acac ligands typically resonate between 1.1 – 2.0 ppm with Pd(II)[38, 169] and between 1.8 – 2.1 with Pt(II).[170, 171] This shift to below 1.0 ppm is most likely due to anisotropic shielding of the methyl group that is directed towards the face of the diisopropyl-phenyl ring. Evaluation of the crystal structures shows this to be a reasonable assessment. In the ^{13}C-NMR spectrum of both complexes the $(CH_3CO)_2CH$ carbon (C33) is found at ~ 100.0 ppm and the two methyl carbons at ~ 26.5 ppm and ~ 25.2 ppm. The proton of the imidazole-2-ylidene ring adjacent to the aryl ring (H17) is also anisotropically shielded. Its signal arises in the spectrum of both complexes at ~ 6.7 ppm which is ~ 1.1 ppm upfield of the neighbouring imidazolyl proton signal.

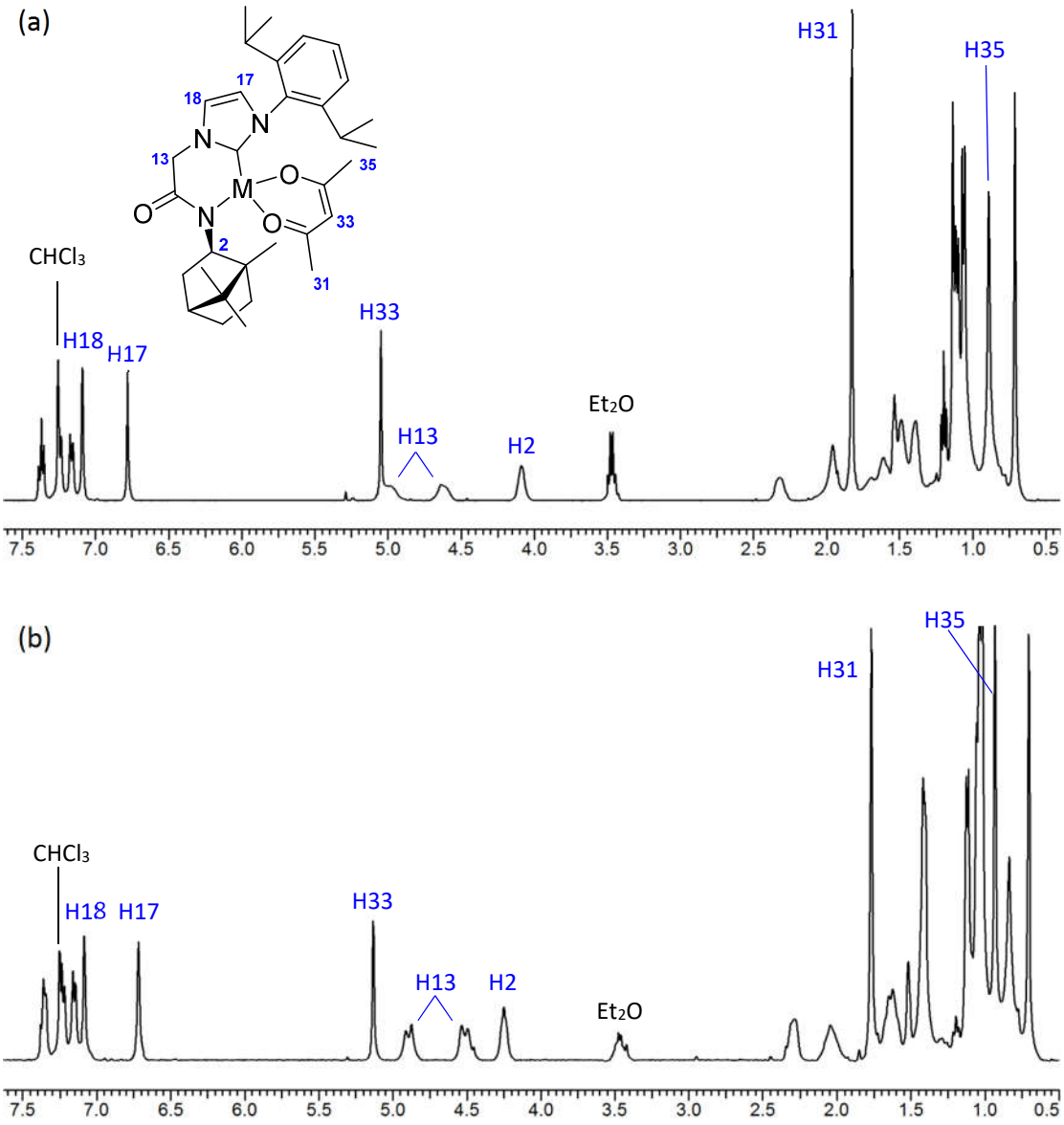

Figure 2.13 (a): *The ^{1}H-NMR spectrum of complex Pd(**2.4 - H**)(O,O'-acac) and,* ***(b)*** *complex Pt(**2.4 - H**)(O,O'-acac). Several of the signals discussed in the text are noted.*

An amide N*H* proton is also missing from the ^{1}H-NMR spectrum. Although this implies that amidate chelation has occurred, this signal can be broadened out by other effects and hence its absence is not definitive evidence of deprotonation. In this case however, the presence of a deprotonated amide moiety was verified by IR spectroscopy. In a coordinated amidate, the amide anion is stabilised by association with the metal and conjugation of the negative charge onto the oxygen atom. This increases its iminol character and the consequent weakening of the carbonyl bond is reflected in the IR-

spectrum as a lowering of its vibrational stretching frequency. In the IR-spectrum of the precursor salt **2.4.HCl** the amide carbonyl stretch occurs at 1687 cm^{-1}. In the complexes Pd(**2.4 - H**)(*O,O'*-acac) and Pt(**2.4 - H**)(*O,O'*-acac) the vibrational energy of the NHC-ligand based carbonyl stretch is reduced to 1575 cm^{-1} and 1574 cm^{-1} as expected. The carbonyl stretch associated with the O-bound acac ligand in each respective complex are 1515 cm^{-1} and 1521 cm^{-1}, closely mirroring the carbonyl stretching frequency recorded for Pd(*O,O'*-acac)$_2$ at 1516 cm^{-1}. In this way, concomitant IR-spectroscopy was used to confirm that the bulk material contained a coordinated amidate moiety.

In addition to structural assignments, the ^{1}H-NMR and ^{13}C-NMR spectrum of complexes Pd(**2.4 - H**)(*O,O'*-acac) and Pt(**2.4 - H**)(*O,O'*-acac) aptly communicate how the **2.4 - H** ligand is sterically restricted yet still conformationally fluxional. The non-equivalence of proton and carbon environments due to the diisopropyl-phenyl moiety and the emergence of diastereotopic methylene proton signals (H13) belies some degree of conformational restraint. However, the severe broadening of all signals associated with the bornane frame and methylene linker is indicative of slow molecular motion relative to the NMR timescale. This conformational dynamism will be explored through comparison of these spectral features with those of the complexes Pd(**3.3 - H**)(*O,O'*-acac) and Pt(**3.3 - H**)(*O,O'*-acac) in section 3.3.1.3. Signal sharpening occurs at elevated temperatures due to acceleration of this motion, for an example of this see Figure 2.15 in section 2.3.1.4.

2.3.1.4. Characterisation of Pd(2.4)(*O,O'*-acac)(γC-acac) and Pt(2.4)(*O,O'*-acac)(γC-acac)

Of the complexes Pd(**2.4**)(*O,O'*-acac)(γC-acac) and Pt(**2.4**)(*O,O'*-acac)(γC-acac), the former was isolated some time before the latter and its identity was not immediately obvious. Despite exhaustive efforts, diffraction quality crystals were unable to be obtained for either complex. The difficulty in characterising Pd(**2.4**)(*O,O'*-acac)(γC-acac) arose from the fact that its mass-spectrum was identical to that of Pd(**2.4 - H**)(*O,O'*-acac) displaying a lone signal at 626.2570 (m/z, [Pd(**2.4 - H**)(*O,O'*-acac) + H]$^{+}$ = 626.2574). On the other hand, its ^{1}H-NMR and ^{13}C-NMR spectra appeared to contain signals due to two

compounds in a 70 : 30 ratio in CD_3CN, neither of which were the chelated complex Pd(**2.4 - H**)(*O,O'*-acac). These compounds were clearly closely related and could not be separated by chromatography. Synthesis of the Pt(II) version enabled identification of the true complex mass by mass spectrometry. For Pt(**2.4**)(*O,O'*-acac)(γC-acac) a single cation of mass 815.3714 is observed which corresponds to a calculated m/z, $[Pt(\mathbf{2.4})(O,O'\text{-acac})(\gamma C\text{-acac}) + H]^+$ = 815.3711. In this way it was determined that these species contain one **2.4** ligand and two acac ligands, one of which is weakly bound given that it dissociates in the mass-spectrum of Pd(**2.4**)(*O,O'*-acac)(γC-acac). A thorough NMR and IR analysis subsequently confirmed the structural identity of these compounds to be of the type shown in Figure 2.14. The two species observed in the NMR spectra were found to be amide rotamers hence are distinguished as having either *Z* or *E*-amide geometries.

For the NMR characterisation of Pd(**2.4**)(*O,O'*-acac)(γC-acac) and Pt(**2.4**)(*O,O'*-acac)(γC-acac) it was beneficial to use spectra collected on a 600 MHz spectrometer to maximise signal resolution. With the exception of a couple of signals, the ^{1}H-NMR and ^{13}C-NMR spectra of Pd(**2.4**)(*O,O'*-acac)(γC-acac) and Pt(**2.4**)(*O,O'*-acac)(γC-acac) compare closely, hence, for convenience, the following analysis will focus on the spectra of the Pd(II) complex. Upfield regions of the ^{1}H-NMR and ^{13}C-NMR spectra of Pd(**2.4**)(*O,O'*-acac)(γC-acac) are shown in Figure 2.14. At a glance, the alkyl regions of these spectra are too congested to be informative to this discussion and hence have been omitted. It is important to note that all alkyl environments are accounted for and have been assigned through careful interpretation with the aid of HSQC, HMBC, COSY and 2D-NOESY experiments.

It is deduced from these that the BA – NHC ligand adopts a monodentate “pendant” motif. This is clear from the presence of an amide hydrogen signal (H11) and the distinctive, geminally coupled doublets of the methylene hydrogen environments (H13). These are observed at 5.43 ppm and 4.75 ppm for the major isomer and at 5.19 ppm and 4.98 ppm for the minor with the $^2J_{H\text{-}H}$ coupling constant of both being 16 Hz. This characteristic AB splitting pattern is routinely used to identify coordination of acetamide-linked NHC ligands in this study.

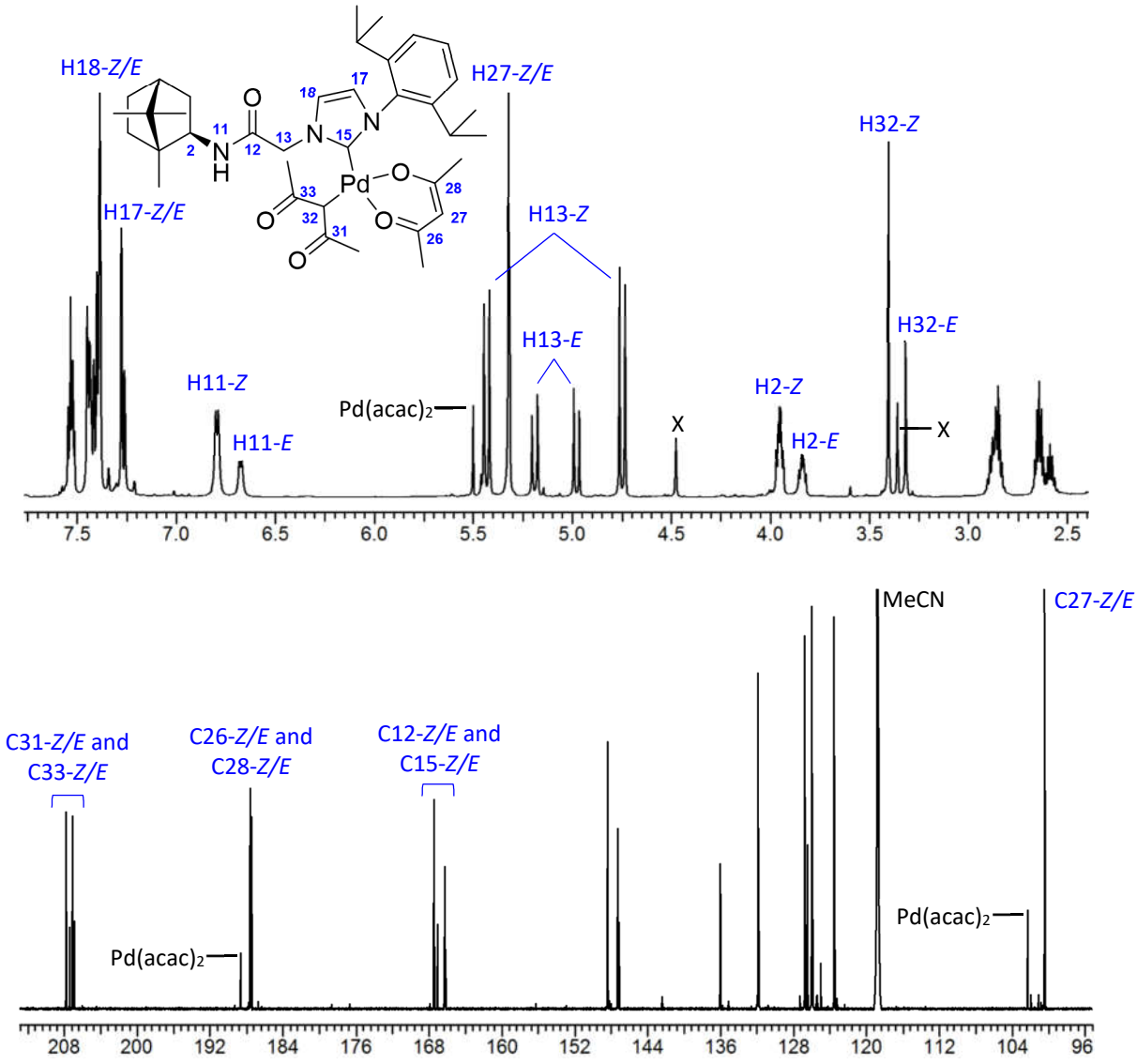

Figure 2.14: *Upfield regions of the ^{1}H-NMR and ^{13}C-NMR spectra of Pd(**2.4**)*(O,O'-*acac)(γC-acac) in CD_3CN. Selected signals are labelled with the suffix* Z *or* E *denoting the amide geometry of the isomer.*

It is further inferred from these spectra that there is one O-bound and one C-bound acac ligand in the complex. The O-bound acac ligand contributes carbonyl-carbon resonances at 188.64 ppm and 187.63 ppm (C27/C28) and the pseudo-aromatic carbon resonance (C27) at 100.38 ppm with its bonded hydrogen (H27) detected at 5.32 ppm in the proton spectrum. More importantly, we find conclusive evidence that a σ-bonded acac ligand occupies the remaining coordination site. The chemical shift of these proton and carbon environments are markedly different to those of the *O,O'*-chelated acac. The ^{13}C-NMR

spectrum is particularly informative with the carbonyl-carbon of γC-acac generating the highest frequency signals between 207.80 ppm – 206.94 ppm (C31/C33). The metal-bonded carbon centre is seen to resonate at a lower frequency when compared with the O-bound acac due to greater nuclear shielding as a result of its sp^3 character. Signals for both isomers due to this environment are found at 48.68 ppm (C32-*Z*) and 48.31 ppm (C32-*E*) and the associated proton resonances are 3.40 ppm (H32-*Z*) and 3.32 ppm (H32-*E*). HMBC analysis shows that the γC*H* signal is correlated to the carbonyl-carbon resonances as expected. Further correlations enabled the two methyl environments to be assigned. In both Pd(**2.4**)(*O,O'*-acac)(γC-acac) and Pt(**2.4**)(*O,O'*-acac)(γC-acac), the ^{1}H-NMR and ^{13}C-NMR chemical shifts agree with reported values for C-bound acac.[38, 169-173]

IR-spectroscopy complemented this structural assignment through identification of several characteristic carbonyl stretching frequencies. Both Pd(**2.4**)(*O,O'*-acac)(γC-acac) and Pt(**2.4**)(*O,O'*-acac)(γC-acac) produced comparable IR spectra with three strong signals at 1672 cm^{-1}, 1578 cm^{-1} and 1515 cm^{-1} for the former and at 1674 cm^{-1}, 1575 cm^{-1} and 1520 cm^{-1} for the latter. The observed signal at $\sim$ 1670 cm^{-1} falls neatly within the range for a typical amide carbonyl stretching frequency (1640 cm^{-1} – 1690 cm^{-1}) and resembles the related stretch at 1687 cm^{-1} observed in the spectrum of the proligand **2.4.HCl**. This strongly suggests that the amido-functionality is not involved in coordination. Stretching of the O-bound acac carbonyl produces the signals at $\sim$ 1520 cm^{-1}, mirroring the equivalent signal observed in the spectrum of Pd(**2.4 - H**)(*O,O'*-acac), Pt(**2.4 - H**)(*O,O'*-acac) and Pd(acac)$_2$ (see section 2.3.1.3). The intermediary stretch is most likely due to the C-bound acac. Several much weaker signals are interspersed amongst these carbonyl stretching frequencies and may be attributed to amide N – H bending, aromatic C – C stretching or to the carbonyl stretches of the minor isomer.

Confident of the structure assigned to Pd(**2.4**)(*O,O'*-acac)(γC-acac) and Pt(**2.4**)(*O,O'*-acac)(γC-acac), attention turned to identifying the perceived mode of isomerism apparent in NMR spectra of these compounds. An equilibrium relationship between the two observed isomers of Pd(**2.4**)(*O,O'*-acac)(γC-acac) and Pt(**2.4**)(*O,O'*-acac)(γC-acac) was anticipated on the basis that they are inseparable and consistently recovered in an identical ratio. Inhibition of free conformational motion due to the bulky bornane

substituent could similarly affect these complexes as it does for the chelate complexes Pd(**2.4 - H**)(*O,O'*-acac) and Pt(**2.4 - H**)(*O,O'*-acac) (section 2.3.1.3). The molecule contains a number of rotatable bonds which could plausibly be restricted by steric interactions to give the two distinct species observed by ^{1}H-NMR (as in Pd(**2.4**)(allyl)Cl, section 2.3.3.2), however, the evidence at hand suggests amide rotamers are a probable cause (Scheme 2.15). The occurrence of *Z* and *E*-amide geometries is a well understood phenomenon arising from the significant π-bond character of the resonance stabilised amide bond.[145]

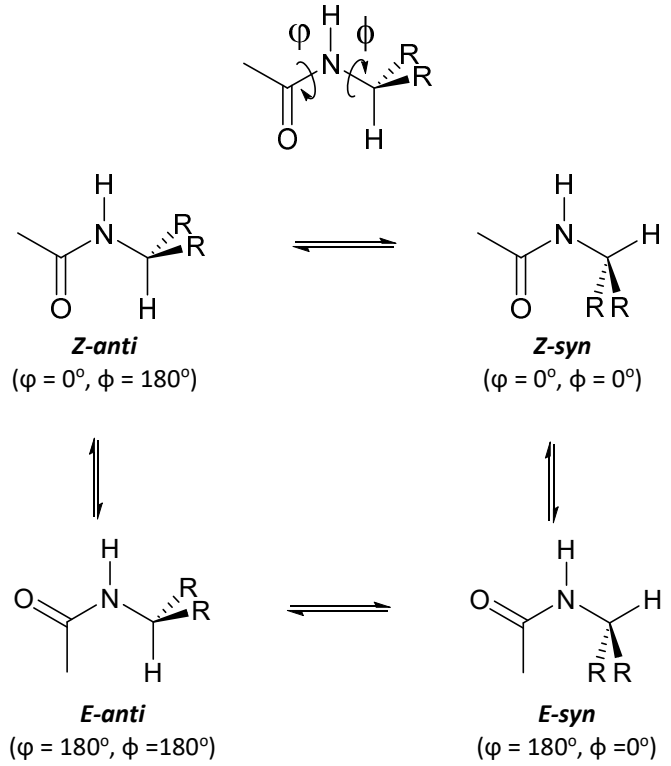

Scheme 2.15: Syn *and* anti-*conformations of the* Z *and* E *geometric isomers of an acetamide derivative.*

An initial indication that such isomerism is taking place in complexes Pd(**2.4**)(*O,O'*-acac)(γC-acac) and Pt(**2.4**)(*O,O'*-acac)(γC-acac) is the position of the proton and carbon NMR resonances for the N – CHα environment. It is well established that secondary *N*-alkyl amides prefer to orient themselves such that the NH proton is *anti*- relative to the

CH proton (Scheme 2.15). When in the *Z-anti* configuration, the amide carbonyl bond anisotropy has a large deshielding influence on Hα whilst shielding Cα.[174] This effect was observed in the spectra of both complexes for which the equivalent bond is labelled N11 – C2 (see Figure 2.14). For (*Z / E*)-Pd(**2.4**)(*O,O'*-acac)(γC-acac), H2 resonates at 3.95 ppm / 3.84 ppm and C2 at 58.41 ppm / 58.81 ppm, and for (*Z / E*)-Pt(**2.4**)(*O,O'*-acac)(γC-acac) at 3.97 ppm / 3.86 ppm and 58.37 ppm / 58.66 ppm. None of the precursor acetamide compounds **2.1** and **2.2** – **2.5**.**HCl** exhibit observable isomerism, nor for that matter, do any reported NHC-acetimide derivatives. Moreover, it is surprising that a distinction between *E / Z* geometries in the ligand **2.4** should arise following an increase in the bulk of the imidazole terminus which, on steric grounds, should overwhelmingly favour the *Z*-amide geometry.

Variable temperature ^{1}H-NMR experiments were used to confirm that the isomers were dynamically interconverting, rotationally related species. Coalescence of signals is expected at elevated temperatures due to accelerated rotation relative to the timescale of the NMR. The analysis was performed using DMSO as the solvent and heating at 10 – 15 ^{o}C increments between from 25 ^{o}C to 130 ^{o}C (Figure 2.15a). CD_3CN was the preferred solvent for these experiments as it produces ^{1}H-NMR spectra with clear resolution of isomeric signals (Figure 2.14). Unfortunately, only minor spectral changes occurred at temperatures approaching its boiling point of 82 ^{o}C necessitating the use of DMSO-*d6* to access higher temperatures.

Resonances were observed to have fully coalesced by 110 ^{o}C. As expected, proton resonances adjacent to the amide bond are most affected. The amide NH proton (H11) and CHα (H2) coalesce neatly to a single peak. Signals due the methylene proton (C13) likewise merge but are not seen at temperatures above 100 ^{o}C. Measuring the spectrum again at 25 ^{o}C after cooling from 130 ^{o}C showed that the original isomeric ratio was restored hence the process is reversible (Figure 2.15b).

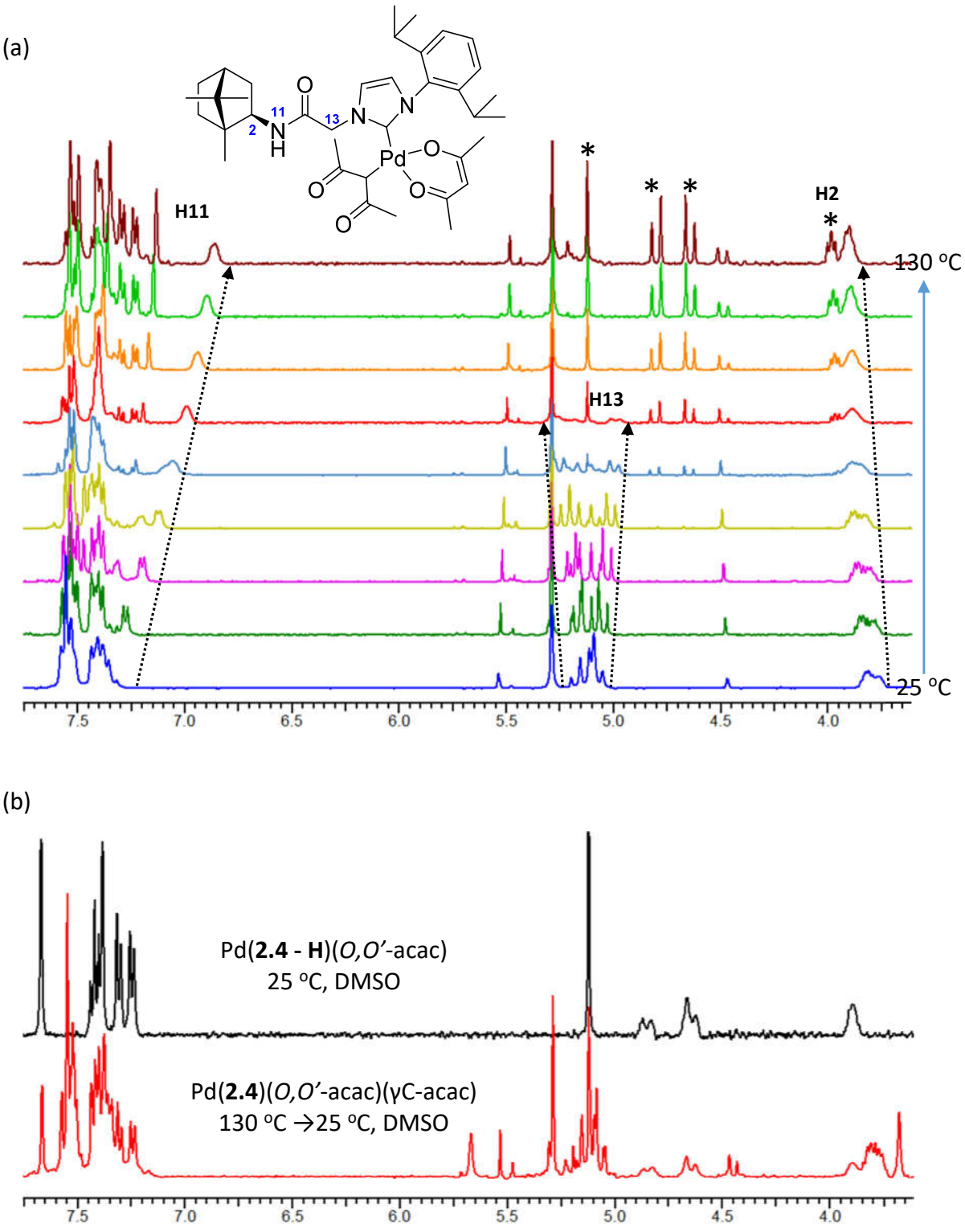

Figure 2.15 (a): *Series highlighting the changes in the ^{1}H-NMR spectrum of Pd(**2.4**)*(O,O'-*acac)(γC-acac) as a function of temperature in DMSO*-d6 *and,* ***(b)*** *its spectrum recorded at 25 °C after heating to 130 °C in comparison with the ^{1}H-NMR spectrum of Pd(**2.4 - H**)*(O,O'-*acac). The formation of the chelated species upon heating of Pd(**2.4**)*(O,O'-*acac)(γC-acac) accounts for the emergence of signals denoted by *. These signals persist upon cooling.*

No attempt was made to quantify the rotational free energy barrier $\Delta G^{\ddagger}$ using the coalescence temperature method.[175, 176] This is complicated by the asymmetry of the compound and conversion to Pd(**2.4 - H**)(*O,O'*-acac) at higher temperature. Observing the reversible coalescence of proton resonances related to the amide moiety is adequate confirmation of interconverting amide rotamers.

Curiously, irreversible formation of the chelated amidate complex Pd(**2.4 - H**)(*O,O'*-acac) emerged as a competing side-process, onset of which occurred at 70 ^{o}C. Diagnostic signals due to this species are denoted by an asterisk in Figure 2.15a and it is shown to persist in solution upon cooling through comparison with the room temperature spectrum of Pd(**2.4 - H**)(*O,O'*-acac) in DMSO-*d6* (Figure 2.15b). Sharp signals due to Pd(**2.4 - H**)(*O,O'*-acac) are observed at elevated temperature due to acceleration of the ring flipping action identified in section 2.3.1.3 and its very formation provides some mechanistic insight as elaborated in section 2.3.1.5.

The effect of solvent polarity on the rotamer equilibrium was studied in an effort to determine why the *E*-amide configuration of ligand **2.4** becomes so prevalent when incorporated in this complex. As mentioned previously, coordination of the NHC represents a large increase in steric bulk which should favour the *Z*-amide. However, while steric interactions are usually the main driving force, electrostatic and entropic factors can be influential.[145, 146, 174, 177, 178] The relative *Z / E* populations were determined by integration of selected proton signals in the ^{1}H-NMR spectra of Pd(**2.4**)(*O,O'*-acac)(γC-acac) in several different solvents. An *E*-amide population of $\sim$ 30% is observed in benzene-*d6*, CD_3CN and CD_3OD but drops slightly to 24 % in chloroform. Signals are too poorly separated in the spectrum recorded using DMSO-*d6* to determine a ratio and the compound is insoluble in D_2O. It is difficult to draw a definitive conclusion based on these findings, but regardless of this, a room temperature *E*-amide population of $\sim$ 30% is large for a secondary amide. It is suspected that the *E*-amide geometry is stabilised by non-polar interactions between the bornane group and the hydrophobic pockets formed between the isopropyl substituents on **2.4** and methyl groups of the acac ligands. A representation of how hydrophobic interactions can increase when in the *E*-

amide configuration compared with the *Z*-amide is shown in Figure 2.16 for both Pd(**2.4**)(*O,O'*-acac)(γC-acac) and a tailor-made literature compound.[178]

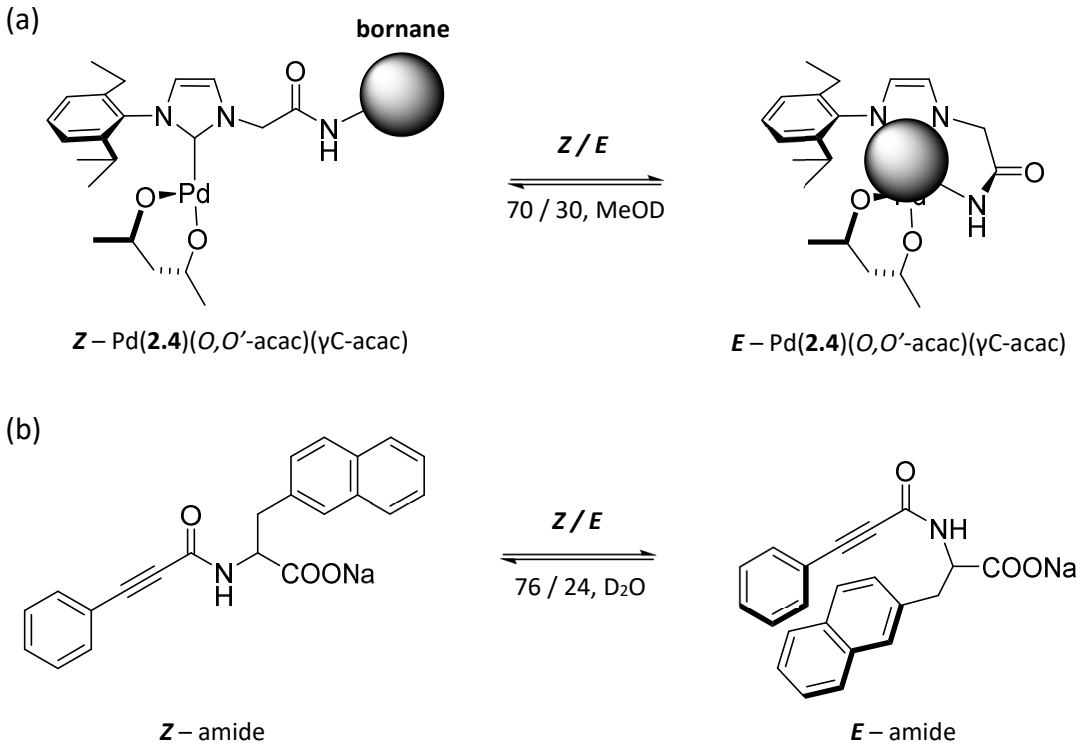

Figure 2.16 (a): E / Z – *amide configurations of Pd(**2.4**)(*O,O'*-acac)(γC-acac) and,* ***(b)*** *a literature compound designed to maximise the* E-*amide population in aqueous media.*

In the conformation shown, the carbonyl group can also participate in hydrophilic interactions with keto-groups of the γC-acac ligand and the amide moiety can be co-planar to the pseudo-aromatic *O,O'*-acac ligand. These complementary intramolecular hydrophilic and hydrophobic interactions may explain why the *Z / E* ratio exhibits only minor solvent dependence. If the driving interaction is predominantly non-polar a polar-protic solvent such as MeOH would be expected to promote association of the hydrophobic surfaces increasing the *E*-amide population compared to say, benzene. This is demonstrated by the example in Figure 2.16b for which the *E*-amide configuration minimises the hydrophobic surface area and exposes hydrophilic contacts. This leads to an *E*-amide population of 24% in D_2O and only 6% in $CDCl_3$.[178] Because intramolecular

contacts such as these reduce the amount of solvent accessible surface area, desolvation upon conversion to the *E*-amide configuration provides an entropic motive.[177] Furthermore, this accounts for why the imidazolium salt proligands **2.2.HCl** – **2.5.HCl** are not observed as amide rotamers; an *E*-amide configuration would bring the highly hydrophobic bornane proximal to the hydrophilic imidazolium salt moiety. The *Z*-amide configuration therefore minimises both steric strain and electrostatic repulsion in **2.2.HCl** – **2.5.HCl**. Conversion into a neutral, coordinated NHC reverses the electrostatic relationship between imidazolyl moiety and the bornane unit. The *E*-configuration which was destabilising to the precursor becomes energetically available in the complex. This has interesting implications for the role for these compounds in asymmetric catalysis. Interaction with the stereodirecting bornane unit via chelation by the amide requires it to be in the *Z*-geometry however, "non-chelated" electrostatic association improves with an *E*-geometry.

Such behaviour has been documented in a number of organic compounds and, most notably, in relation to the study of protein dynamics.[179] Furthermore, hydrophobic/hydrophilic interactions have been exploited to tune *Z* / *E*-amide equilibria in order to understand and control receptor binding of amide-containing compounds for enzyme regulation and inhibition.[179-181]

2.3.1.5. Discussion of reaction conditions and possible improvements

Although complex Pd(**2.4**)(*O,O'*-acac)(γC-acac) proved to be interesting in its own right, the chelated complex Pd(**2.4 - H**)(*O,O'*-acac) was the desired target and considerable effort was invested in its synthesis. The condition sets that were trialled for its preparation by the reaction shown in Scheme 2.16 are summarised in Table 2.1.

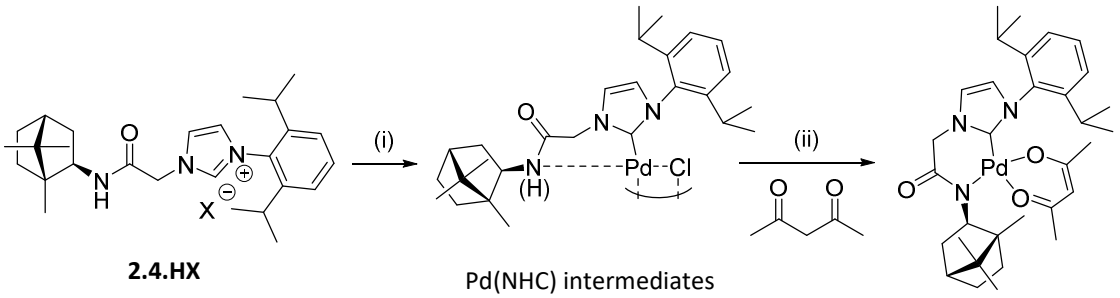

2.4.HX Pd(NHC) intermediates Pd(**2.4 - H**)(O,O'-acac)

Scheme 2.16: *In situ synthesis of Pd(**2.4 - H**)(O,O'-acac) from **2.4.HX** via one or more uncharacterised Pd(NHC) intermediates. The conditions trialled for (i) and (ii) are summarised in Table 2.1.*

Table 2.1: *Conditions sets attempted for the synthesis of Pd(**2.4 - H**)(O,O'-acac) (Scheme 2.16).*

set	X	(i) solvent	Pd(II) source	base	temp (C°)	time (mins)	(ii) time (hrs)	Yield
1	Cl	MeCN	PdCl2	K2CO3	80	0	4	~10%
2	Cl	MeCN	PdCl2	K2CO3	80	10	4	12%
3	Cl	MeCN	PdCl2	K2CO3	80	90	1	trace
4	Cl	MeCN	PdCl2	K2CO3	reflux	45	4	14%
5	PF6	MeCN	Pd(OAc)2	K2CO3	reflux	90	4	~10%
6	Cl	MeCN	PdCl2	NEt3	80	10	4	0
7	Cl	DMSO	Pd(PhCN)2Cl2	K2CO3	110	60	15	0

Condition sets 1, 2, 4 and 5 were the most successful albeit still low yielding. These used K_2CO_3 as base and are similar in that the reaction was heated for 4 hours after the addition of acetylacetone. Condition set 7 which used DMSO at an extreme temperature of 110 °C yielded no product, however, it was likely reacted for too long (15 hours) leading to degradation of the product and reactants. The formation of Pd(**2.4**)(*O,O'*-acac)(γC-acac) as the major product was suspected to occur via reaction of the NHC ligand with Pd(*O,O'*-acac)$_2$.

To support this hypothesis, complex Pd(**2.4**)(*O,O'*-acac)(γC-acac) was prepared in a 59% yield by a targeted synthesis using sodium acetylacetonate as base (Scheme 2.17). This

presumably produces the compound by reorganisation of one O-bound acac ligands of Pd(*O,O'*-acac)$_2$ to accommodate coordination of the NHC in a manner that has been previously acknowledged.[38] Furthermore, this supports the notion that Pd(**2.4**)(*O,O'*-acac)(γC-acac) forms because Pd(*O,O'*-acac)$_2$ is a thermodynamically and kinetically favoured product that forms rapidly under the conditions before coordination by the sterically hindered **2.4** ligand that is formed slowly by comparison.

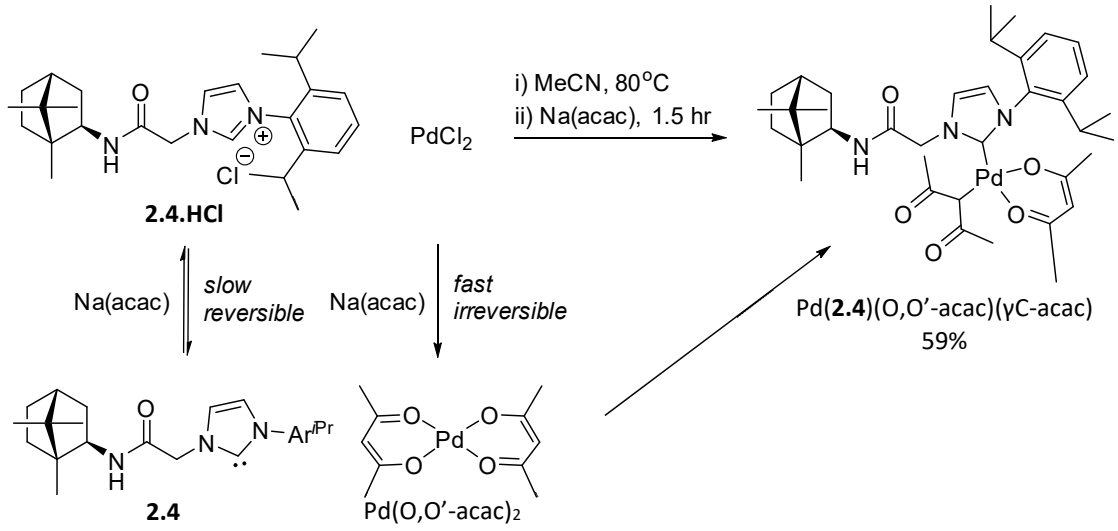

Scheme 2.17: *Targeted synthesis of Pd(**2.4**)(*O,O'*-acac)(γC-acac) and the probable pathway to its formation.*

It is likely that even when not using Na(acac) as base, as per the conditions in Table 2.1, Pd(*O,O'*-acac)$_2$ forms readily. This is despite efforts to pre-form the NHC – Pd bond, as in step (i), Scheme 2.16. Formation of Pd(**2.4**)$_2$ type species, which were detected by mass spectrometry, may be driven by the formation of Pd(*O,O'*-acac)$_2$ after the initial addition of acetylacetone. Because of the extremely hindered nature of **2.4**, the Pd(**2.4**)$_2$ complexes are likely prone to ligand dissociation, availing **2.4** to react with Pd(*O,O'*-acac)$_2$.

Interestingly, attempts made at the synthesis of Pd(**2.2**)(*O,O'*-acac) derivatives using proligand **2.2.HCl** and condition set 4, Table 2.1 and also with Na(acac) as base (as in Scheme 2.17) met with failure. Product mixtures were irresolvable however, low-

resolution mass spectra bore a single major signal at ~ 330.13 which is attributable to $[Pd(\mathbf{2.2})_2]^{2+}$ species (calculated m/z, $[Pd(\mathbf{2.2})_2]^{2+}$ = 328.15). Formation of Pd(**2.2**)$_2$ explains the complexity of the ^{1}H-NMR spectrum of the product mixtures as addressed in section 2.3. The propensity for ligand **2.2** to favour Pd(NHC)$_2$ type complexes is explored further in section 2.3.3.1 in relation to the Pd(**2.2**)(allyl)Cl complex (see Scheme 2.21).

It is likely that the bulky diisopropyl-phenyl group of **2.4** is crucial to disfavouring Pd(NHC)$_2$ coordination, enabling the isolation of mono-NHC complexes Pd(**2.4 - H**)(*O,O'*-acac) and Pd(**2.4**)(*O,O'*-acac)(γC-acac). Mono-NHC complexes could not be isolated using ligand **2.2** highlighting the subtleties of synthesising mono-NHC complexes by this method. This is why acetamide-linked NHC ligands are typically used to prepare M(NHC)$_2$ type complexes or for coordinating an NHC to a stable complex with the desired ancillary ligand pre-coordinated.[120] The latter approach was taken with the directed synthesis of Pd(**2.4**)(*O,O'*-acac)(γC-acac) from Pd(*O,O'*-acac)$_2$ (Scheme 2.17). Variable temperature NMR analysis of Pd(**2.4**)(*O,O'*-acac)(γC-acac) showed the formation of Pd(**2.4 - H**)(*O,O'*-acac) at temperatures above 70 ^{o}C (Figure 2.15). Therefore, synthesising Pd(**2.4**)(*O,O'*-acac)(γC-acac) and then converting it to the chelated form through careful heating is a rational approach. Unfortunately, there was insufficient time to attempt this.

2.3.2. Ag(NHC) intermediary complexes

The complexes discussed in sections 2.3.3, 2.3.4 and 2.3.5 are all prepared via transmetalation of the NHC ligand from an Ag(I) centre, as are many of the complexes prepared in Chapters 3 and 5. This approach is ubiquitous in the field of NHC-complex synthesis, however, because the NHC-Ag(I) complexes are often treated as intermediary species, they are rarely isolated or characterised. However, to provide an appreciation of their reactivity and spectral properties, two complexes Ag(**2.2**)Cl and Ag(**2.3**)Cl, were isolated for analysis. This helped to improve later evaluation of reaction progress and product mixtures obtained following the silver-transmetalation route. As such, during

this study, the ^{1}H-NMR spectra of most other NHC-Ag(I) intermediates were recorded and found to be comparable with the characterised species.

It is worth noting here that because of the geometric ambivalence of Ag(I) complexes it is difficult to predict the structure of the NHC-Ag(I) species, particularly in the presence of the potentially coordinating amide wing. Selecting the appropriate counter-anion of the imidazolium salt proligand affords some degree of control. Halides typically favour neutral, mono-NHC complexes of the type Ag(NHC)X, although, numerous halo-bridged and ion-pair complexes have been reported.[100] Non-coordinating anions such as PF_6 generally form cationic, bis-NHC complexes ($[Ag(NHC)_2][PF_6]$). This is best illustrated by Wang and Lin's early demonstration of this NHC-Ag chemistry as shown in Scheme 2.18.[182]

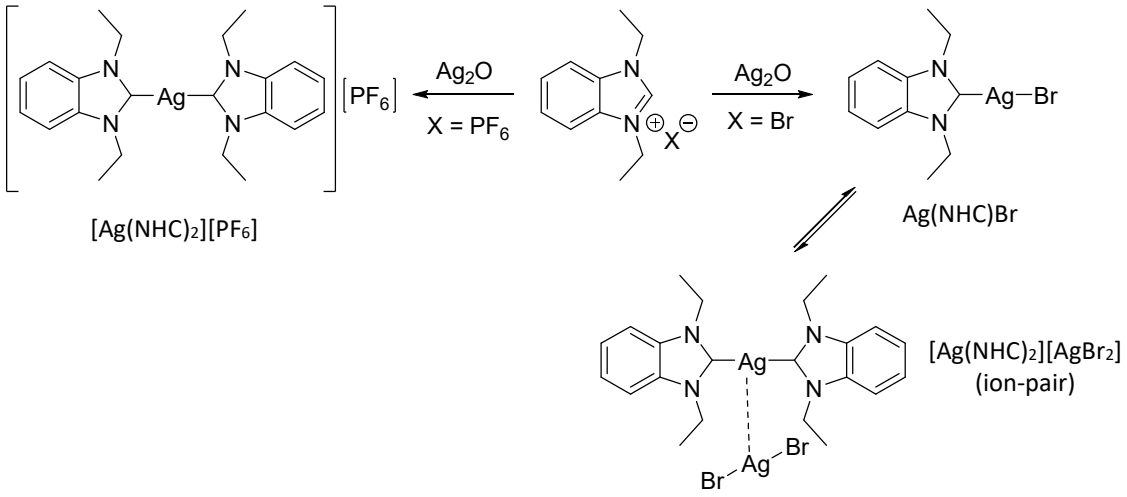

Scheme 2.18: *Coordination behaviour of NHC-Ag complexes with coordinating (Br) and non-coordinating (PF_6) anions.*

The choice of anion is governed by the solubility of the proligand salt (imidazolium halides are typically less organic soluble), solubility of the NHC-Ag(I) intermediate and the nature of the target NHC-M complex. Regardless of the anion, organic solubility was rarely an issue for these bornyl-acetamide compounds because of the bornane component. Solubility problems were more prevalent in the synthesis of metallo-NHC

complexes in Chapter 5. However, it was found that using an imidazolium PF_6 precursor increased the likelihood of forming undesired bis-ligated $M(NHC)_2$ complexes due to the $Ag(NHC)_2$ intermediate (see section 5.3.2.1). Using the chloride salts, as obtained from the proligand synthesis, was therefore preferred. However, without detailed structural characterisation such as an X-ray crystal structure it is difficult to assign the true nature of NHC-Ag(I) complexes prepared from an imidazolium chloride salt. For the sake of this discussion, NHC-Ag(I) complexes are assumed to adopt a linear at metal geometry with a monodentate BA-NHC ligand represented here as Ag(BA)Cl.[100] This assumption has no major experimental basis, it is purely for convenience.

2.3.2.1. Synthesis and Characterisation of Ag(2.2)Cl and Ag(2.3)Cl

Complex Ag(**2.2**)Cl and Ag(**2.3**)Cl were prepared by stirring the corresponding imidazolium chloride proligand in DCM with half a molar equivalent of Ag_2O. Like most Ag(I) complexes, these are light sensitive so reactions are performed in darkness. Reaction progress is seen in the gradual disappearance of the grey Ag_2O into a colourless solution or turbid, white suspension. Reaction time appeared to be dependent on the bulk of the pendant group with synthesis of Ag(**2.4**)Cl taking over 20 hours. For the smaller alkyl-appended species Ag(**2.2**)Cl and Ag(**2.3**)Cl, reactions were complete after 7 hours and 14 hours, respectively. Complex Ag(**2.2**)Cl was isolated after filtering through celite and removing the solvent carefully by rotary-evaporation, avoiding heating and overexposure to light. This provided pure compound as a fluffy white solid in 86% yield. This batch was partitioned and used in separate synthesis of Pd(**2.2**)(allyl)Cl (section 2.3.3.1) and [Ru(**2.2**)(*p*-cymene)Cl][Cl] (section 2.3.5.1). The solid sample was air and moisture stable over a one-week period, however, in solution grey material, probably metallic silver or silver oxide, deposited within two days. Attempts to grow crystals likewise resulted in deposition of a grey powder and this was true for all organic NHC-Ag(I) complexes in this study. Ag(**2.3**)Cl was similarly isolated but only a portion was taken from the reaction mixture for analysis so yields could not be calculated. The remainder of the reaction mixture was used in a synthesis not discussed in this thesis.

Being the simplest NHC complexes prepared in this work, their NMR spectra are suited to comparison with those of the proligands to clearly highlight the changes undergone upon NHC formation. Figure 2.17 shows the ^{1}H-NMR spectra of **2.3.HCl** and Ag(**2.3**)Cl in CD_3CN.

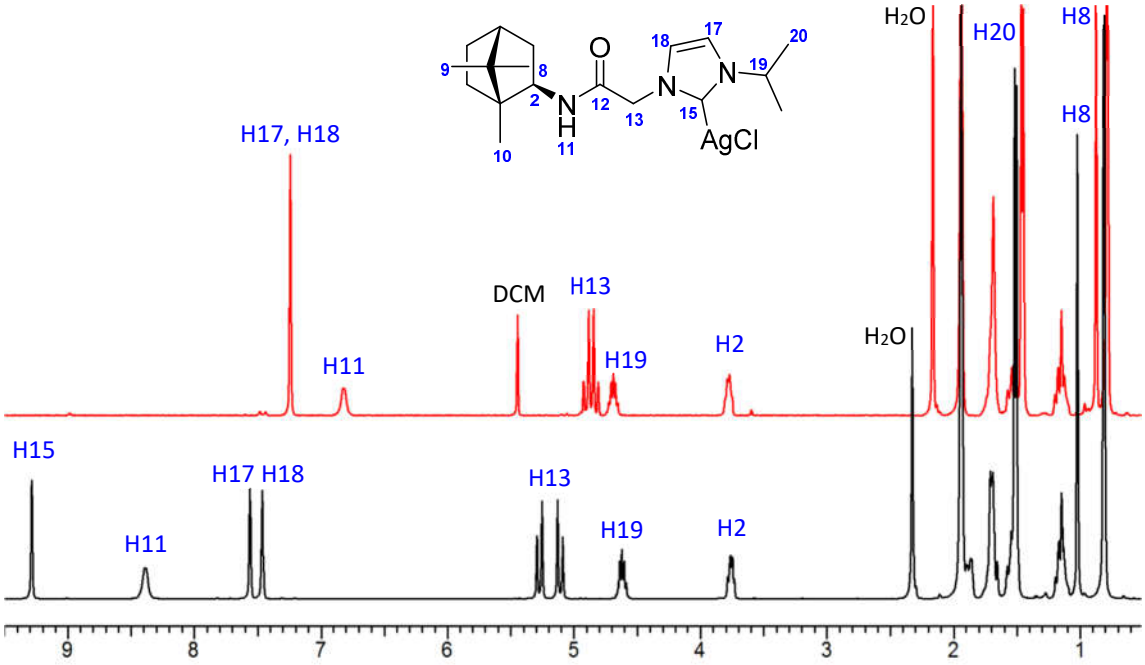

Figure 2.17: *Collated ^{1}H-NMR spectra of Ag(**2.3**)Cl (red) and **2.3.HCl** (black) in CD_3CN with selected signals labelled.*

Here the loss of the NC*H*N (H15) proton signal at 9.28 ppm is conspicuous as is the upfield shift of the amide N*H* (H11) from 8.39 ppm in **2.3.HCl** to 6.83 ppm in Ag(**2.3**)Cl ($\Delta\delta$ = 1.56 ppm). The strongly coupled methylene proton environments (H13) converge slightly and shift modestly upfield ($\Delta\delta \sim 0.30$ ppm). Interestingly, H11 is shifted to a greater extent than H13 despite being more remote to the site of modification. This supports the assertion made in section 2.2.1 that the amide group of imidazolium salt proligands is involved in hydrogen bonding, either between the amide carbonyl and H15 or H11 and the chloride anion (or both). Deprotonation and NHC coordination prevent these interactions, returning the H11 signal to an upfield position (as in **2.1**). Furthermore, the most affected bornane environment is the methyl H8 which juts over the amide. This hints at a change in spatially dependent interactions rather than simple

inductive deshielding considering that H2, which is adjacent to the N*H*, remains unchanged. Irrespective of their origin, it is plain to see the formation of a carbenic species based on these changes.

Each NHC-Ag(I) species was identified by low resolution mass-spectroscopy as a minor signal due to the $[Ag(NHC)_2]^+$ cation at 657.30 for $[Ag(\mathbf{2.2})_2]^+$ and at 715.37 for $[Ag(\mathbf{2.3})_2]^+$ (product of deuterium exchange with NMR solvent) for which the calculated m/z are $[Ag(\mathbf{2.2})_2]^+$ = 657.30 and $[Ag(\mathbf{2.3})_2]^+$ (-2H, +2D) = 715.37. Much larger signals due to the corresponding imidazolium salts ($[\mathbf{2.2}.\mathbf{H}]^+$ or $[\mathbf{2.3}.\mathbf{H}]^+$) were evident in each spectra. This alludes to the acknowledged weakness of the NHC – Ag(I) bond so necessary for transmetalation. Despite NHC – Ag(I) compounds being potentially useful in a variety of applications,[64] in this study they were employed solely as intermediates.

2.3.3. Pd(NHC)(allyl)Cl type complexes

$L_nPd(\eta^3\text{-allyl})$ complexes represent a class of organo-palladium compounds containing a π-bonded, formally anionic allyl(η^3) ligand. An allyl ligand can be variably substituted however, the following synthesis and discussion is concerned solely with the simplest allyl C_3H_5. The canonical forms of the free ligand are reflected in the organometallic bonding of the coordinated species (Figure 2.18). When π-bonded it is considered a bidentate ligand. A fluxional relationship between π and σ coordination modes of allylic ligands is often observed, the nature of which depends on the metal centre, other ligands and the solvent.[183]

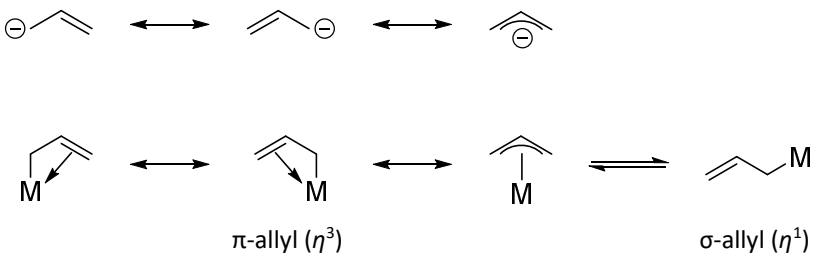

Figure 2.18: *Organometallic bonding of the allyl ligand C_3H_5.*

The selection of an allyl ancillary ligand was decided based upon their synthetic practicality and air and moisture stability. Several Pd(NHC)(allyl)Cl type complexes have been applied as catalysts in Suzuki-Miyaura and Buchwald-Hartwig cross-coupling reactions,[37, 184] the telomerisation of amines[185] and in the α-arylation of ketones.[85] In all cases the authors have noted their efficient pre-catalyst activation.

Reported Pd(NHC)(allyl)Cl complexes are synthesised by reacting the dimeric complex $[Pd(allyl)Cl]_2$ with an NHC source; either the free NHC ligand or an NHC-Ag(I) complex. The latter transmetalation route was employed, in this study, for the synthesis of Pd(BA)(allyl)Cl complexes with ligands **2.2** and **2.4.** This approach is generalised in Scheme 2.19.

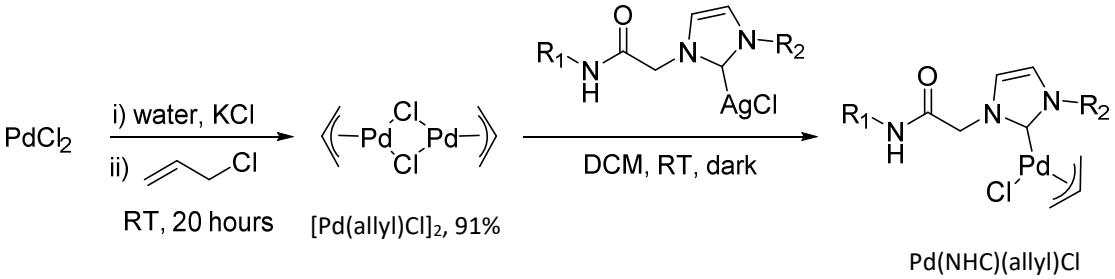

Scheme 2.19: *Conditions for the synthesis of $[Pd(allyl)Cl]_2$ and its reaction to form an Pd(NHC)(allyl)Cl complex by transmetalation of the NHC ligand from an Ag(I) complex.*

The precursor $[Pd(allyl)Cl]_2$ was conveniently prepared by oxidative addition of Pd(0) into the allyl-Cl bond of allylchloride following the method of Nolan *et al.*[37] $PdCl_2$ is stirred with excess allylchloride and KCl in degassed, distilled water under an inert atmosphere at room temperature. After 20 hours the faint yellow suspension is extracted with chloroform which is dried over $MgSO_4$ and the solvent removed providing $[Pd(allyl)Cl]_2$ as a fine yellow powder. This approach relies on the in situ reduction of Pd(II) to Pd(0). Optimal yields of over 90% are achieved by the careful exclusion of oxygen and using freshly distilled allylchloride.

The following sections explore the synthesis and study of Pd(BA)(allyl)Cl complexes prepared from $[Pd(allyl)Cl]_2$ in accordance with Scheme 2.19.

2.3.3.1. Synthesis of Pd(2.2)(allyl)Cl and Pd(2.4)(allyl)Cl

Compounds Pd(**2.2**)(allyl)Cl and Pd(**2.4**)(allyl)Cl were prepared by carbene transfer from their respective NHC-Ag(I) complexes. Complex Pd(**2.2**)(allyl)Cl was prepared from isolated Ag(**2.2**)Cl however, as mentioned in section 2.3.2, it is not always necessary to isolate the NHC-Ag(I) intermediate. For Pd(**2.4**)(allyl)Cl, the Ag(I) precursor was prepared, and reacted onwards in situ. Aside from this exception the two approaches were identical as shown in Scheme 2.20, the quoted yields were calculated from the imidazolium salt. The lower yield for Pd(**2.2**)(allyl)Cl is due to product lost during isolation of Ag(**2.2**)Cl and the requirement for additional purification.

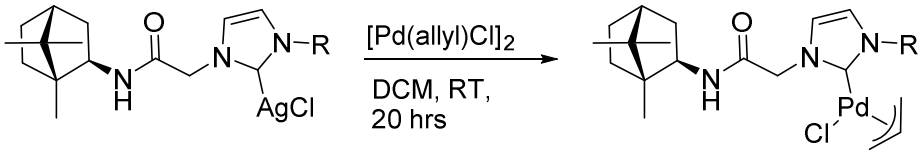

R = Me, Pd(**2.2**)(allyl)Cl, 62%
R = Ar^{iPr}, Pd(**2.4**)(allyl)Cl, 82%

Scheme 2.20: *Synthesis of Pd(**2.2**)(allyl)Cl and Pd(**2.4**)(allyl)Cl by the NHC-Ag(I) transmetalation method.*

The reaction was performed in darkness and under an inert atmosphere by adding a DCM solution of $[Pd(allyl)Cl]_2$ to a stirred DCM solution of the NHC-Ag(I) species. In each case the solution immediately becomes white and cloudy from precipitation of AgCl. After 20 hours transmetalation is complete and products are obtained following the removal of AgCl by filtration of the reaction mixture through celite and evaporation of the solvent. This provided Pd(**2.4**)(allyl)Cl in pure form as a fluffy, faint yellow solid. Like Pd(**2.4**)(*O,O'*-acac)(γC-acac) and Pt(**2.4**)(*O,O'*-acac)(γC-acac), this complex of ligand **2.4** was observed to exist as a mixture of two isomers, contributing to the complexity of its NMR spectra (see section 2.3.3.2).

Purification of methyl-appended version, Pd(**2.2**)(allyl)Cl was impeded by its apparent instability and only a crude yield could be determined. Its ^{1}H-NMR spectrum in chloroform contained numerous broad peaks, although, the ligand **2.2** was clearly present. After several hours the sample had begun to blacken, presumably depositing Pd(0). In DMSO-*d6*, the sample darkened rapidly and two distinct species were observed by ^{1}H-NMR. Pd(**2.2**)(allyl)Cl is assumed to exhibit isomerism also however, in addition to this, its mass-spectrum indicated the presence of two distinct species. The larger signal at 422.1421 corresponds to the desired product with the chloride ligand missing while the smaller signal at 697.3433 is assigned to the cationic complex [Pd(**2.2**)$_2$(allyl)]$^+$ (m/z, [Pd(**2.2**)(allyl)]$^+$ = 422.1424, [Pd(**2.2**)$_2$(allyl)]$^+$ = 697.3421). It is possible to extract the cationic impurity into an aqueous phase by washing an Et_2O solution with water or directly rinsing the solid with water. Addition of KPF_6 solution results in precipitation of a white solid which has a messy ^{1}H-NMR spectrum, albeit clearly indicating the presence of **2.2.** Its mass-spectrum is clean, showing the same two signals for Pd(**2.2**)(allyl)Cl and [Pd(**2.2**)$_2$(allyl)]$^+$, however, the latter signal is now much larger. Analysis of the "purified" Pd(**2.2**)(allyl)Cl shows it to be unchanged. Evidently, ligand **2.2** is moderately labile and an equilibrium exists between Pd(**2.2**)(allyl)Cl and [Pd(**2.2**)$_2$(allyl)]$^+$ which may be exacerbated by nucleophilic solvents (Scheme 2.21). This no doubt contributes to its observed degradation in solution and for this reason complex Pd(**2.2**)(allyl)Cl was not subject to further analysis.

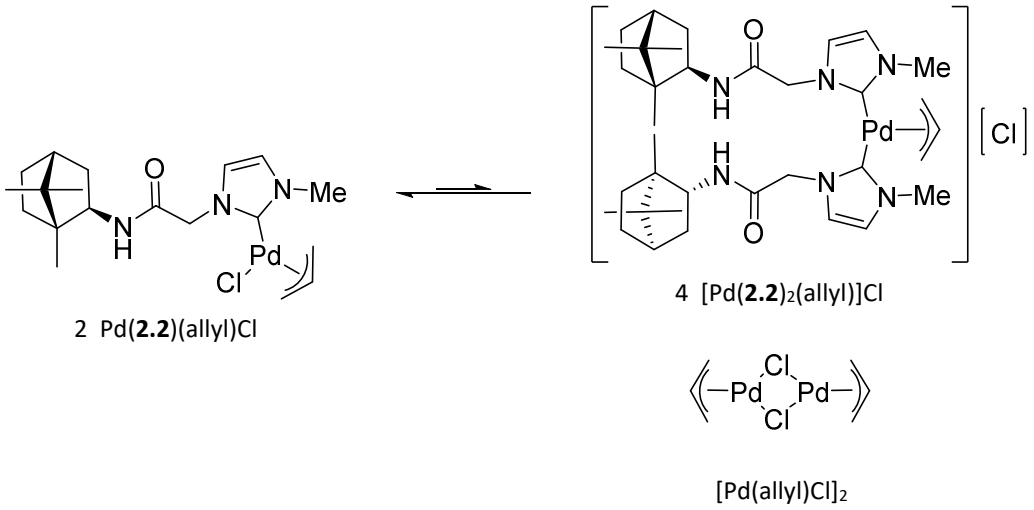

Scheme 2.21: *Possible equilibrium explaining the persistent occurrence of [Pd(**2.2**)$_2$(allyl)]$^+$.*

Transmetalation of carbene ligands between Pd(II)-centres is uncommon but has been explored in a comprehensive study by Canovese *et al.*[186] They demonstrated the exchange of NHC ligands bearing thio-ether or pyridyl groups constituting hemi-labile chelating arms (Scheme 2.22). An associative mechanism of exchange was postulated and suggested to occur via a dimeric intermediate which is reliant on having arm-groups capable of bridging interactions. Only NHC ligands with a methyl substituent underwent ligand interchange. The steric bulk of mesityl- or diisopropyl-phenyl- substituted NHC ligands shielded the Pd(II) centre, preventing associative exchange. There are obvious parallels between these complexes and Pd(**2.2**)(allyl)Cl.

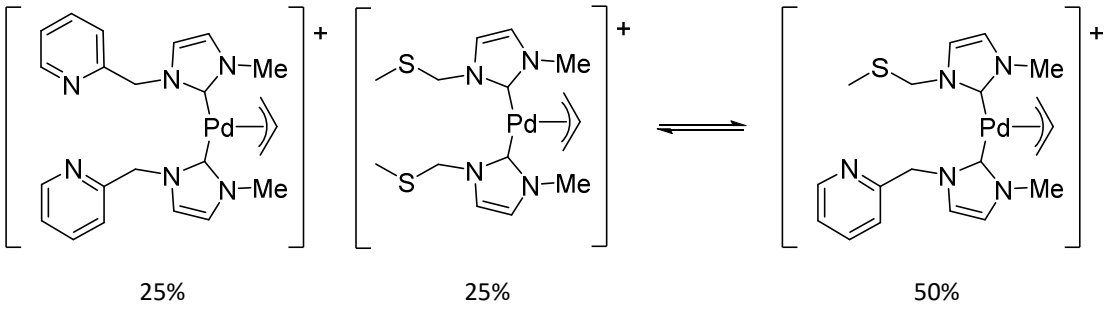

Scheme 2.22: *Pd(II) to Pd(II) transmetalation of NHC ligands with hemi-labile coordinating wing-tips.*

2.3.3.2. Characterisation of Pd(2.4)(allyl)Cl

Complex Pd(**2.4**)(allyl)Cl is sufficiently stable to be isolated in a pure form and demonstrably catalyses the synthesis of hindered biaryls by Suzuki-Miyaura coupling (Chapter 6). Employment of well-defined precatalysts is desired to better predict the structure of the active species making Pd(**2.4**)(allyl)Cl particularly interesting. Full structural assignment was achieved using NMR, IR and mass-spectroscopy. Suitable crystals for X-ray diffraction could not be obtained although the analogous cyclohexyl-derivative Pd(**3.3**)(allyl)Cl was studied by crystallography (section 3.3.2.2).

The complex Pd(**2.4**)(allyl)Cl produced a solitary signal in its mass-spectrum at 568.2533, attributable to the species $[M - Cl]^+$ (calculated m/z, $[Pd(\mathbf{2.4})(allyl)]^+$ = 568.2519). NMR analysis in solvents including $CDCl_3$, CD_3CN and benzene-*d6* show Pd(**2.4**)(allyl)Cl to exist as two interconverting diastereomers, however, only a single species is apparent in the spectrum recorded using DMSO-*d6* alluding to some curious solvent dependent behaviour (Figure 2.19). For the previously discussed complexes Pd(**2.4**)(*O,O'*-acac)(γC-acac) and Pt(**2.4**)(*O,O'*-acac)(γC-acac), the occurrence of isomers was attributed to *Z/E*-amide geometries of ligand **2.4** (2.3.1.4). In Pd(**2.4**)(allyl)Cl the well-studied conformational dynamism of the allyl ligand introduces further modes of isomerism. As will become apparent, it is difficult to assign the exact nature of allyl-isomerism without a lengthy spectroscopic analysis[187-190] hence only preliminary insight is provided herein. For convenience, the structural assignment of Pd(**2.4**)(allyl)Cl will be discussed in relation to the NMR spectra in DMSO-*d6* before evaluating the compound's dynamic behaviour.

The ^{1}H-NMR and ^{13}C-NMR spectra of Pd(**2.4**)(allyl)Cl in DMSO-*d6* clearly present a single species (Figure 2.19a). Ligation by **2.4** is readily confirmed by the presence of signals pertaining to the bornane group in the alkyl-region of each spectrum along with aromatic signals assignable to the diisopropyl-phenyl and imidazolyl moieties. Methylene proton environments (H13) are diastereotopic, presenting as two doublets at 5.16 ppm and ~ 4.97 ppm (overlapping with H26) with a large germinal coupling of 15.7 Hz. NHC coordination is identified by the absence of an NC*H*N proton resonance

and the emergence of a downfield ^{13}C resonance at 182.22 ppm corresponding to the carbene environment (C15).

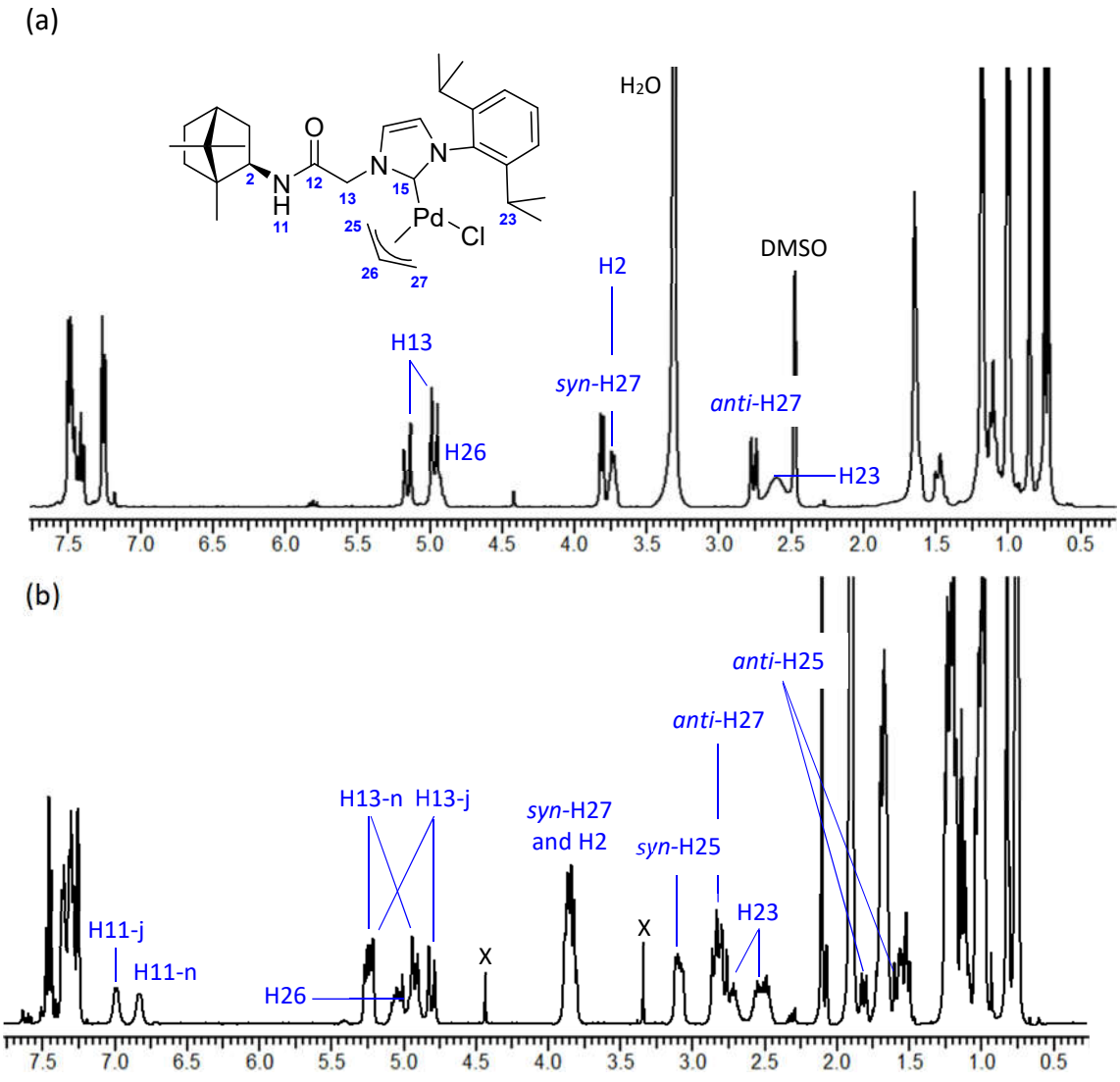

Figure 2.19 (a): *The ^{1}H-NMR spectrum of Pd(**2.4**)(allyl)Cl in DMSO-*d6 *and,* ***(b)*** *in CD_3CN. Selected signals labelled and, where relevant, major and minor isomers denoted by the suffix j and n respectively.*

This assignment was confirmed on the basis of HMBC correlations between this signal and the H13, H17, H18 and H27 proton environments. The signal due to the amide N*H* environment (H11) is concealed under the multiplet at 7.60 ppm – 7.38 ppm but is identifiable by integration over this range and further confirmed to be at around 7.48 ppm by its HMBC correlation to the carbonyl carbon (C12) and bornane Cα (C2) signals

at 167.09 ppm and 56.77 ppm, respectively. The relative peak position of the amide N*H* environment typically varies with solvent hence is observed as a broad singlet or doublet in spectra using $CDCl_3$, CD_3CN and benzene-*d6*. This alludes to "pendant" coordination as verified by IR spectroscopy in which the observed carbonyl-stretching frequency of 1672 cm^{-1} is comparable to the proligand **2.4.HCl** (ν (C=O) = 1687 cm^{-1}).

Proton environments of the allyl auxiliary are observed as a multiplet at ~ 4.95 ppm (H26) and two doublets at 3.81 ppm (*syn*-H27) and 2.76 ppm (*anti*-H27). *Syn* and *anti*-environments relative to the central hydrogen (H26) are distinguished by their coupling constants which fall within the range expected for vicinal coupling of the type $^3J_{cis/rans}$ (*syn*-H27, $^3J_{cis}$ = 7.4 Hz and *anti*-H27, $^3J_{trans}$ = 13.3 Hz).[191, 192] Carbon signals for the allyl ligand are found at 144.79 ppm (C26), 71.22 ppm (C27) and 49.22 ppm (C25). The position of C27 being *trans* to the NHC is reflected in the upfield location of its signal relative to that of C25.[193] Interestingly, the *syn/anti*-CH_2 allyl resonances correlate to C27 and not C25 in the HSCQ-map. The C25 environment is only assignable by three-bond correlation in the HMBC spectrum (Figure 2.20) suggesting that the *syn/anti*-H25 environments are not observable by ^{1}H-NMR in DMSO-*d6.*

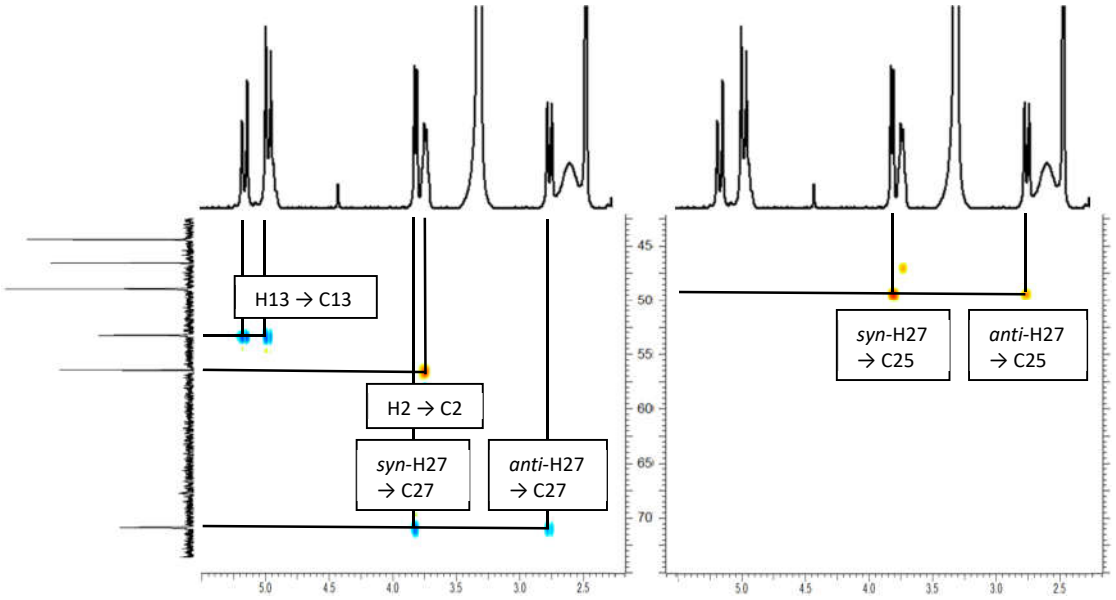

Figure 2.20: *HSQC (left) and HMBC (right) spectra of Pd(**2.4**)(allyl)Cl in DMSO*-d6*. Highlighted correlations show the detection of C25 through a 3-bond correlation with* syn/anti-*H27 while no* syn/anti-*H25 environments are observed.*

They are however, visible in the other solvents used (see Figure 2.19b for CD_3CN).

It is tempting to attribute the *Z/E*-amide geometric isomerism proposed for Pd(**2.4**)(*O,O'*-acac)(γC-acac) and Pt(**2.4**)(*O,O'*-acac)(γC-acac) to the isomerism of Pd(**2.4**)(allyl)Cl. NMR evidence suggests, however, that allyl fluxionality is the sole contributor. This evidence includes; (a) a near 1:1 isomeric ratio, (b) minor chemical shift differences between the two isomers which are only observed for environments associated with the coordinated groups, not the bornyl group and (c) a single species observed by NMR in DMSO-*d6.* These points will be addressed systematically.

Without a strong driving force, such as well-defined intramolecular hydrogen-bonding, a near 1:1 *Z/E* ratio for a secondary acetamide derivative is unheard of.[145, 177] In the ^{1}H-NMR spectrum of Pd(**2.4**)(allyl)Cl using $CDCl_3$, CD_3CN and benzene-*d6*, respective minor isomer populations of 41%, 47% and 43% are observed. In the Pd(**2.4**)(*O,O'*-acac)(γC-acac) complex, it is postulated that electrostatic interactions provide the impetus to overcome the steric strain present in the *E*-amide geometric diastereomer. It is difficult to envisage the compact Pd(allyl)Cl environment supporting the same interactions, especially not to a greater degree.

Inspecting the ^{1}H-NMR spectrum of Pd(**2.4**)(allyl)Cl in CD_3CN (Figure 2.19b) we find five non-isomeric allyl-proton environments corresponding to *syn/anti*-H25, H26 and *syn/anti*-H27 (*syn/anti*-H25 was not observed in DMSO-*d6*). These signals differentiate the two species along with those of the amide N*H* environment (H11), methylene CH_2 (H13) and the methine environments of the diisopropyl-phenyl group (H23). This holds true for the spectra in $CDCl_3$ and benzene-*d6*. Notably, the N – C*H*α (H2) environment is the same for both isomers (~ 3.89 ppm overlapped with *anti*-H27 signal) when *Z/E*-amide isomers have very different N – C*H*α environments (Section 2.3.1.4). Raising the temperature at which the spectra were recorded resulted in reversible coalescence of signals at 55 ^{o}C. This variable temperature NMR analysis was performed using CD_3CN as the solvent and recording spectra at 10 ^{o}C intervals (Figure 2.21).

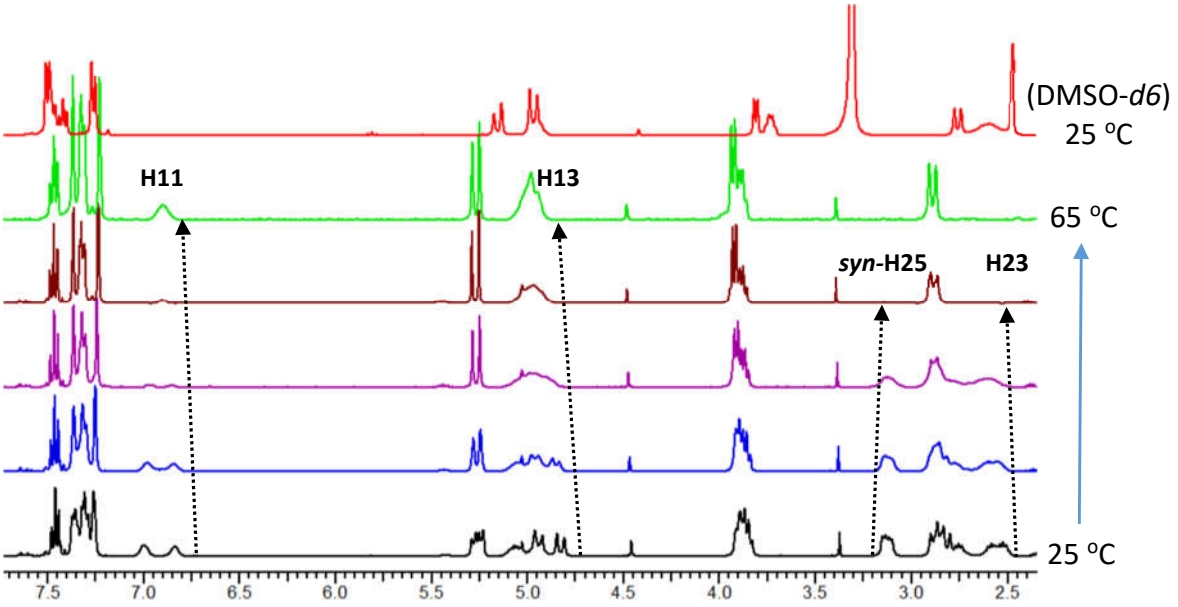

Figure 2.21: *Series showing a portion of the ^{1}H-NMR spectra of Pd(**2.4**)(allyl)Cl as a function of temperature in CD_3CN. Top spectrum in DMSO-*d6 *at 25 °C highlighting its similarity with the spectrum in CD_3CN at 65 °C.*

The low coalescence temperature compared with the 110 °C required for Pd(**2.4**)(*O,O'*-acac)(γC-acac) in DMSO-*d6* implies a much lower energy barrier to free rotation. The amide N*H* and methylene environments coalesce cleanly, however, the methine proton signals appear to dissipate. Interestingly, signals due to the allyl-CH_2 environments pseudo-*trans* to the carbene (*syn/anti*-H27) become strong and well resolved at elevated temperature whereas the pseudo-*cis* allyl-CH_2 (*syn/anti*-H25) merge with the baseline. Scheme 2.23 shows how allyl group pseudo-rotation, referred to here as *syn-anti* interchange, produces chemically distinct forms of Pd(**2.4**)(allyl)Cl.

A diastereomer of isomer 2 can also be produced from isomer 1 by rotation around the Pd – NHC bond (not shown). This may also be a relevant mode of interchange, although, would not be expected to exhibit such dramatic solvent dependence. In the structure depicted, it is clear how accelerating *syn-anti* interchange could cause the abutting methine and *cis*-allyl proton environments (H23 and *syn/anti*-H25) to become convoluted while the pseudo-*trans* allyl-CH_2 proton environments (*syn/anti*-H27) remain largely unchanged.

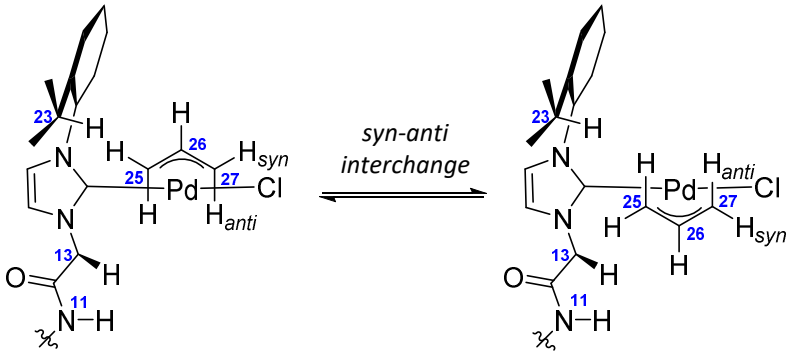

Scheme 2.23: *Depicting isomeric forms of Pd(**2.4**)(allyl)Cl generated by syn-anti interchange of the allyl auxiliary.*

The dynamic nature of Pd(allyl) complexes is an ongoing subject of investigation however, it is generally accepted that an $\eta^3 - \eta^1 - \eta^3$ (alternatively π – σ – π) interconversion is responsible for much of their fluxional behaviour.[188, 189, 193] This mechanism can be applied to allyl *syn-anti* interchange by reorientation of the σ-bonded species (Scheme 2.24).

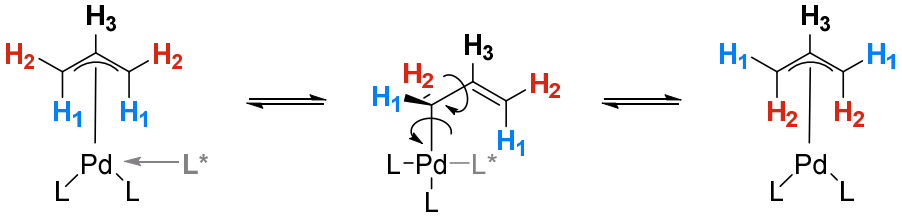

Scheme 2.24: *Mechanism of* syn-anti *interchange. The highlighted ligand (L*) may be an additive or nucleophilic solvent molecule. It is not required for interchange occur but can greatly accelerate the process.*

This behaviour is known to be highly solvent dependent and is accelerated by lewis-acidic solvents, particularly DMSO.[183, 191] This almost certainly accounts for the seemingly anomalous ^{1}H-NMR spectrum recorded in DMSO-*d6*, which at 25 °C shares

similar features with one recorded in CD_3CN at elevated temperature (Figure 2.21). These features include suppression of the methine and *cis*-allyl proton environments (*syn/anti*-H25) which is an understandable consequence of accelerated *syn-anti* interchange.

Often, conformational changes in an allyl auxiliary are analysed through the chemical shift differences between diagnostic proton environments on a "reporter ligand" also bound to Pd(II).[187, 190, 194] In this sense, observance of *syn-anti* interchange through differences in the ligand **2.4** of Pd(**2.4**)(allyl)Cl is reasonable. Of course, further solution studies are necessary to unequivocally prove this hypothesis, although, based on the evidence, it appears much more likely than *E/Z*-amide isomerisation or some other conformational change. Through-space NMR correlation experiments such as NOESY spectra could be used to assign each isomer (*i.e.* isomer 1 and 2 Scheme 2.23) and the precise mode of isomerisation.[195] It may however, be more informative to synthesise an analogue of the compound with a substituted allyl-auxiliary such as 2-methylallyl to emphasise isomeric differences. This remains an interesting challenge for future researchers.

2.3.4. Pd(NHC)Cl_2 type complexes

Chelation as a bidentate NHC-amidate ligand such as is observed for the M(**2.4 - H**)(*O,O'*-acac) complexes (section 2.3.1) is difficult to achieve due to the steric bulk of the bornane-group. On the other hand, monodentate coordination by the NHC is very accessible. However, this "pendant" motif is susceptible to isomeric ambiguities making them less well defined pre-catalysts than their chelated counterparts. Furthermore they are potentially less stable as observed for Pd(**2.2**)(allyl)Cl (section 2.3.3.1). Bulky pendant substituents such as diisopropyl-phenyl (ligand **2.4**) generally improve complex stability and catalytic activity.[65] However, to reduce conformational strain, they promote pendant like coordination by forcing the NHC into an orthogonal orientation to the Pd(II) or Pt(II) ligand plane.

A ligand such as **2.5** (Scheme 2.25) provides a partial remedy to these problems by having a coordinating pendant group in addition to the acetamide moiety. In this case, chelation by the pyridyl substituent stabilises the complex whilst bringing the imidazolyl ring coplanar with the coordination plane. Preventing rotation around the NHC – M bond also reduces the conformations available to the bornyl-acetamide wing-group hence it is anticipated to have more predictable structural attributes. Formation of the NHC – pyridyl chelate would hopefully also have a pre-organising effect, poising the amide-nitrogen to coordinate in a tridentate 5,6-chelate arrangement.

2.3.4.1. Synthesis and Characterisation of Pd(2.5)Cl_2

The pro-ligand **2.5.HCl** was prepared in order to investigate these possibilities and applied to the synthesis of Pd(**2.5**)Cl_2 via the NHC-Ag transmetalation method (see section 2.3.2). No attempt was made to characterise the Ag(**2.5**) intermediate. The reaction was performed by stirring the proligand **2.5.HCl** and Ag_2O in DCM in the absence of light for 12 hours followed by the addition of $Pd(PhCN)_2Cl_2$ as a DCM solution. Immediate precipitation of white AgCl indicated successful transmetalation. After 12 hours the reaction mixture was filtered through celite yielding a faint orange/brown solution which was evaporated to dryness to give an off white solid.

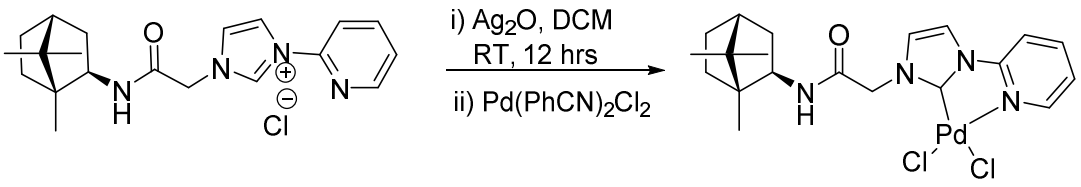

Pd(**2.5**)Cl_2 75%

Scheme 2.25: *Synthesis of Pd(**2.5**)Cl_2 by the NHC-Ag transmetalation method.*

It was noted following the compounds initial synthesis that its solubility in various solvents decreased with subsequent purification steps. For example, despite being

isolated from a DCM solution, it could not be dissolved again in DCM. After several recrystallisation attempts is was only sparingly soluble in warm MeCN or $MeNO_2$ and insoluble in acetone. A crystal structure of Pd(**2.5**)Cl_2 (discussed shortly) was obtained using crystals grown by slow evaporation of a MeCN/toluene solution of the compound. Analysis of these same crystals by NMR in DMSO-*d6* revealed that the observed species was unchanged from that initially isolated. Ultimately, purification by bulk crystallisation of the crude product material by slow evaporation of its MeCN/toluene solution was effective. The resulting white microcrystalline solid was washed with acetone and dried in vacuo to give pure Pd(**2.5**)Cl_2 in a 75% yield.

Mass-spectrometry revealed a myriad of signals due to cations with a mass within the range of m/z $\sim$440 to $\sim$570 and was difficult to assign definitively. A moderately intense signal at 443.1050 could be attributed to the tridentate chelated species (calculated m/z, [Pd(**2.5 - H**)]$^+$ = 443.1063) but the majority of more intense signals appeared to be variously ligated cations of the type [Pd(**2.5**)$(L)_n$]$^+$ and [Pd(**2.5**)(L)Cl]$^+$, where L is MeOH (sample solvent) or water and their deprotonated adducts along with many unassigned signals. Samples prepared from the NMR sample solution contained a major signal at 563.1346 due to a DMSO-*d6* ligated species (calculated m/z, [Pd(**2.5**)(DMSO-*d6*)Cl]$^+$ = 563.1346). This is not present when the solution is prepared from straight MeOH. Fragmentation to this degree is not observed for any of the other NHC – Pd(II) complexes prepared during this work and suggests that substitution of the chloride ligands can occur readily, a feature especially highlighted by the species [Pd(**2.5**)(DMSO-*d6*)Cl]$^+$. This behaviour is likely to be a consequence of the trans-influence of the NHC ligand that has been highlighted in previous discussions. In all previous complexes, the trans-position is occupied by a bidentate ligand, negating any kinetic trans-effect on ligand exchange. Similar behaviour due to this is observed in the mass-spectrum of $[Ru(phen)_2$(Pd{**5.10 - H**}Cl)$][PF_6]_2$ (see section 5.3.2). Despite the mass-spectral evidence, there is no definitive sign of ligand exchange species by NMR.

X-Ray analysis of the crystals obtained as described above was performed using synchrotron radiation of frequency 0.71073 nm (Mo/Kα) due to the small size of the crystals. This revealed the structure of Pd(**2.5**)Cl_2 shown in Figure 2.22 which crystallised

in the non-centrosymmetric orthorhombic space-group $P2_12_12_1$ with two molecules of Pd(**2.5**)Cl_2 (designated A and B) and two toluene solvate molecules in the asymmetric unit.

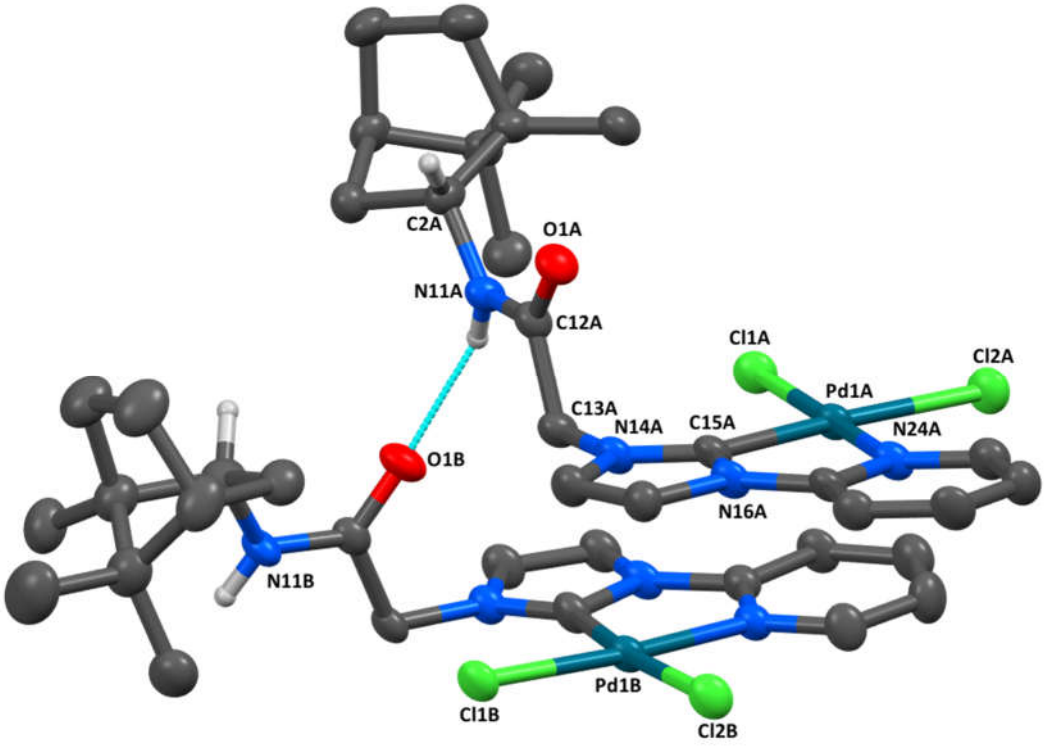

Figure 2.22: *Contents of the asymmetric unit of Pd(**2.5**)Cl_2. All non-bonding hydrogen atoms have been omitted for clarity. Thermal ellipsoids are drawn at a 50% probability level.*

Flack (x) and Hooft (y) parameters of 0.007(6) and 0.004(7) respectively verify that the structure is a resolved chiral species. The Pd(II) centre is bound within the anticipated 5-membered NHC – Py chelate with two chloride ligands completing the neutral complex. A contracted chelate angle C15 – Pd1 – N24 (A / B) of 79.9(2)° / 79.8(2)° causes a distorted square-planar geometry. The remaining bond angles around the Pd(II) centre are (A / B); C15 – Pd1 – Cl1 = 95.9(2)° / 96.2(2)°, N24 – Pd1 – Cl2 = 93.5(2)° / 93.4 (2)° and Cl1 – Pd1 – Cl2 = 90.6(1)° / 90.5(1)°. Metal to ligand bond lengths are as follows (A / B); Pd1 – C15 = 1.972(6) Å / 1.972(6) Å, Pd1 – N24 = 2.052(5) Å / 2.028(5) Å, Pd1 – Cl1 = 2.285(2) Å / 2.292(2) Å and Pd1 – Cl2 = 2.360(2) Å / 2.362(2) Å. Elongation of the Pd1

– Cl2 bond occurs in response to the trans-influence of the NHC ligand. Pd – $C_{carbene}$ and Pd – $N_{pyridyl}$ bond lengths are in agreement with related complexes reported in the literature.[86, 196, 197]

The methylene linkage is oriented such that the CH_2 – C_{amide} bond is perpendicular to the mean-plane of the complex as expressed by the torsion angle C15-N14-C13-C12 (A / B) of 87.8(6)° / 81.2(6)°. The bornane moiety is rotated to bring the C*H*α (C2) into an *anti*-configuration relative to the amide N*H*. Complexes assemble such that the planar organometallic components are stacked with bridging occurring via *Z*-amide supported N*H* ··· O hydrogen bonds (N11A ··· O1B = 2.821(7) Å, N11B ··· O1A = 2.901(2) Å) (Figure 2.22). A stacked packing motif has been noted for related Pd(NHC – Py) complexes as being driven by π – π interactions.[86, 197] Here, formation of a hydrogen-bonded array necessitates staggering of the planar groups causing weak n – π interactions between the chloride ligands and the aromatic pyridyl (Py) or imidazolyl (Im) rings to predominate. These have Cl to centroid distances of; Cl1A ··· PyB = 3.514(3) Å, Cl1B ··· PyA = 3.455(3) Å, Cl2A ··· ImB = 3.498(3) Å and Cl2B ··· ImA = 3.486(3) Å. Weak, non-conventional hydrogen bonds of the type C*H* ··· Cl occurs between the chloride ligand (Cl2) *trans* to the carbene and the imidazolyl-moiety of the adjacent complex (Figure 2.23) (C17A ··· Cl2A = 3.546(6) Å and C17B ··· Cl2B = 3.515(6) Å).

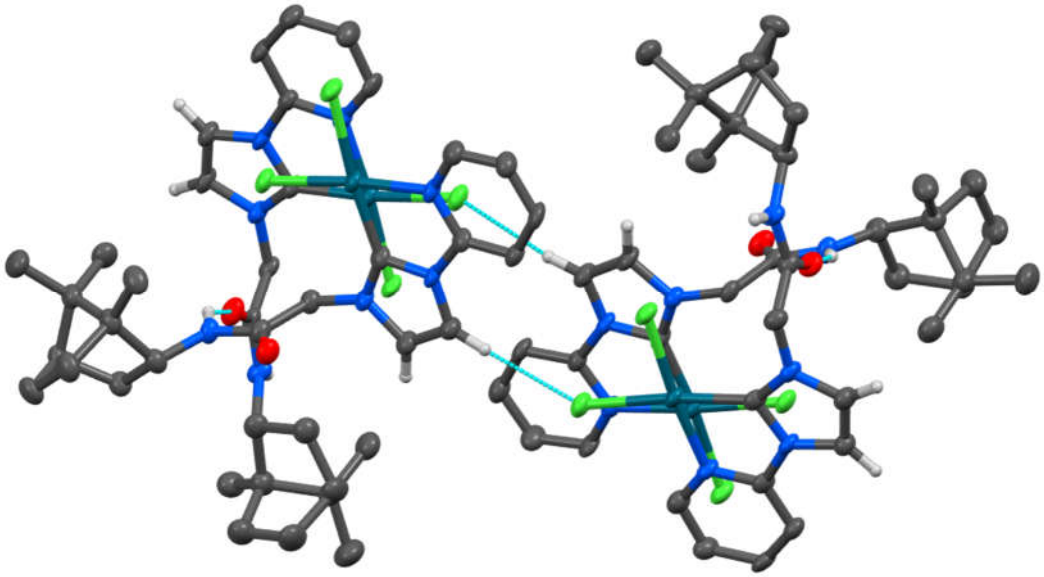

Figure 2.23: *Illustrating some packing features of the extended structure of Pd(**2.5**)Cl_2.*

NMR analysis of the same batch of crystalline material used to obtain the crystal structure of Pd(**2.5**)Cl_2 showed it to be unchanged from the compound initially isolated. The spectra were collected on the sample in DMSO-*d6* as it is only sparingly soluble in the other common deuterated solvents. No isomerism was seen to occur, although, a trace of impurity persisted, seen only in the ^{1}H-NMR spectrum. Impurity signals are particularly visible in the region below ~ 0.75 ppm which are probably related to bornane methyl groups. This may be due to the species [Pd(**2.5**)(DMSO-*d6*)Cl]$^{+}$ observed by mass-spectroscopy but unfortunately, this could not be corroborated by ^{13}C-NMR. The ^{1}H-NMR and ^{13}C-NMR spectra are shown in Figure 2.24 with some key signals noted.

These spectra have no major features that have not been addressed in the previous discussions of Pd(**2.4**)(*O,O'*-acac), Pd(**2.4**)(*O,O'*-acac)(γC-acac) and Pd(**2.4**)(allyl)Cl other than environments related to the pyridyl-group. Conversion of the imidazolium salt **2.5.HCl** into Pd(**2.5**)Cl_2 coincides with a moderate downfield shift of the α-positioned pyrdidine proton (H23) from 8.65 ppm to 9.21 ppm (Δδ = + 0.56 ppm). A minor coordination induced shift of + 0.19 ppm is observed for H21 and changes in H20 and H22 are negligible. Here, NHC – Py chelation augments the downfield shift of the H23

resonance by forcing it into the deshielding environment of the nearby chloride ligand. This effect has been noted in a previous report.[86]

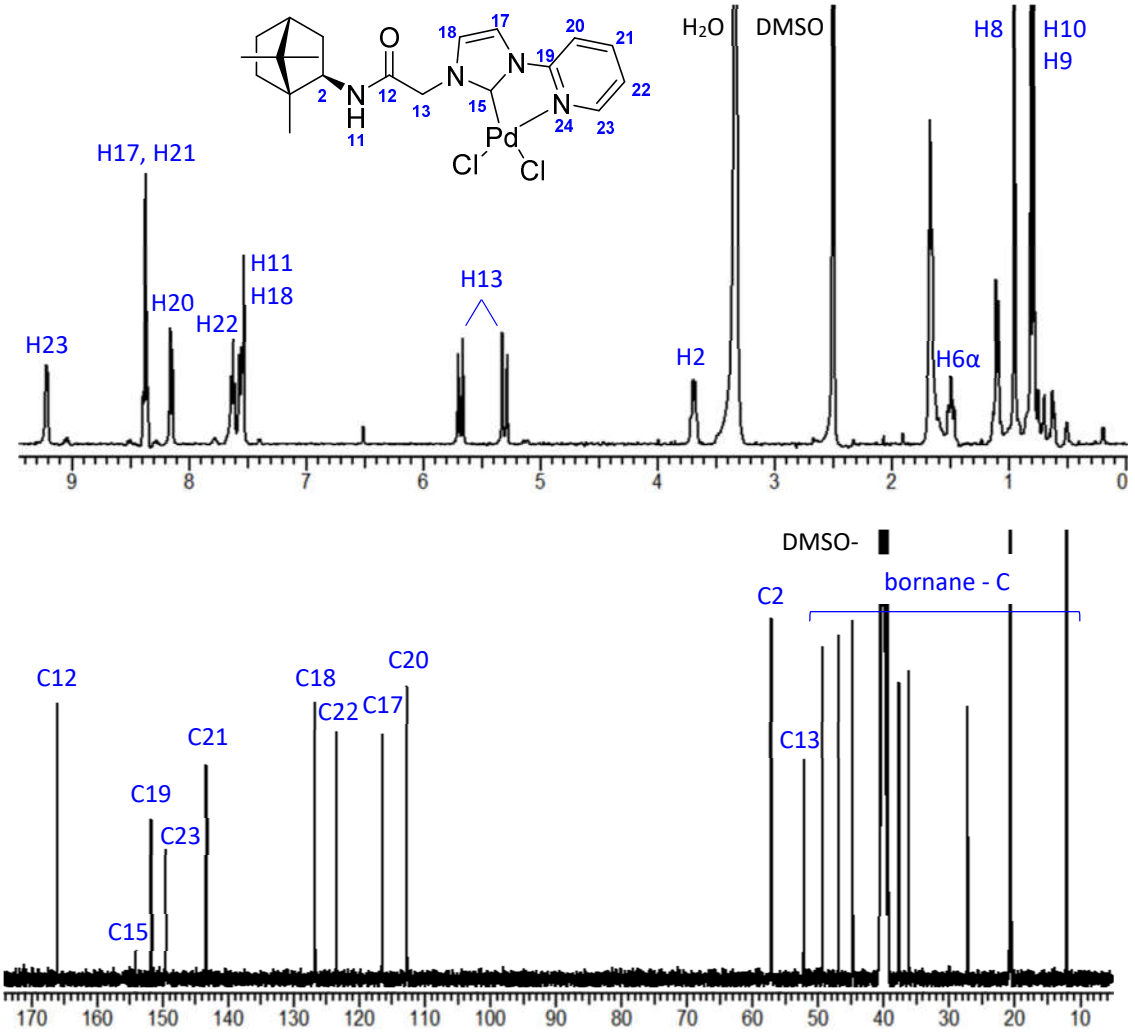

Figure 2.24: *The ^{1}H-NMR and ^{13}C-NMR spectra of Pd(**2.5**)Cl$_2$ in DMSO-*d6 *with selected signals highlighted.*

Resonances due to the methylene-proton (H13) appear similarly affected, although, to a lesser extent. Here the distinctive H13 doublets occur at 5.68 ppm and 5.30 ppm, slightly further downfield than in any of the previously discussed complexes for which the largest equivalent resonance occurs at, or below 5.30 ppm in DMSO-*d6*. Differences also arise in the relative positions of the imidazolyl-proton environments H17 and H18. For complexes of **2.4** these occur between 7.25 ppm – 7.75 ppm with anisotropic shielding of the H17 environment by the orthogonally oriented diisopropyl-phenyl

group, shifting its resonance upfield relative to H18. In Pd(**2.5**)Cl_2, the pyridyl and imidazolyl-rings are coplanar and the resultant anisotropic deshielding of H17 accounts for its chemical shift of 8.37 ppm, downfield of H18 at 7.54 ppm.

In the ^{13}C-NMR spectrum the carbenic carbon signal (C15) is found at 153.85 ppm, having a near identical chemical environment to that of Pd(**2.4**)(*O,O'*-acac) (153.55 ppm). In both complexes the NHC participates in bidentate coordination with a nitrogen donor. However, carbenic resonances are typically difficult to predict on such a basis.

In most cases the pyridyl-group is expected to be the more labile than the NHC,[198] this is indeed crucial for catalysis. Interestingly however, a study by Willans *et al.* reported curious NHC ligand exchange phenomena in their 4-methyl-pyridyl substituted NHC-Py(Me) complex shown in Scheme 2.26.[197] Although the target [Pd(NHC-Py(Me))$_2$Br]Br species was observed by NMR, only the neutral species Pd(NHC-Py)Br_2 was crystallised (crystallisation conditions not specified). Furthermore, the 4-methoxy-pyridyl analogue only produced the mono-NHC species when reacted with 0.5 equivalents of $Pd(OAc)_2$. Only pyridyl-groups with mildly electron donating substituents behaved in this manner implying electronic destabilisation of the trans NHC – Pd bond.

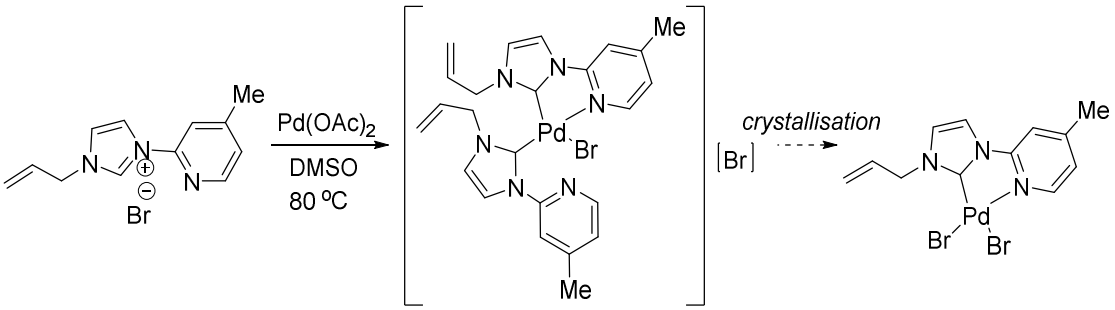

Scheme 2.26: *Observed NHC-Py(Me) dissociation to give an Pd(NHC-Py(Me))Br_2 complex.*

This emphasises that such systems do not necessarily behave predictably. Facile substitution of the halides *trans* to the NHC by MeCN to give cationic complexes of the type $[Pd(NHC)(MeCN)X]^+$ have also been noted in related complexes.[197, 199] Such behaviour may account for the shifting solubility of Pd(**2.5**)Cl_2 and in light of the above discussion, it is not surprising that the neutral complex can be recovered by crystallisation. These complications can be mitigated by using a chelating auxiliary such as an allyl ligand.[195] Complexes of **2.5** with an allyl or acac coligand ligand are interesting synthetic targets with probable catalytic applicability.

2.3.5. Ru(NHC)(arene)Cl type complexes

To demonstrate the compatibility of these ligands with alternative systems the ruthenium-arene complex [Ru(**2.2**)(*p*-cymene)Cl][Cl] was prepared. Ru(II) is a known centre for catalysis and its octahedral geometry provides an alternative architectural scaffold to the square planar Pd(II) and Pt(II) complexes discussed previously. NHC ligands have been employed in a variety of Ru(II) precatalysts,[65, 200, 201] most notably for use in alkene metathesis.[80] In particular, precatalysts with an Ru(NHC)(arene) motif have been shown to catalyse numerous processes including hydrogenation and transfer hydrogenation,[69] cyclopropanation,[202] alkyne dimerization[203] and furan synthesis.[204]

Two reports have shown the coordination of acetamide-linked NHC ligands to an Ru(arene) unit by facile transfer from the NHC – Ag(I) intermediate. In both cases the bidentate NHC-amidate chelate could be produced either by the spontaneous loss of HCl[114] or following treatment of cationic carbonyl-bound species with KOH.[115] These complexes possess a stereogenic centre derived from the pseudo-tetrahedral geometry of the Ru(II)[50] and Sakaguchi and co-workers demonstrated that using one enantiomer of a chirally-functionalised NHC-acetamide ligand produces two diastereomers in an 87 : 13 molar ratio.[115] In the case shown, conversion to the amidate-bound chelate was found to proceed for one diastereomer only generating diastereomerically pure product (Scheme 2.27).

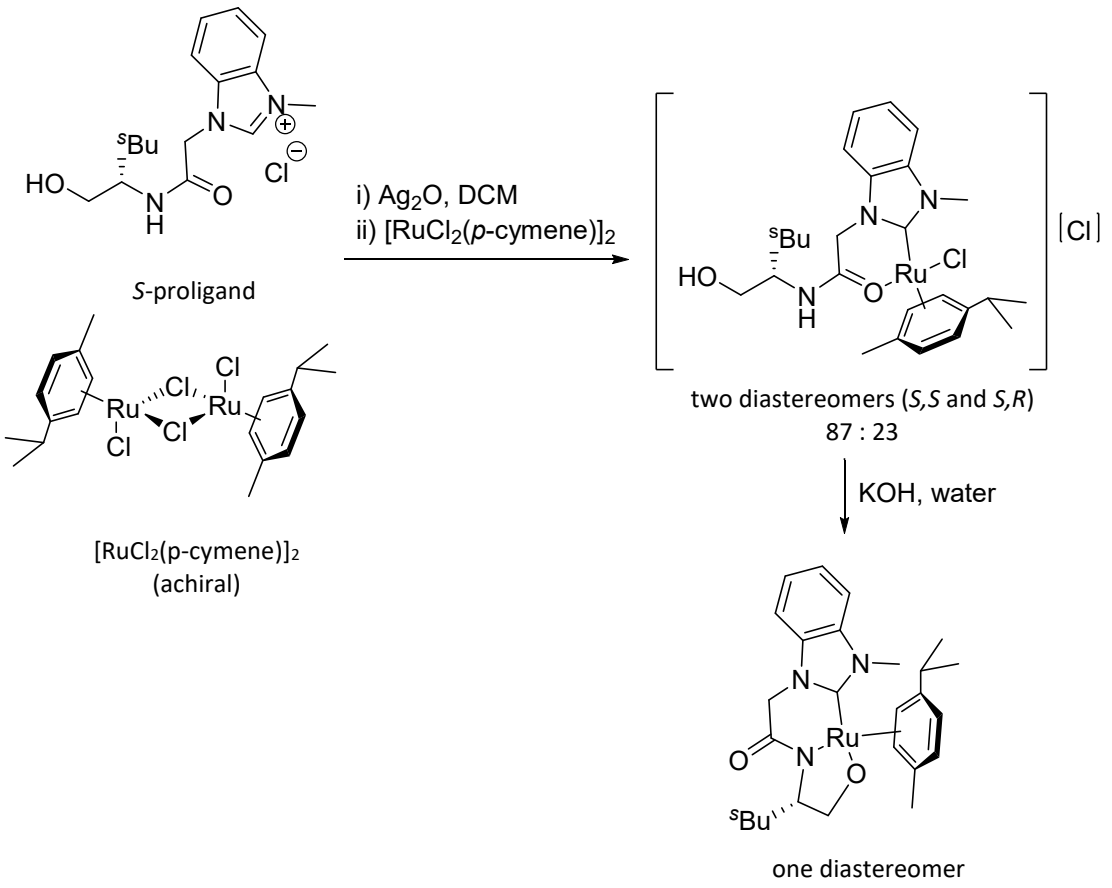

Scheme 2.27: *Sakaguchi's diastereoselective synthesis of Ru(NHC)(arene) complexes using a chirally functionalised NHC-acetamide ligand. No comment on the* SS *or* SR *configuration of the major and minor isomers was made in the report.*

This is because amidate-chelation brings the stereochemical-component of the ligand closer to the chiral coordination sphere of the Ru(II). This observed diastereoselectivity therefore provides a rudimentary assessment the stereodirecting components influence over the metal-centre as in a catalysis scenario. A similar diastereoselective synthesis of an Ru(NHC)(arene) complex has been reported by Gade *et al.* using a chiral NHC – oxazoline ligand.[205]

2.3.5.1. Synthesis and Characterisation of [Ru(2.2)(*p*-cymene)Cl][X]

It was anticipated that utilising a bornyl-acetamide NHC ligand would elicit similar diastereoselectivity. This methodology was applied using proligands **2.2.HCl** and **2.4.HCl**,

however, only the synthesis of [Ru(**2.2**)(*p*-cymene)Cl][Cl] was successful. The failure to synthesise Ru(**2.4**)(*p*-cymene)Cl is attributed to hindrance by the diisopropyl-phenyl group of **2.4** and will not be discussed further.

Complex [Ru(**2.2**)(*p*-cymene)Cl][Cl] was prepared by transmetalation from the isolated complex Ag(**2.2**)Cl (see section 2.3.2) by the previously addressed method (Scheme 2.28). The precursor [Ru(*p*-cymene)Cl_2]$_2$ was synthesised in accordance with a literature procedure and obtained as an orange, microcrystalline solid in a yield of 79%.[206] After removal of the precipitated AgCl by filtration, rotary evaporation of the DCM reaction mixture provided the adequately pure chloride salt as a brown solid (89% yield).

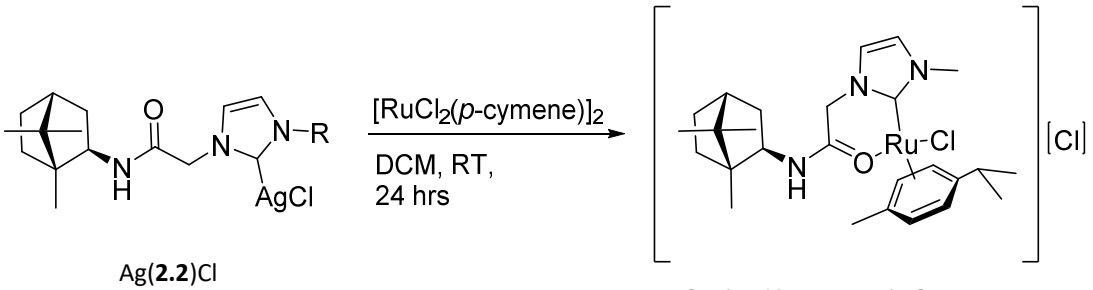

Ag(**2.2**)Cl

[Ru(**2.2**)(p-cymene)Cl]Cl, 89%

Scheme 2.28: *Synthesis of Ru(**2.2**)(*p-*cymene)Cl by the NHC – Ag(I) transmetalation method.*

This could be purified by flash column chromatography (silica, 5% MeOH/DCM) but more expediently so by precipitation as its PF_6 salt from an aqueous solution. The following discussion will focus on this species [Ru(**2.2**)(*p*-cymene)Cl][PF_6], which has been characterised spectroscopically and by X-ray analysis.

Complex [Ru(**2.2**)(*p*-cymene)Cl]$^+$ generates a mass-spectrum with a lone signal at 546.1817 corresponding to the expected cation (calculated m/z, [Ru(**2.2**)(*p*-cymene)Cl]$^+$ = 546.1820). As anticipated, two diastereomers were observed by NMR, however, their occurrence in a 1:1 ratio implies that the ligand does not impart any appreciable selectivity. No attempt to separate these was made. A crystal structure of [Ru(**2.2**)(*p*-

cymene)Cl][PF_6] was obtained with both diastereomers in the asymmetric unit. This will be explored foremost to aid the explanation of their NMR spectra.

Crystallisation of [Ru(**2.2**)(p-cymene)Cl][PF_6] was achieved by slow evaporation of a $CHCl_3$ solution of the compound. It resides in the triclinic space-group *P*1 with four molecules [Ru(**2.2**)(p-cymene)Cl]$^+$, four PF_6 anions and eight molecules of $CHCl_3$ that could be modelled in the asymmetric unit (Figure 2.25). The enantiopure bornane component renders the structure a pure enantiomorph with Flack (x) and Hooft (y) parameters of -0.03(1) and -0.025(4) respectively. Ligand 1.2 is clearly coordinated via the amide-carbonyl oxygen in addition to the NHC and, overall, complex [Ru(**2.2**)(p-cymene)Cl]$^+$ is arranged in the classical three-legged piano stool geometry around the pseudo-tetrahedral Ru(II) centre.

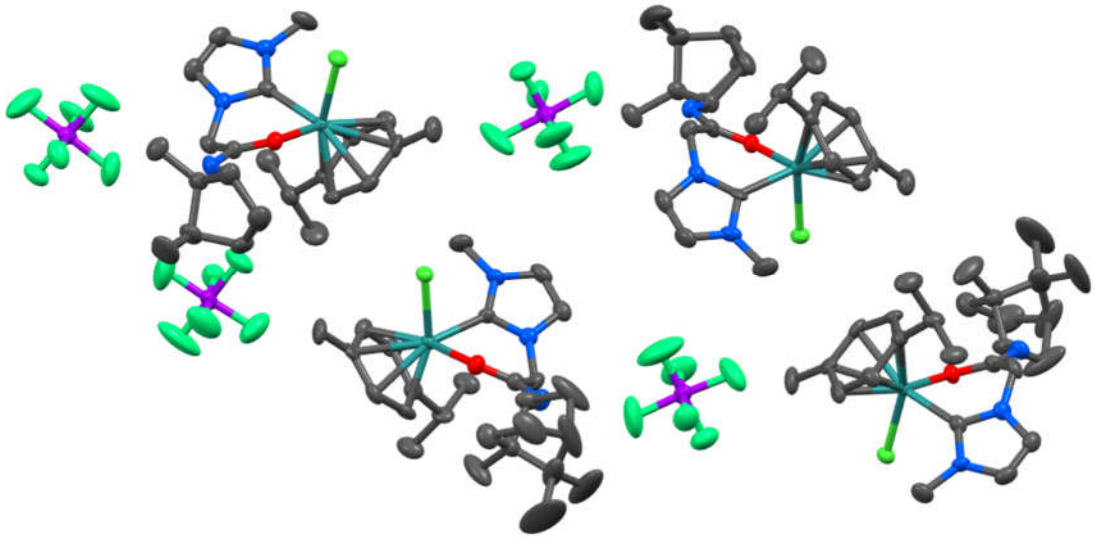

Figure 2.25: *Asymmetric unit of [Ru(**2.2**)(p-cymene)Cl][PF_6], hydrogen atoms and chloroform solvate molecules omitted for clarity. Thermal ellipsoids are drawn at a 50% probability level.*

For the sake of this discussion, the *R* / *S* notation used to define the Ru(II) stereogenic centre is extended to distinguish the two diastereomers (the *R*-diastereomer and the *S*-

diastereomer). As there are two of each diastereomer in the asymmetric unit, these will be defined as *R*-A, *R*-B, *S*-A and *S*-B (Figure 2.26). Bonding to the Ru(II) is characterised by the following bond lengths Ru1 – C15, Ru1 – O1, Ru1 – Cl1 and Ru1 – centroid and angles C15 – Ru1 – O1, C15 – Ru1 – Cl1, O1 – Ru1 – Cl1 which are summarised in Table 2.2 along with bond lengths O1 – C12 and N11 – C12 of the amide (centroid is *p*-cymene centroid, angles related to this are not discussed). Evaluating the key bonding information reveals few differences between the two diastereomers. The Ru1 – C15 bond length is shorter for occupant *R* – (B) by ~ 0.027 Å but there is no obvious reason for this anomaly. The only notable difference between diastereomers is observed for the bonds Ru1 – O1 and O1 – C12 which are slightly elongated in the *S* diastereomer by ~ 0.021 Å. This may be in response to the closer proximity of the bornane-methyl groups to the *p*-cymene ligand in this isomer. Distances for Ru1 – C15, Ru1 – Cl1 and Ru1 – Cent and associated bond angles are in agreement with reported values for piano-stool Ru – NHC complexes of this type.[114, 158, 207]

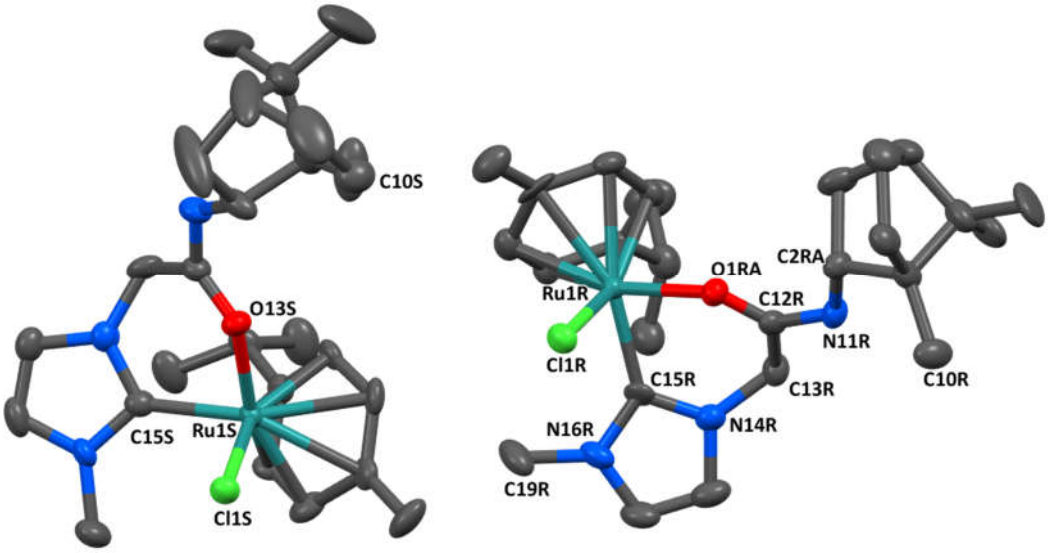

Figure 2.26: *Two diastereomers of [Ru(**2.2**)(*p*-cymene)][PF_6] with label suffix* R *or* S *denoting the stereochemical configuration of the pseudo-tetrahedral ruthenium centre. Hydrogen atoms, anions and solvate molecules have been omitted for clarity*

Weak hydrogen-bonding interactions are prevalent within the asymmetric unit with each PF_6 anion accepting hydrogen-bond donation from the amido-N*H* and supported by a non-conventional interaction with the adjacent methylene-CH_2 (N11 ··· F = 3.04(2) Å, 3.03(2) Å, 3.03(2) Å and 3.04(2) Å and C13 ··· F = 3.25(2) Å, 3.23(2) Å, 3.30(2) Å and 3.31(2) Å). Interactions of the type Cl_3CH ··· Cl occur between each ligated chloride and a chloroform solvate molecule (Cl_3C ··· Cl1 = 3.33(2) Å, 3.33(2) Å, 3.150(3) Å and 3.186(3) Å). There are no perceptible interactions between molecules of [Ru(**2.2**)(*p*-cymene)Cl]$^+$.

Table 2.2: *Summary of relevant X-ray crystallographic measurements for the four molecules of [Ru(**2.2**)(*p*-cymene)]$^+$ occupying the asymmetric unit. Diastereomers are denoted* R *and* S.

		[Ru(**1.2**)(*p*-cymene)Cl]$^+$			
		R - (A)	*R* - (B)	*S* - (A)	*S* - (B)
bond lengths	Ru1 - C15	2.044(9)	2.019(2)	2.045(2)	2.050(9)
	Ru1 - O1	2.126(7)	2.120(7)	2.143(7)	2.144(7)
	Ru1 - Cl1	2.409(2)	2.410(2)	2.412(2)	2.410(2)
	Ru1 - Cent	1.691(4)	1.698(4)	1.701(4)	1.703(4)
	O1 - C12	1.240(2)	1.236(2)	1.256(2)	1.261(2)
	N11 - C12	1.316(2)	1.321(2)	1.328(2)	1.324(2)
bond angles	C15-Ru-O1	83.5(3)	82.9(4)	82.6(3)	82.7(3)
	C15-Ru-Cl1	87.3(3)	87.2(3)	88.1(3)	88.0(3)
	O1- Ru -Cl1	84.0(2)	83.8(2)	84.4(2)	84.4(2)

In the ^{1}H-NMR spectrum of [Ru(**2.2**)(*p*-cymene)Cl][PF_6], the most discernible difference between the two diastereomers is the position of resonances due to the C10 methyl-group. It can be envisaged, based upon the solid state structure, that in the *S*-diastereomer, the C10 methyl-group abuts the *p*-cymene ligand more so than in the *R*-diastereomer hence is subject to greater anisotropic deshielding in the former.

IR-spectroscopy corroborates that the amide-group is involved in chelation with the carbonyl stretching frequency of 1614 cm^{-1} decreased from that of the proligand **2.2.HCl**

(1659 cm^{-1}). This coordination shift has been noted previously for a closely related complex (carbonyl stretch, 1619 cm^{-1})[115] and has been addressed in the discussion of the amidate-chelated complexes Pd(**2.4 - H**)(*O,O'*-acac) and Pt(**2.4 - H**)(*O,O'*-acac) (see section 2.3.1.3). The possibility of amidate coordination in solution is negated by identification of the amide N*H* proton environment (H11) by ^{1}H-NMR spectroscopy. The ^{1}H-NMR and ^{13}C-NMR spectra of [Ru(**2.2**)(*p*-cymene)Cl][PF_6] in $CDCl_3$ are shown in Figure 2.27.

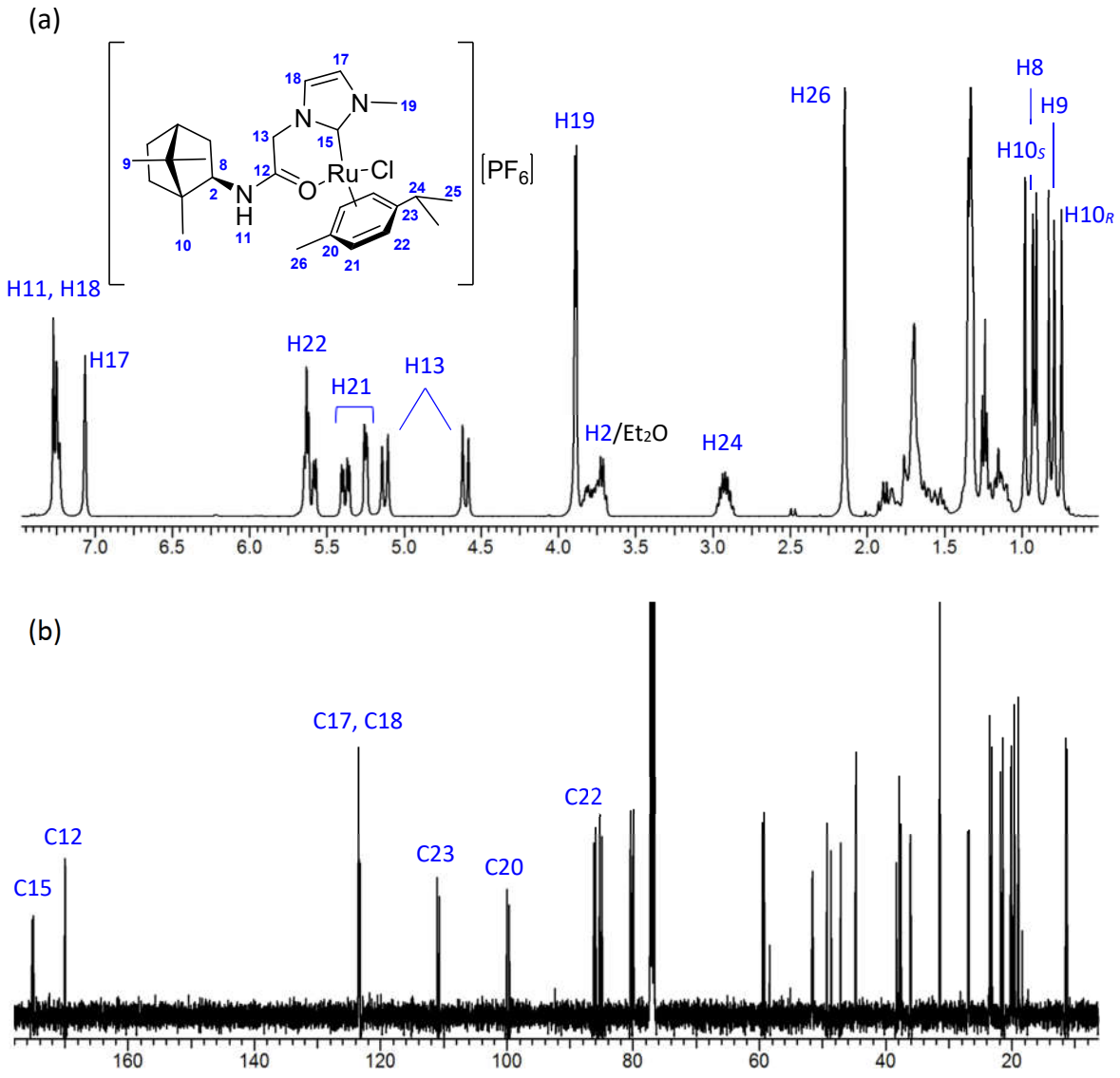

Figure 2.27: *The ^{1}H-NMR and ^{13}C-NMR spectra of Ru(**2.2**)(*p*-cymene)Cl_2 in $CDCl_3$ with selected signals labelled.*

All signals due to ligand **2.2** and *p*-cymene are accounted for. Two diastereomers are discernible and the *R*- or *S*- configurations could be definitively distinguished for the bornane methyl environment H10 and *p*-cymene environments H21 and H22. As noted in the discussion of the crystal structure, the closer proximity of the C10 methyl environment to the field of the arene ligand in the *S*-diastereomer is expected to increase its proton resonances. The downfield position of $H10_S$ (0.98 ppm) relative to $H10_R$ (0.74 ppm) is the realisation of this effect. On the other hand, carbon resonances due to the equivalent nuclei of each diastereomer are very similar; for example, $C10_S$ and $C10_R$ are 11.46 ppm and 11.40 ppm respectively. It is therefore difficult to employ through-bond correlations to H10, such as in the HMBC spectrum, to further assign signals to each diastereomer. Through-space correlation spectra such as NOESY could be used to scrupulously characterise the *R* and *S*-diastereomers although this was not performed here due to time constraints.

The anticipated diastereotopic methylene-CH_2 environments (H13) arise at 5.12 ppm and 4.60 ppm ($^2J_{H\text{-}H}$ = 16.0 Hz). In previous examples, the chemical-shift of these signals has elucidated differences between conformational-isomers, however, in the case of these diastereomers the differences are minor. Both have identical H13 environments and similar C13 resonances ($C13_{(R \text{ or } S)}$ = 51.73 ppm and 51.64 ppm). The carbenic carbon (C15) resonates at 175.24 ppm / 175.00 ppm which is comparable to resonances reported for related NHC – Ru(II) complexes.[158, 205, 208] Coordination of the carbonyl-group to Ru(II) produces a C12 resonance of 170.00 ppm / 169.92 ppm, not unlike those observed for Pd(**2.4 - H**)(*O,O'*-acac) and Pt(**2.4 - H**)(*O,O'*-acac) in $CDCl_3$ (170.29 ppm and 171.56 ppm).

It is surprising that ligand **2.2** affords no stereochemical control over complexation whereas the much less bulky literature example does. It is possible that in the reported case (Scheme 2.27), intermediary association of the hemi-labile hydroxyl moiety guides selectivity by orienting the chiral group during complex formation. It was hoped that conversion of the O-chelated complex [Ru(**2.2**)(*p*-cymene)Cl][Cl] into the neutral amidate-chelated congener Ru(**2.2 - H**)(*p*-cymene)Cl would exhibit some diastereomeric preference. This was attempted, as reported, by addition of two molar equivalents of

KOH(aq) to a stirred, aqueous solution of the salt at room temperature (Scheme 2.29). Unfortunately, the starting material was retained and heating of the solution resulted in decomposition. The bornane group is simply too hindered to allow this transformation.

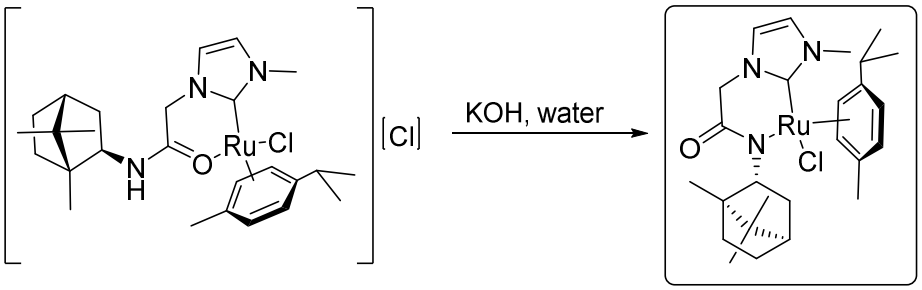

*[Ru(**2.2**)(*p*-cymene)Cl]Cl*

not formed
*Ru(**2.2 - H**)(*p*-cymene)Cl*

Scheme 2.29: *Attempted synthesis of [Ru(**2.2 - H**)(*p*-cymene)Cl]Cl by deprotonation of [Ru(**2.2**)(*p*-cymene)Cl]Cl.*

This is perhaps unsurprising given the steric barrier to coordination of the bornyl-amidate which has been addressed previously in section 2.3.1. It has been established that the application of heat is necessary to achieve this; hence, in the case of Ru(**2.2 - H**)(*p*-cymene)Cl, it may be possible using a different base and/or solvent. However, having already achieved the aim of incorporating ligand **2.2** into an alternative, potentially catalytically active system, this was not pursued.

2.4. Summarising remarks

A series of novel acetamide-linked imidazolium salts derived from *exo*-(-)-isobornylamine have been prepared as precursors to the chiral NHC ligands **2.2** – **2.5**. Investigation of an alternative system based on e*xo*-3-aminoborneol was also undertaken, however, this was hampered by issues during synthesis and difficulty of product isolation. Regardless, a precursor to the very unique, potentially tridentate NHC ligand **2.9** was successfully isolated and characterised.

Bornyl-acetamide NHC proligands were applied to the synthesis of several NHC complexes with Ag(I), Pd(II), Pt(II) and Ru(II). Complex motifs were selected for their potential catalytic activity, particularly in the case of the Pd(II) systems, and to benefit structural elucidation.

Complexes based upon the M(NHC)(*O,O'*-acac) motif provided neutral mono-NHC species with coordination of the deprotonated amide. The diisopropyl-phenyl NHC ligand **2.4** could be used to generate the desired *N*-amidate/NHC chelated species Pd(**2.4 - H**)(*O,O'*-acac) and Pt(**2.4 - H**)(*O,O'*-acac) albeit in low yield. These will be discussed further in Chapter 3. The pendant species Pd(**2.4**)(*O,O'*-acac)(γC-acac) and Pt(**2.4**)(*O,O'*-acac)(γC-acac) formed competitively and were also isolated and characterised. The latter, non-chelated complexes where found to exist as two interconverting species attributed to *E/Z*-amide geometric diastereomers. This was verified by detailed NMR analysis including variable temperature NMR and is extremely interesting given the relatively high proportion (~ 30%) of the sterically disfavoured *E*-amide geometry.

The silver transmetalation route to NHC complexes was successfully employed for the synthesis of Pd(**2.4**)(allyl)Cl, Pd(**2.5**)Cl_2 and Ru(**2.2**)(*p*-cymene)Cl. Properties of NHC-Ag(I) intermediates Ag(**2.2**)Cl and Ag(**2.3**)Cl were explored despite these intermediates not typically being isolated. In complexes Pd(**2.4**)(allyl)Cl and Pd(**2.5**)Cl_2, the amide group is uncoordinated whereas in [Ru(**2.2**)(*p*-cymene)Cl][PF_6] it coordinates via the amide-carbonyl oxygen. Pd(**2.4**)(allyl)Cl exhibits fluxional diastereoisomerism attributable to *syn-anti* interchange of the allyl ancillary ligand. Remarkably, ^{1}H-NMR spectra of Pd(**2.4**)(allyl)Cl performed in DMSO-*d6* are missing some allyl-environments due to solvent-assisted acceleration of this interconversion. Unlike other "pendant" complexes in this study, the pyridyl appended NHC complex Pd(**2.5**)Cl_2 did not exhibit any form of diastereoisomerism. As such, the formation of a pyridyl/NHC chelate had the desired pre-organising effect on the ligand conformation however, possible ligand exchange in Pd(**2.5**)Cl_2 is a source of potential ambiguity. Two diastereomers of Ru(**2.2**)(*p*-cymene)Cl were identified by NMR and X-ray crystallography. These arise due to the formation of

an additional enantiomeric centre at the Ru(II) resulting from its pseudo-tetrahedral piano-stool geometry. Observance of a 1:1 ratio indicates that the bornane moiety imparts no stereochemical control over the geometry of the piano-stool in [Ru(**2.2**)(*p*-cymene)Cl][PF_6]. This implies that *N*-amidate/NHC chelation is required to bring the chiral bornane unit sufficiently close to the active metal centre to provide asymmetric induction in a catalytic scenario.

2.5. Scope and future work

Besides their potential catalytic applications, the NHC complexes prepared in this study offer considerable insight into the organometallic chemistry of acetamide-linked NHC compounds.

It has been demonstrated that the synthesis of imidazolium salts from 2-chloro-*N*-*exo*-bornylacetamide (**2.1**) is tenable to expedient modulation of the pendant group leading to a range of NHC precursors including those synthesised **[2.2.H]**$^+$ – **[2.5.H]**$^+$. Likewise, this study shows that these ligands are compatible with a variety of complex system and, as such, this class of NHC ligand is readily diversifiable and could be applied to generate numerous novel chiral complexes.

Of the complexes synthesised, Pd(**2.4 - H**)(*O,O'*-acac) and Pd(**2.4**)(*O,O'*-acac)(γC-acac) are particularly interesting candidates for further investigation given the demonstrated catalytic ability of the related complex Pd(**3.3 - H**)(*O,O'*-acac) (see Chapter 6). Furthermore, NMR spectra of Pd(**2.4**)(*O,O'*-acac)(γC-acac) collected in DMSO-*d6* reveal that elevated temperatures can cause the irreversible conversion to the chelated form Pd(**2.4 - H**)(*O,O'*-acac). It would be beneficial to study this conversion as a means towards preparing Pd(**2.4 - H**)(*O,O'*-acac) in useable isolated yields or for in situ generation.

Both Pd(**2.4**)(*O,O'*-acac)(γC-acac) and Pd(**2.4**)(allyl)Cl exhibit fluxional stereoisomerism of different origins and could each be the subject of separate investigations. For

example, a detailed NMR analysis of Pd(**2.4**)(*O,O'*-acac)(γC-acac) including NOESY or ROESY NMR would better elucidate the relationship between its *E*/*Z*-amide conformers and the types of interaction that are driving this phenomenon. The synthesis of related Pd(**BA**)(*O,O'*-acac)(γC-acac) systems would also be informative, as would be the successful crystallisation of Pd(**2.4**)(*O,O'*-acac)(γC-acac) or its adducts for X-ray analysis.

This work has established that the steric bulk of the bornane group impedes formation of the *N*-amidate/NHC chelate which may be important for asymmetric induction during catalysis. This being the case, a slightly less hindered, more flexible chiral terpene such as menthol may provide a more suitable scaffold. Synthesis of (+ or -)-menthylamine could be performed as reported[135] and used analogously to *exo*-(-)-isobornylamine in Scheme 2.4 to provide acetamide-linked imidazolium salts for the synthesis of NHC complexes with *N*-amidate/NHC chelation (Scheme 2.30).

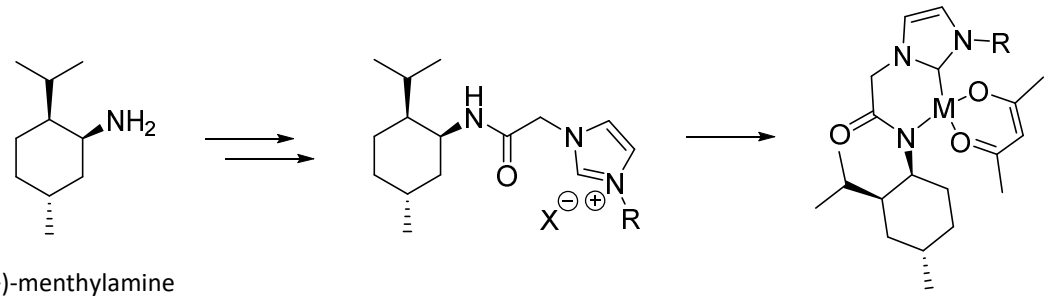

(+)-menthylamine

Scheme 2.30: *General scheme showing the synthesis of an M(NHC)(O'O-acac) type acetamide-linked NHC complex derived from (+)-menthylamine.*

Chapter 3

cyclohexyl-acetamide derivatives; achiral analogues of the bornyl-acetamide system

3.1. Introduction

Several of the complexes bearing bornyl-acetamide NHC ligands displayed interesting structural features arising from the steric bulk and inflexibility of the bornane-skeleton (Chapter 2). An achiral system was targeted to evaluate how these features might translate to catalytic ability. Replacing the chiral bornyl-actamide NHC ligand with an achiral cyclohexyl-acetamide was considered a comparable reference point for some of the NHC complexes. As a cyclic alkane, the cyclohexyl-group is chemically related to bornane and hence tenable to the same synthesis. Furthermore, its reduced steric bulk and rigidity was sought to improve the potential for chelation of the amidate, thus avoiding some of the synthetic handicaps encountered with the bornyl-acetamide derivatives. More importantly, these ligands provided an achiral control against which to reference any enantiomeric-excesses generated during catalysis involving their chiral-counterparts.

3.2. Synthesis of cyclohexyl-NHC proligands

3.2.1. Acetamide-linked cyclohexyl-imidazolium salts

Cyclohexyl-acetamide imidazolium salt proligands **3.2** – **3.4** were prepared in an identical manner to the bornyl-acetamide imidazolium salt proligands **2.2** – **2.5** (Scheme 3.1). Chloroacetylation of cyclohexylamine provided 2-chloro-N-cyclohexylacetamide (**3.1**) by the same method used for **2.1**. An old batch of cyclohexylamine was used because impurities did not badly affect the synthesis and the product was easily isolated. For this reason, no particular care was taken to employ anhydrous conditions as in the synthesis of **2.1**. After 14 hours the reaction mixture was taken up in ethyl-acetate and washed with water followed by brine. The organic phase was dried over $MgSO_4$ and filtered through a silica-plug before removal of the solvent. Recrystallisation of the light brown residue from hot Et_2O provided large white crystals of **3.1** in an overall yield of 70%. Compound **3.1** has been prepared previously by a variety of methods and the characterisation data obtained in this study agrees with that reported.[209]

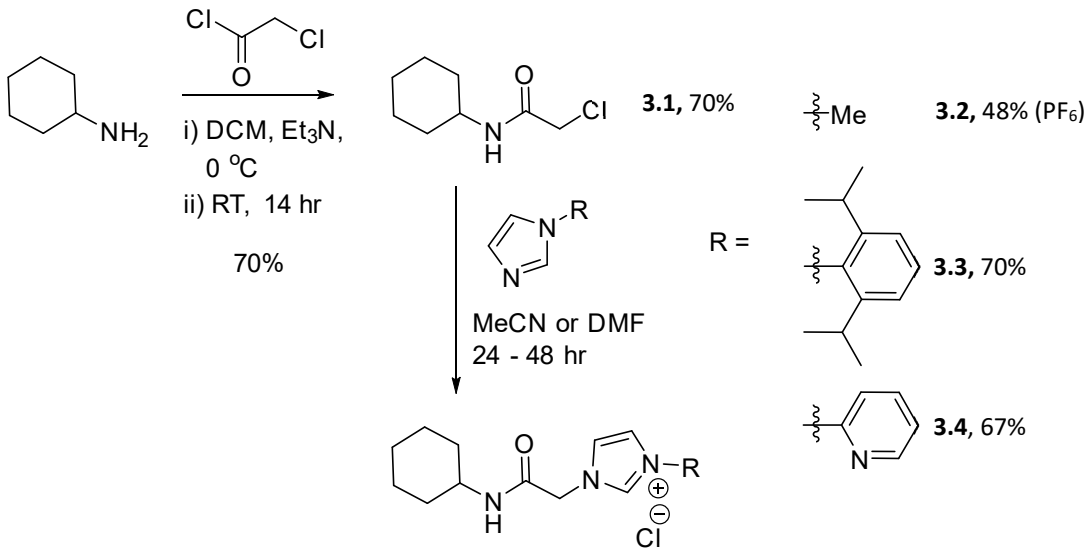

Scheme 3.1: *Synthesis and subsequent substitution of* ***3.1*** *to give 1-[2-(cylclohexyl)-2-oxoethyl]-1H-imidazolium salts* ***3.2.HPF$_6$, 3.3.HCl, 3.4.HCl****.*

As with the bornyl-acetamide proligands, heating the chloroacetamide with the corresponding mono-substituted imidazole provided the desired imidazolium salt (Scheme 3.1). Salts of the methyl derivative **3.2.HCl, 3.2.HBF$_4$** and **3.2.HPF$_6$** have been reported previously in a patent on ionic liquids,[210] however, access could not be gained via the Chinese outlet through which it was published. Here, the compound was isolated as the PF_6 salt due to the unmanageably sticky constitution of the chloride. Some material was lost during these manipulations causing its comparatively low yield of 48%. Salt **3.2.HPF$_6$** has a melting point of 64 ^oC and based on this, it is unsurprising that salts of **[3.2.H]$^+$** have been explored in the context of ionic liquids.

Compounds **3.2.HCl** and **3.3.HCl** are new and all three have been fully characterised. Their spectroscopic features are largely unremarkable. In the ^{1}H-NMR spectrum, signals due to the cyclohexyl group are well resolved into axial and equatorial proton environments suggesting, as expected, that the amide-group favours an equatorial position.[211] The methylene proton environments of the acetamide linker resonate as a singlet at $\sim$ 5 ppm. This is in contrast with the bornyl analogues for which these environments are often observed as two doublets. Because the cyclohexyl group is

achiral these environments are enantiotopic as opposed to diastereotopic as in the case of chiral bornane.

3.3. Synthesis of cyclohexyl-NHC complexes

Complexes of the cyclohexyl-acetamide NHC ligands were prepared as structurally related, achiral analogues of the bornyl-acetamide NHC complexes. Ideally all complex syntheses discussed in Chapter 2 would be repeated for ligands **3.2** – **3.4** but in the interest of time, the most informative and catalytically relevant systems were targeted. Therefore, the following discussion focusses on the complexes Pd(**3.3 - H**)(*O,O'*-acac), Pt(**3.3 - H**)(*O,O'*-acac) and Pd(**3.3**)(allyl)Cl (Figure 3.1).

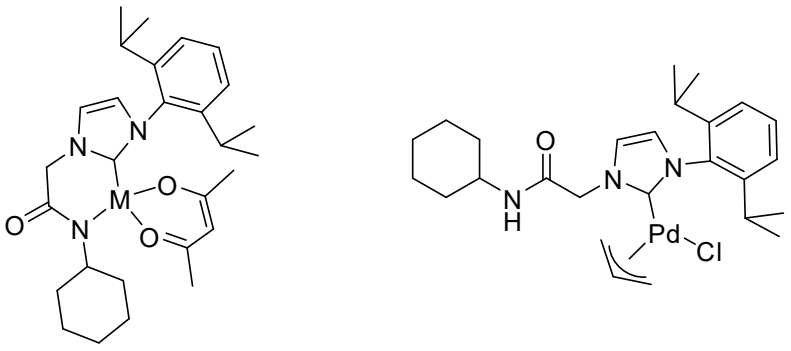

M(**3.3 - H**)(O,O'-acac) Pd(**3.3**)(allyl)Cl

Figure 3.1: *Target compounds explored in this section.*

3.3.1. M(NHC)(acac) type complexes

3.3.1.1. Synthesis of M(3.3 - H)(*O,O'*-acac)

Complexes Pd(**3.3 - H**)(*O,O'*-acac) and Pt(**3.3 - H**)(*O,O'*-acac) were prepared in a similar fashion to their bornane-counterparts, however, the reactions proceeded much more favourably providing each product in yields of 46% and 47%, respectively (Scheme 3.2).

This is compared with the ~ 14% and 22% yields recorded for Pd(**2.4 - H**)(*O,O'*-acac) and Pt(**2.4 - H**)(*O,O'*-acac).

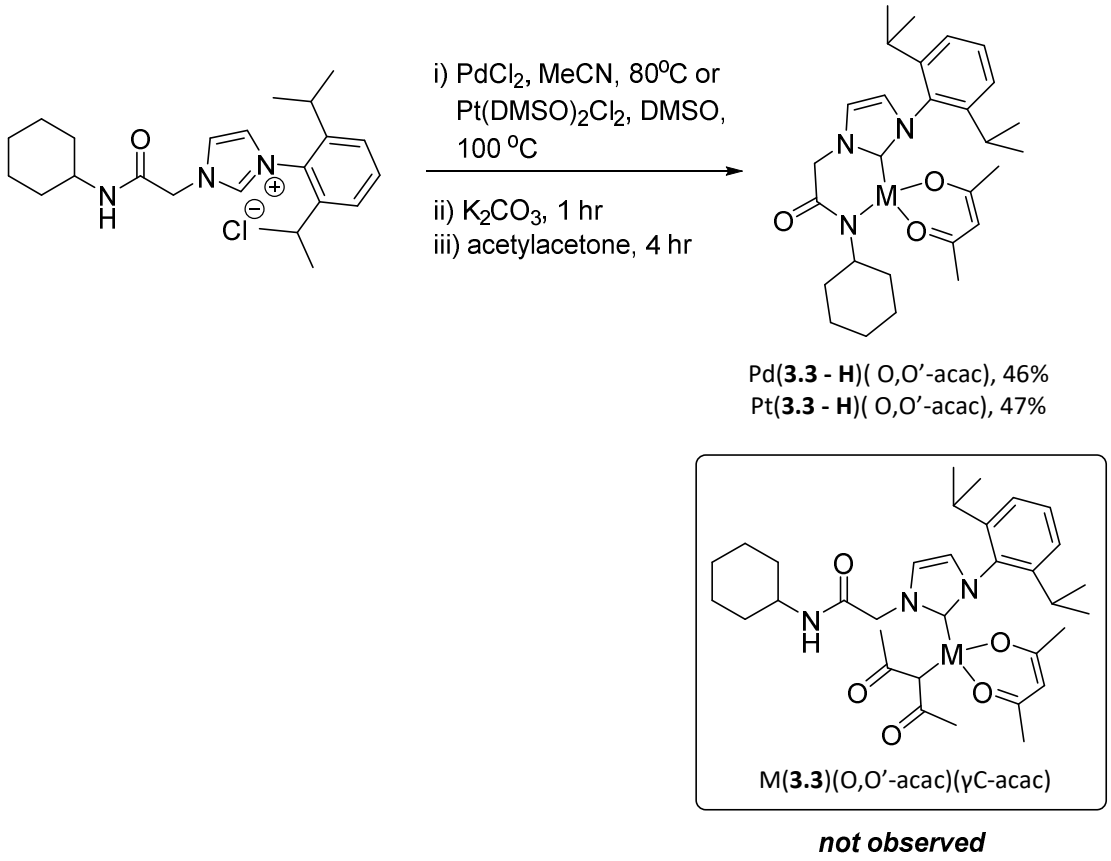

Scheme 3.2: *Synthesis of Pd(**3.3 - H**)(*O,O'*-acac) and Pt(**3.3 - H**)(*O,O'*-acac).*

The Pd(II) complex Pd(**3.3 - H**)(*O,O'*-acac) was isolated after filtration of the cooled reaction mixture and removal of the solvent by triturating the off white residue in pentane. Filtering the material, air drying then rinsing with water and quickly with MeCN provided pure product. Isolation of the Pt(II) congener was achieved by uptake of the reaction mixture into a DCM phase and washing with water and brine to remove the DMSO. After drying over $MgSO_4$, filtering, and removing the solvent, the off white residue was rinsed with cold MeCN to give a faint yellow product. An ^{1}H-NMR analysis of the MeCN rinse revealed that it contains a mixture of products including the desired complex. It is predicted based on this that an improved purification could recover the product in yields upwards of 60%. None of the pendant side product M(**3.3**)(*O,O'*-

acac)(γC-acac) was observed which is unsurprising given that one equivalent of acetylacetone was used. Observing at least 50% conversion to M(**3.3**)(*O,O'*-acac) leaves residual acac to form a maximum of 25% M(**3.3**)(*O,O'*-acac)(γC-acac). No effort was made to synthesise or isolate M(**3.3**)(*O,O'*-acac)(γC-acac).

3.3.1.2. Characterisation of Pd(3.3 - H)(*O,O'*-acac) and Pt(3.4 - H)(*O,O'*-acac)

Complexes Pd(**3.3 - H**)(*O,O'*-acac) and Pt(**3.3 - H**)(*O,O'*-acac) were characterised by NMR, mass-spectrometry and IR analysis. Crystal structures of both compounds were also obtained. Features of the ^{1}H-NMR spectrum of Pd(**3.3 - H**)(*O,O'*-acac) are discussed in section 3.3.1.3 through comparison with Pd(**2.4 - H**)(*O,O'*-acac). Resonances in the ^{13}C-NMR pertaining to the *O,O'*-acac ligand, imidazolyl-moiety and acetamide-linkage are as expected, having been addressed in the previous discussion of the related bornyl-acetamide complexes in section 2.3.1. Interestingly however, the carbenic carbon resonance of Pd(**3.3 - H**)(*O,O'*-acac), found at 145.31 ppm, is upfield of its bornyl counterpart at 153.55 ppm. On the other hand, the equivalent resonances for Pt(**3.3 - H**)(*O,O'*-acac) and Pt(**2.4 - H**)(*O,O'*-acac) are similar (138.80 ppm and 139.25 ppm, respectively). It is unclear why this difference in the carbene resonance is so significant for the Pd(II) complexes. Again, IR was used to support assignment of the *N*-amidate/NHC chelated species through observance of the anticipated coordination induced reduction in the amide carbonyl stretching frequency. This is found at 1575 cm^{-1} for Pd(**3.3 - H**)(*O,O'*-acac) and 1524 cm^{-1} for Pt(**3.3 - H**)(*O,O'*-acac), down from 1672 cm^{-1} in the precursor imidazolium salt **3.3.HCl.**

Crystals of Pd(**3.3 - H**)(*O,O'*-acac) suitable for single crystal diffraction analysis were grown by slow evaporation of an Et_2O solution of the compound. This crystallised in the monoclinic space group $P2_1/c$ with one molecule of the neutral complex Pd(**3.3 - H**)(*O,O'*-acac) in the asymmetric unit (Figure 3.2). The structure reveals that ligand **3.3 - H** is coordinated as a 6-membered chelate that adopts a puckered ring conformation reminiscent of the bornyl-acetamide complexes Pd(**2.4 - H**)(*O,O'*-acac) and Pt(**2.4 - H**)(*O,O'*-acac).

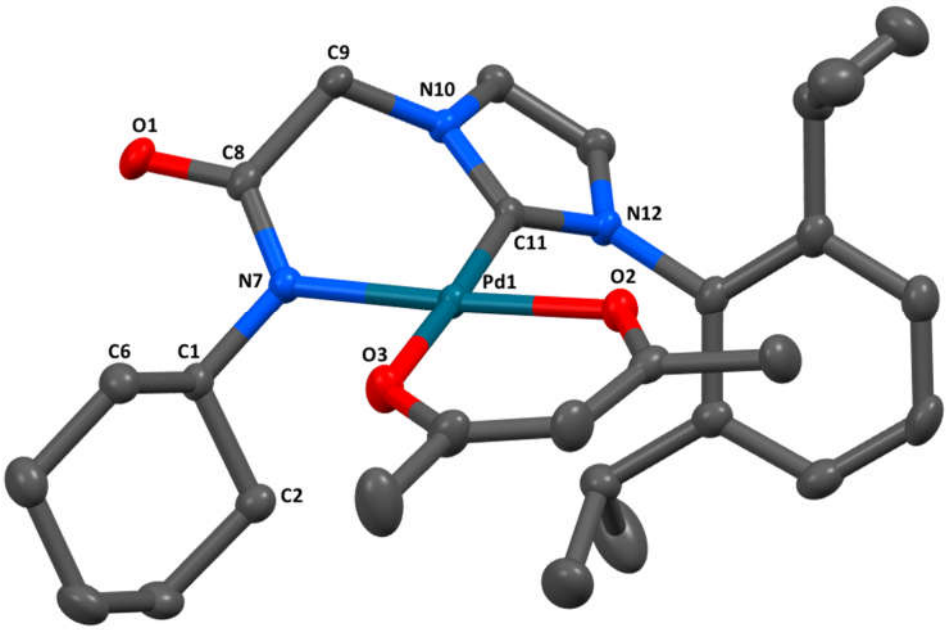

Figure 3.2: *Asymmetric unit of complex Pd(**3.3 - H**)(*O,O'*-acac). Hydrogen atoms have been omitted for clarity. Thermal ellipsoids are drawn at a 50% probability level.*

As before, the extent to which the chelate ring is distorted from the idealised mean-plane of the square-planar Pd(II) centre is represented by the torsion angles C11-Pd1-N7-C8 and N7-Pd1-C11-N10 which are 47.1(2)° and 35.4(2)°, respectively. As discussed in section 2.3, internal chiral axes arise from this fixed solid-state conformation along the C11 – Pd1 and N7 – Pd1 bonds of Pd(**3.3 - H**)(*O,O'*-acac). However, because the molecule contains no permanent stereo-centres, the two conformations are enantiomeric and both enantiomers are present in the unit cell. This point will be expanded in the discussion of the ^{1}H-NMR spectra of these compounds in section 3.3.1.3. The relative position of the methylene group described by the angle θ_{CH2} is 60.91(8)° for Pd(**3.3 - H**)(*O,O'*-acac). The cyclohexyl substituent is found in a well-defined chair conformation with the amido-functionality in the equatorial position as expected. Bond lengths pertaining to the Pd(II) centre are as follows; Pd1 – C11 = 1.956(2) Å, Pd1 – N7 = 2.032(2) Å, Pd1 – O2 = 2.013(2) Å and Pd1 – O3 = 2.044(2) Å. The angles between these bonds are C11 – Pd1 – N7 = 87.10(9)°, C11 – Pd1 – O2 = 90.84(9)°, N7 – Pd1 – O3

= 90.42(8)° and O2 – Pd1 – O3 = 91.61(7)°. The observed disparity in bond lengths has been highlighted in previous discussions and is consistent with the strong bonding and large trans-influence of the NHC ligand. The bite-angle of **3.3 - H** (C11 – Pd1 – N7) is ~ 4.5° smaller than that of the *O,O'*-acac despite both forming 6-membered chelates. It is deemed that contraction of the C11 – Pd1 – N7 bond angle coincides with the puckering of the chelate ring. This occurs in order for the compound to crystallise with the minimum internal steric interactions. The cyclohexyl ring does not engage in close contacts with other atoms of the complex at a distance greater than three bonds apart. This is unlike its bornyl counterpart which contained related contacts as short as 2.839(7) Å. The shortest such contact in Pd(**3.3 - H**)(*O,O'*-acac) is 3.166(3) Å for C6 ··· O3 suggesting that there is less steric strain associated with the cyclohexyl ring.

The Pt(II) complex Pt(**3.3 - H**)(*O,O'*-acac) was also successfully crystallised by slow evaporation of an Et_2O solution of the compound. As with Pd(**3.3 - H**)(*O,O'*-acac), this crystallised in the monoclinic space group $P2_1/c$ with one molecule of the neutral complex Pt(**3.3 - H**)(*O,O'*-acac) in the asymmetric unit (Figure 3.3).

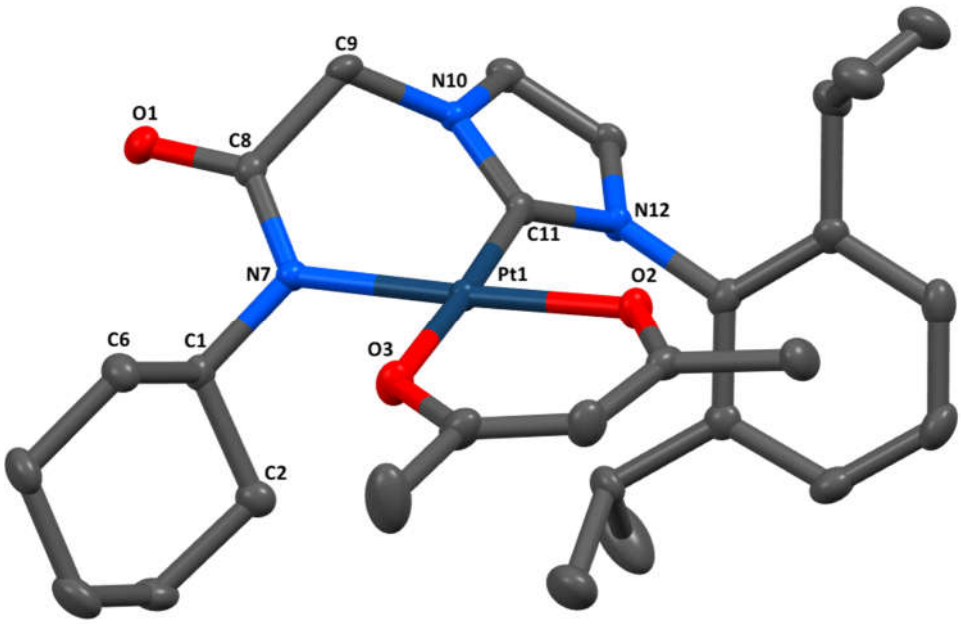

Figure 3.3: *Asymmetric unit of complex Pt(**3.3 – H**)*(O,O'*-acac). Hydrogen atoms have been omitted for clarity. Thermal ellipsoids are drawn at a 50% probability level.*

Complexes Pd(**3.3 - H**)(*O,O'*-acac) and Pt(**3.3 - H**)(*O,O'*-acac) are crystallographically isostructural, sharing many similar bond lengths and angles. The chelate ring is distorted to the same extent with the torsion angles C11-Pd1-N7-C8 and N7-Pd1-C11-N10 of 46.1(3)^{o} and 35.4(3)^{o} respectively, closely matching those of the Pd(II) complex. So too does the angle θ_{CH2} which is 61.0(1)^{o}. Bond lengths and angles pertaining to the Pd(II) centre are as follows; Pt1 – C11 = 1.944(3) Å, Pt1 – N7 = 2.023(3) Å, Pt1 – O2 = 2.012(2) Å and Pt1 – O3 = 2.046(2) Å, C11 – Pt1 – N7 = 87.7(2)^{o}, C11 – Pt1 – O2 = 91.0(2)^{o}, N7 – Pt1 – O3 = 89.7(1)^{o} and O2 – Pt1 – O3 = 91.65(9)^{o}. There are no features that have not been noted in the discussion of Pd(**3.3 - H**)(*O,O'*-acac) above. Many of the crystallographic measurements discussed here are summarised in Table 3.1 in the following section.

Complex Pd(**3.3 - H**)(*O,O'*-acac) was shown to perform acceptably as a precatalyst for the synthesis of hindered biaryls by Suzuki coupling (Chapter 6). The structural characterisation discussed above, and in the next section, therefore fosters an understanding of the active species. Because there was an insufficient amount of the bornyl species Pd(**2.4 - H**)(*O,O'*-acac) remaining to perform a full catalysis study, the applicability of Pd(**3.3 - H**)(*O,O'*-acac) becomes important by analogy. It provides further incentive for a researcher interested in improving the synthesis of Pd(**2.4 - H**)(*O,O'*-acac) and studying its catalysis.

3.3.1.3. A comparative analysis of M(2.4 - H)(*O,O'*-acac) and M(3.3 -H)(*O,O'*-acac)

That the bornane appendage of the M(**2.4 - H**)(*O,O'*-acac) complexes elicits greater steric congestion of the metal-centre is clearly communicated by comparison with the less encumbered cyclohexyl analogues. As has been noted prior, the cyclohexyl-acetamide NHC complexes Pd(**3.3 - H**)(*O,O'*-acac) and Pt(**3.3 - H**)(*O,O'*-acac) are produced in yields $\sim$ 25% larger than the best yields obtained for the bornyl-acetamide NHC complexes Pd(**2.4 - H**)(*O,O'*-acac) and Pt(**2.4 - H**)(*O,O'*-acac) under similar conditions. These larger yields reflect the ready chelation of the cyclohexyl-amide nitrogen compared with the bornyl-amide which is justifiable on steric grounds. One therefore assumes that a

greater degree of conformational strain exists within the complexes M(**2.4 - H**)(*O,O'*-acac) when compared with M(**3.4 - H**)(*O,O'*-acac). This is manifested as a reduction in close contacts between the cyclohexyl moiety and the remainder of the complex when compared with the bornane complex. Scrutiny of the X-ray crystal structures provided several geometric measurements relevant to the conformation of the NHC-amidate ligand (Table 3.1). Typically, the values obtained for the cyclohexyl-amidate complexes are equal to one of, or fall within the range of values obtained for the two diastereomers of each bornyl-amidate complex. Some subtle differences are observed for the bond length M – O3 and the torsion angle N_{am}-M-C_{carb}-N(CH_2). The M – O3 bond length is longer for the bornyl complexes by ≤ 0.01 Å. This may be due to the bulky bornane substituent pushing away the adjacent part of the acac ligand resulting in elongation of the nearby M – O bond.

The torsion angle N_{am}-M-C_{carb}-N(CH_2) represents the twist of the imidazolyl moiety relative to the metal-centred coordination plane. This torsion is greater for the bornyl complexes by upwards of 10° and may be due to twisting of the ligand to accommodate the bulkier substituent. It is in this torsion that the greatest variation between the two crystallised diastereomers of M(**2.4 - H**)(*O,O'*-acac) is observed (A ~ 52° and B ~ 64°). It is touched on in section 2.3.1.3 that, of the two diastereomers, the structure of diastereomer B harbours more destabilising internal steric clashes. Diastereomer B, presumptively the most encumbered of the two, also has the larger N_{am}-M-C_{carb}-N(CH_2) torsion angle. It therefore, may be true that the reduced torsion of ~ 47° observed in the M(**3.3 - H**)(*O,O'*-acac) complexes reflects their less congested nature. It was thought that contortion of the ligand might be quantifiable by the angle θ_{CH2}, however, this was found to be fairly conserved for the four complexes.

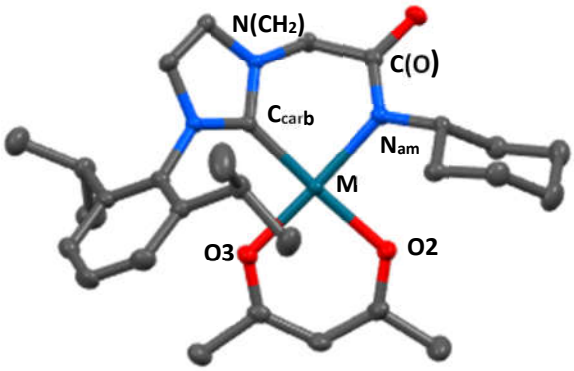

Figure 3.4: *Generalised labelling scheme shown for the structure of Pd(**3.3 - H**)(O,O'-acac).*

Table 3.1: *Summary of relevant X-ray crystallographic measurements for M(**2.4 - H**)(O,O'-acac) and M(**3.3 - H**)(O,O'-acac) complexes based on labelling in Figure 3.4.*

		complexes			
		Pd(BA-N) (*O,O'*-acac) (A / B)	Pt(BA-N) (*O,O'*-acac) (A / B)	Pd(Cy-N) (*O,O'*-acac)	Pt(Cy-N) (*O,O'*-acac)
bond lengths	M - C_{carb}	1.949(5) / 1.945(6)	1.931(5) / 1.937(5)	1.956(2)	1.944(3)
	M - N_{am}	2.030(4) / 2.046(4)	2.022(4) / 2.046(4)	2.032(2)	2.023(3)
	M - O2	2.015(3) / 2.011(3)	2.015(3) / 2.015(3)	2.013(2)	2.012(2)
	M - O3	2.056(4) / 2.058(4)	2.051(3) / 2.053(4)	2.044(2)	2.046(2)
bond angles	C_{carb} - M - N_{am}	87.6(2) / 86.1(2)	88.1(2) / 87.4(2)	87.10(9)	87.71(12)
	C_{carb} - M - O2	89.7(2) / 92.5(2)	92.3(2) / 91.3(2)	90.84(9)	90.97(11)
	N_{am} - M - O3	89.7(2) / 92.5(2)	88.8(2) / 90.8(2)	90.42(8)	89.65(10)
	O2 - M - O3	90.6(2) / 91.3(2)	90.9(2) / 90.7(2)	91.61(7)	91.65(9)
distortion angles	C_{carb} - M - N_{am} - C(O)	52.1(6) / 63.6(5)	50.8(4) / 60.8(4)	60.91(8)	60.95(10)
	N_{am} - M - C_{carb} - $N(CH_2)$	32.0(4) / 35.8(4)	32.5(3) / 35.1(3)	47.1(2)	46.1(3)
	θ_{CH2}	28.4(2) / 30.7(2)	28.6(2) / 30.3(2)	35.4(2)	35.4(3)

The X-ray crystal structures of these complexes shows that, in the solid state, the six-membered chelate ring adopts a puckered conformation with the methylene group directed away from the plane defined by the square planar metal centre. In solution however, the *N*-amidate/NHC chelated ligand is conformationally mobile with the major substituents moving in tandem by "flipping" of the chelate ring as illustrated in Figure 3.5 and Figure 3.6. NMR spectroscopy supports this assessment and, furthermore, implies that transitional energy barrier (ΔE_{TS}) between the two extreme conformations is higher for the bornyl-appended complexes than their cyclohexyl-appended counterparts (Figure 3.7).

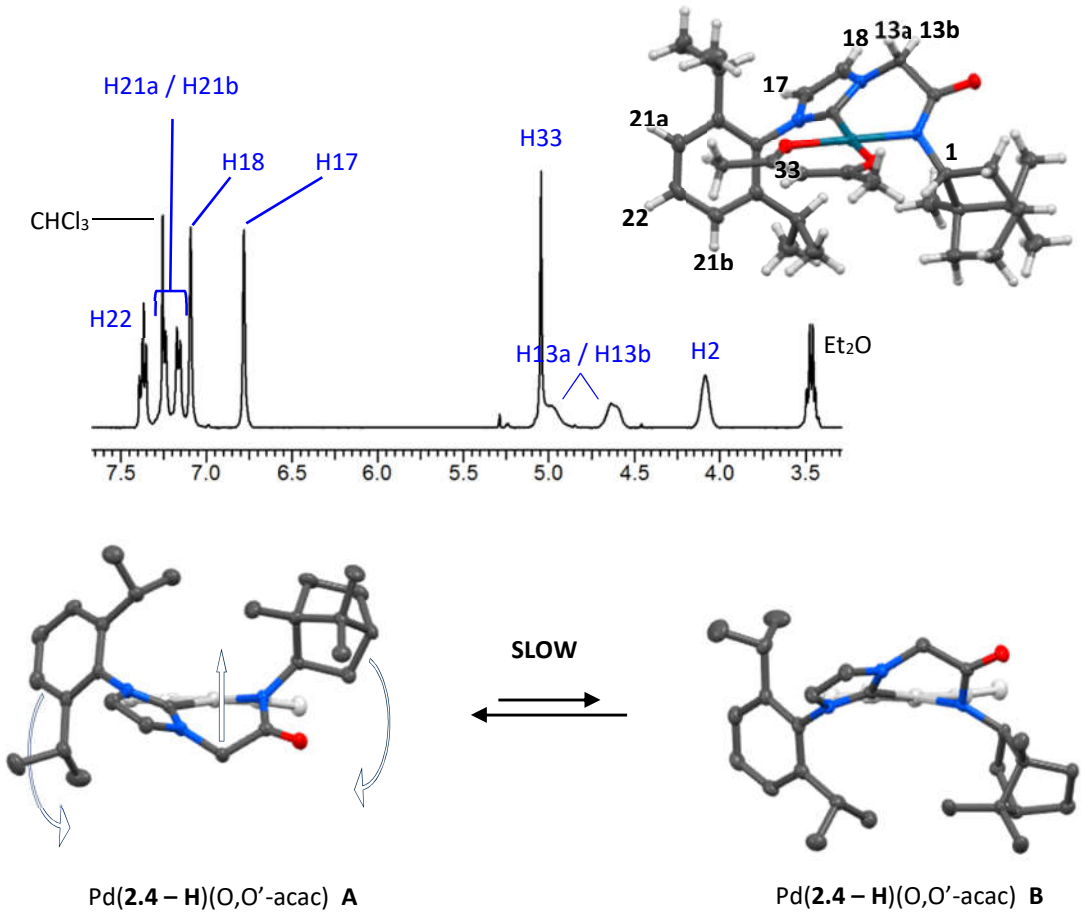

Figure 3.5: *A region of the ^{1}H-NMR spectrum highlighting the limited conformational fluxionality of Pd(**2.4 - H**)*(O,O'-acac) *and its relationship with the solid state structure.*

This implication is made on the basis that, in the ^{1}H-NMR spectra of complexes Pd(**2.4 - H**)(*O,O'*-acac) and Pt(**2.4 - H**)(*O,O'*-acac) at 25 °C, signals pertaining to the acetamide-linker and bornane moiety are observed as broad, featureless mounds. Each of the two diastereotopic methylene hydrogen atoms contribute a separate signal due to occupying chemically distinct positions. The same is true for many of the hydrogen and carbon atom environments of the diisopropyl-phenyl group. Many that are equivalent in the spectra of the complexes Pd(**3.3 - H**)(*O,O'*-acac) and Pt(**3.3 - H**)(*O,O'*-acac) are non-equivalent in the spectra of Pd(**2.4 - H**)(*O,O'*-acac) and Pt(**2.4 - H**)(*O,O'*-acac). These contrasting features are highlighted in the portion of ^{1}H-NMR spectrum shown in Figure 3.5 for complex Pd(**2.4 - H**)(*O,O'*-acac) and in Figure 3.6 for its cyclohexyl analogue Pd(**3.3 - H**)(*O,O'*-acac).

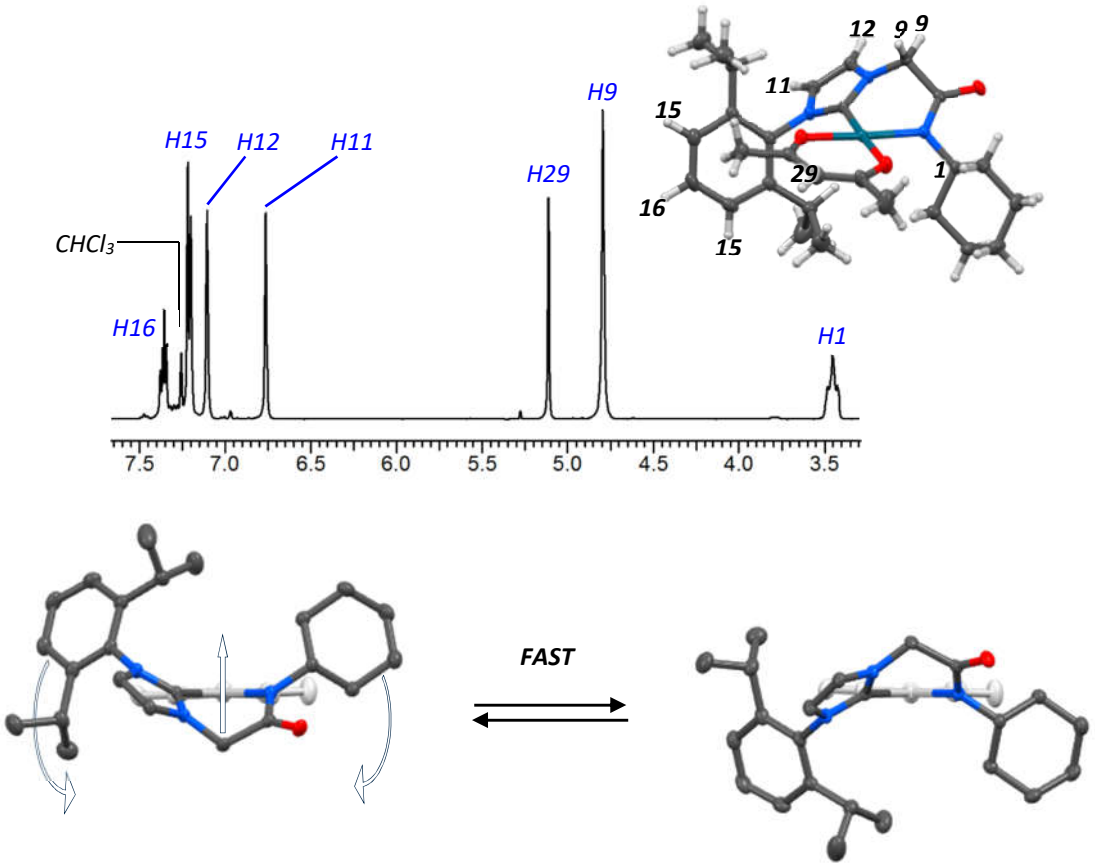

Figure 3.6: *A region of the ^{1}H-NMR spectrum highlighting the conformational fluxionality of Pd(**3.4 - H**)*(O,O'*-acac) and its relationship with the solid state structure.*

For M(**2.4 - H**)(*O,O'*-acac) complexes, the broad, non-equivalent methylene hydrogen atom environments and those of, for example H21a and H21b, strongly suggests that the molecule spends most of its time in the puckered ring arrangement revealed by X-ray crystallography. However, the molecule is still observed to be conformationally mobile, albiet slowly on the NMR timescale as evidenced by the broadening of noted signals. The fact that the two extreme conformation states shown in Figure 3.5 are diastereomeric and hence not degenerate is expected to contribute to the convolution of their NMR spectra. Conversely, the cyclohexyl appended complexes Pd(**3.3 - H**)(*O,O'*-acac) and Pt(**3.3 - H**)(*O,O'*-acac) interconvert rapidly between conformation states causing the enantiotopic methylene hydrogen atoms to generate a singlet proton signal in the ^{1}H-NMR spectrum (Figure 3.6). Also, the environment of the diisopropyl-phenyl H15 resonates as one doublet and signals related to the cyclohexyl moiety are slightly better defined. It is gleaned from these observations that the bornyl-amidate complexes harbour greater internal congestion which hinders their conformational mobility when compared with the cyclohexyl-amidate complexes.

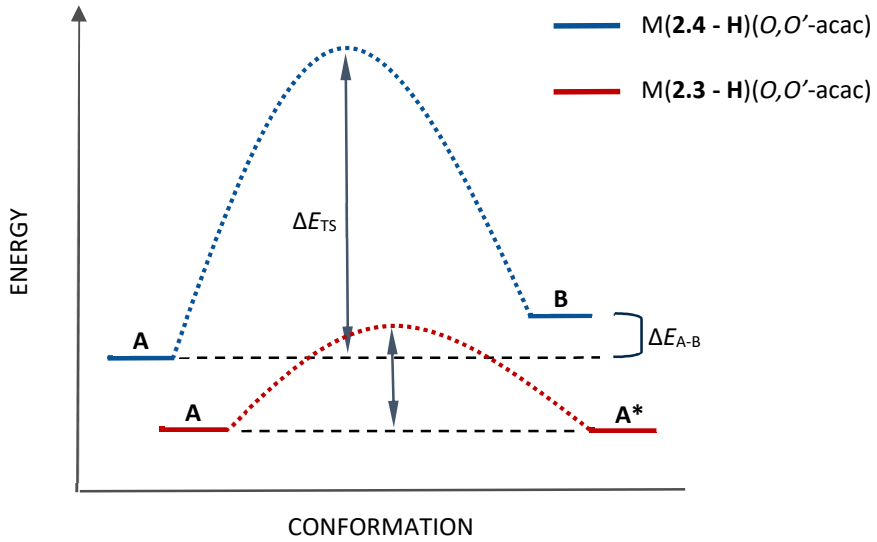

Figure 3.7: *Representative energy profile for conversion between the two extreme conformations of M(**2.4 - H**)*(O,O'-acac) *and M(**3.4 - H**)*(O,O'-acac).

One interesting similarity between the two spectra is the relatively upfield resonance of the imidazolyl-proton adjacent to the diisopropyl-phenyl group (H17/H11 ~ 6.77 ppm). This is attributed to anisotropic shielding by the aromatic ring which is roughly perpendicular to the imidazolyl ring in solution. This analysis clearly establishes that the bornyl-substituent crowds the metal centre to a greater extent than the cylohexyl-group. In light of their intended application in catalysis, this will hypothetically enhance the stereodirecting capabilities of the bornane group.

3.3.2. Pd(NHC)(allyl)Cl type complexes

With regard to application in palladium mediated synthesis, the Pd(NHC)(allyl) family of complexes represent a well-heeled class of precatalyst with predictable catalytic performance. Synthesis of Pd(**2.4**)(allyl)Cl in section 2.3.3 demonstrated selectivity for an unchelated "pendant" motif. It was necessary to determine if this was true also for the cyclohexyl-species which, in light of the above discussion, is shown to be much more receptive to amidate-chelation. It was also important to have a related non-chelated species for comparison with Pd(**3.3 - H**)(*O,O'*-acac) which represents the class of organic, amidate-chelated precatalysts. This would help assess the role of amidate-chelation in active species formation and product conversion.

Successful synthesis of the pendant complex Pd(**3.3**)(allyl)Cl provided the desired "intermediate chelator," something that can chelate under the conditions of a Suzuki coupling, but is selectively isolated in an unchelated form. It finalises the series with the pre-chelated species Pd(**3.3 - H**)(*O,O'*-acac) and one in which chelation is sterically disfavoured, Pd(**2.4**)(allyl)Cl.

3.3.2.1. Synthesis of Pd(3.3)(allyl)Cl

Complex Pd(**3.3**)(allyl)Cl was prepared in an identical manner to Pd(**2.4**)(allyl)Cl via the silver transmetalation method and isolated in a yield of 78% (Scheme 3.3). The reaction was performed under an inert atmosphere in the absence of light. Complete conversion

to the NHC – Ag(I) was indicated by ^{1}H-NMR prior to addition of $[Pd(allyl)Cl]_2$ as a DCM solution. This immediately resulted in the formation of a white precipitate.

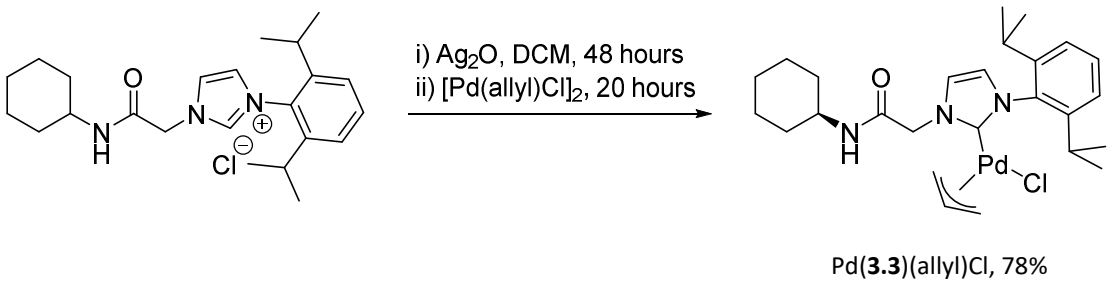

Scheme 3.3: *Synthesis of Pd(**3.3**)(allyl)Cl by the NHC-Ag(I) transmetalation method.*

The completed reaction was filtered through a celite pad and the solvent removed in vacuo to provide a fluffy white mass of pure Pd(**3.3**)(allyl)Cl. Being slightly less organic soluble than the bornyl congener meant it could be purified further by rinsing with pet-ether to provide very pure material for analysis.

3.3.2.2. Characterisation of Pd(3.3)(allyl)Cl

Full characterisation of Pd(**3.3**)(allyl)Cl was successfully performed and NMR analysis revealed the same curious isomerism exhibited by Pd(**2.4**)(allyl)Cl which is attributable to allyl-auxiliary dynamics. Further evidence allying allyl group fluxionality with the observed solution-state isomerism was provided by a crystal structure of Pd(**3.3**)(allyl)Cl.

Crystals of Pd(**3.3**)(allyl)Cl were obtained by slow evaporation of a concentrated Et_2O solution of the compound. This crystallised in the monoclinic spacegroup $P2_1/c$ with one molecule of Pd(**3.3**)(allyl)Cl in the asymmetric unit (Figure 3.8). Ligand **3.3** is seen to coordinate in a monodentate fashion via the NHC with a chloride and the bidentate allyl auxiliary completing the distorted square planar geometry of Pd(II). The acetamide-NHC ligand is oriented perpendicularly such that the inter-planar angle between the coordination plane of Pd(II) and that of the imidazolyl moiety is 102.3(2)°. This limits

contact between the diisopropyl-phenyl substituent and the remainder of the ligand field. Likewise, the acetamide arm and diisopropyl-phenyl substituent are both rotated to be orthogonal to imidazolyl moiety generating an C9-N8-C7-C6 torsion of 91.3(4)° and an inter-planar angle (imidazolyl-phenyl) of 85.1(2)°.

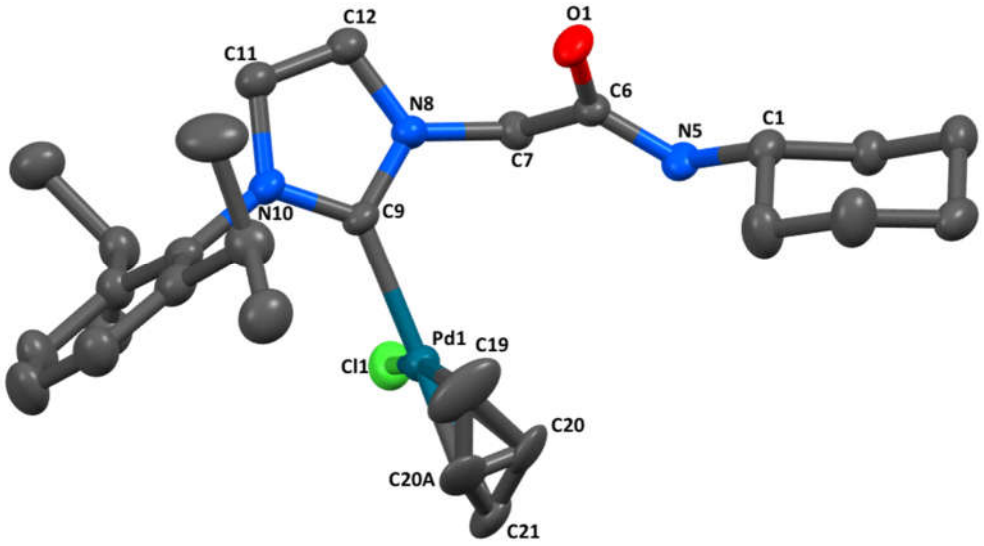

Figure 3.8: *Contents of the asymmetric unit of Pd(**3.3**)(allyl)Cl. Hydrogen atoms have been omitted for clarity. Thermal ellipsoids are drawn at a 50% probability level.*

Coordination to Pd(II) is quantified by the following bond lengths; Pd1 – C9 = 2.047(3) Å, Pd1 – C19 = 2.095(5) Å, Pd1 – C21 = 2.169(4) Å and Pd1 – Cl1 = 2.3643(9) Å, and angles; C9 – Pd1 – C19 = 100.7(2)°, C19 – Pd1 – C21 = 68.8(2)°, C21 – Pd1 – Cl1 = 99.2(2)° and C9 – Pd1 – Cl1 = 91.2(2)°. Palladium to carbon separations for the allyl carbons are differentiated due to the trans influence of the NHC ligand causing the pseudo-*trans* bond Pd1 – C21 to be elongated compared to Pd1 – C19. A crystallographic study performed by Vicui and co-workers on eight simple Pd(NHC)(allyl)Cl complexes reported measurement ranges for related Pd – Ligand bonds.[212] These are; Pd – $C_{carbene}$ = 2.028(4) Å – 2.062(2) Å, Pd – $C_{allyl(cis)}$ = 2.098(6) Å – 2.160(10) Å, Pd – $C_{allyl(trans)}$ = 2.167(3) Å – 2.236(4) Å and Pd – Cl = 2.358(9) Å – 2.419(8) Å. Bond lengths vary considerably depending on the nature of the NHC wing groups however, the Pd – $C_{carbene}$ and Pd – Cl

bond lengths recorded for Pd(**3.3**)(allyl)Cl fall neatly within the reported ranges. Pd – C distances for the allyl ligand, however, are at the low end or outside in the case of Pd1 – C19 and compare more closely with a reported Pd(NHC)(allyl)Br complex.[193] Bond angles are comparable to those reported in the above sources, importantly these corroborate the narrow angle between terminal carbons of the allyl ligand (C19 – Pd1 – C21). The acetamide pendant adopts a *Z*-amide configuration allowing it to participate in bridging hydrogen bonds of the type N*H* ··· O (N5 ··· O1 = 2.878(4) Å, N5 – H ··· O1 = 155.7(2)°) (Figure 3.9). The resultant linearly polymeric packing motif was also seen in the structure of the "pendant" complex Pd(**2.5**)Cl_2. The aromatic diisopropyl-phenyl rings appear to stack, however, the offset is too large to constitute a genuine π ··· π interaction (centroid to centroid = 4.537(4) Å, plane to plane shift = 2.505(8) Å, plane to centroid = 3.782(7) Å).

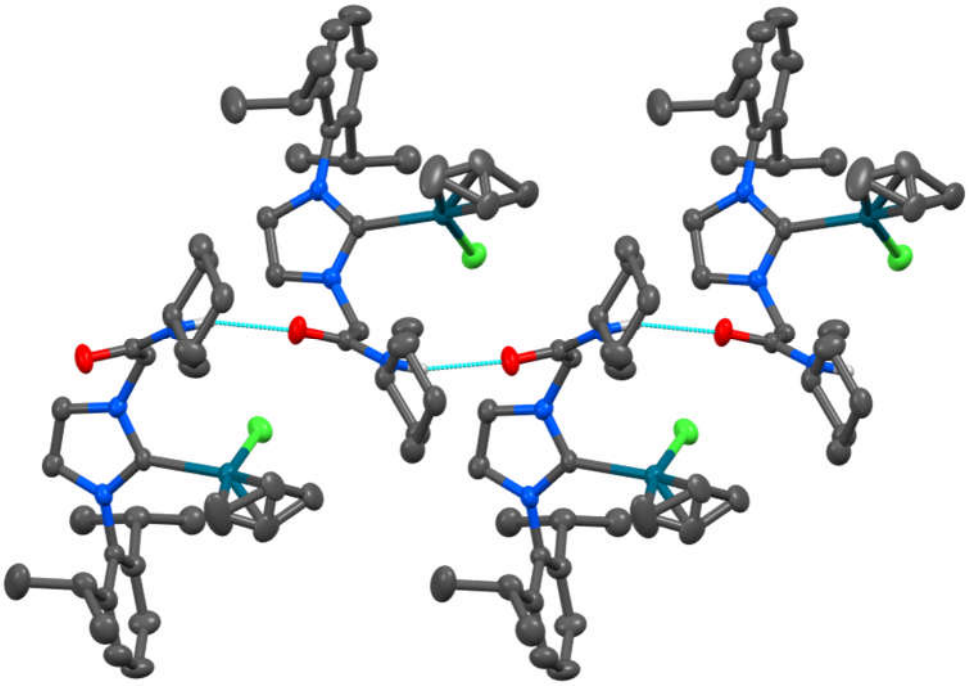

Figure 3.9: *Inter-amide hydrogen bonding in the extended structure.*

The allyl ligand itself exhibits positional disorder of the central carbon C20 which arises due to the *syn-anti* interchange mechanism discussed previously. It is found that the C20 sites are occupied in a 70 : 30 ratio. As has been noted, fixing the position of the allyl group and rotating the Pd – NHC bond produces a different diastereomer to the one observed. Inspection of the crystal structure suggests that this rotation is unrestricted and could occur more rapidly than *syn-anti* interchange making it unlikely to contribute to the isomerism witnessed on the NMR timescale. The two diastereomers shown in Scheme 3.4 are implicated in the observance of two species by NMR. A previous study that observed allyl-group isomerism by NMR also identified these isomers crystallographically.[189]

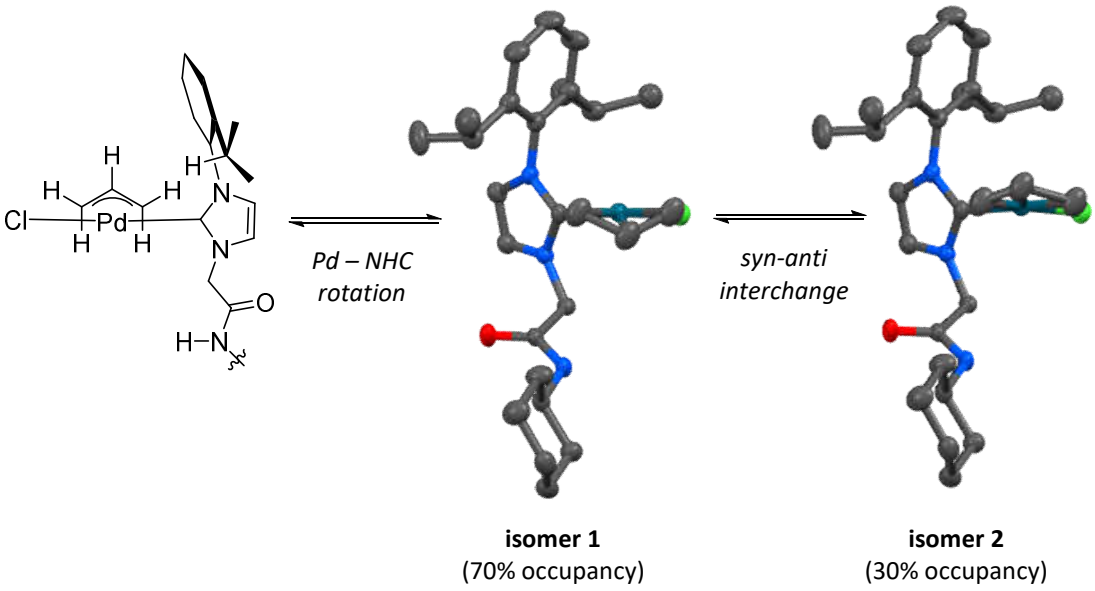

Scheme 3.4: *The diastereomeric products of* syn-anti *interchange by the allyl-auxiliary as observed crystallographically in the form of positional disorder. A different diastereomer is produced by rotation about the Pd – NHC bond which is expected to occur rapidly.*

These conformations of the allyl ligand were witnessed as separate species by NMR in solvents other than DMSO-*d6*. As in the case of the related bornyl-acetamide species, their dynamic behaviour was probed through variable temperature NMR. First however,

it is convenient to address the general characterisation of Pd(**3.3**)(allyl)Cl in relation to the more simplistic DMSO-*d6* NMR spectra before discussing the compounds dynamics.

The mass-spectrum of complex Pd(**3.3**)(allyl)Cl identifies a single species of mass 514.2055 corresponding to the $[M - Cl]^+$ cation (calculated m/z, $[Pd(\mathbf{3.3})(allyl)]^+$ = 514.2050). Features of the ^{1}H-NMR and ^{13}C-NMR spectra of Pd(**3.3**)(allyl)Cl in DMSO-*d6* (Figure 3.10) mirror those of the bornyl-acetamide analogue Pd(**2.4**)(allyl)Cl. Resonances due to the allyl-ligand are found at ~ 4.97 ppm (H20, overlapped with H7), 3.79 ppm (*syn*-H21) and 2.76 (*anti*-H21).

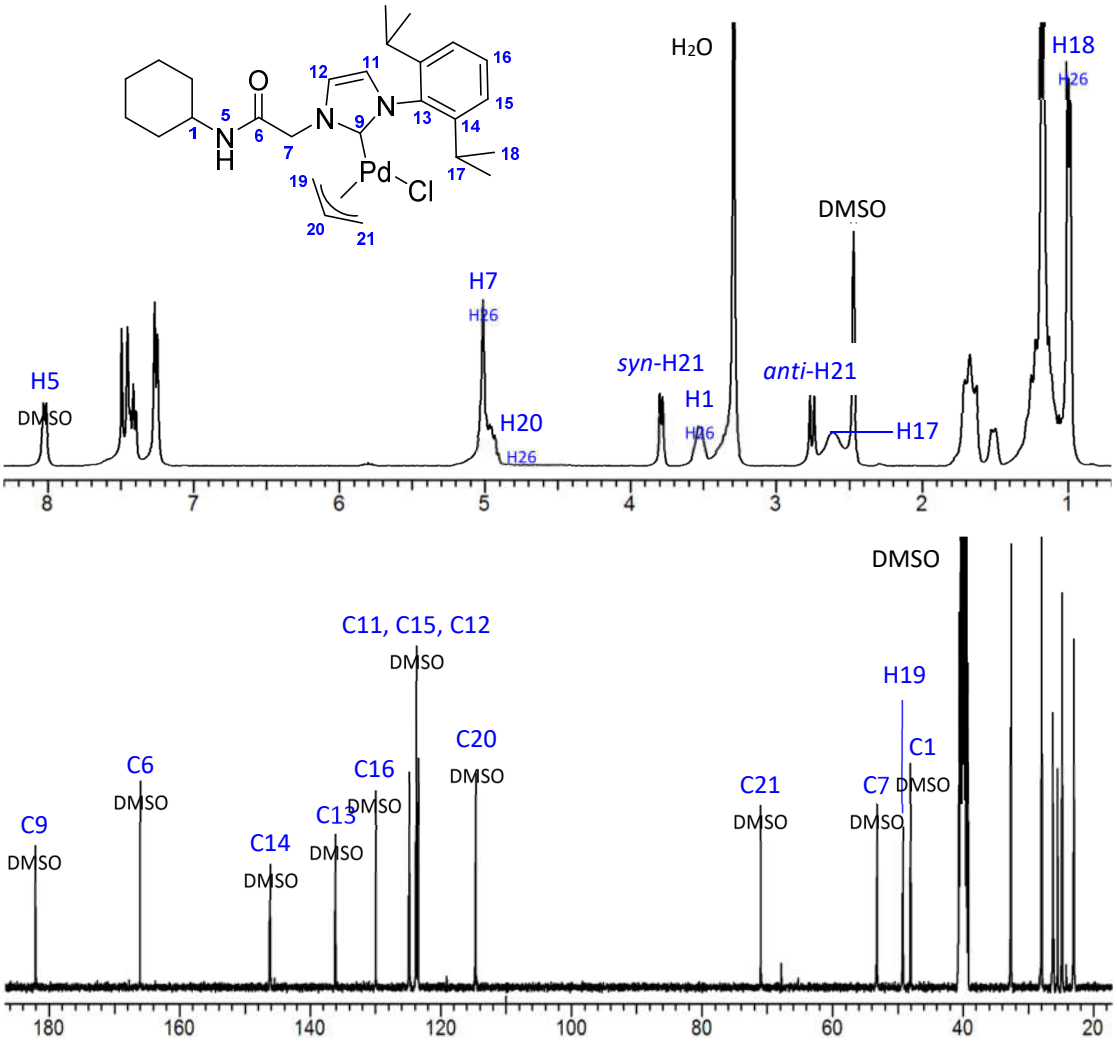

Figure 3.10: *The ^{1}H-NMR and ^{13}C-NMR spectra of Pd(**3.3**)(allyl)Cl in DMSO-*d6 *with selected signals highlighted.*

Note again that the allyl-proton environments pseudo-*cis* to the NHC (H25) are absent in the ^{1}H-NMR spectrum due to rapid allyl *syn*-*anti* interchange induced by the DMSO-*d6* solvent. Broadening of the spatially adjacent diisopropyl-phenyl methine proton signals (H23) is a further consequence of this. All allyl environments are accounted for in the ^{13}C-NMR spectrum at 114.75 ppm (C20), 71.01 (C21) and 49.30 (C19). Ligand **3.3** is readily identifiable by its carbenic carbon signal at 182.15 (C9) and an amide carbonyl resonance at 166.20 (C6). Proton resonances due to **3.3** are as expected with the exception of the amide N*H* environment H5 which resonates at 8.03 ppm, moderately downfield of the equivalent signal in the bornyl-acetamide analogue (~ 7.48 ppm). This is probably occurring because the cyclohexyl-appended amide N*H* is more exposed to hydrogen bond donation to the solvent than the comparatively shielded bornyl-appended amide. A similar relationship is seen in CD_3CN although to a lesser extent.

Isomerism in the ^{1}H-NMR spectrum of Pd(**3.3**)(allyl)Cl in CD_3CN is barely detectible compared with Pd(**2.4**)(allyl)Cl and is only significantly indicated by two singlets for the methylene proton environment (H6) at 5.06 ppm and 5.03 ppm and possible splitting of the H20 environment, although, this is obscured by the H6 signal. Signals due to the diisopropyl-phenyl environments H15 (~ 7.31 ppm) and H18 (~ 1.26 ppm and 1.05 ppm) are observed as multiplets that converge to doublets at higher temperature. Here, all allyl proton environments are observed including H19 which is pseudo-*cis* to the NHC and undetected in DMSO-*d6*. Allyl resonances in CD_3CN are 5.05 ppm (H20, overlapped with H7), 3.91 ppm (*syn*-H21), 3.18 (*syn*-H19), 2.88 ppm (*anti*-H21, overlapped with H17), 1.86 ppm (*anti*-H19). Two distinct methine H17 environments are also observed at 2.84 ppm (overlapped with *anti*-H21) and at 2.59 ppm. Observing separate diisopropyl-phenyl methine environments implies that rotation around the Pd – NHC bond is not occurring as rapidly on the NMR timescale as might be expected. Interestingly, in CD_3CN, the imidazolyl proton environments H11 and H12 at 7.38 ppm and 7.23 ppm couple to one another at a frequency of 1.96 Hz with a slight roof effect. Such coupling was not witnessed elsewhere in this study (or in the wider literature) and it is unknown why it arises for this complex. Because it is retained at high temperatures, it is unlikely to be an artefact of isomerism.

A variable temperature ^{1}H-NMR experiment in CD_3CN was performed to demonstrate the convergence and elimination of signals resulting in a spectrum resembling that in DMSO-*d6* (Figure 3.11). The findings here fortify the assertion that *syn-anti* interchange is a prominent feature of this complexes chemistry.

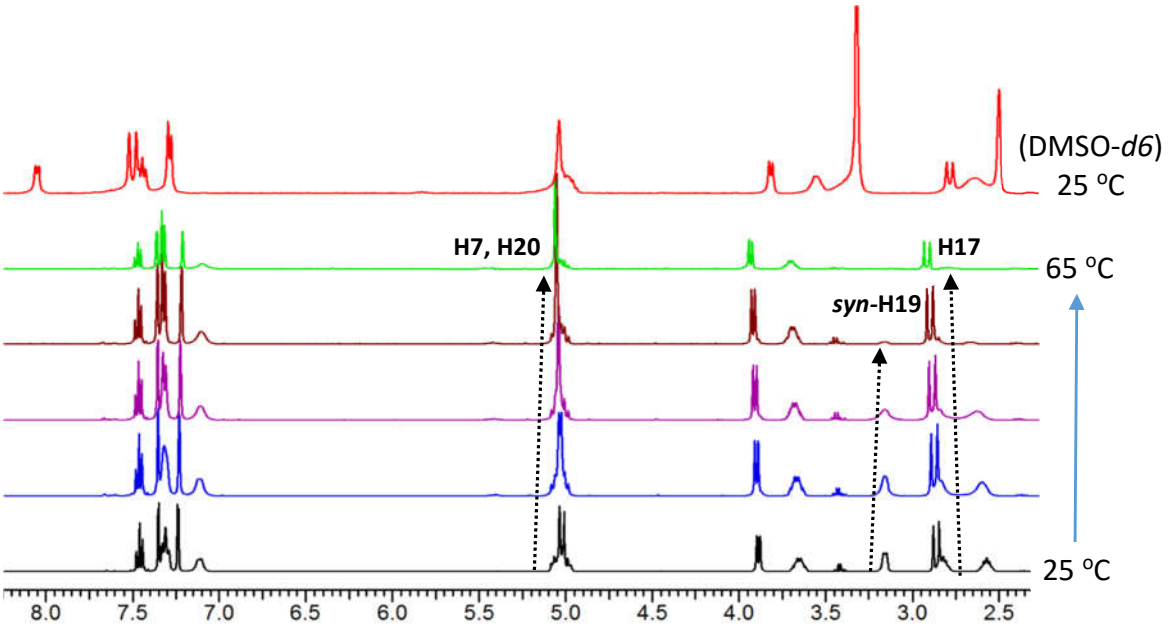

Figure 3.11: *Series showing a portion of the ^{1}H-NMR spectra of Pd(**3.3**)(allyl)Cl as a function of temperature in CD_3CN. Top spectrum in DMSO-*d6 *at 25 °C highlighting its similarity with the spectrum in CD_3CN at 65 °C.*

Convergence to a spectrum resembling that in DMSO-*d6* is observed at 65 °C. At this temperature, the methylene signals (H7) have merged into a neat singlet. Also both *syn* and *anti* H19 ally environments dissipate into the baseline as do the diisopropyl-phenyl methine H17 environments. That both methine signals disappear implies that rotation around the Pd – NHC bond also accelerates which is unsurprising. These observations are shared with the variable temperature analysis of Pd(**2.4**)(allyl)Cl and the conclusion drawn therein apply here.

Complex Pd(**3.3**)(allyl)Cl fulfilled its role as a structural reference for Pd(**2.4**)(allyl)Cl. Much less distinct isomerism due to *syn-anti* interchange is noted for Pd(**3.3**)(allyl)Cl, compared with the bornyl-acetamide species. This is important because it indicates that

the structure of the amide *N*-group influences the immediate ligand sphere of the Pd(II) centre. This is despite it being relatively remote to the Pd(II) in the non-chelated pendant arrangement. Greater differentiation in the electronic environments of the allyl ligand and NHC – acetamide ligand is observed for Pd(**2.4**)(allyl)Cl because the bulkier, more hydrophobic bornane group elicits greater conformation organisation of the overall complex. This restricts key proton environments on ligand **2.4** to report on changes in the allyl ligand (and *visa versa*). Ligand **3.3** can only achieve this to a limited extent.

3.4. Summarising remarks

Complexes Pd(**3.3 - H**)(*O,O'*-acac), Pt(**3.3 - H**)(*O,O'*-acac) and Pd(**3.3**)(allyl)Cl fulfilled their desired function as structural analogues to related complexes in the bornyl-acetamide series. More efficient *N*-amidate/NHC chelation by the less hindered cyclohexyl-amidate allowed Pd(**3.3 - H**)(*O,O'*-acac) and Pt(**3.3 - H**)(*O,O'*-acac) to be obtained in respective yields of 46% and 47%, by un-optimised purification methods. Comparison of X-ray crystal structures of Pd(**3.3 - H**)(*O,O'*-acac) and the bornane appended Pd(**2.4 - H**)(*O,O'*-acac) revealed how significantly the bornane unit crowds the metal centre in the *N*-amidate/NHC chelate form. These steric influences were also identifiable by ^{1}H-NMR contributing to signal broadening in the spectrum of Pd(**2.4 - H**)(*O,O'*-acac) as a result of slow conformational exchange relative to the NMR timescale.

Isolation and subsequent characterisation of Pd(**3.3**)(allyl)Cl bolstered the understanding of this compound class, particularly regarding the *syn-anti* interchange mechanism. This was aided greatly by an X-ray crystal structure of Pd(**3.3**)(allyl)Cl in which both *syn/anti* conformers were identified crystallographically.

3.5. Scope and future work

Cyclohexyl-acetamide NHC proligands have been shown to be applicable to similar synthesis as those used in the bornyl-acetamide NHC series. It is therefore possible to make additional achiral analogues such as the pyridyl/NHC chelated complex Pd(**3.4**)Cl_2 or an Ru(NHC)(arene) derivative such as [Ru(**3.2**)(*p*-cymene)Cl][PF_6]. These would be interesting as the cyclohexyl-amide chelates more readily than the bornyl-amide and hence could provide access to related structures but with an anionic-chelate. It would also be interesting to target the synthesis of Pd(**3.3**)(*O,O'*-acac)(γC-acac) for comparison with Pd(**2.4**)(*O,O'*-acac)(γC-acac) to improve understanding of it curious isomerism. As was true for Pd(**3.3**)(allyl)Cl, it may be possible to obtain a crystal structure of Pd(**3.3**)(*O,O'*-acac)(γC-acac) where it was not possible with Pd(**2.4**)(*O,O'*-acac)(γC-acac).

The availability of cyclohexylamine and relative ease of subsequent synthesis makes this a particularly cheap and accessible NHC ligand system. Furthermore, it is likely that the synthesis of Pd(**3.3 - H**)(*O,O'*-acac) could be developed into a simple, high yielding protocol, providing an abundant source of this organic soluble Pd(II) precatalyst.

Chapter 4

imidazo[4,5-f][1,10]phenanthroline derivatives

4.1. Introduction

NHCs derived from 1*H*-imidazo[4,5-f][1,10]phenanthroline **4.1** (Scheme 4.1) are a class of aromatic, heterodentate ligands capable of linearly bridging two metal centres (Figure 4.1). The imidazo[4,5-f][1,10]phenanthroline core of these compounds will here-in be referred to as IP. Several recent studies have reported the incorporation of IP-NHCs into heteronuclear complexes for applications including; carbon monoxide detection,[213, 214] solar driven hydrogen evolution,[215] in addition to the study of their photophysical properties.[216] Their synthetic utility is based on the selective conversion of the imidazolium component into an NHC ligand. This facilitates the stepwise assembly of dinuclear complexes by enabling the bidentate phenanthroline to be coordinated first, followed by coordination of another metal at the NHC terminus (Figure 4.1).

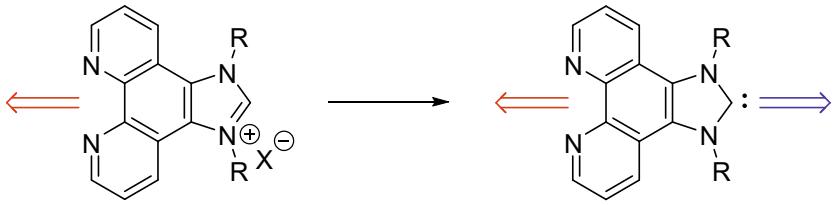

phenanthroline-imidazolium salt ***phenanthroline-NHC***

Figure 4.1: *The stepwise assembly dinuclear complexes with imidazo[4,5-f][1,10]phenanthroline (IP) based NHCs.*

This approach could likewise be applied to the preparation of a ruthenium(II) polypyridyl complex fused to an NHC ligand for metal mediated catalysis (Figure 4.2). This assembly was considered an interesting target for evaluating the electronic influence of the bound ruthenium(II) complex on catalysis more so than its stereochemical influence. It was expected (and has since been established)[216] that the bridging IP ligand would facilitate electronic communication between the two nuclei. However, the relative orientation, and large distance between the catalytic centre and enantiomeric component was deemed too large to enable any form of stereocontrol. Unfortunately, the investigation

of these systems was hampered by synthetic difficulties and ultimately energy was diverted towards systems more amenable to use in enantioselective synthesis. Regardless, several interesting new IP based ligands were developed along with complexes of the type $[Ru(bipy)_2(IP)]^{n+}$. Furthermore, UV-visible and fluorometric analysis on these compounds revealed some curious photophysical properties in several derivatives. Despite recent advances in the literature their application in homogeneous catalysis for organic manipulations remains unexplored.

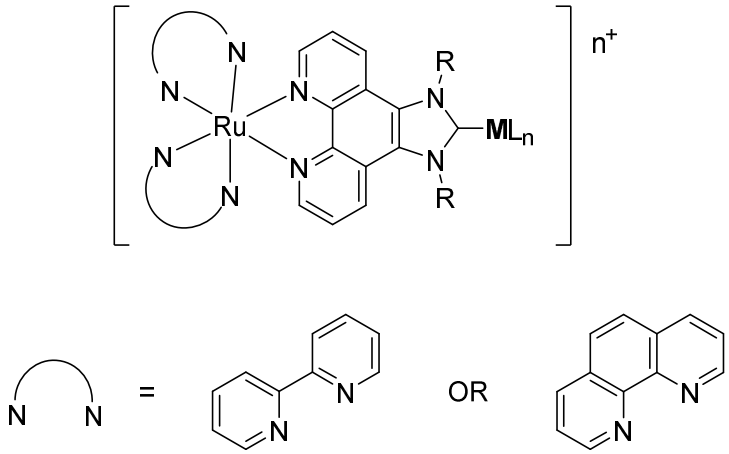

Figure 4.2: *General structure of 1,10-phenanthroline-annelated (IP) NHC complexes with coordinated ruthenium-polypyridine complex and catalytic metal centre M.*

4.2. Synthesis of 1,10-phenanthroline annelated NHC precursors

4.2.1. General route to 1,10-phenanthroline annelated imidazolium salts

Synthesis of several IP imidazolium salts was attempted by stepwise *N*-substitution of 1*H*-imidazo[4,5-f][1,10]phenanthroline (**4.1**) (Scheme 4.1). This approach was appealing because the parent imidazole **4.1** is easily prepared from 1,10-phenanthroline in a two-step process beginning with conversion to 1,10-phenanthro-5,6-dione.[217] Annulation

with ammonium-acetate and formalin in acetic acid gives **4.1** in an overall 82% yield (Step 1, Scheme 4.1).[218]

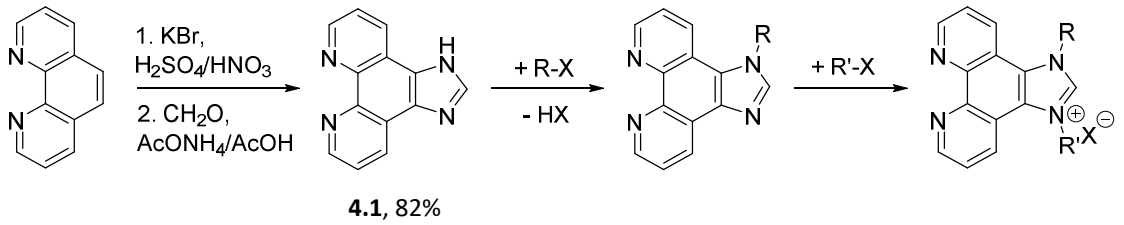

4.1, 82%

Scheme 4.1: *Synthesis of 1,10-phenanthroline annelated imidazolium salts.*

Another possible route by the cyclisation of a substituted diimine (Route A, Scheme 1.12, Chapter 1), was also trialled but found to be infeasible. This was because no 1,10-phenanthroline-5,6-diimines could be prepared from 1,10-phenanthroline-5,6-dione with either aniline or less hindered alkyl-amines. Several imine-condensation protocols were followed including using $TiCl_4$ as a strong Lewis acid, but none provided any evidence of product formation.

4.2.2. *N*-substituted imidazo[4,5-*f*][1,10]phenanthrolines

Three mono-substituted IP derivatives, shown in Figure 4.3 were prepared from **4.1** (Step 3, Scheme 4.1). The mono-benzylated 1-benzyl-imidazo[4,5-*f*][1,10]phenanthroline **4.2** was prepared under dry conditions by the reaction of the parent imidazole with benzylbromide in DMF at 100 ^oC using K_2CO_3 as base. Under these conditions the product **4.2** could react with another equivalent of benzylbromide resulting in di-substituted salts. Loss of product this way may account for the moderate yield of 47%, however, due to the availability of the starting material little effort was made to improve this. The mono-arylated derivatives 1-phenyl-imidazo[4,5-*f*][1,10]phenanthroline (**4.3**) and 1-(2-pyridyl)-imidazo[4,5-*f*][1,10]phenanthroline (**4.4**) were prepared by a pseudo-Ullmann coupling using $Cu(OAc)_2$ as the source of Cu

catalyst. Initially the synthesis of **4.3** was attempted following a literature procedure for arylation of various azoles.[219] The reaction was carried out under conditions similar to those used for **4.2** but with iodobenzene and 1.0 mol% $Cu(OAc)_2$. After 24 hours only a trace amount of product was observed so the reaction was repeated using a 5 mol excess of iodobenzene and a larger catalyst loading of 10 mol% $Cu(OAc)_2$. This provided a product yield of 22% after an aqueous work up and continued modification of the procedure achieved an optimal yield of 60%. It was found that refluxing the reaction mixture for one hour before addition of the $Cu(OAc)_2$ catalyst improved the yield greatly, probably by allowing sufficient time for the relatively insoluble **4.1** to concentrate in solution.

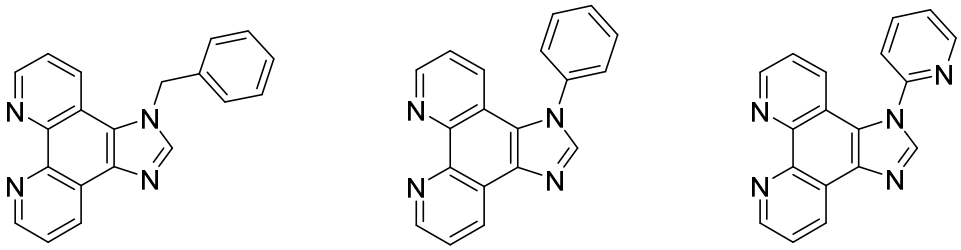

4.2, 47% **4.3**, 60% **4.4**, 45%

Figure 4.3: *Mono-substituted imidazo[4,5-f][1,10]phenanthroline derivatives **4.2**, **4.3**, and **4.4**, and their synthetic yields.*

The same methodology was applied to the synthesis of **4.4** which was obtained in a 45% yield using 2-bromopyridine as the aryl-halide. A more direct synthesis has since been published in which several 1-aryl-imidazo[4,5-*f*][1,10]phenanthroline compounds are prepared from 1,10-phenanthro-5,6-dione by an in situ annulation reaction with an aryl-amine, ammonium-acetate and formalin.[220] This produces **4.3** in a 79% yield. No synthesis of **4.4** has been reported and given the poor nucleophillicity of 2- and 4-aminopyridines preparation by the above mentioned approach would be unsuitable.

The aromatic regions of the ^{1}H-NMR spectra of **4.2**, **4.3** and **4.4** in $CDCl_3$ are shown in Figure 4.4.

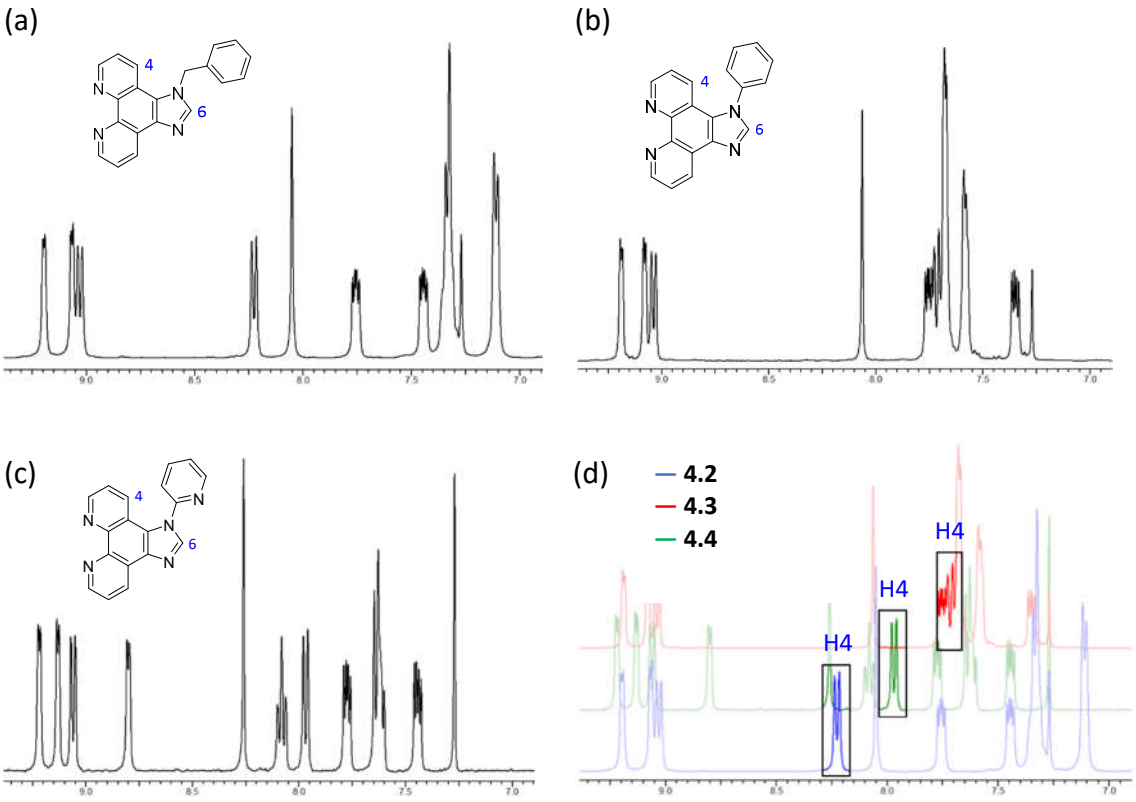

Figure 4.4 (a-c): *Aromatic region of ^{1}H-NMR ($CDCl_3$) spectra of* ***4.2, 4.3*** *and* ***4.4****,* ***(d)*** *collated spectra with H4 proton signals highlighted.*

The chemical shift of signals due to proton environments on the IP core are relatively conserved with the exception of H4 and H6. In the ^{1}H-NMR spectrum of **4.2** the H4 doublet occurs at 8.23 ppm but is shifted upfield in the spectra of **4.3** and **4.4** to 7.72 ppm and 7.93 ppm, respectively. This is most likely the result of anisotropic shielding of the H4 proton by the aryl pendant substituent which will occur if H4 is projected toward the face of the phenyl or pyridyl side-group. The aryl-substituents must therefore be rotated out of the molecular plane. The position of the singlet H6 proton signal is similar in the spectra of **4.2** and **4.3** (8.05 ppm and 8.06 ppm respectively) but is shifted downfield in the spectrum of **4.4** to 8.23 ppm. This is a consequence of electron withdrawal by the π-deficient pyridine substituent and may also explain the higher chemical shift of the H4 proton of **4.4** compared with that of **4.3**.

4.2.3. 1,10-phenanthroline annelated imidazolium salts

Conversion of these N-substituted IP derivatives into imidazolium salts (Step 3, Scheme 4.1) was attempted with varying degrees of success. Synthesis of 1,3-benzyl-1*H*-imidazolium[4,5*f*][1,10]phenanthroline bromide (**4.5.HBr**) was achieved by refluxing **4.2** in chloroform with excess benzylbromide for two days (Scheme 4.2). The resultant precipitate was collected by filtration and washed with additional chloroform to give the pure product in 62% yield. NMR and mass-spectrometry for **4.5.HBr** matched data which was reported after our synthesis.[215] This compound appeared to be unstable under aqueous conditions, isomerising to give other *N*-benzylated salts **[4.6]**$^+$ and **[4.7]**$^+$, or regenerating the mono-substituted precursor **4.2** (Scheme 4.2)**.**

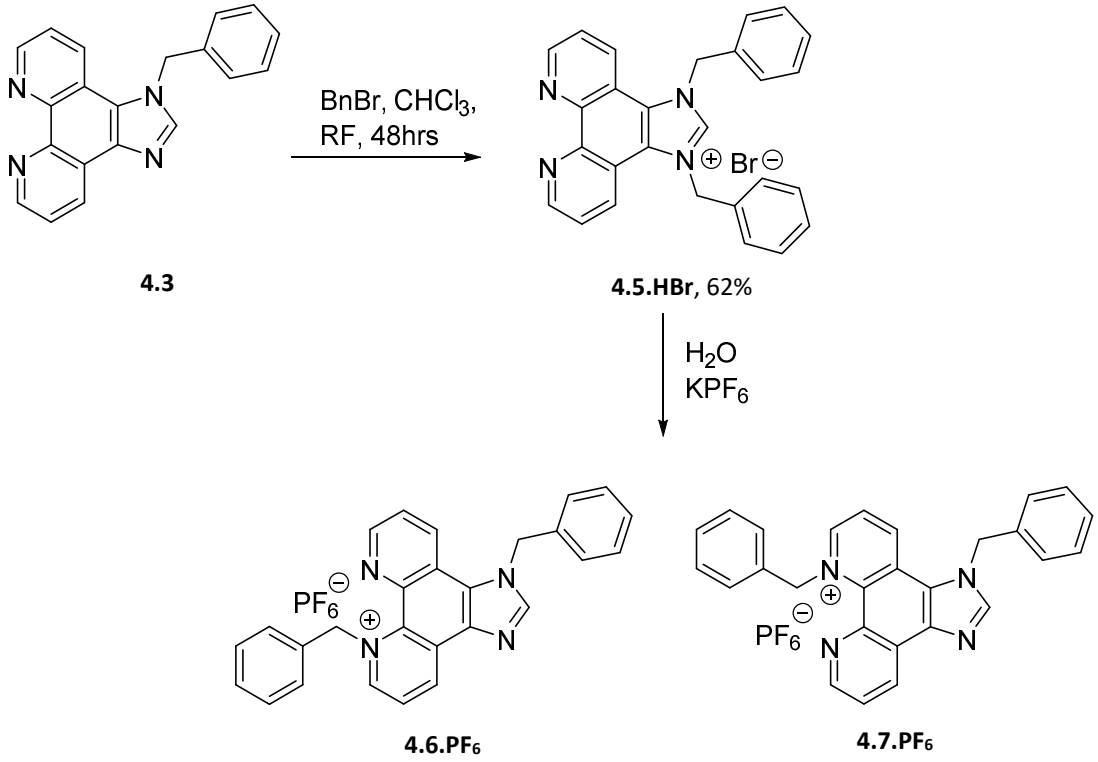

4.3 **4.5.HBr**, 62% **4.6.PF$_6$** **4.7.PF$_6$**

Scheme 4.2: *Synthesis of* ***4.5.HBr*** *and conversion to phenanthrolin-(*N*-benzyl)-ium salts* ***[4.6]***$^+$ *and* ***[4.7]***$^+$ *in aqueous media.*

This was noted when, in an attempt to improve its organic solubility, **[4.5.H]**$^{+}$ was precipitated as its PF_6 salt by addition of KPF_6 to an aqueous solution of **4.5.HBr** at room temperature. The product obtained was bright yellow (instead of the faint orange of **4.5.HBr**) and its ^{1}H-NMR spectrum showed a mixture of several products. The mass-spectrum still showed a major signal which matched **[4.5.H]**$^{+}$ but also a signal due to **4.2**. Using flash column chromatography on alumina with 9:1 DCM/MeOH, **4.2** was separated from the two phenanthrolin-(*N*-benzyl)-ium salts **4.6.PF$_6$** and **4.7.PF$_6$**, which eluted as a single bright yellow band and were obtained as a mixture. No **4.5.HPF$_6$** could be eluted from the column.

Crystals of **4.6.PF$_6$** suitable for single-crystal X-ray diffraction were grown by slow vapour-diffusion of diethyl-ether into a DCM solution of the mixture. Compound **4.6.PF$_6$** crystallised in the monoclinic space group $P2_1/c$, with one molecule of **[4.6]**$^{+}$ and a PF_6 anion present in the asymmetric unit (Figure 4.5).

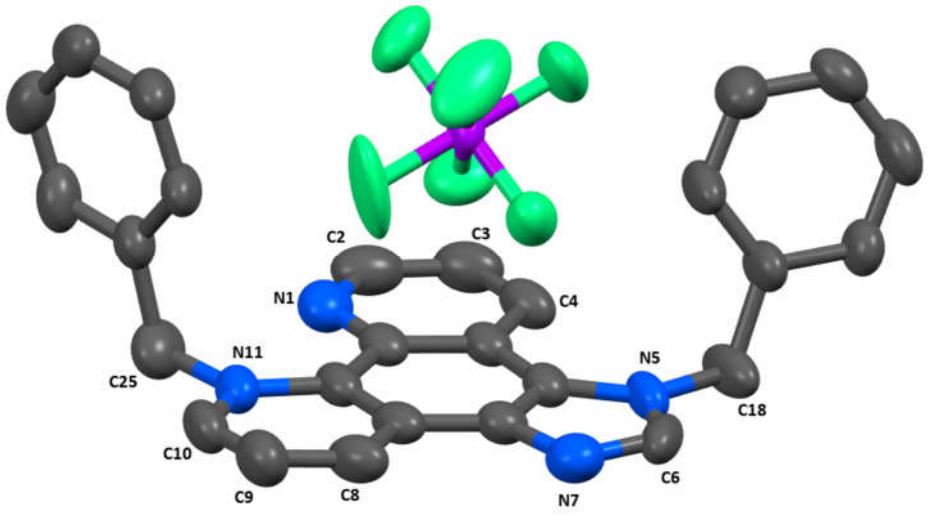

Figure 4.5: *Asymmetric unit of **4.6.PF$_6$**. Hydrogen atoms have been omitted for clarity. Thermal ellipsoids are drawn at a 50% probability level.*

This structure unambiguously shows benzyl substitution at the N11 position instead of at the desired N7 position and the presence of a PF_6 counter-ion provides further

evidence of salt formation. The nitrogen atoms N5 and N11 that are each bonded to a methylene carbon remain conjugated as indicated by their trigonal planar geometry and the internal angles around the N5 and N11 centres which sum to 360.0(4)° and 359.8(4)°, respectively. A layered packing arrangement arises from the surficial alignment of the planar IP cores. Each layer has a front-to-front interface where the benzyl-groups face towards the opposing surface and a back-to-back interface where they face away. At the front-to-front interface, edge-to-face π – π interactions occur between the N5 and N11 benzyl groups (C to centroid distance = 3.538(6) Å and 3.742(6) Å) and N1 pyridyl ring and N11 benzyl group (C to centroid distances = 3.720(6) Å) of opposite molecules. A slipped face-to-face interaction between the imidazole and N11 pyridyl ring (centroid to centroid distances 3.569(3) Å) occurs at the back-to-back interface. Each PF_6 anion is involved in a number of short C*H* ··· F contacts with five molecules of **[4.6]**$^+$ (C ··· F = 3.198(6) Å to 3.600(6) Å) and is participating in weak hydrogen bonding with H6 (C ··· F = 3.206(5), C – H ··· F angle = 160.0(4)°).

These same crystals were used in NMR and mass-spec analysis allowing **4.6.PF$_6$** to be fully characterised. Although isomer **4.7.PF$_6$** was unable to be isolated the remaining, unassigned signals in the ^{1}H-NMR spectrum of the mixture could be attributed to the proposed structure (Figure 4.6).

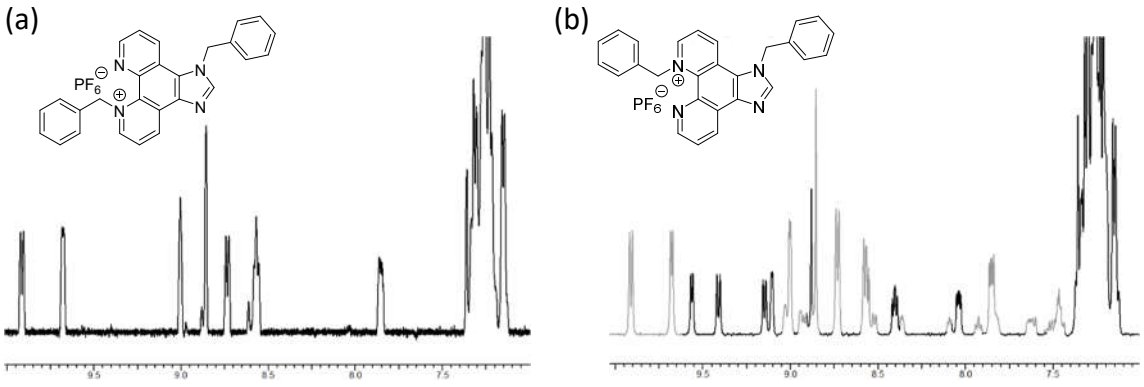

Figure 4.6 (a): *Aromatic region of ^{1}H-NMR (DMSO-*d6*) spectra of **4.6.PF$_6$** and, **(b)** of the mixed material with signals due to **4.7.PF$_6$** highlighted.*

The isomerisation and decomposition reactions undergone by **[4.5.H]**$^{+}$ are understandable considering the well-known lability of benzyl substituents especially when appended to a quaternary azole nitrogen.[221] Although this conversion was not explored in depth the evident instability of **[4.5.H]**$^{+}$ suggested that benzyl pendant groups are unsuitable for NHC precursors in this system. This assessment is explored further in section 4.4.2.

Phenyl-appended imidazolium salts based on **4.3** were identified as useful NHC precursors because the phenyl pendant offers greater steric shielding of the carbene centre when compared with benzyl and *n*-alkyl groups. The synthesis of several such derivatives including a 1-Phenyl-3-butyl-1*H*-imidazolium[4,5*f*][1,10]phenanthroline salt **[4.8.H]**$^{+}$ and 1-Phenyl-3-methyl-1*H*-imidazolium[4,5*f*][1,10]phenanthroline salt **[4.9.H]**$^{+}$ and a symmetrical 1,3-bis-phenyl-1*H*-imidazolium[4,5*f*][1,10] phenanthroline salt **[4.10.H]**$^{+}$ was attempted (Figure 4.7).

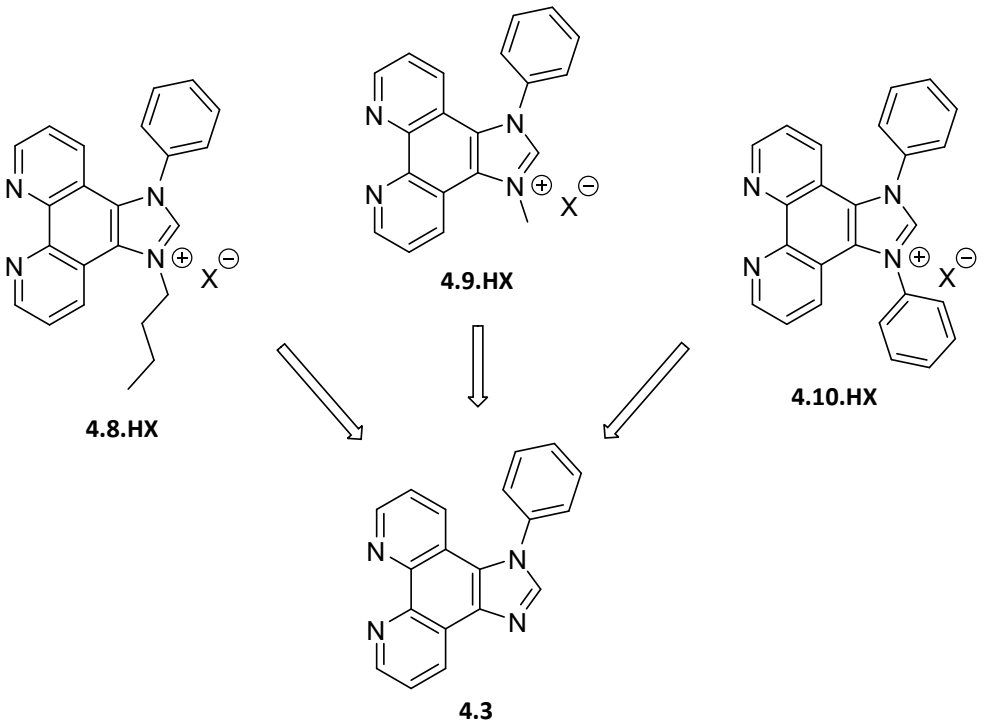

Figure 4.7: *Imidazolium[4,5*f*][1,10]phenanthroline salts derived from* ***4.3.***

The synthesis of **4.8.HI** was attempted based on a procedure for appending an *n*-butyl group to form a similar compound.[213] Surprisingly, using these conditions with **4.3** and excess 1-iodobutane, only the phenanthrolin-(*N*-butyl)-ium iodide salts **4.11.I** and **4.12.I** were formed (Scheme 4.3). The ^{1}H-NMR spectrum of the product mixture showed that these were present in a 2.2:1 ratio of **4.11.I**: **4.12.I**. Some starting material was retained but none of the desired **4.8.HI** was detected. Gradient flash chromatography on alumina with 2% - 5% MeOH/DCM provided a sufficient amount of pure **4.11.I** and **4.12.I** for characterisation, however, poor chromatographic resolution meant the majority remained mixed. The overall yield of **4.11.I** and **4.12.I** was 53%.

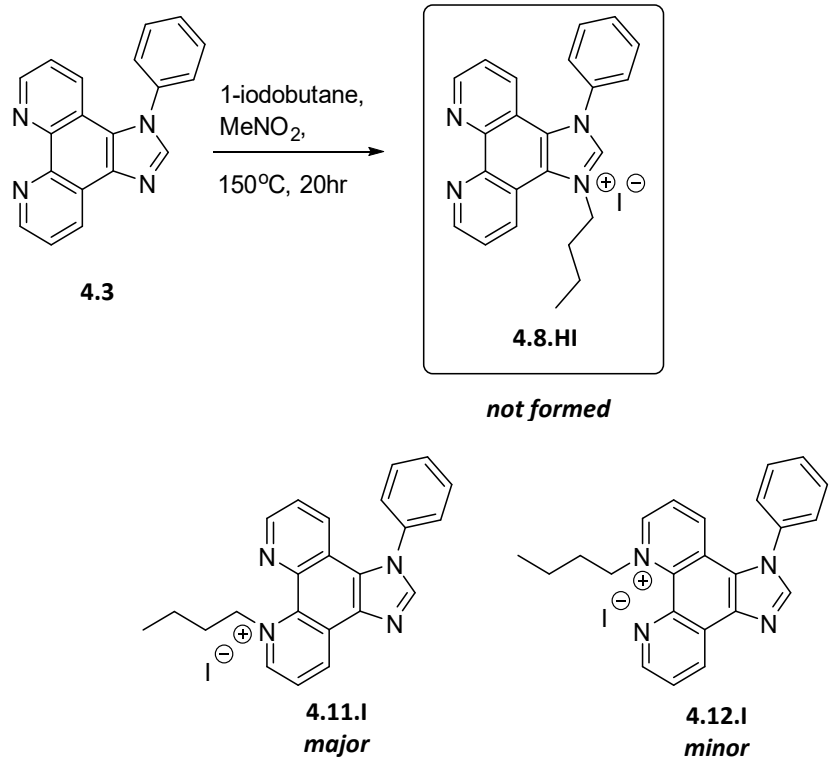

Scheme 4.3: *Formation of **4.11.I** and **4.12.I** from the attempted synthesis of **4.8.HI**.*

Both products gave identical mass-spectra as expected but could be clearly distinguished by ^{1}H-NMR spectroscopy (Figure 4.8). In each case all signals due to protons bonded to the core IP unit were shifted downfield relative to those of the

starting material **4.3.** However, protons bonded to the *N*-substituted pyridine ring were shifted to the greatest extent (Δδ > 0.7 ppm) with the most affected signals being those of the proton environments adjacent to the newly quaternised nitrogen centre. For **4.11.I** this signal (H10) arrived at 10.33 ppm, shifted from 9.19 ppm in **4.3** (Δδ = 1.14 ppm) and for **4.12.I** (H2), at 10.16 ppm from 9.08 ppm in **4.3** (Δδ = 1.08 ppm).

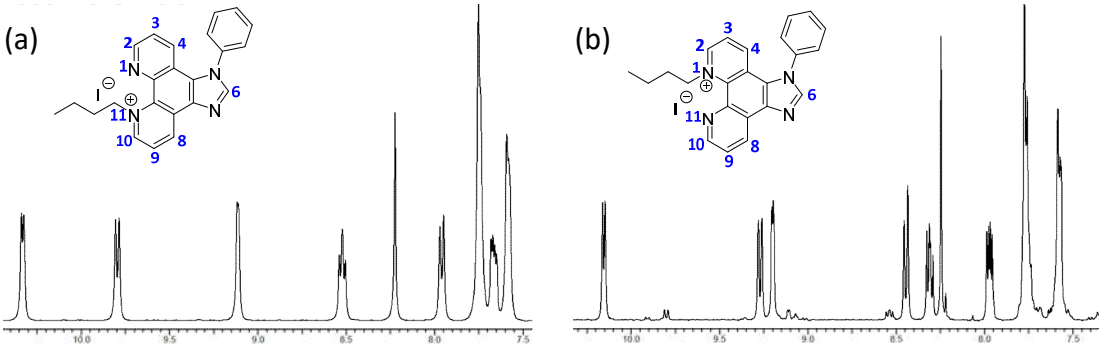

Figure 4.8 (a): *Aromatic region of ^{1}H-NMR spectra of* ***4.11.I*** *in $CDCl_3$ and,* ***(b)*** *of* ***4.12.I.***

The structure of **4.11.I** was verified by single-crystal X-ray analysis for which suitable crystals were grown by slow evaporation chloroform solution spiked with toluene. Compound **4.11.I** crystallised in the triclinic space group $P\bar{1}$, with two molecules of **[4.11]**$^{+}$ (A and B) and two iodine anions present in the asymmetric unit (Figure 4.9). Molecules A and B are differentiated by their butyl chain conformations as well as numerous other bond lengths and angles. The lengths of bonds to the quaternary nitrogen are N11 – C10 (A / B) = 1.351(4) Å / 1.349(4) Å and N11 – C17 (A/B) = 1.389(3) Å / 1.393(3) Å. These are elongated when compared with the same bond lengths in unsubstituted 1*H*-imidazo[4,5-f][1,10]phenanthroline (1.326(3) Å and 1.355(3) Å)[222] due to a reduction in π-bonding character as a result of the nitrogen cation. The observed warping of the polyaromatic IP core is represented by several moderate torsion angles including (A / B) C18-N5-C14-C13 = 25.3(4)° / 20.4(3)°, N5-C14-C13-C4 = 8.6(4)° / 11.5(4)° and N1-C12-C17-N11 = 14.5(3)° / 14.8(3)°. This is evidence of the steric strain imposed by the *N*-substituents, however, the differences in the torsion angles across the same

bonds in molecules A and B suggests that maximisation of π – π surface contacts is also partially responsible.

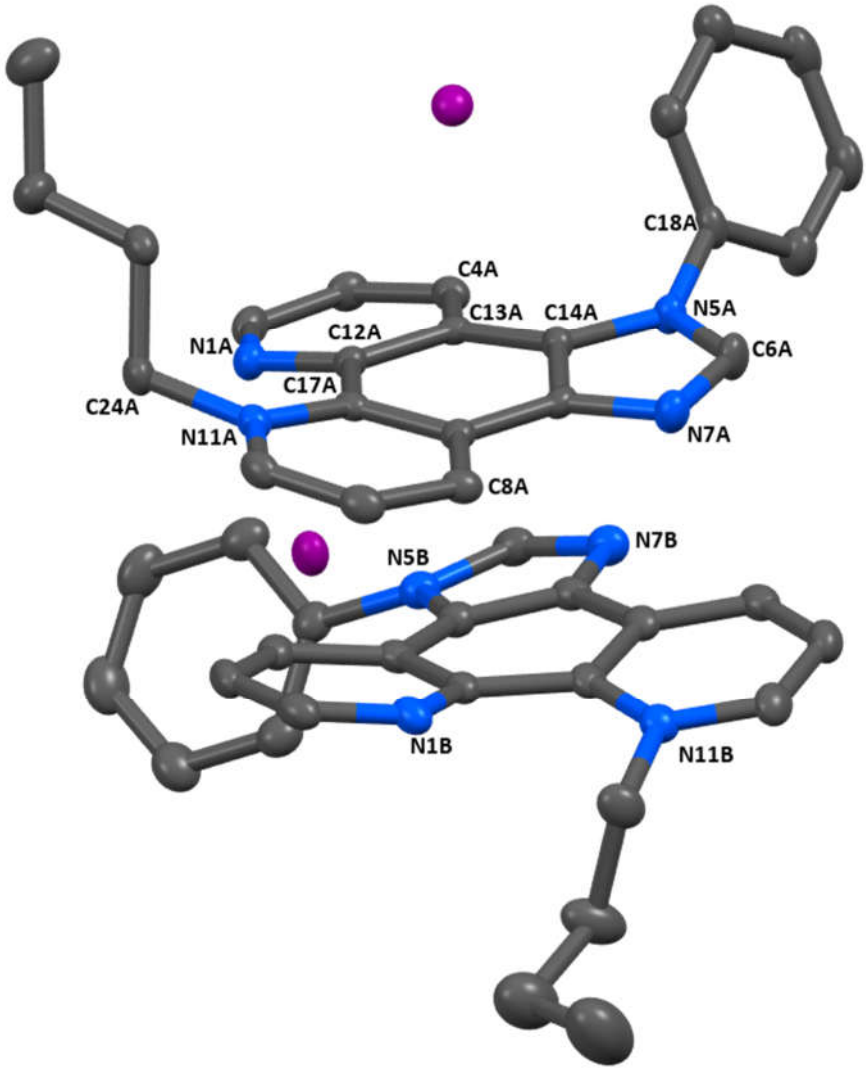

Figure 4.9: *Asymmetric unit of* ***4.11.I****. Hydrogen atoms have been omitted for clarity. Thermal ellipsoids drawn at 50% probability.*

Close, face-to-face π – π stacking occurs between the central benzenoid rings of each IP unit (centroid-to-centroid distance [shift] = 3.5073(15) Å [0.572(4) Å / 0.400(4) Å]). The peripheral rings are also in close contact but with a larger offset (centroid to centroid distance [shift] = 3.510(2) Å [1.409(4) Å / 0.980(4) Å], 3.821(2) Å [1.511(4) Å / 1.196(5) Å] and 3.601(2) Å [1.336(5) Å / 1.323(4) Å]). Various π – π, C*H* ··· π and C*H* ··· I interactions

are observed in the packed structure. Hydrogen bonding between N7 and H8 is also observed (C8 ··· N5 = 3.367(4) Å, C8 – H8 ··· N5 angle = 171.6(2)^{o}). The electron deficiency of C8 due to mesomeric electron withdrawal onto the pyridinium nitrogen renders it a feasible hydrogen bond donor.[223]

Despite the clear regioselectivity issues associated with these molecules, success could be had with a slightly more potent electrophile. This was demonstrated by substituting 1-iodobutane with iodomethane to produce **4.9.HI** in a 32% yield under analogous conditions (Scheme 4.4).

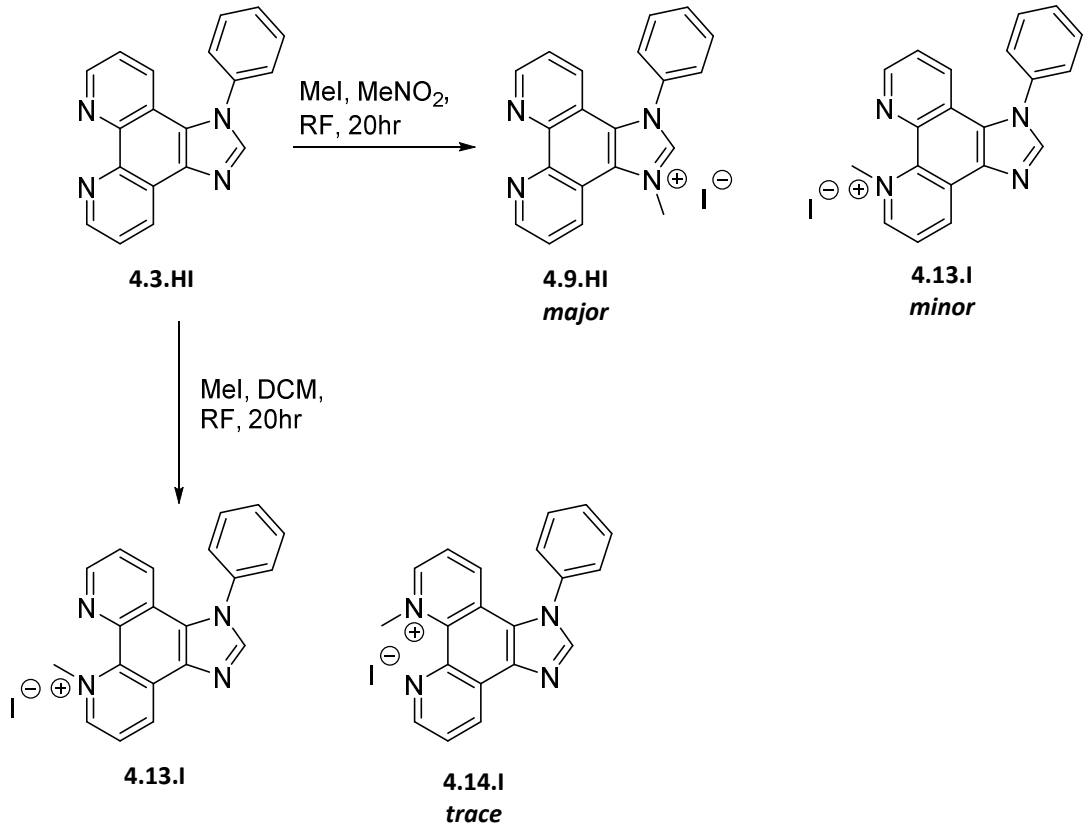

Scheme 4.4: *Synthesis of* ***4.9.HI*** *and the regioisomeric phenanthrolin-(*N*-methyl)-ium salt* ***4.13.I.***

A crude material which was precipitated from the reaction mixture by addition of Et_2O, was shown by ^{1}H-NMR to be a mixture of both **4.9.HI** and **4.13.I** in a 2:1 ratio. Washing

with warm DCM removed **4.13.I** into a bright yellow filtrate leaving pure **4.9.HI** as an off white solid. When the reaction was performed in refluxing DCM no imidazolium salt was formed and the only material isolated, other than starting material, was **4.13.I** although, a trace amount of **4.14.I** was detected by NMR.

Again NMR was indispensable in distinguishing which regiosomers had formed. As well as the emergence of a signal due to methyl-protons, compound **4.9.HI** could be readily identified by the downfield singlet that is characteristic of the imidazolium NC*H*N proton (H6). This was found at 10.15 ppm (Figure 4.10a). Likewise, **4.13.I** produced an ^{1}H-NMR spectrum with the anticipated large downfield shift of protons in the vicinity of the formal positive charge. The most downfield signal, at 10.38 ppm, belonged to the proton adjacent to the methylated nitrogen (H10) as expected (Figure 4.10b).

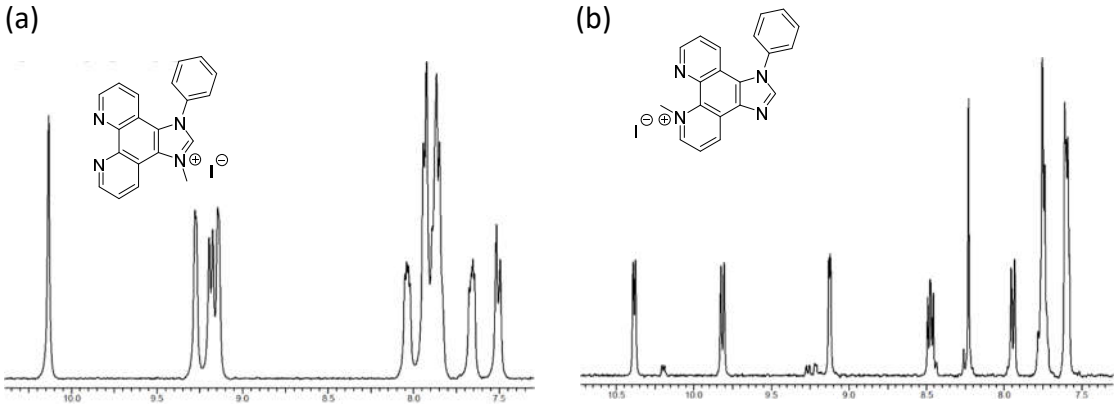

Figure 4.10 (a): *Aromatic region of ^{1}H-NMR spectra of **4.9.HI** in CD_3CN and, **(b)** of **4.13.I** in $CDCl_3$ with a signals due to **4.14.I** evident along the baseline.*

Remarkably, neither synthesis produced more than a trace amount of the third possible regioisomer **4.14.I**. Of the two phenanthrolinium salts the one formed by substitution at the phenanthroline nitrogen nearest the substituted nitrogen of the imidazole (N1) is less favoured in both examples (**4.12.I** and **4.14.I**). Neither position offers any obvious advantages for electronic stabilisation of the pyridinium-cation hence the selectivity may have a steric basis. The x-ray crystal structure of **4.11.I** shows a pronounced warping of the IP body structure to accommodate substitution of the phenanthroline nitrogen

(Figure 4.9). It is probable that substitution at the phenanthroline nitrogen furthest from the phenyl ring as in **4.11.I** and **4.13.I** invokes a less strained distortion than when it occurs at the nearest site as in **4.12.I** and **4.14.I**.

Of the three target phenyl-appended imidazolium salts, **[4.10.H]$^+$** is expected to be the most stable and, the much bulkier phenyl group should favour substitution at the imidazole nitrogen, surmounting the regioselectivity issues discussed previously. Typically, bis-aryl imidazolium salts such as **[4.10.H]$^+$** are formed through an annulation reaction between an aryl-diimine and a C1-electrophile but, as mentioned previously, this approach is not applicable to this system. Therefore, the preparation of **[4.10.H]$^+$** from **4.3** requires *N*-aryl quarternisation of the imidazole nitrogen. This can be performed using a very electron deficient aryl-halide such as 2,4-dinitrochlorobenzene,[224] or some pyridyl-halides,[101] but for a poor aryl electrophile such as benzene an extremely effective leaving group is necessary. The hypervalent-iodine compound diphenyliodonium triflate, in which iodobenzene acts as the leaving group, has been demonstrated as a useful reagent for forming phenyl-substituted imidazolium salts assisted by a Cu(II) catalyst.[225] Such a procedure was adapted for the synthesis of **4.10.HOTf** (Scheme 4.5), however, despite observing the consumption of diphenyliodonium triflate by ^{1}H-NMR, the starting material was conserved.

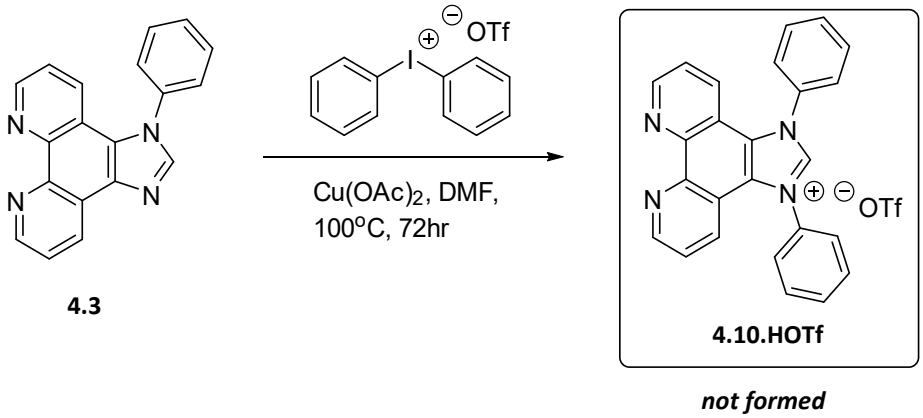

4.3

4.10.HOTf

not formed

Scheme 4.5: *Attempted synthesis of* ***4.10.HOTf****.*

Although this is a synthetically interesting approach, fine tuning was clearly needed and given the various difficulties already encountered with this system it was not pursued further. A more robust strategy for *N*-aryl quarternisation which emerged after this attempt employs coupling using arylboronic acids to prepare imidazolium salts.[226]

The synthesis of imidazolium salts using **4.4** will be discussed in section 4.4.2.

4.3. Photophysical properties of substituted IP derivatives

Interestingly, substitution of the phenanthroline nitrogen to form the phenanthrolinium salts **4.6.PF$_6$**, **4.7.PF$_6$**, **4.11.I**, **4.12.I** and **4.13.I** induced a colour change from the very faint yellow/off-white of the mono-substituted precursors **4.2** and **4.3**, to a vivid yellow. The imidazolium salts **4.5.HBr** and **4.9.HI** on the other hand were a faint yellow/brown. To better understand and quantify this observation an analysis of the absorption and emission properties of these compounds was undertaken. The key spectral features are summarised in Table 4.1.

Table 4.1: *Summary of the absorption and emission maxima of IP derivatives.*

	absorption		emission		absorption		emission
	λ_{max} (nm)	ε (Lmol^{-1}cm^{-1})	λ_{max} (nm)		λ_{max} (nm)	ε (Lmol^{-1}cm^{-1})	λ_{max} (nm)
4.2	252, 283 340, 355	25780, 13074 1130, 819	388	**4.11.I**	257, 301 389	31374, 30465 2954	482
4.3	253, 283 339, 354	32596, 11269 1034, 697	388	**4.12.I**	227, 252 303, 391	23185, 22134 17366, 1626	499
4.4	282, 337 354	15838, 679 368	388	**4.13.I**	235, 255 302, 389	22738, 20801 15675, 1945	482
4.9.HI[a]	244, 270(sh) 319, 336	69147, 20580 943, 547	462				

[a] Recorded in MeCN, all others recorded in DCM.

The UV-visible absorption spectra of the three mono-substituted derivatives (Figure 4.11a) display similar absorption maxima at ~ 384 nm and ~ 255 nm, however, compound **4.4** produced a significantly broadened curve. Having an *N*-appended aryl substituent (**4.3** and **4.4**) caused no appreciable increase in molar absorptivity when compared with the benzyl-appended **4.2**. This suggests that neither aryl π-system is significantly conjugated with the IP core, further evidence that the two ring systems are anti-planar in solution. The aryl substituents do, however, increase absorption below ~ 250 nm. All spectra exhibit weak absorption features at ~ 338 nm and ~ 354 nm which contribute to their faint yellow colouration. Evidently the electronic structure of the electron rich IP core is not sensitive to these differences in the imidazole nitrogen substituent.

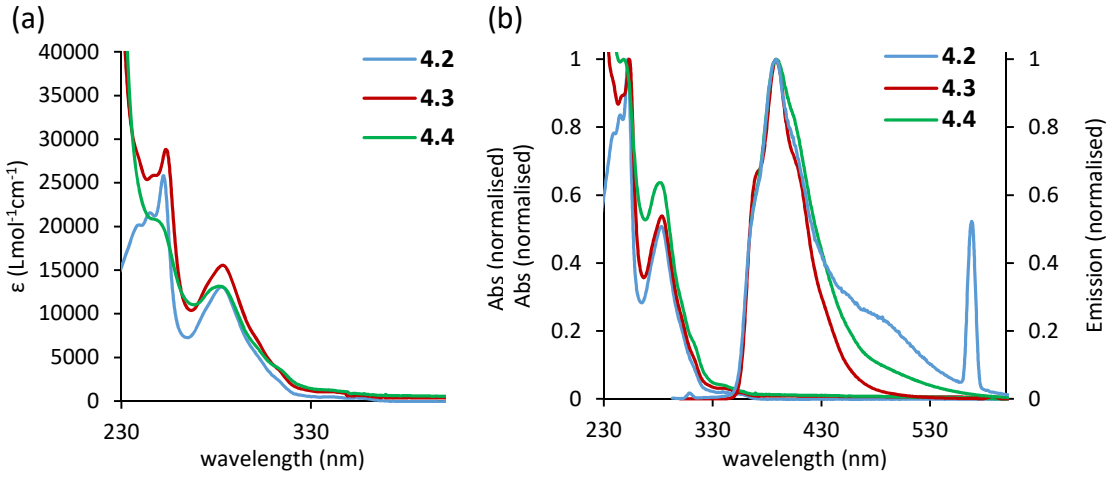

Figure 4.11 (a): *UV-visible spectra and,* ***(b)*** *UV-visible with overlaid photoluminescence spectra of* ***4.2***, ***4.3***, *and* ***4.4*** *in DCM at room temperature, concentration ~ 10^{-5} molL^{-1}.*

Excitation at ~ 284 nm results in emission at λ_{max} = 388 nm for all three derivatives (Figure 4.11b). Compounds **4.3** and **4.4** produce fairly sharp emission curves with **4.3** displaying an emerging fine structure. The spectrum of **4.2** however, is distinguishable by a shoulder of emissive intensity around ~ 490 nm. This may be because the flexible benzyl group of **4.2** enables more vibrational relaxation pathways than the conformationally restricted aryl rings of **4.3** and **4.4**.

The UV-visible absorption spectra of the three phenanthrolinium salts derived from **4.3** is shown in Figure 4.12a. These all feature similar intense absorption in the ultraviolet region with λ_{max} ~ 235 nm and ~ 255 nm. The lowest energy $\pi - \pi^*$ transition which occurs at 283 nm in **4.3** is slightly red-shifted to ~ 300 nm in **4.11.I**, **4.12.I** and **4.13.I**. This is consistent with a lowering of the LUMO energy due to the electron acceptor ability of the pyridinium cation. Furthermore, torsional distortion, such as that observed in the XRD structure of **4.11.I**, may contribute to HOMO destabilisation by reducing the π-orbital overlap.[6] Compound **4.11.I** absorbs at twice the intensity of **4.12.I** and **4.13.I**, the reason for this is not yet understood.

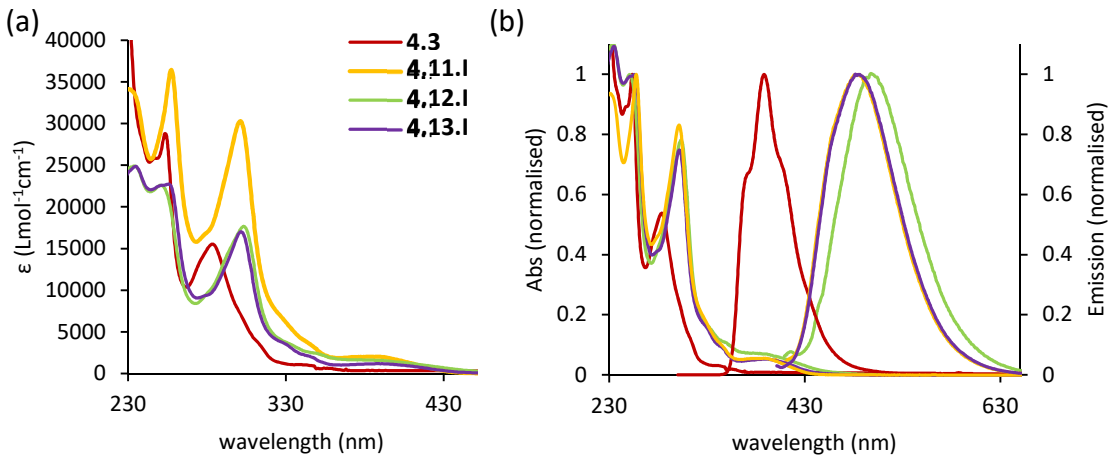

Figure 4.12 (a): *UV-visible spectra and,* ***(b)*** *UV-visible with overlaid photoluminescence spectra of* ***4.11.I***, ***4.12.I***, *and* ***4.13.I*** *in DCM at room temperature, concentration ~ 10^{-5} $molL^{-1}$.*

The emission spectra, more-so than the absorption spectra, highlights the subtle electronic differences between the N1 and N11 substituted salts. The N1 salt **4.12.I** emits at a slightly lower energy (λ_{max} = 499 nm, 20000 cm^{-1}) than the N11 salts **4.11.I** and **4.13.I** which have near identical emission curves (λ_{max} = 482 nm, 20700 cm^{-1}). Substitution of the phenanthroline nitrogen induces a large bathochromic shift of greater than 5030 cm^{-1} from the emission maxima of the precursor **4.3**.

The bright yellow colour of these phenanthrolinium salts is due to a moderately intense absorption around ~ 390 nm which is not present in the neutral precursor. This may be attributed to intramolecular charge transfer (ICT) between the substituted imidazole nitrogen donor and the quarternary nitrogen acceptor or a π(*N*-Ph) – π*(pyridinium) transition. This is analogous behaviour to other systems in which pyridinium rings have been incorporated for their π-electron acceptor ability most notably in the hemicyanine stilbazolium salt family.[227-231] Ionic ICT based organic dyes are of interest for their potential non-linear optical (NLO) properties which have been applied in optoelectronic and photonic devices.[227] Unfortunately, however, the ICT absorption band of compounds **4.11.I**, **4.12.I** and **4.13.I** are weak (ε_{max} ~ 1000 – 2000 $Lmol^{-1}cm^{-1}$) when compared with literature pyridinium based dyes (typically, ε_{max} > 20000 $Lmol^{-1}cm^{-1}$).[227, 228] One possible reason for this low molar-absorptivity is illustrated by a comparison of the ICT excited states of compound **4.13.I** and the stilbazolium salt *trans*-4'-(dimethylamino)-*N*-methyl-4-stilbazolium hexfluorophosphate ([DAST][PF_6]) (Figure 4.13).[227, 229] Neither excited state is aromatic, however, aromaticity is lost in four rings of **4.13.I** instead of just two in $[DAST]^+$. Furthermore, steric strain in the excited state of **4.11.I** due to the rigidity of the fused-imidazole may supresses the donor ability of the imidazole nitrogen.

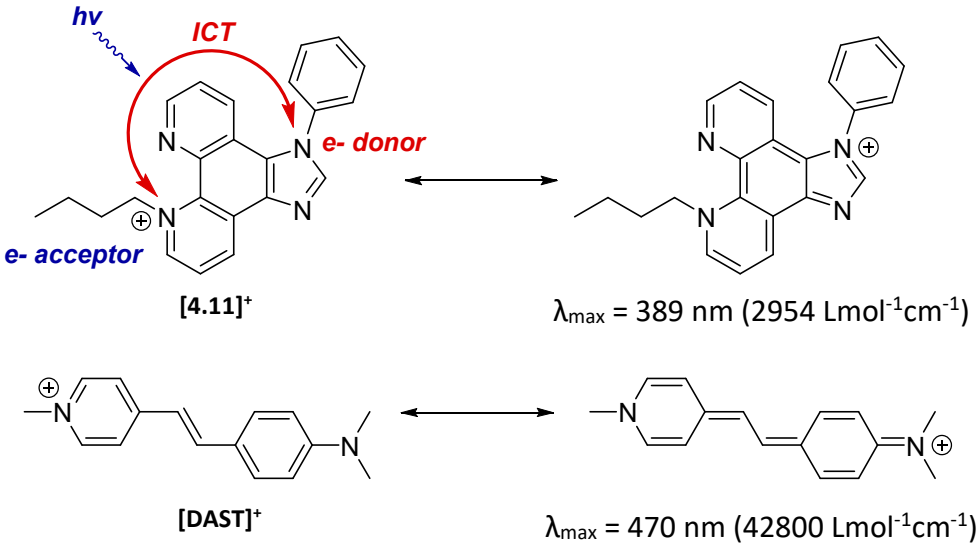

Figure 4.13: *Probable ICT excited state resonance forms of a 1-phenyl-imidazo[4,5-f][1,10]phenanthrolinium cation (**4.11.I**) and a stilbazolium cation ($[DAST]^+$).*

The $\pi - \pi^*$ ICT excitation depicted in Figure 4.13 invokes a large charge displacement hence these molecules are inevitably highly polarizable and probably exhibit solvatochromism.[228] Their application as solvatochromic agents has yet to be studied.

The imidazolium salt **4.9.HI** is insoluble in DCM and had to be studied as a MeCN solution meaning its absorption and emission spectra are not amenable to direct comparison with the previously discussed compounds. Regardless, the UV-visible spectrum did show this unsymmetrical imidazolium salt only absorbs significantly in the far ultra-violet ($\lambda <$ 330 nm) in contrast to the phenanthrolinium salts.

4.4. Synthesis of [Ru(2,2'-bipyridine)$_2$(IP)]$^{n+}$-type complexes

4.4.1. Complexes with *N*-substituted imidazo[4,5-*f*][1,10]phenanthroline ligands

Complexes [Ru(bipy)$_2$(**4.2** – **4.4**)][PF$_6$]$_2$ were prepared by reacting the corresponding N-substituted IP ligand with Ru(bipy)$_2$Cl$_2$ in a microwave reactor using ethylene-glycol as the solvent (Scheme 4.6). The reactions typically required 5 – 10 minutes of microwave irradiation before all ligand and Ru(bipy)$_2$Cl$_2$ were consumed as indicated by TLC (silica, 4:1:1 DMF/water/1 M NH_4Cl).

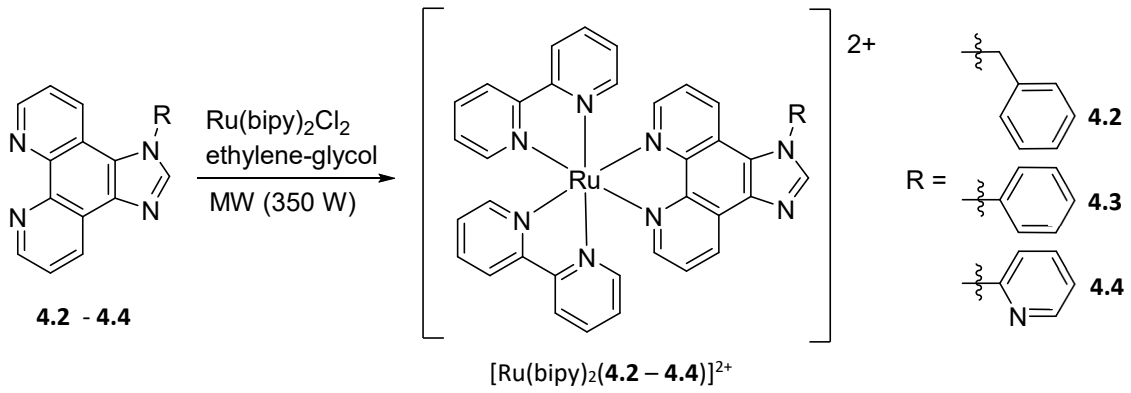

Scheme 4.6: *Synthesis of complexes [Ru(bipy)$_2$(**4.2** – **4.4**)]$^{2+}$.*

After cooling, the reaction mixture was poured onto water and the aqueous solution filtered through celite. Although all products were ultimately isolated as PF_6 salts, TLC analysis of the reaction mixture of $[Ru(bipy)_2(\mathbf{4.2})]^{+2}$ indicated that a minor by-product was present. This is potentially $[Ru(bipy)_2(\mathbf{4.1})]^{+2}$, formed by loss of the benzyl substituent. Therefore, the aqueous solution was first loaded onto a column of sephadex – C25 ion-exchange resin which was eluted with 0.00 – 0.20 M NaCl solution. This rigorous purification was later found to be unnecessary as each product could be adequately purified simply by precipitating it as a PF_6 salt then washing the collected solid with water. Recrystallisation from a hot MeOH/water mixture could also be performed if desired.

Crystals of $[Ru(bipy)_2(\mathbf{4.2})][PF_6]_2$ suitable for single-crystal X-ray analysis were grown by slow vapour-diffusion of iPr_2O into an MeOH solution of the compound. Complex $[Ru(bipy)_2(\mathbf{4.2})][PF_6]_2$ crystallised in the monoclinic space group $P2_1/c$ with one molecule of $[Ru(bipy)_2(\mathbf{4.2})]^{2+}$ and two PF_6 anions present in the asymmetric unit (Figure 4.14). A region occupied by disordered solvent was also present. This was adequately modelled as containing one iPr_2O and four MeOH molecules, all of which displayed partial occupancy. Hydrogen atoms bonded to MeOH molecules could not be satisfactorily modelled and all attempts to calculate their positions resulted in poor refinement. The structure of $[Ru(bipy)_2(\mathbf{4.2})]^{2+}$ shows an octahedral ruthenium centre with the expected propeller arrangement of polypyridyl ligands. The bite angles for the three ligands, N1 – Ru – N11, N1A' – Ru – N1A'' and N1B' – Ru – N1B'' are 79.46(8)°, 78.99(8)° and 78.92(9)° respectively and Ru – N bond lengths fall within a narrow range between 2.060(2) Å for Ru – N1B' and 2.065(2) Å for Ru – N1. The C6 – N7 bond (1.309(4) Å) is shorter than the C6 – N5 bond (1.354(4) Å) due to its greater double-bond character as expected for a mono-substituted imidazole. The benzyl ring projects away from the mean plane of the IP core at an angle of 85.10(5)°.

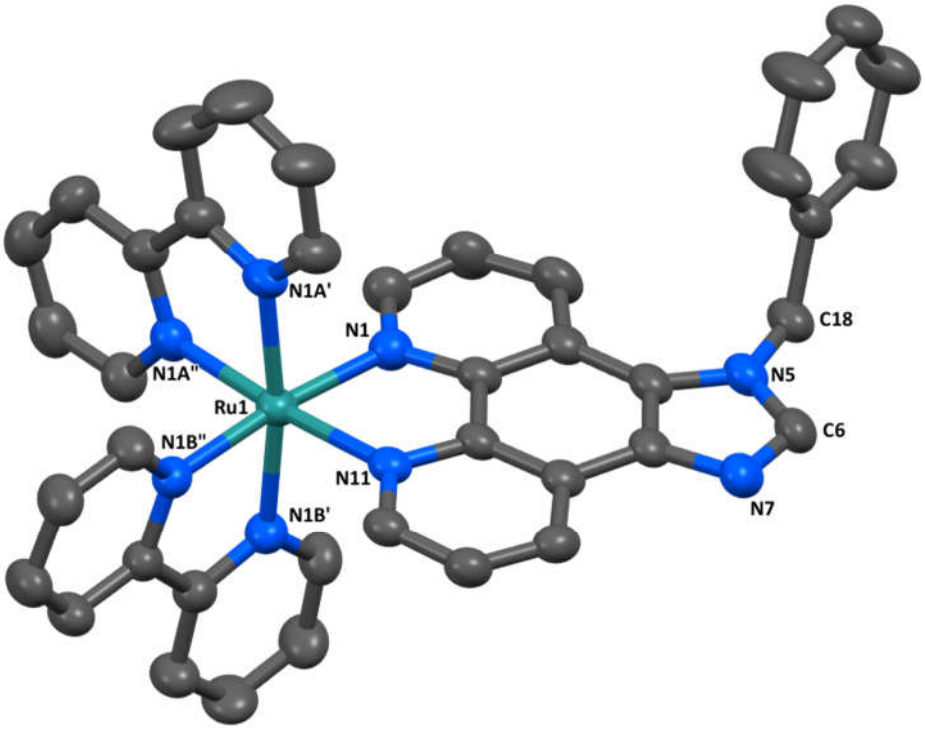

Figure 4.14: *Asymmetric unit of [Ru(bipy)$_2$(**4.2**)][PF$_6$]$_2$. Hydrogen atoms, PF$_6$ anions and solvent molecules have been omitted for clarity. Thermal ellipsoids drawn at 50% probability.*

An X-ray structure of [Ru(bipy)$_2$(**4.3**)][PF$_6$]$_2$ was obtained using crystals grown by slow vapour-diffusion of Et$_2$O into a MeCN solution of the complex. This crystallised in the triclinic space group $P\bar{1}$ with one molecule of [Ru(bipy)$_2$(**4.3**)]$^{2+}$ and two PF$_6$ anions in the asymmetric unit (Figure 4.15) along with three molecules of MeCN and one of Et$_2$O. The bite angles for the three ligands around the octahedral ruthenium centre N1 – Ru – N11, N1A' – Ru – N1A'' and N1B' – Ru – N1B'' are 79.35(6)°, 78.78(8)° and 78.72(7)° respectively and Ru – N bond lengths fall within a narrow range between 2.057(2) Å for Ru – N1 and 2.068(2) Å for Ru – N11. The phenyl ring is rotated out of the plane of the IP core by 58.42(9)°. As with [Ru(bipy)$_2$(**4.2**)]$^{2+}$, bond length asymmetry also exists between C6 – N7 (1.309(3) Å) and C6 – N5 (1.373(3) Å) due to the greater double-bond character of C6 – N7.

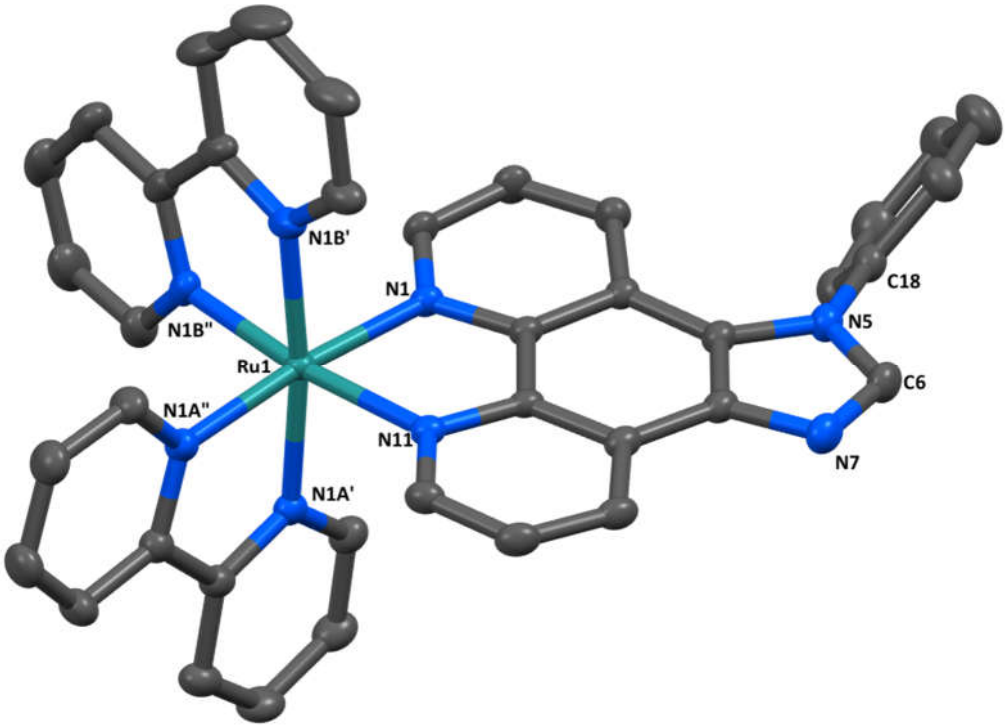

Figure 4.15: *Asymmetric unit of [Ru(bipy)$_2$(**4.3**)][PF$_6$]$_2$. Hydrogen atoms, PF$_6$ anions and solvent molecules have been omitted for clarity. Thermal ellipsoids are drawn at 50% probability.*

The compact nature of ligand **4.3** allows [Ru(bipy)$_2$(**4.3**)]$^{2+}$ cations to adopt a closely packed configuration in which several intermolecular π – π contacts are observed. Each of the two molecules in the unit-cell arrange such the IP cores are parallel with N7 of the imidazole adjacent to the plane of the N11 pyridine subunit (N7-to-centroid distance = 3.534(2) Å). Also observed is an edge-to-face interaction between the C6 – N7 edge of the imidazole and the N1A' pyridine subunit (N7-to-centroid distance = 3.377(2) Å). This is unlike [Ru(bipy)$_2$(**4.2**)]$^{2+}$ in which tight packing of the cations is obstructed by the benzyl arm.

Crystals of [Ru(bipy)$_2$**4.4**][PF$_6$]$_2$ were unable to be grown despite numerous attempts.

4.4.2. Complexes with 1,10-phenanthroline annelated imidazolium salt ligands

The two possible routes for preparing ruthenium coordinated imidazolium salts based on IP ligands are defined by whether imidazolium salt formation occurs "pre-complexation" or "post-complexation" (Scheme 4.7). Both routes were explored in the course of this investigation and it was found that any preference was ultimately system dependent.

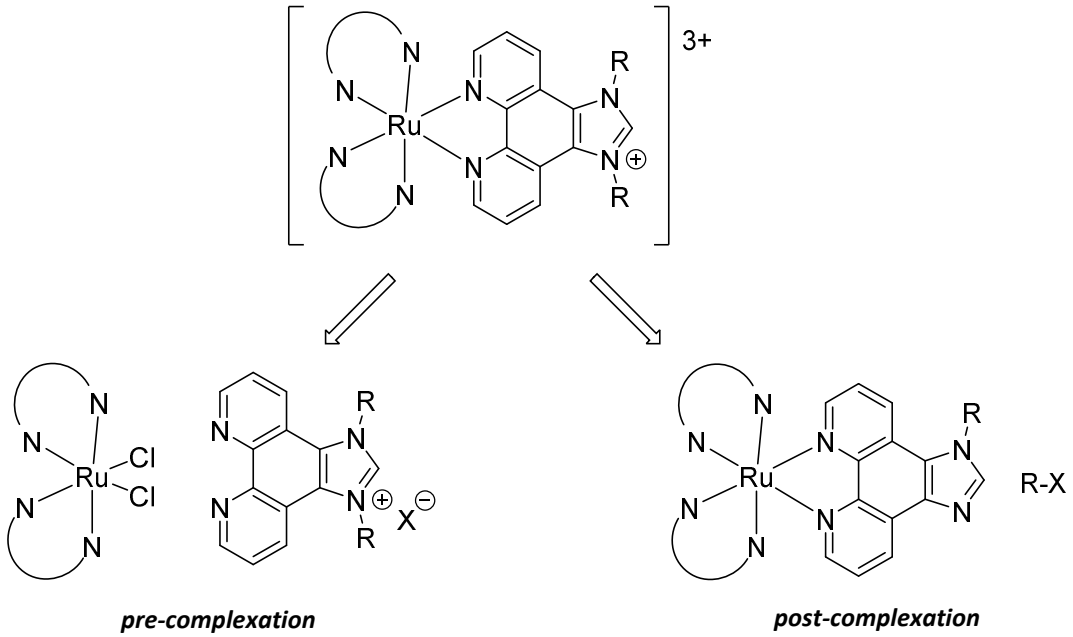

Scheme 4.7: *Retrosynthetic "pre-complexation" and "post-complexation" routes to ruthenium coordinated imidazolium salts.*

Successful application of the pre-complexation route hinges on the stability of the imidazolium salt and judicious choice of reaction conditions. This pathway was first attempted for the synthesis of $[Ru(bipy)_2(\mathbf{4.5.H})]^{3+}$. Having recognised that isomerisation of $\mathbf{[4.5.H]^+}$ can occur in aqueous media (see section 4.2.3) it was hoped that "protecting" the phenanthroline nitrogen by coordination to ruthenium might negate this issue. Synthesis of $[Ru(bipy)_2(\mathbf{4.5.H})]^{3+}$ was attempted using a microwave

reactor (350 W) (Scheme 4.8, route A) with the same conditions as those used for the synthesis of $[Ru(bipy)_2(\mathbf{4.2} - \mathbf{4.4})]^{2+}$. Complex formation and the consumption of $Ru(bipy)_2Cl_2$ was monitored by TLC (silica, 4:1:1 DMF/water/1 M NH_4Cl), consumption of **4.5.HBr** was also monitored by TLC (alumina, 1:4 MeOH/DCM). After three 2 minute bursts of microwave radiation **4.5.HBr** could no longer be observed by TLC, however, a spot due to $Ru(bipy)_2Cl_2$ persisted and a bright orange product spot had emerged. This product was obtained as a PF_6 salt after successful isolation by sephadex – C25 ion-exchange chromatography eluting with 0.00 – 0.20 M NaCl solution.

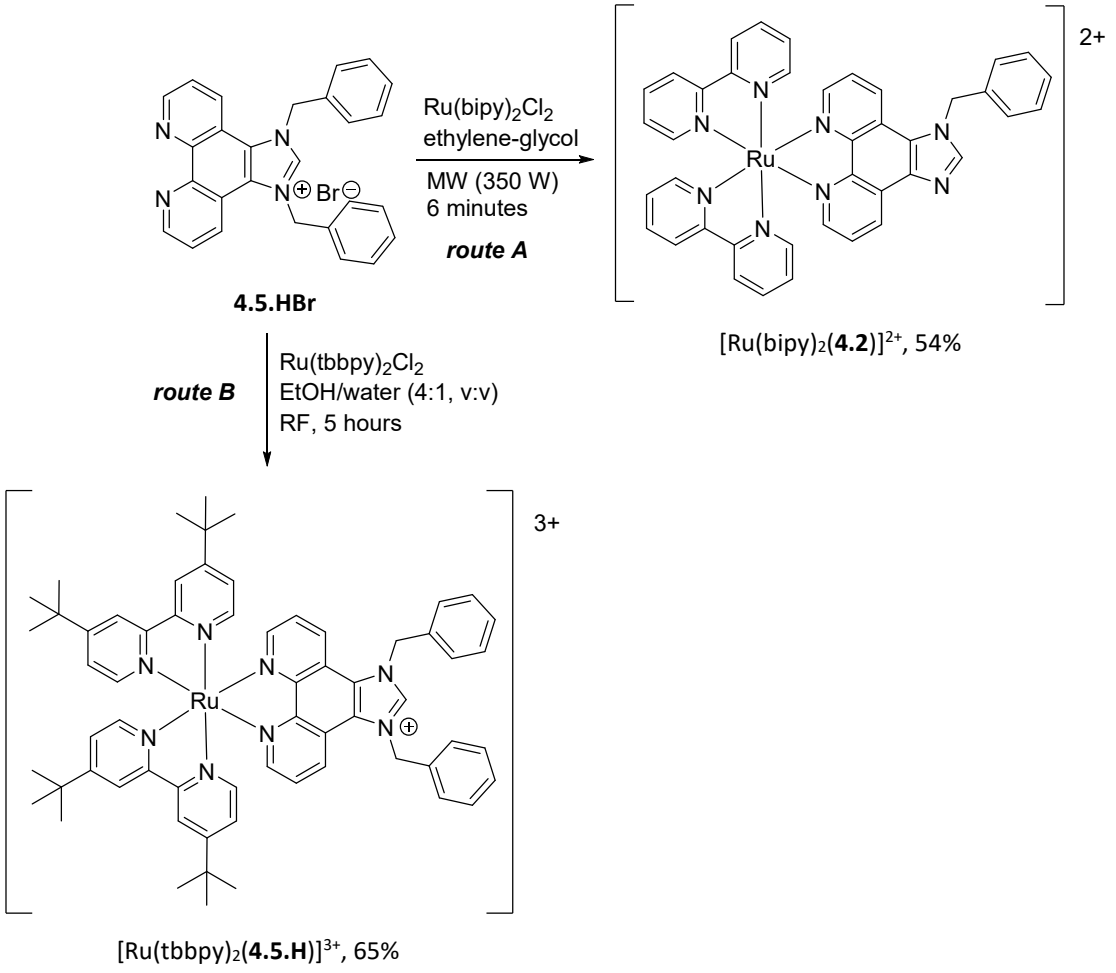

Scheme 4.8: *Attempted synthesis of* $[Ru(bipy)_2(\mathbf{4.5.H})]^{3+}$ *(route A) and successful synthesis of* $[Ru(tbbpy)_2(\mathbf{4.5.H})]^{3+}$ *reported by Peuntinger et al. (route B).*

Subsequent NMR and mass-spectrometric analysis on the bright orange material revealed this to be $[Ru(bipy)_2(\mathbf{4.2})][PF_6]_2$ (acquired in a 53.7% yield) instead of the desired complex $[Ru(bipy)_2(\mathbf{4.5.H})][PF_6]_3$. Other diffuse yellow bands collected from the column were shown by mass-spectrometry to contain $[Ru(bipy)_2(\mathbf{4.2})]^{2+}$ and other unidentified species of various mass. As with during the purification of ligand **4.5.HBr**, the lability of the benzyl pendant proved to be a tremendous liability. Milder reaction conditions such as refluxing in an EtOH/water mixture, were not considered because it was anticipated that the prolonged reaction time and aqueous solvent would lead to decomposition of the **[4.5.H]$^+$** ligand. It therefore came as a surprise when work published by Peuntinger *et al.* demonstrated the reaction of **4.5.HBr** with $Ru(tbbpy)_2Cl_2$ to form $[Ru(tbbpy)_2(\mathbf{4.5.H})][PF_6]_3$ in a 65% yield under harsh microwave conditions in a EtOH/water solution (Scheme 4.8, route B).[215]

Decomposition of **[4.5.H]$^+$** in route A was probably facilitated by excessive heating (ethylene-glycol boils at 197 ^{o}C). As route B shows, **[4.5.H]$^+$** is compatible with polar-protic solvents including water, just not to extreme temperatures. This partially contradicts the observation that **[4.5.H]$^+$** isomerises in the presence of water at room temperature, however, this finding may have been misleading. Other factors, such as a solubility driven equilibrium shift caused by association of the PF_6 anion may have been more influential than the solvent itself. The synthesis of $[Ru(bipy)_2(\mathbf{4.5.H})][PF_6]_3$ was not revisited using milder conditions because success was being had with the more durable ligand **[4.9.H]$^+$**. This was successfully reacted with $Ru(bipy)_2Cl_2$ to give the complex $[Ru(bipy)_2(\mathbf{4.9.H})]^{3+}$ under conditions analogous to those reported for the synthesis of $[Ru(tbbpy)_2(\mathbf{4.5.H})]^{3+}$, however, heating was performed on a hot-plate rather than in a microwave (Scheme 4.9). The product was isolated as a PF_6 salt after flash chromatography (silica, 9:1.5:1 MeCN/water/saturated $KNO_{3(aq)}$) giving $[Ru(bipy)_2(\mathbf{4.9.H})][PF_6]_3$ as a bright orange powder in a 70.8% yield.

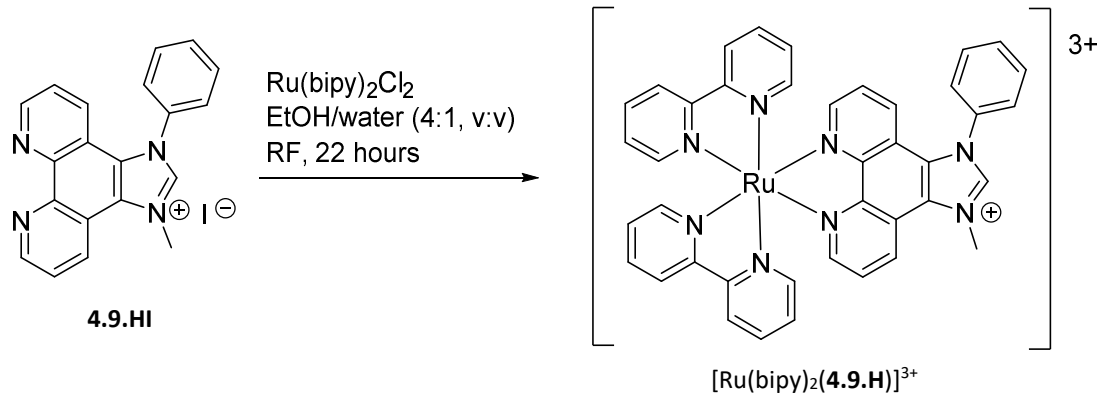

4.9.HI

[Ru(bipy)$_2$(**4.9.H**)]$^{3+}$

Scheme 4.9: *Synthesis of [Ru(bipy)$_2$(**4.9.H**)]$^{3+}$.*

The characterisation of [Ru(bipy)$_2$(**4.9.H**)][PF$_6$]$_3$ was aided by X-ray diffraction analysis which was performed on a crystal grown by slow-vapour diffusion of Et$_2$O into a MeCN solution of the complex. Complex [Ru(bipy)$_2$(**4.9.H**)][PF$_6$]$_3$ crystallised in the monoclinic space group P2$_1$/*c* with one molecule of [Ru(bipy)$_2$(**4.9.H**)]$^{3+}$ in the asymmetric unit (Figure 4.16). One of the three PF$_6$ anions present resides on a special position and there is one solvate molecule of MeCN. The bite angles for the three ligands around the octahedral ruthenium centre N1 – Ru – N11, N1A' – Ru – N1A'' and N1B' – Ru – N1B'' are 79.14(7)°, 78.38(8)° and 78.80(8)° respectively and Ru – N bond lengths fall within a range between 2.047(2) Å for Ru – N11 and 2.066(2) Å for Ru – NA'. The average of the Ru – N(IP) bond lengths (Ru – N1 and Ru – N11) in this structure is 2.054(2) Å which is slightly shorter than those in the complexes with mono-substituted IP ligands [Ru(bipy)$_2$**4.2**]$^{2+}$ (2.064(2) Å) and [Ru(bipy)$_2$**4.3**]$^{2+}$ (2.063(2) Å). This observation is in alignment with the average Ru – N(IP) bond lengths reported for similar compounds.[215, 232] Also unlike [Ru(bipy)$_2$(**4.2**)]$^{2+}$ and [Ru(bipy)$_2$(**4.3**)]$^{2+}$ this structure exhibits symmetric bond lengths between C6 – N5 and C6 – N7 (1.329(3) Å and 1.322(3) Å respectively) as expected for an imidazolium salt. In the packed structure, H6 of the electron deficient C6 carbon participates in hydrogen bonding with the fluorine of one PF$_6$ anion (C ⋯ F = 3.034(3), C – H ⋯ F angle = 170.85(15)°).

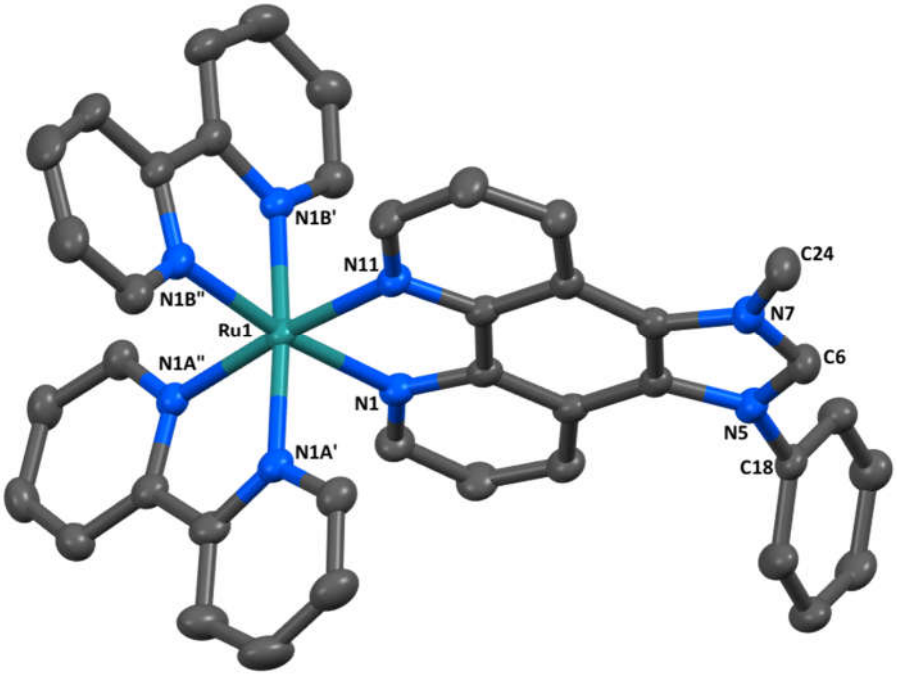

Figure 4.16: *Asymmetric unit of [Ru(bipy)$_2$(**4.9.H**)][PF$_6$]$_3$. Hydrogen atoms, PF$_6$ anions and solvent molecules have been omitted for clarity. Thermal ellipsoids have been drawn at 50% probability.*

In addition to [Ru(bipy)$_2$(**4.9.H**)][PF$_6$]$_3$, a ruthenium bound imidazolium salt based on the 2-pyridyl substituted IP ligand **4.4** was sought as a proligand for chelation stabilised NHC complexes. In light of the difficulties associated with regioisomer formation discussed in section 4.2.3, the post-complexation route holds obvious advantages. Coordination to ruthenium renders the nitrogen of the phenanthroline terminus unable to compete with the imidazole nitrogen as the reactive nucleophile. This is particularly pertinent to the synthesis of imidazolium salts from **4.4** which can be substituted at the pyridyl nitrogen in addition to the three nitrogen of the IP core. Applying this logic, methylation of complex [Ru(bipy)$_2$(**4.4**)]$^{+2}$ to give [Ru(bipy)$_2$(**4.15.H**)]$^{+3}$ was attempted using ten-fold excess of iodomethane in DMF at 100 ^{o}C (Scheme 4.10). These conditions were based on those reported for the synthesis of a similar compound.[216] The low boiling point of iodomethane (42 ^{o}C), necessitated the use of a sealed tube to prevent its loss while reacting at 100 ^{o}C. This meant that the reaction was unable to be monitored by TLC without returning to room-temperature and as a result when the reaction was stopped

after 48 hours it was found that only a small amount of product had formed. Rather than resuming the reaction the complex was isolated for analysis using flash chromatography (silica, 9:1.5:1 MeCN/water/saturated $KNO_{3(aq)}$) and obtained by precipitation as a PF_6 salt. Complex $[Ru(bipy)_2(\mathbf{4.15.H})][PF_6]_3$ was obtained in a 21% yield and 69% of the original mass of starting material was recovered.

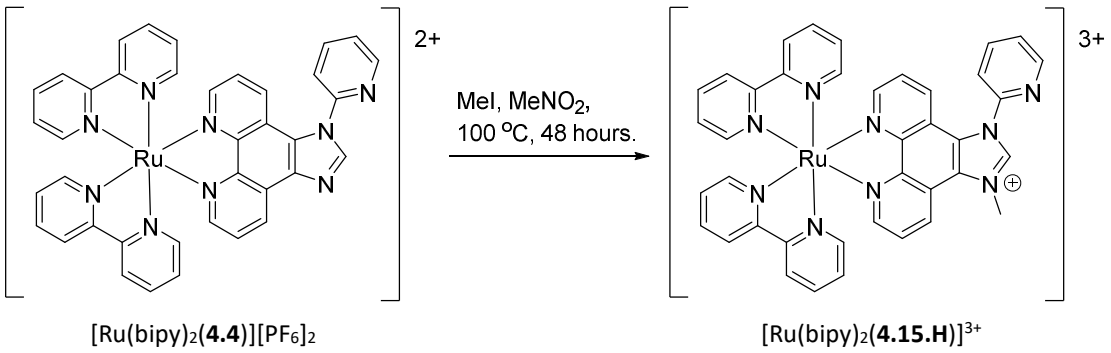

$[Ru(bipy)_2(\mathbf{4.4})][PF_6]_2$ $[Ru(bipy)_2(\mathbf{4.15.H})]^{3+}$

Scheme 4.10: *Synthesis of $[Ru(bipy)_2(\mathbf{4.15.H})]^{3+}$ by post-complexation methylation of $[Ru(bipy)_2(\mathbf{4.4})][PF_6]_2$.*

Comparison of the ^{1}H-NMR spectrum of the starting material $Ru(bipy)_2(\mathbf{4.4})][PF_6]_2$ with that of the product revealed the hallmark downfield shift of the imidazolyl proton signal (H6) associated with imidazolium salt formation (Figure 4.17). This singlet moved from 8.59 ppm to 9.51 ppm in the product spectrum confirming that methylation had occurred to produce the desired imidazolium salt $[Ru(bipy)_2(\mathbf{4.15.H})]^{+3}$, rather than the regioisomeric pyridinium salt.

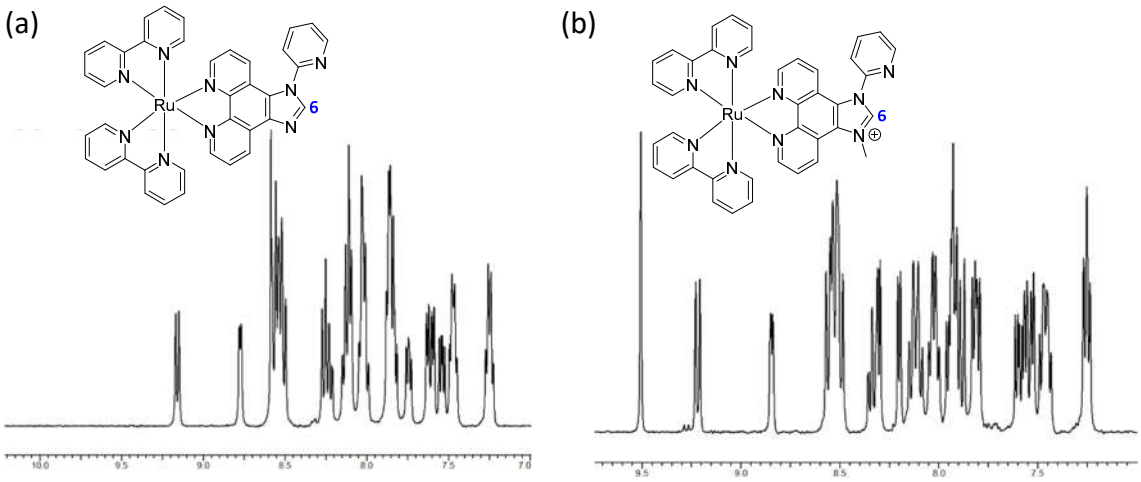

Figure 4.17 (a): *Aromatic region of ^{1}H-NMR spectra of [Ru(bipy)$_2$(**4.4**)][PF$_6$]$_2$ in CD$_3$CN and,* ***(b)*** *that of [Ru(bipy)$_2$(**4.15.H**)][PF$_6$]$_3$.*

With regards to the low yield there are several possible explanations. The kinetic handicap of electronic repulsion between the doubly-cationic nucleophile and the electrophile could be sufficient to slow the reaction in which case a longer reaction time would be required. The reaction may also be in an equilibrium which favours the starting material. Alternatively, the iodomethane may simply have been lost to the system, either being consumed through side reactions with the DMF solvent and its degradation products or by escaping through the seal. Some of these issues could be circumvented by using a less volatile methylating agent such as dimethyl-sulfate which would allow elevated temperatures to be used without requiring a sealed tube. However, as an adequate quantity of analytically pure [Ru(bipy)$_2$(**4.15.H**)][PF$_6$]$_3$ had already been obtained this synthesis was not amended in practice.

4.5. Photophysical properties of [Ru(2,2'-bipyridine)$_2$(IP)]$^{n+}$ type complexes

The photophysical properties of ruthenium-polypyridine type complexes remain a subject of interest despite having been studied intensively for decades.[124, 126, 233, 234] Of these complexes, the [Ru(bipy)$_3$]$^{2+}$-type motif is the most commonly encountered. These typically absorb strongly in the visible region (~ 450 nm) due to a metal-to-ligand charge

transfer state (MLCT) which is generated by photoexcitation of one electron from a metal-centred t_{2g} orbital to a ligand-centred π^* orbital. As such, the absorption wavelength associated with the MLCT is an indicator of the HOMO-LUMO energy gap in these complexes.[233] The resulting excited state is long lived (~ 600 ns) and can be described as having a ruthenium(III) centre with one bipy ligand that has undergone a single electron reduction.[235]

The optical properties of a handful of $[Ru(bipy)_2(IP)]^{2+}$-type complexes have also been investigated and applied in various roles. Complexes of the type shown in Figure 4.18a have been employed as pH-dependent luminescence probes[236] and as photoactive DNA binding agents.[237-239] Moreover, work by Park *et al.* has demonstrated that the ruthenium bound IP-imidazolium salt shown in Figure 4.18b can act as both the photosensitiser and electron mediator for photocatalytic hydrogen evolution from water.[232]

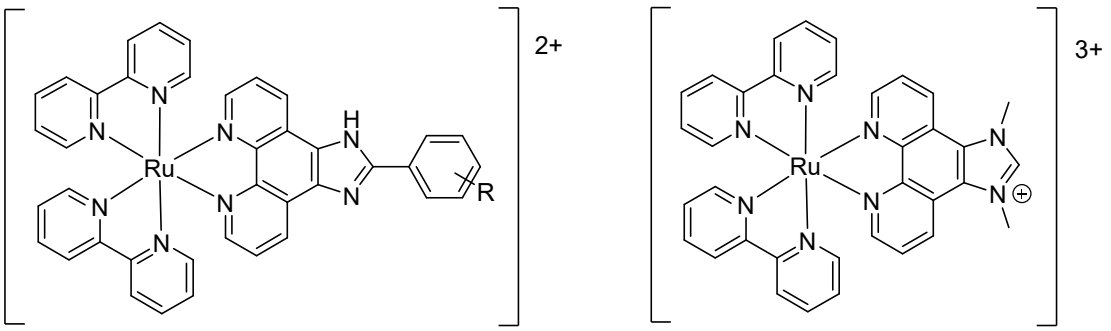

Figure 4.18 (a): *Luminescent pH-sensor and DNA-probe,* ***(b)*** *photocatalyst for hydrogen generation.*

The new $[Ru(bipy)_2(IP)]^{2+}$ derivatives prepared during this research project were studied by UV-visible and fluorescence spectroscopy to assess their viability as photochemical agents for applications such as those discussed above. Data for these complexes is collated in Table 4.2 along with that of the prototypical parent complex $[Ru(bipy)_3]^{2+}$.

Table 4.2: *Summary of the absorption and emission maxima of complexes [Ru(bipy)$_2$(**L**)][PF$_6$]$_3$ recorded in MeCN and [Ru(bipy)$_3$]$^{2+}$ (**A**) in water.*

		absorption		emission		absorption		emission
		λ_{max} (nm)	ε (Lmol^{-1}cm^{-1})	λ_{max} (nm)		λ_{max} (nm)	ε (Lmol^{-1}cm^{-1})	λ_{max} (nm)
[Ru(bipy)$_2$(**L**)][PF$_6$]$_n$	**4.2**	254, 284 425(sh), 454	50249, 79328 12877, 17540	601	**4.9.H**	245, 275 285, 436 269(sh)	123125, 120123 119060, 30263 23871	632
	4.3	254, 285 425(sh), 454	50176, 80317 13542, 17008	599	**4.15.H**	245, 276 285, 437 469(sh)	89274, 92572 97858, 20499 16942	633
	4.4	253, 284 425(sh), 453	49825, 80872 13313, 17390	599	**A**	238, 250(sh) 285, 423(sh) 451	30000, 25000 87000, 12000 14000	607

[a] data for [Ru(bipy)$_3$][Cl]$_2$ in water[240]

The three complexes with N-substituted IP ligands, [Ru(bipy)$_2$(**4.2** – **4.4**)][PF$_6$]$_2$ produce UV-visible spectra that differ only in their molar absorptivity (Figure 4.19a). The UV-region is dominated by ligand-centred (LC) transitions at ~ 254 nm and ~ 284 nm with the characteristic visible MLCT absorption occurring at ~ 454 nm with a shoulder at ~ 425 nm. The emission spectra of the three complexes are identical with λ_{max} ~ 600 nm (Figure 4.19b). These spectral features are analogous to those reported for [Ru(bipy)$_3$]$^{+2}$ (Table 4.2).

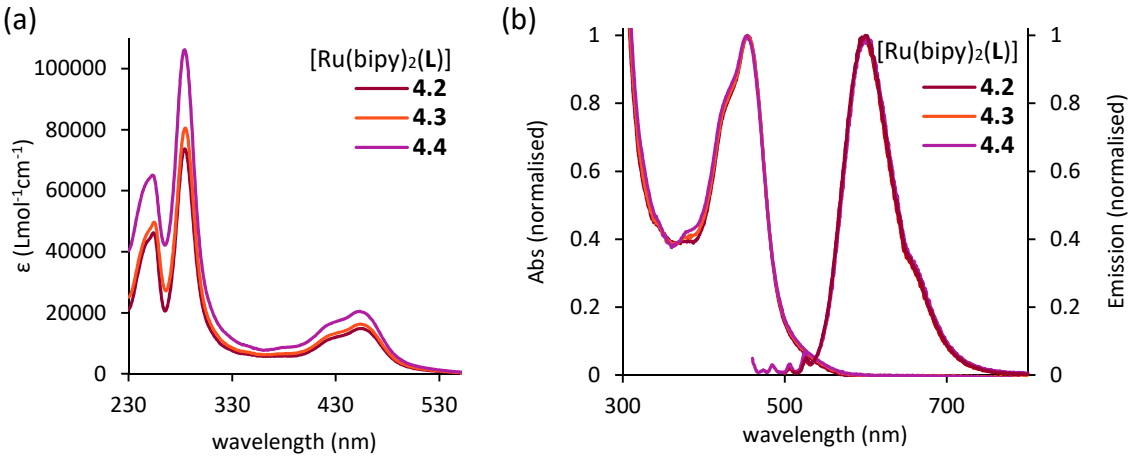

Figure 4.19 (a): *UV-visible spectra and,* ***(b)*** *UV-visible (visible region) with overlaid photoluminescence spectra of [Ru(bipy)$_2$(**4.2** – **4.4**)][PF$_6$]$_2$ in MeCN at room temperature, concentration ~ 10^{-6} molL^{-1}.*

The visible region of the UV-visible absorption spectrum of the complexes $[Ru(bipy)_2(\mathbf{4.9.H})][PF_6]_3$ and $[Ru(bipy)_2(\mathbf{4.15.H})][PF_6]_3$ are shown in Figure 4.20. Not shown, are absorption maxima at ~ 245 nm and ~ 285 nm that are similar to those observed in the spectra of $[Ru(bipy)_2(\mathbf{4.2} - \mathbf{4.4})][PF_6]_2$ and $[Ru(bipy)_3]^{+2}$, an additional absorption at ~ 275 nm can therefore be attributed to an IP-imidazolium ligand centred $\pi - \pi^*$ transition. A broad absorption band in the visible region (360 nm – 530 nm with λ_{max} ~ 437 nm) is ascribed to multiple overlapping MLCT transitions. In particular, excitation from the ruthenium-centre onto the imidazolium salt ligand would explain the shoulder of intensity occurring in both spectra at ~ 469 nm. Less energy is required to promote an electron onto the cationic entity due to the reduction in the energy of the LUMO that is elicited by imidazolium salt formation. This assessment is supported by the emission spectra of $[Ru(bipy)_2(\mathbf{4.9.H})][PF_6]_3$ and $[Ru(bipy)_2(\mathbf{4.15.H})][PF_6]_3$ shown in Figure 4.20. Here the maximum emission value for both spectra (λ_{max} ~ 632 nm, 15800 cm^{-1}) undergoes a bathochromic shift of ~ 844 cm^{-1} from the emission maxima observed for complexes $[Ru(bipy)_2(\mathbf{4.2} - \mathbf{4.4})][PF_6]_2$. This correlates to a lowering in energy of the emissive state i.e. the LUMO.

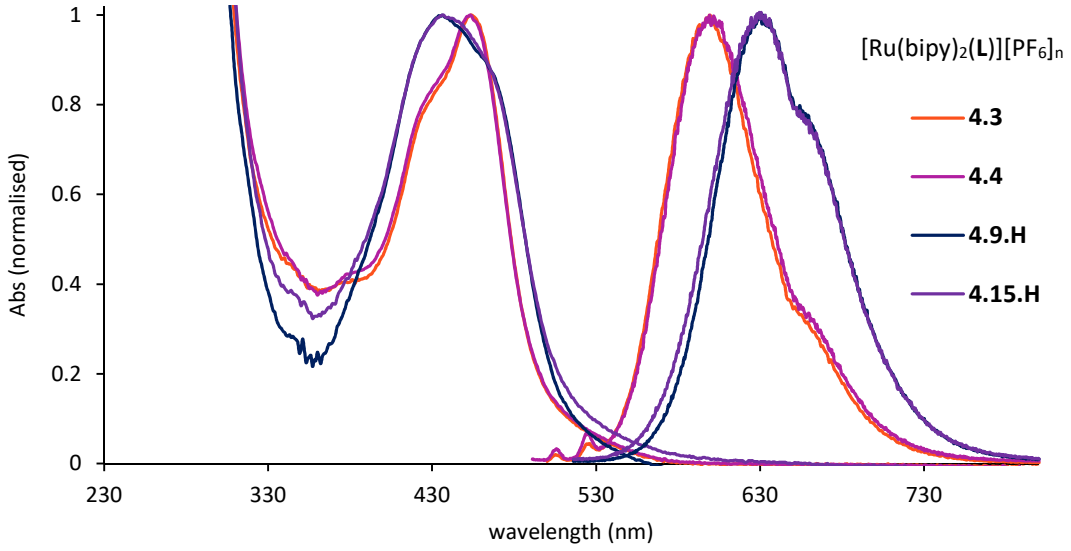

Figure 4.20 (a): *UV-visible (visible region) with overlaid photoluminescence spectra of* $[Ru(bipy)_2(\mathbf{4.9.H})][PF_6]_3$ *and* $[Ru(bipy)_2(\mathbf{4.15.H})][PF_6]_3$ *with* $[Ru(bipy)_2(\mathbf{4.3})][PF_6]_3$ *and* $[Ru(bipy)_2(\mathbf{4.4})][PF_6]_3$ *for comparison. Recorded in MeCN at room temperature, concentration ~* 10^{-6} *molL*$^{-1}$.

The electronic absorption and photoluminescence properties of the new complexes discussed above are in agreement with the properties of conventional $[Ru(bipy)_3]^{2+}$ type complexes and may therefore be amenable to many of the same applications.

4.6. Summarising remarks

The investigation of NHC precursors with an imidazo[4,5-f][1,10]phenanthroline core and backbone ruthenium-polypyridine functionality was undertaken. Two new metallo-NHC proligands, $[Ru(bipy)_2(\mathbf{4.9.H})][PF_6]_3$ and $[Ru(bipy)_2(\mathbf{4.10.H})][PF_6]_3$ were identified.

N-Quaternisation of *N*-substituted imidazo[4,5-f][1,10]phenanthroline derivatives to give imidazolium salts encountered regioselectivity issues associated with *N*-substitution of the phenanthroline nitrogen instead of the imidazole. Several of the resulting phenanthrolinium salts, **4.11.I**, **4.12.I** and **4.13.I**, were able to be characterised. A post-complexation approach was investigated whereby the imidazolium salt is prepared after coordination of the phenanthroline to ruthenium leading to effective protection of the phenanthroline nitrogen. This was successfully employed for the synthesis of $[Ru(bipy)_2(\mathbf{4.10.H})][PF_6]_3$ although, a low yield of 21% was obtained.

The photochemical properties of ruthenium-polypyridine complexes with imidazo[4,5-f][1,10]phenanthroline derived ligands have been studied in the literature for use in various applications. New complexes of the type $[Ru(bipy)(IP)]^{n+}$ prepared in this work were studied by UV-visible and fluorescence spectroscopy and found to conform to established norms. Uncoordinated imidazo[4,5-f][1,10]phenanthroline derivatives have been less studied in this context prompting their photochemistry to be examined also. Of particular interest are the unusual phenanthrolinum salts which were revealed by UV/vis to possess a moderately intense absorption around $\sim$ 390 nm that is not present in the neutral precursor **4.3**. This is attributed to intramolecular charge transfer (ICT) which gives rise to the yellow colouration of these compounds. ICT capable salts such as these are amenable to various photochemical applications, although, the extinction

coefficient of the phenanthrolinium salts is much weaker than those of reported ICT salts such as $[DAST]^+$.

4.7. Scope and future work

This section introduced two new unsymmetrical metallo-NHC proligands $[Ru(bipy)_2(\mathbf{4.9.H})][PF_6]_3$ and $[Ru(bipy)_2(\mathbf{4.15.H})][PF_6]_3$ which are of particular interest both as NHC proligands[213-215] and potential photocatalysts.[232] Although related NHC-complexes have been prepared, their application as ligands in metal-mediated couplings have not been explored. These could be easily introduced into the protocol developed in Chapter 6 to study their behaviour in Suzuki couplings but could not be conducted here due to time limitations. Synthesis of a PEPPSI palladium precatalyst using an $[Ru(bipy)_2(\mathbf{IP})]^{2+}$ type NHC ligand could also be an achievable and interesting endeavour. This would provide a known system with which to study the effect of the coordinated ruthenium on the activity of the palladium centre.

It has been noted previously that IP derived systems are interesting for their optoelectronic properties. The identification, characterisation and photophysical analysis of the phenanthrolinium salts **4.6.PF$_6$**, **4.7.PF$_6$**, **4.11.I**, **4.12.I** and **4.13.I** represents a previously unexplored aspect of IP chemistry. Their bright yellow colouration, quantified by a moderately intense absorption around ~ 390 nm in the UV/vis spectrum, is attributed to an ICT event. It would be worthwhile to investigate the probable solvatochromism of these systems as they are soluble in a wide range of solvents.

Chapter 5

metal-centred chirality;
ruthenium-polypyridine derivatives

5.1. Introduction

The previous chapter introduced a 1,10-phenanthroline fused NHC system in which the ruthenium-polypyridine moiety occupies a peripheral site relative to the NHC centre. It was proposed that increasing the steric interplay of the enantiomeric Ru(II) moiety and NHC node would improve the stereodirecting capabilities of such metallo-NHC ligands. Affixing the NHC moiety closer to the phenanthroline coordination site is one way of achieving this objective. Otherwise, an acetamide tether could be utilised similarly to the bornyl-acetamide NHC complexes in Chapter 1, to exploit *N*-amidate/NHC chelation as a means of interacting the chiral and catalytic environments. Derivatives of 3-imidazole-1,10-phenanthroline were targeted as representatives of the "appended" sub-class with acetamide-linked 1,10-phenanthroline derivatives forming the basis of the "tethered" category (Figure 5.1). In this chapter, the shorthand expressions 3-IMP and 5-PA are used to indicate ligands derived from 3-imidazole-1,10-phenanthroline and 5-acetamido-1,10-phenanthroline, respectively.

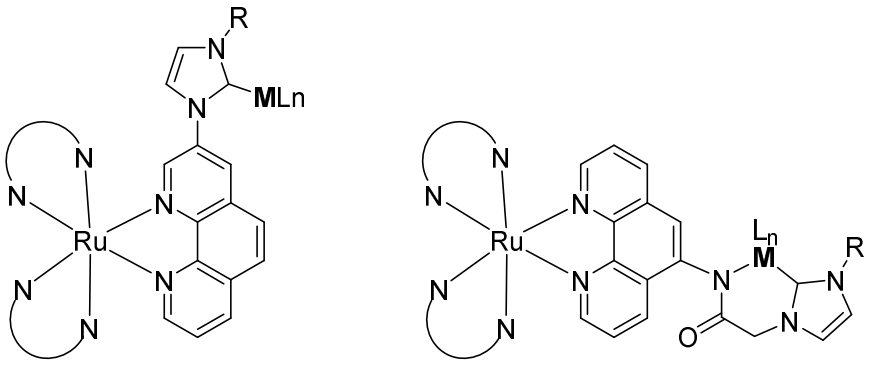

appended metallo-NHC complex ***tethered metallo-NHC complex***

Figure 5.1: *Target metallo-NHC prototype systems*

The development and application of some general and specific protocols for the enantiomeric resolution of metallo-NHC proligands is also detailed in this section. It is generally accepted that resolution of the Δ/Λ-enantiomers of octahedral ruthenium complexes are more efficient for those with 1,10-phenanthroline ancillary ligands

compared with 2,2'-bipyridine ligands. This prompted 2,2-bipyridine, which is more affordable, to be exchanged with 1,10-phenanthroline for the synthesis of "tethered-imidazolium" compounds. Effectively the precursor $Ru(bipy)_2Cl_2$ was substituted with $Ru(phen)_2Cl_2$ in later syntheses.

5.2. Synthesis of metallo-NHC proligands

5.2.1. Appended 1,10-phenanthroline NHC precursors and their ruthenium-polypyridine complexes

Previous researchers have demonstrated that imidazolyl-appended polypyridine compounds can be obtained by substitution of a halo-polypyridine precursor. In the context of NHC ligands, this has been demonstrated by Liu and co-workers who prepared 2,9-diimidazolium-1,10-phenanthroline salts by substitution of 2,9-diiodo-1,10-phenanthroline, either by quaternising an imidazole-phenanthroline intermediate (route A, Scheme 5.1) or by direct reaction with an *N*-substituted imidazole (route B, Scheme 5.1).[101] Similarly, 3,8-diimidazol-1,10-phenanthroline has been prepared as a supramolecular synthon.[241]

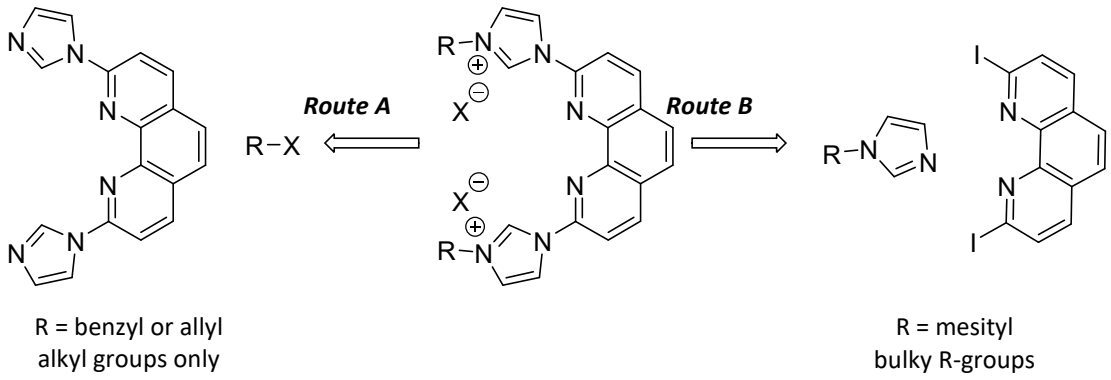

Scheme 5.1: *Synthetic routes to 2,9-diimidazolium-1,10-phenanthroline successfully employed by Liu and coworkers.*

The 2,9-diiodo-1,10-phenanthroline mentioned above is prepared by a non-trivial multi-step synthesis. A more direct approach was sought for this study, ideally using mono-imidazolyl-1,10-phenanthroline derivatives to avoid an unnecessarily complicated system. A mono-halogenated polypyridine precursor was therefore required, however, preparations of halogenated 1,10-phenanthrolines and 2,2'-bipyridines are typically low yielding and produce poly-halogenated products.[242] A suitable starting point was found in 3-bromo-1,10-phenanthroline which could reportedly be obtained in a 33% yield from 1,10-phenanthroline along with 3,8-dibromo-1,10-phenanthroline (17% yield).[243] The reaction was performed by heating 1,10-phenanthroline mono-hydrochloride in nitrobenzene at 140 °C for 3 hours following the dropwise addition of bromine to the heated solution. Purification by careful chromatography provided both 3-bromo-1,10-phenanthroline and 3,8-dibromo-1,10-phenanthroline in yields of 24% and 5.5%, respectively.

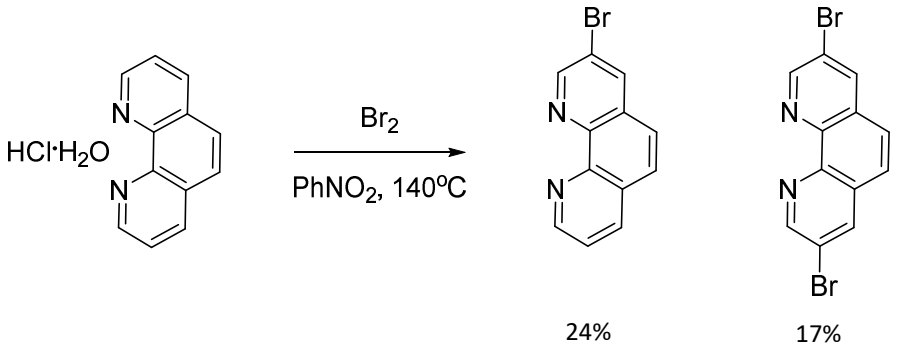

Scheme 5.2: *Bromination of 1,10-phenanthroline to provide 3-bromo and 3,8-dibromo-1,10-phenanthroline.*

The route taken by Lui *et al.* which enabled access to bulky aryl pendant imidazolium salts (route B, Scheme 5.1) was not viable. This is because halides in the 3-position of 1,0-phenanthroline are less reactive to nucleophilic substitution than those in the 2 and 4-positions and using bromine in place of iodine further reduces this reactivity.[244] Synthesis via the imidazole was the only option, however, this meant the system would be limited to substitution by unhindered alkyl pendant groups.

5.2.1.1. Imidazolium salts derived from 3-imidazo-1,10-phenanthroline

The 3-bromo-1,10-phenanthroline was reacted under conditions outlined for the synthesis of 3,8-diimidazol-1,10-phenanthroline[241] to provide 3-imidazol-1,10-phenanthroline (**5.1**), which has not been reported (Scheme 5.3). This required heating the 3-bromo-1,10-phenanthroline in an imidazole melt at 180 °C with K_2CO_3 and 2.5 mol% anhydrous $CuSO_4$ under an inert atmosphere. The product was isolated analogously to 3,8-diimidazol-1,10-phenanthroline by stirring the reaction mixture in water and extracting into chloroform. This procedure was greatly hampered by formation of a green emulsion making the organic extracts difficult to recover. Regardless, pure **5.1** was obtained from the dried extracts in a 55% yield. Difficulties with the extraction may have been avoided by employing an aqueous ammonium hydroxide solution to sequester any Cu(II) and better solubilise residual imidazole.

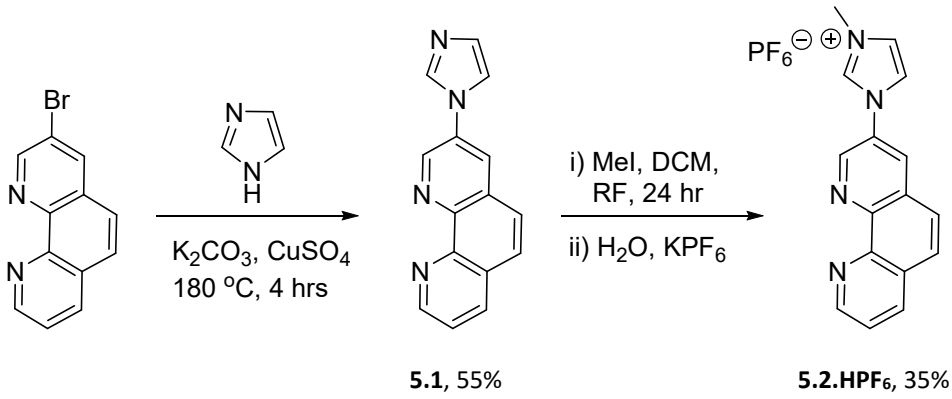

Scheme 5.3: *Synthesis of* ***5.2.HPF$_6$*** *from 3-bromo-1,10-phenanthroline via* ***5.1****.*

Quaternisation of the base imidazole **5.1** by reaction with excess iodomethane in refluxing DCM provided the methyl imidazolium salt 3-(1-methylimidazolium)-1,10-phenanthroline iodide (**5.2.HI**) (Scheme 5.3). Refluxing was performed for 24 hours, with the highly volatile iodomethane being topped up after 14 hours. Crude **5.2.HI** precipitates during the reaction and can be collected by filtration and washed with DCM and Et_2O providing material suitable for synthesis. If desired, further purification is achieved by dissolving this in water and precipitating as a PF_6 salt, providing **5.2.HPF$_6$** in an overall yield of 35% following filtering and drying. As with the 1,10-phenanthroline

annelated imidazoles discussed in Chapter 4, substitution of the phenanthroline nitrogen to form phenanthrolinum salts instead of the desired imidazolium salt may occur competitively. In the case of **5.2.HI**, the dark yellow complexion of the initial reaction mixture and DCM washes may indicate the presence of such impurities which have been proven to be highly coloured (see section 4.3).

This procedure could be optimised by using a sealed tube reaction to minimise the loss of the iodomethane and access higher temperatures. However, there is a risk of displacing the imidazolyl moiety at elevated temperatures as noted in the following section. To avoid formation of phenanthrolinium salt biproducts a post-complexation quartenisation pathway could be adopted as demonstrated for the synthesis of $[Ru(bipy)_2(\mathbf{4.9.H})][PF_6]_3$ from $[Ru(bipy)_2(\mathbf{4.4})][PF_6]_2$ (section 4.4.2). Here, the imidazole precursor **5.1** would be coordinated to Ru(II) and the resulting complex $[Ru(bipy)_2(\mathbf{5.1})][PF_6]_2$ reacted onward to form the imidazolium salt. Using a more reactive alkylating agent such as benzylbromide could also be advantageous. These advancements were not attempted due to time limitations.

Both $\mathbf{5.2.HPF_6}$ and its precursor **5.1** were characterised spectroscopically and an X-ray structure of $\mathbf{5.2.HPF_6}$ was obtained. The ^{1}H-NMR and ^{13}C-NMR spectra of both are as expected (^{1}H-NMR spectrum of $\mathbf{5.2.HPF_6}$, Figure 5.3a). As is commonplace, a downfield shift is noted for the imidazolyl NC*H*N proton (H16) upon formation of the imidazolium salt, going from 8.06 ppm in **5.1** ($CDCl_3$) to 9.07 ppm in $\mathbf{5.2.HPF_6}$ (CD_3CN). A new signal attributed the methyl group arises in the ^{1}H-NMR and ^{13}C-NMR spectra of $\mathbf{5.2.HPF_6}$ at 4.04 ppm and 36.51 ppm, respectively.

Crystals of $\mathbf{5.2.HPF_6}$ suitable for single crystal diffraction analysis were grown by slow vapour diffusion of THF into a MeCN solution of the compound. This crystallised in the monoclinic space group $P2_1/c$ with one molecule of $\mathbf{[5.2.H]^+}$ and one PF_6 counter-anion in the asymmetric unit (Figure 5.2). A shorter bond length between the imidazolyl-nitrogen and phenanthroline N15 – C3 of 1.425(3) Å compared with the methyl group bond N17 – C20 of 1.464(2)° is observed due to conjugation between the aromatic rings. This is despite the imidazolyl ring being twisted out of the phenanthroline plane by

31.4(2)°. This twist enables intermolecular hydrogen bonding between the imidazolium proton on C19 and the phenanthroline nitrogen atoms of neighbouring molecules (C19 ··· N1 = 3.519(2) Å and C19 ··· N10 = 3.246(2) Å). These occur in a reciprocal manner forming a weakly H-bonded dimer. Additionally, phenanthroline units are stacked such that face-to-face π – π interactions are observed between the central benzenoid ring and N10 rings generating a centroid-to-centroid distance of 3.567(1) Å shifted by 1.069(3) Å / 1.141(3) Å.

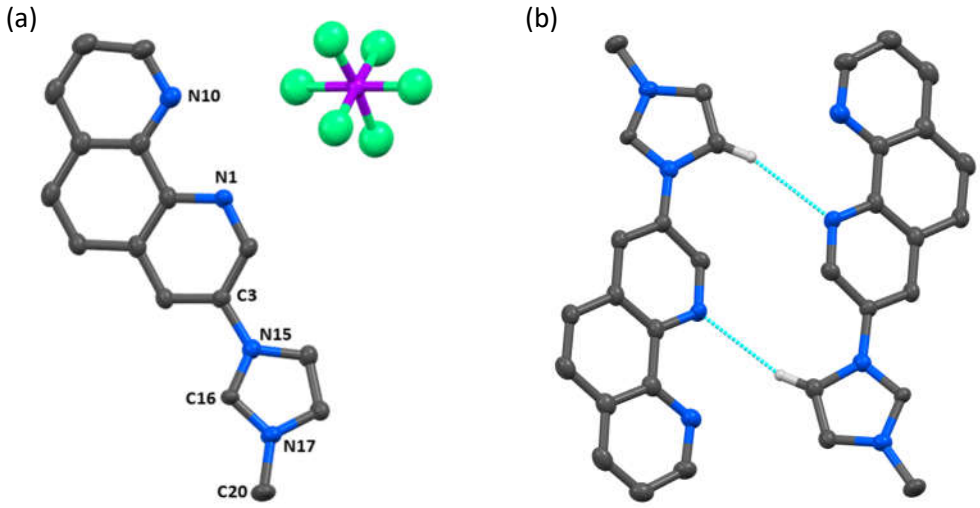

Figure 5.2 (a): *Asymmetric unit of* ***5.2.HPF$_6$*** *and,* ***(b)*** *Complementary C*H *··· N hydrogen bonding between molecules of* ***[5.2.H]$^+$****. Hydrogen atoms not involved in H-bonding have been omitted for clarity. Thermal ellipsoids are drawn at a 50% probability level.*

Ligand **5.2.HPF$_6$** was carried forward into synthesis of [Ru(bipy)$_2$(**5.2.H**)][PF$_6$]$_3$. The methodology described above allows for salts of **5.1** to be prepared with other alkyl pendant groups, however, this was not deemed necessary.

5.2.1.2. Synthesis of [Ru(2,2'-bipyridine)$_2$(5.2.H)][PF$_6$]$_3$

Target complex [Ru(bipy)$_2$(**5.2.H**)][PF$_6$]$_3$ was successfully prepared by the reaction of **5.2.HPF$_6$** with Ru(bipy)$_2$Cl$_2$ in ethylene-glycol using a microwave reactor and monitoring by TLC (silica, 4:1:1 DMF/water/1 M NH_4Cl). In an initial attempt, reagents were

combined in ethylene-glycol and the mixture heated by microwave irradiation (450 W) in 2 minute bursts, requiring a total of 6 minutes to dissolve the $Ru(bipy)_2Cl_2$ and react all material. Two products were isolated following ion-exchange chromatography with gradient elution (sephadex – C25, 0 to 0.20 M NaCl) and found to be the desired product $[Ru(bipy)_2(\mathbf{5.2.H})][PF_6]_3$ (28% yield) and the ethylene-glycol adduct $[Ru(bipy)_2(\mathbf{5.3})][PF_6]_2$ (40% yield) (Scheme 5.4).

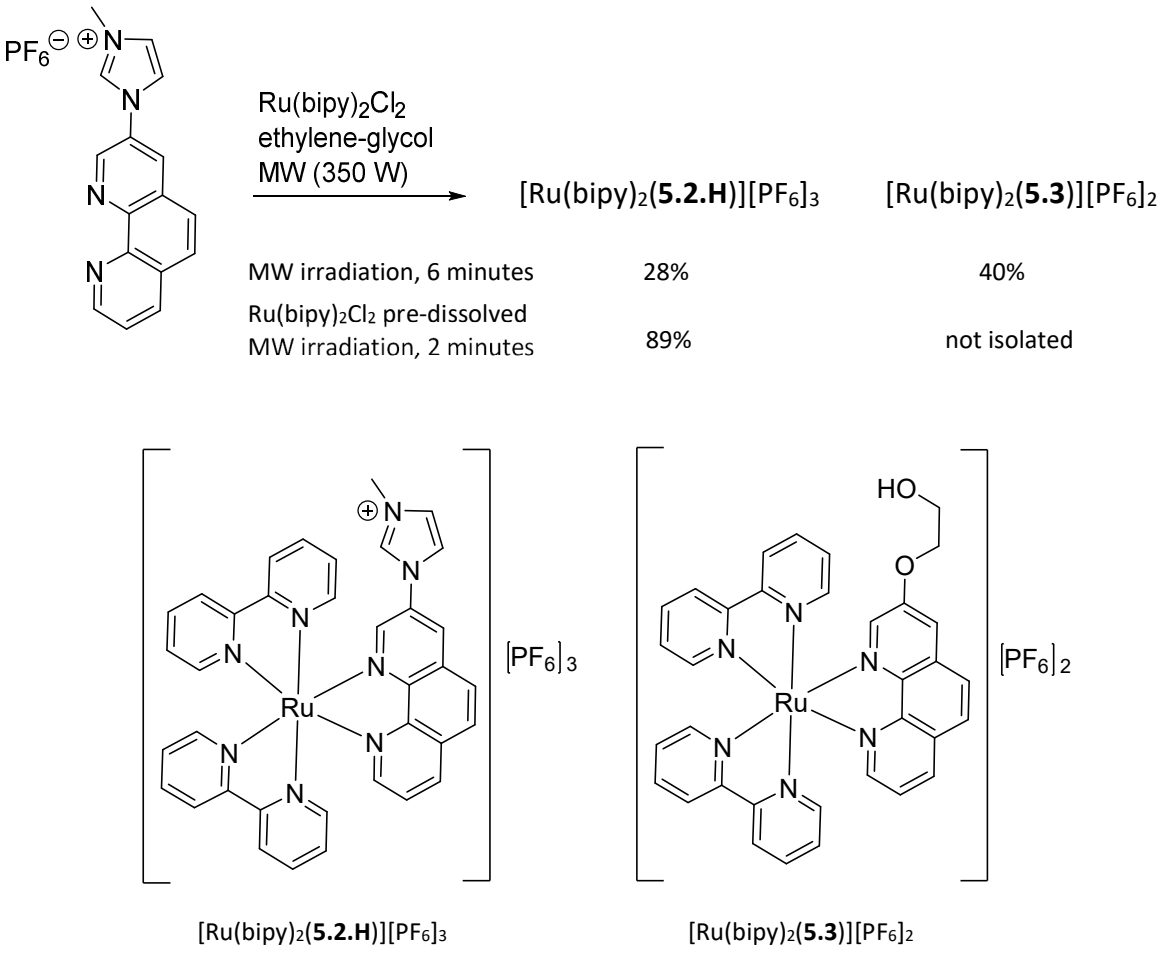

$[Ru(bipy)_2(\mathbf{5.2.H})][PF_6]_3$ $[Ru(bipy)_2(\mathbf{5.3})][PF_6]_2$

Scheme 5.4: *Synthesis of $[Ru(bipy)_2(\mathbf{5.2.H})][PF_6]_3$ and the solvolysis product $[Ru(bipy)_2(\mathbf{5.3})][PF_6]_2$.*

Formation of $[Ru(bipy)_2(\mathbf{5.3})]^{2+}$ undoubtedly occurs by substitution of the imidazolium moiety by an ethylene-glycol solvent molecule under the highly energetic reaction conditions. Modifying the approach so that the reaction mixture was pre-heated to dissolve the $Ru(bipy)_2Cl_2$ then adding **5.2.HPF$_6$** and irradiating for only 2 minutes

provided $[Ru(bipy)_2(\mathbf{5.2.H})][PF_6]_3$ in an 89% yield. In this instance the product was isolated as its PF_6 salt following the reaction and purified by washing with water and methanol.

Given the formation of $[Ru(bipy)_2(\mathbf{5.3})]^{2+}$, the synthesis of $[Ru(bipy)_2(\mathbf{5.2.H})]^{3+}$ may have suited milder conditions such as the refluxing EtOH/water method used for the synthesis of $[Ru(bipy)_2(\mathbf{4.9.H})]^{3+}$ (section 4.4.2) and the acetamide tethered complexes discussed shortly. However, sufficient product was obtained by truncating the reaction time so this was not attempted.

The complex $[Ru(bipy)_2(\mathbf{5.2.H})][PF_6]_3$ and the solvolysis product $[Ru(bipy)_2(\mathbf{5.3})][PF_6]_2$ were both fully characterised and their structures unambiguously confirmed by X-ray crystallography. Four cations attributable to the complex $[Ru(bipy)_2(\mathbf{5.2.H})][PF_6]_3$ were identified by mass spectrometry with the two most intense signals at 225.0476 and 410.0532 belonging to $[Ru(bipy)_2(\mathbf{5.2.H})]^{3+}$ and $[[Ru(bipy)_2(\mathbf{5.2.H})][PF_6]]^{2+}$ (calculated m/z, $[Ru(bipy)_2(\mathbf{5.2.H})]^{3+}$ = 225.0517 and $[Ru(bipy)_2(\mathbf{5.2.H})][PF_6]^{2+}$ = 410.0599). Interestingly, a less intense signal due to the free NHC species $[Ru(bipy)_2(\mathbf{5.2})]^{2+}$ was found at 337.0682 (calculated m/z, $[Ru(bipy)_2(\mathbf{5.2})]^{2+}$ = 337.0739). A minor signal due to $[[Ru(bipy)_2(\mathbf{5.2.H})][PF_6]_2]^{+}$ was also observed.

Comparison of the ^{1}H-NMR spectrum of $[Ru(bipy)_2(\mathbf{5.2.H})][PF_6]_3$ and the free ligand **5.2.HPF$_6$** revealed several notable coordination induced shifts (Figure 5.3). As is typical of Ru(II) polypyridine complexes, proton environments adjacent to the pyridyl nitrogen shift significantly upfield upon coordination as a result of anisotropic shielding by adjacent rings of pyridyl ligands. For **5.2.HPF$_6$**, the H2 and H9 resonances shifted from 9.32 ppm and 9.21 ppm to 8.22 ppm and ~ 8.13 ppm in $[Ru(bipy)_2(\mathbf{5.2.H})][PF_6]_3$ ($\Delta\delta$ = -1.10 ppm and ~ -1.08 ppm, respectively). Interestingly, proton environments on the imidazolium moiety also shifted upfield, albeit to a lesser extent. Signals for H16, H18 and H19 shifted from 9.07 ppm, 7.67 ppm and 7.96 ppm to 8.77 ppm, 7.58 ppm and 7.71 ppm upon coordination ($\Delta\delta$ = -0.30 ppm and -0.09 ppm and -0.25 ppm, respectively). The methyl environment undergoes a small upfield shift of -0.09 ppm. Again, anisotropic shielding is accountable and explains why greater shifts are observed for H16 and H19,

which are directed towards the face of the geometrically *cis*-pyridyl ring of a 2,2-bipyridine ligand, unlike H18 and H20. This is obvious from the crystal structure (Figure 5.4). Environments H4, H5, H6 and H7 which are further afield from the ligand sphere of the complex exhibit downfield shifts of 0.17 ppm, 0.31 ppm, 0.21 ppm and 0.20 ppm as a consequence of electron density withdrawal onto Ru(II).

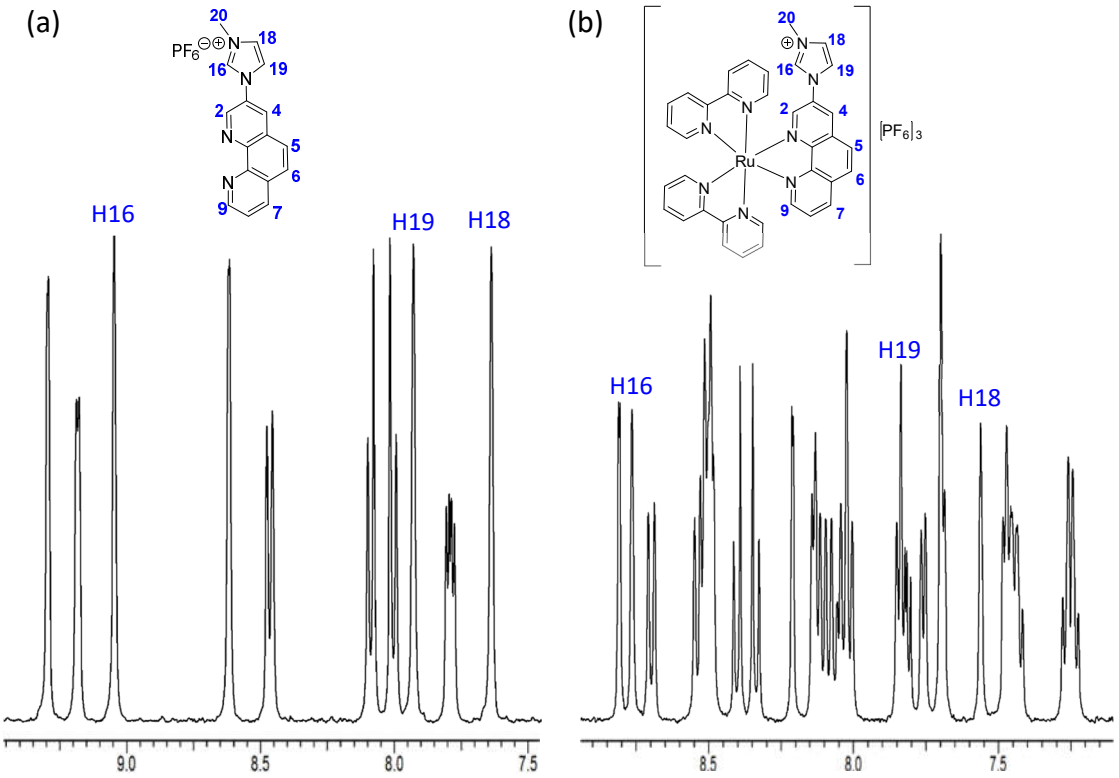

Figure 5.3 (a): *Aromatic region of the ^{1}H-NMR spectra of* ***5.2.HPF$_6$*** *and,* ***(b)*** *[Ru(bipy)$_2$(**5.2.H**)][PF$_6$]$_3$ in CD$_3$CN.*

The ^{1}H-NMR and ^{13}C-NMR spectra of [Ru(bipy)$_2$(**5.3**)][PF$_6$]$_2$ was also fully assigned and the ethylene-glycol appendage confirmed by two ethylene proton multiplets at 4.22 ppm and 3.84 ppm and a singlet due to the hydroxyl proton at 3.00 ppm as well as ethylene carbon signals at 72.09 ppm and 60.83 ppm.

X-ray diffraction analysis was performed on [Ru(bipy)$_2$(**5.2.H**)][PF$_6$]$_3$ using crystals grown by slow vapour diffusion of benzene into a MeCN solution of the compound. This crystallised in the monoclinic space group $P2_1/c$ with one molecule of [Ru(bipy)$_2$(**5.2.H**)]$^{+}$

and three PF_6 anions in the asymmetric unit (Figure 5.4). The octahedral ruthenium centre supports the expected propeller arrangement of bidentate ligands. The bite angles for the three ligands, N1 – Ru – N10, N1A' – Ru – N1A'' and N1B' – Ru – N1B'' are 79.95(9)°, 78.58(9)° and 79.02(9)°, respectively and Ru – N bond lengths fall within a narrow range between 2.055(2) Å for Ru – N1B'' and 2.072(2) Å for Ru – N1B'. A twist of the imidazolyl-ring out of the phenanthroline plane by 35.8(3)° is similar in magnitude to that observed in the crystal structure of the free ligand, **5.2.HPF$_6$**. Bond lengths related to the imidazole including N15 – C3 = 1.433(3) Å and N17 – C20 = 1.468(3) Å are also largely unchanged.

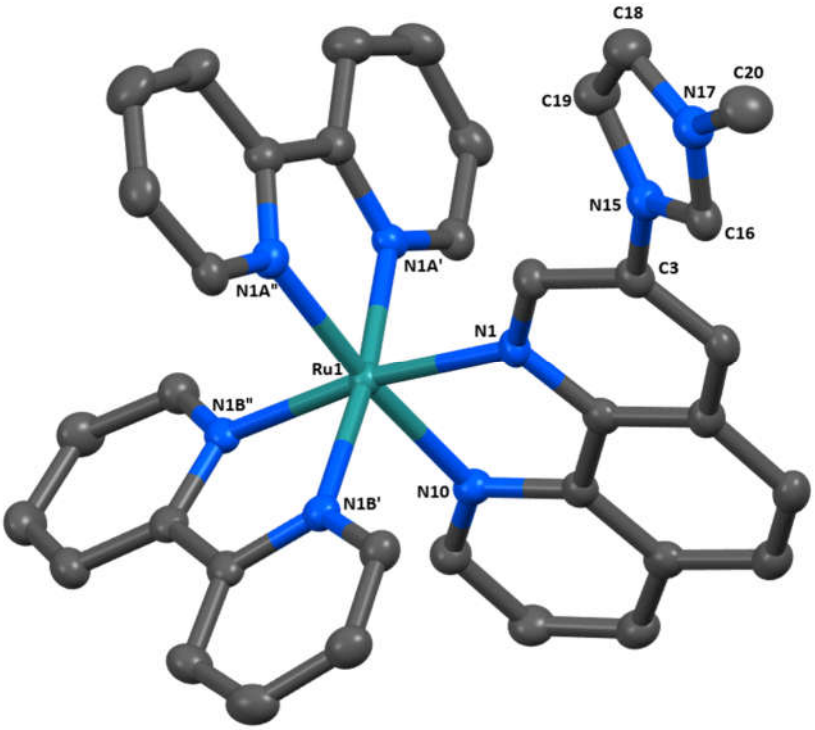

Figure 5.4: *Asymmetric unit of [Ru(bipy)$_2$(**5.2.H**)][PF$_6$]$_3$. Hydrogen atoms and PF$_6$ anions have been omitted for clarity. Thermal ellipsoids have been drawn at 50% probability.*

Packing of the extended structure is characterised by numerous short C*H* ··· F contacts involving electron poor carbon environments such as C19 ··· F = 3.163(4) Å, C16 ··· F = 3.397(4) Å and C6A' ··· F = 3.220(3) Å. A largely offset but still face-to-face π – π

interaction is seen between phenanthroline components of neighbouring **[5.2.H]**$^{+}$ ligands with corresponding benzenoid rings and N1-pyridyl rings at a centroid-to-centroid distance of 3.650(2) Å and plane-to-centroid shift of 1.515(4) Å / 1.454(4) Å. The shortest carbon-to-plane distances are C4 ··· plane = 3.344(3) Å and C5 ··· plane = 3.335(3) Å.

The crystal structure of [Ru(bipy)$_2$(**5.3**)][PF$_6$]$_2$ was obtained using crystals grown by slow vapour diffusion of benzene into a MeCN solution of the compound. This crystallised in the triclinic spacegroup $P\bar{1}$ with one molecule of [Ru(bipy)$_2$(**5.3**)]$^{2+}$, two PF$_6$ anions and one benzene solvate molecule in the asymmetric unit (Figure 5.5). This clearly shows an ethylene-glycol group in the 3-position of the phenanthroline ligand.

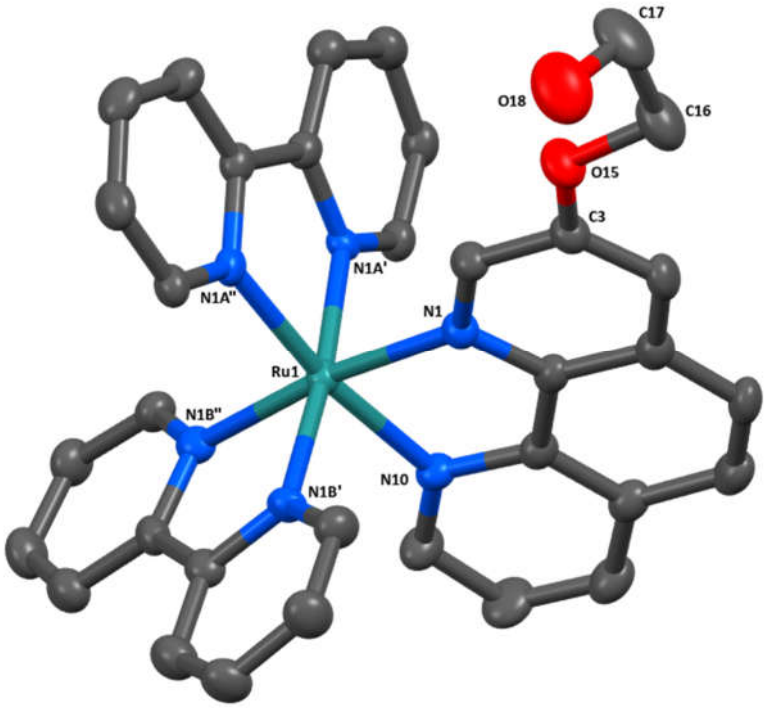

Figure 5.5: *Asymmetric unit of [Ru(bipy)$_2$(**5.3**)][PF$_6$]$_2$. Hydrogen atoms, PF$_6$ anions and the benzene solvate molecule have been omitted for clarity. Thermal ellipsoids have been drawn at 50% probability.*

The octahedral coordination geometry of the Ru(II) is characterised by the bond angles N1 – Ru – N10, N1A' – Ru – N1A'' and N1B' – Ru – N1B'' are 80.2(2)°, 78.6(2)° and 78.7(2)°,

respectively. Ru – N bond lengths fall within the range of 2.047(3) Å for Ru – N1B'' and 2.076(3) Å for Ru – N10. Oxygens of the ethylene-glycol group are gauche to one another as expressed by the O15-C16-C17-O18 torsion angle of 61.9(4)°. As with $[Ru(bipy)_2(\mathbf{5.2.H})][PF_6]_3$ there are numerous hydrogen bonding contacts with PF_6 flourine acceptors most notably; O18 ⋯ F = 2.987(6) Å, C7 ⋯ F = 3.317(5) Å and C6A' ⋯ F = 3.322(4) Å. Likewise, adjacent phenanthroline units of the **5.3** ligand stack such that the benzenoid rings are overlapped, having a centroid-to-centroid distance of 3.684(3) Å at an offset of 1.493(6) Å and centroid-to-plane distance of 3.368(4) Å. The N1A' pyridyl rings of adjacent 2,2'-bipyridine ligands also associate in a face-to-face manner with a centroid-to-centroid distance of 3.805(3) Å at an offset of 1.735(6) Å and centroid-to-plane distance of 3.387(4) Å.

This pathway was eventually disfavoured in place of the acetamide derivatives which are ripe for variation of the opposing pendant group and are much easier to synthesise. Furthermore, the acetamide methodology is more adaptable to other systems for comparison such as the bornyl and cyclohexyl systems (Chapter 1 and Chapter 2).

5.2.2. Acetamide tethered 1,10-phenanthroline NHC precursors and their ruthenium-polypyridine complexes

It has been shown in previous chapters that the use of an acetamide linking unit lends itself to exploration of tethered NHC compounds because it is highly adaptable and tolerant to variation of the imidazolyl moiety. As with the bornyl-acetamide and cyclohexyl-acetamide derivatives, this approach hinges on the synthesis of a chloroacetamide electrophile from an amine of the core compound, in this case 1,10-phenanthroline. By far the most well documented and synthetically accessible amine for this is 5-amino-1,10-phenanthroline however, preparations for 2-amino-1,10-phenanthroline[245] and 4-amino-1,10-phenanthroline[246] can be found along with 4,7-diamino-1,10-phenanthroline[247] and 5,6-diamino-1,10-phenanthroline.[248] These offer interesting opportunities for modulation of this system.

Following reported procedures, 1,10-phenanthroline was nitrated to give 5-nitro-1,10-phenanthroline[249, 250] (90% yield) which was subsequently reduced using hydrazine hydrate and 10% Pd/C to provide 5-amino-phenanthroline[251] in an 81% yield. Chloroacetylation of 5-amino-1,10-phenanthroline to give 2-chloro-N-1,10-phenanthrolin-5-yl-acetamide **5.4** has been reported, however, the preparations followed were found to require some modifications. For one synthesis of **5.4**, 5-amino-1,10-phenanthroline was reacted with chloroacetyl-chloride in MeCN using $NaHCO_3$ as the base.[251] Supposedly **5.4** could be collected by filtration at the conclusion of the reaction, however, the solid material was found to be a mixture of **5.4** and its protonated adduct along with inorganic contaminants including unreacted $NaHCO_3$. After rinsing the solid with water, additional product was isolated by basifying the filtrate and collecting the precipitated product which provided crude **5.4** in an overall yield of 70%. A more succinct approach was found in which a suspension of 5-amino-1,10-phenanthroline and triethylamine in THF was cooled to 0 ^oC and treated with chloroacetyl-chloride under anhydrous and oxygen free conditions (Scheme 5.5).[252] After an hour the beige material was filtered, washed with water and dried immediately afterwards in a vacuum desiccator.

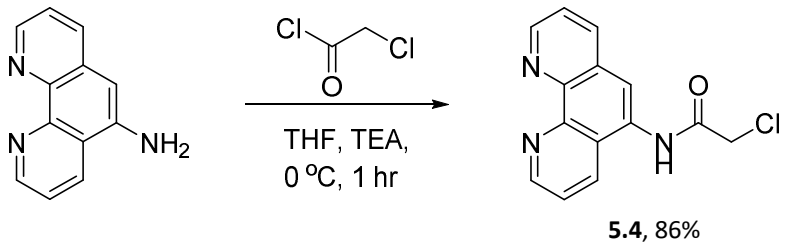

5.4, 86%

Scheme 5.5: *Synthesis of 2-chloro-*N*-1,10-phenanthrolin-5-yl-acetamide (**5.4**) from 5-amino-1,10-phenanthroline.*

Again, it was found that addition of 10% NaOH to the filtrate provided an additional crop of product, giving **5.4** in an overall yield of 86%. This source suggested that the compound is air sensitive, although, the nature of this sensitivity was not elaborated. It was noted, however, that when using the earlier preparation method, different coloured samples of **5.4** were isolated ranging from light orange to dark brown and

sometimes pink. Sample isolated after avoiding exposure to air remained a beige powder as described.

5.2.2.1. Acetamide tethered 1,10-phananthroline imidazolium salts

Acetamide tethered 1,10-phenanthroline imidazolium salts were prepared from the chloroacetamide **5.4** by reaction with several *N*-substituted imidazoles. This is in analogy to the synthesis of bornyl-acetamide and cyclohexyl-acetamide imidazolium salts described previously. The salts **5.5.HX**, **5.6.HX**, **5.7.HX**, **5.8.HX**, **5.9.HX** and **5.10.HX** were prepared as shown in Scheme 5.6 and were isolated as either their Cl or PF_6 salts depending on the purification method or desired product solubility.

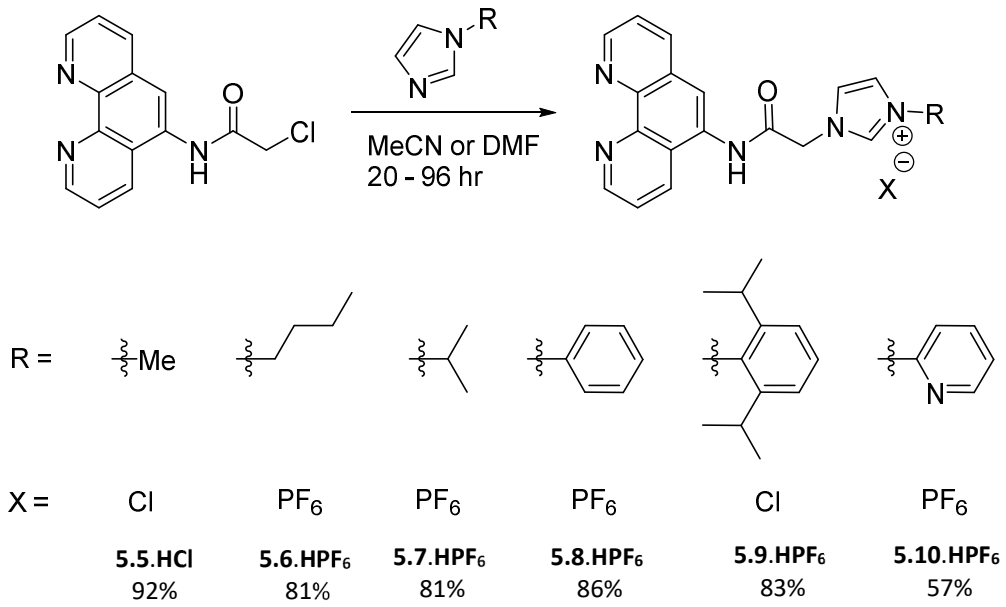

Scheme 5.6: *Synthesis of acetamide tethered 1,10-phenanthroline imidazolium salts* ***5.5.HX****,* ***5.6.HX****,* ***5.7.HX****,* ***5.8.HX****,* ***5.9.HX*** *and* ***5.10.HX*** *from* ***5.4****. Yields shown for most conveniently isolated salts (Cl or* PF_6*).*

Compound **5.4** was heated in MeCN or DMF with an excess of *N*-substituted imidazole until all **5.4** had been consumed as determined by ^{1}H-NMR. Compounds **5.6.HPF$_6$**, **5.7.HPF$_6$** and **5.8.HPF$_6$** were prepared by refluxing in MeCN for 20 hours under an inert

atmosphere. After this time the solvent was removed by rotary-evaporation and the residue taken up in water, filtered and washed with DCM to remove unreacted **5.4** and by-products, then washed with Et_2O. Precipitating the product by addition of excess solid KPF_6 and stirring for 30 minutes before filtering provided pure material as fine white powders in yields of 80% – 86%. The methyl compound **5.5.HPF$_6$** was also prepared by this method using DMF at 100 ^oC for 2 hours. Although isolated in an 83% yield, it precipitated very slowly with the PF_6 salt being isolated in several crops by condensing the aqueous solution. It was more easily isolated as **5.5.HCl** (93% yield) by refluxing in MeCN for 24 hours and collecting the resultant precipitate by filtration and washing with DCM. Likewise, the diisopropyl-phenyl derivative **5.9.HX** was better isolated as its chloride salt. Because **5.9.HCl** is soluble in DCM, washing the aqueous solution of the reaction mixture with DCM resulted in the product being distributed between both phases. Instead it was found that filtering the aqueous solution through a plug of alumina and rinsing through with additional water provided a filtrate of pure **5.9.HCl** that could simply be rotary evaporated (86% yield) or precipitated as **5.9.HPF$_6$**. It is likely that this approach could also be applied to purification of the other imidazolium salts. Using MeCN as the reaction solvent was preferable to DMF because it could be easily removed making workup more straightforward. However, synthesis of **5.9.HX** required 96 hours in refluxing MeCN as opposed to 24 hours using DMF at 100 ^oC. Synthesis of the pyridyl appended **5.10.HX** was not attempted in MeCN but took 48 hours to complete in DMF at 100 ^oC. It was isolated the same manner as compounds **5.6.HPF$_6$**, **5.7.HPF$_6$** and **5.8.HPF$_6$**, giving **5.10.HPF$_6$** as a yellow powder in a 57% yield.

These salts were spectroscopically characterised and crystal structures of **5.7.HPF$_6$** and **5.8.HPF$_6$** were obtained. Aside from differences derived from their pendant group functionality, salts of **5.5.HX**, **5.6.HX**, **5.7.HX**, **5.8.HX**, **5.9.HX** and **5.10.HX** exhibit similar ^{1}H-NMR, ^{13}C-NMR, IR and mass-spectral features. NMR features of these ligands are discussed in relation to their Ru(II) complexes [Ru(phen)$_2$(**5.5.H – 5.10.H**)][PF_6]$_3$ in the next section. ^{1}H-NMR spectra of **5.5HPF$_6$** is shown in Figure 5.11a and some chemical shifts values for **5.5HPF$_6$** and **5.9.HCl** are given in Table 5.1.

Crystals of imidazolium salt **5.7.HPF$_6$** were grown by slow vapour diffusion of Et_2O into a MeCN solution of the compound. It crystallised in the monoclinic space group $P2_1/n$ with four molecules of [**5.7.H**]$^+$, four PF_6 anions and four MeCN solvate molecules in the asymmetric unit (Figure 5.6). The four molecules of [**5.7.H**]$^+$, are distinguished by the suffix A, B, C or D. A *Z*-configuration of the amide is observed and bond lengths related to the amide as follows (A / B / C / D); O1 – C16 = 1.227(5) Å / 1.231(5) Å / 1.220(5) Å / 1.231(5) Å, N15 – C16 = 1.338(5) Å / 1.336(6) Å / 1.358(6) Å / 1.347(5) Å, N15 – C5 = 1.409(6) Å / 1.420(6) Å / 1.421(5) Å / 1.415(6) Å. In addition to characterisation, this structure is interesting for its extended architecture which arises from mutual hydrogen-bonding and π – π stacking interactions between molecules of [**5.7.H**]$^+$.

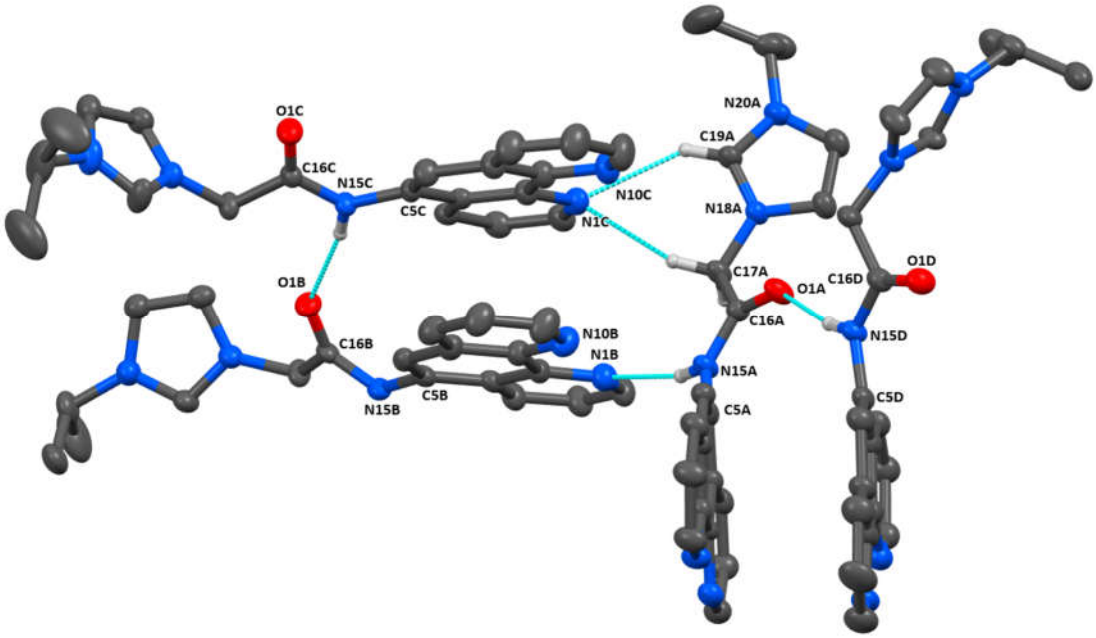

Figure 5.6: *Contents of the asymmetric unit of* ***5.7.HPF$_6$*** *with hydrogen bonding interactions highlighted. Hydrogen atoms not involved in intermolecular contacts have been omitted for clarity along with PF_6 counter anions and MeCN solvate molecules. Thermal ellipsoids have been drawn at 50% probability.*

Several examples of crystal structures where acetamide compounds have uncoordinated amides such as this are explored in Chapters 1 and 2. In all of these cases the *Z*-amide supports bridged hydrogen bonds between the amide-N*H* and amide-O of

adjacent molecules resulting in unidimensional hydrogen bonded polymers (see **2.1**, section 2.2.1 for a representative case). In this structure, however, the N1 nitrogen of two out of the four unique phenanthroline-moieties accepts a hydrogen bond from an amide-N*H* (N15A ··· N1B = 2.841(5) Å and N15B ··· N1A = 2.950(5) Å), terminating chain formation. Instead a helical arrangement of [**5.7.H**]$^+$ molecules occurs, resulting in rectangular channels of 6.942(4) Å by 7.504(4) Å that propagate along the crystallographic b axis (Figure 5.7). These are occupied by acetonitrile.

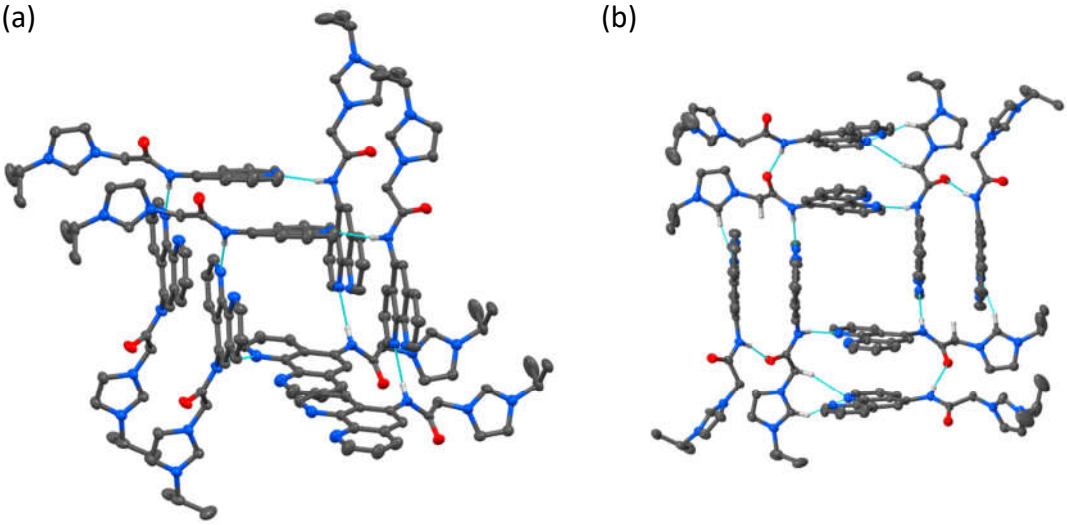

Figure 5.7 (a): *N*H ··· *N bonding resulting in a helical motif and,* ***(b)*** *view along the crystallographic b axis revealing a rectangular channel. Molecules of MeCN occupying the channel are not shown.*

All four sides of these channels are insulated by another molecule of [**5.7.H**]$^+$ that is emplaced by a hydrogen bond of the type N*H* ··· O between amide units (N15C ··· O1B = 2.817(5) Å and N15D ··· O1A = 2.774(5) Å). Each pair of phenanthroline groups stack such that they are almost overlaid at a plane-to-plane distance of 3.480(3) Å (B-to-C) and 3.427(3) Å (A-to-D) (Figure 5.7b). Interestingly, this pairing of phenanthroline units appears to be stabilised by a hydrogen bond donating clip formed between the imidazolyl NC*H*N donor and amide N*H* donor as seen in Figure 5.6. Relative to the solvent channel, this supporting C*H* ··· N interaction occurs between the NC*H*N of the "inner" [**5.7.H**]$^+$ and the phenanthroline N1 of the "outer" [**5.7.H**]$^+$. Internuclear distances

related to this secondary association are C19A ··· N1C = 3.337(6) Å and C19B ··· N1D = 3.135(6) Å. It is difficult to determine whether this clip-like behaviour has a significant effect on templating the arrangement observed here as this structural motif is not present in the crystal structure of **5.8.HPF$_6$**.

Single crystal X-ray diffraction was performed on **5.8.HPF$_6$** using crystals grown by slow vapour diffusion of Et_2O into MeCN. Unlike **5.7.HPF$_6$**, this crystallises with unit cell contents of a single molecule of [**5.8.H**]$^+$, one PF_6 anion and one water molecule in the orthorhombic space group *Pbca* (Figure 5.8). As expected the amide crystallises in its *Z*-configuration and is characterised by the bond lengths C16 – O1 = 1.225(5) Å, C16 – N15 = 1.337(5) Å and C5 – N15 = 1.428 Å all of which are comparable with those recorded for [**5.7.H**]$^+$.

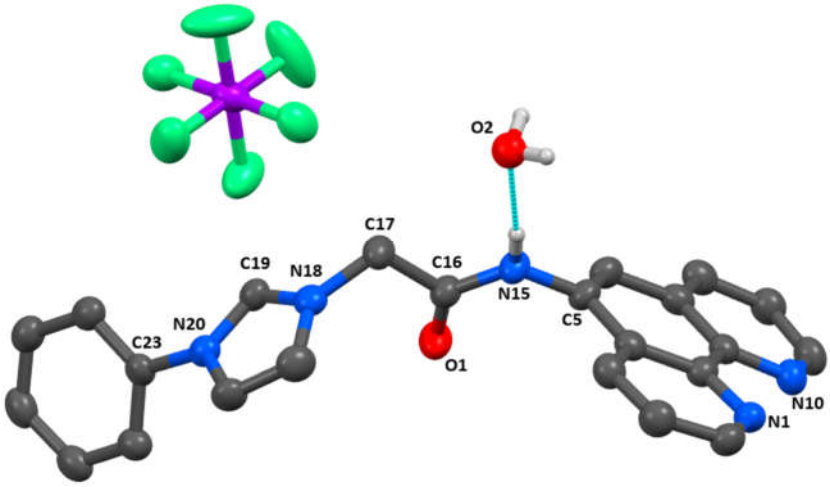

Figure 5.8: *Contents of the asymmetric unit of* ***5.8.HPF$_6$*** *Hydrogen atoms not involved in intermolecular contacts have been omitted for clarity. Thermal ellipsoids have been drawn at 50% probability.*

The acetamide linkage is rotated such that it is perpendicular to the plane of the imidazolyl ring as represented by the torsion angle C19-N18-C17-C16 of 95.9(4)°. Hydrogen bonding in the packed structure is exclusively mediated by the water molecule which is an O*H* donor in two interactions O2 ··· O1 = 2.819(5) Å and O2 ··· N10 = 2.831(5)Å and an acceptor to the amide N*H* for the interaction N15 ··· O2 = 2.816(5) Å (Figure 5.9).

Stacking of the phenanthroline groups is much less notable, with only the benzenoid ring and N1-pyridyl ring slightly overlapped at a centroid-to-centroid distance of 3.717 Å and shift distance of 1.192 Å. Molecules of [**5.8.H**]$^+$, hydrogen bonded via the N15*H* ··· O2*H* ··· O1 chain are arranged such that the phenyl pendant of one molecule, and imidazolyl ring of the other are co-planar but largely offset. Their centroid-to-centroid distance is 4.266(3) Å with a shift of 2.590(7) Å however, the plane-to-centroid distance is 3.293(5) Å. Perhaps it is because the aromatic phenyl pendant of [**5.8.H**]$^+$ can participate in additional interactions that a different packing arrangement is observed when compared with the structure of **5.7.HPF$_6$**.

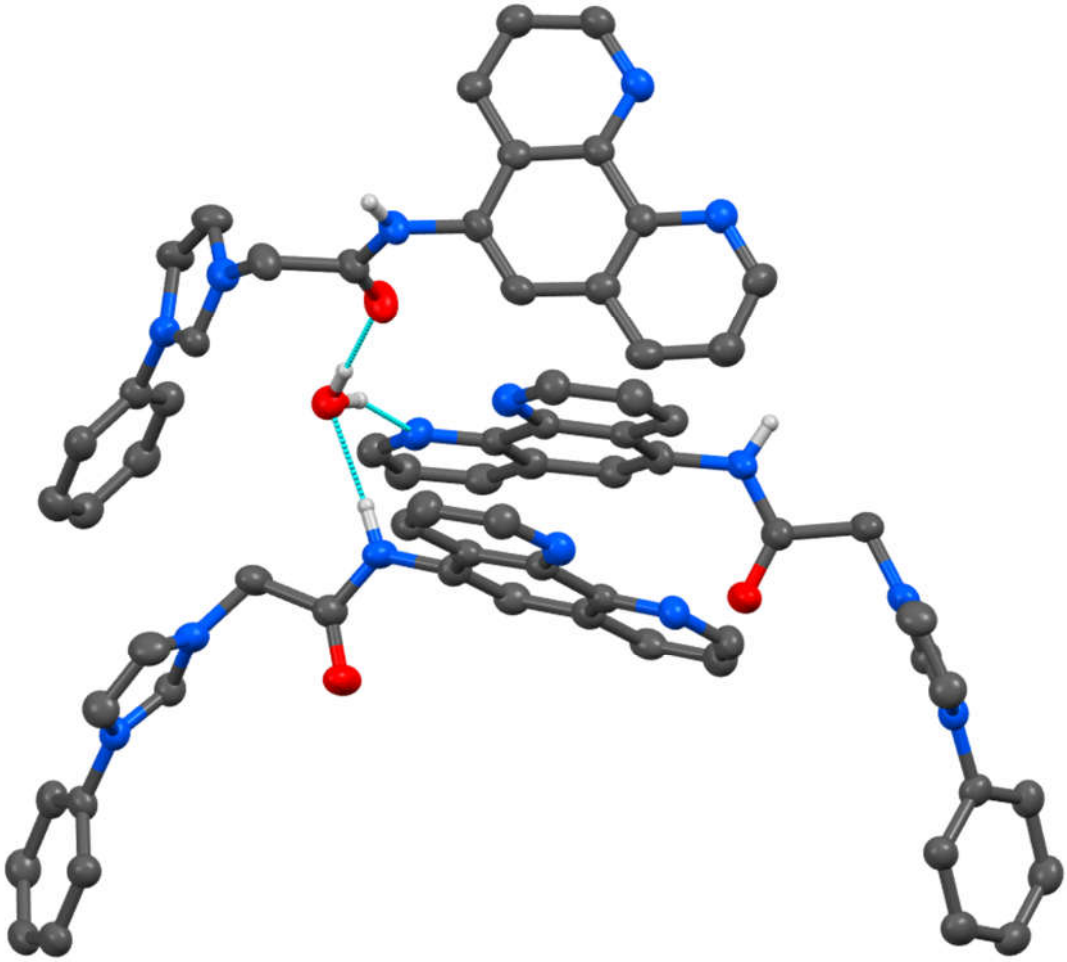

Figure 5.9: *Highlighting the role of the water molecule in hydrogen bonding within the packed structure.*

5.2.2.2. Synthesis of acetamide linked metallo-NHC proligands

Complexes of the type $[Ru(phen)_2(5\text{-}PA)][PF_6]_3$ were sought as prospective NHC metalloproligands from which Δ / Λ enantiomers could be resolved or synthesised from resolved precursors. Racemic forms of these were prepared in the first instance to provide material for analysis and to assess their applicability as proligands in palladium mediated catalysis. Synthesis and characterisation of the racemic complexes $[Ru(phen)_2(\mathbf{5.5.H})][PF_6]_3$, $[Ru(phen)_2(\mathbf{5.6.H})][PF_6]_3$, $[Ru(phen)_2(\mathbf{5.7.H})][PF_6]_3$, $[Ru(phen)_2(\mathbf{5.8.H})][PF_6]_3$, $[Ru(phen)_2(\mathbf{5.9.H})][PF_6]_3$ and $[Ru(phen)_2(\mathbf{5.10.H})][PF_6]_3$ will be discussed here. Enantiomeric resolution of $[Ru(phen)_2(\mathbf{5.9.H})][PF_6]_3$ into Δ - $[Ru(phen)_2(\mathbf{5.9.H})][PF_6]_3$ and Λ - $[Ru(phen)_2(\mathbf{5.9.H})][PF_6]_3$ is explored in section 5.7.

Preparation of complexes $[Ru(phen)_2(\mathbf{5.5.H} – \mathbf{5.10.H})][PF_6]_3$ was achieved by refluxing one of the imidazolium salt ligands **5.5.HX** – **5.10.HX** with $Ru(phen)_2Cl_2$ in a 4 : 1 EtOH/water mixture (Scheme 5.7). Before use, the EtOH/water mixture was degassed with bubbling argon and all reactions were performed under an argon atmosphere with reaction progress monitored by TLC (silica, 9:1.5:1 MeCN/water/saturated $KNO_{3(aq)}$). Several of these reactions were allowed to reflux overnight for ~ 20 hours, however, it was typically found that 2 – 4 hours was sufficient for total conversion to product. All complexes were isolated by flash chromatography on silica, eluting with 9:1.5:1 MeCN/water/saturated $KNO_{3(aq)}$ solution. Pure material was obtained by condensing the appropriate fractions which were then taken up in water and treated with aqueous KPF_6 solution. The resultant precipitate was collected by filtration providing the PF_6 salt of the product as a bright orange powder. Yields were typically between 70% – 80% except for $[Ru(phen)_2(\mathbf{5.10.H})][PF_6]_3$ which was 58%. Yields returned for the pyridyl-pendant imidazolium salt compounds $[Ru(phen)_2(\mathbf{5.10.H})][PF_6]_3$ and ligand **5.10.HPF$_6$** were always lower than the other imidazolium salts. This continues a trend of lower yields for pyridyl-substituted derivatives beginning with the synthesis of **2.5.HCl** (55% yield) and **2.5.HCl** (67% yield). Such variations in yield may be caused by the electron deficient pyridine unit rendering 1-(2-pyridyl)-imidazole less nucleophilic than its alkyl or phenyl appended counterparts. Furthermore, it is postulated that the inherently basic pyridine substituent could deprotonate the imidazolium salt under the reaction conditions

leading to decomposition via the NHC. The latter decomposition pathway may be exacerbated under the aqueous reaction conditions employed in the synthesis of $[Ru(phen)_2(\mathbf{5.10.H})][PF_6]_3$. Coordination of the pyridyl-pendant to the ruthenium starting material is another possible route to undesired products.

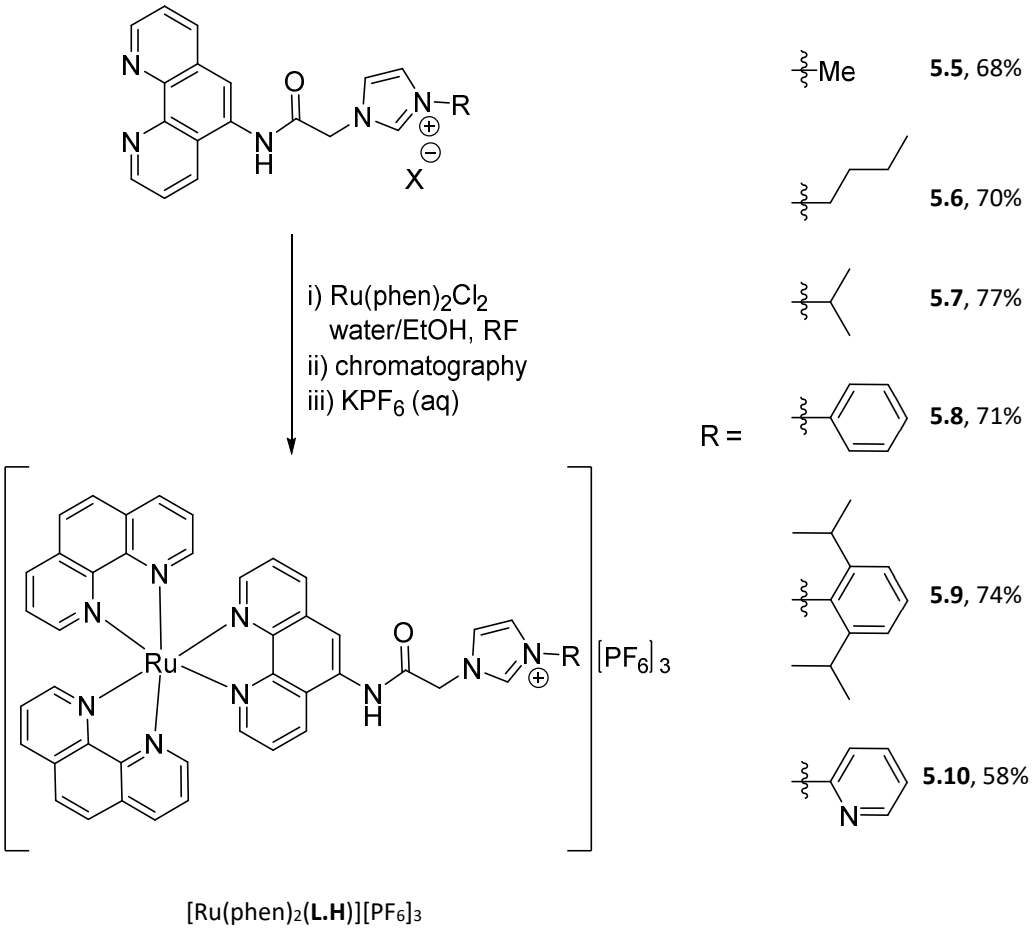

$[Ru(phen)_2(\mathbf{L.H})][PF_6]_3$

Scheme 5.7: *Synthesis of complexes* $[Ru(phen)_2(\mathbf{5.5.H} - \mathbf{5.10.H})][PF_6]_3$.

Besides differences derived from their pendant group functionality, the complexes $[Ru(phen)_2(\mathbf{5.5.H} - \mathbf{5.10.H})][PF_6]_3$ exhibit similar ^{1}H-NMR, ^{13}C-NMR, IR and mass-spectral features. Table 5.1 summarises the key proton and carbon resonances for the phenanthroline-acetamide imidazolium salt ligand.

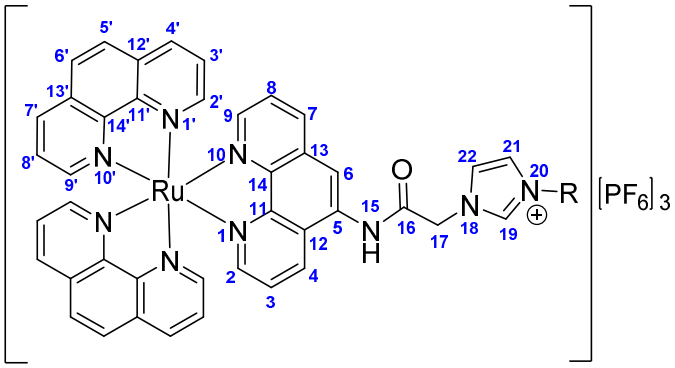

Figure 5.10: *Structure of [Ru(phen)$_2$(5-PA)][PF$_6$]$_3$ type complex with atoms labelled.*

Table 5.1: *Selected proton and carbon NMR resonances for complexes [Ru(phen)$_2$(**5.5.H - 5.10.H**)][PF$_6$]$_3$ and two free ligands. Atomic labelling shown in Figure 5.10.*

			Complexes [Ru(phen)$_2$(**L**)][PF$_6$]$_3$						Ligands	
			5.5.H	**5.6.H**	**5.7.H**	**5.8.H**	**5.9.H**	**5.10.H**	**5.5.HPF$_6$**	**5.9.HCl**
proton and carbon environments DMSO-*d6* (ppm)	acetamide	H15	11.00	11.00	11.00	11.06	11.15	11.06	10.74	—
		H17	5.46	5.45	5.45	5.55	5.61	5.58	5.46	5.47
		C16	166.13	166.13	166.08	165.75	165.96	165.33	165.34	165.88
		C17	51.96	51.82	52.88	52.14	52.30	51.83	51.20	53.21
	imidazolyl	H19	9.13	9.20	9.27	9.86	9.54	10.14	~ 9.17	9.65
		H21	~ 7.73	~ 7.80	7.95	~ 8.37	~ 8.13	~ 8.58	~ 7.82	~ 8.21
		H22	~ 7.77	~ 7.84	~ 7.80	~ 8.05	~ 8.09	~ 8.05	7.74	8.11
		C19	138.39	137.39	136.67	137.23	139.97	136.42	137.95	139.66
		C21	123.68	124.39	124.56	121.37	125.03	118.85	123.13	124.68
		C22	124.47	124.65	124.75	125.50	125.32	125.40	124.03	125,37
	5-amido-phen	H2	8.10	8.12	8.13	8.13	~ 8.12	~ 8.12	~ 9.17	9.07
		H9	7.99	7.99	8.00	8.00	8.01	7.99	9.07	8.94
		H4	8.91	8.91	8.92	8.92	8.94	8.92	8.75	8.87
		H7	8.70	~ 8.71	~ 8.71	~ 8.72	~ 8.77	~ 8.73	8.53	8.34
		H6	8.56	8.57	8.59	8.59	8.57	~ 8.58	8.21	~ 8.21
		C2	153.22	153.49	153.51	153.55	153.54	153.10	150.06	149.98
		C9	153.19	153.19	152.55	152.60	152.59	152.17	149.22	148.80
		C4	132.83	132.87	132.80	133.24	132.94	132.82	132.07	132.70
		C7	136.87	136.77	136.81	136.83	136.88	136.89	136.82	135.74
		C5	133.14	—	132.83	—	133.25	132.43	124.50	123.48
		C6	120.73	121.89	120.47	120.66	120.97	120.28	120.18	118.75

Also contained in Table 5.1 are related environments for uncoordinated ligands **5.5.HPF$_6$** and **5.9.HCl** which provide representative examples of PF_6 and Cl ligand salts and a reference point for coordination induced shifts. Not shown in the table are resonances due to the 1,10-phenanthroline ancillary ligands which have conserved signals at ~ 8.75 ppm (H4' / H7'), ~ 8.37 ppm (H5' / H6'), ~ 8.05 ppm (H2' / H9') and ~ 7.76 ppm (H3' / H8'). Their carbon environments are similarly conserved. Also absent are environments related to the pendant group and environments H3 and H8 which are consistently found in a multiplet between 7.83 – 7.70 ppm.

Unsurprisingly, chemical shifts of proton and carbon environments of the imidazolyl moiety are most affected by changes to the pendant group. The proton resonant frequencies are lower for alkyl-appended imidazolium groups than their aryl counterparts and the H19 and H21 environments differ most. Of the aryl appended species, the diisopropyl-phenyl derivative [Ru(phen)$_2$(**5.9.H**)][PF$_6$]$_3$ displays lower H19 and H21 frequencies (9.54 ppm and ~ 8.13 ppm, respectively) than the phenyl-appended and pyridyl-appended derivatives ([Ru(phen)$_2$(**5.8.H**)][PF$_6$]$_3$, 9.86 ppm and ~ 8.37 ppm; and [Ru(phen)$_2$(**5.10.H**)][PF$_6$]$_3$, 10.14 ppm and ~ 8.37 ppm). This is presumably because the rotation around the N – Ar bond is restricted by the isopropyl groups in [Ru(phen)$_2$(**5.9.H**)][PF$_6$]$_3$, forcing it the spend more time orthogonal to the imidazolium-ring. Therefore the H19 and H21 environments experience less anisotropic deshielding due to the aromatic pendant than in [Ru(phen)$_2$(**5.8.H**)][PF$_6$]$_3$ and [Ru(phen)$_2$(**5.10.H**)][PF$_6$]$_3$. Modulation of the pendant group affects the imidazolium carbon environments to a much lesser extent. All other environments are largely conserved. The phenanthroline carbon environment bonded to the amide (C5) was not always detectable but in some cases a small signal at ~ 132.8 ppm could be found with assistance from an HMBC correlation to H4.

Coordination induced shifts are as predicted for a phenanthroline based ligand that is coordinated to a ruthenium-polypyridine system. Such behaviour has been addressed for ligand **5.2.HPF$_6$** and its complex [Ru(bipy)$_2$(**5.2.H**)][PF$_6$]$_3$ in section 5.2.1.2 and will be reiterated here using the example of **5.5.HPF$_6$** and its complex [Ru(phen)$_2$(**5.5.H**)][PF$_6$]$_3$.

The ^{1}H-NMR spectra of **5.5.HPF$_6$** and [Ru(phen)$_2$(**5.5.H**)][PF$_6$]$_3$ in DMSO-*d6* are shown in Figure 5.11.

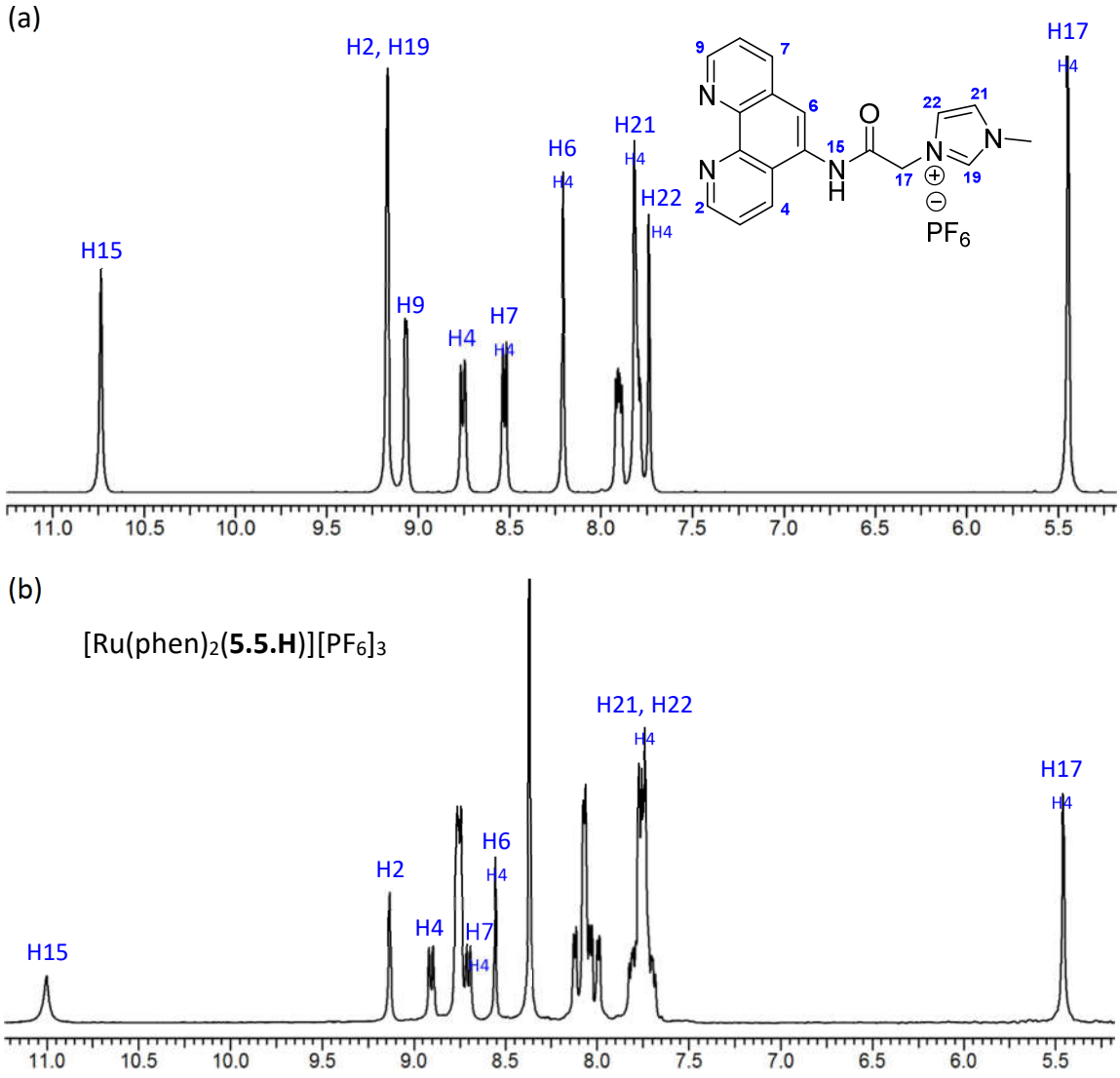

Figure 5.11 (a): *^{1}H-NMR spectra of the uncoordinated ligand* ***5.5.HPF$_6$*** *and,* ***(b)*** *its complex [Ru(phen)$_2$(**5.5.H**)][PF$_6$]$_3$ with some key signals highlighted.*

As expected, anisotropic shielding of the proton environments H2 and H9 by the phenanthroline ancillary ligands causes them to shift upfield by ~ 1.1 ppm. Signals due to H3 and H8 are also shifted upfield but only very slightly. Environments H4 and H7 are not influenced by through space magnetisation and instead shift downfield by ~ 0.2 ppm as a result of electron density withdrawal onto the Ru(II). The most important shift to the ensuing analysis is that of the amide N*H* environment which relocates 0.26 ppm

downfield upon coordination of ligand **5.5.HPF$_6$** to Ru(II). The observed deshielding of this environment supports the assertion that coordination to Ru(II) withdraws electron density from the amide proton through the conjugated π-system (see Figure 5.23). Stabilisation of the amidate conjugate base in this manner means that the amide proton will be more acidic in the coordinated ligand (see Scheme 5.16). The nearby H6 environment also responds with a downfield shift of similar magnitude (Δδ = + 0.35 ppm) which verifies this cross-ligand influence. The amide carbonyl carbon environment C16 only changes marginally. Environments associated with the imidazolium-moiety including its pendants remain unchanged as expected due to their remoteness to the site of coordination.

Phenanthroline-acetamide imidazolium salts were prepared with various pendant functionalities (**5.5.HX** – **5.10.HX**) in order to illustrate the versatility of this approach. It was also necessary to have options with which to attempt the synthesis of NHC complexes because, as has been discussed, the nature of the pendant group can be highly influential. It was originally intended that the impact of different pendent groups on catalysis would be assessed as well, however, this could not be attempted in the time available. NHC complexes in the bornyl-acetamide and cyclohexyl-acetamide series were obtained with methyl, diisopropyl-phenyl and pyridyl pendant ligands. For this reason, PA-NHC complexes with ligands **5.5**, **5.9** and **5.10** were targeted exclusively.

5.3. Synthesis of [Ru(1,10-phenanthroline)$_2$(5-PA)]$^{3+}$ derived NHC complexes

5.3.1. [Ru(1,10-phenanthroline)$_2$(Pd{5.9 - H}{allyl})][PF$_6$]$_2$

The Ru(ppy)$_3$ – NHC – Pd(II) complex [Ru(phen)$_2$(Pd{**5.9**}{allyl}Cl)][PF$_6$]$_2$ was targeted to finalise the series with Pd(**2.4**)(allyl)Cl and Pd(**3.3**)(allyl)Cl. This would provide NHC – acetamide complexes with an achiral-organic, enantiopure-organic and enantiopure-metal-centred component. Rewardingly, instead of isolating the pendant complex as is the case for Pd(**2.4**)(allyl)Cl and Pd(**3.3**)(allyl)Cl, the *N*-amidate/NHC chelated species

$[Ru(phen)_2(Pd\{\mathbf{5.9}\text{ - }\mathbf{H}\}\{allyl\})][PF_6]_2$ was obtained (Scheme 5.8). Spontaneous amidate coordination under mild conditions without additional base has been noted for some NHC – Ru(II) acetamide complexes[114, 158] but never with Pd(II). Such behaviour is recurrent for all $Ru(ppy)_3$ – NHC – Pd type complexes in this study and the reasons for this are examined in section 5.6. It is significant because, to the authors knowledge, no examples of Pd(allyl) complexes with anionic chelating ligands exist. This is because conditions under which a proligand is deprotonated to give the anionic chelate are typically too harsh for the allyl auxiliary to withstand. Therefore, this ligand system opens up an entire enclave of unexplored Pd(allyl) chemistry.

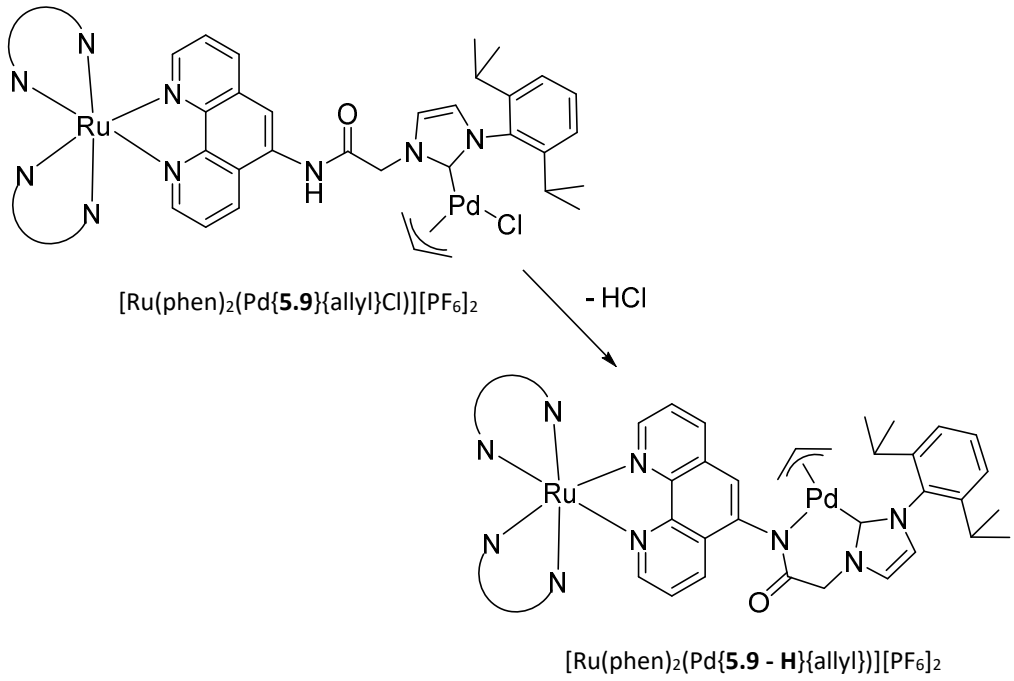

$[Ru(phen)_2(Pd\{\mathbf{5.9}\}\{allyl\}Cl)][PF_6]_2$

$[Ru(phen)_2(Pd\{\mathbf{5.9}\text{ - }\mathbf{H}\}\{allyl\})][PF_6]_2$

Scheme 5.8: *Conversion of the expected complex $[Ru(phen)_2(Pd\{\mathbf{5.9}\}\{allyl\}Cl)][PF_6]_2$ to the isolated NHC – amidate chelated complex $[Ru(phen)_2(Pd\{\mathbf{5.9}\text{ - }\mathbf{H}\}\{allyl\})][PF_6]_2$.*

Because *N*-amidate/NHC chelation occurs readily for the metalloligand $[Ru(phen)_2(\mathbf{5.9})]^{2+}$, it presents an opportunity to understand how this influences catalysis when using NHC – acetamide ligands. A detailed structural analysis of the related bornane functionalised ligand **2.4** revealed chelation to be disfavoured on a steric basis, whereas its cyclohexyl functionalised cousin **3.3** would chelate under basic conditions. Now with $[Ru(phen)_2(\mathbf{5.9})]^{2+}$, which exhibits preferential chelation, it is

possible to study a complete range of amidate coordination ability and it effect on catalysis.

5.3.1.1. Synthesis and characterisation of [Ru(1,10-phenanthroline)$_2$(Pd{5.9 - H}{allyl})][PF$_6$]$_2$

Complex [Ru(phen)$_2$(Pd{**5.9 - H**}{allyl})][PF$_6$]$_2$ was synthesised from the metalloproligand [Ru(phen)$_2$(**5.9.H**)][PF$_6$]$_3$ by transmetalation from an intermediary NHC – Ag(I) complex (Scheme 5.9). This synthesis was performed similarly to that which produced Pd(**2.4**)(allyl)Cl and Pd(**3.3**)(allyl)Cl but with some minor modifications. Unlike the other [Ru(phen)$_2$(5-PA)][PF$_6$]$_3$ metalloproligands, [Ru(phen)$_2$(**5.9.H**)][PF$_6$]$_3$ is adequately soluble in DCM because of its diisopropyl-phenyl pendant and this is the favoured solvent for NHC – Ag(I) transmetalation. DCM accommodates clean, proligand conversion by Ag_2O to provide NHC – Ag(I) for subsequent transmetalation and its volatility simplifies work up of potentially sensitive products. However, while the PF_6 salt salts solubilises well, the chloride salt of [Ru(phen)$_2$(**5.9.H**)]$^{3+}$ is poorly organic soluble. This is important because it has been mentioned previously that having a coordinating anion such as chloride present can improve the synthesis of mono-NHC products via the Ag(I) transmetalation approach. This is because chloride favours mono-NHC intermediate of the type Ag(NHC)Cl as opposed to the bis-NHC [Ag(NHC)$_2$]$^+$ type complexes favoured by non-coordinating counteranions such as PF_6. The impact of this is examined further in section 5.3.2.1 regarding the synthesis of [Ru(phen)$_2$(Pd{**5.10 - H**}Cl)][PF$_6$]$_2$. Because it was not possible to use a chloride salt of the metallo-NHC proligand, the synthesis of [Ru(phen)$_2$(Pd{**5.9 - H**}{allyl})][PF$_6$]$_2$ was modified from previous works to include addition of a molar equivalent of tetraethyl-ammonium chloride as a source of coordinating anion. Although sparingly soluble in DCM, only a small quantity tetraethyl-ammonium chloride was required relative to the volume of solvent. It was found to serve its function, however, the more suitably soluble tetrabutyl-ammonium chloride would have been used if available and is recommended for future syntheses.

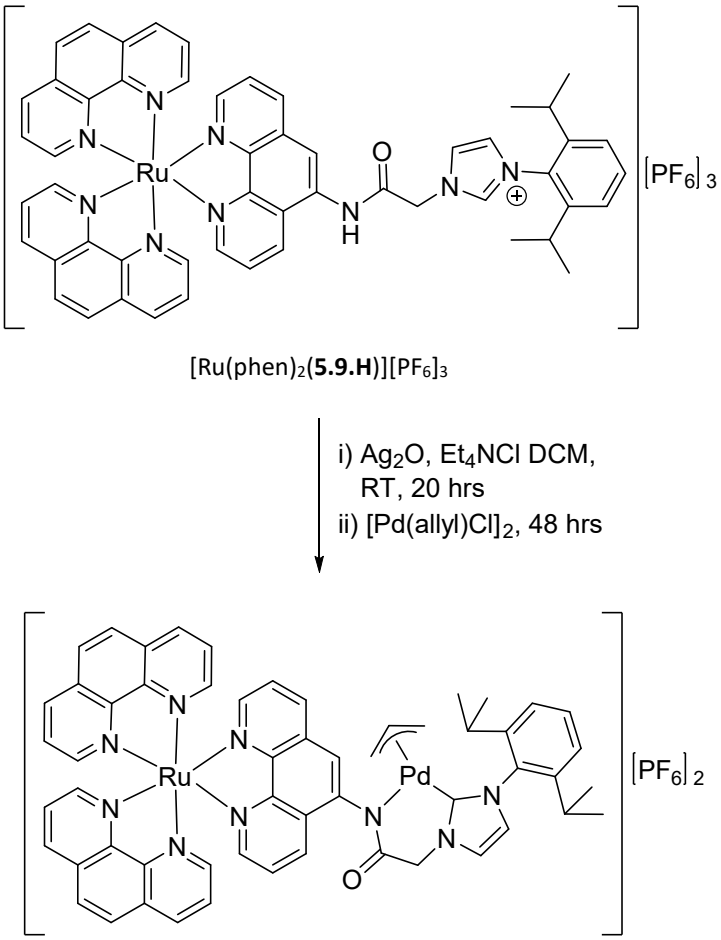

[Ru(phen)$_2$(**5.9.H**)][PF$_6$]$_3$

[Ru(phen)$_2$(Pd{**5.9 - H**}{allyl})][PF$_6$]$_2$, 64%

Scheme 5.9: *Synthesis of [Ru(phen)$_2$(Pd{**5.9 - H**}{allyl})][PF$_6$]$_2$ from [Ru(phen)$_2$(**5.9.H**)][PF$_6$]$_3$ by the NHC-Ag(I) transmetalation method*

The reaction was performed once by stirring [Ru(phen)$_2$(**5.9.H**)][PF$_6$]$_3$ and an equivalent of tetraethyl-ammonium chloride in anhydrous DCM under an inert atmosphere. Once the solution was homogeneous, half an equivalent of Ag_2O was added under a blanket of nitrogen and the reaction stirred in darkness. After 15 hours the reaction mixture was seen to be a bright red solution with some suspended solid. An aliquot analysed by ^{1}H-NMR showed it to be a mixture of starting material and NHC product in a 1 : 2 ratio. Because NHC – Ag(I) intermediates are not always stable it is difficult to say whether or not the observed starting material was regenerated from the product by, for example, removing a proton from water in the NMR solvent. Stirring was continued for a further 5 hours followed by the addition of an equivalent of [Pd(allyl)Cl]$_2$ as a solution in DCM.

After stirring for a further 48 hours the mixture was filtered through celite to remove a light grey precipitate and the filtrate rotary-evaporated to provide a flaky red solid.

The ^{1}H-NMR spectrum of this material was messy with only baseline-level signals attributable to allyl ligand environments and evidence of significant tetraethyl-ammonium salt contamination. It did, however, contain definite Ru(ppy)$_3$ environments and no imidazolium NC*H*N or amide N*H* signals. It is now known that the product [Ru(phen)$_2$(Pd{**5.9 - H**}{allyl})][PF$_6$]$_2$ has an intrinsically complex spectrum due to the dynamic allyl group and, in fact, the material recovered here is relatively pure with the exception of the tetraethyl-ammonium salt. Likewise, the low resolution mass-spectrum of this crude confirmed the presence of the desired complex with large signals at 357.41 and at 535.61 corresponding to the cations [Ru(phen)$_2$(Pd{**5.9**}{allyl})]$^{3+}$ and [Ru(phen)$_2$(Pd{**5.9 - H**}{allyl})]$^{2+}$ (m/z calculated, [Ru(phen)$_2$(Pd{**5.9**}{allyl})]$^{3+}$ = 357.41 and [Ru(phen)$_2$(Pd{**5.9 - H**}{allyl})]$^{3+}$ = 535.61). There was also an equally intense signal due to starting material at 308.76 (m/z calculated, [Ru(phen)$_2$(**5.9.H**)]$^{3+}$ = 308.76).

Unfortunately, the tetraethyl-ammonium salt had similar solubility to the desired product and could not be removed by solvent washes or precipitation. Instead the batch of material was halved for separate purification attempts. First, ion-exchange chromatography was attempted using sephadex-C25 and gradient elution with NaCl solution. In order to load the material it was converted into a water soluble chloride form by stirring in MeOH with AmberliteR IRA-400 (chloride form) ion exchange resin for several hours then filtering and removing the solvent. The leading band was collected by elution with 0.15 M NaCl solution and found to be a small quantity of imidazolium salt proligand. The material that followed this streaked extensively down the column and was collected in many dilute fractions over a range of high NaCl eluent concentrations (0.2 M – 1.0 M). After obtaining the material as its PF$_6$ salt it was analysed by ^{1}H-NMR and found contain slightly more aromatic impurities than the crude material but with no tetraethyl-ammonium contamination. Being in aqueous media for several days no-doubt contributed to the emergence of additional impurities however, the product remained largely intact. In retrospect, the observed smearing of the product along the sephadex resin was a consequence of allyl-group fluxionality (exacerbated by

chloride anions) and product degradation. Despite this, similar chromatography has been applied successfully to the isolation of $[Ru(phen)_2(Pd\{\mathbf{5.10 - H}\}Cl)][PF_6]_2$.

Instead traditional flash chromatography (alumina, 2% MeOH/chloroform) was performed on a separate portion of the original crude material with greater success. Again the product band smeared broadly but was able to be collected cleanly, providing pure $[Ru(phen)_2(Pd\{\mathbf{5.9 - H}\}\{allyl\})][PF_6]_2$. Scaling the isolated product to the overall synthesis gave $[Ru(phen)_2(Pd\{\mathbf{5.9 - H}\}\{allyl\})][PF_6]_2$ in a yield of 64%.

The identity of this species was confirmed by X-ray crystallography and NMR analysis. Mass-spectrometry was also performed on the same batch of crystals. It was important to do so given that the allyl environments were difficult to identify by NMR but were unambiguously verified crystallographically and with support from mass-spec. Crystals of $[Ru(phen)_2(Pd\{\mathbf{5.9 - H}\}\{allyl\})][PF_6]_2$ were grown by slow evaporation of an acetone solution of the compound spiked with a small amount of benzene. It was found that larger samples of the compound, such as the impure material obtained from the sephadex column, could be purified by crystallising similarly. After drying the crystallisation vessel under vacuum, pure crystalline product could be shaken out leaving behind non-crystalline impurity residues fused to the interior.

Samples for X-ray analysis were best prepared by slow evaporation of an acetone/benzene mixture with some benzene anti-solvent in the outer-vial to ensure the crystals remained solvated. Crystals grown in this manner were clusters of thin diamond platelets too small for analysis by diffraction of home-source X-rays and were therefore analysed using synchrotron radiation of frequency 0.71073 nm (Mo/Kα). Complex $[Ru(phen)_2(Pd\{\mathbf{5.9 - H}\}\{allyl\})][PF_6]_2$ crystallises in the monoclinic space group *P*2/*c* with one molecule of $[Ru(phen)_2(Pd\{\mathbf{5.9 - H}\}\{allyl\})]^{2+}$ and two PF_6 anions in the asymmetric unit (Figure 5.12). One water molecule is hydrogen bonded to the amide and resides on single site however, voids in the lattice are occupied by a benzene molecule and at least four water molecules, all of which are highly disordered and difficult to model. Poor data collection contributed to challenges in modelling solvate associated electron density. The structure provides unambiguous confirmation that the

Pd(II) centre remains coordinated to the allyl ligand and that the amide nitrogen is coordinated as an amidate.

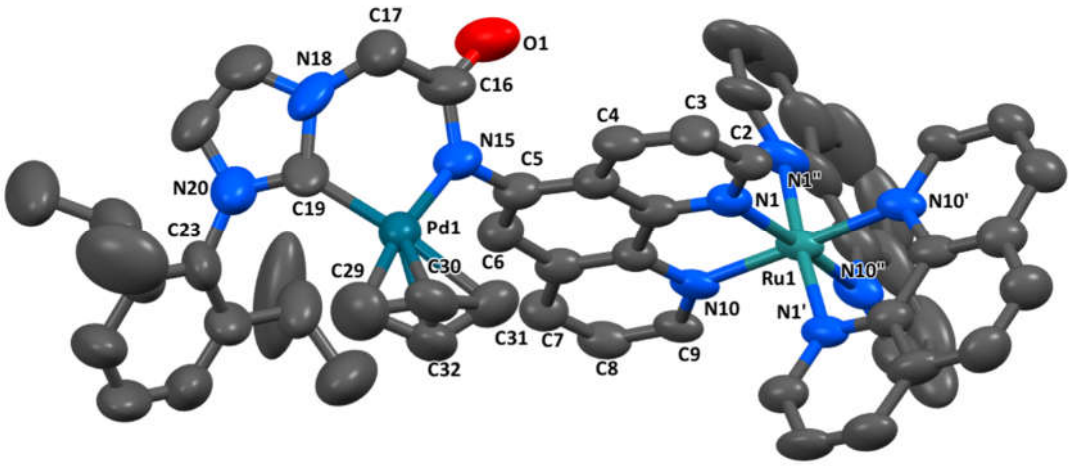

Figure 5.12: *Asymmetric unit of [Ru(phen)$_2$(Pd{**5.9 - H**}{allyl})][PF$_6$]$_2$. Hydrogen atoms, PF$_6$ anions and solvate molecules have been omitted for clarity. Thermal ellipsoids have been drawn at 50% probability.*

As seen for Pd(**3.3**)(allyl)Cl, the allyl group is disordered over two positions with site occupancies for the central carbon of 60 : 40, C30 : C32. A distorted square-planar geometry of the Pd(II) centre is observed due to the constricted chelate angle of the allyl ligand, C29 – Pd1 – C31 of 69.8(5)°. For the NHC – amidate chelate, C17 – Pd1 – N15 is 86.4(4)° and the Pd(II) – ligand bond lengths are as follows; Pd1 – C19 = 2.002(11) Å, Pd1 – N15 = 2.101(8) Å, Pd1 – C29 = 2.075(14) Å and Pd1 – C29 = 2.153(10) Å. As is routinely observed the NHC – metal bond is shortest and the bond trans to it is longest. Interestingly, the Pd – amidate bond, Pd1 – N15 is long compared with those of related compounds in this study. For Pd(**2.4 - H**)(*O,O'*-acac) and Pd(**3.3 - H**)(*O,O'*-acac) this bond is 2.030(4) Å / 2.046(4) Å and 2.032(2) Å respectively and, for the related Ru(ppy)$_3$ – NHC complexes [Ru(phen)$_2$(Pd{**5.10 - H**}Cl)][PF$_6$]$_3$ and [Ru(phen)$_2$(Pd{**5.12 - H**}Cl)][PF$_6$]$_3$ these are 2.026(10) Å / 2.007(11) Å and 2.035(6) Å. This is because the carbon donor allyl-ligand, like the NHC, is a strongly σ-donating,[192] hence the Pd – amidate bond also experiences a trans-influence. This is similarly why the NHC – Pd bond is slightly longer for complexes with allyl-auxiliaries such as Pd(**3.3**)(allyl)Cl and related literature

compounds.[184, 186, 193] The six membered NHC – amidate chelate ring is slightly puckered with the apical methylene C17 raised from the Pd(II) mean-plane at an angle of 11.1(2)°. Puckering in this fashion minimises steric interactions between the diisopropyl-phenyl pendant an the allyl ligand. The octahedral coordination geometry of the Ru(II) is characterised by the bond angles N1 – Ru – N10, N1A' – Ru – N1A'' and N1B' – Ru – N1B'' are 80.2(2)°, 78.6(2)° and 78.7(2)°, respectively. Ru – N bond lengths fall within the range of 2.047(3) Å for Ru – N1B'' and 2.076(3) Å for Ru – N10. The Δ enantiomer of this stereochemical propeller arrangement is shown in Figure 5.12 though the structure is racemic overall. As will be elaborated further in section 5.3.2.1, the orthogonal orientation of the Pd(II) complex relative to the phenanthroline plane of ligand **5.9 - H** results in a stereochemical axis along the N15 – C5 bond generating M or P enantiomers. As such, the plane defined by ligand donor sites around the Pd(II) centre is twisted at an angle of 69.3(3)° to the phenanthroline plane and has an M-stereochemical axis along the N15 – C5 bond. Because the complex has two stereochemical components (Δ, Λ and M, P), it is capable of forming diastereomers. Diastereoisomerism of this type may contribute to the convolution of the compounds NMR spectra as will be discussed. One well-defined water molecule participates in bridging hydrogen bond donation between the amide-carbonyl groups of two $[Ru(phen)_2(Pd\{\mathbf{5.9 - H}\}\{allyl\})]^{3+}$ molecules at an internuclear distance of O1 ··· O2 = 2.830(13) Å. Several C*H* ··· F type interactions are also noted, the shortest of which having C ··· F distances of 3.296(10) Å, 3.298(11) Å and 3.311(12) Å.

As with the crude material, mass spectrometry performed on the crystallised sample showed three strong signals at 357.4077, 535.6089 and 549.1136. The former two have been accounted for previously (m/z calculated, $[Ru(phen)_2(Pd\{\mathbf{5.9}\}\{allyl\})]^{3+}$ = 357.4076 and $[Ru(phen)_2(Pd\{\mathbf{5.9 - H}\}\{allyl\})]^{3+}$ = 535.6072), however, the final signal, which was also noted in the crude, has not been discussed. Surprisingly, this mass corresponds to that of a cyanide ligated cation $[Ru(phen)_2(Pd\{\mathbf{5.9}\}\{allyl\}CN)]^{2+}$ which has a calculated m/z of 549.1136 (Figure 5.13). The occurrence of similar cyanide complexes is also noted for the other Ru(ppy) – NHC – Pd(II) complexes in this study.

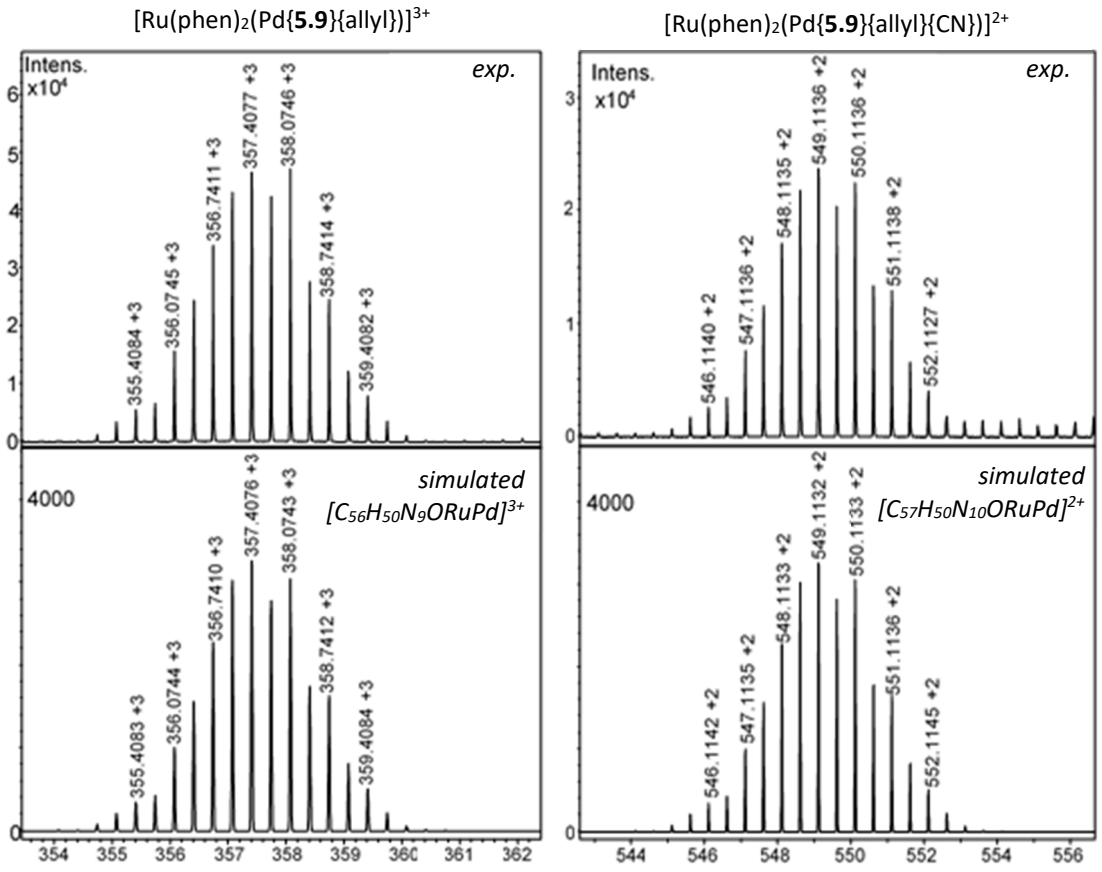

Figure 5.13: *Experimental and simulated mass-spectra identifying fragments [Ru(phen)(Pd{**5.9**}{allyl})]$^{3+}$ and [Ru(phen)(Pd{**5.9**}{allyl}{CN})]$^{2+}$.*

MeCN is known to contain trace quantities of cyanide and these samples were all run as, or at least prepared from, a MeCN solution. Because cyanide forms strong complexes with Pd(II)[253] it is clearly able to displace the amidate. Given the low concentrations of compound required for mass-spectrometry it may be possible to detect the NHC – Pd(CN) complex at a meaningful intensity, especially if the complex is actively "picking up" cyanide. Furthermore, this system is attuned to the detection of such species because of the permanently cationic [Ru(ppy)]$^{2+}$ component which behaves like a mass-spectral antenna, allowing the detection of adducts that would otherwise be neutral. It is this principle that allows the detection of the free-NHC fragment in the mass-spectrum of the Ru(ppy)-imidazolium salt proligands.

The mass-spectrum affirms that the bulk sample contains a Pd(allyl) moiety although, this cannot be verified by ^{1}H-NMR and ^{13}C-NMR analysis of the crystalline sample. Peak suppression in the NMR is a consequence of both *syn-anti* interchange of the allyl group and, conformational flipping of the 6-membered *N*-amidate/NHC chelate. Both of these concepts have been explored previously in Chapters 1 and 2. After standing the CD_3CN NMR solution of $[Ru(phen)_2(Pd\{\mathbf{5.9 - H}\}\{allyl\})][PF_6]_2$ for two weeks and analysing again, three large signals, possibly attributable to the allyl functionality emerge at 3.53 ppm, 3.42 ppm and 3.28 ppm. The ^{1}H-NMR spectrum of both the fresh, and weeks old sample of $[Ru(phen)_2(Pd\{\mathbf{5.9 - H}\}\{allyl\})][PF_6]_2$ is shown in Figure 5.14. Interestingly there is minimal difference in the aromatic region of the two spectra suggesting that the overall structure is conserved. In both cases the diagnostic acetamide methylene environment (H17) is completely supressed, registering as a nub at 4.85 ppm. This environment will also be heavily affected by chelate ring flipping. These observations imply that the compound has not lost the Pd(allyl) group but it is instead involved in an equilibrium that has slowly become established, allowing certain environments to be viewed. Coordinating solvents such as MeCN are known to influence *syn-anti* interchange and this may be true here also. However, it is important to note that the same analysis performed in the non-coordinating solvents acetone-*d6* and $CDCl_3$ did not improve the clarity of the spectra. It is probable that the allyl group of $[Ru(phen)_2(Pd\{\mathbf{5.9 - H}\}\{allyl\})][PF_6]_2$ is intrinsically mobile, irrespective of the solvent, unlike Pd(**2.4**)(allyl)Cl and Pd(**3.3**)(allyl)Cl which are static, or very slowly interchanging, in these solvents. Additional conformational changes can occur in the form of chelate ring flipping and rotation around the C5 – N15 bond to produce different atropisomeric diastereomers. Spectral convolution as a consequence of this dynamic behaviour made the spectrum difficult to assign. This also contributed to being unable to obtain a high quality ^{13}C-NMR spectrum. However, environments belonging to the 1,10-phenanthroline ancillary ligands, and some of the phenanthroline component of ligand **5.9** could be identified. This was assisted by comparison with the fully assigned ^{1}H-NMR and ^{13}C-NMR spectra of the metalloproligand $[Ru(phen)_2(\mathbf{5.9.H})][PF_6]_3$.

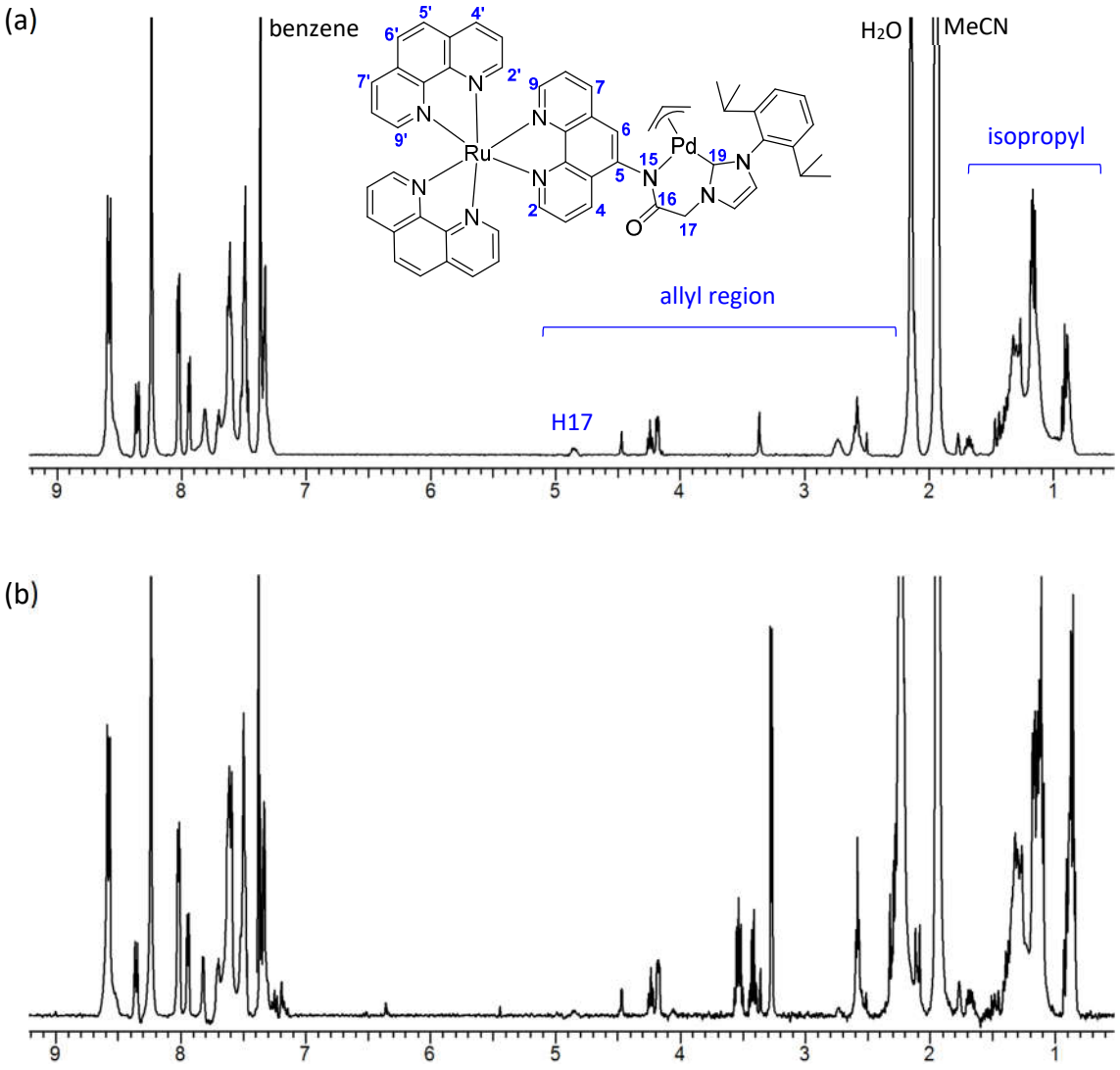

Figure 5.14 (a): *The ^{1}H-NMR spectrum of [Ru(phen)$_2$(Pd{**5.9 - H**}{allyl})][PF$_6$]$_2$ in CD$_3$CN and **(b)** the same solution after two weeks, showing new signals in the allyl region.*

In the aromatic region of the original CD$_3$CN ^{1}H-NMR spectra there are four well defined doublets, the largest at 8.58 ppm and 8.03 ppm attributable to the respective H4' / H7' and H2' / H9' proton of the 1,10-phenanthroline ancillaries. Smaller doublets at 8.36 ppm and 7.94 ppm belong to H4 or H7 and H2 or H9 of the **5.9** phenanthroline. Any environments in the vicinity of the Pd(II) ligands sphere, including H6 and H7 are seen as severely broadened peaks. Although the ^{13}C-NMR spectrum was difficult to assign, a signal at 170.13 ppm due the amide carbonyl environment (C16) was identified as well as one at 57.30 ppm due to the acetamide methylene (C17). The carbenic carbon environment (C19) can usually be identified by HMBC correlation to the methylene

proton resonance and those of the two imidazolyl proton H21 and H22. However, this was not possible here due to signal broadening.

In previous analysis of NHC-acetamide complexes, IR spectroscopy provided insight into the amide's coordination state by evaluating any changes in the compound's carbonyl C=O stretching frequency from that of the free ligand. Unfortunately, for all of the $Ru(ppy)_3$ – NHC – M type complexes in this study, this was not possible. Both the free metalloproligands and $Ru(ppy)_3$ – NHC – M complexes produced unhelpful IR spectra due to the fact that only weak, broad signals in the diagnostic region between 2000 – 1000 cm^{-1} were observed. Signals due to the PF_6 anion were distinguishable in all spectra, particularly the strong PF_6 asymmetric stretch at $\sim$ 830 cm^{-1}, a weaker symmetric stretch between 624 – 680 cm^{-1} and PF_6 scissor bending below 600 cm^{-1}, all of which are in accordance with the literature.[254, 255]

Despite inconclusive NMR support, the assigned structure of $[Ru(phen)_2(Pd\{\textbf{5.9 - H}\}\{allyl\})][PF_6]_2$ was deemed correct on the basis of its crystal structure and mass-spectrum. Further evaluation of its structural and chemical attributes is undertaken in section 5.6.

5.3.2. $[Ru(1,10\text{-phenanthroline})_2(M\{\textbf{5.10 - H}\}Cl)][PF_6]_2$

A $Ru(ppy)_3$ analogue of the pyridyl pendant bornyl-acetamide complex Pd(**2.5**)Cl_2 was sought in the hope that the ordering influence of NHC – Py chelation would support more structurally defined NHC – Pd(II) core, unlike the allyl-ligated $[Ru(phen)_2(Pd\{\textbf{5.9 - H}\}\{allyl\})][PF_6]_2$. As such, the complex $[Ru(phen)_2(Pd\{\textbf{5.10}\}Cl_2)][PF_6]_2$ was targeted with the expectation that the amidate-chelated complex $[Ru(phen)_2(Pd\{\textbf{5.10 - H}\}Cl)][PF_6]_2$ would be isolated. This would provide valuable insight into the structural attributes of these truly unique Ru(ppy) – NHC – Pd(II) systems. To some extent this ambition was achieved; Synthesis of $[Ru(phen)_2(Pd\{\textbf{5.9 - H}\}\{allyl\})][PF_6]_2$ proceeded with spontaneous chelation of the amidate, giving complex $[Ru(phen)_2(Pd\{\textbf{5.10 - H}\}Cl_2)][PF_6]_2$ (Figure 5.15)

however, the isolated species was found to be mixture of diastereoisomers in an 2:1 ratio, the origin of which is discussed in the next section.

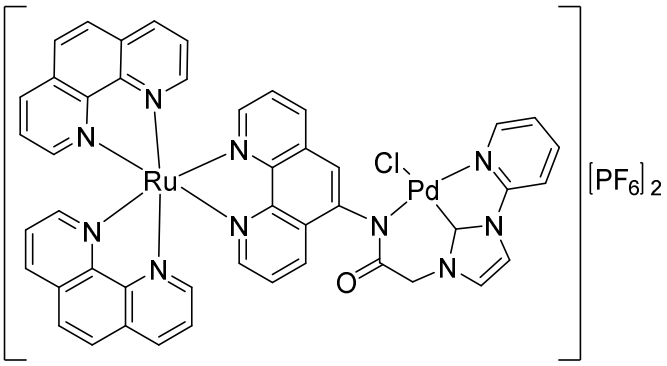

[Ru(phen)$_2$(Pd{**5.10 - H**}Cl)][PF$_6$]$_2$

Figure 5.15: *Structure of complex [Ru(phen)$_2$(Pd{**5.10 - H**}Cl)][PF$_6$]$_2$*

5.3.2.1. Synthesis and characterisation of [Ru(1,10-phenanthroline)$_2$(Pd{5.10 - H}Cl)][PF$_6$]$_2$

Synthesis of [Ru(phen)$_2$(Pd{**5.10 - H**}Cl$_2$)][PF$_6$]$_2$ was performed by transmetalation from an intermediate NHC-Ag(I) complex to Pd(MeCN)$_2$Cl$_2$ or Pd(PhCN)$_2$Cl$_2$ as per the generic method shown in Scheme 5.10. The metallo-NHC proligand for this synthesis, [Ru(phen)$_2$(**5.10.H**)][PF$_6$]$_3$, is not DCM soluble as was the case with [Ru(phen)$_2$(**5.9.H**)][PF$_6$]$_3$ hence the alternative solvents MeCN and DMSO were trialled. This being the case, there were no solubility advantages to using the PF$_6$ salt over chloride as both are soluble in these solvents. Using the precursor chloride salt [Ru(phen)$_2$(**5.10.H**)]Cl$_3$ provides coordinating chloride anions without the addition of tetraalkyl-ammonium salts as these introduce a persistent impurity as was found in the work-up of [Ru(phen)$_2$(Pd{**5.9 - H**}{allyl})][PF$_6$]$_2$. Because all of the metallo-NHC proligand complexes were isolated as their PF$_6$ salts, obtaining chloride salts does add another synthetic step.

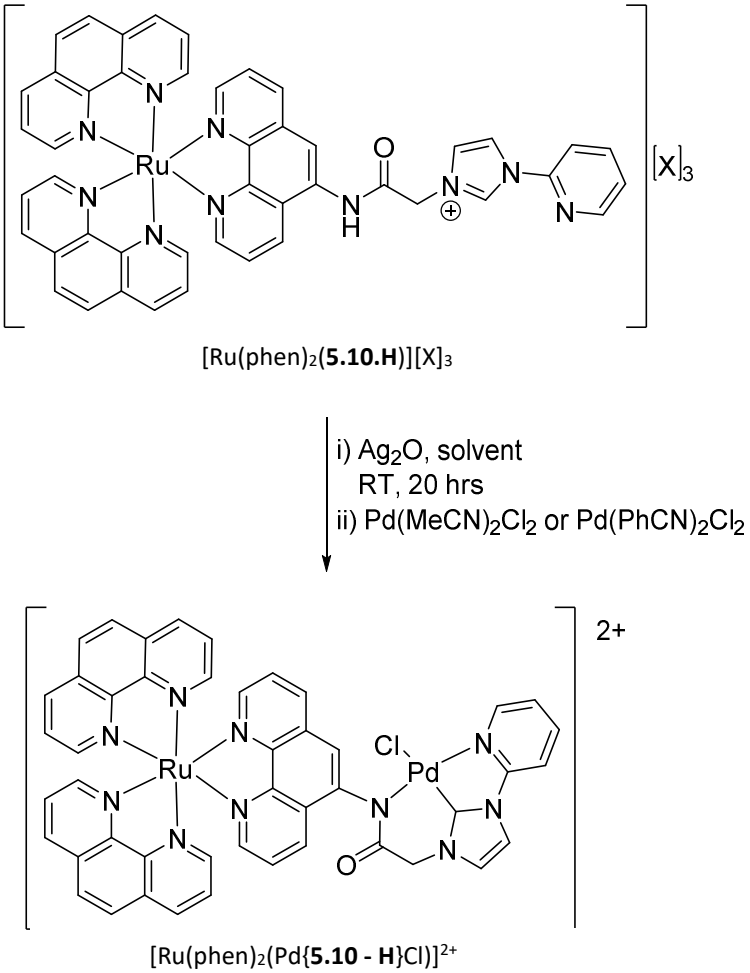

[Ru(phen)$_2$(**5.10.H**)][X]$_3$

[Ru(phen)$_2$(Pd{**5.10 - H**}Cl)]$^{2+}$

Scheme 5.10: *General method for the synthesis of [Ru(phen)$_2$(Pd{**5.10 - H**}Cl]$^{2+}$ by the silver-transmetalation method.*

Synthesis of the desired Ru(ppy)$_3$ – NHC – Pd(II) complex was successfully achieved using the chloride salt of the metallo-NHC proligand [Ru(phen)$_2$(**5.10.H**)]Cl$_3$ in DMSO as will be discussed shortly. Following this, the synthesis was repeated using the PF_6 salt of the proligand without chloride present to determine whether this conversion step was necessary. It was incorrectly predicted that steric and electronic repulsion between the large, cationic [Ru(phen)$_3$]$^{2+}$ pendant functionalities of the [Ru(phen)$_2$(**5.10.H**)]$^{2+}$ ligands would disfavour formation of bis-NHC complexes (Figure 5.16). After addition of Pd(PhCN)$_2$Cl$_2$ to the NHC – Ag(I) intermediate solution and stirring for 20 hours, ^{1}H-NMR analysis of the reaction mixture revealed an extremely complicated aromatic region and a broad, highly irregular methylene environment. The reaction was allowed to continue

for a further 24 hours, however, the constitution of the ^{1}H-NMR spectrum remained unchanged. Crude material was isolated simply by pouring the reaction mixture into water and precipitating as the PF_6 salt.

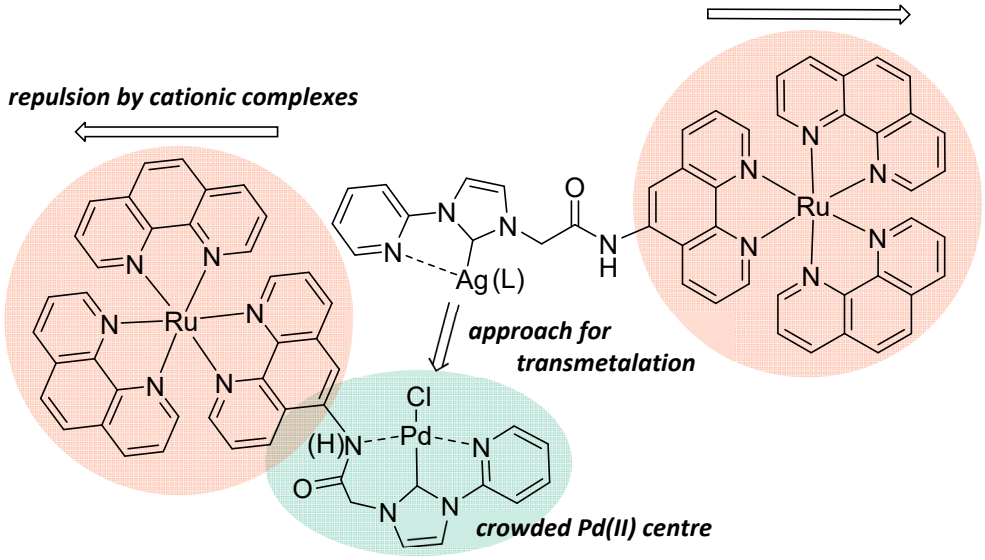

Figure 5.16: *Highlighting why formation of bis-NHC complexes is unexpected on the basis of steric and electronic repulsion between ligands of* $[Ru(phen)_2(\mathbf{5.10})]^{2+}$ *during the transmetalation step.*

The mass-spectrum of this material, as with those of the reaction mixtures, showed a dominant signal at 447.0651 corresponding to the bis-NHC 4+ cation $\{Pd[Ru(phen)_2(\mathbf{5.10 - H})]_2\}^{4+}$ for which m/z is calculated to be 447.0622. At two-thirds the intensity was a signal attributable to the desired product then a smaller signal at 644.4081 due to $[Pd(Ru\{phen\}_2\{\mathbf{5.10 - H}\})_2][PF_6]^{3+}$ (m/z calculated, $[Pd(Ru\{phen\}_2\{\mathbf{5.10 - H}\})_2][PF_6]^{3+}$ = 644.4045). Evidently, one or more bis-NHC species is prevalent in the product mixture which explains the ambiguity observed in the ^{1}H-NMR spectrum. A small portion of the desired complex was selectively crystallised by bulk slow vapour diffusion of diisopropyl-ether into a MeCN solution of the crude product and recovered in a 12% yield. No attempt was made to isolate or quantify any of the bis-NHC products. This exercise

proved the importance of having chloride present in order to avoid the formation of bis-NHC complexes when using the silver-transmetalation method.

Conversion of $[Ru(phen)_2(\mathbf{5.10.H})][PF_6]_3$ into its chloride salt was initially performed using Amberlite® IRA-400 (chloride form) anion exchange resin, an approach commonly used throughout this work. It involves stirring a weighed quantity of the original complex in MeOH and adding a portion of amberlite resin, approximately 0.400 grams of amberlite to 0.100 moles of sample in 20 mL of MeOH. Removal of PF_6 by the resin can be monitored using ^{19}F-NMR on an aliquot of sample. Upwards of 24 hours was necessary for quantitative conversion of $[Ru(phen)_2(\mathbf{5.10.H})][PF_6]_3$ to $[Ru(phen)_2(\mathbf{5.10.H})]Cl_3$. However, this is only necessary if one wishes to have a batch of pure $[Ru(phen)_2(\mathbf{5.10.H})]Cl_3$ from which to accurately calculate molar quantities. For the purposes here it was only required that sufficient chloride be present to improve formation of mono-nuclear Ag(NHC)Cl intermediates and to produce a water soluble product, which proved important to the workup. Only 2 hours was necessary to achieve this level of exchange and, provided losses of material were minimised, the amount of $[Ru(phen)_2(\mathbf{5.10.H})]^{3+}$ could be estimated based on the mass of $[Ru(phen)_2(\mathbf{5.10.H})][PF_6]_3$ used initially.

Salt metathesis was eventually found to be a more expedient method of obtaining chloride salts of these compounds.[256] This was achieved by dropwise addition of saturated tetraethyl-ammonium chloride solution in acetone into an acetone solution of $[Ru(phen)_2(\mathbf{5.10.H})][PF_6]_3$ ($\sim$ 0.100 mmol in 20 mL) and collecting the resultant precipitate. After rinsing with cold acetone the fine orange powder was dried in vacuo providing $[Ru(phen)_2(\mathbf{5.10.H})]Cl_3$ quantitatively, although, ^{19}F-NMR was not performed to confirm the absence of all PF_6.

The first attempt at the synthesis of $[Ru(phen)_2(Pd\{\mathbf{5.10 - H}\}Cl)][PF_6]_2$ was performed in MeCN as per the approach shown in Scheme 5.10 but was unsuccessful because the NHC – Ag(I) intermediate precipitated as a brick-red solid after stirring in darkness for 20 hours. The supernatant remained red also so $Pd(PhCN)Cl_2$ in MeCN was added in the hope that sufficient NHC – Ag(I) material was dissolved to perform the reaction. An aliquot of the mixture was analysed by ^{1}H-NMR after 2 hours which confirmed no

starting material was present, however, there was clearly a complicated mixture of NHC – Pd(II) and NHC – Ag(I) products. After reacting for a further 20 hours the mixture was analysed again by NMR but the mixture remained complicated. It was decided to repeat the synthesis in DMSO to avoid complications arising due to the insolubility of the NHC – Ag(I) intermediate. Although this does provide an effective route to synthesising and isolating the intermediate species, presumed to be $[Ru(phen)_2(Ag\{\mathbf{5.10}\}Cl_2)]Cl_2$, if desired for future investigation.

Using DMSO as the solvent proved effective; proligand $[Ru(phen)_2(\mathbf{5.10.H})]Cl_3$ and half an equivalent of Ag_2O were combined under an inert atmosphere and DMSO added by syringe. The reaction was stirred in darkness for 20 hours before adding an equivalent of $Pd(MeCN)_2Cl_2$ as a solution in DMSO and stirring for a further 24 hours. No AgCl precipitated as is commonly observed, however, NMR indicated that the reaction was complete. Pouring the reaction mixture into water and stirring for several hours still did not prompt precipitation of AgCl as expected, potentially due to the formation of an Ag-DMSO adduct. It was found that the presence of Ag(I) hampered purification by the preferred method of crystallisation so it was necessary to remove it at an early stage. This was achieved by taking an aqueous solution of the reaction mixture and loading it onto a short plug of sephadex-C25 ion-exchange resin. After rinsing with water the desired product was eluted using a steep gradient going from 0.1 – 0.5 M NaCl solution and precipitated by addition of KPF_6 solution. Filtering and drying provided moderately pure $[Ru(phen)_2(Pd\{\mathbf{5.10 - H}\}Cl)][PF_6]_2$ as a brick-red powder. Pure material was obtained by bulk slow vapour diffusion of diisopropyl-ether into a MeCN solution. Collecting the crystalline material by filtration provided $[Ru(phen)_2(Pd\{\mathbf{5.10 - H}\}Cl)][PF_6]_2$ in an overall yield of 51%. Note that to obtain crystals suitable for X-ray analysis this crystallisation process had to be repeated. Employing a Sephadex-C25 plug allowed the removal of both DMSO and AgCl with elution by NaCl solution ensuring the complex remained ligated by chloride.

Complex $[Ru(phen)_2(Pd\{\mathbf{5.10 - H}\}Cl)][PF_6]_2$ was obtained in a highly pure form and its identity confirmed by X-ray crystallography, mass-spectrometry and NMR analysis. As with $[Ru(phen)_2(Pd\{\mathbf{5.9 - H}\}\{allyl\})][PF_6]_2$, the IR spectrum was not a useful

characterisation tool due to supressed transmittance of signals informative of the core structure. Remarkably, the mass-spectrum contained a dominant peak belonging to the cyanide adduct $[Ru(phen)_2(Pd\{\mathbf{5.10 - H}\}\{CN\})]^{2+}$ in which the chloride ligand has been substituted. This arises at 486.5405 (m/z calculated, $[Ru(phen)_2(Pd\{\mathbf{5.10 - H}\}\{CN\})]^{2+}$ = 486.5396). Often this signal is accompanied by relatively minor, M^{2+} peaks. One at 474.0390 is likely related to a fragment without the chloride ligand, $[Ru(phen)_2(Pd\{\mathbf{5.10 - H}\})]^{3+}$, however, this yields a disparate mass to charge ratio. A hydride adduct of this, $[Ru(phen)_2(Pd\{\mathbf{5.10 - H}\}\{H\})]^{2+}$ has the correct calculated m/z of 474.0420, although, this presents another unusual fragment. The other at 495.5338 is similar to that of the hydrated cyanide adduct $[Ru(phen)_2(Pd\{\mathbf{5.10}\}\{CN\}\{OH_2\})]^{2+}$ which has a calculated m/z of 495.5449.

Rationalising the features of the NMR spectra was tremendously benefited by X-ray crystallography. Therefore, the crystallographic attributes of $[Ru(phen)_2(Pd\{\mathbf{5.10 - H}\}Cl)][PF_6]_2$, particularly regarding its conformational arrangement, will be discussed foremost.

As mentioned above, crystals suitable for X-ray diffraction were grown by slow vapour diffusion of diisopropyl-ether into a MeCN solution of $[Ru(phen)_2(Pd\{\mathbf{5.10 - H}\}Cl)][PF_6]_2$. This crystallised in the triclinic space group $P\bar{1}$ with two molecules of $[Ru(phen)_2(Pd\{\mathbf{5.10 - H}\}Cl)]^{2+}$ (designated by the suffixes A and B) and four PF_6 anions in the asymmetric unit (Figure 5.17). The structure contains moderate solvent accessible void space occupied by numerous, highly disordered MeCN molecules causing a poor overall refinement (R_f = 12.90%). The molecules of interest are well represented by the model.

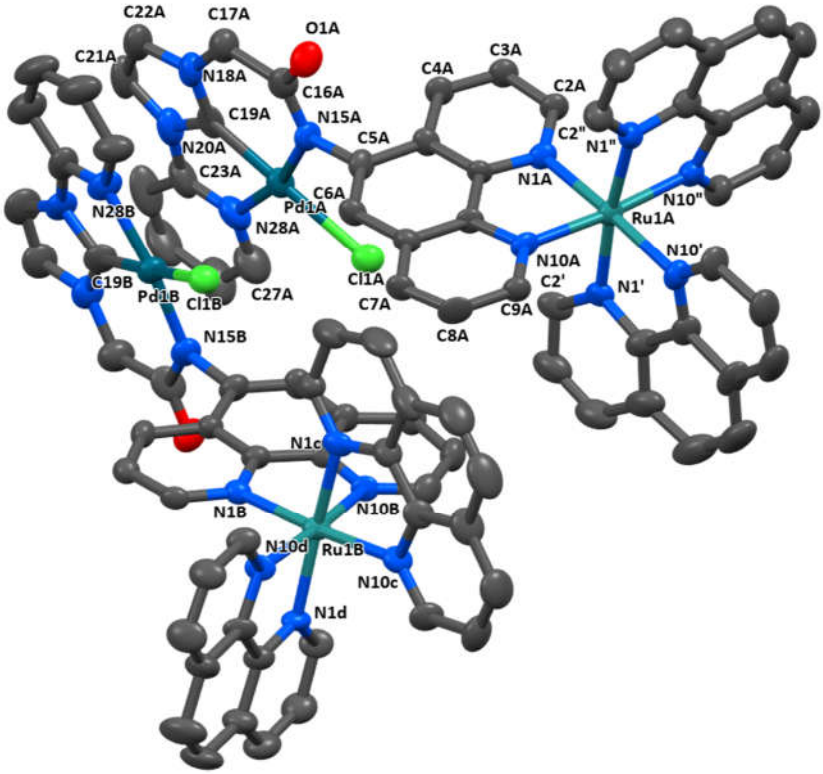

Figure 5.17: *Contents of the asymmetric unit of [Ru(phen)$_2$(Pd{**5.10 - H**}Cl)][PF$_6$]$_2$ with hydrogen atoms, PF$_6$ anions and MeCN solvate molecules omitted for clarity. Thermal ellipsoids have been drawn at 50% probability.*

The Ru(phen)$_3$ complex component is observed as a distorted octahedron represented by the bond angles N1 – Ru – N10, N1' – Ru – N10' and N1" – Ru – N10" (A / B) of 79.4(3)° / 80.2(3)°, 79.5(4)° / 80.5(4)° and 79.6(4)° / 79.9(4)°. Ru – N bond lengths falling within the range 2.060(9) Å (Ru1B – N1B) and 2.106(8) Å (Ru1B – N10B). The incorporation of a Pd(II) centre is unambiguously verified, adopting a characteristic square planar geometry. Distortion of this geometry occurs due to the NHC – Py chelate ring having a less than 90° bite angle of 78.8(5)° / 79.2(5)° along with the NHC – amidate chelate (C19 – Pd1 – N15 = 87.2(5)° / 87.1(5)°). Interestingly, the NHC – amidate chelate ring exhibits a planar conformation, in stark contrast to the puckered ring-structures of previously discussed NHC – amidate complexes including [Ru(phen)$_2$(Pd{**5.9 - H**}{allyl})]$^{2+}$, Pd(**2.4 - H**)(*O,O'*-acac) and Pd(**3.3 - H**)(*O,O'*-acac). This is quantified by θ_{CH2} which describes the angle between the line intersecting Pd1 and the methylene carbon C17, and the plane

defined by N15, C19 and Pd. Here, θ_{CH2} is 1.5(2)° / 1.8(2)° but for [Ru(phen)$_2$(Pd{**5.9 - H**}{allyl})]$^{2+}$ it is 11.1(2)° and Pd(**2.4 - H**)(*O,O'*-acac) it is 28.4(2)°. For [Ru(phen)$_2$(Pd{**5.10 - H**}Cl)]$^{2+}$, ligand **5.10 - H** coordinates in a 5,6-tridenate motif in which the planarity of the 5-membered NHC – Py chelate is imposed on the more flexible 6-membered chelate in order to retain the correct coordination geometry. Bond distances to the Pd(II) centre are as follows; Pd1 – C19 = 1.901(12) Å / 1.909(12) Å, Pd1 – N15 = 2.026(10) Å / 2.007(11) Å, Pd1 – N28 = 2.089(11) Å / 2.057(10) Å and Pd1 – Cl1 = 2.385(3) Å / 2.393(3) Å. As is commonly observed, the Pd – NHC bond is shortest and causes a lengthening in the opposite bond due to its trans influence. The planar Pd(NHC)Cl fragment is oriented perpendicular to the phenanthroline ligand to which it is appended producing a twist angle between the phenanthroline ligand plane and that of the 6-membered chelate ring of 90.9(3)° / 80.4(4)°. This directs the chloride ligand towards the front edge of one of the phenanthroline ancillaries resulting in a Cl1 ··· C2' distance of 4.194(14) Å / 4.153(13) Å. In this conformation, the two [Ru(phen)$_2$(Pd{**5.10 - H**}Cl)]$^{2+}$ molecules within the asymmetric unit can align such that the faces of the Pd(NHC)Cl moieties are coplanar whilst the N10 pyridyl rings of the phenanthroline are stacked at a centroid-to-plane distance of 3.380(14) Å / 3.855(12) Å, shifted by 2.602(17) Å / 1.855 Å (Figure 5.18).

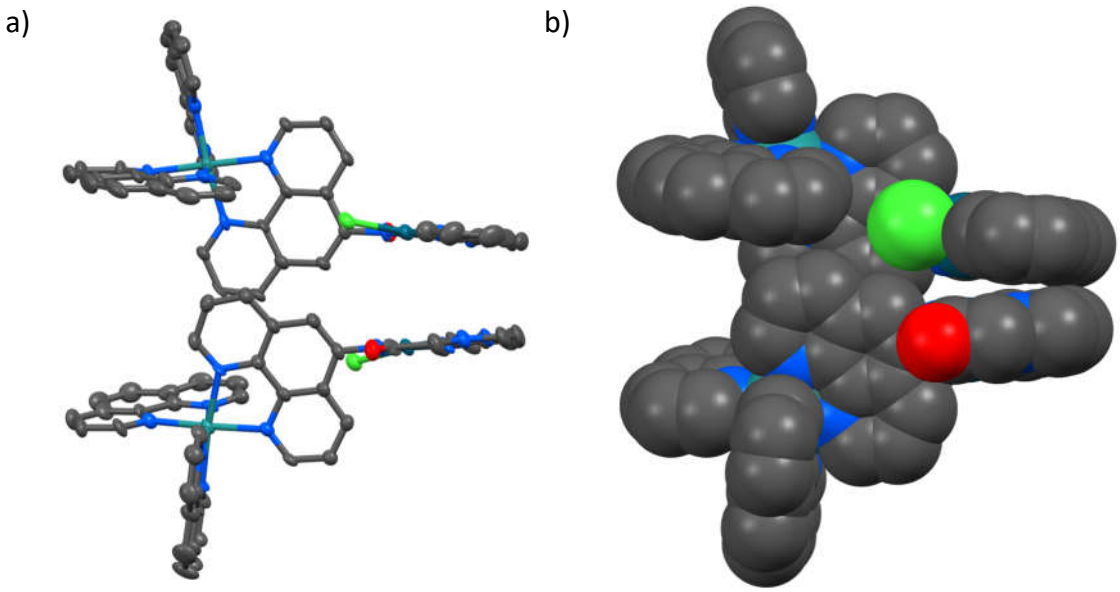

Figure 5.18 (a): *An alternative view of the asymmetric unit clarifying the face-stacked arrangement of the Pd(II) complex units and,* ***(b)*** *the related spacefill model highlighting the steric constraints within the complex.*

The NHC-pyridyl ring overlaps with the opposing NHC ring at an inter-planar distance of 3.428(15) Å / 3.518(15) Å with related plane-to-plane shifts of 2.16(2) Å / 2.01(3) Å. A distance of 4.0128 Å is noted between Pd(II) centres. The H21 hydrogen atoms of adjacently stacked NHC rings participate in separate C*H* ··· F interactions with two fluorine atoms of a single PF_6 anion at a C ··· F of 3.026(15) Å and 3.089(16) Å.

The relative conformation of the planar phenanthroline and Pd(NHC)Cl units is atropisomeric, possessing either an M or P stereochemical axis along the C5 – N15 bond. Coupling this with the Δ or Λ stereochemistry of the octahedral Ru(II) produces Δ,M and Λ,M enantiomers which are diastereomers of the Δ,P and Λ,P configurations and responsible for the two species observed by NMR, as will be discussed shortly. The Δ,M and Λ,M enantiomers have been crystallised here. A steric evaluation of the crystal structure strongly suggests that the stereochemical axis cannot freely interconvert when in solution. Viewing the complex as a spacefill model helps to illustrate this point (Figure 5.18b). Converting between the M and P configurations of $[Ru(phen)_2(Pd\{\textbf{5.10 - H}\}Cl)]^{2+}$ relies on rotation around the C5 – N15 bond which appears to be prevented by the chloride ligand and to a lesser extent, on the opposite side by the amide oxygen. Having only crystallised one diastereomer it is difficult to determine which of the two might be favoured on a steric basis.

NMR analysis reveals that the compound exists as a mixture of two diastereomers in a 2 : 1 ratio. The same ratio of products is always observed, whether it is a crude reaction mixture or crystalline sample. Generally speaking, this diastereoisomerism is the product of two stereogenic components; the (Δ/Λ) – $Ru(phen)_3$ group and an axial-enantiomer designated M or P arising from the fixed configuration of the Pd(NHC-Py)Cl fragment relative to the phenanthroline. This stereochemical-axis was referenced in the discussion of the compounds crystal structure as occurring along the C5 – N15 bond. Figure 5.19 illustrates both diastereomeric conformations in relation to the Λ stereoisomer.

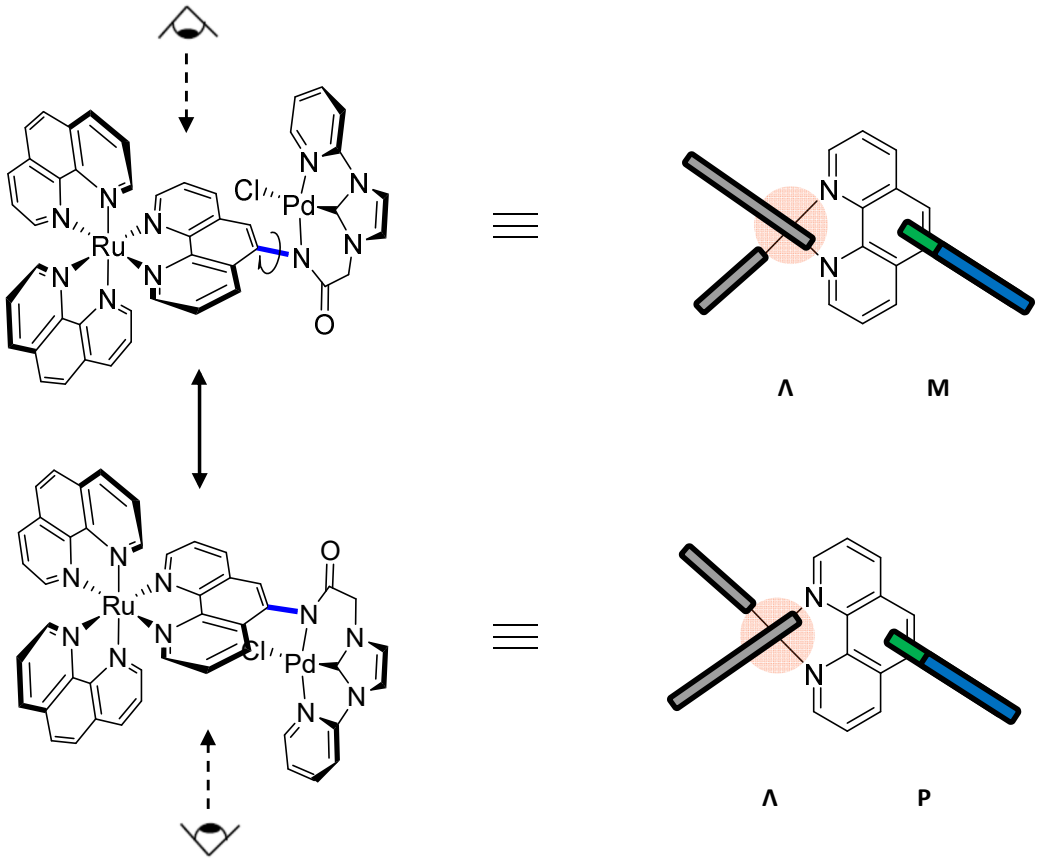

Figure 5.19: *Depiction of Λ,M and Λ,P diastereoisomers of [Ru(phen)$_2$(Pd{**5.10 - H**}Cl)]$^{2+}$ that arise due to restricted rotation around the C – N bond as shown. Projections of these along the vertical axis highlight the relative orientations of the Pd(NHC)Cl moiety (blue/green) and the phenanthroline ancillary ligands (grey) in each diastereomer.*

The following discussion will focus on the structural confirmation of [Ru(phen)$_2$(Pd{**5.10 - H**}Cl)][PF$_6$]$_2$ and justifying the aforementioned mode of stereoisomerism with supplementary analysis performed in section 5.6.1. Aromatic regions of the ^{1}H-NMR and ^{13}C-NMR spectra of [Ru(phen)$_2$(Pd{**5.10 - H**}Cl)][PF$_6$]$_2$ are shown in Figure 5.20. Where relevant, the major and minor isomers are denoted by the suffix *j* or *n*, respectively. Interestingly the acetamide methylene proton (H17) resonances at 5.12 ppm are observed as a singlet with the two diastereomers being barely distinguishable. This is despite the two protons being confined to separate, diastereotopic chemical environments by *N*-amidate/NHC chelation. It is presumed that these environments are chemically identical due to the planarity of the chelate and directed away from the bulk

of the complex. This also explains why little distinction between diastereomers is observed for this environment including for the corresponding carbon resonance at 54.18 ppm / 54.14 ppm (C17-n / C17-j).

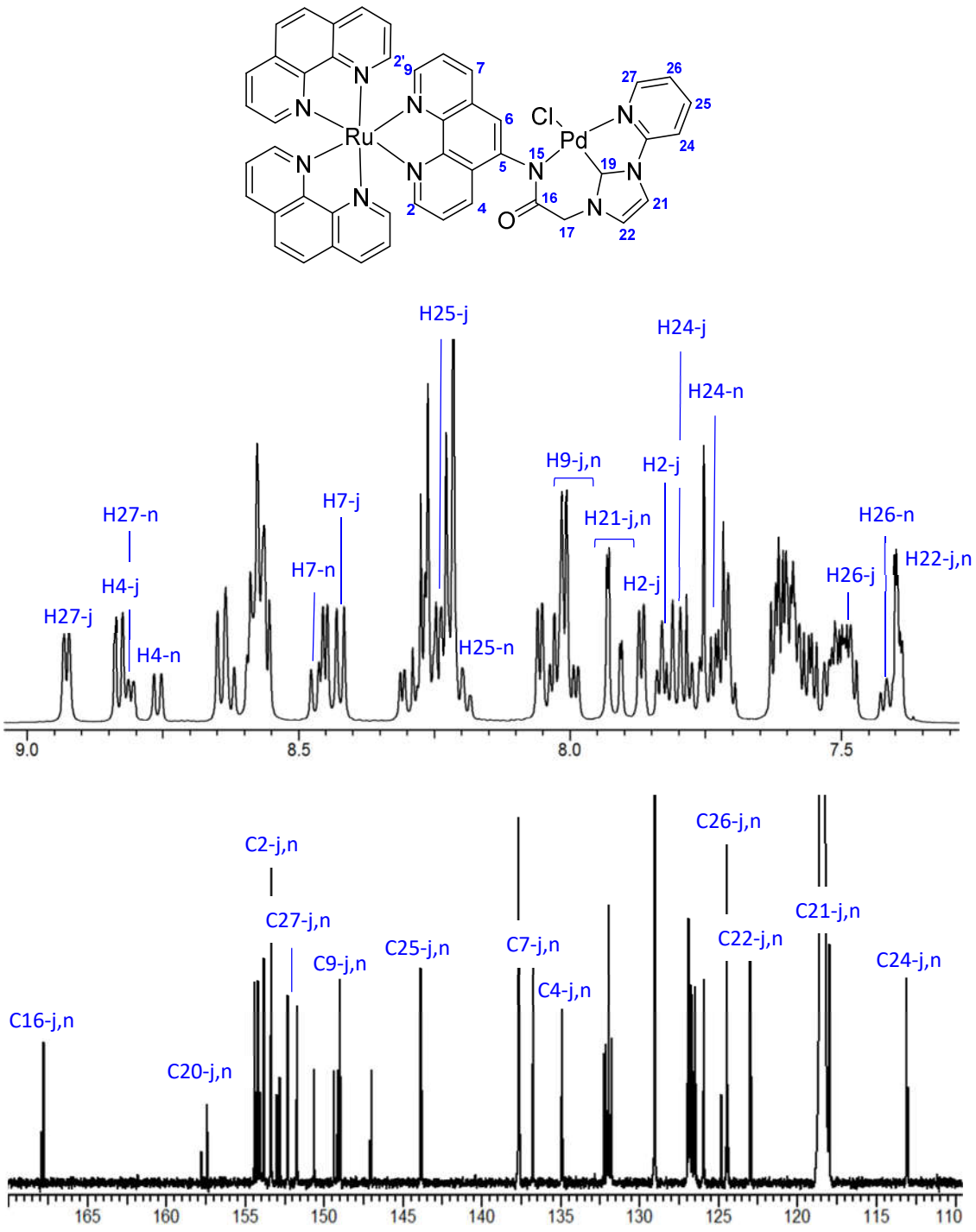

Figure 5.20: *The ^{1}H-NMR and ^{13}C-NMR spectra of [Ru(phen)$_2$(Pd{**5.10 - H**}Cl)][PF$_6$]$_3$ with selected signals highlighted.*

Unlike many of the proton environments, carbon nuclei were not greatly affected by the differences in diastereomer conformation. This allowed detection of connectively identical but chemically distinct proton environments by HSQC, HSQC-TOCSY and HMBC correlation to the comparatively localised diastereomeric carbon resonances. HMBC correlation with the methylene H17 was used to identify the amide carbonyl carbon environment at the predictably downfield position of 167.92 ppm / 167.80 ppm (C16-n / C16-j) and the carbenic carbon environment at 157.79 ppm / 157.44 ppm (C19-n / C19-j). Correlation to C19 signals enable detection of the other imidazolyl-proton environments at 7.93 ppm / 7.91 ppm (H21-j /H21-n) and ~ 7.40 ppm (H22). These imidazolyl-environments appear as doublets (J_{H-H} = 2.0 Hz) which is rarely observed. The typically downfield H27 environment of the pyridyl pendant group displays a significant difference between the diastereomers producing doublets at 8.93 ppm (H27-j) and ~ 8.81 ppm (H27-n) (Δδ ~ 0.12 ppm). COSY-NMR enabled assignment of the other proton in this ring system at ~ 7.48 ppm / ~ 7.42 ppm (H26-n / H26-j, Δδ ~ 0.06 ppm), ~ 8.24 ppm / ~ 8.20 ppm (H25-j / H25-n, Δδ ~ 0.04 ppm), and ~ 7.80 ppm / ~ 7.76 ppm (H24-j / H24-n, Δδ ~ 0.04 ppm). A significant difference between the major and minor H27 environments, followed by H26 is a result of their proximity to the stereochemical zone. Similarly, the H4 major and minor environments are distinct at ~ 8.83 and 8.76 ppm (Δδ ~ 0.07 ppm). The H2' environments of the phenanthroline ancillary ligand facing into the Pd(II) complex fragment are found at 8.45 ppm (H2'-j) and 8.31 (H2'-n), notably downfield of the other related phenanthroline environments H2, H4, H2' and H2'' which resonate between 8.06 – 7.82 ppm. This results from the interaction between this proton and the chloride ligand of the Pd(II) which, as mentioned regarding the crystal structure, are spatially adjacent. In the Λ,M and Δ,P enantiomers the H2' proton is directed towards the chloride ligand which is expected to enable greater deshielding than in the Λ,P and Δ,M enantiomers where H2' is pointed orthogonally. It is tentatively deduced from this that the major diasteriomers are Λ,M and Δ,P-[Ru(phen)$_2$(Pd{**5.10 - H**}Cl)][PF_6]$_2$.

Carbon environments adjoining most of the hydrogen nuclei discussed above are labelled on the ^{13}C-NMR spectrum in Figure 5.20. Besides the carbenic carbon environment C19, these exhibit small differences between the major and minor

diastereomers. Resonances due to C5, C6 and H6 would have been informative to this discussion however, due to the complexity of the spectra, they could not be confidently assigned without a scrupulous and time-consuming analysis.

The occurance of diatereoisomers that are distinguishable by NMR demonstrates that the stereochemistry of the $Ru(phen)_3$ unit does influence the stereochemical environment of the NHC – complex, at least when chelated via the amidate. Not only that, they show selectivity for one diastereomer over the other, boding well for their eventual application as stereodirecting metalloligands in asymmetric catalysis. This isomerism will be discussed further in section 5.6.1 through comparison with complexes $[Ru(phen)_2(Pd\{$**5.9 - H**$\}\{allyl\})][PF_6]_3$ and $[Ru(phen)_2(Pd\{$**5.12 - H**$\}Cl)][PF_6]_3$.

5.4. Synthesis of 2,2'-bipyridine derived metallo-NHC proligands

It was identified in section 5.3.2.1 that the metallo-NHC complex [Ru(1,10-phenanthroline)$_2$(Pd[**5.10 - H**]Cl)][PF_6]$_2$ exists as a 2:1 mixture of atropisomeric diastereomers. These isomers arise due to restricted rotation around the phenanthroline – N(amide) bond and are differentiated by the extent of the steric interaction between the 1,10-phenanthroline ancillary ligands and the chloride ligand of the NHC – Pd(II) fragment. It was envisaged that moving the NHC – Pd(II) fragment to the 4-position of 1,10-phenanthroline would maximise the interaction with the Ru(II)-polypyridine ligand sphere, increasing selectivity for one diastereomeric product (Figure 5.21).

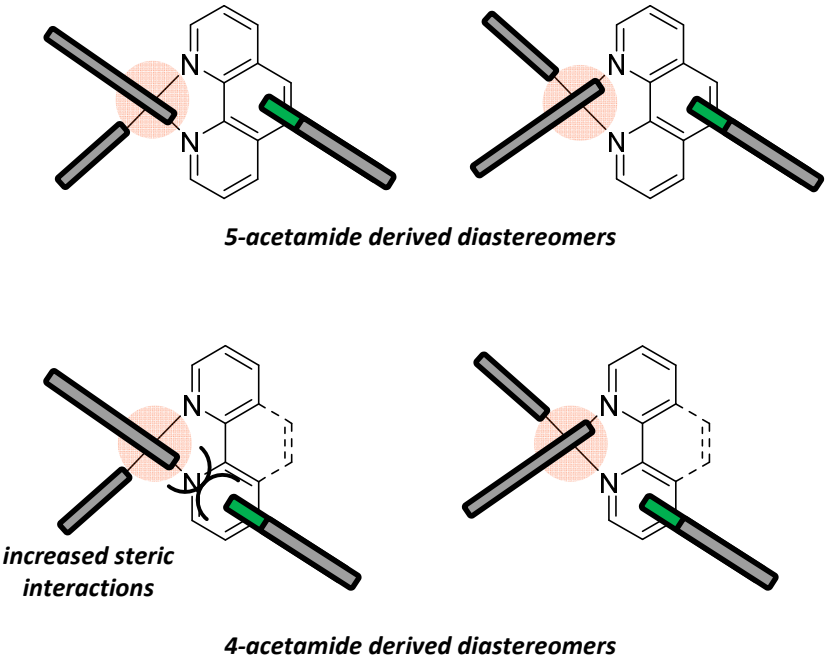

Figure 5.21: *Projections of [Ru(phen)$_2$(Pd{**5.10 - H**}Cl)]$^{2+}$ type diastereomers highlighting a difference in the relative proximity of groups between the 5-functionalised and 4-functionalised derivatives.*

Because the required amine precursor, 4-amino-1,10-phenanthroline, cannot be sourced easily, it was necessary to proceed via 4-amino-2,2'-bipyridine which can be prepared from 2,2-bipyridine. This necessitated the switch to a 2,2-bipyridyl-acetamide basis to target the complex [Ru(phen)$_2$(Pd{**5.12 - H**}Cl)][PF$_6$]$_2$ (Figure 5.22). Ligands derived from 4-acetamido-2,2'-bipyridine are generically referred to as 4-BipA derivatives herein.

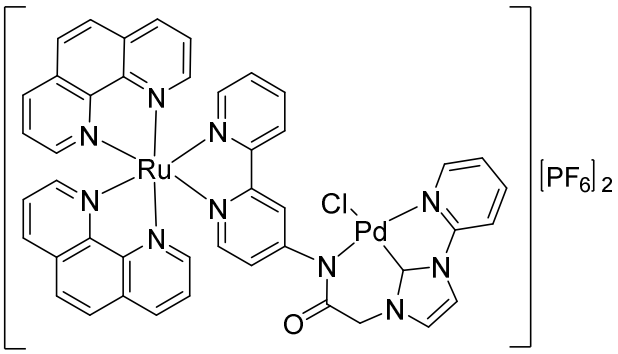

[Ru(phen)$_2$(Pd{**5.12 - H**}Cl)][PF$_6$]$_2$

Figure 5.22: *Target compound [Ru(phen)$_2$(Pd{**5.12 - H**}Cl)][PF$_6$]$_2$.*

Both 5-acetamido-phenanthroline and 4-acetamido-bipyridine systems can stabilise the amidate anion through conjugation onto the pyridine nitrogen, however, their electron distribution is markedly different. This is illustrated through a comparison of resonance structures of their respective core amines in which the amino lone-pair is delocalised onto the pyridine-nitrogen (Figure 5.23). As shown, 5-amino-1,10-phenanthroline exhibits a large charge separation, sacrificing aromaticity in all three rings whereas charge separation is small for 4-amino-2,2'-bipyridine derivatives and aromaticity is maintained in one ring. The amino hydrogen of 4-amino-pyridine derivatives are well known to be more acidic than 3-amino-pyridines and anilines.[221, 244, 246] On the basis of mesomeric electron withdrawal, 4-amino-2,2'-bipyrdine is also expected to have a more acidic, less nucleophilic amine than 5-amino-1,10-phenanthroline. This concept underpins many of the assertions made in the following discussion.

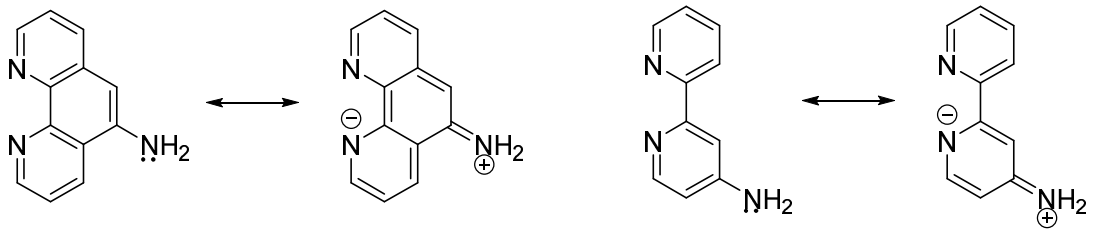

5-amino-phenanthroline ***4-amino-bipyridine***

Figure 5.23: *Resonance form of 5-amino-1,10-phenanthroline and 4-amino-2,2'-bipyridine in which the amine lone pair is delocalised onto a pyridine nitrogen.*

5.4.1. Acetamide tethered 2,2'-bipyridine NHC precursors and their ruthenium-polypyridine complexes.

Synthesis of 4-amino-2,2'bipyridine from 2,2'-bipyridine was achieved in three steps (Scheme 5.11), the first of which being the formation of 2,2'-bipyridine-*N*-oxide. A variety of literature preparations for this exist, the most efficient of which employ hydrogen peroxide in either acetic acid,[257] or tri-fluoroacetic acid,[258] which form a potentially explosive per-acid intermediate. Milder approaches employ excess MCPBA,[259] which is expensive on the large scale required here. Hence, a safe and

affordable synthesis was designed using potassium monopersulfate (oxone) as the oxidant in a MeOH/water mixture as solvent.

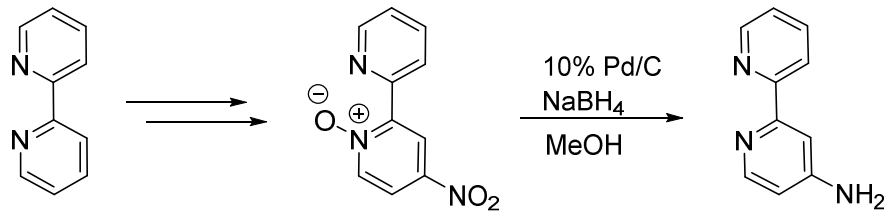

Scheme 5.11: *Synthesis of 4-amino-2,2'bipyridine from 2,2'-bipyridine in three steps. The 4-nitro-2,2'-bipyridine is obtained by nitration of the 2,2'-bipyridine*-N-*oxide.*

After 48 hours a crude material containing 2,2'-bipyridine and 2,2'-bipyridine-*N*-oxide is recovered by extraction of the aqueous reaction mixture with chloroform after the removal of MeOH. This is then evaporated and the resulting light brown oil run through a short alumina plug with Et_2O which recovers the 2,2'-bipyridine then 2,2'-bipyridine-*N*-oxide is eluted with 10% MeOH / DCM. Pure *N*-oxide is consistently isolated in 40-50% yields and, although this is low compared with other techniques, the unreacted 2,2'-bipyridine can be recycled. Spectra of 2,2'-bipyridine-*N*-oxide isolated by this method are consistent with those reported.[258]

The nitration of 2,2'-bipyridine-*N*-oxide to give 4-nitro-2,2'-bipyridine-*N*-oxide was initially performed following a literature procedure[259] using concentrated H_2SO_4 and KNO_3, however, 4-nitro-2,2'-bipyridine and 4-nitro-2,2'-bipyridine-*N*-oxide were isolated together in low, inconsistent yields. Yields upwards of 40% were obtained via an alternative preparation using concentrated H_2SO_4 and fuming HNO_3.[257] The subsequent reduction of 4-nitro-2,2'-bipyridine-*N*-oxide to give 4-amino-2,2'-bipyridine was performed efficiently by a previously reported method.[260]

Chloroacetylation of 4-amino-2,2'-bipyridine to produce 2-chloro-N-(4-amino-2,2'-bipyridine)-acetamide (**5.11**) has not been reported. This was performed similarly to the

synthesis of **5.4**, however, anhydrous DCM was used in place of THF due to its availability at the time (Scheme 5.12). Surprisingly, **5.11** was only recovered in a 26% yield despite previous acetamide syntheses in this study proceeding smoothly. Upon addition of the chloroacetyl-chloride to the cooled reaction mixture the solution immediately turned brown and proceeded to deposit a brown/black precipitate.

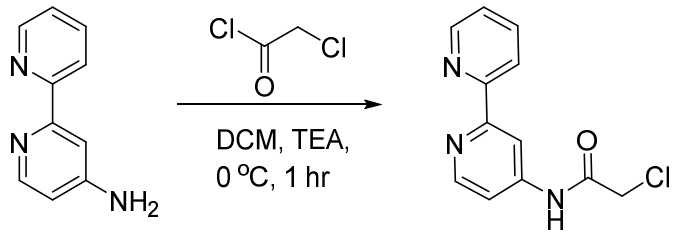

5.11, 26%

Scheme 5.12: *Synthesis of 2-chloro-*N*-2,2'-bypyridin-4-yl acetamide (**5.11**) from 4-amino-2,2'-bipyridine.*

At the conclusion of the reaction the dark solid was removed by filtration and the DCM filtrate washed with water before drying over $MgSO_4$ and removing the solvent by rotary evaporation. This material was also almost black but was identified as crude **5.11** by ^{1}H-NMR. Pure **5.11** was obtained as a terracotta powder following flash chromatography (alumina, 1% MeOH/DCM). The dark brown/black precipitate was only sparingly soluble in DMSO and produced messy, uninformative NMR and mass-spectra. Having obtained a sufficient quantity of material no effort was made to improve this preparation.

The adverse reactivity of 4-amino-2,2'-bipyridine to chloroacetylation is likely the result of the decreased nucleophilicity of the amine when compared with 5-amino-1,10-phenanthroline, as noted above. Likewise, the comparatively labile amide-proton makes it susceptible to further substitution under the basic reaction conditions. The product **5.11** may undergo additional acetylation of the amide-nitrogen or even substitution of the chloride to form polymeric species. However, chloroacetylation of the related 4-amino-pyridine has been reported under similar conditions (58% yield)[261] but it has been shown that using bromoacetyl-bromide instead proceeds more cleanly, producing 2-Bromo-*N*-pyridin-4-yl-acetamide in a 76% yield.[262]

5.4.1.1. Synthesis of a 4-BipA imidazolium salt

Only the pyridyl-imidazolium salt **5.12.HCl** of the 2,2-bipyridine-acetamide was prepared for the express purpose of comparison with the complex [Ru(1,10-phenanthroline)$_2$(Pd{**5.10 - H**}Cl)][PF_6]$_2$. It was synthesised in the same manner as **5.10.HPF$_6$** by refluxing **5.11** with a two-fold excess of 1-(2-pyridyl)-imidazole in MeCN under an inert atmosphere. Consumption of the precursor acetamide **5.11** was monitored by TLC (alumina, 1% MeOH/DCM) and after 48 hours the reaction was cooled to room temperature. Work-up was simplified by pouring the reaction mixture onto Et_2O and stirring, then collecting the resultant white precipitate and washing with addition of Et_2O. This provided pure **5.12.HCl** in a 78% yield without the intervening conversion to the PF_6 salt.

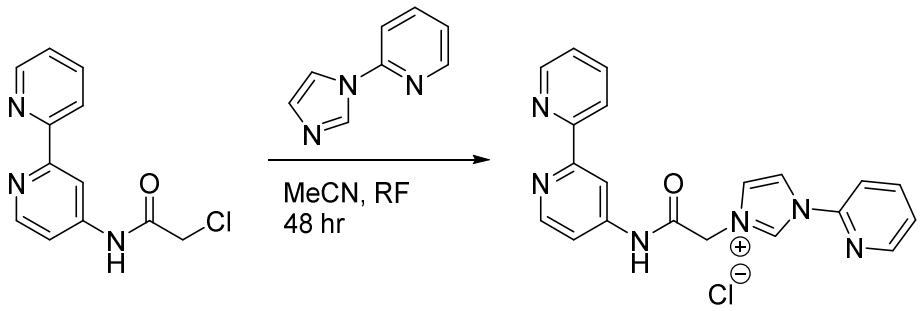

5.11 **5.12.HCl**, 78%

Scheme 5.13: *Synthesis of the acetamide tethered 2,2'-bipyridine imidazolium salt* ***5.12.HCl****.*

Compound **5.12.HCl** was identifiable as three signals in the mass-spectrum with the most intense at 357.1458 corresponding to the [**5.12.H**]$^+$ cation (m/z calculated, [**5.12.H**]$^+$ = 357.1458). Lesser signals at 713.2863 and 749.2627 belong to dimeric clusters [**5.12** + **5.12.H**]$^+$ and [**5.12.H** + **5.12.HCl**]$^+$ respectively (m/z calculated, [**5.12** + **5.12.H**]$^+$ = 713.2838 and [**5.12.H** + **5.12.HCl**]$^+$ = 749.2611). Isolating and analysing the chloride salt benefitted collection of a clear IR spectrum as it did not suffer from dilution of [**5.12.H**]$^+$ signals due to a large PF_6 anion. This revealed a prominent amide C = O stretching mode at 1709.63 cm^{-1} which lies beyond the routinely reported range of 1680

– 1630 cm^{-1}.[263] For the PA-imidazolium salts the carbonyl stretching frequency was comparatively stunted and broad, even for the chloride salts and cover a range of 1688 – 1711 cm^{-1} which encompasses the above value. This may be due to the competition of the imino-resonance form (Figure 5.23), meaning the carbonyl has greater π-character than in an unconjugated amide. IR analysis of a related *N*-pyridin-4-yl-acetamido imidazolium salt system reported C = O stretching frequencies of 1794 cm^{-1} (methyl pendant) and 1795cm^{-1} (isopropyl pendant).[158] This supports that the C = O stretching frequency probably increases as a result of imino-conjugation, although, no discussion was provided in the text.[158] Surprisingly the carbonyl-stretch is less intense than five sharp stretches within 1594 – 1535cm^{-1} corresponding the aromatic C – C and C – N stretching.[263]

NMR spectra of **5.12.HCl** were fully assigned with expected downfield signals in the ^{1}H-NMR belonging to the amide N*H* and imidazolyl NC*H*N signals 11.98 ppm and 10.27 ppm respectively. The acetamide group is represented in the ^{1}H-NMR and ^{13}C-NMR spectra by the methylene environment at 5.56 ppm and 52.13 ppm respectively as well as the carbonyl-carbon C14 signal at 164.90 ppm. Functionalisation of the 4-position of 2,2-bipyridine is confirmed by assignment of the C4 resonance at 146.21 ppm by HMBC correlation with H6 and H13 (amide N*H*). A singlet resonance at 8.76 ppm exhibits a one-bond HSQC correlation to 109.99 ppm which is confirmed to belong to H3 by HMBC correlation to the H5 and H6 environments. All remaining pyridyl-environments were assigned similarly by correlation NMR.

5.4.1.2. Synthesis of $[Ru(phen)_2(5.11)][PF_6]_3$

The metallo-NHC proligand $[Ru(phen)_2($**5.12.H**$)][PF_6]_3$ was synthesised from acetamide tethered 2,2'-bipyridine imidazolium salt ligand **5.12.HCl** by the same method used for the preparation of complexes $[Ru(phen)_2($**5.5.H - 5.10.H**$)][PF_6]_3$ (Scheme 5.14) .

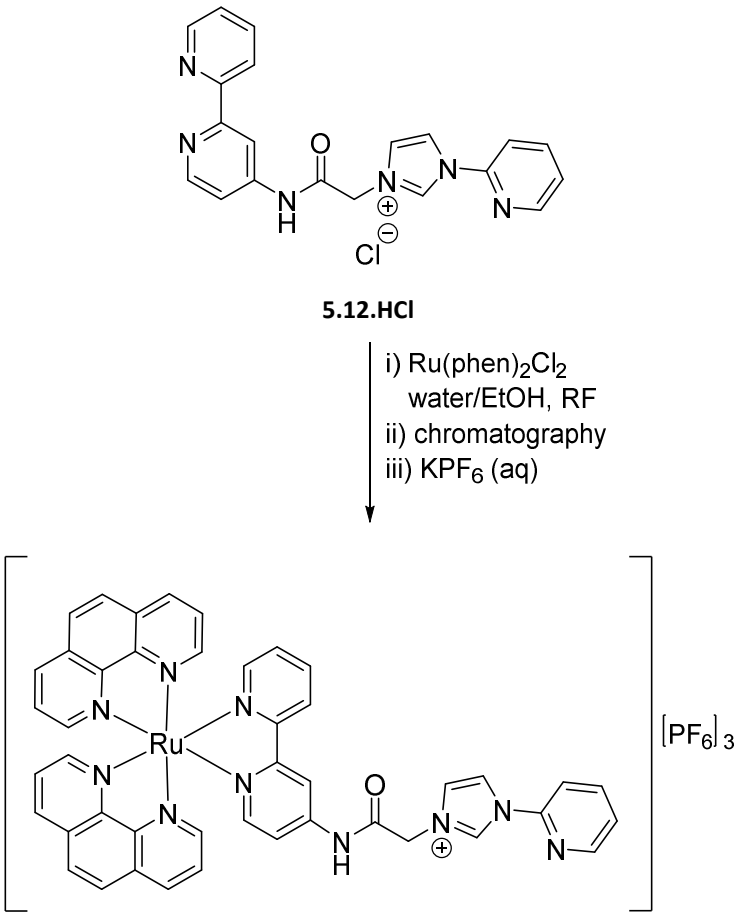

Scheme 5.14: *Synthesis of the complex [Ru(phen)$_2$(**5.12.H**)][PF$_6$]$_3$*

Complex [Ru(phen)$_2$(**5.12.H**)][PF$_6$]$_3$ was characterised spectroscopically, producing NMR spectra with the expected attributes (^{1}H-NMR spectrum, Figure 5.24). Proton resonances due to the imidazolium ring are found at 10.07 ppm (H17), 8.58 ppm (H19) and ~ 7.96 ppm. Figure 5.24 compares the ^{1}H-NMR spectra of [Ru(phen)$_2$(**5.12.H**)][PF$_6$]$_3$ with its pyridyl-pendant, 5-acetamido phenanthroline analogue [Ru(phen)$_2$(**5.10.H**)][PF$_6$]$_3$. For [Ru(phen)$_2$(**5.12.H**)][PF$_6$]$_3$, the amide N*H* resonance is found at 11.54 ppm (H13), markedly downfield of the equivalent resonance in [Ru(phen)$_2$(**5.10.H**)][PF$_6$]$_3$ which arises at 11.06 ppm ($\Delta\delta$ = 0.48 ppm). The 4-substituted 2,2'-bipyridine core facilitates greater electron donation from the amide N*H* onto the Ru(II) centre as has been explained. Differences in the N*H* chemical shift of

[Ru(phen)$_2$(**5.12.H**)][PF$_6$]$_3$ compared with [Ru(phen)$_2$(**5.10.H**)][PF$_6$]$_3$ arise as a result of this. The difference observed between the carbonyl carbon environments of these two compounds is much less distinct at 165.58 ppm and 165.33 ppm respectively.

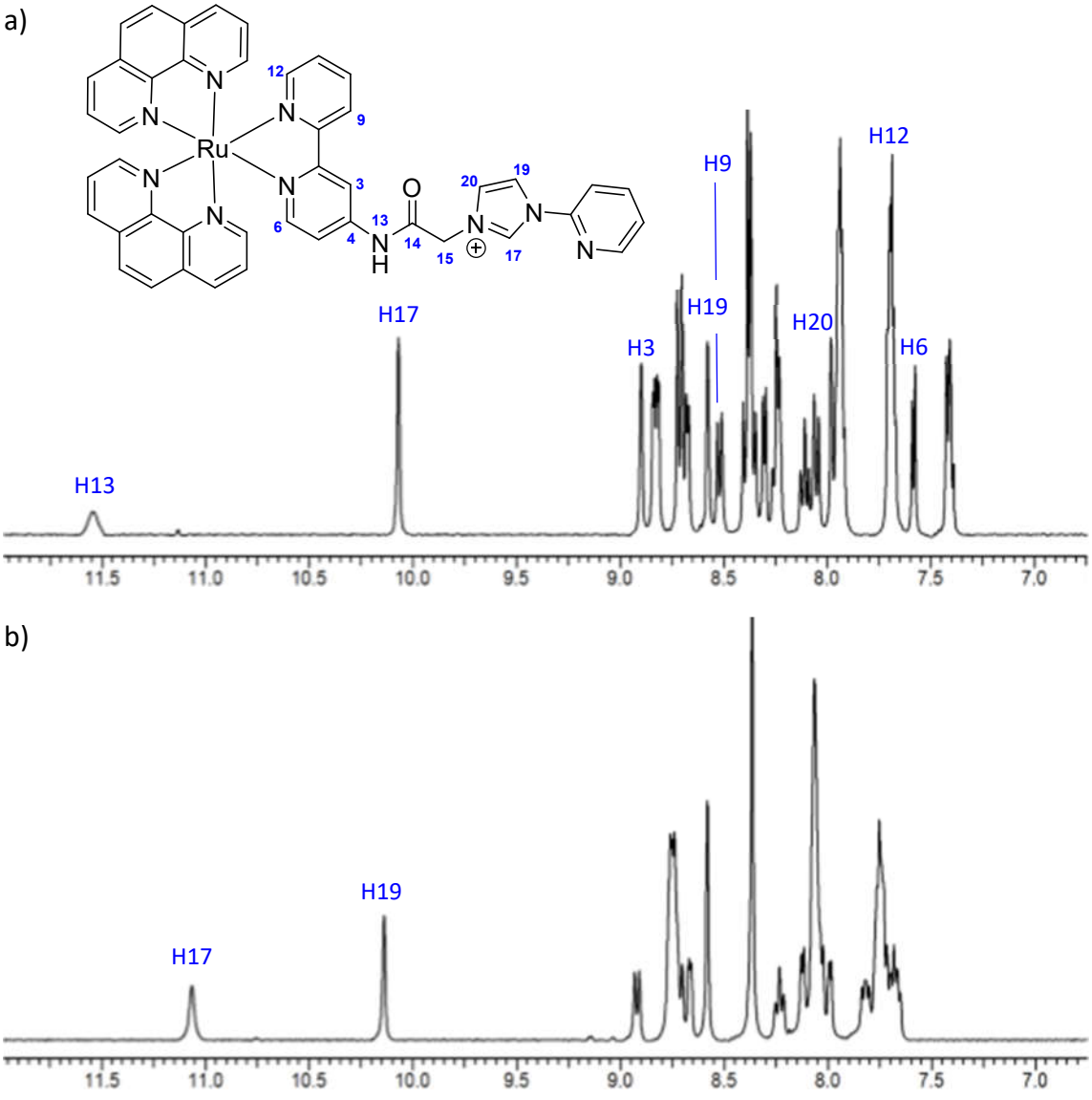

Figure 5.24 (a): *The ^{1}H-NMR spectrum of [Ru(phen)$_2$(**5.12.H**)][PF$_6$]$_3$ and,* ***(b)*** *of the related complex [Ru(phen)$_2$(**5.10.H**)][PF$_6$]$_3$. Selected signals have been highlighted.*

As expected, proton environments adjacent to the pyridyl-nitrogen H6 and H12 exhibit dramatic upfield coordination induced shifts of 1.00 ppm and 0.97 ppm. This is respective to the uncoordinated ligand **5.12.HCl** for which these signals arise at 7.58 ppm and ~ 7.69 ppm. Conversely, proton resonances due to H3 and H9 are shifted

slightly upfield relative to the free ligand with H3 repositioned from 8.76 ppm to 8.90 ppm (Δδ = 0.14 ppm) and H9 from 8.37 ppm to 8.52 ppm (Δδ = 0.15 ppm). This reflects the affixing of the 2,2-bipyridine ligand such that these environments are now anisotropically deshielded by the neighbouring ring. Proton and carbon environments attributable to the 1,10-phenanthroline ancillary ligands and the pyridyl-pendant are accounted for.

Confirmation was provided by mass spectrometry in which complex $[Ru(phen)_2(\mathbf{5.12.H})][PF_6]_3$ is identifiable by two signals at 273.0608 and 409.0897. These are attributable to $[Ru(phen)_2(\mathbf{5.12.H})]^{3+}$ and the free carbene adduct $[Ru(phen)_2(\mathbf{5.12})]^{2+}$ which have calculated m/z values of 273.0626 and 409.0900 respectively.

5.5. Synthesis of $[Ru(1,10\text{-phenanthroline})_2(4\text{-BipA})]^{3+}$ derived NHC complexes

5.5.1. $[Ru(1,10\text{-phenanthroline})_2(Pd\{5.12 - H\}Cl)][PF_6]_2$

Synthesis of complex $[Ru(phen)_2(Pd\{\mathbf{5.12 - H}\}Cl)][PF_6]_2$ was attempted using the metallo-NHC proligand $[Ru(phen)_2(\mathbf{5.12.H})]Cl_3$ by the procedure used for the preparation of $[Ru(phen)_2(Pd\{\mathbf{5.10 - H}\}Cl)][PF_6]_2$ (Scheme 5.15). In this case however, a mixture of the "chelate" complex $[Ru(phen)_2(Pd\{\mathbf{5.12 - H}\}Cl)]^{2+}$ and "pendant" complex $[Ru(phen)_2(Pd\{\mathbf{5.12}\}\{L\}Cl)]^{n+}$ was obtained.

Isolation was performed by dissolving the DMSO reaction mixture in water and filtering the deep red, turbid solution through celite. This was then loaded onto a short plug of Sephadex C25 cation exchange resin and eluted with a gradient of 0 – 0.1 mol/L NaCl solution. Three fractions were collected; the first was a mixture of both chelate and pendant complexes, the second was pure pendant and the final fraction was again a mixture of the two complexes. Complexes were isolated as PF_6 salts. Given the high concentration of NaCl solution used in the work-up, it is likely that the additional ligand,

L of $[Ru(phen)_2(Pd\{\mathbf{5.12}\}\{L\}Cl)]^{n+}$, is chloride. The isolated form would therefore be $[Ru(phen)_2(Pd\{\mathbf{5.12}\}Cl_2)][PF_6]_2$ (as was true for Pd(**2.5**)Cl_2), although, this was not confirmed by elemental analysis. Assuming this is the case, complex $[Ru(phen)_2(Pd\{\mathbf{5.12}\}Cl_2)][PF_6]_2$ was isolated in a 36% yield.

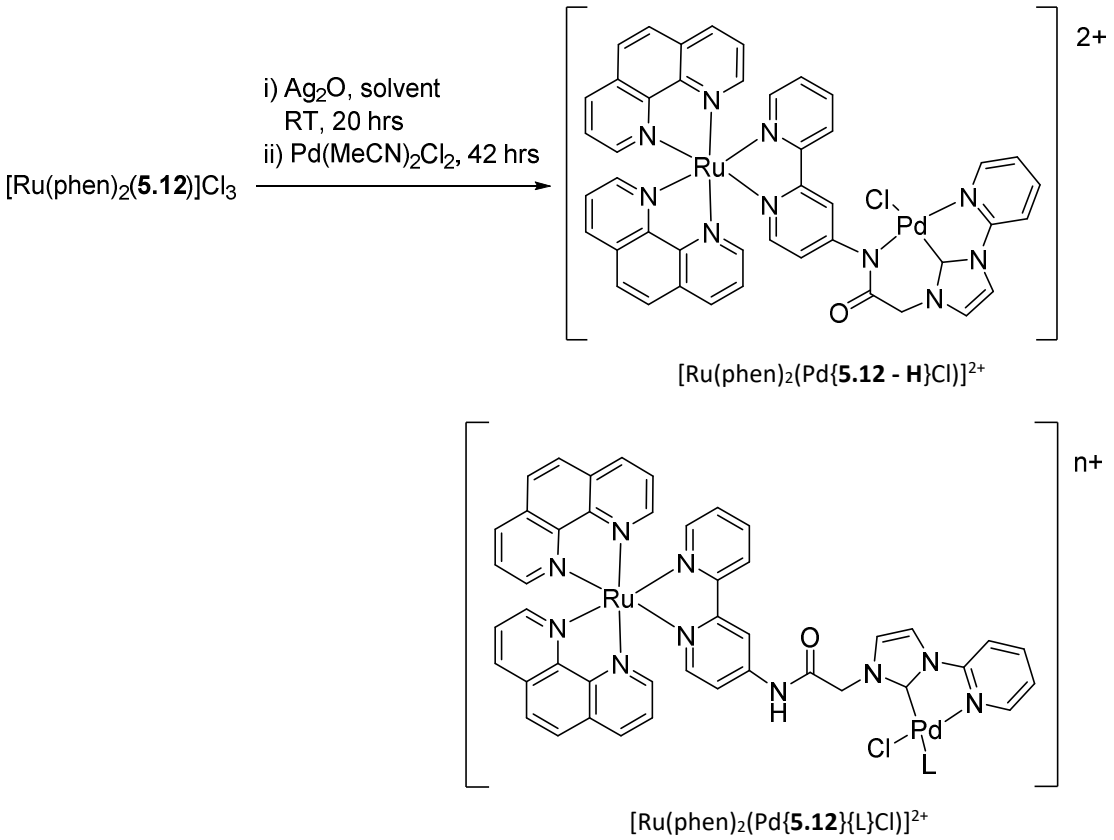

Scheme 5.15: *Synthesis of $[Ru(phen)_2(Pd\{\mathbf{5.12}\ \mathbf{-}\ \mathbf{H}\}Cl]^{2+}$ and $[Ru(phen)_2(Pd\{\mathbf{5.12}\}\{L\}Cl]^{2+}$ by the silver-transmetalation method.*

Characterisation of the pendant complex $[Ru(phen)_2(Pd\{\mathbf{5.12}\}Cl_2)][PF_6]_2$ was performed by ^{1}H-NMR, ^{13}C-NMR, mass-spectrometry and X-ray crystallography along with IR and UV-vis spectroscopy. Interestingly, while the NMR clearly indicated pendant type coordination, the crystal structure obtained was that of the chelated species $[Ru(phen)_2(Pd\{\mathbf{5.12}\ \mathbf{-}\ \mathbf{H}\}Cl)][PF_6]_2$. The mass-spectrum also indicated chelation with a dominant signal at 474.5393 corresponding to the cyanide ligated adduct of the *N*-

amidate/NHC chelated form $[M - HCl + CN]^{2+}$ (calculated m/z, 474.5399). This motif is reminiscent of that observed for the 5-phenanthroline chelated complex $[Ru(phen)_2(Pd\{\mathbf{5.10 - H}\}Cl)][PF_6]_2$.

Crystallisation of $[Ru(phen)_2(Pd\{\mathbf{5.12}\}Cl_2)][PF_6]_2$ was attempted by slow vapour diffusion, however, the crystal selected for analysis was found to be $[Ru(phen)_2(Pd\{\mathbf{5.12 - H}\}Cl)][PF_6]_2$. An ^{1}H-NMR analysis on the same crop of crystals showed it to be a mixture of both pendant and chelate forms of the complex. It appears likely that crystallisation of the chelated form is thermodynamically favoured with chelation reversible in solution. This is explored further in section 5.6.1.

Crystals of complex $[Ru(phen)_2(Pd\{\mathbf{5.12 - H}\}Cl)][PF_6]_3$ suitable for X-ray diffraction analysis were grown by slow vapour diffusion of Et_2O into a MeCN solution of $[Ru(phen)_2(Pd\{\mathbf{5.12}\}Cl_2)][PF_6]_2$. It crystallised in the monoclinic space group *I*2/*a* with one molecule of $[Ru(phen)_2(Pd\{\mathbf{5.12 - H}\}Cl)]^{2+}$ and two PF_6 anions in the asymmetric unit (Figure 5.25) along with numerous disordered solvent molecules.

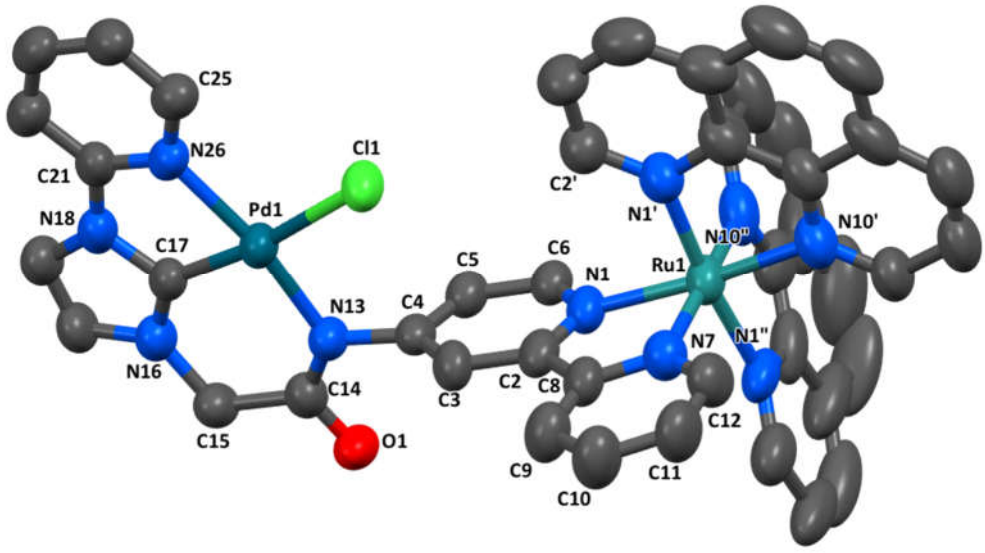

Figure 5.25: *Asymmetric unit of $[Ru(phen)_2(Pd\{\mathbf{5.12 - H}\}Cl)][PF_6]_2$. Hydrogen atoms, PF_6 anions and solvate molecules have been omitted for clarity.*

Three MeCN molecules were modelled adequately, however, a portion of the residual electron density was dealt with using OLEX2 solvent mask function. For the unit cell, a total of 1608.4 $Å^3$ (13.5%) of solvent accessible volume containing 419 electrons was masked, equating to 2.2 MeCN molecules per asymmetric unit. It may also be assigned, in part, to water or an Et_2O molecule.

Complex $[Ru(phen)_2(Pd\{\mathbf{5.12 - H}\}Cl)]^{2+}$ shares many structural attributes with the 5-acetamido phenanthroline based $[Ru(phen)_2(Pd\{\mathbf{5.10 - H}\}Cl)]^{2+}$ complex. The $Ru(ppy)_3$ component is in the expected octahedral geometry with the Λ-enantiomer shown in Figure 5.25. An intrachelate bond angle, N1 – Ru – N7 of 78.5(3)° is observed for the 2,2-bipyridine of **5.12 - H** and N1' – Ru – N10', and N1" – Ru – N10" angles of 80.0(3)° and 80.7(4)° for the two phenanthroline ligands. Ru – N bond lengths are as follows; Ru1 – N1 = 2.064(6) Å, Ru1 – N7 = 2.048(8) Å, Ru1 – N1' = 2.061(7) Å, Ru1 – N10' = 2.076(6) Å, Ru1 – N1" = 2.068(7) Å and Ru1 – N10" = 2.086(9) Å. Ligand **5.12 - H** coordinates to the Pd(II) in a tridentate motif of the type *N*-amidate – NHC – Py enforcing a distorted square planar geometry with a chloride ligand occupying the fourth site. Distortion occurs due to the narrow NHC – Py bite angle C17 – Pd1 – N26, of 78.9(3)° whereas the 6-membered *N*-amidate/NHC chelate is more conducive to 90° coordination with a C17 – Pd1 – N13 angle of 88.2(3)°. Bond angles relative to the chloride are C26 – Pd1 – Cl1 = 93.8(2)° and N13 – Pd1 – Cl1 = 99.0(2)°. Metal to ligand distances for the Pd(II) centre are Pd1 – C17 = 1.897(7) Å, Pd1 – N13 = 2.035(6) Å, Pd1 – N26 = 2.059(6) Å and Pd1 – Cl1 = 2.375(2) Å. Relative bond lengths are as expected given coordinating ability of each ligand. Again it is noted that the NHC – amidate chelate ring is planar as a result of 5,6-tridentate chelation resulting in a θ_{CH2} of 1.79(9)°. The NHC – amidate coordination plane is oriented at 97.6(2)° relative to the N1 pyridyl ring of the bipyridine. As with $[Ru(phen)_2(Pd\{\mathbf{5.10 - H}\}Cl)]^{2+}$ this is an atropisomeric relationship defined by the stereochemical axis along the C4 – N13 bond and is designated, in this case, as the P enantiomer. Thus, the complex depicted is the Λ,P-diastereomer.

In the extended structure, the planar Pd(II) complex components of neighbouring $[Ru(phen)_2(Pd\{\mathbf{5.12 - H}\}Cl)]^{2+}$ are overlaid in a similar packing motif to $[Ru(phen)_2(Pd\{\mathbf{5.10 - H}\}Cl)]^{2+}$, albeit with a different relative orientation. The observed

orientation appears to maximise stabilising intermolecular hydrogen bonding contacts (Figure 5.26).

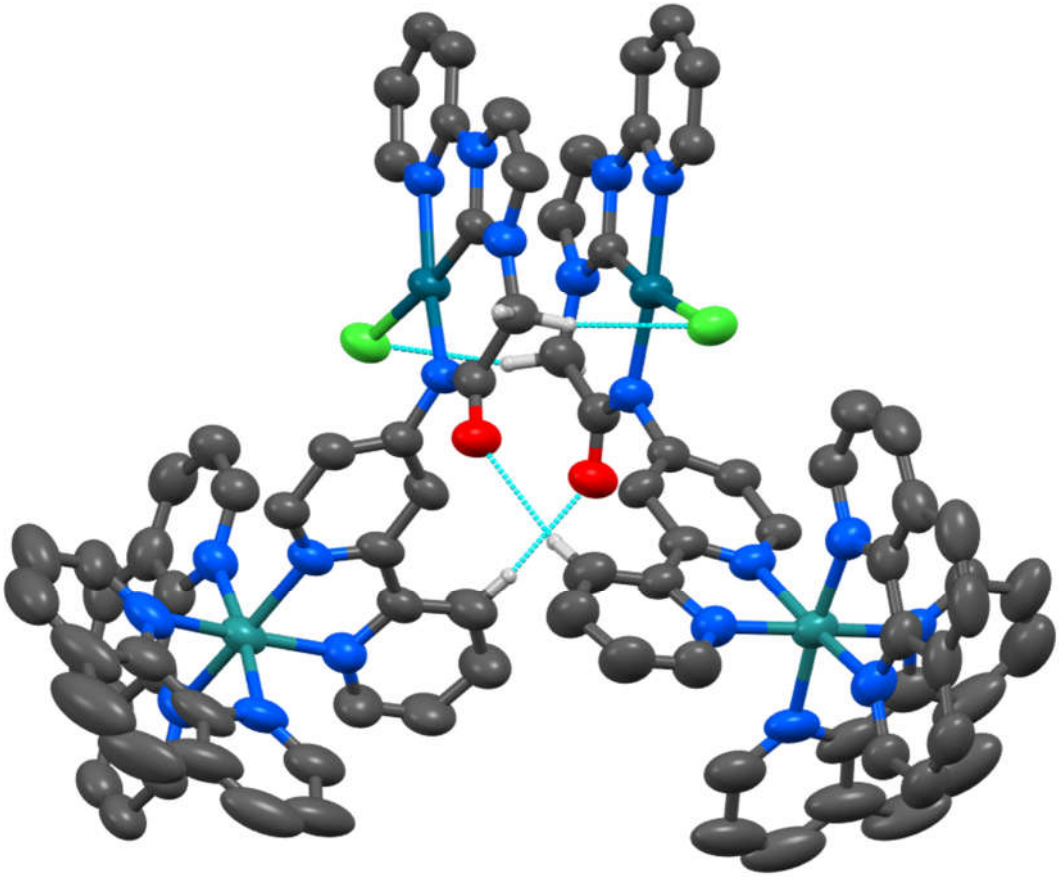

Figure 5.26: *Dimeric packing arrangement of* $[Ru(phen)_2(Pd\{$***5.12 - H***$\}Cl)]^{2+}$ *with hydrogen bonding interactions highlighted.*

Opposing Pd(NHC)Cl fragments, as defined by the Pd(II) coordination plane, have a plane-to-plane centroid distance of 3.508(9) Å at a relative twist angle of 20.0(6)°. The internuclear distance between Pd(II) centres, Pd1 – Pd1 is 3.966(2) Å. A strong C*H* ··· O type interaction is noted between H9 of 2,2-bipyridine and the amide-carbonyl of neighbouring complexes such that C9 ··· O1 = 3.193(11) Å. There is also an apparent supporting interaction between the chloride ligand and methylene hydrogen, C14 ··· Cl1 = 3.638(10) Å. Beyond this dimeric-structure the most significant interaction is a face-to-face π – π stack between the pendant pyridyl and N10'-pyridyl ring of an adjacent

phenanthroline at a plane-to-plane centroid distance of 3.443(8) Å / 3.339(8) Å with a shift of 1.50(2) Å / 1.723(2) Å. Interactions with the PF_6 anion occur in the form of C*H* ··· F contacts, the shortest of which with an appropriate geometry being C8" ··· F = 3.276(17) Å and C20 ··· F = 3.321(11) Å.

Unlike ligand **5.10 - H**, the functionalised pyridyl-ring of **5.12 - H** has no ortho-substituents relative to the acetamide group making free rotation around the C4 – N13 bond more likely when in solution. However, the crystallised diastereomer of $[Ru(phen)_2(Pd\{\mathbf{5.12 - H}\}Cl)]^{2+}$ has the chloride ligand of the Pd(NHC)Cl fragment situated much closer to the front edge of the phenanthroline auxiliary resulting in a Cl1 ··· C2' distance of 3.581(9) Å. This is significantly shorter than the 4.194(14) Å / 4.153(13) Å seen for $[Ru(phen)_2(Pd\{\mathbf{5.10 - H}\}Cl)]^{2+}$ confirming that moving the Pd(NHC)Cl moiety to the 4-position has maximised its interaction with the stereochemical $Ru(ppy)_3$ component as desired. Figure 5.27 compares the spacefilled models of $[Ru(phen)_2(Pd\{\mathbf{5.10 - H}\}Cl)]^{2+}$ and $[Ru(phen)_2(Pd\{\mathbf{5.12 - H}\}Cl)]^{2+}$ to better illustrate this point.

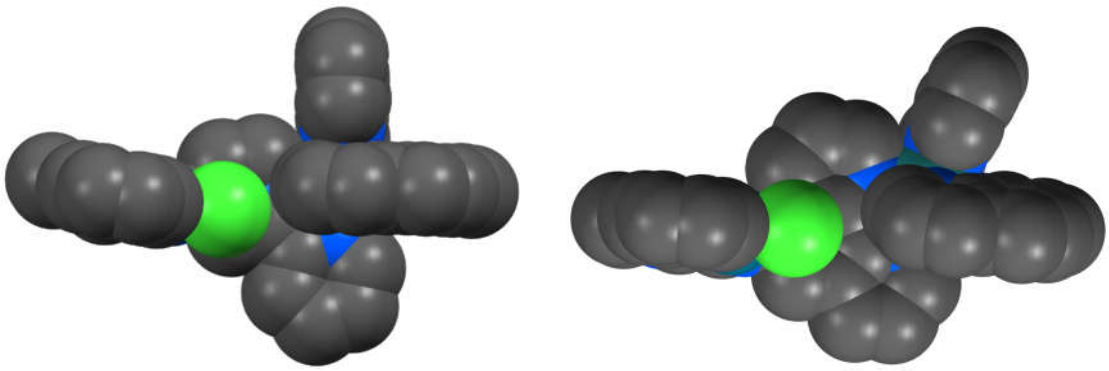

$[Ru(phen)_2(Pd\{\mathbf{5.12 - H}\}Cl)]^{2+}$ $[Ru(phen)_2(Pd\{\mathbf{5.10 - H}\}Cl)]^{2+}$

Figure 5.27: *Perspective view highlighting the potential for increased steric interactions between the Pd(NHC)Cl and $Ru(ppy)_3$ components of $[Ru(phen)_2(Pd\{\mathbf{5.12 - H}\}Cl)]^{2+}$ when compared with $[Ru(phen)_2(Pd\{\mathbf{5.10 - H}\}Cl)]^{2+}$ as observed crystallographically.*

Pendant type coordination in the chromatographically isolated sample of $[Ru(phen)_2(Pd\{\mathbf{5.12}\}Cl_2)][PF_6]_2$ was confirmed by NMR analysis. Furthermore, it was found that simply adding solid K_2CO_3 to the NMR sample of $[Ru(phen)_2(Pd\{\mathbf{5.12}\}Cl_2)][PF_6]_2$ in CD_3CN achieved conversion to the chelated form $[Ru(phen)_2(Pd\{\mathbf{5.12 - H}\}Cl)][PF_6]_2$ after 24 hours. The ^{1}H-NMR spectra of the two compounds are shown in Figure 5.28, note that the spectrum of $[Ru(phen)_2(Pd\{\mathbf{5.12}\}Cl_2)][PF_6]_2$ contains a small amount of chelate impurity.

Upon going from $[Ru(phen)_2(Pd\{\mathbf{5.12}\}Cl_2)][PF_6]_2$ to $[Ru(phen)_2(Pd\{\mathbf{5.12 - H}\}Cl)][PF_6]_2$ a disappearance of the diagnostic amide N*H* (H13) proton resonance at 9.82 ppm is observed as expected. Further evidence of *N*-amidate/NHC chelation is seen in the upfield shift of the methylene H15 signal from 5.74 ppm to 4.99 ppm due to shielding by the adjacent anionic moiety. The H3 environment responds similarly, shifting upfield from 8.83 ppm to 8.20 ppm as does H5 which shifts from the region between 7.40 – 7.50 ppm to 6.98 ppm. In the pendant form, both phenanthroline ancillary ligands are magnetically equivalent, however, they become non-equivalent in the chelated form as a result of interaction with the Pd(NHC)Cl component. Hence we see H4' shift from a doublet at 8.65 ppm in $[Ru(phen)_2(Pd\{\mathbf{5.12}\}Cl_2)][PF_6]_2$ to two separate doublets in $[Ru(phen)_2(Pd\{\mathbf{5.12 - H}\}Cl)][PF_6]_2$ at 8.68 pm and 8.65 ppm. A similar effect is also seen for H2' and H3'. Importantly, only one of the two possible diastereomers of $[Ru(phen)_2(Pd\{\mathbf{5.12 - H}\}Cl)][PF_6]_2$ is observed implying that conversion of $[Ru(phen)_2(Pd\{\mathbf{5.12}\}Cl_2)][PF_6]_2$ to $[Ru(phen)_2(Pd\{\mathbf{5.12 - H}\}Cl)][PF_6]_2$ is diastereoselective. Furthermore, it must be fixed as one diastereomer because the two phenanthroline ligands are distinguished by unique H2', H3' and H4' environments. If rotation around the C4 – N14 bond was occurring rapidly on the NMR timescale such that the diastereomers were interconverting rapidly, these proton environments would appear as equivalent.

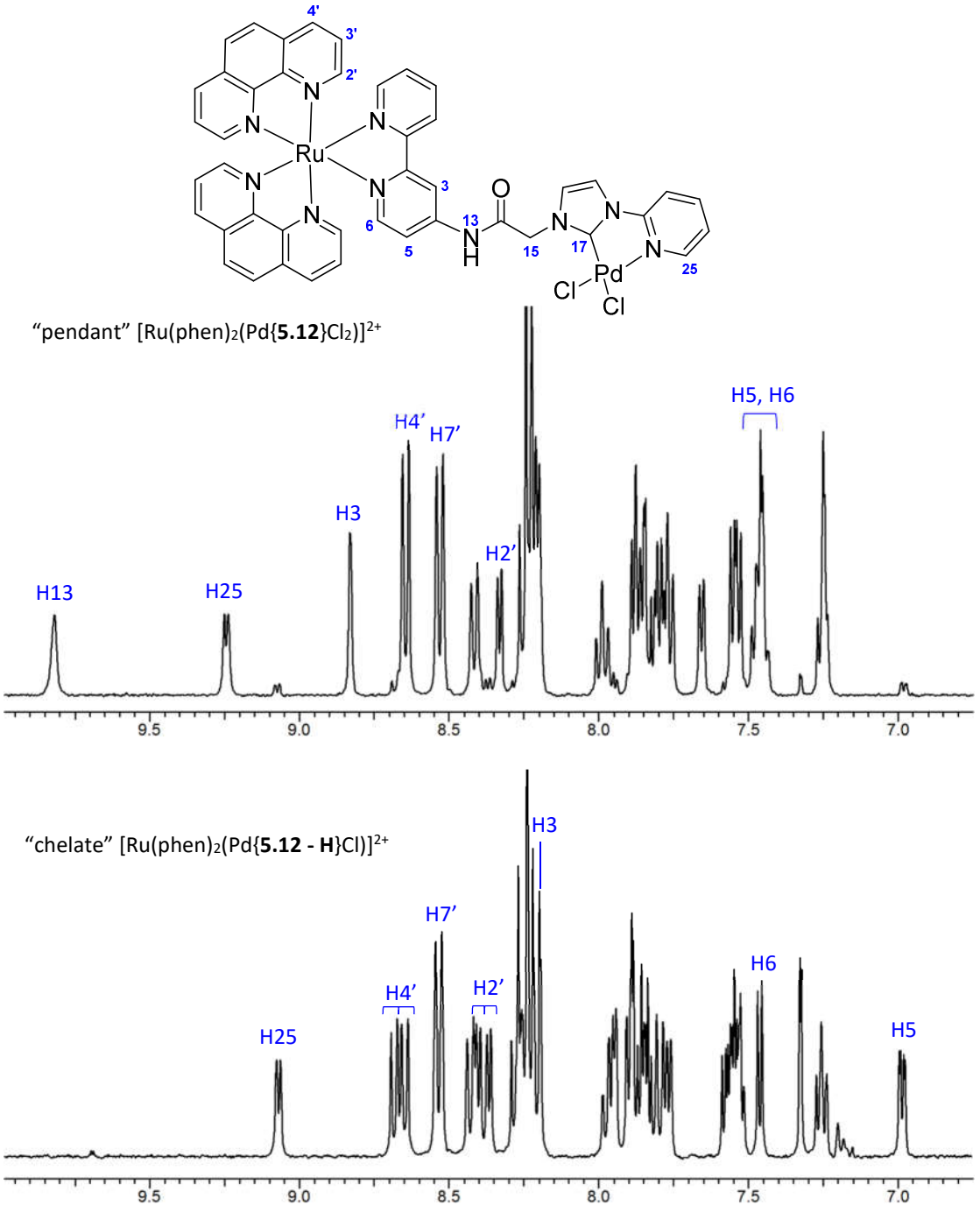

Figure 5.28: *Aromatic region of the ^{1}H-NMR spectrum of [Ru(phen)$_2$(Pd{**5.12**}Cl$_2$)][PF$_6$]$_2$ and again following treatment with base to give [Ru(phen)$_2$(Pd{**5.12 - H**}Cl)][PF$_6$]$_2$.*

It appears that the pendant and chelated forms can exist in an equilibrium which is dependent on the pH or thermodynamic transformations such as crystallisation. This, in part, would explain why chromatographic isolation provided a fraction of pure pendant compound in between fractions of pendant/chelate mixtures.

5.6. Comparative analysis of Ru – NHC – Pd complexes

Conjugate stabilisation of the amidate anion is crucial to the properties of the metallo-NHC complexes $[Ru(phen)_2(Pd\{\mathbf{5.9 - H}\}\{allyl\})][PF_6]_2$, $[Ru(phen)_2(Pd\{\mathbf{5.10 - H}\}Cl)][PF_6]_2$ and $[Ru(phen)_2(Pd[\mathbf{5.12 - H}]Cl)][PF_6]_2$. It has been shown that the 5-acetamido-phenanthroline derivatives $[Ru(phen)_2(Pd\{\mathbf{5.9 - H}\}\{allyl\})][PF_6]_2$ and $[Ru(phen)_2(Pd\{\mathbf{5.10 - H}\}Cl)][PF_6]_2$ form an *N*-amidate/NHC chelate through spontaneous deprotonation of the amide (section 5.3). However, this process is not as dominant for the 4-acetamido-bipyridine analogue which was isolated in both chelate and pendant forms, $[Ru(phen)_2(Pd[\mathbf{5.12 - H}]Cl)][PF_6]_2$ and $[Ru(phen)_2(Pd[\mathbf{5.12}]Cl_2)][PF_6]_2$, respectively. It is reasonable to assume that the amide of the 4-acetamido-bipyrdine will be more acidic than the 5-acetamido-phenanthroline amide due better resonance stabilisation of the conjugate base amidate as noted previously. With regard to the metallo-NHC proligands, stabilisation of the amidate-anion is enhanced tremendously by delocalisation onto the pyridine-nitrogen coordinated to ruthenium. Deprotonation also serves to decrease the overall charge of the system. Scheme 5.16 depicts this scenario in terms of the Ru(II) coordinated acetamide-ligand to reiterate this point.

For both 5-acetamido-phenanthroline and 4-acetamido-bipyrdine ligands, the anion participates in stabilising donation to the Ru(II) centre, however, the stability penalty in terms of loss of aromaticity is much greater for the 5-amino-1,10-phenanthroline system. Scheme 5.17 illustrates two possible canonical forms, A and B, of the bimetallic 4-acetamido-bipyrdine complex $[Ru(phen)_2(Pd[\mathbf{5.12 - H}]Cl)][PF_6]_2$. Delocalisation of the anion onto the oxygen is not shown. For the reasons stated above, resonance structure B contributes more and, as a result, the amidate is less basic and has a weaker coordination bond to palladium in the NHC complex. The observed interchangeability between the chelate and pendant forms in $[Ru(phen)_2(Pd[\mathbf{5.12 - H}]Cl)][PF_6]_2$ is attributed to weakening of the Pd – N bond and is important to the isolation of a single diastereomer as discussed shortly.

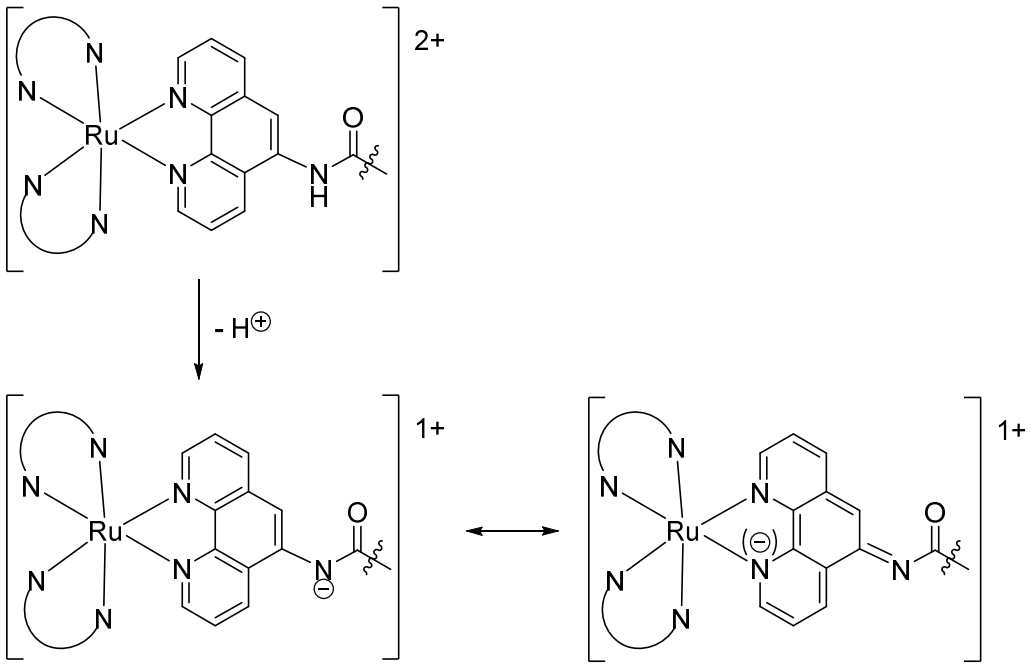

Scheme 5.16: *Showing deprotonation of a ruthenium bound 5-phenanthroline-acetamide derivative and resonance stabilisation of the resultant amidate.*

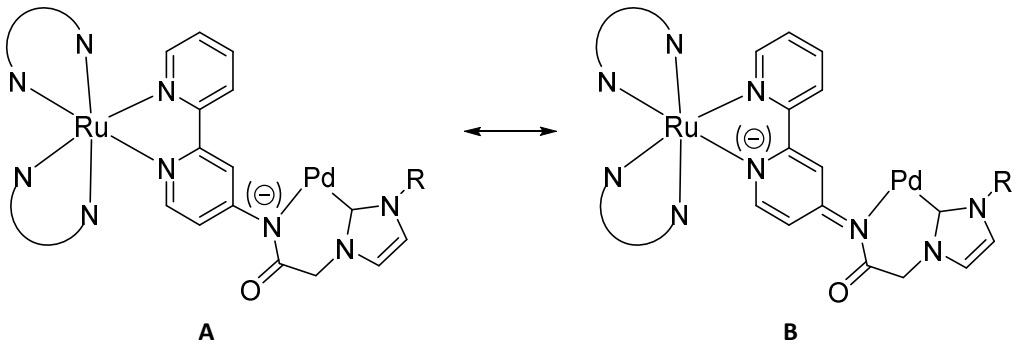

Scheme 5.17: *Two possible resonance forms, A and B, of complex [Ru(phen)$_2$(Pd[**5.12 - H**]Cl)][PF$_6$]$_2$.*

5.6.1. Atropisomerism and system dynamics

Two diastereomers of the complex $[Ru(phen)_2(Pd\{\mathbf{5.10 - H}\}Cl)][PF_6]_2$ occur due to the presence of two enantiomeric components; the metal-centred Δ/Λ-$Ru(phen)_3$ and a P/M chiral axis along the bond conjoining the planar Pd(NHC)Cl moiety to the phenanthroline ligand. On the other hand, the related bipyridine derivative $[Ru(phen)_2(Pd\{\mathbf{5.12 - H}\}Cl)][PF_6]_2$ is isolated as a single diastereomer in its chelated form. Similarly, the allyl complex $[Ru(phen)_2(Pd\{\mathbf{5.9 - H}\}\{allyl\})][PF_6]_2$ does not exhibit the same diastereoisomerism due to the chiral axis, although, it is difficult to say definitively based on its NMR spectra.

The two diastereomers of $[Ru(phen)_2(Pd\{\mathbf{5.10 - H}\}Cl)][PF_6]_2$, referred to as (Δ/Λ),M and (Δ/Λ),P, form in a 2 : 1 ratio. Evidently the major diastereomer is favoured on steric grounds, however, it is yet to be assigned to (Δ/Λ),M or (Δ/Λ),P forms. For $Ru(phen)_2(Pd\{\mathbf{5.10 - H}\}Cl)][PF_6]_2$ it is proposed that either; (a) *N*-amidate chelation occurs irreversibly locking the compound in one of two diastereomeric configurations or, (b) the two configurations are in equilibrium. It seems unlikely, however, that there is a pathway for bond rotation, or on-off *N*-amidate chelation, which would enable an equilibrium to exist.

In $[Ru(phen)_2(Pd\{\mathbf{5.9 - H}\}\{allyl\})][PF_6]_2$ and $[Ru(phen)_2(Pd\{\mathbf{5.12 - H}\}Cl)][PF_6]_2$, there may be a pathway leading to the prevalence of one diastereomer. It was noted for $[Ru(phen)_2(Pd\{\mathbf{5.12 - H}\}Cl)][PF_6]_2$ that *N*-amidate/NHC chelation appears to be reversible during synthesis and work-up. Treating the pendant form, $[Ru(phen)_2(Pd\{\mathbf{5.12}\}Cl_2)][PF_6]_2$, with base leads to a single diastereomer of $[Ru(phen)_2(Pd\{\mathbf{5.12 - H}\}Cl)][PF_6]_2$. Reversibility of chelation could lead to formation of a single diastereomer under thermodynamic control as per the mechanism in Scheme 5.18. This is possible due to the weaker *N*-amidate coordination detailed in the above section. Alternatively, it may simply be that only one diastereomer is sterically favourable (or possible) given the shorter distance between the Pd(NHC)Cl group and the phenanthroline ancillary ligands as shown previously in Figure 5.27.

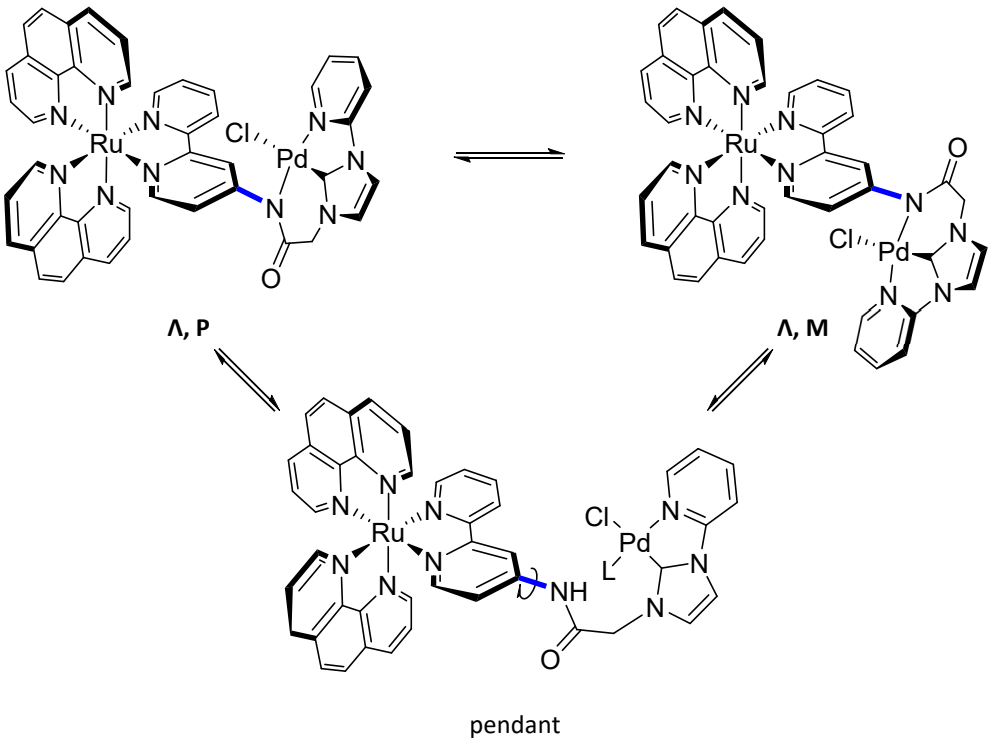

Scheme 5.18: *Possible route to interconversion between P and M atropisomers of [Ru(phen)$_2$(Pd{**5.12 - H**}Cl)][PF$_6$]$_2$ via the pendant form.*

The 5-phananthroline based ligands in Ru(phen)$_2$(Pd{**5.10 - H**}Cl)][PF$_6$]$_2$ and allyl complex [Ru(phen)$_2$(Pd{**5.9 - H**}{allyl})][PF$_6$]$_2$ are expected to have the same *N*-amidate/NHC chelation properties. However, in [Ru(phen)$_2$(Pd{**5.9 - H**}{allyl})][PF$_6$]$_2$ rotation about the chiral axis may be enabled as a result of allyl-group *syn-anti* interchange. Effectively, movement of the allyl group could "unlock" the axial-bond, allowing rotation to generate the favoured diastereomer (Scheme 5.19). Looking at the crystal structure of [Ru(phen)$_2$(Pd{**5.9 - H**}{allyl})][PF$_6$]$_2$ it appears as though the allyl-group has less interaction with the phenanthroline ancillary ligands compared with Ru(phen)$_2$(Pd{**5.10 - H**}Cl)][PF$_6$]$_2$ and [Ru(phen)$_2$(Pd{**5.12 - H**}Cl)][PF$_6$]$_2$.

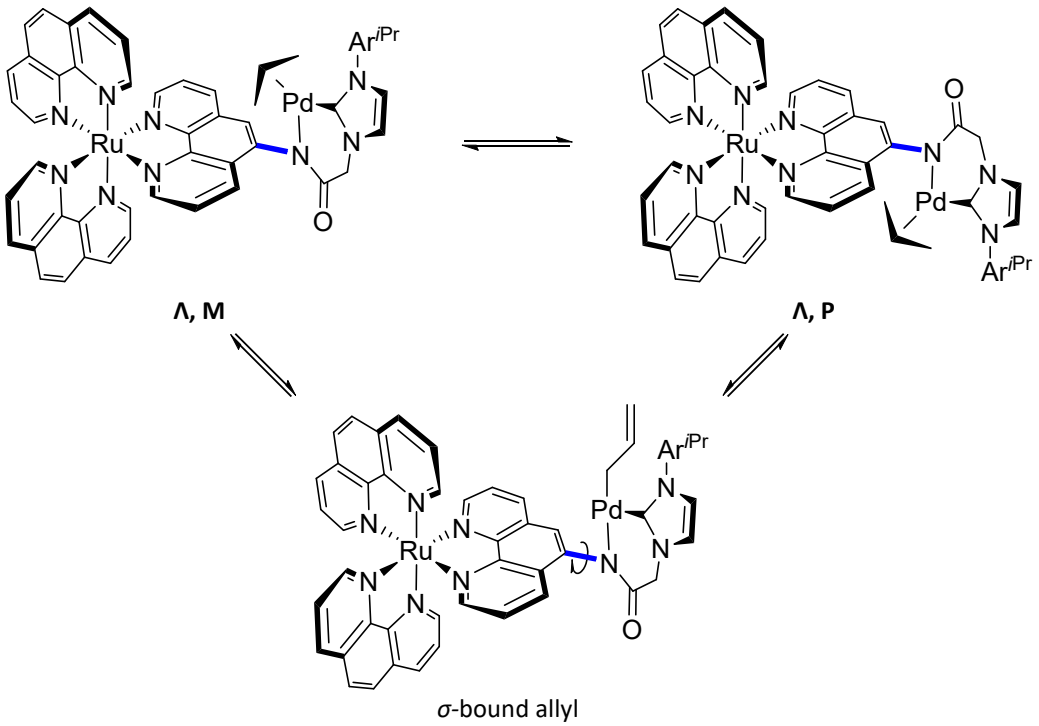

Scheme 5.19: *Possible route to interconversion between M and P atropisomers of [Ru(phen)$_2$(Pd{**5.9 - H**}{allyl})][PF$_6$]$_2$ via the less hindered σ-bound allyl form.*

It is important to consider possible pathways for diastereomeric interconversion of these compounds for their application as asymmetric catalysts. Essentially, substrates bound to the palladium centre during the catalytic cycle need to be selectively arranged in one diastereomeric configuration for consistent asymmetric induction. In this sense, it is promising that the 2,2'-bipyridine derivative [Ru(phen)$_2$(Pd{**5.12 - H**}Cl)][PF$_6$]$_2$ forms as a single diastereomer and there is no reason why this would not also be true in a catalytic scenario. For compounds with 5-phenanthroline cores as in [Ru(phen)$_2$(Pd{**5.9 - H**}{allyl})][PF$_6$]$_2$ and Ru(phen)$_2$(Pd{**5.10 - H**}Cl)][PF$_6$]$_2$, diastereoselectivity could be improved by a larger ligand at palladium. This would increase steric interactions between the two complex-fragments. In the case of Suzuki coupling, the aryl substrate would hopefully constitute a large enough ligand to invoke the desired level of interaction for diastereoselectivity.

5.7. Enantiomeric Resolution

Methods for the enantiomeric resolution of chiral, tris-bidentate octahedral complexes are well established, particularly for ruthenium-polypyridine complexes of the type $[Ru(ppy)_3]^{n+}$.[15, 45, 264] These approaches are summarised in Scheme 5.20, as applied to the complexes in this study.

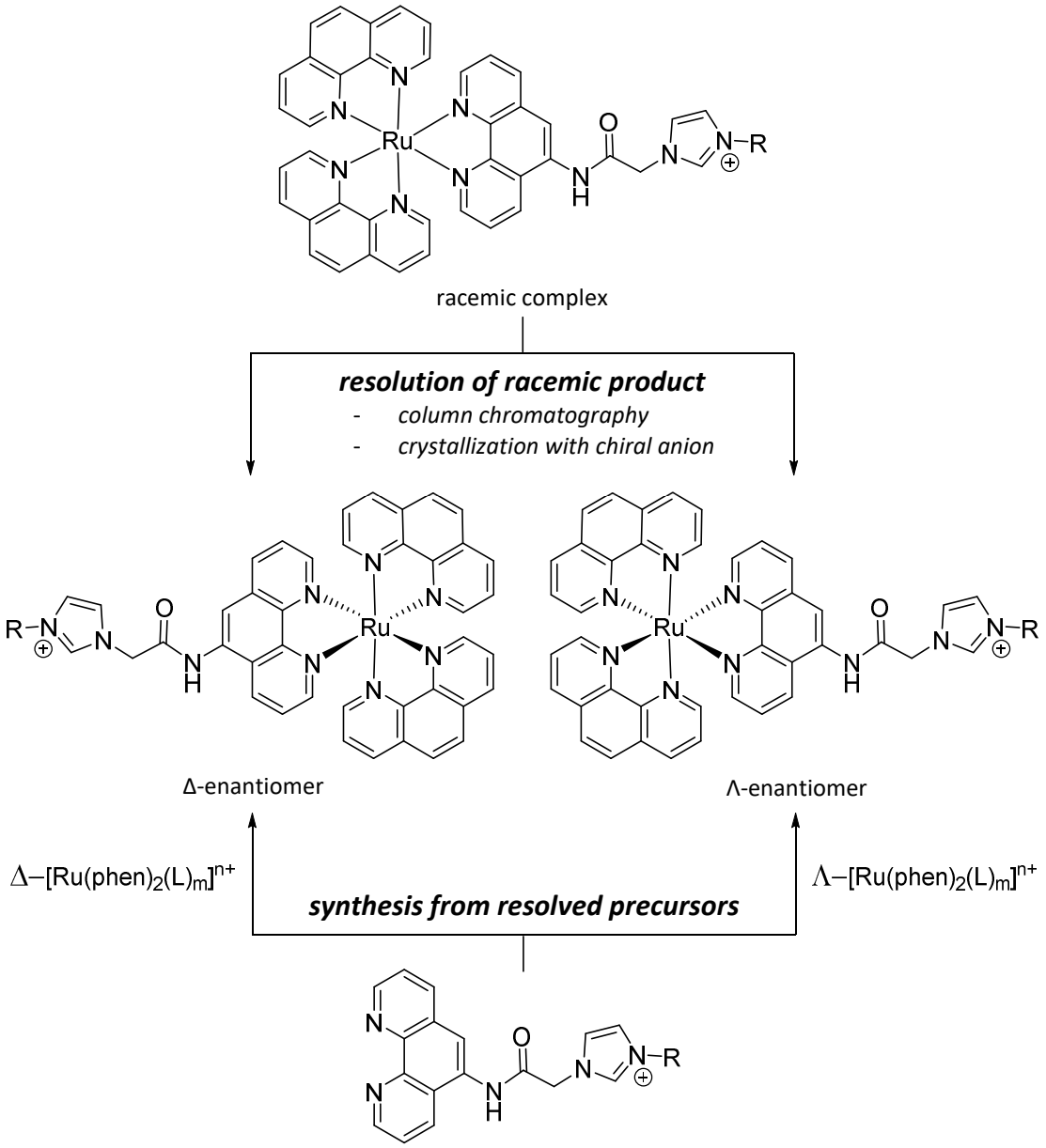

Scheme 5.20: *Routes employed for the resolution of acetamide-linked metallo-NHC proligands in this study.*

In essence, these are all forms of the resolution techniques introduced in Chapter 1, section 1.1.2, this includes chiral chromatography, synthesis from resolved precursors and classical resolution. Enantiomeric precursors are usually obtained by classical resolution and can be enriched through synthesis using a chiral auxiliary ligand.[265] The latter approach was not explored in this study. The following sections outline approaches to resolve the Δ and Λ enantiomers of diisopropyl-phenyl appended complex $[Ru(phen)_2(\mathbf{5.9.H})]^{3+}$.

5.7.1. Resolution of $[Ru(phen)_2(5.9.H)]^{3+}$

5.7.1.1. Chromatographic resolution

Chromatographic resolution is advantageous because it can provide both enantiomers in a single step. Methods for the resolution of ruthenium-polypyridine type complexes by low pressure ion-exchange chromatography have been comprehensively established by Keene and co-workers.[264, 266-268] This is performed using a column of Sephadex-C25 cation-exchange resin and eluting with an aqueous solution of a chiral anion such as sodium (—)-*O,O'*-di-benzoyl-L-tartrate, sodium (+)-*O,O'*-di-benzoyl-D-tartrate, sodium (—)-*O,O'*-di-*p*-toluoyl-L-tartrate or sodium (+)-*O,O'*- di-*p*-toluoyl-D-tartrate. As well as the eluent, the dextran-derived sephadex-C25 support is also chiral. Separation therefore occurs on the basis of a three-way interaction between complex, chiral eluent and the Sephadex support. Efficiency of resolution by this method is difficult to predict and large variations are often observed between different eluents (and eluent concentrations) for the same complex and between different complexes for the same eluent. However, some general trends have been noted, for example, a larger degree of aromaticity typically improves resolution ($[Ru(phen)_3]^{2+}$ > $[Ru(bipy)_3]^{2+}$) and the presence of hydrophobic groups increases the length of column required for resolution by causing a stronger association of the complex with the stationary phase.

In this investigation, low pressure chromatographic resolution was attempted following procedures outlined in the above references. SP Sephadex C-25 cation exchange resin which was housed in a column approximately 120 cm long and 1.7 cm in diameter. Both

ends of the column were sealed with a capillary tube port. Eluent flow was regulated with a peristaltic pump and during separations a flow rate of 1.5 mL/min was used, although, this could be adjusted as desired. Conjoining the two ends of capillary tubing via the peristaltic pump allows eluent to be recycled through the column. If a "longer column" is needed, the product can be reticulated through more than one column length. Achieving this requires there to be no solvent head-space between the capillary intake and the stationary phase to prevent band mixing. The "effective column length" (ECL) is the overall length of column through which the compound passes before effective separation is achieved and provides a measure of separation efficiency.

Eluent solutions of sodium *O,O'*-di-benzoyl-tartrate or sodium *O,O'*-di-*p*-toluoyl-tartrate where prepared by neutralisation of their respective acids with NaOH. Stock solutions of these were prepared and diluted to the desired concentration prior to use.

The instrumental set-up was trialled for the resolution of Δ/Λ-$[Ru(phen)_3]^{2+}$ using a 0.075 mol/L solution of sodium (—)-*O,O'*-di-benzoyl-L-tartrate as specified in the literature.[268] Separation is reportedly observed at an ECL of 60 cm. A Sephadex column was packed using distilled water and after settling to a constant height, was rinsed with flowing distilled water to ensure even packing. A sample of racemic $[Ru(phen)_3][PF_6]_2$ was converted to the water soluble chloride salt using Amberlite® IRA-400 (chloride form) anion exchange resin. It was then loaded onto a short Sephadex plug and rinsed with distilled water before eluting with dilute NaCl solution. This removes impurities before attempting chromatographic resolution, helping to minimise the accumulation of contaminants through re-use of the column. The solution of $[Ru(phen)_3]Cl_2$ was loaded and rinsing with distilled water continued for a further two hours before beginning elution with 0.075 mol/L sodium (—)-*O,O'*-di-benzoyl-L-tartrate solution at 1.5 mL/min. The increased ionic strength of the anion solution causes compaction of the sephadex medium resulting in shortening of the column. It can be necessary to add additional sephadex to reduce solvent head-space for product reticulation. The red product band travelled cleanly and separation began to be observed after 50 cm as it approached the end of the column. Total separation of Δ-$[Ru(phen)_3]^{2+}$ and Λ-$[Ru(phen)_3]^{2+}$ would have required further circulation and, as this was slow, it was not allowed to continue. Instead

the material was rinsed off and the column prepped for re-use by rinsing with saline solution followed by distilled water.

Resolution of racemic [Ru(phen)$_2$(**5.9.H**)]$^{3+}$ was attempted similarly as above, although, this was met with some complications. A sample of [Ru(phen)$_2$(**5.9.H**)]Cl$_3$ (0.040 g) was run through the preliminary sephadex plug, however, this required a higher NaCl concentration of 0.3 mol/L for elution. It was necessary to dilute this to 0.001 mol/L NaCl (800 mL) to ensure the product did not run on the column during loading. Loading such a large volume was slow and minor compacting of the column was noted due to the ionic strength of the loading solution. To accelerate the process, the flow rate was increased to 2 mL/min, however, this caused drying and cracking of the column near the base. Once loaded the column was rinsed with distilled water causing the column to re-expand and the product band to broaden as a result. Regardless, elution with 0.075 mol/L sodium (—)-*O,O'*-di-benzoyl-L-tartrate solution was conducted and the band travelled well. Unfortunately, due to the initial broadening of the compound band following loading, and cracks in the column media, it seemed unlikely clean separation could be achieved. Instead the product was collected for re-use and the separation repeated.

It was decided to skip the initial Sephadex plug and load a distilled water solution of [Ru(phen)$_2$(**5.9.H**)]Cl$_3$ directly, leaving some brown residue at the top of the column. The compound was loaded and rinsed expediently, providing a neat band which travelled cleanly when eluted with 0.075 mol/L sodium (—)-*O,O'*-di-benzoyl-L-tartrate solution at 1.5 mL/min. Over time, the bright orange band began to broaden, however, there was no indication of band separation. It was necessary to cycle the compound through another column length, although, whilst the band grew larger, no separation occurred. This process required two working days and, for over-night periods, the flow rate was slowed to 0.5 mL/min. It is likely that a more concentrated sodium (—)-*O,O'*-di-benzoyl-L-tartrate eluent solution could provide separation over a shorter ECL, reducing the time for diffusion and mixing of product bands. This would increase interactions of the complex with the anion, especially since [Ru(phen)$_2$(**5.9.H**)]$^{3+}$ has a higher 3+ charge

state than $[Ru(phen)_3]^{2+}$. Changing the chiral anion in addition to manipulating the eluent concentration is also possible.

Despite these insights, it had been found concurrently that enantiomers of $[Ru(phen)_2(\mathbf{5.9.H})]^{3+}$ could be isolated by synthesis from a resolved precursor and fractional crystallisation with a chiral anion. For this reason, chromatographic resolution was not pursued further. It was, however, successfully demonstrated that the set-up and methodology used here are operable and warrants further attention.

5.7.1.2. Synthesis from a resolved precursor

It is possible to obtain enantiomers of a ruthenium-polypyridine complex by synthesis using a previously resolved precursor. For $[Ru(phen)_2(L)]^{n+}$ type complexes this can be achieved using resolved Δ or Λ $[Ru(phen)_2(py)_2]^{2+}$. This approach was executed successfully for the synthesis of Δ-(—)-$[Ru(phen)_2(\mathbf{5.9.H})][PF_6]_3$ using Δ-$[Ru(phen)_2(py)_2]$[As-(—)-Otart]$_2$ which was obtained via a literature procedure. [269] [270]

The racemic precursor complex $[Ru(phen)_2(py)_2]Cl_2$ was prepared by refluxing $Ru(phen)_2Cl_2$ in aqueous pyridine (pyridine/water, 1:2) for three hours.[269] The reaction mixture is cooled, filtered, washed with water and dried in vacuo. Crystallisation of the crude solid from an MeOH solution by addition of Et_2O provides pure $[Ru(phen)_2(py)_2]Cl_2$ as a burnt-orange microcrystalline powder in 97% yield. Complex $[Ru(phen)_2(py)_2]Cl_2$ is resolved into its Δ and Λ optical isomers by precipitation with sodium arsenyl-L-(—)-tartrate (As-(—)-Otart) and sodium arsenyl-D-(+)-tartrate respectively (As-(+)-Otart) (Scheme 5.21).

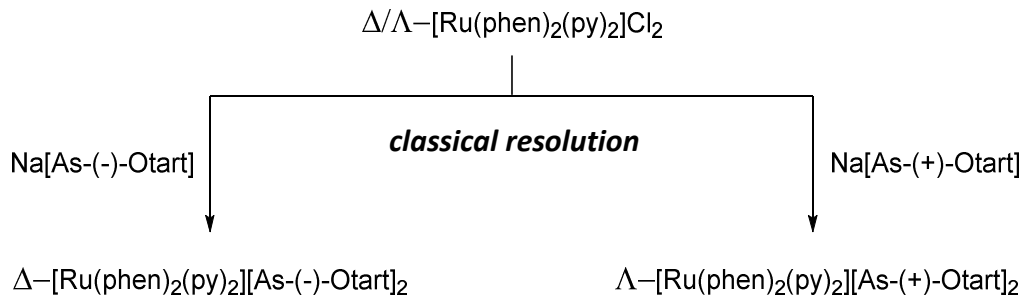

Scheme 5.21: *Enantiomeric resolution of Δ/Λ-$[Ru(phen)_2(py)_2]^{2+}$ by crystallisation with arsenyl-tartrate.*

An aqueous solution of sodium arsenyl-tartrate (0.80 M, 2.5 equivalents) is warmed to 60 °C and added to an aqueous solution of racemic $[Ru(phen)_2(py)_2]Cl_2$, also at 60 °C. Crystals of the diastereoisomer form upon cooling slowly to room temperature. The mixture is refrigerated at 4 °C for 24 hours before filtering and washing with water and acetone. This was only performed for Δ-$[Ru(phen)_2(py)_2][As\text{-}(—)\text{-}Otart]_2$ which was obtained in a 48.5% yield. Its optical rotation was recorded in a 0.0003 g/mL solution in MeCN at 20 °C giving a $[\alpha]_D$ of – 174° which agrees with the reported value.[271] The opposite, Λ-$[Ru(phen)_2(py)_2]^{2+}$ enantiomer can be isolated from the filtrate by further manipulations,[269] although, this was not performed. Light was excluded from all preparations and analysis with Δ-$[Ru(phen)_2(py)_2][As\text{-}(—)\text{-}Otart]_2$ to minimise the risk of photo-racemisation.

Synthesis of Δ-(—)-$[Ru(phen)_2($**5.9.H**$)][PF_6]_3$ from Δ-$[Ru(phen)_2(py)_2][As\text{-}(—)\text{-}Otart]_2$ was undertaken by adapting a literature procedure.[256] Ligand **5.9.HCl** and Δ-$[Ru(phen)_2(py)_2][As\text{-}(—)\text{-}Otart]_2$ were combined under an inert atmosphere and dissolved in an ethylene-glycol/water (9:1) mixture. This was heated at 110 °C and, after 6 hours the reaction was stopped and the reaction mixture run through a column of Sephadex C-25 cation-exchange resin eluting with a 0 – 0.4 mol/L NaCl solution gradient. The desired product was collected and isolated as the PF_6 salt in a 20% yield. A moderated proportion of the 5-amino-1,10-phenanthroline complex $[Ru(phen)_2($5-amino-phen$)][PF_6]_2$ was also isolated (19% yield) indicating that the amide bond is

cleaved under these conditions. A similar outcome was noted previously for the attempted synthesis of [Ru(phen)$_2$(**5.5.H**)][PF$_6$]$_3$ in ethylene-glycol with microwave irradiation. Employing the less energetic conditions of refluxing EtOH/water (4:1) failed to provide any product. Evidently, substitution of the pyridine ligands of [Ru(phen)$_2$(py)$_2$]$^{2+}$ requires more heat input than with neutral Ru(phen)$_2$Cl$_2$. Unfortunately, such conditions contribute to decomposition of the acetamide linking unit of the NHC proligand.

Isolation of enantiomeric Δ-(—)-[Ru(phen)$_2$(**5.9.H**)][PF$_6$]$_3$ was confirmed by polarimetry, having a $[\alpha]_D$ value of – 678^o for a 0.004 g/mL solution in MeCN at 20 ^{o}C. With an analytical sample of Δ-(—)-[Ru(phen)$_2$(**5.9.H**)][PF$_6$]$_3$ in hand, resolution of Δ/Λ-[Ru(phen)$_2$(**5.9.H**)]$^{3+}$ by direct crystallisation with sodium arsenyl-L-(—)-tartrate was sought as a more efficient, high yielding method.

5.7.1.3. Crystallisation with a chiral anion; classical resolution

Enantiomeric resolution of Δ-[Ru(phen)$_2$(**5.9.H**)]$^{3+}$ and Λ-[Ru(phen)$_2$(**5.9.H**)]$^{3+}$ was performed analogously to the above isolation of Δ-[Ru(phen)$_2$(py)$_2$][As-(—)-Otart]$_2$. Racemic Δ/Λ-[Ru(phen)$_2$(**5.9.H**)]Cl$_3$ was dissolved in a minimum of warm water and a solution of sodium arsenyl-L-(—)-tartrate in warm water (3.6 equivalents, 0.13 mol/L) was added resulting in immediate precipitate formation. The solution was heated at 80 ^{o}C and water added dropwise until all material had dissolved, it was then allowed to crystallise slowly before refrigerating for 24 hours. The resultant bright orange microcrystalline powder was collected by filtration and washed with cold water then acetone before drying in vacuo to give Δ-[Ru(phen)$_2$(**5.9.H**)][As-(—)-Otart]$_3$ in a 43% yield. Material in the aqueous filtrate was recovered by precipitation of the PF$_6$ salt and extraction into DCM. This is enriched with Λ-[Ru(phen)$_2$(**5.9.H**)]$^{3+}$ and following conversion back into the chloride salt, could be subjected to the above procedure with sodium arsenyl-D-(+)-tartrate to recover the opposite enantiomer, Λ-[Ru(phen)$_2$(**5.9.H**)][As-(+)-Otart]$_3$. This was not performed due to time limitations.

A portion of Δ-[Ru(phen)$_2$(**5.9.H**)][As-(—)-Otart]$_3$ was dissolved in hot water and precipitated as the PF$_6$ salt. The mixture was extracted with DCM and the organic

extracts dried over $MgSO_4$ before removal of the solvent. This provided Δ-[Ru(phen)$_2$(**5.9.H**)][PF_6]$_3$ for analysis by polarimetry. In this case it is necessary to remove the chiral anion to ensure that any observed optical rotation is attributable to enantiomeric enrichment of the chiral complex itself without interference from the anion. The product was found to have an $[\alpha]_D$ value of – 526^o for a 0.005 g/mL solution in MeCN at 20 ^{o}C which is lower than the – 678^o recorded for Δ-[Ru(phen)$_2$(**5.9.H**)][PF_6]$_3$ obtained in the previous section. This suggests that obtaining Δ-[Ru(phen)$_2$(**5.9.H**)][PF_6]$_3$ from a well resolved precursor yields a superior enantiomeric excess than direct crystallisation with sodium arsenyl-L-(—)-tartrate as performed here. The latter approach demonstrates that an enriched sample of the metallo-NHC proligand can be obtained expediently and in high yield. Better enrichment might be achieved following further method development.

5.8. Summarising remarks

The synthesis and isolation of a novel, appended metallo-NHC proligand [Ru(bipy)$_2$(**5.2.H**)][PF_6]$_3$ has been outlined, however, this approach was encumbered by challenges in obtaining the necessary 1,0-phenanthroline halides and subsequent reactions of the 3-imidazole-1,10-phenanthroline derivatives. Comparatively, acetamide linked species [Ru(phen)$_2$(**5.5.H** – **5.10.H**)][PF_6]$_3$ and [Ru(phen)$_2$(**5.12.H**)][PF_6]$_3$ were prepared expediently from the readily accessible amine precursor 5-amino-1,10-phenanthroline and 4-amino-2,2'-bipyridine, respectively. Ultimately, only the acetamide-linked class of metallo-NHC proligands were carried forward into catalysis trials. Irrespective of this, the 3-imidazolyl-1,10-phenanthroline system retains interest due to the close proximity of the NHC to the enantiomeric ruthenium-polypyridine complex. Being monodentate NHC ligands may also be advantageous to catalysis. This is in light of the poor performance of acetamide linked [Ru(phen)$_2$(5-PA)]$^{2+}$ type NHC ligands in palladium mediated Suzuki coupling which is attributed to their chelating ability (see Chapter 6).

Several remarkable hetero-dinuclear NHC complexes were prepared from these metallo-NHC proligands and subject to a detailed structural evaluation. Complex $[Ru(phen)_2(Pd\{\mathbf{5.9}\}\{allyl\}Cl)][PF_6]_2$ represents a unique example of a Pd(allyl) system with an anionic-chelating ligand and provides an excellent demonstration of how spontaneous *N*-amidate/NHC chelation occurs for these acetamide linked metallo-NHC ligands under mild conditions. Similarly, complex $[Ru(phen)_2(Pd\{\mathbf{5.10 - H}\}Cl)][PF_6]_2$ also exhibits a previously un-reported coordination motif, having a Pd(II) centre bound within a tridentate *N*-amidate – NHC – Py chelate. Unusual conformational diastereomers of $[Ru(phen)_2(Pd\{\mathbf{5.10 - H}\}Cl)][PF_6]_2$ arise through steric interplay of the enantiomeric $Ru(phen)_3$ component with the atropisomeric Pd(**5.10 - H**)Cl fragment. These are identified as existing in a 2:1 ratio in solution and are not thought to be interchangeable. Synthesis of a 4-acetamido-2,2'-bipyridine based system was undertaken to prove that this isomeric relationship could be manipulated by increasing the steric interaction between the complex groups. In practice, both the chelated and pendant forms, $[Ru(phen)_2(Pd\{\mathbf{5.12 - H}\}Cl)][PF_6]_2$ and $[Ru(phen)_2(Pd\{\mathbf{5.12}\}Cl_2)][PF_6]_2$, were obtained. Chelation could be promoted by treating the pendant form with base and gives $[Ru(phen)_2(Pd\{\mathbf{5.12 - H}\}Cl)][PF_6]_2$ as a single diastereomer. The reversibility of *N*-amidate binding in the 4-BipA systems is thought to allow isolation of the thermodynamically favoured diastereomeric conformation which is desirable for application in asymmetric catalysis. That one diastereomer is favoured in both $[Ru(phen)_2(Pd\{\mathbf{5.10 - H}\}Cl)][PF_6]_2$ and $[Ru(phen)_2(Pd\{\mathbf{5.12 - H}\}Cl)][PF_6]_2$ represents the accomplishment of this chapter's underpinning objective; to prepare a metallo-NHC ligand in which an enantiomeric ruthenium-polypyridine moiety has stereochemical influence over a catalytic centre.

Effective protocols for the enantiomeric resolution of the metallo-NHC proligand $[Ru(phen)_2(\mathbf{5.9.H})][PF_6]_3$ were established leading to isolation of Δ-(—)-$[Ru(phen)_2(\mathbf{5.9.H})][PF_6]_3$. This was achieved either by synthesis from the resolved precursor Δ-$[Ru(phen)_2(py)_2][As\text{-}(—)\text{-}Otart]_2$ or by selective crystallisation of racemic $[Ru(phen)_2(\mathbf{5.9.H})][PF_6]_3$ with a chiral anion, arsenyl-(—)-tartrate. Methods were also emplaced for resolution by chiral chromatography, although, this could not be achieved in the required timeframe. Chromatographic resolution seems accomplishable through further application of the methods established herein.

Overall, this chapter outlines the synthesis of metallo-NHC ligands bearing an enantiomerically resolved ruthenium-polypyridine unit. That these are capable of coordinating to a catalytically active centre is supported by the synthesis of several plausible Pd(II) precatalysts.

5.9. Scope and future work

In light of the diastereoselective synthesis of $[Ru(phen)_2(Pd\{\mathbf{5.12 - H}\}Cl)][PF_6]_2$, the 4-BipA derived NHC ligands show tremendous promise going forward in the context of asymmetric catalysis. It would be extremely interesting to prepare other BipyA derivatives such as an analogue of the Pd(allyl) complex $[Ru(phen)_2(Pd\{\mathbf{5.9}\}\{allyl\}Cl)][PF_6]_2$.

With regard to the isolation of enantiomerically resolved metallo-NHC proligands, it was demonstrated that synthesis of Δ-$[Ru(phen)_2(\mathbf{5.9.H})][PF_6]_3$ from the resolved precursor Δ-$[Ru(phen)_2(py)_2][As\text{-}(—)\text{-}Otart]_2$ was achievable yet low yielding due to the instability of the acetamide-linked ligand $[\mathbf{5.9.H}]^+$ under the required conditions. A more effective approach would be to use this synthesis to prepare resolved enantiomers of a 5-amino-1,10-phenanthroline precursor complex, Δ-$[Ru(phen)_2(5\text{-amino-phen})]^{2+}$ or Λ-$[Ru(phen)_2(5\text{-amino-phen})]^{2+}$ (Scheme 5.22). These could then be used to synthesise resolved metallo-NHC proligands including Δ-$[Ru(phen)_2(\mathbf{5.9.H})][PF_6]_3$ and Λ-$[Ru(phen)_2(\mathbf{5.9.H})][PF_6]_3$, similarly to the preparation of the free ligand **5.9.HCl**. Chloroacetylation of $[Ru(phen)_2(5\text{-amino-phen})][PF_6]_2$ to give $[Ru(phen)_2(\mathbf{5.4})][PF_6]_2$ has been reported previously.[272] This could no doubt be adapted for 4-amino-2,2-bipyridine also.

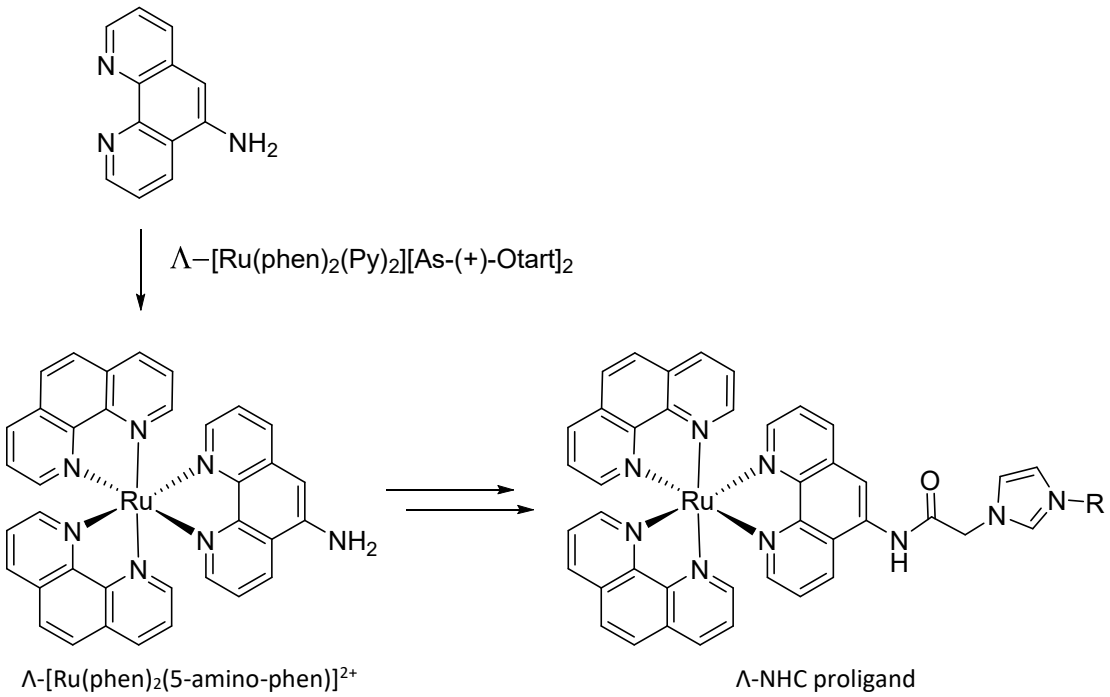

Scheme 5.22: *Route to enantiomerically resolved metallo-NHC proligands prepared from resolved [Ru(phen)$_2$(5-amino-phen)]$^{2+}$ by established methods.*

Being heteroleptic bridging ligands, these species are potential supramolecular synthons and ripe for diversification of the metal centre at either the polypyridine terminus, NHC terminus or both. Focussing on the metallo-NHC ligands [Ru(phen)$_2$(**5.5** – **5.10**)][PF$_6$]$_3$ already developed, these could be applied to use in different catalytic systems with metals such as with Ni(II), Pt(II) or Ru(II). Additionally, NHCs have been employed to affix functional groups to metallic surfaces including gold nano-particles.[273] These ligands could therefore provide a means of tethering a photoactive ruthenium-polypyridine moiety to a metallic substrate for photochemical applications.

Chapter 6

performance in palladium mediated Suzuki coupling

6.1. Introduction

Several of the NHC proligands and complexes prepared in the preceding chapters were trialled in the asymmetric synthesis of axially chiral biaryl compounds by Suzuki cross-coupling. Rotationally hindered biaryls such as BINOL and BINAP possess a chiral axis along the biaryl-bond, enantiomers resulting from this are known as atropisomers (see section 1.1). Enantiomeric biaryl motifs are important structural components in numerous natural products, several of which have demonstrable therapeutic properties including those shown in Figure 6.1.[274] As such, the targeted synthesis of atropisomeric natural products and therapeutics by asymmetric coupling reactions is an appealing prospect.

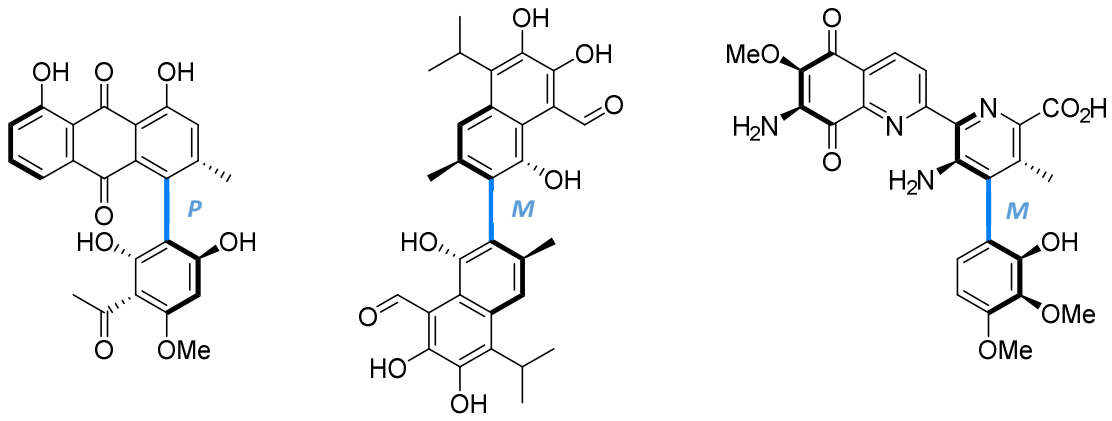

(+)-knipholone (-)-gossypol streptonigrin

Figure 6.1: *Natural product therapeutics with enantiomerically defined biaryl units.*

Atroposelective Suzuki couplings were first reported in 2000, nearly simultaneously, by Buchwald *et al.*[275] and Cammidge *et al.*[276] Both demonstrated the synthesis of enantiomeric *bis*-2,2'-naphthalene derivatives using existing chiral ligands. Since then, the application of asymmetric Suzuki couplings have graduated to more complex systems, although, enantioselective couplings with chiral ligands remain fairly uncommon.[92] A successful example, shown in Scheme 6.1, demonstrates the enantioselective synthesis of a cumyl-amide substituted biaryl compound.[277] Removal

of the cumyl protecting group provides a primary amide precursor to natural product alkaloid analogues.

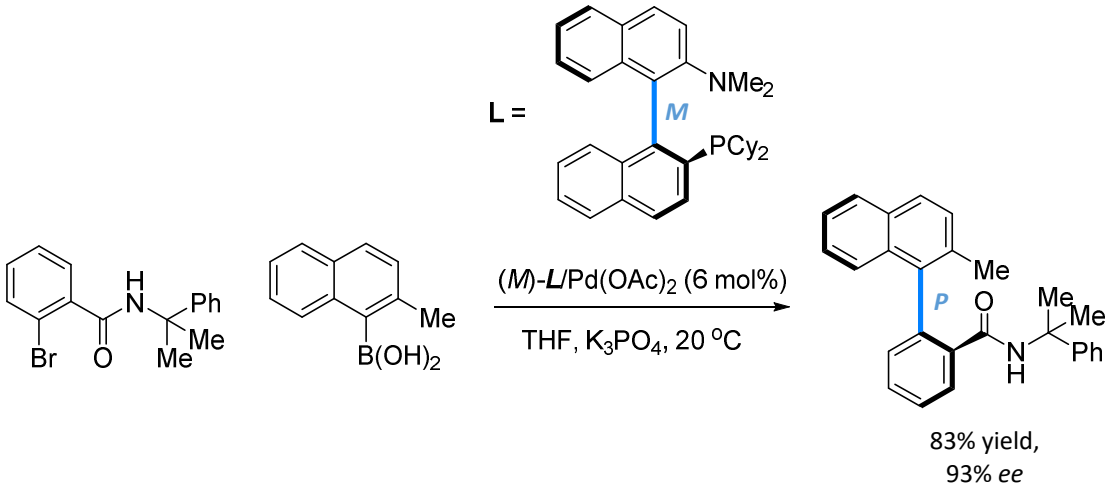

Scheme 6.1: *Enantioselective Suzuki coupling to give a useful atropisomeric subcomponent.*

Physical separation of atropisomers is accomplishable if racemisation is slow at a given temperature, that is, the free energy barrier to rotation is sufficiently high. The configurational stability of an axially chiral biaryl compound is determined by the steric demand of substituents in proximity to the axis. Rotation may also be prevented by bridging units. Interconversion of atropisomeric enantiomers is often thermally driven, however, may be chemically or photochemically induced depending on the compound.

Thermal stability in non-bridged biaryls is governed by the number and size of ortho-substituents. Typically, the rotational energy barrier in di-*ortho*-substituted biaryls with methyl-groups and larger are stable to resolution.[274] Moderately hindered tetra-*ortho*-substituted biaryl compounds are practically inert to thermally induced rotation, however, di-*ortho*-substituted aryl substrates are much more challenging coupling partners. The simple di-*ortho*-substituted biaryl 1-*o*-tolyl-naphthalene and 1,1'-binaphtalene was targeted in this study as they are rotationally stable enough to allow measurement of enantiomeric enrichment by chiral HPLC while being synthetically achievable. Once catalysis had been demonstrated using these substrates, graduation

to more hindered systems was intended to ensure reliable measurement of enantiomeric excess.

Performing these catalysis trials proved to be extremely time consuming in addition to the time spent establishing a working methodology. Time limitations restricted the breadth of NHC ligands trialled and prevented the screening of more substrates and reaction conditions. Likewise, evaluating catalysis of 1,1'-binaphtalene formation was abandoned for this reason. Most unfortunate of all, progress was halted before enantiomeric resolution of product mixtures could be performed by chiral HPLC and therefore, enantiomeric excesses are not calculated. However, several new chiral NHC ligands were proven to be operable in catalysis of Suzuki couplings. Preliminary insight into the effect of *N*-amido substituents on catalysis was also obtained. Most importantly however, the emplacement of methodologies and instrumentation with which to experimentally evaluate asymmetric catalysis will allow future investigators to continue this work.

6.2. Control system

Wholescale screening of homogenous catalysts is not regularly attempted in the University of Canterbury chemistry department and hence there is no existing precedent for this. As such, methodologies were developed to replicate literature analyses as best possible. To ensure the efficacy of this, a published NHC catalyst based on the PEPPSI system (see section 1.3.3) was used as a control. The PEPPSI precatalyst **6.1** was prepared following a literature procedure in which the imidazolium salt is heated with $PdCl_2$ and K_2CO_3 in neat pyridine (Scheme 6.2).[87]

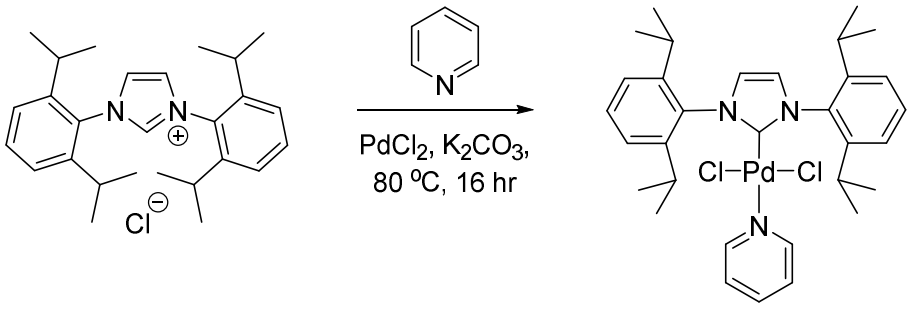

IPr.HCl

6.1, 88 %

Scheme 6.2: *Synthesis of PEPPSI precatalyst* ***6.1****.*

Pyridine was used instead of 3-chloropyridine, as reported, due to availability. Employing a pyridine ligated precatalyst was not expected to greatly impact the overall yield of the Suzuki coupling because the slightly more electron deficient 3-chloropyridine ligand is typically used to improve precatalyst initiation rates.[278] The NHC proligand used for this was 1,3-bis(2,6-diisopropylphenyl)imidazolium chloride (IPr.HCl), which was prepared by an established method.[279]

Precatalyst **6.1** was applied to the synthesis of 1-*o*-tolyl-naphthalene and 1,1'-binaphtalene to provide sample for the standardisation and calibration of the GC-FID used in the analysis of reaction mixtures (see section 6.3.2). This was performed as reported for PEPPSI type catalysts.[87] A sample of 1-*o*-tolyl-naphthalene was obtained by stirring **6.1** and *t*-BuOK in isopropanol for 20 minutes before adding naphthalene-1-boronic acid and *o*-bromo-toluene. These initial syntheses were monitored by TLC. After 1.5 hours it appeared that all *o*-bromo-toluene had been consumed, however, it was later found that it was not well visualised on the TLC plate. Pure 1-*o*-tolyl-naphthalene was obtained by flash chromatography (silica, pentane) in a modest yield of 50% due to the incomplete reaction.

The synthesis of 1,1'-binaphthalene was also attempted under the above conditions using naphthalene-1-boronic acid and 1-bromo-naphthalene, however, this was found to proceed slowly. Instead K_2CO_3 was used as the base and the reaction heated at 60 °C. After 4 hours the reaction was complete, however, it was left to continue for 24 hours.

Flash chromatography (silica, pet ether) provided 1,1'-binaphtalene in an isolated yield of 83%. In addition to providing analyte samples of 1-*o*-tolyl-naphthalene and 1,1'-binaphtalene, these reactions served as preliminary trials of reaction conditions and proved **6.1** to be a relevant model catalyst.

6.3. Methodology and experimental set-up

6.3.1. Conditions and instrumentation

Each catalysis trial reaction was performed in a microscale conical reaction vial sealed with screw cap and septum. Custom made aluminium blocks were used to house up to eight reaction vials at a time. Placing the block on a heater/stirrer allowed stirring of the reaction mixtures and heating when necessary. Blocks were pre-heated to the desired temperature before studying reactions at elevated temperature. Reactions were performed under an argon atmosphere administered through a Schlenk line. Gas hosing was split into multiple lines ending with syringe needles to provide gas-flow through the septum of each vial. Undecane was used as an internal standard for the GC-FID analysis. Stock solutions of precatalysts were prepared prior to the reaction and were used within 2 days of preparation. Pre-formed precatalyst solutions were prepared in the reaction solvent such that 1.0 mL delivered the desired mol%. When using unformed precatalysts, the NHC proligand and palladium source were introduced as a combined solution in MeCN and 0.30 mL of solution provided the desired mol%. Using MeCN was necessary to ensure solubilisation of all components, particularly when using the metallo-NHC proligands. A smaller volume was used to minimise the influence of the MeCN solvent.

All trials were duplicated and typically performed as follows; the boronic acid (1.2 equiv.) and base (equivalents depend on base and catalyst) were weighed into a microscale conical reaction vial equipped with a spin vane. Solvent was added (2.0 mL for preformed precatalysts or 2.7 mL for unformed precatalysts) followed by undecane (0.10 mL). The vial was loosely capped and placed in a stirring block without heating.

Argon was bubbled through the sample for 15 minutes before the aryl-halide was added (1 equiv.) followed by the precatalyst solution (1.0 mL or 0.30 mL). The vial cap was tightened and the argon needle raised from solution but left in the septum. Gas flow was switched to a static pressure to maintain an inert atmosphere. If heating was required, the vial was transferred to a heated block. The total solvent and internal standard volume was 3.1 mL. These conditions were adapted from published procedures.[37, 87, 122]

Most aspects of sample analysis are not well described in the literature and had to be developed from scratch. Sampling for analysis was performed by removing 0.1 mL aliquots of reaction mixture by syringe and injecting onto a short silica plug. This was rinsed through into an autosampler vial with 1 mL of HPLC grade Et_2O and sealed for later analysis. Silica plugs for this purpose were prepared by plugging a Pasteur pipette with a small amount of glass wool and adding silica to a height of ~ 1.5 cm. This step is important for removal of insoluble material and boronic acid prior to GC-FID analysis as these can damage the auto-injector needle and/or contaminate the column.

Sampling was initially performed hourly to provide an accurate reaction profile for calculation of TON and TOF, however, this proved to be incredibly laborious. Focus eventually shifted to simply assessing the product yield as a measure of system performance as these were, after all, preliminary and explorative trials. For this purpose, it was sufficient to sample at zero minutes (immediately after catalyst added), 3 hours, 24 hours, 48 hours and so forth if necessary. This also allowed greater trial throughput. The zero-minute sample was useful for error checking, ensuring the GC-FID trace was as expected with an internal standard present *etcetera*.

6.3.2. Analysis by GC-FID

Aliquots were subjected to GC-FID analysis to determine the amount of aryl-halide converted and the product yield. GC-FID (Gas Chromatography with a Flame Fonisation Detector) provides a trace output with intensity peaks produced at various intervals as

compounds are eluted. Gradually raising the column temperature drives the analyte into the helium carrier gas (mobile phase) causing them to elute. The time at which they are detected is the compounds retention time and this is used to differentiate the species in the mixture. It is important that analyte signals are well resolved, that is, their retention times are very different. Retention times are best tuned by adjusting the rate at which the column temperature increases and can include pauses where the temperature is fixed for an interval. At the end of each GC-FID run the column temperature was held at 300 ^{o}C for 5 minutes to ensure all sample was eluted before the next run. The column standby temperature was set at 150 ^{o}C to avoid adsorption of water.

Individual stock solutions of the key analytes *o*-bromo-toluene, 1-bromo-naphthalene and 1-*o*-tolyl-naphthalene and the internal standard undecane were used to identify the retention times of these compounds. A solution containing all four components was then used to obtain a heating profile which provided good compound resolution. This method was used for all analyses and provided average retention times, in minutes, of 8.11, 9.36, 13.86 and 16.17 for undecane, *o*-bromo-toluene, 1-bromo-naphthalene and 1-*o*-tolyl-naphthalene, respectively. Analyses that did not adequately conform to these retention times were repeated to minimise signal drift as this can indicate a source of instrumental error.

The molar quantity of eluted compound is proportional to the area of the signal peak and is measured by integration. As signal areas differ between compounds at a given concentration, a calibration curve must be obtained for each analyte. This was performed by measuring the signal area of the compound at various concentrations over a range that encompasses the experimental concentration of the analyte in a sample. For experimental samples, the compound concentration is calculated by relating the peak integral to the calibration curve equation. In addition to the initial calibration, GC-FID traces of a stock mixture containing a known concentration of undecane, *o*-bromo-toluene, 1-bromo-naphthalene and 1-*o*-tolyl-naphthalene was regularly collected as an external standard. This was at the beginning and end of each batch of samples and at regular intervals during larger batches. In some cases, integrals had to be adjusted

against this external standard. At the conclusion of a batch of samples, an aliquot of MeOH was run to purge the column before standby.

Yields and conversion were calculated as follows; integrals of relevant signals in the GC-FID trace were measured and tabulated. These were normalised against the undecane internal standard signal. The calibration equation obtained as above was used to calculate the number of moles of analyte compound present in the aliquot solution. Based on the volume of the original aliquot removed (0.10 mL), its concentration in the reaction mixture was determined and from that, yield and conversion. Although solution volumes were kept as regular as possible, the undecane internal standard ensured that fluctuations were corrected for. It was only critical to strictly maintain the original reaction mixture volume.

6.4. Results of catalysis trials

For the following discussion the catalyst systems trialled are subdivided into separate categories. One being “preformed NHC-Pd precatalyst systems” which are NHC-Pd complexes that have been synthesised an characterised previously. The other is “NHC proligand systems” which is where the imidazolium salt NHC proligand and Pd(II) source are introduced to form an active NHC-Pd complex in situ. Compounds analysed in this section have been renamed as shown in Figure 6.2 and Figure 6.3. This is for the benefit of clarity in this discussion, and to simplify the results tables.

6.4.1. Preformed NHC-Pd precatalyst systems

Preformed precatalyst systems were trialled first as these possess NHC-Pd moieties known for their activity in Suzuki couplings including Pd(NHC)(*O,O’*-acac) and Pd(NHC)(allyl)Cl. The systems studied here are shown in Figure 6.2 and include the control precatalyst **6A**. Having been fully characterised, their structural features are well-defined enabling clearer assessment of any structure-function relationships.

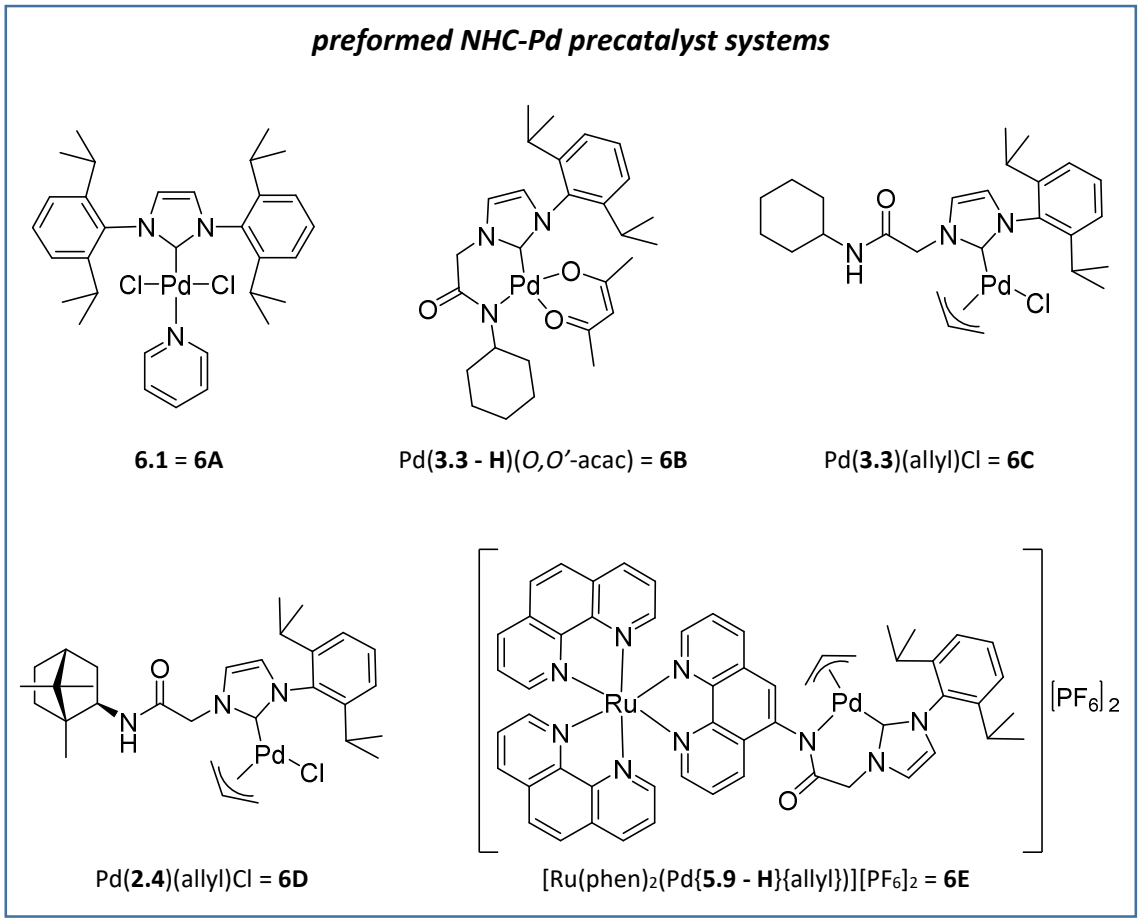

Figure 6.2: *Preformed NHC-Pd precatalyst systems trialled. Relabelling also shown.*

A preliminary set of reactions were performed using the literature standard **6A** and the organic, achiral *N*-amidate/NHC complex **6B** as per the methodology given in section 6.3.1. Table 6.1 provides the conversion and yield percentages for this series of reactions. Again in the interest of time, only a limited survey of solvents and bases could be performed based closely on what is known to work for related systems. It was found that the conditions reported for the use of the literature precatalyst **6A** (entry 5, Table 6.1) also suited **6B** (entry 6, Table 6.1). It was heartening to find that the control compound **6A** performed as well as reported with regard to yield (83%),[87] albeit over a longer time period. This is unsurprising given that pyridine ligated PEPPSI catalysts are known to initiate more slowly than their 3-chloro-pyridine counterparts. The results for **6A** confirm that the procedures and analysis used provide an accurate measure of yield.

Table 6.1: *Condition sets trialled with precatalyst systems* ***6A*** *and* ***6B*** *for the synthesis of 1-o-tolyl-naphthalene.*

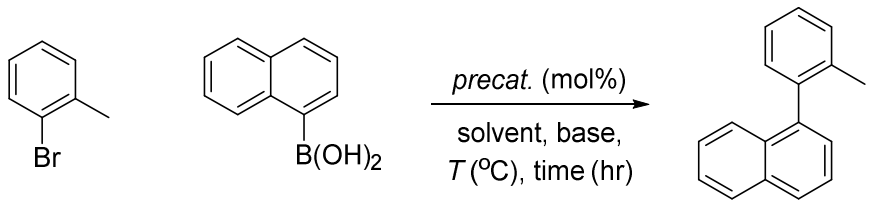

entry	cat	Loading [mol%]	base (equiv)	solvent	*T* [°C]	time [hr]	Conv [%]	yield [%]
1	**6A**	1	*t*-BuOK (1.3)	iPrOH	20	24	90	65
2	**6B**	2	*t*-BuOK (1.3)	iPrOH	60	5	69	55
3	**6B**	2	K_2CO_3 (3)	iPrOH	60	24	49	18
4	**6B**	2	*t*-BuOK (1.3)	1,4-diox	60	24	36	26

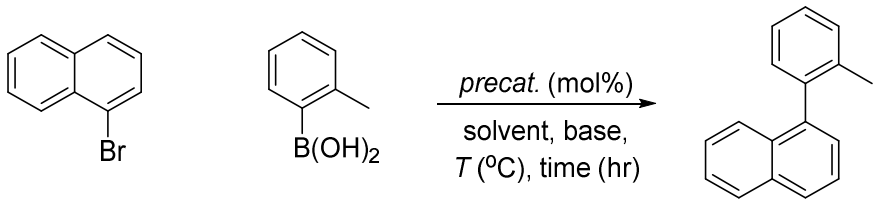

entry	cat	Loading [mol%]	base (equiv)	solvent	*T* [°C]	time [hr]	Conv [%]	yield [%]
5	**6A**	1	*t*-BuOK (1.3)	iPrOH	20	2	100	83
6	**6B**	2	*t*-BuOK (1.3)	iPrOH	60	4	100	79
7	**6B**	2	K_2CO_3 (3)	iPrOH	60	24	78	42
8	**6B**	2	*t*-BuOK (1.3)	1,4-diox	60	24	28	0

Precatalyst **6B** performed comparably to **6A** producing a yield of 79%, although, this required 24 hours and it was necessary to heat reactions with **6B** at 60 °C. Presumably heating is required for **6B** because its initiation is slowed by the more stable acac "throw-away" ligand. This has been noted in other Pd(NHC)(acac) precatalyst systems and is a common trade-off for greater precatalyst stability.[38, 162] Better yields for both **6A** and **6B** were obtained in isopropanol, when using 1-bromo-naphthalene as the aryl-halide with *o*-tolyl-boronic acid as opposed to the other way around. Using 1,4-dioxane and *t*-BuOK with **6B** resulted in a dark-grey/brown slurry forming after 2 hours and analysis revealed that the reaction stopped with incomplete conversion due to apparent deactivation of the catalyst. Using K_2CO_3 as base with 1,4-dioxane resulted in immediate deposition of dark-grey material and no reaction progress was observed (not shown).

Satisfied that the experimental set-up, analysis and condition sets were performing as desired, the trial was expanded to include the Pd(NHC)(allyl) systems **6C**, **6D** and the metallo-NHC precatalyst **6E** the results of which are summarised in Table 6.2.

Table 6.2: *Condition sets trialled with precatalyst systems **6C**, **6D** and **6E** for the synthesis of 1-*o*-tolyl-naphthalene.*

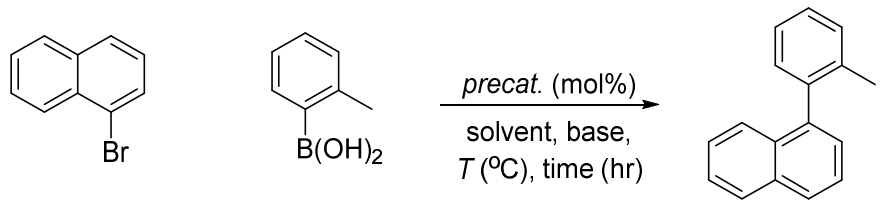

entry	cat	Loading [mol%]	base (equiv)	solvent	*T* [°C]	time [hr]	Conv [%]	yield [%]
1	**6C**	2	*t*-BuOK (1.3)	iPrOH	20	24	78	61
2	**6D**	2	*t*-BuOK (1.3)	iPrOH	20	24	80	60
3	**6D**	2	*t*-BuOK (1.3)	iPrOH	60	3	99	67
4	**6E**	2	*t*-BuOK (1.3)	iPrOH	20	24	15	0
5	**6E**	2	*t*-BuOK (1.3)	iPrOH	60	24	24	0

The organic NHC derivatives **6C** and **6D** performed moderately well producing yields of ~ 60 % after 24 hours at room temperature. This was accelerated for **6D** to give the same result after 3 hours by heating at 60 °C. After 24 hours, the product yield was unchanged suggesting that catalysis had terminated, the 99% conversion suggest that the 1-bromo-naphthalene was consumed in other side reactions. Additional signals in the GC-FID trace does support this although no characterisation of these was performed. Addition of precatalysts **6C** and **6D** to the colourless reaction mixture solutions resulted in a rapid change to pink before fading back to colourless. A white suspension formed shortly thereafter. A similar white suspension was observed for reactions with **6A** and **6B** under analogous conditions and proved to be a useful visual indicator of a healthy reaction. The metallo-NHC precatalyst **6E** produced no product at room temperature or with heating at 60 °C. After 24 hours at room temperature, the reaction mixture remained a bright orange, homogenous solution. Performing the reaction at 60 °C resulted in immediate darkening of the solution upon heating and deposition of a dark brown solid after 24 hours. Heating is probably necessary for initiation of **6E**, as was the case also

with **6B**, because of the stabilising *N*-amidate/NHC chelate which is not initially present in **6C** and **6D**. However, it appears under these conditions heating facilitated decomposition of the catalyst species. Unfortunately, there was not enough **6E** available for further trials. It is possible a mild base such as K_2CO_3 would be more successful as *t*-BuOK is highly reactive and may contribute to catalyst breakdown. Also, **6E** was on the cusp of solubility in isopropanol, solvents such as MeCN and DMF might be better suited for use with **6E** as was the case with **6H** in the next section. Reasons for the inactivity of **6E** are discussed further in section 6.4.3.

Further tuning of conditions to improve the yield of **6C** and **6D** was not performed as the current conditions produced an analysable amount of product. Product mixtures from reactions with the chiral precatalyst **6D** were rotary evaporated to give a crude solid material. These were set aside for chiral HPLC analysis to determine their enantiomeric excess which, in the end, could not be performed.

6.4.2. NHC proligand systems

Attention turned to establishing an operational system using NHC proligands with a Pd(II) source. Those trialled are shown in Figure 6.3, all of which are diisopropyl-phenyl appended species. These were chosen to examine first as NHCs with a diisopropyl-phenyl pendant group are generally reliable for catalytic applications.[280] Employing NHC proligands was aimed, in particular, at finding a condition set in which the metallo-NHC complexes might function as it is easier to use the proligand than to synthesise the metallo-NHC-Pd precatalysts. It was hoped at least some product could be obtained using a metallo-NHC system in order to measure their enantiomeric excess and gauge the influence of the chiral metal complex moiety on asymmetric induction.

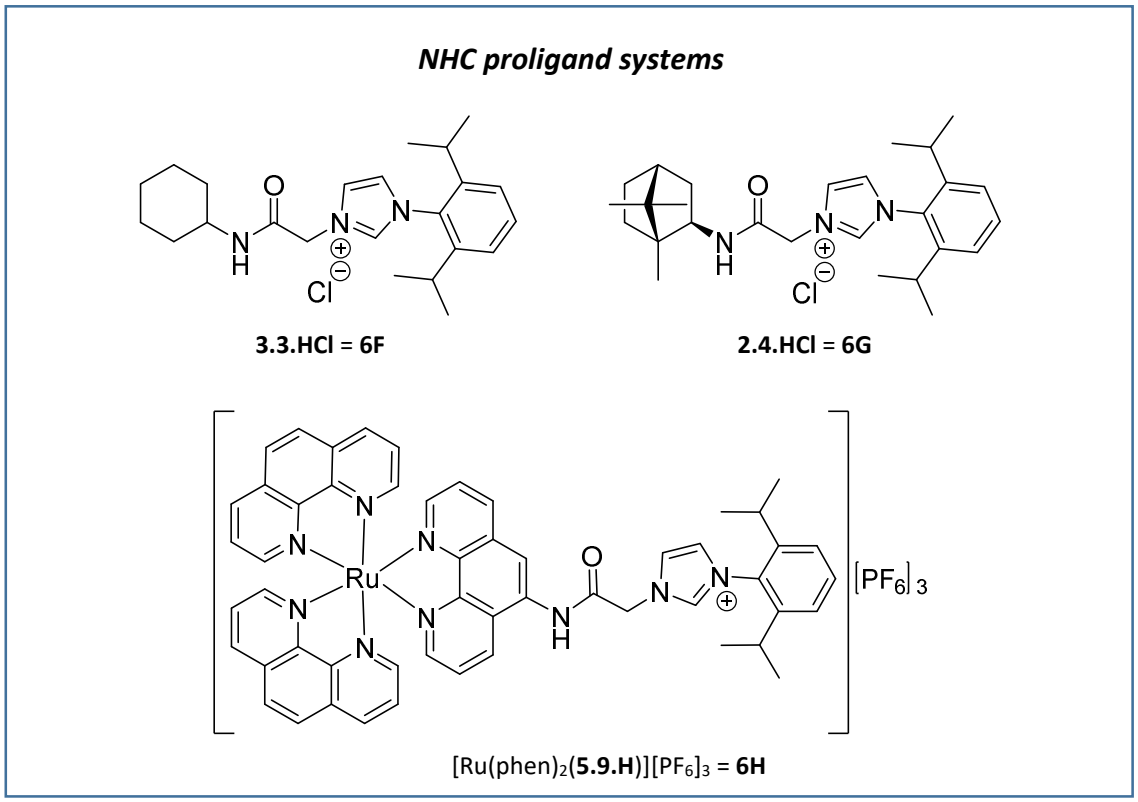

Figure 6.3: *NHC proligands used with $PdCl_2$ in catalysis trials. Relabelling also shown.*

Reactions were performed following the methodology given in section 6.3.1, however, *t*-BuOK was avoided as the base. Instead milder bases such as K_2CO_3 and NaOH were favoured as was the case in the published example of Suzuki couplings performed with addition of an *N*-amide/NHC proligand (see section 1.4.1).[122] These bases are also better suited to in situ precatalyst formation without degradation of the NHC ligand. Trials were performed using NHC proligands **6F**, **6G** and **6H** with $PdCl_2$ under various conditions**.** Some successful condition sets are summarised in Table 6.3. Solvents including toluene and MeCN were also surveyed without success as was the use of NaOH as a base. These less informative trials will not be discussed further in the interest of providing a succinct analysis.

Table 6.3: *Condition sets trialled with NHC proligand systems* ***6F****,* ***6G*** *and* ***6H*** *with* $PdCl_2$ *for the synthesis of 1-*o*-tolyl-naphthalene. Entry 4 is a run with* $PdCl_2$ *and no proligand.*

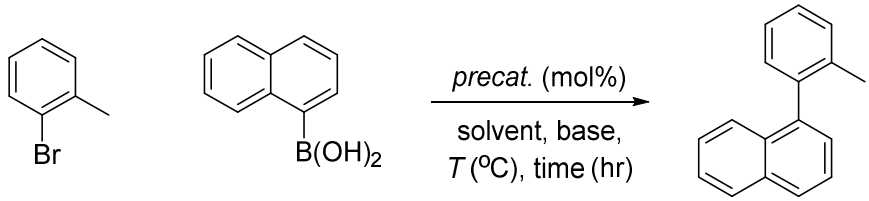

entry	proligand $PdCl_2$	Loading [mol%]	base (equiv)	solvent	*T* [°C]	time [hr]	Conv [%]	yield [%]
1	**6F**	2	K_2CO_3 (3)	iPrOH/H_2O (5/1)	60	24	40	5
2	**6G**	2	K_2CO_3 (3)	iPrOH/H_2O (5/1)	60	24	38	22
3	**6H**	2	K_2CO_3 (3)	iPrOH/H_2O (5/1)	60	24	28	2

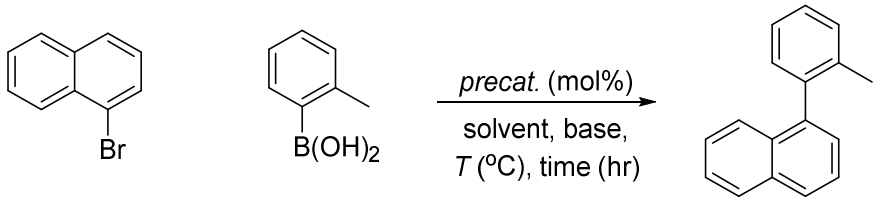

entry	proligand (+ $PdCl_2$)	Loading [mol%]	base (equiv)	solvent	*T* [°C]	time [hr]	Conv [%]	yield [%]
4	x	2	K_2CO_3	iPrOH/H_2O (5/1)	60	3	10	2
5	**6F**	2	K_2CO_3	iPrOH/H_2O (5/1)	60	3	85	42
6	**6G**	2	K_2CO_3	iPrOH/H_2O (5/1)	60	3	72	67
7	**6G**	2	K_2CO_3	DMF/H_2O (5/1)	60	3	100	95
8	**6H**	2	K_2CO_3	iPrOH/H_2O (5/1)	60	24	14	2
9	**6H**	2	K_2CO_3	DMF/H_2O (5/1)	60	24	48	5
10	**6H**	2	K_2CO_3	DMF/H_2O (5/1)	120	24	24	0
11	**6H**	2	NaOH	DMF/H_2O (5/1)	120	24	32	0

It was found that addition of water was crucial for a successful reaction. Without water, reactions in isopropanol and DMF produced negligible product with **6F** and **6G**. Addition of water is common for Suzuki couplings and aids solubilisation of inorganic bases and formation of the reactive boronate coupling partner. As with the preformed precatalyst systems, there was an obvious preference for using 1-bromo-naphthalene and *o*-tolyl-boronic acid instead of *o*-bromo-toluene and naphthyl-1-boronic acid. When the latter was used, the solution immediately darkened to grey upon addition of the proligand/$PdCl_2$ mixture and the reaction did not proceed. The **6G**/$PdCl_2$ combination operated acceptably, producing a 67% yield in isopropanol/water and 95% yield in

DMF/water after 24 hours. As before, these reaction mixtures were rotary-evaporated and set aside for chiral HPLC analysis. The achiral system **6F**/$PdCl_2$ was slightly less efficient, providing a 42% yield in isopropanol/water. Reactions with organic proligands **6F** and **6G** begun as colourless solutions, sometimes with a separated aqueous phase, and became grey slurries over the 3-hour period. Measuring conversion/yields again after 24 hours showed them to be unchanged, suggesting the reactions had ceased. Catalyst deactivation likely occurs by precipitation of metallic Pd(0) and its adducts, explaining the greying of the mixture. A dummy run using only $PdCl_2$ and no proligand (entry 4, Table 6.3) produced a trace amount of product confirming that an NHC ligand is required.

Metallo-NHC proligand **6H** could, at best, produce a trace amount of product comparable to when only $PdCl_2$ was used. Some of the trialled condition sets are shown in entry 8 – 11, Table 6.3. MeCN and MeCN/water as solvent was trialled with K_2CO_3 and NaOH as base but these were equally unsuccessful. Interestingly, when performing reactions with **6H**/$PdCl_2$ at 60 ^oC, the bright orange solution remained homogenous; no grey/black material deposited as happens when **6F** and **6G** are used. Performing the reaction at 120 ^oC instead of 60 ^oC also failed to promote the reaction, however, after 48 hours the solution had darkened slightly. This suggests that the in situ NHC-Pd species formed with **6H** is more stable than **6F** and **6G**. It is likely that this heightened NHC-Pd complex stability contributes to the inactivity of metallo-ligand NHC systems as demonstrated with **6E** and **6H**.

A qualitative investigation of the synthesis of biphenyl using bromo-benzene or iodo-benzene with phenyl-boronic acid was perfomed using **6H** to determine whether the steric bulk of the substrates, or the reactivity of the aryl-halide could be influential. This was initially performed using **6G**/$PdCl_2$ in isopropanol/water with K_2CO_3 and bromo-benzene as the aryl halide at 60 ^oC. GC-FID analysis showed all bromo-benzene had been consumed and a lone spike due to biphenyl was present after 3 hours. Repeating this reaction with **6H** produced a small spike due to biphenyl and after 48 hours, minimal consumption of bromo-benzene was observed. Repeating with iodo-benzene proved to be successful and, after 48 hours only a small signal due to iodo-benzene was present in

the GC-FID trace compared with a large signal due to biphenyl. Evidently, turnover with **6H** occurs slowly but can be achieved with the more reactive aryl-iodide and the catalyst does not appear to degrade over this long reaction time. It may also be possible to perform the synthesis of more hindered biaryls using **6H** and aryl-iodides to assess asymmetric induction.

6.4.3. Preliminary insights

The key insight provided by these catalysis trials is that the metallo-NHC systems do not function under the same conditions as their organic-NHC counterparts. This supports the assertion that the nature of the *N*-amido group is extremely influential. This has been noted by Lee *et al.* (see scheme 1.17, section 1.4.1), albeit to a lesser extent.[122] This is particularly evident for the Pd(allyl) precatalyst systems **6C**, **6D** and **6E** which have been well characterised. It was found that while the cyclohexyl-acetamide and bornyl-acetamide derivatives **6C** and **6D** turned over yields of ~ 60%, no product was observed using **6E** under the same conditions (at room temperature), or with heating. Of these, **6E** is the only one with the Pd(II) centre bound within an *N*-amidate/NHC chelate. However, successful trials using the Pd(acac) derivative **6B** proved that having a preformed *N*-amidate/NHC chelate does not negate catalysis. As explained in the previous chapter, synthesis of the metallo-NHC complexes $[Ru(phen)_2(Pd\{$**5.9 - H**$\}\{allyl\})][PF_6]_2$ (**6E**) and $[Ru(phen)_2(Pd\{$**5.10 - H**$\}Cl)][PF_6]_2$ proceeded with spontaneous deprotonation of the amide. Clearly this process is highly favourable and, during catalysis, it could compete heavily with substrate binding. This also explains why the metallo-NHC proligand system **6H** was able to function, albeit slowly, with the more reactive phenyl-iodide. For this reason, a BipA system related to $[Ru(phen)_2(Pd\{$**5.12 - H**$\}Cl)][PF_6]_2$ might be better suited as it is suspected these engender weaker *N*-amidate coordination to Pd(II).

The results of trials using an N-amido/imidazolium salt NHC proligand with $PdCl_2$ tentatively imply that the favourability of *N*-amidate/NHC chelation correlates to the recorded yield (Scheme 6.3). Here, the best performing proligand was bornyl acetamide

derivative **6G** which gave a yield of 67% after 3 hours, compared with 42% for the cyclohexyl analogue **6F**. As discussed in Chapters 1 and 2, *N*-amidate coordination is sterically disfavoured by the bulky bornane of **6G** (NHC ligand **2.4**) more so than the cyclohexyl group of **6F** (NHC ligand **3.3**). In the extreme case of the readily chelating metallo-NHC proligand **6H** (NHC ligand [Ru(phen)(**5.9**)]$^{2+}$), negligible biaryl product was generated after 24 hours.

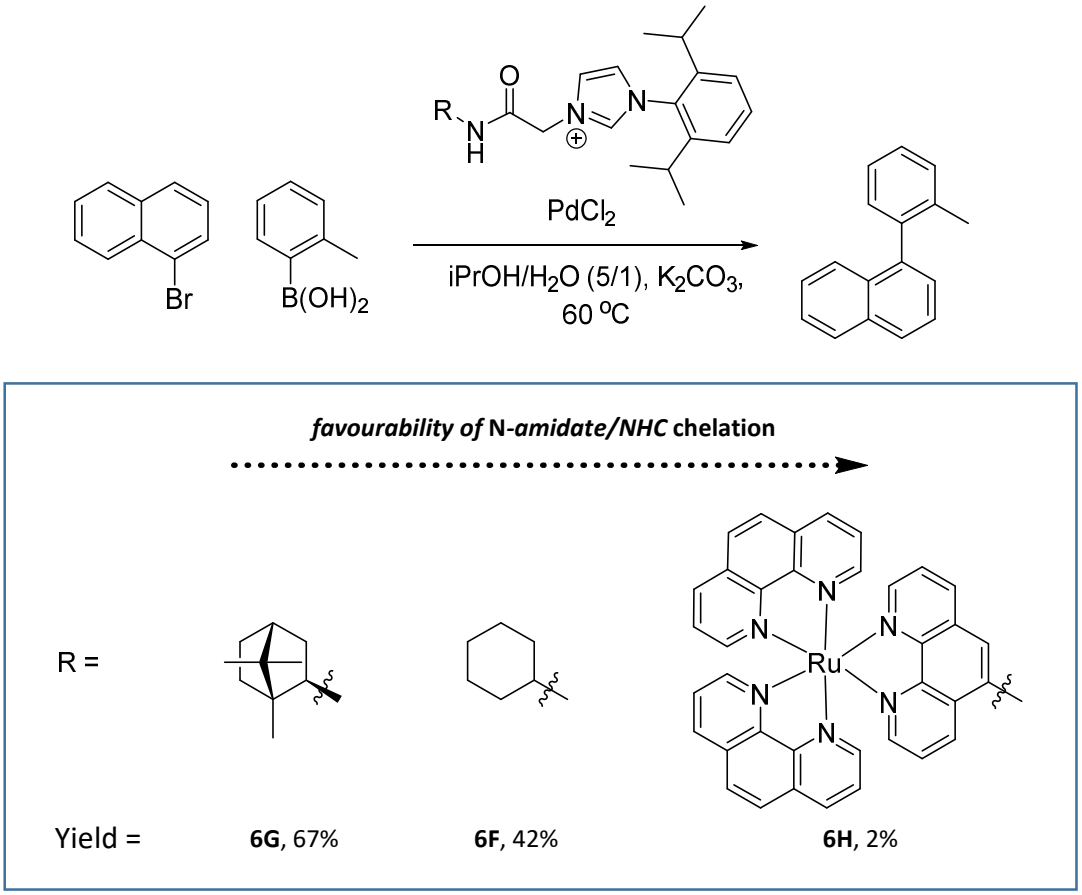

Scheme 6.3: *Comparison of yields for proligand systems **6F**, **6G** and **6H** in relation to the favourability of* N-*amidate/NHC chelation*

When using **6F** and **6G** a grey aggregate due to Pd(0) material deposited, however, this is not observed with **6H** suggesting that the in situ generated precatalyst species is resistant to degradation. The prolonged, 48-hour trial synthesis of biphenyl using **6H**/$PdCl_2$ showed that the metallo-NHC ligand supports a long lived active species but this stability consequently inhibits efficient turnover.

6.5. Summarising remarks

The performance of several novel NHC precatalyst and proligand systems in palladium mediated Suzuki cross-coupling was investigated successfully. Procedures and analysis techniques were established on the basis of reported methods and referenced against a known PEPPSI precatalyst, **6A.** Trials were performed for the synthesis of moderately hindered atropisomeric biaryl compounds, however, enantiomeric excesses were unable to be calculated within the available timeframe.

Organic NHC precatalysts **6B** (Pd(**3.3 - H**)(*O,O'*-acac)), **6C** (Pd(**3.3**)(allyl)) and **6D** (Pd(**2.4**)(allyl)) provided satisfactory yields of the product 1-*o*-tolyl-naphthalene comparable to related literature systems.[37] Organic proligands **6F** and **6G** were also able to generate product but all trials performed using metallo-NHC derivatives (**6E** and **6H**) failed to produce any 1-*o*-tolyl-naphthalene. This has been attributed to *N*-amidate coordination outcompeting substrate binding when using the metallo-NHC ligands. This is supported by experimental observations discussed in previous chapters.

6.6. Scope and future work

Determination of enantiomeric excesses for reactions involving enantiomeric NHC ligands is the critical next step for the evaluation asymmetric induction and can be performed by chiral HPLC. Bornyl-acetamide systems trialled above have provided sample that could be analysed for this purpose.

Several NHC ligands possessing an enantiomeric ruthenium-polypyridine group as the stereodirecting component were prepared however, only catalysis using $[Ru(phen)_2(\mathbf{5.9})]^{2+}$, could be studied in the time available. This was unsuccessful for asymmetric Suzuki couplings however, further screening of conditions sets, metallo-NHC ligands and the use of different substrates is required before ruling out the activity of this system.

The 4-acetamido-2,2-bipyridine (BipA) derived metallo-NHC system is a promising candidate due its weaker *N*-amidate coordination. This may allow substrate conversion to occur unlike in the 5-acetamido-1,10-phenanthroline based derivatives. It would also be beneficial to trial some of the novel monodentate metallo-NHC systems including the fused IP NHC proligand $[Ru(bipy)_2(\mathbf{4.9.H})][PF_6]_3$ or the appended 3-imidazol-phenanthroline species $[Ru(bipy)_2(\mathbf{5.2.H})][PF_6]$. This would inform on whether chelation is involved in quenching catalysis or if some other process involving the ruthenium centre is responsible.

Finally, all metallo-NHC proligands and precatalysts developed in this work could be applied to one of numerous other palladium (or other metal) mediated syntheses such as Buchwald-Hartwig couplings, Heck couplings or α-Ketone arylation, not necessarily looking at asymmetric induction. The scope for further catalytic studies with the ligand systems presented in this thesis is seemingly boundless.

Chapter 7

conclusions and future perspectives

7.1. Conclusions

Presented in this thesis is the synthesis and characterisation of thirty-three previously un-reported imidazolium salts (and precursors) including; six new bornane-derivatives, two new cyclohexyl-derivatives and twelve new organic 1,10-phenanthroline-derivatives. Incorporation of the 1,10-phenanthroline-derived species into ruthenium-polypyridine complexes generated thirteen novel metallo-NHC proligands and precursors. Imidazolium salts were employed in the synthesis of NHC-complexes, fourteen of which were isolated, characterised and subject to a comprehensive structural evaluation.

A majority of the compounds introduced in this work are of the acetamide-tethered family and are capable of coordinating to a metal in an *N*-amidate/NHC motif. Chapter 1 introduces the new bornyl-acetamide NHC ligands **2.2** – **2.5** and explores the structure and properties of their complexes prepared with catalytically relevant metal centres Pd(II), Pt(II) and Ru(II) as well as several Ag(I) precursor complexes. One important insight presented is that the steric bulk of the bornane *N*-amido substituent disfavours *N*-amidate/NHC chelation. The synthesis of less hindered cyclohexyl-acetamide analogues in Chapter 2 helped to support this assertion, in particular through comparison of the synthetic yields, NMR spectra and X-ray crystal structures of the chelated complexes Pd(**2.4 - H**)(*O,O'*-acac) and Pd(**3.3 - H**)(*O,O'*-acac). Consequently, it was synthetically challenging to generate *N*-amidate/NHC chelated complexes in the bornyl-acetamide series. A succinct demonstration of this was provided by the unsuccessful conversion of an *O*-amidate/NHC chelated bornyl-species, [Ru(**2.2**)(*p*-cymene)Cl][PF_6], to the *N*-amidate/NHC chelated [Ru(**2.2 - H**)(*p*-cymene)Cl][PF_6] complex using a methodology reported for a related compound.

Developing NHC-ligands incorporating an enantiomeric ruthenium-polypyridine moiety was one of the central objectives of this work. Synthesis of phenanthroline-annelated NHC derivatives in Chapter 3 identified several of the regiosynthetic obstacles to preparing poly-heterocyclic imidazolium salts by *N*-substitution. This is exemplified by

the isolation and characterisation of compounds **4.11.I**, **4.12.I** and **4.13.I** which formed by the undesired *N*-alkylation of the phenanthroline nitrogen. A post-complexation methodology in which the imidazolium salt is prepared following coordination of the phenanthroline-terminus to ruthenium was demonstrated as a plausible mitigating approach. UV/visible and fluorometric analysis of the previously unexplored phenanthrolinum salts implicates intramolecular charge transfer as the cause of their unusually intense yellow colouration.

Avoidance of the synthetic issues identified in Chapter 3 was achieved by adopting an acetamide linking unit. This provided a diverse selection of metallo-NHC proligands $[Ru(phen)_2($**5.5.H** – **5.10.H**$)][PF_6]_3$ and $[Ru(phen)_2($**5.12.H**$)][PF_6]_3$ and the NHC complexes $[Ru(phen)_2(Pd\{$**5.9 - H**$\}\{allyl\})][PF_6]_2$, $[Ru(phen)_2(Pd\{$**5.10 - H**$\}Cl)][PF_6]_2$, $[Ru(phen)_2(Pd\{$**5.12**$\}Cl_2)][PF_6]_2$ and $[Ru(phen)_2(Pd\{$**5.12 - H**$\}Cl)][PF_6]_2$. The latter were prepared by the silver-transmetalation method and proceeded with deprotonation of the amide to give *N*-amidate/NHC chelated complexes without the use of additional base. Here, *N*-amidate formation is promoted by conjugate stabilisation of the anion and the reduction in molecular charge that deprotonation affords, neither of which is possible with bornane or cyclohexyl-amido substituents. This led to previously unseen coordination motifs including tridentate coordination of an *N*-amidate-NHC-pyridine chelate. In addition to the chiral ruthenium-polypyridine moiety, these complexes possess an internal chiral axis leading to diastereomers. In the 2,2'-bipyridine derivative $[Ru(phen)_2(Pd\{$**5.12 - H**$\}Cl)][PF_6]_2$, the probable reversibility of *N*-amidate chelation enables a single diastereomer to be obtained as the thermodynamic product.

Chapter 6 outlines the screening of precatalyst and proligand systems in an asymmetric Suzuki-coupling producing atropisomeric biaryl compounds. Organic NHC precatalysts Pd(**3.3 - H**)(*O,O'*-acac), Pd(**3.3**)(allyl) and Pd(**2.4**)(allyl) provided satisfactory yields of the product 1-*o*-tolyl-naphthalene comparable to yields reported for related systems. Organic proligands **2.4.HCl** and **3.3.HCl** were also able to generate product but all trials performed using metallo-NHC derivatives ($[Ru(phen)_2(Pd\{$**5.9 - H**$\}\{allyl\})][PF_6]_2$ and $[Ru(bipy)_2($**5.9.H**$)][PF_6]_3$) were unsuccessful. Inhibition of catalysis has been attributed to *N*-amidate coordination by the metallo-NHC ligands outcompeting substrate binding.

Evidently, the coordination ability of the *N*-amidate has implications for product turnover during catalysis.

7.2. Future perspectives

Avenues for further investigation are outlined at the conclusion of each chapter with a focus on transition metal catalysis. However, the novel NHC proligands developed in this work have by no means been studied to their full potential and are not limited to use in metal-mediated processes.

For example, no acetamide coupled NHCs have been reported in an organocatalytic role and hence the novel NHC proligands developed here provide an excellent start-point. Of particular interest is the potential for hydrogen-bonding by the amide unit to participate in transformations. It is plausible that acetamide-triazole derivatives could be prepared by the methods established in this work to provide interesting chiral-precatalysts for asymmetric benzoin condensation.

The synthesis of *f*-block NHC complexes stabilised by *N*-amidate/NHC chelation is another novel pursuit. Numerous *f*-block metal complexes with NHCs have been reported in which the NHC ligand bears an anionic chelating arm.[281] Stabilisation by anionic groups is often essential for maintaining NHC coordination to highly electropositive lanthanide and actinide centres.[111] Surprisingly, amidate-based chelation has not been explored in this context. Acetamide linked metallo-NHC ligands of the type introduced in Chapter 5 could be particularly effective in this role as they are proven to be proficient *N*-amidate chelators. These would be highly unusual and interesting hetero-dinuclear complexes.

Chapter 8

experimental data and methods

8.1. General information

Unless otherwise specified, all reagents and starting materials were reagent grade, purchased from standard suppliers and used as received. Water was purified by reverse osmosis *in-house*. Anhydrous solvents were either obtained from a commercial source or, HPLC-grade solvent was dried via the *in-house* solvent system by passing over a sealed column of activated alumina. All air and water sensitive manipulations were carried out under either an argon or nitrogen atmosphere using standard Schlenk techniques. Melting points were recorded on an electrothermal melting point apparatus and are uncorrected. The following compounds were prepared following literature procedures: *exo*-(-)-isobornylamine,[135] *exo*-3-aminoborneol,[149] 1-isopropyl-imidazole,[282] 1-(2,6-diisopropyl)phenyl-imidazole,[283] 1-(2-pyridyl)-imidazole,[284] 1-phenyl-imidazole,[285] 1-(2-bromoethyl)-3-methylimidazolium bromide (**2.9.HBr**),[154] 1,10-phenanthro-5,6-dione,[217] imidazo[4,5-*f*][1,10]phenanthroline (**4.1**),[218] 3-bromo-1,10-phenanthroline,[243] 5-amino-1,10-phenanthroline,[251], 4-amino-2,2'-bipyridine,[260] *cis*-$Ru(bipy)_2Cl_2$ and *cis*-$Ru(phen)_2Cl_2$,[286] *cis*-$[Ru(phen)_2(py)_2]Cl_2$ and Δ-$[Ru(phen)_2(py)_2][As-(—)-Otart]_2$,[269] [Pd(allyl)Cl],[37] $[Ru(p\text{-cymene})Cl_2]_2$,[206] 1,3-bis(2,6-diisopropyl-phenyl)imidazolium chloride,[279] napthalene-1-boronic acid and tolyl-*o*-boronic acid.[275]

Nuclear Magnetic Resonance Spectroscopy (NMR)

Spectra were recorded on a Varian VNMRS 600, Varian INOVA 500 or an Agilent 400-MR instrument operating at 600, 500 and 400 MHz, respectively, for ^1H, and at 150, 125, and 100 MHz, respectively, for ^{13}C. Experiments using the 600 MHz instrument were performed externally by Ian Vorster at Victoria University, Wellington. All samples were dissolved in commercially available deuterated solvents and spectra were referenced to the residual solvent peak. When required, COSY, HSQC, HMBC, and TOCSY experiments were employed, using standard Varian and Agilent pulse sequences.

Mass spectrometry (ESI-MS)

Mass spectra were recorded by Dr. Marie Squire, Dr. Alexander Goroncy and Dr. Amelia Albrett on either a DIONEX Ultimate 3000 or Bruker MaXis 4G spectrometer, operated in high resolution positive ion electrospray mode. Samples were prepared in HPLC grade MeCN, MeOH or water.

Infra-red spectroscopy (FT-IR)

FT-IR spectra were recorded using on a Bruker ALPHA Platinum ATR FT-IR spectrometer in the range of 4000 – 550 cm^{-1} using a solid sample of the analyte. Abbreviations used to describe signal intensity are as follows; strong (s), medium (m), weak (w) and broad (br).

UV/visible spectroscopy (UV-vis)

UV/Visible spectra were recorded on an Agilent Cary 300 spectrophotometer over a 200 - 800 nm range using spectroscopy grade MeCN or DCM solutions. Samples were measured at room temperature in quartz cuvettes of path length 1 cm.

Fluorometry

Emission spectra were recorded on a Horiba Fluorolog-3 spectrometer over 300 - 800 nm range using spectroscopy grade MeCN or DCM solutions. Samples were measured at room temperature in quartz curvettes of path length 1 cm.

Polarimetry

Optical rotation values were recorded on a Perkin Elmer polarimeter (Model 341) using a sodium lamp producing D-line radiation of 589.3 nm. Samples were prepared in spectroscopy grade MeCN or MeOH and measured at room temperature in a cell of path length 10 cm.

Elemental Analysis

Elemental analysis was carried out by Campbell Microanalytical Laboratory, University of Otago.

X-Ray Crystallography

X-ray crystallographic data collection and refinement was carried out on an Oxford-Agilent SuperNova instrument with focussed microsource Cu Kα (λ = 1.5418 Å) radiation or Mo Kα (λ = 0.71073 Å) and ATLAS CCD area detector. All structures were solved using direct methods with SHELXS or SHELXT and refined on F2 using all data by full matrix least-squares procedures with SHELXL within OLEX-2.3. Non-hydrogen atoms were refined with anisotropic displacement parameters. Hydrogen atoms were included in calculated positions, or were manually assigned from residual electron density where appropriate, with isotropic displacement parameters 1.2 times the isotropic equivalent of their carrier atoms. The functions minimized were $\Sigma w(F^2_o - F^2_c)$, with $w = [\sigma^2(F^2_o) + aP_2 + bP] - 1$, where $P = [\max(F_o)^2 + 2F^2_c]/3$. Graphical representations of crystallographic data were prepared using Mercury. Crystallographic data for all compounds is available in .cif format if required.

Gas Chromatography (GC-FID)

GC-FID traces were recorded using a Shimadzu GC-2010 gas chromatograph with FID detector and a Shimadzu AOC-20i auto injector set at a 1 µL injection volume. Samples were prepared in HPLC grade Et_2O. A helium carrier gas was used at flow rate of 5 mL/min. The FID detector required hydrogen and air at a flow rate of 20 mL/min and 4000.0 mL/min, respectively.

8.2. Chapter 2

8.2.1. Bornyl-acetamide (BA) and amino-borneol derivatives

2-chloro-*N*-*exo*-bornylacetamide (2.1)

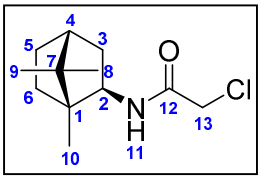

In a 100 mL round-bottom flask and under an argon atmosphere, *exo*-bornylamine (2.27 g, 14.8 mmol) was dissolved in DCM (50 mL) and cooled to 0 °C. Freshly distilled triethylamine (3.1 mL, 22.2 mmol) was added followed by the dropwise addition of chloroacetyl-chloride (1.3 mL, 16.3 mmol) in DCM (25 mL). The reaction mixture was stirred for 1 hour at 0 °C then for a further 14 hours at room temperature. To the brown mixture was added Et_2O (100 mL) and the precipitated triethylamine.HCl salt filtered off and rinsed with Et_2O (50 mL). Rotary-evaporation of the filtrate gave an oily brown, semi-crystalline residue which was purified by flash chromatography (silica, 3:2 Et_2O/pet-ether). The desired product **2.1** was obtained as a white, crystalline solid. Yield 2.751 g (81%). **MP**: 88 – 89 °C. **^{1}H NMR** (400 MHz, DMSO-*d6*): δ 7.50 (1H, d, J = 6.7 Hz, H11), 4.07 (1H, d, J = 12.5 Hz, H13a), 4.01 (1H, d, J = 12.5 Hz, H13b), 3.68 (1H, dd, J = 8.2 Hz, 5.9 Hz, H2), 1.69 – 1.56 (4H, m, H3α, H3β, H4, H5α), 1.51 – 1.43 (1H, m, H6α), 1.16 – 1.03 (2H, m, H5β, H6β), 0.87 (3H, s, H8), 0.76 (3H, s, H9), 0.73 (3H, s, H10). **^{13}C NMR** (100 MHz, DMSO-*d6*): δ 166.15 (C12), 56.93 (C2), 49.31 (C1), 46.91 (C7), 44.70 (C4), 43.18 (C13), 37.48 (C3), 36.14 (C6), 27.11 (C5), 20.72 (C8), 20.37 (C9), 11.84 (C10). **FT-IR** ν/cm^{-1} (intensity)**:** 3366 (w), 3323 (m), 2955 (m), 2938 (m), 2878 (w), 1673 (m), 1652 (s), 1550 (m), 1527 (s), 1458 (m), 1432 (m), 1393 (m), 1156 (w), 1081 (w), 790 (w), 678 (m), 571 (m). **ESI-MS**: Found $[MH]^+$ 230.1263, $[2M + H]^+$ 459.2466. $[C_{12}H_{21}NOCl]^+$ requires 230.1312, $[C_{24}H_{41}N_2O_2Cl_2]^+$ requires 459.2545. **$[\alpha]_D$** (MeOH, 20 °C): - 32.68°.

1-methyl-3-[*N-exo*-(2-bornyl)acetamido]-1*H*-imidazolium chloride (2.2.HCl)

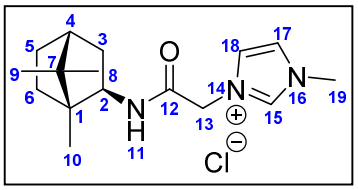

In a 50 mL round-bottom flask and under a nitrogen atmosphere, **2.1** (0.526 g, 2.29 mmol) and 1-methyl-imidazole (0.56 mL, 7.00 mmol) were dissolved in MeCN (25 mL). The colourless solution was refluxed for 24 hours then cooled to room temperature and concentrated by rotary-evaporation. The product was precipitated from the concentrate by addition of Et_2O (80 mL) with stirring then collected by filtration and washed further with Et_2O. The slightly tacky solid was re-crystallised from hot DCM to give **2.2.HCl** as colourless rectangular plates. Yield 0.629 g (88%). **MP:** 190 – 192 °C. **^{1}H NMR** (400 MHz, DMSO-*d6*): δ 9.23 (1H, s, H15), 8.32 (1H, d, J = 7.4 Hz, H11), 7.71 (2H, br.s, H17, H18), 5.10 (2H, s, H13), 3.88 (3H, s, H19), 3.67 (1H, m, H2β), 1.84 – 1.67 (1H, m, H3α), 1.67 – 1.57 (3H, m, H3β, H4, H5α), 1.47 (1H, m, H6α), 1.21 – 0.99 (2H, m, H5β, H6β), 0.93 (3H, s, H8), 0.75 (6H, s, H9, H10). **^{13}C NMR** (100 MHz, DMSO-*d6*): δ 165.20 (C12), 138.07 (C15), 124.00 (C18), 123.43 (C17), 57.32 (C2), 51.09 (C13), 49.31 (C1), 46.91 (C7), 44.72 (C4), 37.29 (C3), 36.20 (C19), 36.19 (C6), 27.15 (C5), 20.80 (C9), 20.65 (C8), 12.05 (C10). **FT-IR** ν/cm^{-1} (intensity)**:** 3372 (w), 2948 (m), 2878 (m), 1689 (m), 1659 (s), 1535 (m), 1458 (w), 1389 (w), 1372 (w), 1188 (w), 1170 (m), 739 (w), 701 (w), 619 (m), 450 (m). **ESI-MS:** Found $[M]^+$ 276.1785, $[2M + Cl]^+$ 587.3234, $[3M+2Cl]^+$ 898.5616. $[C_{16}H_{26}N_3O]^+$ requires 276.2070, $[C_{32}H_{52}N_6O_2Cl]^+$ requires 587.3829, $[C_{48}H_{78}N_9O_3Cl_2]^+$ 898.5588. **$[\alpha]_D$** (MeOH, 20 °C): - 13.44°.

1-isopropyl-3-[*N-exo*-(2-bornyl)acetamido]-1*H*-imidazolium chloride (2.3.HCl)

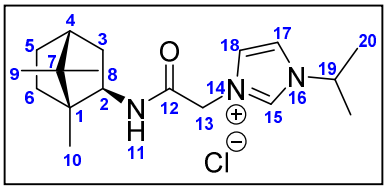

In a 50 mL round-bottom flask and under a nitrogen atmosphere, **2.1** (0.264 g, 1.15 mmol) and 1-isopropyl-imidazole (0.40 mL, 3.50 mmol) were dissolved in MeCN (15 mL). The faint yellow solution was refluxed for 24 hours then cooled to room temperature and concentrated by rotary-evaporation. The product was precipitated from the amber coloured concentrate by addition of Et_2O (80 mL), with stirring, then collected by filtration and washed further with Et_2O. Air drying gave **2.3.HCl** as a fine white powder. Yield 0.349 g (89%). **MP:** 226 – 229 °C. **^{1}H NMR** (400

MHz, DMSO-*d6*): δ 9.34 (1H, s, H15), 8.19 (1H, d, J = 7.4 Hz, H11), 7.91 (1H, s, H17), 7.71 (1H, s, H18), 5.04 (2H, s, H13), 4.67 (1H, spt, J = 6.5 Hz, H19), 3.72 – 3.63 (1H, m, H2β), 1.79 – 1.54 (4H, m, H3α, H3β, H4, H5α), 1.52 – 1.41 (7H, m, H6α, H20), 1.13 – 0.99 (2H, m, H5β, H6β), 0.92 (3H, s, H8), 0.75 (3H, s, H9), 0.74 (3H, s, H10). **^{13}C NMR** (100 MHz, DMSO-*d6*): δ 165.16 (C12), 136.44 (C15), 124.35 (C18), 120.35 (C17), 57.29 (C2), 52.64 (C19), 51.08 (C13), 49.28 (C1), 46.91 (C7), 44.68 (C4), 37.38 (C3), 36.17 (C6), 27.13 (C5), 22.79 (C20a), 22.77 (C20b), 20.79 (C9), 20.58 (C8), 12.04 (C10). **FT-IR** ν/cm^{-1} (intensity)**:** 3208 (w), 3065 (w), 2952 (m), 2925 (w), 2874 (w), 1683 (m), 1673 (s), 1556 (m), 1539 (m), 1458 (w), 1264 (m), 1212 (m), 1180 (m), 897 (w), 778 (m), 624 (m), 605 (m). **ESI-MS**: Found $[M]^+$ 304.2072, $[2M + Cl]^+$ 643.3803. $[C_{18}H_{30}N_3O]^+$ requires 304.2383, $[C_{36}H_{60}N_6O_2Cl]^+$ requires 643.4455. **[α]$_D$** (MeOH, 20 °C): - 10.91°.

1-(2,6-diisopropyl)phenyl-3-[*N-exo*-(2-bornyl)acetamido]-1*H*-imidazolium chloride (2.4.HCl)

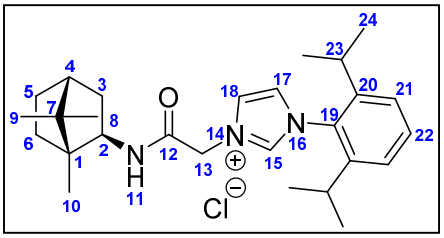

Synthesis performed as reported for **2.3.HCl** using **2.1** (0.530 g, 2.31 mmol) and 1-(2,6-diisopropyl)phenyl-imidazole (1.00 g, 4.36 mmol) in MeCN (50 mL). Compound **2.4.HCl** was obtained as a fine white powder. Yield 0.945 g (89%). **MP**: 159 °C with decomposition. **^{1}H NMR** (400 MHz, DMSO-*d6*): δ 9.60 (1H, s, H15), 8.30 (1H, d, J = 7.4 Hz, H11), 8.06 (1H, s, H17), 8.04 (1H, s, H18), 7.61 (1H, t, J = 7.8 Hz, H22), 7.43 (2H, d, J = 7.8 Hz, H21), 5.20 (2H, s, H13), 3.76 – 3.69 (1H, m, H2β), 2.29 (2H, dq, J = 13.1 Hz, 6.6 Hz, H23), 1.75 – 1.61 (4H, m, H3α, H3β, H4, H5α), 1.54-1.43 (1H, m, H6α), 1.13 (14H, m, H5β, H6β, H24), 0.96 (3H, s, H8), 0.77 (6H, s, H9, H10). **^{13}C NMR** (100 MHz, DMSO-*d6*): δ 165.03 (C12), 145.59 (C20), 139.57 (C15), 131.87 (C22), 131.02 (C19), 125.02 (C18), 124.82 (C21), 124.73 (C17), 57.36 (C2), 51.74 (C13), 49.37 (C1), 46.95 (C7), 44.74 (C4), 37.38 (C3), 36.17 (C6), 28.44 (C23), 27.16 (C5), 24.28 (C24a), 24.20 (C24b), 20.81 (C9), 20.68 (C8), 11.98 (C10). **FT-IR** ν/cm^{-1} (intensity)**:** 3208 (w), 3018 (w), 2960 (m), 2928 (m), 2872 (w), 1687 (s), 1548 (s), 1459 (m), 1367 (m), 1256 (w), 1168 (m), 1066 (w), 816 (m), 766 (w), 672 (w). **ESI-MS**: Found $[M]^+$ 422.2739, $[2M + Cl]^+$ 879.5132. $[C_{27}H_{40}N_3O]^+$ requires 422.3166, $[C_{54}H_{80}N_6O_2Cl]^+$ requires 879.6020. **[α]$_D$** (MeOH, 20 °C): - 1.93°.

1-(2-pyridyl)-3-[*N*-*exo*-(2-bornyl)acetamido]-1*H*-imidazolium chloride (2.5.HCl)

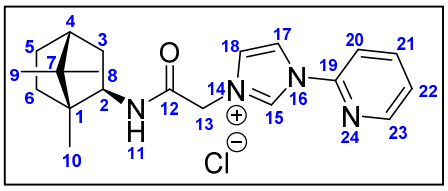

Synthesis performed as reported for **2.3.HCl** using **2.1** (0.265 g, 1.15 mmol) and 1-(2-pyridyl)-imidazole (0.250 g, 1.73 mmol) in MeCN (15 mL).. Compound **2.5.HCl** was obtained as a fine white powder. Yield 0.236 g (55%). **MP**: 256 – 258 °C. **^{1}H NMR** (400 MHz, DMSO-*d6*): δ 10.15 (1H, s, H15), 8.65 (1H, m, H23), 8.55 (1H, s, H17), 8.24 – 8.13 (2H, m, H11, H21), 8.08 (1H, d, J = 8.2 Hz, H20), 7.98 (1H, s, H18), 7.65 (1H, t, J = 5.3 Hz, H22), 5.19 (2H, s, H13), 3.72 (1H, m, H2β), 1.69 (4H, m, H3α, H3β, H4, H5α), 1.51 (1H, m, H6α), 1.06 (2H, m, H5β, H6β), 0.96 (3H, s, H8), 0.80 (6H, s, H9, H10). **^{13}C NMR** (100 MHz, DMSO-*d6*): δ 164.59 (C12), 149.52 (C23), 146.50 (C19), 140.91 (C21), 136.33 (C15), 125.55 (C22), 125.34 (C18), 118.86 (C17), 114.51 (C20), 57.22 (C2), 51.45 (C13), 49.11 (C1), 46.73 (C7), 44.51 (C4), 37.29 (C3), 35.99 (C6), 26.92 (C5), 20.58 (C9), 20.37 (C8), 11.87 (C10). **FT-IR** ν/cm^{-1} (intensity)**:** 3238 (w), 3067 (w), 2985 (m), 2880 (m), 1673 (s), 1599 (m), 1544 (s), 1477 (m), 1447 (s), 1233 (s), 1158 (m), 968 (w), 794 (m), 784 (m), 701 (w), 619 (m). **ESI-MS:** Found $[M]^+$ 339.2187. $[C_{20}H_{27}N_4O]^+$ requires 339.2179. **$[\alpha]_D$** (MeOH, 20 °C): - 2.78°.

2.10.2HBr and **2.13.2HBr**

In an oven dried Schlenk tube, *exo*-3-aminoborneol (0.100 g, 3.90 mmol) was dissolved in anhydrous DMSO (1 mL) and freshly distilled trimethylamine added (0.62 mL, 4.43 mmol). A solution of 1-(2-bromoethyl)-3-methylimidazolium bromide (**2.9.HBr**) (0.800 g, 2.96 mmol) in DMSO (2 mL) was added dropwise. The colourless solution was stirred for 48 hours at room temperature, becoming a cloudy, faint yellow suspension. After this time the reaction mixture was pipetted into vigorously stirring EtOAc (150 mL) resulting in deposition of a sticky white solid. The supernatant was decanted off, acetone added (100 mL) and stirring continued until the residue became a powdered solid which was collected by filtration. This material (0.270 g) was shown by ^{1}H-NMR to contain both the bis-imidazolium bromide salt **2.12.2HBr** and the desired product **2.10.2HBr** in a 1.5 : 1 ratio. Recrystallisation from hot MeCN provided pure **2.10.2HBr** as a white powder

(0.101 g). The initial EtOAc supernatant was condensed by rotary evaporation and THF (100 mL) added producing a faint yellow solution. Treatment with an HBr solution in THF (~ 0.5 M, 3 mL) resulted in immediate precipitation of a white solid that was collected by filtration and rinsed with THF. The material (0.153 g) was found by ^{1}H-NMR to be a mixture of **2.10.2HBr** and the camphidine derivative **2.13.2HBr**. Washing the material with DCM left behind pure **2.10.2HBr** (0.105 g), taking **2.13.2HBr** into the filtrate which, after removal of the solvent, was obtained as a fine white, hygroscopic powder (0.0063 g).

2.10.2HBr

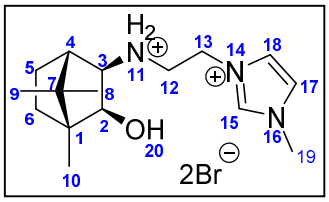

Overall yield 0.207 g (15.9%). **^{1}H NMR** (400 MHz, CD_3OD): δ 9.17 (1H, s, H15), 7.81 (1H, s, H18), 7.73 (1H, s, H17), 4.72 (2H, m, H13), 3.98 (3H, s, H19), 3.93 (1H, d, J = 7.4 Hz, H2β), 3.69 (2H, t, J = 7.0 Hz, H12), 3.49 (1H, d, J = 7.4 Hz, H3β), 2.19 (1H, d, J = 4.3 Hz, H4), 1.89 – 1.69 (1H, m, H5α), 1.55 (1H, td, J = 12.4 Hz, 3.7 Hz, H6α), 1.24 (1H, m, H5β), 1.13 (4H, m, H6β, H8), 0.97 (3H, m, H9), 0.89 (3H, m, H10). **^{13}C NMR** (100 MHz, CD_3OD): δ 138.86 (C15), 125.30 (C17), 123.89 (C18), 77.96 (C2), 67.07 (C3), 50.58 (C1), 49.87 (C4), 49.39 (C12), 47.91 (C7), 46.03 (C13), 36.80 (C19), 32.90 (C6), 27.31 (C5), 21.77 (C9), 21.15 (C8), 11.35 (C10). **ESI-MS**: Found M^+ 278.2229. $[C_{16}H_{28}N_3O]^+$ requires 278.2221.

2.13.2HBr

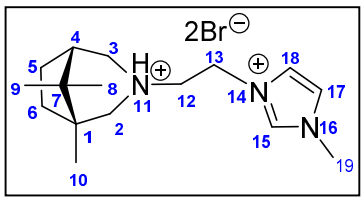

Yield 0.0063 g (0.5%). **^{1}H NMR** (400 MHz, CD_3OD): δ 9.14 (1H, s, H15), 7.80 (1H, s, H18), 7.64 (1H, s, H17), 4.82 (2H, m, H13), 3.97 (3H, s, H19), 3.73 (2H, m, H12), 3.43 (2H, m, H3), 3.26 (1H, d, J = 12.5 Hz, H2a), 3.16 (1H, d, J = 12.5 Hz, H2b), 2.17 – 1.95 (3H, m, H4, H5α, H6α), 1.94 – 1.80 (2H, m, H5β, H6β), 1.15 (3H, s, H8), 1.00 (3H, m, H9), 0.96 (3H, m, H10). **^{13}C NMR** (100 MHz, CD_3OD): δ 138.99 (C15), 125.55 (C17), 124.08 (C18), 61.47 (C2), 56.75 (C3), 56.57 (C12), 45.47 (C4), 44.87 (C13), 44.16

(C1), 42.69 (C7), 36.93 (C19), 34.14 (C6), 25.32 (C5), 23.62 (C9), 18.78 (C8), 17.37 (C10). **ESI-MS**: Found M^+ 262.2281. $[C_{16}H_{28}N_3]^+$ requires 262.2278.

8.2.2. NHC complexes of bornyl-acetamide derivatives

Pd(2.4 - H)(*O,O'*-acac)

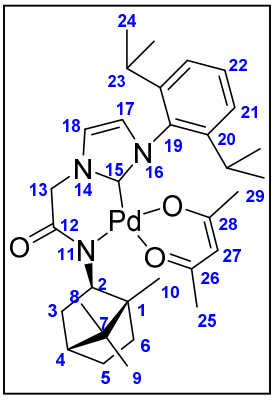

In an oven dried Schlenk tube, **2.4.HCl** (0.0916 g, 0.200 mmol) and $PdCl_2$ (0.337 g, 0.190 mmol) were combined and the vessel sparged with nitrogen. Dry MeCN (3 mL) was added by syringe and the solution heated at 80 °C until the $PdCl_2$ had dissolved. Finely powdered, oven dried K_2CO_3 (0.197 g, 1.43 mmol) was added under flowing nitrogen and allowed to react for 1 hour before adding acetylacetone (20.5 µL, 0.200 mmol). Heating was continued for 4 hours before cooling to room temperature and stirring overnight. The off-white mixture was filtered through celite and the filtrate condensed by rotary evaporation. The residue was then taken up in Et_2O and again filtered and the solvent removed before triturating the material in pentane for 2 hours to give Pd(**2.4 - H**)(*O,O'*-acac) as a fine light-brown solid. Crystals suitable for X-ray diffraction were grown by slow evaporation of an Et_2O solution. Yield 0.0266 g (14%). **MP**: 192 °C with decomposition. **^{1}H NMR** (400 MHz, $CDCl_3$): 7.37 (1H, m, H22), 7.22 (1H, d, J = 7.4 Hz, H21a), 7.16 (1H, d, J = 7.4 Hz, H21b), 7.09 (1H, s, H18), 6.78 (1H, s, H17), 5.05 (2H, m, H13a, H27), 4.63 (1H, br.s, H13b), 4.09 (1H, br.s, H2), 2.32 (1H, br.s, H3α), 1.89 (3H, s, H25), 1.76-1.32 (9H, m, H3β, H4, H5α, H6α, H23), 1.17 – 0.98 (17H, m, H5β, H6β, H24, H29), 0.89 (6H, s, H8, H9/H10), 0.71 (3H, s, H9/H10). **^{13}C NMR** (100 MHz, $CDCl_3$): δ 185.98 (C26/28), 184.44 (C26/C28), 170.29 (C12), 153.55 (C15), 146.28 (C20a), 145.10 (C20b), 134.42 (C19), 129.31 (C22), 124.73 (C17), 123.65 (C21a), 123.54 (C21b), 120.13 (C18), 99.50 (C27), 63.00 (C2), 55.66 (C13), 52.66 (C1/C7), 46.85 (C1/C7), 45.28 (C4), 41.32 (C3), 36.25 (C6), 28.32 (C23a), 28.28 (C23b), 27.62 (C5), 26.47 (C25/C29), 25.21 (C25/C29), 25.00 (C24a), 24.88 (C24b), 23.63 (C24c), 20.77 (C8/C9/C10), 20.56 (C8/C9/C10). **FT-IR** ν/cm^{-1} (intensity): 2951 (w), 2925 (w), 2870 (m), 1575 (s), 1515 (s), 1459 (m), 1421 (w),

1382 (m), 1289 (w), 1269 (w), 1058 (w), 907 (w), 802 (w), 727 (s), 690 (w). **ESI-MS**: Found $[MH]^+$ 626.2592. $[C_{32}H_{46}N_3O_3Pd]^+$ requires 626.2570.

Pd(2.4)(*O,O'*-acac)(γC-acac)

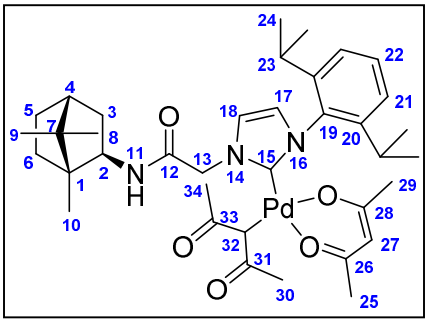

In an oven dried Schlenk tube, **2.4.HCl** (0.0911 g, 0.199 mmol) and $PdCl_2$ (0.347 g, 0.196 mmol) were combined and the vessel sparged with nitrogen. Dry MeCN (4 mL) was added by syringe and the solution heated at 80 °C until the $PdCl_2$ had dissolved. Finely powdered, oven dried sodium-acetylacetonate (0.124 g, 1.02 mmol) was added under flowing nitrogen and allowed to react for 1.5 hours before cooling to room temperature. The faint yellow suspension was stirred at room temperature for a further 16 hours. The reaction mixture was taken up in Et_2O (20 mL) and filtered, washing through with additional Et_2O. The filtrate was condensed, dissolved in a minimum of Et_2O then pentane (30 mL) added resulting in a turbid solution which was filtered through celite. The filtrate solvent was removed giving the Pd(**2.4**)(*O,O'*-acac)(γC-acac) as a fluffy, banana yellow solid. Yield 0.0957 g (59%). **MP**: 130 – 135 °C. **^{1}H NMR** (600 MHz, CD_3CN) δ 7.53 (1H, m, H22-j,n), 748 – 7.36 (3H, m, H21-j,n, H18-j,n), 7.28 (0.7, s, H17-j), 7.25 (0.3H, s, H17-n), 6.79 (0.7H, d, J = 7.6 Hz, H11-j), 6.67 (0.3H, d, J = 7.6 Hz, H11-n), 5.34 (0.7H, d, J = 15.8 Hz, H13a-j), 5.32 (0.7H, s, H27-j), 5.32 (0.3H, s, H27-n), 5.19 (0.3H, d, J = 15.8 Hz, H13a-n), 4.98 (0.3H, d, J = 15.8 Hz, H13b-n), 4.75 (0.7H, d, J = 15.8 Hz, H13b-j), 3.95 (0.7H, m, H2-j), 3.84 (0.3H, m, H2-n), 3.40 (0.7H, s, H32-j), 3.32 (0.3H, s, H32-n), 2.86 (1H, m, H23a), 2.70 – 2.54 (1H, m, H23b), 2.24 (2.1H, s, H30/H34-j), 2.23 (0.9H, s, H30/H34-n), 2.00 – 2.06 (0.7H, m, H3α-j), 1.83 (3.4H, m, H3α-n, H25/H29), 1.79 (3H, s, H25/H29), 1.77 – 1.55 (4H, m, H3β, H4, H5α, H6α), 1.32 – 1.12 (12.8H, m, H5β, H6β, H24a, H24b, H24c), 1.08 (3H, m, H30/H34), 0.99 (3H, m, H24d), 0.91 (4H, s, H8, H10-n), 0.88 (2.5H, s, H10-j), 0.83 (1.5H, s, H9-n), 0.82 (2.2H, s, H9-j). **^{13}C NMR** (150 MHz, CD_3CN): 207.80 (C31/C33-j), 207.44 (C31/C33-n), 207.11 (C31/C33-j), 206.94 (C31/C33-n), 187.63 (C26/C28), 187.40 (C26/C28), 167.41 (C12-j), 167.05 (C12-n), 166.26 (C15-j), 166.18 (C15n), 148.36 (C20a), 147.24 (C20b-j), 147.11 (C20b-n), 136.01 (C19n), 135.96 (C19-j), 131.82 (C22-j), 131.76 (C22-n), 126.70 (C17-j),

126.39 (C17-n), 125.95 (C21a-j), 125.94 (C21a-n), 125.92 (C21b-j), 125.89 (C21b-n), 123.49 (C18), 100.38 (C27), 58.81 (C2-n), 58.41 (C2-j), 55.32 (C13-j), 54.57 (C13-n), 50.66 (C1/C7-j), 49.87 (C1/C7-n), 48.68 (C32-j), 48.31 (C32-n), 48.14 (C1/C7-n), 47.95 (C1/C7-j), 46.20 (C4), 39.84 (C3-n), 37.86 (C3-j), 37.48 (C6-n), 37.17 (C6-n), 31.19 (C30/C34-j), 31.12 (C30/C34-n), 30.42 (C30/C34), 29.94 (C23a-j), 29.90 (C23a-n), 29.87 (C23b-n), 29.49 (C23b-j), 28.67 (C30/C34), 28.20 (C5-j), 28.08 (C5-n), 27.95 (C30/C34-n), 27.74 (C30/C34-j), 27.16 (C24a-n), 27.08 (C24a-j), 26.28 (C24b-n), 26.20 (C24b-j), 23.74 (C24c-j), 23.65 (C24c-n), 23.51 (C24d-j), 23.47 (24d-n), 21.23 (C9-j), 21.09 (C8-n), 21.02 (C9-n), 20.42 (C8-j), 12.83 (C10-j), 12.77 (C10-n). **FT-IR** ν/cm^{-1} (intensity): 2956 (w), 2928 (w), 2870 (w), 1672 (s), 1626 (w), 1578 (s), 1541 (w), 1515 (s), 1458 (w), 1386 (s), 1354 (w), 1265 (w), 1157 (w), 1019 (w), 933 (w), 804 (w), 739 (w). **ESI-MS**: Found [M - acac]$^+$ 626.2570. $[C_{32}H_{46}N_3O_3Pd]^+$ requires 626.2574. **Micro-analysis** (%): Found C, 60.74; H, 7.58; N, 5.79. Calc. for $C_{37}H_{53}N_3O_5Pd$ C, 61.19; H, 7.36; N, 5.79.

Pt(2.4 - H)(*O,O'*-acac) and **Pt(2.4)(*O,O'*-acac)(γC-acac)**

In an oven dried Schlenk tube **2.4.HCl** (0.0910 g, 0.199 mmol) and $Pd(DMSO)_2Cl_2$ (0.0853 g, 0.202 mmol) were combined and the vessel sparged with nitrogen. Dry DMSO (3mL) was added by syringe and the solution heated at 80 ^oC. Finely powdered, oven dried K_2CO_3 (0.138 g, 1.00 mmol) was added under flowing nitrogen and allowed to react for 1 hour before adding sodium-acetylacetonate (0.0366 g, 0.300 mmol). The temperature was elevated to 110 ^oC and reacted for 4 hours before cooling to room temperature and stirring overnight. The brown suspension was taken up in DCM (20 mL), filtered through celite then washed with water (3 x 10 mL) and brine (2 x 10 mL) before drying over $MgSO_4$ and removing the solvent by rotary evaporation. The light brown residue was dissolved in a minimum of Et_2O and Pt(**2.4 - H**)(*O,O'*-acac) precipitated by the addition of pet-ether (30 mL). This was collected by filtration, air dried and obtained as a fine off-white powder of satisfactory purity. Crystals of Pt(**2.4 - H**)(*O,O'*-acac) suitable for X-ray diffraction were grown by slow vapour diffusion of pentane into a toluene solution of the compound. Rotary evaporation of the pet-ether filtrate provided adequately pure compound Pt(**2.4**)(*O,O'*-acac)(γC-acac) as a faint yellow powder. An extremely pure sample for analysis was obtained by dissolving a small portion of the compound in MeCN

and extracting into pentane. Evaporation of the pentane extract gave Pt(**2.4**)(*O,O'*-acac)(γC-acac) as a white, microcrystalline solid.

Pt(2.4 - H)(*O,O'*-acac)

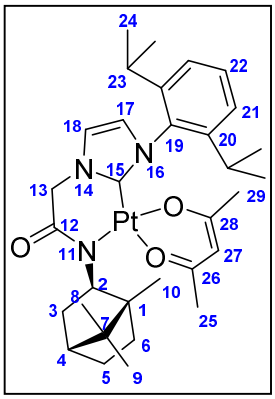

Yield, 0.0310 g (22%). **MP**: Decomposition onset at 208 °C. **^{1}H NMR** (400 MHz, $CDCl_3$): δ 7.36 (1H, m, H22), 7.22 (1H, m, H21a), 7.15 (1H, d, J = 7.0 Hz, H21b), 7.08 (1H, s, H16), 6.72 (1H, s, H15), 5.13 (1H, s, H27), 4.89 (1H, d, J = 15.3 Hz, 13a), 4.52 (1H, d, J = 15.3 Hz, 13b), 4.25 (1H, br.s, H2), 2.81 (1H, br.s, H3α), 1.77 (3H, s, H25/29), 1.71 – 1.55 (2H, m, H3β, H5α), 1.52 (1H, br.s, H4), 1.48 – 1.23 (6H, m, H6α, H23, H24a), 1.17 – 0.97 H5β, H6β, H24b, H25/H29), 0.84 (3H, s, H8), 0.78 (3H, br.s, H10), 0.71 (3H, s, H9). **^{13}C NMR** (100 MHz, $CDCl_3$): δ 183.56 (C26/C28), 182.64 (C26/C28), 171.56 (C12), 146.59 (C20a), 145.02 (C20b), 139.25 (C15), 134.52 (C19), 129.17 (C22), 123.95 (C17), 123.64 (C21a), 123.53 (C21b), 119.78 (C18), 101.18 (C27), 63.87 (C2), 55.50 (C13), 52.46 (C1/C7), 46.69 (C1/C7), 45.21 (C4), 40.14 (C3), 36.35 (C6), 28.25 (C24a), 28.13 (C24b), 27.51 (C5), 26.57 (C25/C29), 25.19 (C25/C29), 25.01 (C24c), 24.81 (C24d), 23.54 (C23a), 23.44 (c23b), 20.76 (C8/C9/C10), 20.69 (C8/C9/C10). **FT-IR** v/cm^{-1} (intensity): 2956 (w), 2927 (w), 2870 (m), 1574 (s), 1521 (s), 1458 (m), 1421 (m), 1383 (m), 1311 (w), 1289 (w), 1190 (w), 1057 (w), 936 (m), 802 (w), 726 (s), 698 (m). **ESI-MS**: Found $[MH]^+$ 715.3185. $[C_{32}H_{46}N_3O_3Pt]^+$ requires 715.3184.

Pt(2.4)(*O,O'*-acac)(γC-acac)

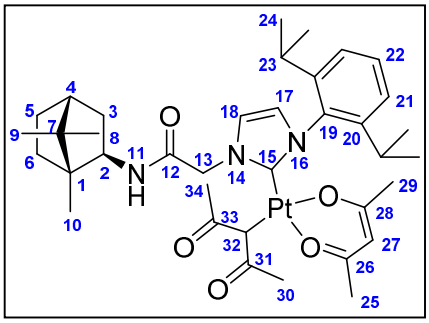

Yield 0.0957 g (59%). **MP**: 133 – 135 °C. **^{1}H NMR** (600 MHz, CD_3CN) δ 7.54 – 7.47 (1H, m H22), 7.42 – 7.29 (3H, H18, H21), 7.22 (0.7H, s, H17-j), 7.21 (0.3H, s, H17-n), 6.58 (0.7H, d, J = 7.6 Hz, H11-j), 6.43 (0.3H, d, J = 7.3 Hz, H11-n), 5.50 (0.7H, d, J = 15.8 Hz, H13a-j), 5.41 (1H, m, H27) 5.14 (0.3H, d, J = 16.1 Hz, H13a-n), 5.08 (0.3H, d, J = 16.1 Hz, H13b-n), 4.74 (0.7H, d, J = 15.8 Hz, H13b-j), 4.01 – 3.91 (1.4H,

m, H32-j, H2-j), 3.89 (0.3H, s, H32-n), 3.84 (0.3H, m, H2-n), 2.82 (1H, m, H23a), 2.77 – 2.64 (1H, m, H23b), 2.17 (3H, m, H30/H34), 2.04 (0.7H, m, H3α-j), 1.82 (0.3H, m, H3α-n), 1.79 - 1.50 (4H, m, H3β, H4, H5α, H6α), 1.32 - 1.13 (11H, m, H5β, H6β, H24a, H24b, H24c), 1.10 (3H, m, H30/H34), 0.98 (3H, m, H24d), 0.97 (2.1H, s, H8-j), 0.89 (1.8H, s, H8-n, H10-n), 0.88 (2.1H, s, H10-j), 0.83 (2.1H, s, H9-j), 0.82 (0.9H, s, H9-n). **^{13}C NMR** (150 MHz, CD_3CN): δ 210.38 (C31/C33-n), 209.89 (C31/C33-j), 209.72 (C31/C33-j), 209.07 (C31/C33-n), 185.6 (C26/C28-j), 185.55 (C26/C28-n) 185.25 (C26/C28-j), 185.19 (C26/C28-n), 167.49 (C12-j), 167.18 (C12-n), 148.46 (C20a-j), 148.44 (C20a-n), 148.19 (C15), 147.11 (C20b-j), 146.96 (C20b-n), 136.10 (C19-n), 136.02 (C19-j), 131.55 (C22-j), 131.50 (C22-n), 126.05 (C17-j), 125.75 (C17-n), 125.72 (C21a), 125.71 (C21b-j), 125.65 (C21b-n), 122.67 (C18-n), 122.56 (C18-j), 102.09 (C27-n), 102.06 (C27-j), 58.66 (C2-n), 58.37 (C2-j), 54.39 (C13-j), 53.75 (C13-n), 50.6 (C1/C7-j), 49.87 (C1/C7-n), 48.09 (C1/C7-j), 47.93 (C1/C7-n), 46.18 (C4), 40.07 (C32-j), 39.79 (C3-n), 39.52 (C32-n), 37.83 (C3-j), 37.36 (C6-n), 37.12 (C6-j), 30.25 (C30/C34), 30.17 (C30/C34), 29.83 (C23a-j), 29.8 (C23a-n), 29.53 (C23b-n), 29.48 (C23b-j), 29.42 (C30/C34-n), 28.38 (C20/C34-j), 28.16 (C5-j), 28.02 (C5-n), 27.97 (C24a-n), 27.75 (C24a-j), 27.27 (C24b-n), 27.16 (C24b-j), 23.44 (C24c-j), 23.39 (C24c -n), 23.22 (C24d-j), 23.14 (C24d-n), 21.17 (C9-j), 21.05 (C8-n), 20.96 (C9-n), 20.39 (C8-j), 12.78 (C10-j), 12.69 (C10-n). **FT-IR** ν/cm^{-1} (intensity): 2957 (w), 2937 (w), 2872 (m), 1674 (s), 1641 (m), 1575 (m), 1520 (s), 1389 (m), 1353 (m), 1273 (w), 1242 (m), 1021 (w), 934 (m), 801 (m), 741 (w), 616 (w). **ESI-MS**: Found $[MH]^+$ 815.3714. $[C_{37}H_{53}N_3O_5Pt]^+$ requires 815.3711. **Micro-analysis** (%): Found C, 54.33; H, 6.87; N, 4.80. Calc. for $C_{37}H_{53}N_3O_5Pt$ C, 54.53; H, 6.56; N, 5.16.

Pd(2.4)(allyl)Cl

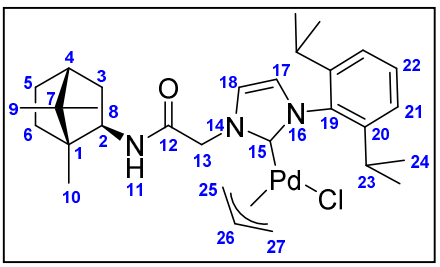

In a Schlenk tube, **2.4.HCl** (0.0916 g, 0.200 mmol) and Ag_2O (0.0255 g, 0.110 mmol) were combined under nitrogen. DCM (5 mL) was added and the suspension stirred in the absence of light for 48 hours. A solution of $[Pd(allyl)Cl]_2$ (0.0366 g, 0.100 mmol) in DCM (2 mL) was added to the cloudy white solution and stirring continued for a further 20 hours. The white suspension was filtered through a celite pad and the

solvent removed by rotary evaporation providing Pd(**2.4**)(allyl)Cl in a pure form as a fluffy, faint yellow solid. Yield 0.102 g (82%). **MP:** 89 – 96 °C**. ^{1}H NMR** (400 MHz, DMSO-*d6*): δ 7.60 – 7.38 (4H, m, H11, H17, H18, H22), 7.26 (1H, d, J = 7.8 Hz, H21), 5.16 (1H, d, J = 15.7 Hz, H13a), 4.97 (2H, m, H13b, H26), 3.81 (1H, d, J = 7.4 Hz, H27syn), 3.72 (1H, m H2), 2.76 (1H, d, J = 13.3 Hz, 27anti), 2.60 (2H, br.s, H23), 1.65 (4H, br.s, H3α, H3β, H4, H5α), 1.47 (1H, m, H6α), 1.18 (6H, d, J = 6.3 Hz, H24a), 1.09 (2H, m, H5β, H6β), 0.99 (6H, d = 6.3 Hz, 24b), 0.85 (3H, s, H8), 0.74 (3H, s, H10), 0.71 (3H, s, H9). **^{13}C NMR** (100 MHz, DMSO-*d6*): δ 182.22 (C15), 167.09 (C12), 146.29 (C20), 136.18 (C19), 130.09 (C22), 125.23 (C17), 123.94 (C21a), 123.86 (C21b), 123.17 (C18), 114.79 (C26), 71.22 (C27), 56.77 (C2), 53.58 (C13), 49.22 (C25, C7), 46.85 (C1), 44.69 (C4), 37.37 (C3), 36.09 (C6), 28.02 (C23), 27.14 (C5), 26.31 (C18a), 23.11 (C18b), 23.03 (C18c), 20.76 (C9), 20.34 (C8), 11.9 (C10). **FT-IR** ν/cm^{-1} (intensity): 3264 (w), 2956 (m), 2872 (w), 1672 (s), 1536 (m), 1458 (m), 1411 (w), 1384 (w), 1363 (w), 1220 (w), 1179 (w), 935 (w), 804 (m), 762 (m), 733 (w), 690 (m). **ESI-MS:** Found $[M - Cl]^+$ 568.2533. $[C_{30}H_{44}N_3OPd]^+$ requires 568.2519.

Pd(2.5)Cl$_2$

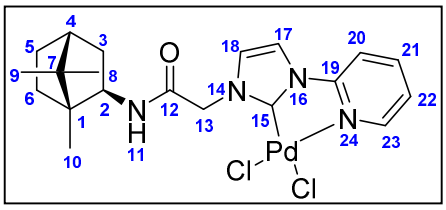

In a Schlenk tube, **2.5.HCl** (0.0760 g, 0.200 mmol) and Ag_2O (0.0255 g, 0.110 mmol) were combined under nitrogen. DCM (5 mL) was added and the suspension stirred in the absence of light for 20 hours. A solution of $Pd(PhCN)_2Cl_2$ (0.0767 g, 0.200 mmol) in DCM (2 mL) was added to the cloudy white solution and stirring continued for a further 12 hours. The light yellow suspension was filtered through a celite pad and the solvent removed by rotary evaporation. The light brown residue was rinsed with Et_2O (20 mL) then water (30 mL) and dried in a desiccator under vacuum. It was purified further by bulk slow vapour diffusion of toluene into a MeCN solution of the compound. The resultant white microcrystalline deposit was collected by filtration and washed with acetone giving Pd(**2.5**)Cl_2 as an off-white powder. Yield 0.077 g (75%). **MP**: Decomposition onset at 250 °C. **^{1}H NMR** (400 MHz, DMSO-*d6*): δ 9.21 (1H, br.s, H23), 8.37 (2H, m, H17, H21), 8.15 (1H, d, J = 8.2 Hz, H20), 7.63 (1H, t, J = 6.7 Hz, H22), 7.53 (2H, m, H18, H11), 5.68 (1H, d, J = 16.2 Hz, H13a), 5.30 (1H, d, J = 16.2 Hz, H13b), 3.71 (1H, m, H2), 1.68 (4H, m, H3α,

H3β, H4, H5α), 1.49 (1H, m, H6α), 1.11 (2H, m, H5β, H6β), 0.95 (3H, s, H8), 0.81 (3H, s, H10), 0.79 (3H, s, H9). **^{13}C NMR** (100 MHz, DMSO-*d6*): δ 165.66 (C12), 153.78 (C15), 151.38 (C19), 149.18 (C23), 142.99 (C21), 126.35 (C18), 123.08 (C22), 116.11 (C17), 112.32 (C20), 56.71 (C2), 51.77 (C13), 48.89 (C7), 46.46 (C1), 44.29 (C4), 37.26 (C3), 35.77 (C6), 26.75 (C5), 20.38 (C9), 20.12 (C8), 11.77 (C10). **FT-IR** ν/cm^{-1} (intensity): 3326 (w), 3101 (w), 2948 (w), 2876 (w), 1665 (s), 1615 (w), 1530 (m), 1492 (s), 1459 (m), 1383 (m), 1333 (m), 1245 (w), 1141 (w), 1101 (w), 780 (s), 717 (s), 687 (w). **ESI-MS:** Found $[MH]^+$ 230.1263, $[2M + H]^+$ 459.2466. $[C_{12}H_{21}NOCl]^+$ requires 230.1312, $[C_{24}H_{41}N_2O_2Cl_2]^+$ requires 459.2545.

[Ru(2.2)(*p*-cymene)Cl][PF$_6$]

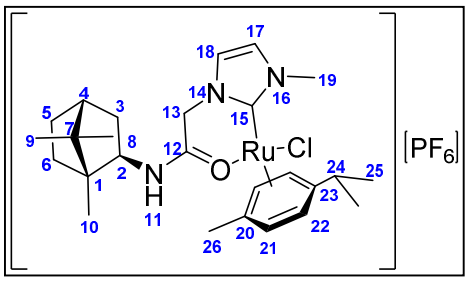

In a Schlenk tube and in the absence of light, Ag(**2.2**)Cl (0.0912 g, 0.218 mmol) was dissolved in DCM (5mL) under an argon atmosphere. A solution of [Ru(*p*-cymene)Cl$_2$]$_2$ (0.0726 g, 0.119 mmol) in DCM (3 mL) was added and the resulting turbid mixture stirred in darkness for 24 hours. The orange suspension was filtered through a celite pad and the solvent removed by rotary evaporation. Adequately pure [Ru(**2.2**)(*p*-cymene)Cl]Cl was recovered by this method (Yield 0.164 g, 89%). The brown solid was purified further by dissolving in water (5 mL) and precipitating it as a PF_6 salt by addition of saturated KPF_6 solution. The solid was collected by filtration, washed with water then Et_2O and dried in a vacuum desiccator to give pure [Ru(**2.2**)(*p*-cymene)Cl][PF_6] as a fine orange/yellow powder. Yield 0.113 g (75%). **MP:** 256 – 258 °C. **^{1}H NMR** (400 MHz, $CDCl_3$): δ 7.25 (4H, m, H11, H18), 7.07 (2H, s, H17), 5.63 (3H, m, H22), 5.58 (1H, d, J = 5.6 Hz, H22), 5.40 (1H, d, J = 5.4 Hz, H21), 5.36 (1H, d, J = 5.4 Hz, H21), 5.25 (2H, d, J = 5.9 Hz, H21), 5.12 (2H, d, J = 16.0 Hz, H13a), 4.60 (2H, d, J = 16.0 Hz, H13b), 3.89 (2H, s, H19), 3.88 (3H, s, H19), 3.81 (3H, s, H2), 2.92 (2H, sept, J = 7.0, H24), 2.15 (6H, s, H26), 1.96 – 1.46 (10H, m, H3α, H3β, H4, H5α, H6α), 1.33 (12H, m, H25), 1.25 – 1.04 (4H, m, H5β, H6β), 0.98 (3H, s, H10a), 0.93 (3H, s, H8b) 0.91 (3H, s, H8a), 0.83 (3H, s, H9a), 0.79 (3H, s, H9b), 0.74 (3H, s, H10b). **^{13}C NMR** (100 MHz, $CDCl_3$): δ 175.24 (C15), 175.00 (C15), 170.00 (C12), 169.92 (C12), 123.5 (C17), 123.38 (C18), 123.25 (C18),

111.11 (C23), 110.80 (C23), 100.03 (C20), 99.61 (C20), 86.26 (C22), 85.92 (C22), 84.99 (C22), 80.48 (C21), 80.37 (C21), 80.00 (C21), 79.94 (C21), 59.54 (C2), 59.27 (C2), 51.73 (C13), 51.64 (C13), 49.33 (C7a), 48.68 (C7b), 47.15 (C1), 47.12 (C1), 44.84 (C4), 44.76 (C4), 38.37 (C3), 37.95 (C19), 37.92 (C19), 37.65 (C3), 36.18 (C6), 36.06 (C6), 31.48 (C24), 26.97 (C5), 26.84 (C5), 23.53 (C24), 23.23 (C24), 21.84 (C24), 21.48 (C24), 20.18 (C9), 20.09 (C9), 19.66 (C8), 19.62 (C8). 19.08 (C26), 19.06 (C26), 11.46 (C10), 11.40 (C10). **FT-IR** v/cm^{-1} (intensity): 2956 (w), 2875 (w), 1614 (s), 1557 (m), 1459 (m), 1390 (w), 1345 (w), 1243 (w), 1192 (w), 1115 (w), 832 (s), 737 (m), 681 (m). **ESI-MS:** Found $[M]^+$ 546.1817. $[C_{26}H_{39}N_4OClRu]^+$ requires 546.1820.

8.3. Chapter 3

8.3.1. Cyclohexyl-acetamide (CyA) derivatives

1-methyl-3-[*N*-(cyclohexyl)acetamido]-imidazolium hexafluorophosphate (3.2.HPF$_6$)

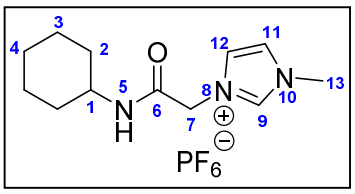

In an oven dried Schlenk flask, 1-methyl-imidazole (1.60 mL, 20.0 mmol) was added to a stirred solution of 2-chloro-N-cyclohexylacetamide (**3.1**) (1.755 g, 9.99 mmol) in MeCN (50 mL). The system was flushed with nitrogen and heated at reflux for 48 hours. The reaction mixture was allowed to cool and the solvent removed by rotary-evaporation. The resultant residue was dissolved in water (50 mL) and a tacky white solid was deposited following addition of excess KPF_6 solution. After decanting off the supernatant and washing with additional portions of water the residue was dissolved in a minimum of MeCN and transferred to a 250 mL round-bottom flask before removing the solvent and drying under high-vacuum. The colourless oily residue was triturated in 150 mL chloroform with vigorous stirring. After 2 hours **3.2.HPF$_6$** had become a white crystalline solid which was collected by filtration and rinsed with chloroform then Et_2O. Yield 1.750 g (48%). **MP:** 64 °C. **^{1}H NMR** (400 MHz, DMSO-*d6*): δ 9.04 (1H, s, H9), 8.29 (1H, d, J = 7.0 Hz, H5), 7.66 (2H, s, H11, H12), 4.92 (2H, s, H7), 3.88 (3H, s, H13), 3.55 (1H, br.s, H1), 1.87 – 1.61 (4H, m, H2*e*, H3*e*), 1.55 (1H, d, J = 11.0, H4*e*),

1.35 – 1.08 (17H, m, H2*a*, H3*a*, H4*a*). **^{13}C NMR** (100 MHz, DMSO-*d6*): δ 163.65 (C6), 137.67 (C9), 123.76 (C12), 124.42 (C15), 122.91 (C11), 50.47 (C7), 48.06 (C1), 35.77 (13), 32.23 (C2), 25.07 (C4), 24.32 (C3). **FT-IR** ν/cm^{-1} (intensity)**:** 3287 (w), 2942 (w), 2856 (w), 1657 (m), 1567 (m), 1450 (w), 1375 (w), 1276 (w), 1176 (m), 954 (w), 826 (s), 719 (m), 624 (m), 583 (w), 555 (s). **ESI-MS:** Found $[M]^+$ 222.1608. $[C_{12}H_{20}N_3O]^+$ requires 222.1606.

1-(2,6-diisopropyl)phenyl-3-[*N-exo*-(cyclohexyl)acetamido]-1*H*-imidazolium chloride (3.3.HCl)

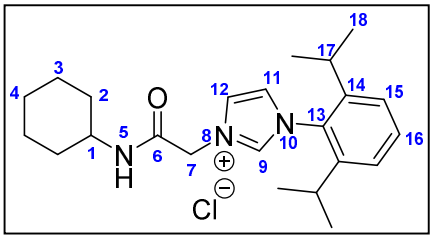

In an oven dried Schlenk flask 1-(2,6-diisopropyl)-imidazole (1.259 g, 5.51 mmol) was added to a stirred solution of 2-chloro-N-cyclohexylacetamide (**3.1**) (0.880 g, 5.03 mmol) in DMF (20 mL). The system was flushed with nitrogen and heated at 100 °C for 48 hours. The reaction mixture was allowed to cool and the solvent removed by rotary-evaporation. The resultant residue was dissolved in a minimum amount of DCM and added dropwise to stirring Et_2O (150 mL). The resulting green/grey gelatinous solid was collected by filtration and allowed to air dry. The crude material was purified by recrystallisation from acetone giving **3.3.HCl** as a white microcrystalline solid. Yield 1.410 g (69%). **MP**: 259 °C. **^{1}H NMR** (400 MHz, DMSO-*d6*): δ 99.65 (1H, s, H9), 8.88 (1H, d, J = 6.7 Hz, H5), 8.10 (1H, s, H12), 8.06 (1H, s, H11), 7.62 (1H, t, J = 7.8 Hz, H16), 7.45 (2H, d, J = 7.8 Hz, H15), 5.17 (2H, s, H7), 3.59 (1H, br.s, H1), 2.31 (2H, sept, J = 6.7 Hz, H17), 1.86 – 1.62 (4H, m, H2*e*, H3*e*), 1.55 (1H, d, J = 11.0 Hz, H4*e*), 1.41 – 1.01 (17H, m, H2*a*, H3*a*, H4*a*, H18). **^{13}C NMR** (100 MHz, DMSO-*d6*): δ 163.56 (C6), 145.19 (C14), 139.25 (C9), 131.51 (C16), 130.59 (C13), 124.60 (C12), 124.42 (C15), 124.30 (C11), 51.13 (C7), 48.21 (C1), 32.29 (C2), 28.04 (C17), 25.15 (C4), 24.40 (C3), 23.86 (C18a), 23.80 (C18b). **FT-IR** ν/cm^{-1} (intensity)**:** 3186 (w), 3035 (w), 2961 (m), 2922 (m), 1672 (s), 1560 (s), 1544 (m), 1459 (w), 1365 (w), 1315 (w), 1254 (m), 1188 (w), 1066 (m), 944 (w), 807 (s), 761 (m). **ESI-MS**: Found $[M]^+$ 368.2693, $[2M+Cl]^+$ 771.5085. $[C_{23}H_{34}N_3O]^+$ requires 368.2702, $[C_{46}H_{68}N_6O_2]^+$ requires 771.5092.

1-(2-pyridyl)-3-[*N-exo*-(cyclohexyl)acetamido]-1*H*-imidazolium chloride (3.4.HCl)

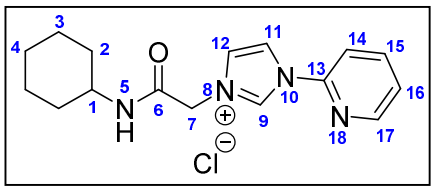

In an oven dried Schlenk tube 1-(2-pyridyl)-imidazole (0.800 g, 5.51 mol) was added to a stirred solution of 2-chloro-N-cyclohexylacetamide (**3.1**) (0.888 g, 5.06 mmol) in DMF (10 mL). The system was flushed with nitrogen and heated at 100 °C for 24 hours. The reaction mixture was allowed to cool and the solvent removed by rotary-evaporation. The resultant residue was stirred vigorously with Et_2O (50 mL) for 1 hour then the off white solid collected by filtration. Washing with acetone give the pure **3.4.HCl** as a white powder. Yield 1.079 g (67%). **MP**: 212 °C. **^{1}H NMR** (400 MHz, DMSO-*d6*): 10.15 (1H, s, H9), 8.67 (1H, d, J = 7.0 Hz, H17), 8.63 (1H, d, J = 4.3 Hz, H5), 8.54 (1H, s, H11), 8.19 (1H, m, H15), 8.07 (1H, d, J = 8.2Hz, H14), 7.92 (1H, s, H12), 7.62 (1H, dd, J = 7.0 Hz, 5.1Hz, H16), 5.11 (2H, s, H7), 3.55 (1H, br.s, H1), 1.83 – 1.60 (4H, m, H2*e*, H3*e*), 1.52 (1H, d, J = 11.3 Hz, H4*e*), 1.33 – 1.07 (5H, m, H2*a*, H3*a*, H4*a*). **^{13}C NMR** (100 MHz, DMSO-*d6*): δ 163.36 (C6), 149.27 (C17), 146.68 (C13), 140.66 (C15), 136.14 (C9), 125.29 (C12), 125.12 (C16), 118.60 (C11), 114.28 (C14), 51.15 (C7), 48.16 (C1), 32.21 (C2), 25.11 (C4), 24.33 (C3). **FT-IR** ν/cm^{-1} (intensity)**:** 3213 (w), 3048 (m), 2929 (w), 2850 (w), 1690 (s), 1603 (m), 1538 (s), 1478 (m), 1446 (m), 1345 (w), 1282 (m), 1232 (m), 1056 (s), 788 (m), 715 (m). **ESI-MS:** Found $[M]^+$ 285.1704. $[C_{16}H_{21}N_4O]^+$ requires 285.1715.

8.3.2. NHC complexes of cyclohexyl-acetamide derivatives

Pd(3.3 - H)(*O,O'*-acac)

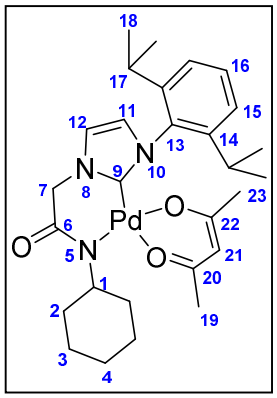

In an oven dried Schlenk tube **3.3.HCl** (0.204 g, 0.505 mmol) and $PdCl_2$ (0.887 g, 0.499 mmol) were combined and the vessel sparged with nitrogen. Dry MeCN (8 mL) was added by syringe and the solution heated at reflux until the $PdCl_2$ had dissolved. Finely powdered, oven dried K_2CO_3 (0.346 g, 2.50 mmol) was added under flowing nitrogen and allowed to react for 1 hour before adding acetylacetone (51.3 µL, 0.500 mmol). Heating was continued for 4 hours before cooling to room temperature and stirring overnight. The off-white mixture was filtered and the solvent removed under vacuum. The resultant residue was stirred in pentane then filtered and the collected solid rinsed with water then quickly with MeCN to give Pd(**3.3 - H**)(*O,O'*-acac) as a fine white powder. Crystals suitable for X-ray diffraction were grown by slow evaporation of an Et_2O solution. Yield 0.145 g (46%). **MP**: Decomposition onset at 198 °C. **^{1}H NMR** (400 MHz, $CDCl_3$): δ 7.35 (1H, t, J = 7.4 Hz, H16), 7.20 (2H, d, J = 7.4 Hz, H15), 7.10 (1H, s, H12), 6.75 (1H, s, H11), 5.07 (1H, s, H21), 4.75 (2H, s, H7), 3.39 (1H, m, H1), 2.89 (2H, m, H17), 2.12 – 1.96 (2H, m, H2*e*), 1.88 (3H, s, H19), 1.82 – 1.61 (4H, m, H2*a*, H3*e*), 1.54 (1H, d, J = 12.1 Hz, H4*e*), 1.44 – 1.18 (8H, m, H3*a*, H18*a*), 1.14 (3H, s, H23), 1.07 (7H, m, H4*a*, H18b). **^{13}C NMR** (100 MHz, $CDCl_3$): δ 183.87 (C22), 185.40 (C20), 168.01 (C6), 145.31 (C9), 134.58 (C14), 134.58 (C13), 129.28 (C16), 123.81 (C15), 123.68 (C11), 120.88 (C12), 99.82 (C21), 58.76 (C1), 57.81 (C7), 32.52 (C2), 28.41 (C17), 26.53 (C19), 26.50 (C3), 26.20 (C4), 25.35 (C23), 24.99 (C18b), 23.50 (C18a). **FT-IR** ν/cm^{-1} (intensity): 3121 (w), 3093 (w), 2963 (w), 2927 (w), 2849 (m), 1575 (s), 1543 (s), 1519 (s), 1428 (s), 1317 (w), 1297 (w), 1271 (w), 1024 (w), 937 (m), 815 (w), 776 (w), 767 (w), 743 (m), 689 (w). **ESI-MS**: Found $[MH]^+$ 572.2117. $[C_{28}H_{40}N_3O_3Pd]^+$ requires 572.2110.

Pt(3.3 - H)(*O,O'*-acac)

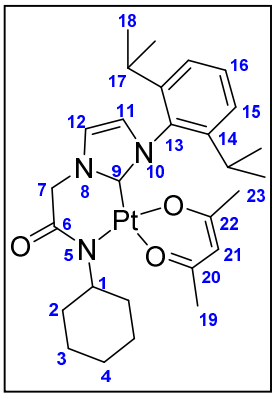

In an oven dried Schlenk tube **3.3.HCl** (0.202 g, 0.500 mmol) and $Pt(DMSO)_2Cl_2$ (0.211 g, 0.500 mmol) were combined and the vessel sparged with nitrogen. Dry DMSO (5 mL) was added by syringe and the solution heated to 100 °C. Finely powdered, oven dried K_2CO_3 (0.420 g, 3.00 mmol) was added under flowing nitrogen and allowed to react for 1 hour before adding acetylacetone (51.3 µL, 0.500 mmol). Heating was continued for 4 hours before cooling to room temperature and stirring overnight. The off-white suspension was then poured onto 40 mL of DCM and filtered through a celite pad. The filtrate was washed with water (2 x 20 mL) then brine (2 x 20 mL), dried over $MgSO_4$ and the solvent removed by rotary-evaporation. The off-white residue was washed quickly with cold MeCN and filtered giving Pt(**3.3 - H**)(*O,O'*-acac) as a fine white powder. Crystals suitable for X-ray diffraction were grown by slow evaporation of an Et_2O solution. Yield 0.156 g (47%). **MP**: Decomposition onset at 215 °C. **^{1}H NMR** (400 MHz, $CDCl_3$): δ 7.35 (1H, t, J = 7.8 Hz, H16), 7.19 (2H, d, J = 7.8 Hz, H15), 7.09 (1H, s, H12), 6.73 (1H, s, H11), 5.16 (1H, s, H21), 4.70 (2H, s, H7), 3.52 (1H, m, H1), 2.92 (2H, m, H17), 2.06 (2H, m, H2*e*), 1.83 (3H, s, H19), 1.70 (4H, m, H2*a*, H3*e*), 1.56 (1H, d, J = 12.1 Hz, H4*e*), 1.25 (8H, m, H3*a*, H18*a*), 1.08 (10H, m, H4*a*, H18b, H23). **^{13}C NMR** (100 MHz, $CDCl_3$): δ 183.59 (C22), 183.55 (C20), 167.73 (C6), 145.61 (C14), 138.8 (C9), 134.54 (C13), 129.20 (C16), 123.64 (C15), 123.07 (C11), 120.40 (C12), 101.52 (C21), 59.57 (C1), 56.85 (C7), 32.44 (C2), 28.35 (C17), 26.61 (C19), 26.54 (C3), 26.24 (C4), 25.38 (C23), 25.01 (C18b), 23.38 (C18a). **FT-IR** ν/cm^{-1} (intensity)**:** 3123 (w), 3093 (w), 2962 (w), 2928 (w), 2871 (m), 1598 (m), 1574 (s), 1551 (m), 1524 (s), 1390 (s), 1298 (w), 1255 (w), 1153 (w), 1028 (w), 939 (m), 807 (w), 780 (m), 741 (m), 699 (m). **ESI-MS**: Found $[MH]^+$ 661.2710. $[C_{28}H_{40}N_3O_3Pt]^+$ requires 661.2714.

Pd(3.3)(allyl)Cl

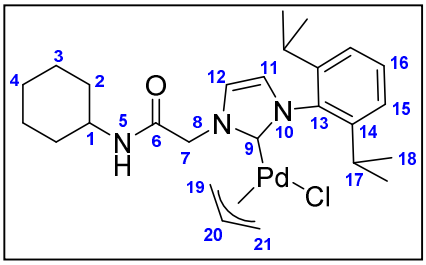

In an oven dried Schlenk tube **3.3.HCl** (0.108 g, 0.268 mmol) and Ag_2O (0.0311 g, 0.134 mmol) were combined under nitrogen. DCM (5 mL) was added and the suspension stirred in the absence of light for 48 hours. A solution of $[Pd(allyl)Cl]_2$ (0.0490 g, 0.134 mmol) in DCM (2 mL) was added to the cloudy white solution and stirring continued for a further 20 hours. The white suspension was filtered through a celite pad and the solvent removed by rotary evaporation. This gave the desired complex Pd(**3.3**)(allyl)Cl in a pure form as a fluffy, faint yellow solid. Yield 0.115 g (78%). **MP**: Decomposition onset at 165 °C. **^{1}H NMR** (400 MHz, DMSO-*d6*): δ 8.03 (1H, d, J = 7.4 Hz, H5), 7.49 (1H, s, H12), 7.45 (1H, s, H11), 7.42 (1H, t, J = 7.8 Hz, H16), 7.26 (2H, d, J = 7.8 Hz, H15), 4.97 (3H, m, H7, H20), 3.79 (1H, d, J = 7.4 Hz, H21syn), 3.52 (1H, m, H1), 2.76 (1H, d, J = 13.7 Hz, H21anti), 2.61 (2H, br.s, H17), 1.67 (4H, m, H2e/H3e), 1.51 (1H, d, J = 11.7 Hz, H4e), 1.39 – 1.07 (14H, m, H2a, H3a, H4a, H18a), 1.00 (6H, d, J = 6.7 Hz, H8b). **^{13}C NMR** (100 MHz, DMSO-*d6*): δ 182.15 (C9), 166.20 (C6), 146.23 (C14), 136.22 (C13), 130.04 (C16), 124.96 (C11), 123.87 (C15), 123.55 (C12), 114.75 (C20), 71.01 (C21), 53.24 (C7), 49.30 (C19), 48.11 (C1), 32.71 (C2), 27.99 (C17), 26.28 (C18b), 25.60 (C4), 24.82 (C3), 23.06 (18a). **FT-IR** ν/cm^{-1} (intensity)**:** 3292 (w), 2963 (w), 2933 (m), 2856 (w), 1651 (s), 1544 (m), 1469 (m), 1446 (m), 1413 (m), 1363 (w), 1255 (m), 1224 (w), 1153 (w), 959 (w), 892 (w), 804 (w), 763 (w), 735 (w), 704 (w), 690 (w). **ESI-MS:** Found $[M - Cl]^+$ 514.2055. $[C_{26}H_{38}N_3OPd]^+$ requires 514.2050.

8.4. Chapter 4

8.4.1. Imidazo[4,5-f][1,10]phenanthroline (IP) derivatives

1-benzyl-imidazo[4,5-*f*][1,10]phenanthroline (4.2)

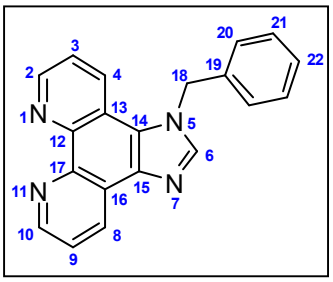

In an oven dried Schlenk tube imidazo[4,5-*f*][1,10]phenanthroline (**4.1**) (0.440 g, 2.00 mmol) and oven dried K_2CO_3 (0.830 g 6.00 mmol) were combined and anhydrous DMF (8 mL), and benzylbromide (0.35 mL, 2.94 mmol) added by syringe. A condenser was fitted and the system sparged with argon. The reaction was heated at 100 °C for 48 hours then allowed to cool to room-temperature. DCM (20 mL) was added to the dark brown mixture which was then filtered, washed with additional DCM (20 mL) and the combined organic filtrates washed with water (3 x 20 mL). The organic phase was then extracted with HCl solution (0.5 M, 3 x 20 mL). The combined light yellow acid extracts were neutralised with solid K_2CO_3 and extracted back into DCM (3 x 25 mL). The combined organic extracts were dried over $MgSO_4$, the solvent removed and the oily residue washed with Et_2O and filtered giving **4.2** as a fine, light peach powder. Yield 0.288 g (47%). **MP**: 195 – 197 °C **^{1}H NMR** (400 MHz, DMSO-*d6*): δ 9.03 (1H, d, J = 3.3 Hz, H10), 8.93 (2H, m, H8, H2), 8.57 (1H, s, H6), 8.51 (1H, d, J = 8.6 Hz, H4), 7.82 (1H, dd, J = 7.8 Hz, 4.3 Hz, H9), 7.62 (1H, dd, J = 8.6 Hz, 4.3 Hz, H3), 7.31 (2H, t, J = 7.4 Hz, H21), 7.24 (1H, t, J = 7.1 Hz, H22), 7.12 (2H, d, J = 7.4 Hz, H20), 6.05 (2H, s, H18). **^{13}C NMR** (100 MHz, DMSO-*d6*): δ 148.76 (C10), 147.89 (C2), 145.60 (C6), 144.16 (C12), 144.00 (C17), 137.22 (C15), 137.09 (C19), 130.03 (C8), 129.71 (C4), 129.43 (C21), 128.14 (C22), 126.44 (C20), 124.26 (C16), 124.21 (C14), 124.15 (C9), 123.1 (C3), 119.77 (C13), 50.3 (C18). **ESI-MS**: Found $[MH]^+$ 311.1294, $[C_{20}H_{15}N_4]^+$ requires 311.1297. **UV-vis** (DCM) λmax/nm (ε, 10^3 $M^{-1}cm^{-1}$): 252 (25.8), 283 (13.1), 340 (1.1), 353 (0.8). **Fluorometry** (DCM) λmax: 388 nm.

1-phenyl-imidazo[4,5-*f*][1,10]phenanthroline (4.3)

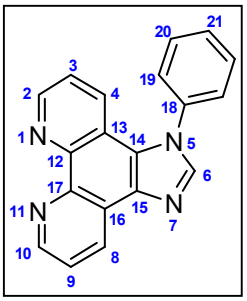

In an oven dried Schlenk tube imidazo[4,5-*f*][1,10]phenanthroline (**4.1**) (0.440 g, 2.0 mmol) and oven dried K_2CO_3 (0.607 g, 4.00 mmol) were combined and anhydrous DMF (5 mL), and iodobenzene (1.12 mL, 10.0 mmol) added by syringe. A condenser was fitted and the system sparged with argon. The reaction was heated to reflux for one hour then $Cu(OAc)_2.H_2O$ (0.040 g 0.20 mmol) was added under an argon blanket causing the yellow suspension to bubble vigorously and turn dark brown. Refluxing was continued for 48 hours then upon cooling to room temperature solid EDTA.2Na (0.101 g, 0.300 mmol) was added and the mixture stirred briefly before pouring onto DCM (40 mL). The mixture was filtering through a celite pad and rinsed through with additional DCM (10 mL). The organic filtrate was washed with water (30 mL) and brine (30 mL), then condensed by rotary evaporation. The oily dark brown residue was purified by column chromatography (alumina, 2% MeOH/DCM) to give **4.3** as a fine off white powder. Yield 0.352 g (60%). **MP**: 225 – 227 ^oC. **^{1}H NMR** (500 MHz, CD_3OD): δ 9.04 (1H, dd, J = 4.4 Hz, 1.7 Hz, H10), 8.97 (1H, dd, J = 8.2 Hz, 1.6 Hz, H8), 8.93 (1H, dd, J = 4.4 Hz, 1.5 Hz, H2), 8.38 (1H, s, H6), 7.83 (1H, dd, J = 8.0 Hz, 4.4 Hz, H9), 7.75 – 7.74 (3H, m, H20, H21), 7.72 – 7.70 (3H, m, H4, H19), 7.44 (1H, dd, J = 8.5 Hz, 4.2 Hz, H3). **^{13}C NMR** (125 MHz, CD_3OD): δ 148.23 (C10), 147.69 (C2), 143.83 (C17), 143.70 (C6), 143.45 (C12), 136.68 (C18), 135.50 (C15), 130.17 (C8, C21), 130.14 (19), 128.54 (C4), 127.04 (C20), 124.89 (C14), 123.74 (C9), 123.61 (C16), 122.43 (C3), 119.39 (C13). **ESI-MS**: Found $[MH]^+$ 297.1135, $[C_{19}H_{13}N_4]^+$ requires 297.1140. **UV-vis** (DCM) λmax/nm (ε, 10^3 $M^{-1}cm^{-1}$): 253 (32.6), 283 (11.2), 339 (1.0), 354 (0.7). **Fluorometry** (DCM) λmax: 388 nm.

1-(2-pyridyl)-imidazo[4,5-*f*][1,10]phenanthroline (4.4)

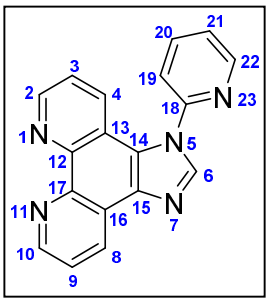

Synthesis performed as reported for **4.3** using imidazo[4,5-*f*][1,10]phenanthroline (**4.1**) (0.220 g, 0.999 mmol) and 2-bromo-pyridine (0.48 mL, 5.00 mmol). Column chromatography (alumina, 2% MeOH/DCM) provided **4.4** as a fine off white powder. Yield 0.134 g (45%). **MP**: 224 °C. **^{1}H NMR** (400 MHz, $CDCl_3$): δ 9.18 (1H, d, J = 4.3 Hz, H10), 9.10 (1H, d, J = 4.3 Hz, H2), 9.02 (1H, d, J = 7.9 Hz, H8), 8.77 (1H, d, J = 4.3 Hz, H22), 8.23 (1H, s, H6), 8.05 (1H, t, J = 7.4 Hz, H20), 7.93 (1H, d, J = 8.2 Hz, H4), 7.74 (1H, dd, J = 4.3 Hz, 8.3 Hz, H9), 7.60 (2H, m, H19, H21), 7.41 (1H, dd, J = 4.3 Hz, 8.3 Hz, H3). **^{13}C NMR** (100 MHz, $CDCl_3$): δ 150.17 (C22), 150.04 (C18), 149.20 (C10), 148.45 (C2), 144.95 (C12), 144.50 (C17), 144.62 (C6), 139.57 (C20), 137.54 (C15), 130.57 (C8), 129.49 (C4), 124.69 (C21), 124,39 (C14), 124.03 (C16), 123.60 (C9), 122.03 (C3), 120.21 (C19), 119.49 (C13). **ESI-MS**: Found $[MH]^+$ 298.1061, $[C_{18}H_{12}N_5]^+$ requires 298.1093. **UV-vis** (DCM) λmax/nm (ε, 10^3 $M^{-1}cm^{-1}$): 282 (15.8), 337 (0.7), 368 (0.4). **Fluorometry** (DCM) λmax: 388 nm.

1-phenyl-1*H*-imidazol[4,5*f*][1,10]phenanthrolin-(*N'/N"*-butyl)-ium Iodide (4.11.I/4.12.I)

In an oven dried pressure tube **4.3** (0.0988 g, 0.333 mmol) was dissolved in $MeNO_2$ (0.5 mL) and 1-iodiobutane (1.0 mL, 8.7 mmol) was added. The tube was sealed and heated at 150 °C for 3 hours. Upon returning to room temperature the dark orange solution was poured onto pet ether (30 mL) and the resultant bright yellow precipitate was collected by filtration and the products isolated by gradient flash chromatography (alumina, 2% - 5% MeOH/DCM). Evaporation of the appropriate fractions gave **4.11.I** and **4.12.I** as bright yellow powders. Several fractions bore a mixture of isomers which had a combined mass of 0.0513 g and an overall isomeric ratio of 1 : 2.2, **4.11.I** : **4.12.I**. Overall yield (**4.11.I** and **4.12.I**) 0.0849 g (53%).

1-phenyl-1*H*-imidazol[4,5*f*][1,10]phenanthrolin-(*N'*-butyl)-ium Iodide (4.11.I)

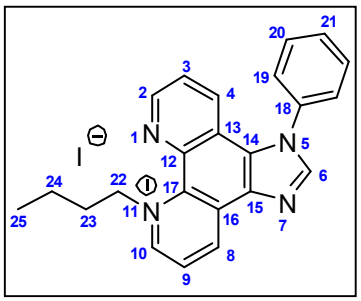

Isolated yield 0.0255 g (16%). **MP**: 188 °C. **^{1}H NMR** (400 MHz, $CDCl_3$): δ 10.33 (1H, d, J = 5.5 Hz, H10), 9.80 (1H, d, J = 8.3 Hz, H8), 9.11 (1H, d, J = 3.5 Hz, H2), 8.52 (1H, m, H9), 8.23 (1H, s, H6), 7.96 (1H, d, J = 8.2 Hz, H4), 7.75 (3H, m, H20, H21), 7.67 (1H, dd, J = 4.3H z, 8.7 Hz, H3), 7.59 (2H, m, H19), 6.16 (2H, m, H22), 2.15 (2H, m, H23), 1.65 (2H, m, H24), 1.02 (3H, m, H25). **^{13}C NMR** (100 MHz, $CDCl_3$): δ 150.85 (C10), 147.48 (C2), 145.06 (C6), 139.80 (C8), 138.67 (C12), 135.73 (C15), 134.63 (C17), 131.19 (C21), 130.99 (C20), 129.57 (C4), 128.49 (C16), 126.91 (C18, C19), 126.84 (C14), 125.73 (C9), 124.74 (C3), 122.56 (C13), 64.93 (C22), 33.96 (C23), 19.75 (C24), 13.84 (C25). **ESI-MS**: Found M^+ 353.1754, $[C_{23}H_{21}N_4]^+$ requires 353.1766. **UV-vis** (DCM) λmax/nm (ε, 10^3 $M^{-1}cm^{-1}$): 257 (31.4), 301 (30.5), 389 (3.0). **Fluorometry** (DCM) λmax: 482 nm.

1-phenyl-1*H*-imidazol[4,5*f*][1,10]phenanthrolin-(*N''*-butyl)-ium Iodide (4.12.I)

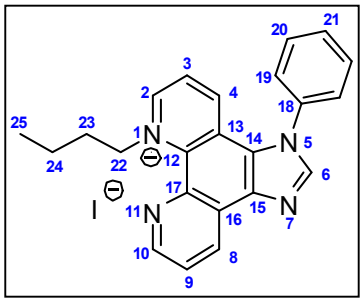

Isolated yield 0.0081 g (5%). **MP**: insufficient sample. **^{1}H NMR** (400 MHz, $CDCl_3$): δ 10.16 (1H, d, J = 5.9 Hz, H2), 9.27 (1H, dd, J = 8.3 Hz, 1.5 Hz, H8), 9.20 (1H, dd, J = 4.2 Hz, 1.7 Hz, H10), 8.45 (1H, d, J = 7.8 Hz, H4), 8.31 (1H, dd, J = 8.6 Hz, 5.9 Hz, H3), 8.25 (1H, s, H6), 7.97 (1H, dd, J = 8.2 Hz, 4.3 Hz, H9), 7.77 (3H, m, H20, H21), 7.58 (2H, m, H19), 6.16 (2H, t, J = 7.8 Hz, H22), 2.19 (2H, p, J = 7.8 Hz, H23), 1.65 (2H, m, H24), 1.05, (3H, t, J = 7.5 Hz, H25). **^{13}C NMR** (100 MHz, $CDCl_3$): δ 150.20 (C2), 148.05 (C10), 145.81 (C6), 136.59 (C4), 131.79 (C8), 131.42 (C21), 131.30 (C20), 126.86 (C19), 125.59 (C9), 125.30 (C3), 65.72 (C22), 33.91 (C23), 19.73 (C24), 13.75 (C25). **ESI-MS**: Found M^+ 353.1756, $[C_{23}H_{21}N_4]^+$ requires 353.1766. **UV-vis** (DCM) λmax/nm (ε, 10^3 $M^{-1}cm^{-1}$): 227 (23.2), 252 (22.1), 303 (17.4), 391 (1.6). **Fluorometry** (DCM) λmax: 499 nm.

1-Phenyl-3'-methyl-1*H*-imidazolium[4,5*f*][1,10]phenanthroline Iodide (4.9.HI)

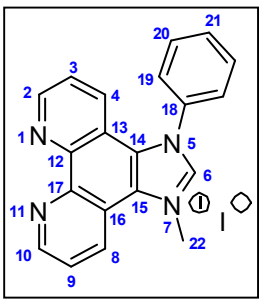

In an oven dried Schlenk tube **4.3** (0.149 g, 0.503 mmol) was dissolved in $MeNO_2$ (0.75 mL) under an argon atmosphere. Iodomethane (1.00 mL, 16.1 mmol) was added and the solution heated to reflux. After 20 hours a yellow suspension had formed which was cooled to room temperature and Et_2O (20 mL) added resulting in a yellow precipitate. This was collected by filtration and washed with warm DCM (2 x 5 mL) to give **4.9.HI** as a fine, pale brown powder. Yield 0.0707 g (32%). **MP**: 270 – 272 °C. **^{1}H NMR** (400 MHz, DMSO-*d6*): δ 10.15 (1H, s, H6), 9.29 (1H, d, J = 3.9Hz, H10), 9.21 (1H, d, J = 8.2 Hz, H8), 9.16 (1H, d, J = 3.5 Hz, H2), 8.06 (1H, 1, dd, J = 8.2 Hz, 4.3 Hz, H9), 7.96 – 7.87 (5H, m, H19, H20, H21), 7.68 (1H, dd, J = 8.1 Hz, 4.1 Hz, H3), 7.53 (1h, d, J = 8.2 Hz, H4), 4.64 (3H, s, H22). **^{13}C NMR** (100 MHz, DMSO-*d6*): δ 151.07 (C2), 151.05 (C10), 145.08 (C17), 144.97 (C12), 143.86 (C6), 134.80 (C18), 132.55 (C21), 131.32 (C20), 131.23 (C8), 128.93 (C4), 127.73 (C19), 125.59 (C14), 125.29 (C15), 124.71 (C9), 124.22 (C3), 118.57 (C16), 117.97 (C13), 38.41 (C22). **ESI-MS**: Found M^+ 311.1290, $[C_{20}H_{15}N_4]^+$ requires 311.1297. **UV-vis** (MeCN) λmax/nm (ε, 10^3 $M^{-1}cm^{-1}$): 244 (69.1), 270(sh) (20.6), 319 (0.9), 336 (0.5). **Fluorometry** (MeCN) λmax: 462 nm.

1-phenyl-1*H*-imidazol[4,5*f*][1,10]phenanthrolin-(*N*'-methyl)-ium Iodide (4.13.I)

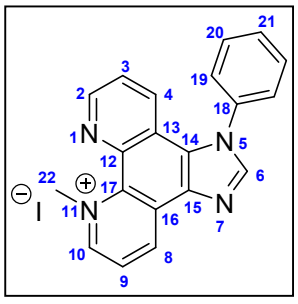

In an oven dried Schlenk tube **4.3** (0.0996 g, 0.336 mmol) was dissolved in DCM (10 mL) under an argon atmosphere. Iodomethane (25 uL, 0.40 mmol) was added and the solution heated to reflux. After 24 hours an additional equivalent of iodomethane (25 uL, 0.40 mmol) was added and refluxing continued for 20 hours. The yellow solution was then cooled to room temperature the solvent removed by rotary evaporation. Isolation of the product from the resultant yellow residue was achieved by flash chromatography (alumina, 2.5% MeOH/DCM) and evaporation of the appropriate fractions gave **4.13.I** as a flaky dark yellow solid. Yield 0.0171 g (12%). **MP**: 172 – 174 °C. **^{1}H NMR** (400 MHz, $CDCl_3$): δ 10.38

(1H, d, J = 5.8 Hz, H10), 9.82 (1H, d, J = 7.8 Hz, H8), 9.12 (1H, dd, J = 4.1 Hz, 1.8 Hz, H2), 8.47 (1H, dd, J = 8.2 Hz, 5.9 Hz, H9), 8.23 (1H, s, H6), 7.94 (1H, dd, J = 8.6 Hz, 1.6 Hz, H4), 7.75 (3H, m, H20, H21), 7.60 (3H, m, H3, H19), 5.56 (3H, s, H22). **^{13}C NMR** (100 MHz, $CDCl_3$): δ 151.36 (C10), 147.15 (C2), 144.92 (C6), 139.82 (C8), 131.01 (C21), 130.82 (C20), 129.16 (C4), 126.87 (C19), 125.37 (C9), 124.27 (C3), 55.75 (C22). **ESI-MS**: Found M^+ 311.1299, $[C_{20}H_{15}N_4]^+$ requires 311.1297. **UV-vis** (DCM) λmax/nm (ε, 10^3 $M^{-1}cm^{-1}$): 235 (22.7), 255 (20.8), 302 (15.7), 389 (1.9). **Fluorometry** (DCM) λmax: 482 nm.

8.4.2. [Ru(2,2'-bipyridine)$_2$(IP)]$^{n+}$ type complexes

[Ru(bipy)$_2$(4.2)][PF$_6$]$_2$

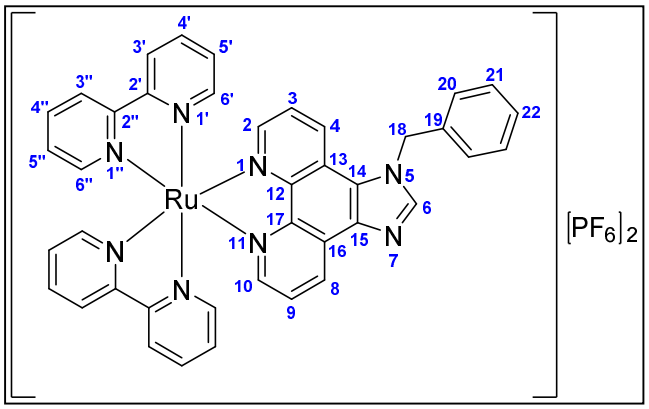

In a round-bottom flask, **4.2** (0.103 g, 0.322 mmol), $Ru(bipy)_2Cl_2$ (0.156 g, 0.322 mmol) and ethylene-glycol (15 mL) were combined and placed in a microwave reactor (350 W), with condenser fitted. The reaction was heated in 2 minute bursts with complex formation and ligand consumption monitored by TLC (silica, 4:1:1 DMF/water/1 M NH_4Cl). After two, 2 minute bursts the ligand had been consumed. Water (50 mL) was added to the solution, filtered through celite and washed through with additional water (20 mL). The product was isolated by ion-exchange chromatography (sephadex – C25, 0 to 0.20 M NaCl). Solid KPF_6 was added to the appropriate, dark orange fraction and stirred for 30 minutes. The resultant precipitate was collected by filtration and washed with KPF_6 solution then water and dried with Et_2O to give $[Ru(bipy)_2$(**4.2**)$][PF_6]_2$ as a fine, bright orange powder. Yield 0.219 g (67%). **MP:** 240 °C. **^{1}H NMR** (400 MHz, Acetone-*d6*): δ 9.16 (1H, d, J = 8.3 Hz, H8), 8.89 – 8.76 (5H, m, H4, H3', H3''), 8.72 (1H, s, H6), 8.36 (1H, d, J = 5.5 Hz, H10), 8.30 (1H, d, J = 5.1 Hz, H2), 8.23 (2H, dd, J = 7.9 Hz, 7.8 Hz, H4''), 8.14 – 8.09 (4H, m, H4', H6''), 7.96 (1H, dd, J = 8.2 Hz, 5.5 Hz, H9), 7.87 (1H, d, J = 5.5, H6'), 7.84 (1H, d, J = 5.5 Hz, H6'), 7.79 (1H, dd, J

= 8.6 Hz, 5.4 Hz, H3), 7.61 (2H, dd, J = 6.6 Hz, 6.3 Hz, H5''), 7.39 – 7.31 (7H, m, H20, H21, H22, H5'), 6.21 (2H, s, H18). **^{13}C NMR** (100 MHz, Acetone-*d6*): δ 157.42 (C2''), 157.37 (C2''), 157.23 (C2'), 157.22 (C2'), 151.95 (C6''), 151.90 (C6'), 150.72 (C10), 150.14 (C2), 146.64 (C6), 146.05 (C12), 145.92 (C17), 138.51 (C15), 138.09 (C4''), 137.94 (C4'), 135.70 (C19), 130.75 (C8), 130.25 (C4), 129.21 (C21), 128.24 (C22), 127.86 (C5''), 127.84 (C5''), 127.70 (C5'), 127.66 (C5'), 126.71 (C16), 126.58 (C9), 126.54 (C20), 125.75 (C3), 125.47 (C14), 124.42 (C3'/C3''), 124.34 (C3'/C3''), 121.94 (C13), 50.62 (C18). **ESI-MS**: Found M^{2+} 362.0824, $[M + PF_6]^+$ 869.1283, $[C_{40}H_{30}N_8Ru]^{2+}$ requires 362.0819, $[C_{40}H_{30}F_6N_8PRu]^+$ requires 869.1284. **UV-vis** (MeCN) λmax/nm (ε, 10^3 $M^{-1}cm^{-1}$): 254 (50.3), 284(79.3), 425(sh) (12.9), 454 (17.5). **Fluorometry** (MeCN) λmax: 601 nm.

[Ru(bipy)$_2$(4.3)][PF$_6$]$_2$

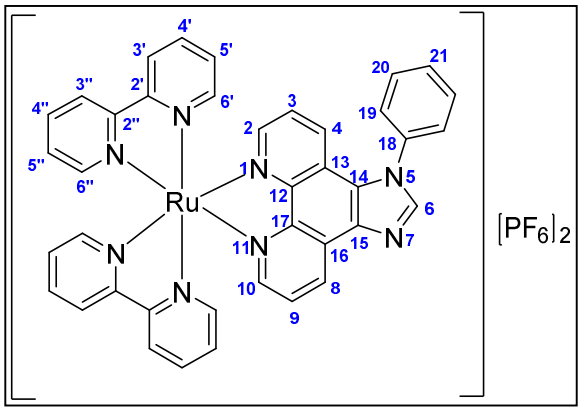

Performed as reported for [Ru(bipy)$_2$(**4.2**)][PF$_6$]$_2$ using **4.3** (0.0499 g, 0.168 mmol), Ru(bipy)$_2$Cl$_2$ (0.0811 g, 0.167 mmol) and ethylene-glycol (7 mL). After two, 2 minute bursts the ligand and Ru(bipy)$_2$Cl$_2$ had been consumed. The solution was poured onto water (25 mL), filtered through celite and washed through with additional water (20 mL). With stirring, saturated KPF_6 solution was added in excess resulting in immediate precipitate formation. This was stirred for 30 minutes then cooled in a refrigerator overnight. The resultant precipitate was collected by filtration, washed with water and Et_2O then dried in a vacuum desiccator to give [Ru(bipy)$_2$(**4.3**)][PF$_6$]$_2$ as a fine orange powder. Yield 0.1551 g (93%). **MP:** + 300 °C. **^{1}H NMR** (400 MHz, Acetone-*d6*): δ 9.20 (1H, d, J = 8.6 Hz, H8), 8.86 – 8.79 (4H, m, H3', H3''), 8.62 (1H, s, H6), 4.43 (1H, d, J = 5.1 Hz, H10), 8.32 (1H, d, J = 5.5 Hz, H2), 8.24 (2H, m, H4''), 8.14 (4H, m, H4', H6''), 7.99 (2H, m, H4, H9), 7.93 (1H, d, J = 5.9 Hz, H6'), 7.88 (1H, d, J= 5.9 Hz, H6'), 7.80 (5H, m, H19, H20, H21), 7.70 – 7.59 (3H, m, H3, H5''), 7.40 (2H, m, H5'). **^{13}C NMR** (100 MHz, Acetone-*d6*): δ 157.44 (C2''), 157.36 (C2''), 157.25 (C2'), 151.97 (C6''), 151.94 (C6'), 150.88 (C10), 150.46 (C2), 146.30

(C12), 146.06 (C17), 145.71 (C6), 138.11 (C4''), 137.98 (C4'), 137.68 (C15), 136.27 (C18), 130.86 (C8), 130.67 (C21), 130.57 (C19), 128.08 (C4), 127.89 (C5''), 127.87 (C5''), 127.75 (C5'), 127.71 (C5'), 127.20 (C20), 126.70 (C9), 126.60 (C16), 126.22 (C14), 125.66 (C3), 124.44 (C3''), 124.37 (C3'), 121.99 (C13). **ESI-MS**: Found M^{2+} 355.0743, $[M + PF_6]^+$ 855.1131, $[C_{39}H_{28}N_8Ru]^{2+}$ requires 355.0740, $[C_{39}H_{28}F_6N_8PRu]^+$ requires 855.1122. **UV-vis** (MeCN) λmax/nm (ε, 10^3 $M^{-1}cm^{-1}$): 254 (50.2), 284 (80.3), 425(sh) (13.5), 454 (17.0). **Fluorometry** (MeCN) λmax: 599 nm.

$[Ru(bipy)_2(4.4)][PF_6]_2$

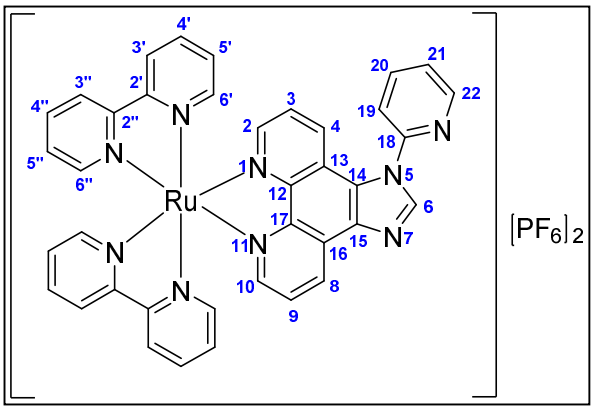

In a round-bottom flask $Ru(bipy)_2Cl_2$ (0.0791 g, 0.163 mmol) and ethylene-glycol (6 mL) were combined and placed in a microwave reactor (350 W), with condenser fitted. The mixture was heated for 2 minutes to give a homogeneous solution then **4.4** (0.0497 g, 0.167 mmol) was added. The solution was heated in 2 minute bursts with complex formation and starting material consumption monitored by TLC (silica, 4:1:1 DMF/water/1 M NH_4Cl). After two, 2 minute bursts the starting material had been consumed. Water (20 mL) was added to the solution, filtered through celite and washed through with additional water (20 mL). With stirring, saturated KPF_6 solution was added in excess resulting in immediate precipitate formation. This was stirred for 30 minutes then cooled in a refrigerator overnight. The resultant precipitate was collected by filtration, washed with water and Et_2O, and dried in a vacuum desiccator to give $[Ru(bipy)_2($**4.4**$)][PF_6]_2$ as a fine orange powder. Yield 0.1118 g (67%). **MP:** 239 – 244 °C. **^{1}H NMR** (400 MHz, CD_3CN): δ 9.16 (1H, d, J = 7.8 Hz, H8), 8.77 (1H, d, J = 2.9 Hz, H22), 8.63 – 8.45 (5H, m, H6, H3', H3''), 8.30 – 8.19 (2H, m, H4, H20), 8.18 – 8.07 (3H, m, H10, H4''), 8.07 – 7.97 (3H, m, 2H, H4'), 7.93 – 7.79 (4H, m, H9, H19, H6''), 7.74 (1H, dd, J = 7.4 Hz, 5.1 Hz, H21), 7.63 (1H, d, J = 5.5 Hz, H6'), 7.59 (1H, d, J = 5.5 Hz, H6'), 7.54 (1H, dd, J = 8.6 Hz, 5.1 Hz, H3), 7.46 (2H, m, H5'', H5''). **^{13}C NMR** (100 MHz, CD_3CN): δ 158.29 (C2''), 158.25 (C2''), 158.06 (C2'), 153.08 (C6'/C6''), 153.02 (C6'/C6''), 152.96 (C6'/C6''), 152.92

(C6′/C6″), 152.00 (C10), 151.59 (C2), 151.99 (C22), 150.27 (C18), 147.38 (C12), 147.29 (C17), 146.45 (C6), 141.54 (C20), 139.32 (C15), 138.93 (C4″), 138.79 (C4′), 132.00 (C4, C8), 128.64 (C5″), 128.50 (C5′), 127.55 (C16), 127.45 (C9), 126.59 (C14, C21), 126.25 (C3), 125.33 (C3″), 125.25 (C3′), 123.20 (C13), 121.71 (C19). **ESI-MS**: Found M^{2+} 355.5706, $[C_{38}H_{27}N_9Ru]^{2+}$ requires 355.5716. **UV-Vis** (MeCN) λmax/nm (ε, 10^3 $M^{-1}cm^{-1}$): 253 (49.8), 284 (80.9), 425(sh) (13.3), 453 (17.4). **Fluorometry** (MeCN) λmax: 599 nm.

$[Ru(bipy)_2(4.9.H)][PF_6]_3$

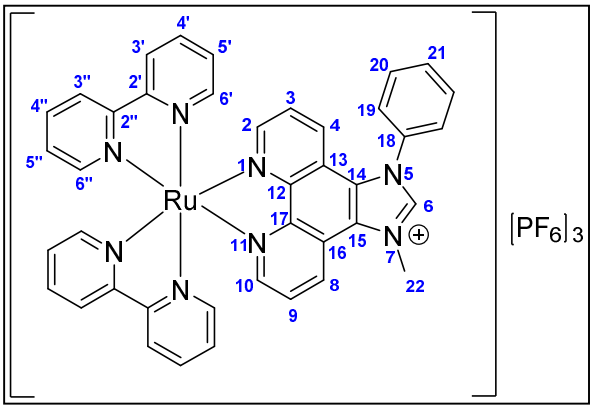

Argon was bubbled through a stock solution of 4:1 EtOH/water for 30 minutes to degas. Ligand **4.9.HI** (0.0219 g, 0.0507 mmol) and $Ru(bipy)_2Cl_2$ (0.0242 g, 0.0502 mmol) were combined in a 25 mL round-bottom flask, a condenser fitted and an argon blanket applied. Degassed EtOH/water (5 mL) was added by syringe and the reaction mixture refluxed for 22 hours in the absence of light. The dark red solution was cooled to room temperature and condensed by rotary-evaporation. The residue was purified by flash chromatography (silica, 9:1.5:1 MeCN/water/saturated $KNO_{3(aq)}$) with the desired product eluting as a bright orange band. The appropriate fractions were combined and condensed by rotary-evaporation then dissolved in a minimum of distilled water and precipitated by addition of a saturated KPF_6 solution. The resultant precipitate was collected by filtration and washed with saturated KPF_6 solution, water and Et_2O to give pure $[Ru(bipy)_2$(**4.7.H**)$][PF_6]_3$ as a fine orange powder. Yield 0.0412 g (71%). **MP:** + 300 °C. **^{1}H NMR** (400 MHz, CD_3CN): δ 9.49 (1H, s, H6), 9.24 (1H, d, J = 8.6 Hz, H8), 8.62 – 8.50 (4H, m, H3′, H3″), 8.33 (1H, d, J = 5.1 Hz, H10), 8.24 – 8.00 (5H, m, H2, H4′, H4″), 7.99 – 7.79 (7H, m, H9, H19, H20, H6″), 7.74 (2H, m, H4, H21), 7.61 – 7.53 (3H, m, H3, H6′), 7.48 (2H, m, H5″), 7.28 (2H, m, H5′), 4.66 (3H, s, H22). **^{13}C NMR** (100 MHz, CD_3CN): δ 158.11 (C2′/C2″), 158.08 (C2′/C2″), 158.03 (C2′/C2″), 157.98 (C2′/C2″), 154.42 (C10), 154.4 (C2), 152.99 (C6′/6″), 152.92 (C6′/C6″), 148.61 (C12), 148.57 (C17), 145.00 (C6), 139.29

(C4′/C4″), 139.25 (C4′/C4″), 139.19 (C4′/C4″), 139.17 (C4′/C4″), 134.61 (C18), 132.33 (C19), 132.16 (C8), 130.68 (C4), 128.82 (C5′/C5″), 128.78 (C5′/C5″), 128.61 (C5′/C5″), 128.60 (C5′/C5″), 128.06 (C9, C20, C21), 127.96 (C14), 127.80 (C3), 127.54 (C15), 125.53 (C3′/C3″), 125.50 (C3′/C3″), 125.49 (C3′/C3″), 125.46 (C3′/C3″), 122.23 (C16), 121.96 (C13), 39.23 (C22). **ESI-MS:** Found M^{3+} 241.7178, $[M + PF_6]^{2+}$ 435.0582, $[M + 2PF_6]^{+}$ 1015.0820. $[C_{40}H_{31}N_8Ru]^{3+}$ requires 241.7238, $[C_{40}H_{31}N_8F_6PRu]^{2+}$ requires 435.0679, $[C_{40}H_{31}N_8OF_{12}P_2Ru]^{+}$ requires 1015.0999. **UV-Vis** (MeCN) λmax/nm (ε, 10^3 $M^{-1}cm^{-1}$): 245 (123.1), 275 (122.9), 285 (119.1), 437 (30.3), 269(sh) (23.9). **Fluorometry** (MeCN) λmax: 632 nm.

[Ru(bipy)$_2$(4.9.H)][PF$_6$]$_3$

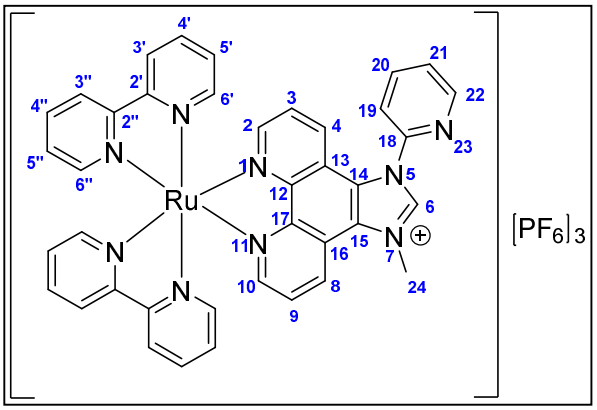

Complex [Ru(bipy)$_2$(**4.4**)][PF$_6$]$_2$ (0.0469 g, 0.0468 mmol) was weighed into a pressure tube and dissolved in dry DMF (2 mL) that had been degassed by bubbling argon prior use. Iodomethane (31.2 µL, 0.500 mmol) was added and the tube sealed with a Teflon screw-top. The reaction was heated to 100 °C for 48 hours after which time the reaction was cooled to room temperature. TLC (silica, 9:1.5:1 MeCN/water/saturated $KNO_{3(aq)}$) revealed minimal product formation, however, the reaction was not continued. The mixture was taken up in 20 mL of water, saturated KPF_6 solution added and the resulting precipitate collected by filtration. Flash chromatography (silica, 9:1.5:1 MeCN/water/saturated $KNO_{3(aq)}$) was used to isolate the desired product as well as recover the remaining starting material. The appropriate fractions were combined and condensed by rotary-evaporation then dissolved in a minimum of distilled water and precipitated by the addition of a saturated KPF_6 solution. The resultant precipitate was collected by filtration and washed with saturated KPF_6 solution, water and Et_2O to give pure [Ru(bipy)$_2$(**4.9.H**)][PF$_6$]$_3$ as a fine orange powder. Yield = 0.0116 g (21%). **MP:** + 300 °C. **^{1}H NMR** (400 MHz, CD_3CN): δ 9.51 (1H, s, H6), 9.22 (1H, d, J = 8.6 Hz, H8), 8.84 (1H, d, J = 3.9 Hz, H22), 8.58 – 8.40 (4H, m, H3′, H3″), 8.36 – 8.29 (2H, m, H10, H20), 8.20 (1H, d,

J = 5.1 Hz, H2), 8.13 (2H, m, H4''), 8.02 (2H, m, H4'), 7.98 – 7.86 (4H, m, H4, H9, H19, H21), 7.80 (1H, d, J = 5.5 Hz, H6''), 7.80 (1H, d, J = 5.5 Hz, H6''), 7.63 – 7.55 (2H, m, H3, H6'), 7.53 (1H, d, J = 5.5 Hz, H6'), 7.50 – 7.41 (2H, m, H5''), 7.25 (2H, t, J = 6.5 Hz, H5'), 4.65 (3H, s, H22). **^{13}C NMR** (100 MHz, CD_3CN): δ 158.40 (C2'/C2'', C2'/C2''), 158.33 (C2'/C2''), 158.28 (C2'/C2''), 154.95 (C2), 154.91 (C10), 153.44 (C6'/6''), 153.35 (C6'/C6''), 153.31 (C6'/C6''), 153.24 (C6'/C6''), 152.37 (C22), 149.00 (C12/C17), 148.97 (C12/C17), 147.83 (C18), 145.19 (C6), 142.90 (C20), 139.59 (C4''), 139.57 (C4''), 139.49 (C4', C4'), 132.51 (C8), 132.17 (C4), 129.38 (C21), 129.12 (C5''), 129.09 (C5''), 128.89 (C5'), 128.87 (C5'), 128.35 (C9) 128.25 (C15), 128.09 (C3), 127.49 (C14), 125.83 (C3'/C3''), 125.79 (C3'/C3''), 125.78 (C3'/C3''), 125.75 (C3'/C3''), 123.30 (C19), 122.55 (C16), 121.03 (C13), 39.88 (C22). **ESI-MS:** Found M^{3+} 242.0527. $[C_{39}H_{30}N_9Ru]^{3+}$ requires 242.0556. **UV-Vis** (MeCN) λmax/nm (ε, 10^3 $M^{-1}cm^{-1}$): 245 (89.3), 276 (92.6), 285 (97.9), 437 (20.5), 469(sh) (16.9). **Fluorometry** (MeCN) λmax: 633 nm.

8.5. Chapter 5

8.5.1. 3-imidazole phenanthroline (3-ImP) derivatives

3-imidazole-1,10-phenanthroline (5.1)

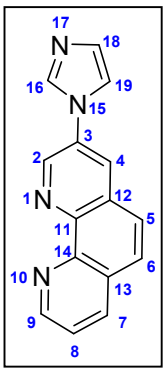

An oven dried Schlenk tube was charged with 3-bromo-1,10-phenanthroline (0.350 g, 1.35 mmol), imidazole (0.153 g, 2.25 mmol) and anhydrous $CuSO_4$ (0.008 g, 0.05 mmol). The vessel sparged with nitrogen heated at 180 °C forming a dark brown melt. After 4 hours the mixture was cooled and the resultant pellet crushed and stirred in water (15 mL) until all large chunks had dissolved, then extracted into chloroform. This was made difficult by formation of an emulsion and washes had to be filtered to remove green solid. Eventually organic extracts were obtained and dried over $MgSO_4$ before removal of the solvent. The off white residue was triturated in acetone (10 mL) for 30 minutes before filtering and air drying to provide **5.1** as a white powder. Yield 0.183 (55%). **MP**: 252 °C with decomposition. **^{1}H NMR** (400 MHz, $CDCl_3$): δ 9.28

(1H, d, J = 2.3 Hz, H2), 9.22 (1H, d, J = 3.9 Hz, H9), 8.29 (1H, d, J = 8.2 Hz, H7), 8.23 (1H, d, J = 2.3 Hz, H4), 8.06 (1H, s, H16), 7.91 (1H, d, J = 9.0 Hz, H6), 7.85 (1H, d, J = 9.0 Hz, H5), 7.68 (1H, dd, J = 8.2 Hz, 4.3 Hz, H8), 7.49 (1H, s, H18), 7.34 (1H, s, H19). **^{13}C NMR** (100 MHz, $CDCl_3$): δ 150.92 (C9), 145.83 (C14), 145.08 (C11), 143.53 (C2), 136.17 (C7), 135.75 (C16), 132.62 (C3), 131.44 (C19), 128.71 (C12), 128.61 (C13), 128.49 (C6), 126.81 (C4), 125.84 (C5), 124.15 (C8), 118.24 (C18). **ESI-MS**: Found $[MH]^+$ 247.0986, $[C_{15}H_{11}N_4]^+$ requires 247.0984.

3-(1-methylimidazolium)-1,10-phenanthroline hexafluorophosphate (5.2.HPF$_6$)

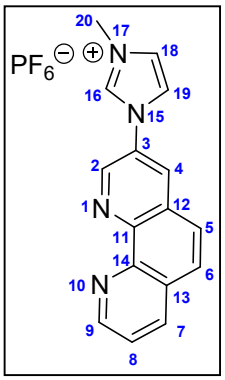

An oven dried Schlenk tube was charged with **5.1** (0.101 g, 0.411 mmol) and sparged with nitrogen. Anhydrous DCM (10 mL) was added by syringe followed by iodomethane (0.13 mL, 2.09 mmol). The stirred solution was heated to reflux and, after 14 hours, additional iodomethane was added (0.13 mL, 2.09 mmol). After refluxing for a further 6 hours the yellow mixture was cooled to room temperature and the solid collected by filtration and washed with DCM (30 mL) and Et_2O (30 mL) before drying under vacuum. The fine, light brown powder was dissolved in water (20 mL) and the turbid mixture filtered through celite. The desired product was precipitated from the colourless filtrate as a PF_6 salt by addition of excess solid KPF_6 and collected by filtration. The solid was washed with cold water followed by Et_2O and dried under vacuum providing pure **5.2.HPF$_6$** as a fine white powder. Recrystallisation from hot methanol provided extremely pure material for analysis. Yield 0.0591 (35%). **MP**: decomposition onset at 150 ^oC. **^{1}H NMR** (400 MHz, CD_3CN): δ 9.32 (1H, d, J = 2.3 Hz, H2), 9.21 (1H, d, J = 4.3 Hz, H9), 9.07 (1H, s, H16), 8.65 (1H, d, J = 1.9 Hz, H4), 8.50 (1H, d, J = 8.6 Hz, H7), 8.22 (1H, d, J = 9.0 Hz, H6), 8.04 (1H, d, J = 9.0 Hz, H5), 7.96 (1H, s, H19), 7.82 (1H, dd, J = 8.3 Hz, 4.4 Hz, H8), 7.67 (1H, s, H18), 4.04 (3H, s, H20). ^{13}C NMR (100 MHz, CD_3CN): δ 150.85 (C9), 146.47 (C11), 146.09 (C14), 143.51 (C2), 136.48 (C7), 135.88 (C16), 130.35 (C3), 129.87 (C4), 129.62 (C12), 129.25 (C6), 128.31 (C13), 125.99 (C5), 124.96 (C18), 124.15 (C8), 122.22 (C19), 36.51 (C20). **ESI-MS**:

Found $[MH]^{2+}$ 131.0604, M^{+} 261.1136. $[C_{16}H_{14}N_4]^{2+}$ requires 131.0609, $[C_{16}H_{13}N_4]^{+}$ requires 261.1140.

8.5.2. [Ru(2,2-bipyridine)$_2$(3-ImP)]$^{n+}$ type complexes

[Ru(bipy)$_2$(5.2.H)][PF$_6$]$_3$

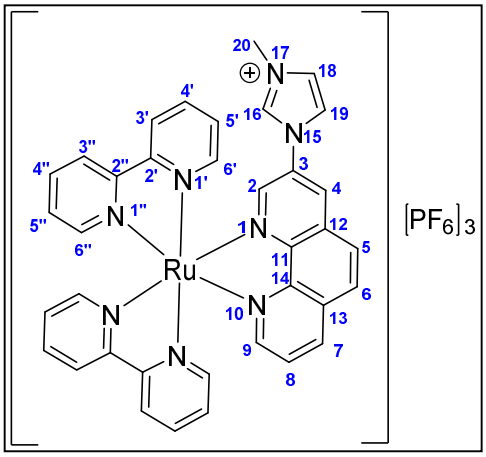

In a round-bottom flask $Ru(bipy)_2Cl_2$ (0.113 g, 0.232 mmol) and ethylene-glycol (5 mL) were combined and placed in a microwave reactor (350 W) with condenser fitted. This was irradiated until all $Ru(bipy)_2Cl_2$ had dissolved. Ligand **5.2.HPF$_6$** (0.0922 g, 0.238 mmol) was added and the solution was irradiated for a further 2 minutes. The cooled solution was poured onto water (10 mL) filtered through celite and washed through with additional water (15 mL). Saturated KPF_6 solution was added in excess to the aqueous solution and stirred for 30 minutes. The resulting precipitate was then filtered and washed with saturated KPF_6 solution followed by distilled water (15 mL), methanol (15 mL) and Et_2O to give [Ru(bipy)$_2$(**5.2.H**)][PF$_6$]$_3$ as a fine, orange powder. Yield 0.0229 g (89%). **MP:** + 300 ^{o}C. **^{1}H NMR** (400 MHz, CD_3CN): δ 8.82 (1H, d, J = 1.6 Hz, H4), 8.77 (1H, s, H16), 8.71 (1H, d, J = 8.2 Hz, H7), 8.57 – 8.50 (4H, m, H3', H3''), 8.42 (1H, d, J = 9.0 Hz, H6), 8.35 (1H, d, J = 9.0 Hz, H5), 8.22 (1H, d, J = 1.9 Hz, H2), 8.16 – 8.02 (5H, m, H9, H4', H4''), 7.87 – 7.82 (2H, m, H8, H6''), 7.77 (1H, d, J = 5.5 Hz, H6''), 7.71 (2H, m, H18/H19, H6'), 7.58 (1H, s, H18/H19), 7.50 – 7.43 (3H, m, H6', H5''), 7.27 (2H, dd, J = 15.2 Hz, 7.3 Hz, H5'), 3.95 (3H, s, H20). **^{13}C NMR** (100 MHz, CD_3CN): δ 157.20 (C2'/C2''), 157.15 (C2'/C2''), 156.87 (C2'/C2''), 153.39 (C9), 152.33 (C6'/C6''), 152.16 (C6'/C6''), 151.99 (C6'/C6''), 151.84 (C6'/C6''), 148.09 (C11), 147.50 (C2), 146.99 (C14), 138.18 (C4'/C4''), 138.05 (C4'/C4''), 138.04 (C4'/C4''), 138.02 (C4'/C4''), 137.19 (C7), 136.27 (C16), 132.07 (C13), 131.60 (C4), 130.28 (C12), 130.09 (C6), 127.82 (C5), 127.71 (C5''), 127.67 (C5''), 127.45 (C5'), 127.37 (C5'), 126.93 (C8), 124.87 (C18/C19), 124.38 (C3'/C3''), 124.33 (C3'/C3''), 124.28

(C3'/C3''), 122.79 (C18/C19), 36.54 (C20). **ESI-MS**: Found M^{3+} 225.0476, $[M - H]^{2+}$ 337.0682, $[M + PF_6]^{2+}$ 410.0532, $[M + 2PF_6]^{+}$ 965.0666. $[C_{36}H_{29}N_8Ru]^{3+}$ requires 225.0517, $[C_{36}H_{28}N_8Ru]^{2+}$ requires 337.0739, $[C_{36}H_{29}F_6N_8PRu]^{2+}$ requires 410.0599, $[C_{36}H_{29}F_{12}N_8P_2Ru]^{+}$ requires 965.0846. **UV-vis** (MeCN) λmax/nm (ε, 10^3 $M^{-1}cm^{-1}$): 235 (43.6), 273 (72.2), 284 (68.8), 438 (15.5).

$[Ru(bipy)_2(5.2.H)][PF_6]_3$ and **$[Ru(bipy)_2(5.3)][PF_6]_2$**

In a round-bottom flask **5.2.HPF$_6$** (0.0313 g, 0.0770 mmol), $Ru(bipy)_2Cl_2$ (0.0353 g, 0.0729 mol) and ethylene-glycol (9 mL) were combined and placed in a microwave reactor (350 W), with condenser fitted. The reaction was heated in 2 minute bursts and complex formation and ligand consumption monitored by TLC (silica, 4:1:1 DMF/water/1 M NH_4Cl). After three, 2 minute bursts the $Ru(bipy)_2Cl_2$ had been consumed. The solution was poured onto water (10 mL) filtered through celite and washed through with additional water (20 mL). The product was isolated by ion-exchange chromatography with gradient elution (sephadex – C25, 0 to 0.20 M NaCl). Complex $[Ru(bipy)_2($**5.3**$)]^{2+}$ was collected in the leading band and $[Ru(bipy)_2($**5.2.H**$)]^{3+}$ was collected in the final band with 0.4 M NaCl washes. Both were isolated as their PF_6 salts by addition of saturated KPF_6 solution to the appropriate fractions with stirring. The resulting bright orange, turbid suspensions were each extracted with DCM (3 x 20 mL), dried over $MgSO_4$ and the solvent removed under vacuum to give $[Ru(bipy)_2($**5.2.H**$)][PF_6]_3$ and $[Ru(bipy)_2($**5.3**$)][PF_6]_2$ as bright orange solid.

$[Ru(bipy)_2(5.2.H)][PF_6]_3$

Isolated yield 0.0192 g (28%).

[Ru(bipy)$_2$(5.3)][PF$_6$]$_2$

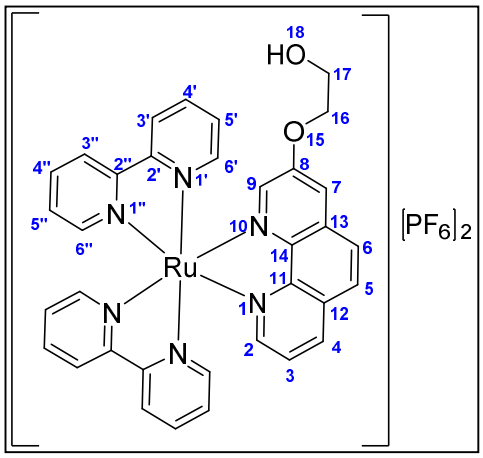

Isolated yield 0.0322 g (40%). **MP:** + 300 °C. **^{1}H NMR** (400 MHz, CD_3CN): δ 8.57 – 8.47 (5H, m, H7, H3', H3''), 8.18 (1H, d, J = 9 Hz, H6), 8.14 – 8.06 (4H, m, H5, H4, H4"), 8.02 – 7.97 (3H, m, H9, H4'), 7.85 (1H, d, J = 5.5 Hz, H6''), 7.82 (1H, d, J = 5.5 Hz, H6''), 7.71 (1H, d, J = 2.7 Hz, H2), 7.66 – 7.61 (2H, m, H8, H6'), 7.53 (1H, d, J = 5.1 Hz H6'), 7.44 (2H, m, H5''), 7.23 (2H, m, H5'), 4.22 (2H, m, H17), 3.84 (2H, m, H16), 3.00 (1H, m, H18). **^{13}C NMR** (100 MHz, CD_3CN): δ 158.33 (C2'/C2''), 158.27 (C2'/C2''), 157.99 (C2'/C2''), 157.92 (C2'/C2''), 157.59 (C3), 153.17 (C9), 153.11 (C6''), 152.95 (C6''), 152.92 (C6'), 152.79 (C6'), 148.62 (C14), 145.70 (C2), 142.46 (C11), 138.85 (C4'/C4''), 138.78 (C4'/C4''), 138.69 (C4'/C4''), 138.66 (C4'/C4''), 137.78 (C7), 133.20 (C12), 130.27 (C13), 129.48 (C6), 128.60 (C5), 128.47 (C5'/C5''), 128.39 (C5'/C5''), 128.32 (C5'/C5''), 125.85 (C8), 125.23 (C3'/C3''), 125.20 (C3'/C3''), 125.17 (C3'/C3''), 125.08 (C3'/C3''), 117.65 (C4), 72.09 (C17), 60.83 (C16). **ESI-MS**: Found M^{2+} 327.0653, $[M + PF_6]^+$ 799.0946. $[C_{34}H_{28}N_6O_2Ru]^{2+}$ requires 327.0659, $[C_{34}H_{28}F_6N_6O_2PRu]^{2+}$ requires 799.0959. **UV-vis** (MeCN) λmax/nm (ε, 10^3 $M^{-1}cm^{-1}$): 232 (39.8), 243(sh) (38.4), 285 (60.3), 428(sh) (13.1), 442 (15.0).

8.5.3. 1,10-Phenanthrolyl-acetamide (5-PA) derivatives

1-methyl-3-[2-(1,10 phenanthrolin-5-ylamino)-2-oxoethyl]-1*H*-imidazolium hexafluorophosphate (5.5.HPF$_6$)

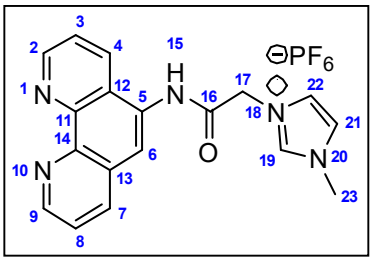

In an oven dried Schlenk tube 1-methyl-imidazole (0.23 mL, 2.9 mmol) was added to a stirred solution of 2-chloro-*N*-[1,10]-phenanthrolin-5-yl-acetamide (**5.4**) (0.0803 g, 0.296 mmol) in DMF (1 mL). The system was flushed with nitrogen and heated 100 °C for 2 hours. The reaction

mixture was dissolved in water (10 mL) and washed with EtOAc (3 x 10 mL). Excess solid KPF_6 was added to the aqueous phase which was stirred for 30 minutes then placed in the refrigerator overnight. The fine white precipitate that was deposited was collected by filtration and washed with saturated KPF_6 solution, water and Et_2O to give 0.0772 g of pure **5.5.HPF$_6$** as a fine white powder. A second crop of 0.0361 g was obtained by taking the original aqueous filtrate and condensing by rotary-evaporation then refrigerating overnight and collecting the precipitate as reported above. Overall yield 0.113 g (83%). **MP:** 264 ^oC. **^{1}H NMR** (400 MHz, CD_3CN): δ 9.68 (1H, s, H15), 8.95 (2H, m, H2, H9), 8.76 (1H, s, H19), 8.54 (1H, d, J = 8.2 Hz, H4), 8.29 (1H, d, J = 7.5 Hz, H7), 8.10 (1H, s, H6), 8.42 (3H, m, H3, H8, H21), 7.44 (1H, s, H22), 5.37 (2H, s, H17), 3.93 (3H, s, H18). **^{13}C NMR** (100 MHz, CD_3CN): δ 165.85 (1C), 150.83 (C2), 150.56 (C9), 146.75 (C11), 145.02 (C14), 138.50 (C19), 137.16 (C7), 132.30 (C4), 131.56 (C5), 129.01 (C13), 125.53 (C12), 124.91 (C21), 124.53 (C8), 124.16 (C22), 123.78 (C3), 121.76 (C6), 52.41 (C17), 37.02 (C23). **FT-IR** ν/cm^{-1} (intensity)**:** 3217 (w), 3100 (w), 2974 (w), 1705 (m), 1681 (w), 1555 (s), 1480 (w), 1456 (w), 1390 (m), 1225 (m), 1179 (m), 874 (m), 788 (m), 735 (s), 630 (m). **ESI-MS:** Found $[MH]^{2+}$ 159.5715, M^+ 318.1353. $[C_{18}H_{17}N_5O]^{2+}$ requires 159.5711, $[C_{18}H_{16}N_5O]^+$ requires 318.1349.

1-methyl-3-[2-(1,10 phenanthrolin-5-ylamino)-2-oxoethyl]-1*H*-imidazolium chloride (5.5.HCl)

In an oven dried Schlenk tube 1-methyl-imidazole (0.15 mL, 1.9 mmol) was added to a stirred suspension of 2-chloro-N-[1,10]-phenanthrolin-5-yl-acetamide (**5.4**) (0.102 g, 0.374 mmol) in MeCN (3 mL). The system was flushed with nitrogen and heated to reflux for 12 hours. The reaction mixture was allowed to cool to room temperature and the resulting precipitate collected by filtration. This was washed with DCM and Et_2O and left to dry giving pure **5.5.HCl** as a fine white powder. Yield 0.121 g (92%).

1-butyl-3-[2-(1,10 phenanthrolin-5-ylamino)-2-oxoethyl]-1*H*-imidazolium hexafluorophosphate (5.6.HPF$_6$)

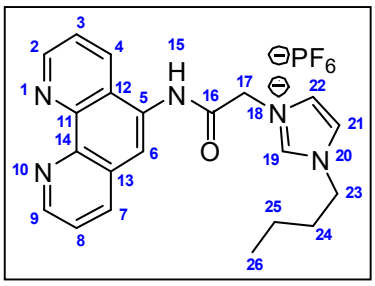

In an oven dried Schlenk tube 1-butyl-imidazole (0.25 mL, 1.9 mmol) was added to a stirred solution of 2-chloro-*N*-[1,10]-phenanthrolin-5-yl-acetamide (**5.4**) (0.105 g, 0.387 mmol) in MeCN (3 mL). The system was flushed with nitrogen and heated at reflux for 20 hours. The reaction mixture was allowed to cool and the solvent removed by rotary-evaporation. The resultant residue dissolved in water (20 mL) and washed with DCM (3 x 10 mL) then with Et_2O (10 mL). Excess solid KPF_6 was added to the aqueous phase resulting in immediate precipitation. This was stirred for 30 minutes and the solid material was collected by filtration and washed with saturated KPF_6 solution, water and after drying, was washed with DCM and Et_2O to give **5.6.HPF$_6$** as a fine white powder. Yield 0.157 g (81%). **MP:** 198 – 204 °C. **^{1}H NMR** (400 MHz, CD_3CN): δ 9.79 (1H, s, H15), 8.95 (2H, m, H2, H9), 8.89 (1H, s, H19), 8.54 (1H, d, J = 8.2 Hz, H4), 8.29 (1H, d, J = 7.5 Hz, H7), 8.12 (1H, s, H6), 7.63 – 7.60 (2H, m, H8, H22), 7.54 (1H, dd, J = 8.2 Hz, 4.3 Hz, H3), 7.49 (1H, s, H21), 5.42 (2H, s, H17), 4.23 (2H, t, J = 7.3 Hz, H23), 1.85 (2H, m, H24), 1.34 (2H, m, H25), 0.93 (3, t, J = 7.5 Hz, H26). **^{13}C NMR** (100 MHz, CD_3CN): δ 164.97 (C16), 149.91 (C2), 149.65 (C9), 145.99 (C11), 142.25 (C14), 137.12 (C19), 136.16 (C7), 131.31 (C4), 130.75 (C5), 128.14 (C13), 124.64 (C12), 124.20 (1C, C22), 123.61 (C8), 122.84 (C3), 121.93 (C21), 120.76 (C6), 51.62 (C17), 49.56 (C23), 31.51 (C24), 18.93 (C25), 12.61 (C26). **FT-IR** ν/cm^{-1} (intensity)**:** 3167 (w), 2962 (w), 1710 (w), 1678 (m), 1558 (m), 1459 (w), 1314 (w), 1271 (w), 1231 (w), 1170 (w), 829 (s), 738 (m), 628 (m). **ESI-MS**: Found $[MH]^{2+}$ 180.5948, M^+ 360.1823. $[C_{21}H_{23}N_5O]^{2+}$ requires 180.5946, $[C_{21}H_{22}N_5O]^+$ requires 360.1819.

1-isopropyl-3-[2-(1,10 phenanthrolin-5-ylamino)-2-oxoethyl]-1*H*-imidazolium hexafluorophosphate (5.7.HPF$_6$)

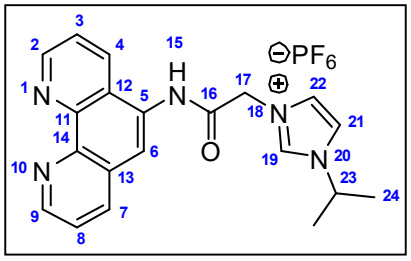

Synthesis performed as reported for **5.6.HPF$_6$** using 2-chloro-*N*-[1,10]-phenanthrolin-5-yl-acetamide (**5.4**) (0.103 g, 0.378 mmol) and 1-isopropyl-imidazole (0.21 mL, 1.8 mmol). The product **5.7.HPF$_6$** was obtained as a fine white powder. Yield 0.151 g (81 %). **MP:** 153 ^{o}C. **^{1}H NMR** (400 MHz, CD_3CN): δ 9.31 (1H, s, H15), 9.09 (2H, m, H2, H9), 8.80 (1H, s, H19), 8.57 (1H, d, J = 8.2 Hz, H4), 8.35 (1H, d, J = 7.8 Hz, H7), 8.16 (1H, s, H6), 7.70 (2H, m, H3, H8), 7.57 (2H, m, H21, H22), 5.32 (2H, s, H17), 4.70 (1H, m, H23), 1.57 (6H, m, H24). **^{13}C NMR** (100 MHz, CD_3CN): δ 164.67 (C16), 150.13 (C2), 149.88 (C9), 146.33 (C11), 144.59 (C14), 136.06 (C7), 135.75 (C19), 131.04 (C4), 130.59 (C5), 128.17 (C13), 124.57 (C12), 124.24 (C22), 123.64 (C8), 122.90 (C3), 121.75 (C6), 120.10 (C21), 53.43 (C17), 51.58 (C23), 21.58 (C24). **FT-IR** v/cm^{-1} (intensity)**:** 3154 (w), 3025 (w), 1711 (m), 1561 (m), 1456 (w), 1314 (w), 1244 (w), 1156 (w), 1132 (w), 835 (s), 738 (m), 649 (w), 629 (w). **ESI-MS**: Found $[MH]^{2+}$ 173.5870, M^{+} 346.1665. $[C_{20}H_{21}N_5O]^{2+}$ requires 173.5868, $[C_{20}H_{20}N_5O]^{+}$ requires 346.1662.

1-phenyl-3-[2-(1,10 phenanthrolin-5-ylamino)-2-oxoethyl]-1*H*-imidazolium hexafluorophosphate (5.8.HPF$_6$)

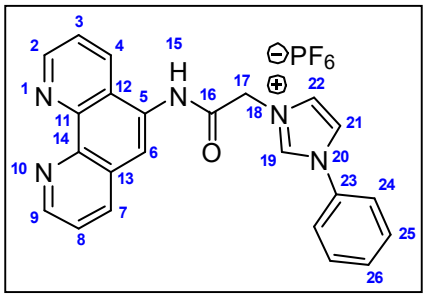

Synthesis performed as reported for **5.6.HPF$_6$** using 2-chloro-*N*-[1,10]-phenanthrolin-5-yl-acetamide (**5.4**) (0.109 g, 0.401 mmol) and 1-phenyl-imidazole (0.23 mL, 1.8 mmol). The product **5.8.HPF$_6$** was obtained as a fine white powder. Yield 0.232 g (86%). **MP:** 164 ^{o}C. **^{1}H NMR** (400 MHz, CD_3CN): δ 9.95 (1H, s, H15), 9.59 (1H, s, H19), 8.86 (2H, m, H2, H9), 8.48 (1H, d, J = 8.2 Hz, H4), 8.24 (1H, d, J = 8.2 Hz, H7), 8.08 (1H, s, H6), 7.88 (1H, s, H21), 7.84 (1H, s, H22), 7.65 – 7.56 (6H, m, H8, H24, H25, H26), 7.49 (1H, dd, J = 8.5 Hz, 4.0 Hz, H3), 5.54 (2H, s, H17). **^{13}C NMR** (100 MHz, CD_3CN): δ 165.90 (C16), 150.99 (C2), 150.71 (C9), 146.96 (C11), 145.20 (C14), 137.84 (C19), 137.50 (C7), 136.02 (C23), 132.55 (C4),

131.89 (C5), 131.60 (C26), 131.56 (C24), 129.32 (C13), 126.17 (C22), 125.75 (C12), 124.82 (C8), 124.02 (C3), 123.67 (C25), 122.51 (C21), 121.88 (C6) 53.13 (C17). **FT-IR** ν/cm^{-1} (intensity)**:** 3162 (w), 1688 (m), 1589 (m), 1422 (w), 1312 (w), 1260 (w), 1220 (w), 1085 (w), 826 (s), 773 (m), 695 (m). **ESI-MS:** Found $[MH]^{2+}$ 190.5794, M^+ 380.1509, $[MH][PF_6]^+$ 526.1230. $[C_{23}H_{19}N_5O]^{2+}$ requires 190.5792, $[C_{23}H_{18}N_5O]^+$ requires 380.1506, $[C_{23}H_{19}F_6N_5OP]^+$ requires 526.1226.

1-(2,6-diisopropyl)phenyl-3-[2-(1,10 phenanthrolin-5-ylamino)-2-oxoethyl]-1*H*-imidazolium chloride (5.9.HCl)

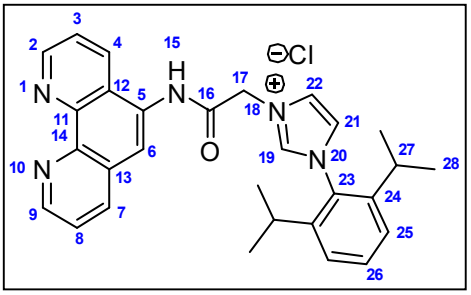

In an oven dried Schlenk tube 1-(2,6-diisopropyl)phenyl-imidazole (0.882 g, 3.86 mmol) was added to a stirred solution of 2-chloro-*N*-[1,10]-phenanthrolin-5-yl-acetamide (**5.4**) (0.875 g, 3.22 mmol) in MeCN (50 mL). The system was flushed with nitrogen and heated at reflux for 96 hours. The resultant peach coloured slurry was allowed to cool and the solvent removed by rotary-evaporation. The residue was washed with Et_2O, dissolved in water (40 mL), filtered through a short alumina plug and washed through with additional water. The aqueous filtrate was rotary-evaporated to dryness, dissolved in a minimum of acetone and precipitated by addition of Et_2O. This was collected by filtration giving pure **5.9.HCl** as a very fine mustard yellow powder. Yield 1.317 g (83%). **MP:** 190 - 208 ^oC with decomposition. **^{1}H NMR** (400 MHz, DMSO-*d*6): δ 9.65 (1H, s, H19), 9.07 (1H, d, J = 4.3Hz, H2), 8.94 (1H, d, J = 4.3 Hz, H9) 8.87 (1H, d, J = 8.2 Hz, H4), 8.34 (1H, d, J = 7.8 Hz, H7), 8.21 (2H, m, H6, H21), 8.11 (1H, s, H22), 7.74 (1H, dd, J = 8.2 Hz, 4.3Hz, H3), 7.67 (1H, dd, J = 8.2 Hz, 4.3 Hz, H8), 7.61 (1H, t, J = 7.8 Hz, H26), 7.44 (2H, d, J = 7.8 Hz, H25), 5.47 (2H, s, H17), 2.37 (2H, m, H27), 1.12 (12H, m, H28). **^{13}C NMR** (100 MHz, DMSO-*d6*): δ 165.88 (C16), 149.98 (C2), 148.80 (C9), 146.44 (C11), 145.66 (C24), 143.11 (C14), 139.66 (C19), 135.74 (C7), 132.70 (C4), 131.88 (C26), 131.10 (C23), 129.12 (C13), 126.36 (C12), 125.37 (C22), 124.84 (C25), 124.68 (C21), 123.83 (C8), 123.48 (C5), 122.91 (C3), 118.75 (C6), 53.21 (C17), 28.44 (C27), 24.25 (C28). **FT-IR** ν/cm^{-1} (intensity)**:** 3363 (w), 2965 (w), 1696 (w), 1625 (w), 1546 (s), 1458 (w), 1421 (m), 1315 (w), 1244 (m), 1196 (m), 1068 (w), 878 (w),

806 (m), 740 (s), 626 (m). **ESI-MS**: Found $[MH]^{2+}$ 232.6270, M^+ 464.2454. $[C_{29}H_{31}N_5O]^{2+}$ requires 232.6262, $[C_{29}H_{30}N_5O]^+$ requires 464.2445.

1-(2-pyridyl)-3-[2-(1,10-phenanthrolin-5-ylamino)-2-oxoethyl]-1*H*-imidazolium hexafluorophosphate (5.10.HPF$_6$)

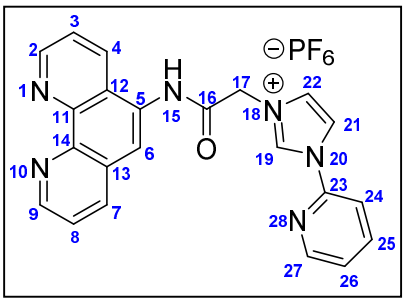

In an oven dried Schlenk tube 1-(2-pyridyl)-imidazole (0.270 g, 1.86 mmol) was added to a stirred solution of 2-chloro-*N*-[1,10]-phenanthrolin-5-yl-acetamide (**5.4**) (0.142 g, 0.523 mmol) in DMF (2 mL). The system was flushed with nitrogen and heated at reflux for 48 hours. The reaction mixture was allowed to cool and the solvent removed by rotary-evaporation. The resultant residue was dissolved in water (20 mL) and filtered through celite, washing through with additional water (20 mL). The dark yellow filtrate was washed with DCM (3 x 20 mL) then with Et_2O (20 mL). Excess solid KPF_6 was added to the aqueous phase resulting in immediate precipitation. This was stirred for 30 minutes then solid material collected by filtration and washed with saturated KPF_6 solution, water and after drying, with Et_2O to give **5.10.HPF$_6$** as a fine mustard yellow powder. Yield 0.156 g (57%). **MP:** 175 ^oC with decomposition. **^{1}H NMR** (400 MHz, CD_3CN): δ 9.78 (1H, s, H15), 9.69 (1H, s, H19), 8.94 (1H, m, H2, H9), 8.65 (1H, d, J = 8.6 Hz, H4), 8.56 (1H, d, J = 4.7 Hz, H27), 8.47 (1H, d, J = 8.2 Hz, H7), 8.23 (1H, s, H6), 8.16 (1H, s, H21), 8.08 (1H, t, J = 7.8 Hz, H25), 7.85 – 7.71 (3H, m, H8, H22, H24), 7.69 (1H, dd, J = 8.2 Hz, 4.3 Hz, H3), 7.56 (1H, m, H26), 5.52 (1H, s, H17). **^{13}C NMR** (100 MHz, CD_3CN): δ 165.76 (C16), 150.78 (C2), 150.56 (C27), 149.21 (C9), 147.44 (C23), 144.65 (C11), 142.52 (C14), 141.57 (C25), 139.65 (C7), 136.81 (C19), 133.58 (C4), 132.41 (C5), 129.68 (C13), 126.62 (C26), 126.31 (C22), 126.95 (C12), 125.31 (C8), 124.85 (C3), 121.28 (C6), 120.06 (C21), 115.30 (C24), 53.21 (C17). **FT-IR** ν/cm^{-1} (intensity): 3158 (w), 1697 (w), 1602 (m, 1477 (w), 1330 (s), 1230 (m), 1079 (w), 968 (w), 841 (s), 780 (m), 737 (m), 626 (w). **ESI-MS**: Found M^+ 381.1454. $[C_{22}H_{17}N_6O]^+$ requires 381.1458.

8.5.4. [Ru(1,10-phenanthroline)$_2$(5-PA)][PF$_6$]$_3$ type complexes

[Ru(phen)$_2$(5.5.H)][PF$_6$]$_3$

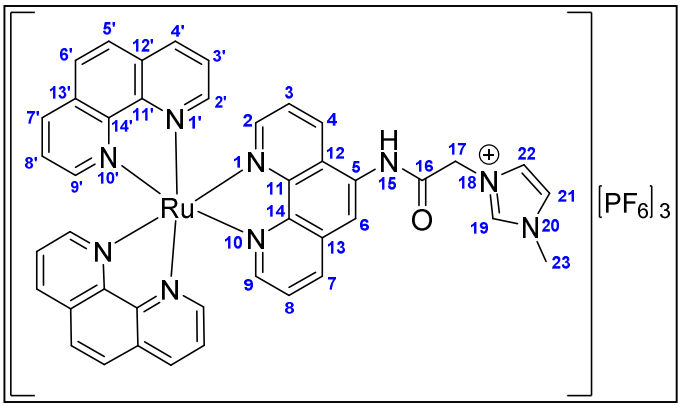

Argon was bubbled through a stock solution of 4:1 EtOH/H_2O for 30 minutes to degas. Ligand **5.5.HCl** (0.0498 g, 0.141 mmol) and an equivalent of Ru(phen)$_2$Cl$_2$ (0.0752 g, 0.141 mmol) were combined in a 25 mL round-bottom flask, a condenser fitted and an argon blanket applied. Degassed EtOH/H_2O (7 mL) was added by syringe and the reaction mixture heated to reflux in the absence of light and monitored by TLC (silica, 9:1.5:1 MeCN/water/saturated $KNO_{3(aq)}$). After 4 hours no starting material was detected. The dark red solution was cooled to room temperature and condensed by rotary-evaporation. The residue was purified by flash chromatography (silica, 9:1.5:1 MeCN/water/saturated $KNO_{3(aq)}$) with the desired product eluting as a bright orange band. The appropriate fractions were combined and condensed by rotary-evaporation then dissolved in a minimum of distilled water and precipitated by addition of a saturated KPF_6 solution. The resultant precipitate was collected by filtration and washed with saturated KPF_6 solution, water and Et_2O to give pure [Ru(phen)$_2$(**5.5.H**)][PF$_6$]$_3$ as a fine orange powder. Yield 0.116 g (68%). **MP:** decomposition onset at 230 °C, melted at 241 °C. **^{1}H NMR** (400 MHz, DMSO-*d6*): δ 11.00 (1H, s, H15), 9.13 (1H, s, H19), 8.91 (1H, d, J = 8.2 Hz, H4), 8.78 – 8.75 (4H, m, H4', H7'), 8.70 (1H, d, J = 7.9 Hz, H7), 8.56 (1H, s, H6), 8.37 (4H, s, H5', H6'), 8.10 (1H, d, J = 5.5 Hz, H2), 8.07 (3H, m, H2'/H9'), 8.04 (1H, d, J = 5.1 Hz, H2'/H9'), 7.99 (1H, d, J = 5.1 Hz, H9), 7.83 – 7.69 (8H, m, H3, H8, H22, H21, H3', H8'), 5.46 (2H, s, H17), 3.93 (3H, s, H23). **^{13}C NMR** (100 MHz, DMSO-*d6*): δ 166.13 (C16). 153.22 (C2), 153.19 (C9, C2', C9'), 148.19 (C11', C14'), 147.66 (C11', C14'), 138.39 (C19), 137.33 (C4', C7'), 136.82 (C7), 133.14 (C5), 132.83 (C4), 130.92 (C12', C13'), 128.51 (C5', C6'), 126.77 (C3', C8'), 126.22 (C14), 124.47 (C22), 123.68 (C21), 120.73 (C6), 51.96 (C17), 36.00 (C23). **FT-IR** v/cm^{-1} (intensity)**:** 1710

(w), 1561 (w), 1426 (w), 1316 (w), 1243 (w), 1180 (w), 823 (s), 722 (m), 625 (w). **ESI-MS**: Found M^{3+} 260.0590, $[M - H]^{2+}$ 389.5850. $[C_{42}H_{32}N_9ORu]^{3+}$ requires 260.0589, $[C_{42}H_{31}N_9ORu]^{2+}$ requires 389.5848. **UV-vis** (MeCN) λmax/nm (ε, 10^3 $M^{-1}cm^{-1}$): 223 (53.5), 263 (74.7), 422 (18.8), 447 (19.4).

$[Ru(phen)_2(5.6.H)][PF_6]_3$

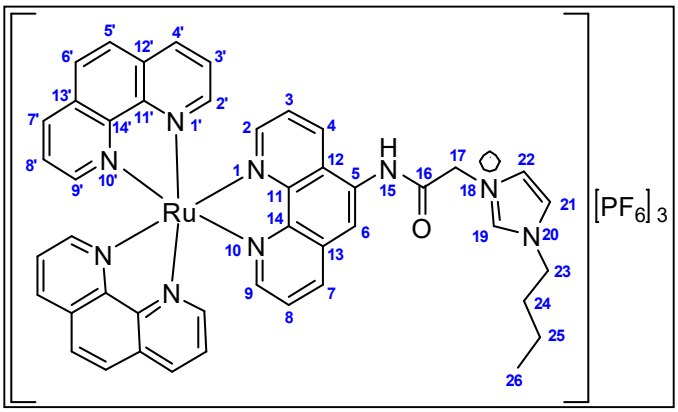

Performed as described for $[Ru(phen)_2$(**5.5.H**)$][PF_6]_3$ using ligand **5.6.HPF$_6$** (0.0243 g, 0.0500 mmol) and reacting for 22 hours. The product was obtained as a fine orange powder. Yield 0.0442 g (70%). **MP:** 202 – 220 °C. **^{1}H NMR** (400 MHz, DMSO-*d6*): δ 11.00 (1H, s, H15), 9.20 (1H, s, H19), 8.91 (1H, d, J = 8.6 Hz, H4), 8.76 – 8.70 (5H, m, H7, H4', H7'), 8.57 (1H, s, H6), 8.37 (4H, s, H5', H6'), 8.12 (1H, d, J = 5.1 Hz, H2), 8.19 (4H, m, H2', H9'), 7.99 (1H, d, J = 4.3 Hz, H9), 7.83 – 7.68 (8H, m, H3, H8, H21, H22, H3', H8'), 5.45 (2H, s, H17), 4.25 (2H, t, J = 7.1 Hz, H23), 1.79 (2H, m, H24), 1.27 (2H, m, H25), 0.90 (3H, t, J = 7.5 Hz, H26). **^{13}C NMR** (100 MHz, DMSO-*d6*): δ 166.13 (C16), 153.49 (C2), 153.19 (C9, C2', C9'), 147.69 (C11'/C14'), 147.64 (C11'/C14'), 137.89 (C19), 137.33 (C4', C7'), 136.77 (C7), 132.82 (C4), 130.91 (C12', C13'), 128.49 (C5', C6'), 126.76 (C3', C8'), 126.69 (C8), 126.15 (C3), 124.65 (C22), 124.39 (C21), 121.89 (C6), 51.82 (C17), 49.16 (C23), 31.86 (C24), 19.18 (C25), 13.71 (C26). **FT-IR** ν/cm^{-1} (intensity)**:** 1711 (w), 1632 (w), 1557 (w), 1428 (w), 1172 (w), 828 (s), 722 (m), 630 (w). **ESI-MS**: Found M^{3+} 274.0745, $[M - H]^{2+}$ 410.6092, $[M + PF_6]^{2+}$ 483.5957, $[M + 2PF_6]^{+}$ 1112.1624. $[C_{45}H_{38}N_9ORu]^{3+}$ requires 274.0747, $[C_{45}H_{37}N_9ORu]^{2+}$ requires 410.6083, $[C_{45}H_{38}F_6N_9OPRu]^{2+}$ requires 483.5943, $[C_{45}H_{38}F_{12}N_9OP_2Ru]^{+}$ requires 1112.1526. **UV-vis** (MeCN) λmax/nm (ε, 10^3 $M^{-1}cm^{-1}$): 222 (69.5), 263 (82.3), 426 (14.9), 446 (17.2).

[Ru(phen)$_2$(5.7.H)][PF$_6$]$_3$

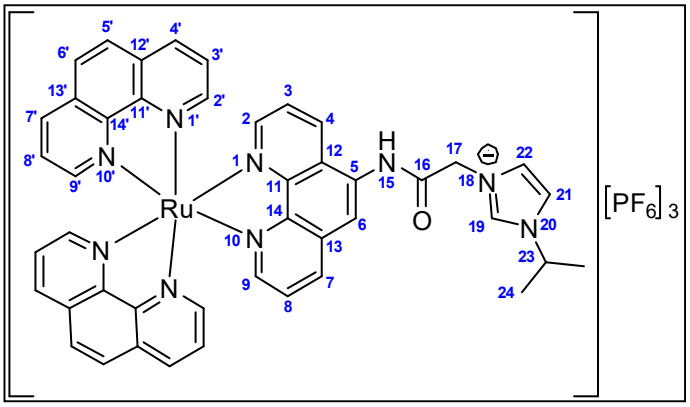

Performed as described for [Ru(phen)$_2$(**5.5.H**)][PF$_6$]$_3$ using ligand **5.7.HPF$_6$** (0.0244 g, 0.0497 mmol) and reacting for 22 hours. The product was obtained as a fine orange powder. Yield 0.0474 g (77%). **MP:** 220 – 230 ^{o}C. **^{1}H NMR** (400 MHz, DMSO-*d6*): δ 11.00 (1H, s, H15), 9.27 (1H, s, H19), 8.92 (1H, d, J = 8.2 Hz, H4), 8.77 – 8.71 (5H, m, H7, H4', H7'), 8.59 (1H, s, H6), 8.38 (4H, s, H5', H6'), 8.13 (1H, d, J = 5.0 Hz, H2), 8.06 (4H, m, H2', H9'), 8.00 (1H, d, J = 4.7 Hz, H9), 7.95 (1H, s, H21), 7.81-7.69 (7H, m, H3, H8, H22, H3', H8'), 5.45 (2H, s, H17), 4.74 (1H, spt, J = 6.3 Hz, H23), 1.51 (6H, d, J = 6.3 Hz, H24). **^{13}C NMR** (100 MHz, DMSO-*d6*): δ 166.08 (C16), 153.51 (C2), 153.19 (C2', C9'), 152.55 (C9), 148.10 (C11), 147.65 (C11', C14'), 145.70 (C14), 137.33 (C4', C7'), 136.81 (C7), 136.67 (C19), 132.83 (C5), 132.80 (C4), 130.92 (C12', C13'), 128.50 (C5', C6'), 126.98 (C8), 126.77 (C3', C8'), 126.18 (C3), 124.75 (C22), 124.56 (C21), 120.47 (C6), 52.88 (C17), 51.81 (C23), 22.79 (C24). **FT-IR** ν/cm^{-1} (intensity)**:** 1711 (w), 1631 (w), 1556 (w), 1428 (w), 1316 (w), 1243 (w), 1183 (w), 828 (s), 722 (m), 654 (w). **ESI-MS**: Found M^{3+} 269.4013, [M – H]$^{2+}$ 403.5990, [M + PF$_6$]$^{2+}$ 476.5850, [M + 2PF$_6$]$^{+}$ 1098.1389. [C$_{44}$H$_{36}$N$_9$ORu]$^{3+}$ requires 269.4029, [C$_{44}$H$_{35}$N$_9$ORu]$^{2+}$ requires 403.6004, [C$_{44}$H$_{36}$N$_9$OF$_6$PRu]$^{2+}$ requires 476.5864, [C$_{44}$H$_{36}$N$_9$OF$_{12}$P$_2$Ru]$^{+}$ requires 1098.1370. **UV-vis** (MeCN) λmax/nm (ε, 10^3 M^{-1}cm^{-1}): 222 (76.0), 263 (92.4), 427 (16.1), 447 (17.2).

[Ru(phen)$_2$(5.8.H)][PF$_6$]$_3$

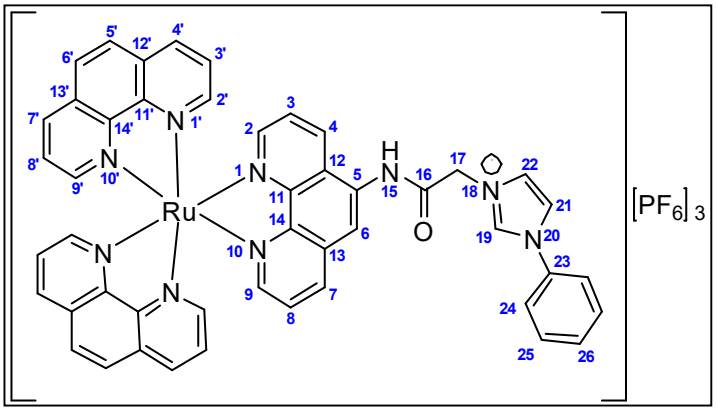

Performed as described for [Ru(phen)$_2$(**5.5.H**)][PF$_6$]$_3$ using ligand **5.8.HPF$_6$** (0.0298 g, 0.0567 mmol) and reacting for 20 hours. The product was obtained as a fine orange powder. Yield 0.0513 g (71%). **MP:** 222 °C. **^{1}H NMR** (400 MHz, DMSO-*d6*): δ 11.06 (1H, s, H15), 9.86 (1H, s, H19), 8.92 (1H, d, J = 8.2 Hz, H4), 8.76 – 8.70 (5H, m, H7, H4', H7'), 8.59 (1H, s, H6), 8.37 (5H, s, H21, H5', H6'), 8.13 (1H, d, J = 5.0 Hz, H2), 8.05 (5H, m, H22, H2', H9'), 8.00 (1H, d, J = 4.7 Hz, H9), 7.99 – 7.62 (11H, m, H3, H8, H24, H25, H26, H3', H8'), 5.55 (2H, s, H17). **^{13}C NMR** (100 MHz, DMSO-*d6*): δ 165.75 (C16), 153.55 (C2), 153.19 (C2', C9'), 152.60 (C9), 147.67 (C11'/C14'), 147.64 (C11'/C14'), 137.34 (C4', C7'), 137.23 (C19), 136.83 (C7), 133.24 (C4), 130.92 (C12', C13'), 130.85 (C24), 130.56 (C26), 128.49 (C5', C6'), 127.00 (C8), 126.76 (C3', C8'), 126.22 (C3), 125.50 (C22), 122.41 (C25), 121.37 (C21), 120.66 (C6), 52.14 (C17). **FT-IR** ν/cm^{-1} (intensity)**:** 1709 (w), 1632 (w), 1600 (w), 1554 (w0, 1496 (w), 1428 (w), 1316 (w), 1210 (w), 1075 (w), 830 (s), 722 (m), 651 (w). **ESI-MS**: Found M^{3+} 280.7305, [M – H]$^{2+}$ 420.5924, [M + PF$_6$]$^+$ 493.5781. [C$_{47}$H$_{34}$N$_9$ORu]$^{3+}$ requires 280.7309, [C$_{47}$H$_{33}$N$_9$ORu]$^{2+}$ requires 420.5926, [C$_{47}$H$_{33}$F$_6$N$_9$OPRu]$^{2+}$ requires 493.5785. **UV-vis** (MeCN) λmax/nm (ε, 10^3 M^{-1}cm^{-1}): 222 (70.8), 263 (81.7), 427 (14.8), 446 (15.5).

[Ru(phen)$_2$(5.9.H)][PF$_6$]$_3$

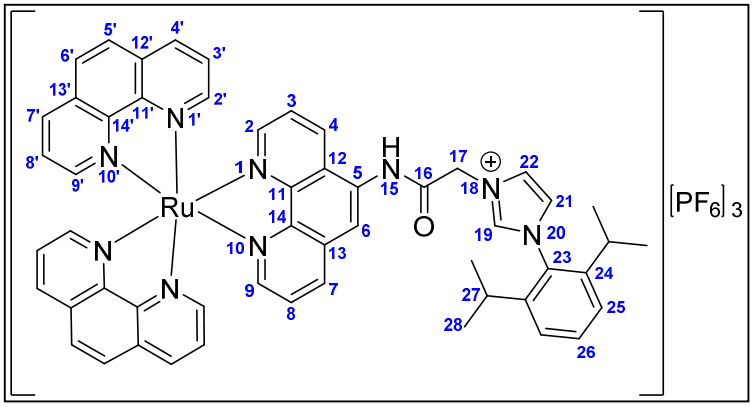

Performed as described for [Ru(phen)$_2$(**5.5.H**)][PF$_6$]$_3$ using ligand **5.9.HPF$_6$** (0.602 g, 0.988 mmol) and reacting for 3 hours. The product was obtained as a fine orange powder. Yield 1.00 g

(74%). **MP:** 224 – 232 °C. **^{1}H NMR** (400 MHz, DMSO-*d6*): δ 11.15 (1H, s, H15), 9.54 (1H, s, H19), 8.94 (1H, d, J = 8.6 Hz, H4), 8.77 (5H, m, H7, H4', H7'), 8.57 (1H, s, H6), 8.38 (4H, s, H5', H6'), 8.15 – 8.08 (6H, m, H2, H22, H21, H2', H9'), 8.05 (1H, d, J = 4.7 Hz, H2'/H9'), 8.01 (1H, d, J = 5.1 Hz, H9), 7.82 (1H, dd, J = 8.6 Hz, 5.1 Hz, H3), 7.79 – 7.70 (5H, m, H8, H3', H8'), 7.63 (1H, t, J = 7.8 Hz, H26), 7.47 (2H, d, J = 7.8 Hz, H25), 5.61 (2H, s, H17), 2.35 (2H, spt, J = 6.3 Hz, H27), 1.15 (12H, d, J = 6.3 Hz, H28). **^{13}C NMR** (100 MHz, DMSO-*d6*): δ 165.96 (C16), 153.54 (C2), 153.22 (C2', C9'), 152.59 (C9), 148.15 (C11), 147.67 (C11'/C14'), 147.65 (C11'/C14'), 145.82 (C14), 145.59 (C24), 139.79 (C19), 137.33 (C4', C7'), 136.88 (C7), 133.25 (C5), 132.94 (C4), 132.01 (C26), 131.01 (C23), 130.92 (C12', C13'), 130.44 (C13), 128.50 (C5', C6'), 126.95 (C8), 126.90 (C12), 126.77 (C3', C8'), 126.18 (C3), 125.32 (C21), 125.03 (C22), 124.93 (C25), 120.97 (C6), 52.30 (C17), 28.48 (C27), 24.28 (C28). **FT-IR** ν/cm^{-1} (intensity)**:** 1709 (w), 1549 (w), 1427 (w0, 1196 (w), 828 (s), 721 (w), 629 (w). **ESI-MS**: Found M^{3+} 308.7626, $[M - H]^{2+}$ 462.6397, $[M + PF_6]^{2+}$ 535.6258. $[C_{53}H_{46}N_9ORu]^{3+}$ requires 308.7623, $[C_{53}H_{45}N_9ORu]^{2+}$ requires 462.6396, $[C_{53}H_{45}F_6N_9OPRu]^{2+}$ requires 535.6256. **UV-vis** (MeCN) λmax/nm (ε, 10^3 M^{-1}cm^{-1}): 221 (65.7), 263 (74.0), 427 (sh), 446 (14.4).

[Ru(phen)$_2$(5.10.H)][PF$_6$]$_3$

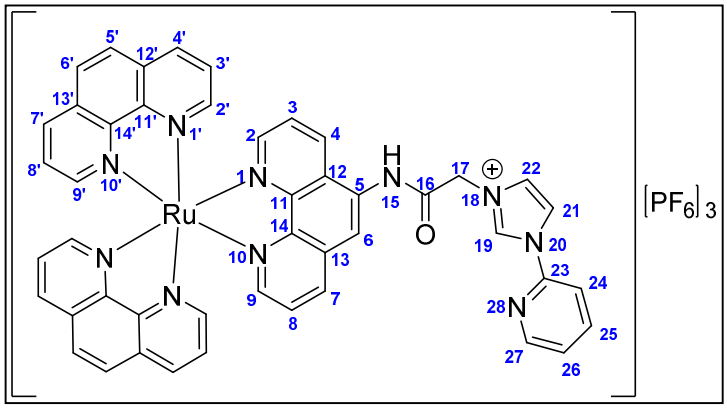

Performed as described for [Ru(phen)$_2$(**5.5.H**)][PF$_6$]$_3$ using ligand **5.10.HPF$_6$** (0.105 g, 0.200 mmol) and reacting for 4 hours. The product was obtained as a fine orange powder. Yield 0.150 g (58%). **MP:** decomposition onset at 219 °C. **^{1}H NMR** (400 MHz, DMSO-*d6*): δ 11.06 (1H, s, H15), 10.14 (1H, s, H19), 8.92 (1H, d, J = 8.2 Hz, H4), 8.79 – 8.69 (5H, m, H7, H4', H7'), 8.66 (1H, d, J = 4.3 Hz, H27), 8.58 (2H, s, H6, H21), 8.36 (4H, s, H5', H6'), 8.23 (1H, t, J = 7.8 Hz, H25), 8.12 (1H, d, J = 5.1 Hz, H2), 8.09 – 8.01 (6H, m, H22, H24, H2', H9'), 7.99 (1H, d, J = 5.1 Hz, H9), 7.82 (1H, m, H3), 7.80 – 7.58 (6H, m, H8, H26, H3', H8'), 5.58 (2H, s, H17). **^{13}C NMR** (100 MHz, DMSO-*d6*): δ 165.33 (C16), 153.10 (C2), 152.74 (C2', C9'), 152.17

(C9), 149.41 (C27), 147.67 (C11), 147.24 (C11'/C14'), 147.20 (C11'/C14'), 146.26 (C23), 145.33 (C14), 140.81 (C25), 136.89 (C7, C4', C7'), 136.42 (C19), 132.82 (C4), 132.43 (C5), 130.47 (C12', C13'), 129.96 (C13), 128.08 (C5', C6'), 126.25 (C12), 125.78 (C3), 125.52 (C26), 125.40 (C22), 120.28 (C6), 118.85 (C21), 114.28 (C24), 51.83 (C17). **FT-IR** ν/cm^{-1} (intensity)**:** 1708 (w), 1631 (w), 1543 (w), 1477 (w), 1428 (w), 1317 (w), 1214 (w), 830 (s), 722 (m), 624 (w). **ESI-MS**: Found M^{3+} 281.0625, $[M - H]^{2+}$ 421.0901, $[M + PF_6]^{2+}$ 494.0762. $[C_{46}H_{33}N_{10}ORu]^{3+}$ requires 281.0626, $[C_{46}H_{32}N_{10}ORu]^{2+}$ requires 421.0900, $[C_{46}H_{33}F_6N_{10}OPRu]^{2+}$ requires 494.0760. **UV-vis** (MeCN) λmax/nm (ε, 10^3 $M^{-1}cm^{-1}$): 222 (96.3), 263 (114.9), 428 (18.3), 446 (20.1).

8.5.5. 2,2'-Bipyridyl-acetamide (4-BipyA) derivatives

2-chloro-*N*-(4-amino-2,2'-bipyridine)-acetamide (5.11)

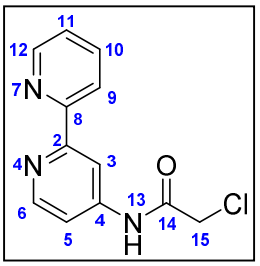

An oven dried Schlenk flask was charged with 4-amino-2,2'-bipyridine (0.286 g, 1.70 mmol) and sparged with nitrogen. Anhydrous DCM (20 mL) was added by cannula followed by freshly distilled trimethylamine (0.24 mL, 1.70 mmol) and the solution cooled to 0 °C. A solution of chloroacetyl-chloride (0.14 mL, 1.70 mmol) in anhydrous DCM (5 mL) was added dropwise resulting in a dark brown/black mixture. Stirring at 0 °C was continued for 1 hour before warming to room temperature. The black/brown suspension was filtered and the solid rinsed with DCM (25 mL). The combined organic phase was washed with water (3 x 30 mL) and dried over $MgSO_4$ before removal of the solvent. Purification of the black residue was achieved by flash column chromatography (alumina, 1% MeOH/DCM) providing **5.11** as a fine, off white powder. Yield, 0.109 g (26%). MP: 142 °C. ^{1}H NMR (400 MHz, $CDCl_3$): δ 8.74 (1H, br.s, H13), 8.67 (1H, d, J = 4.3 Hz, H12), 8.63 (1H, d, J = 5.5 Hz, H6), 8.41 (1H, d, J = 8.2 Hz, H9), 8.28 (1H, m, H3), 7.99 (1H, m, H5), 7.84 (1H, t, J = 7.2 Hz, H10), 7.35 (1H, m, H11), 4.25 (2H, s, H15). ^{13}C NMR (100 MHz, $CDCl_3$): δ 164.63 (C14), 156.98 (C2), 155.03 (C8), 150.37 (C6), 149.110 (C12), 145.06 (C4), 137.13 (C10), 124.20 (C11), 121.19 (C9), 113.72 (C5), 110.77 (C3), 42.84 (C15). FT-IR ν/cm^{-1} (intensity): 3268 (w), 3186 (w), 3109 (w), 2949 (w),

1681 (m), 1597 (m), 1581 (m), 1561 (m), 1530 (m), 1462 (s), 1397 (m), 1331 (w), 1247 (m), 1216 (m), 1179 (w), 991 (m), 928 (w), 882 (w), 836 (m), 791 (s), 743 (m), 731 (m), 661 (w), 632 (m), 616 (m). ESI-MS: Found $[M+H]^+$ 248.0589. $[C_{12}H_{21}N_3OCl]^+$ requires 248.0591.

1-methyl-3-[*N*-(4-amino-2,2'-bipyridine)-acetamido]-1*H*-imidazolium chloride (5.12.HCl)

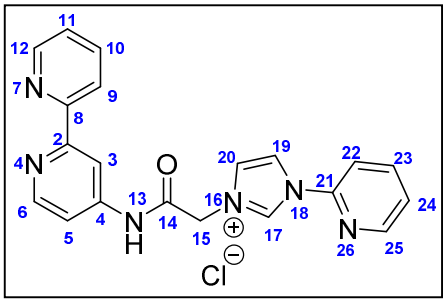

An oven dried Schlenk flask was charged with **5.11** (0.100 g, 0.404 mmol) and 1-(2-pyridyl)-imidazole (0.119 g, 0.820 mmol), and sparged with nitrogen. MeCN (10 mL) was added by syringe and the solution heated to reflux with consumption of **5.11** monitored by TLC (alumina, 1% MeOH/DCM). After 48 hours the reaction was cooled to room temperature and added to Et_2O (50 mL) with stirring. The resulting white precipitate was collected by filtration, washed with Et_2O and dried under vacuum providing **5.12.HCl** as a fine white powder. Yield 0.124 g (78%). **MP:** 154 °C. **^{1}H NMR** (400 MHz, DMSO-*d6*): δ 11.98 (1H, s, H13), 10.27 (1H, s, H17), 8.76 (1H, s, H3), 8.66 (3H, m, H12, H19, H25), 8.58 (1H, d, J = 5.1 Hz, H6), 8.37 (1H, d, J = 7.8 Hz, H9), 8.23 (1H, m, H23), 8.12 (2H, m, H20, H22), 7.93 (1H, t, J = 3.9 Hz, H10), 7.73 (1H, d, J = 3.9 Hz, H5), 7.66 (1H, dd, J = 4.9 Hz, 7.2 Hz, H24), 7.45 (1H, m, H11), 5.56 (2H, s H15). **^{13}C NMR** (100 MHz, DMSO-*d6*): δ 164.90 (C14), 156.36 (C2), 154.97 (C8), 150.22 (C6), 149.29 (C12), 149.19 (C25), 146.25 (C21), 146.21 (C4), 140.67 (C23), 137.23 (C10), 136.43 (C17), 125.33 (C24), 125.30 (C20), 124.30 (C11), 120.47 (C9), 118.67 (C19), 114.28 (C22), 113.46 (C5), 109.99 (C3), 52.13 (C15). **FT-IR** ν/cm^{-1} (intensity): 3058 (w), 2940 (w), 2894 (w), 2824 (w), 1710 (s), 1594 (s), 1579 (s), 1565 (s), 1552 (s), 1525 (s), 1478 (m), 1459 (m), 1442 (m), 1401 (m), 1319 (m), 1239 (s), 1176 (m), 1083 (m), 991 (w), 796 (m), 775 (s), 734 (m), 617 (m). **ESI-MS**: Found M^+ 357.1458, $[2M - H]^+$ 713.2863, $[2M + Cl]^+$ 749.2627. $[C_{20}H_{17}N_6O]^+$ requires 357.1458, $[C_{40}H_{33}N_{12}O_2]^+$ requires 713.2838, $[C_{40}H_{34}N_{12}O_2Cl]^+$ requires 749.2611.

8.5.6. [Ru(1,10-phenanthroline)$_2$(4-BipyA)][PF$_6$]$_3$ type complexes

[Ru(phen)$_2$(5.12.H)][PF$_6$]$_3$

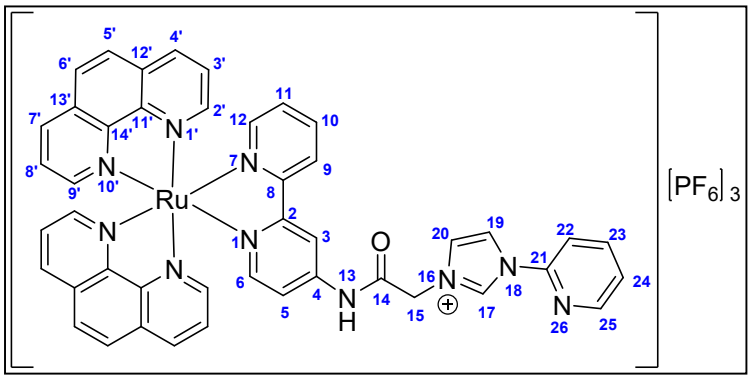

Synthesis performed as described for [Ru(phen)$_2$(**5.5.H**)][PF$_6$]$_3$ using ligand **5.12.HCl** (0.0999 g, 0.0254 mmol) and Ru(phen)$_2$Cl$_2$ (0.107 g, 0.0254 mmol) and reacting for 2 hours. The product was obtained as a fine orange powder. Yield 0.0442 g (70%). Yield 0.195 g (61%). **MP:** 204 °C with decomposition. **^{1}H NMR** (400 MHz, DMSO-*d6*): δ 11.54 (1H, br.s, H13), 10.07 (1H, s, H17), 8.90 (1H, s, H3), 8.83 (2H, dd, J = 8.2 Hz, 3.5 Hz, H4'/H7'), 8.78 – 8.64 (3H, m, H25, H4'/H7'), 8.58 (1H, s, H19), 8.52 (1H, d, J = 8.2 Hz, H9), 8.47 – 8.33 (4H, m, H5', H6'), 8.30 (1H, d, J = 5.1 Hz, H2'/H9'), 8.24 (2H, m, H23, H2'/H9'), 8.11 (1H, t, J = 7.8 Hz, H10), 8.05 (1H, d, J = 8.2 Hz, H22), 8.02 – 7.86 (5H, m, H20, H2'/H9', H3'/H8'), 7.78 – 7.62 (4H, m, H12, H24, H3'/H8'), 7.58 (1H, d, J = 6.3 Hz, H6), 7.51 – 7.22 (2H, m, H5, H11), 5.43 (2H, s, H15). **^{13}C NMR** (100 MHz, DMSO-*d6*): δ 165.58 (C14), 157.39 (C2), 156.59 (C8), 152.55 (C2'/C9'), 152.45 (C6), 151.98 (C12), 149.46 (C25), 147.30 (C11'/C14'), 147.26 (C11'/C14'), 147.08 (C11'/C14'), 146.98 (C20), 146.25 (C4), 140.87 (C23), 138.12 (C10), 136.94 (C4'/C7'), 136.79 (C4'/C7'), 136.41 (C17), 130.56 (C12'/C13'), 130.52 (C12'/C13'), 128.10 (C5'/C6'), 127.98 (C11), 126.37 (C3'/C8'), 125.62 (C24), 125.37 (C20), 124.08 (C9), 118.97 (C19), 116.96 (C5), 114.36 (C22), 113.06 (C3), 52.08 (C15). **FT-IR** v/cm^{-1} (intensity): 1721 (w), 1602 (w), 1527 (w), 1476 (w), 1428 (w), 1333 (w), 1272 (w), 1234 (w), 827 (s), 783 (m), 721 (m), 625 (w). **ESI-MS**: Found M^{3+} 273.0608, $[M-H]^{2+}$ 409.0897. $[C_{44}H_{33}N_{10}ORu]^{3+}$ requires 273.0626, $[C_{44}H_{32}N_{10}ORu]^{2+}$ requires 409.0900.

8.5.7. NHC complexes of ruthenium-polypyridine derivatives

$[Ru(phen)_2(Pd\{5.9 - H\}\{allyl\})][PF_6]_2$

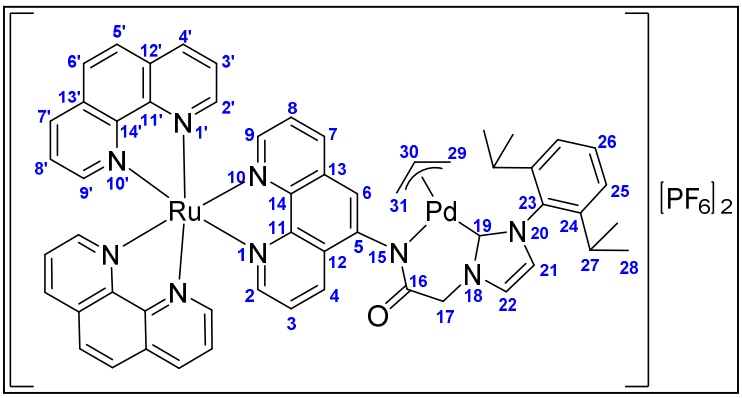

A 50 mL Schlenk flask was charged with $[Ru(phen)_2$ (**5.9.H**)$][PF_6]_3$ (0.136 g, 0.100 mmol) and tetraethyl-ammonium chloride hydrate (0.0184 g, 0.100 mmol), and the flask sparged with nitrogen. Dry DCM (20 mL) was added and the mixture stirred until it became homogeneous. Ag_2O (0.0116 g, 0.050 mmol) was then added and stirring continued at room temperature in the absence of light for 20 hours. A solution of $[Pd(allyl)Cl]_2$ (0.0183 g, 0.050 mmol) in dry DCM (2 mL) was added dropwise and stirring continued as above for a further 48 hours. After this time the red suspension was filtered through celite and solvent removed under vacuum providing material shown by ^{1}H-NMR to be a mixture of NHC products and tetraethyl-ammonium salt (0.164 g). A portion of this (0.0813 g) was purified by flash chromatography (alumina, 2% MeOH/chloroform). The desired product eluted as a broad band that was collected in several fractions providing pure $[Ru(phen)_2(Pd\{$**5.9 - H**$\}\{allyl\})][PF_6]_2$ as a bright red powder. Yield 0.0432 g (64%). Extremely pure material for analysis was obtained by bulk slow evaporation of an acetone/benzene solution of the compound and collecting the resulting crystals. **MP:** decomposition onset at 289 °C. **^{1}H NMR** (400 MHz, CD_3CN): δ 8.56 (6H, m), 8.36 (1H, d, J = 8.2 Hz), 8.24 (5H, m), 8.03 (2H, d, J = 5.1 Hz), 7.94 (1H, d, J = 5.1 Hz), 7.81 (1H, br.s), 7.76 – 7.42 (12H, m), 7.41 – 7.21 (6H, m), 4.85 (0.1H, m), 4.47 (0.2H, s), 4.24 (0.4H, t, J = 6.7 Hz), 4.18 (0.6H, dd, J = 2.5 Hz, 5.7 Hz), 3.36 (0.3H, m), 2.73 (0.5H, m), 2.66 – 2.47 (1.5H, m), 1.77 (0.25H, m), 1.68 (0.5H, m), 1.55 – 0.78 (25.6H, m). **^{13}C NMR** (100 MHz, CD_3CN): δ 170.13, 153.94, 151.80, 149.02, 137.72, 136.60, 132.35, 132.04, 131.24, 129.80, 129.08, 126.90, 126.44, 126.03, 124.89, 124.18, 123.73, 108.35, 57.32, 29.35, 24.65. **FT-IR** ν/cm^{-1} (intensity): 2962 (w), 1720.22 (w), 1624 (w), 1576 (m), 1456 (w), 1427

(m), 1384 (w), 1290 (w), 827 (s), 721 (m), 680 (m). **ESI-MS:** Found $[MH - Cl]^{3+}$ 357.4115, $[M - Cl]^{2+}$ 535.6089, $[MH - Cl + CN]^{2+}$ 549.1136. $[C_{56}H_{50}N_9ORuPd]^{3+}$ requires 357.4072, $[C_{56}H_{49}N_9ORuPd]^{2+}$ requires 535.6072, $[C_{57}H_{50}N_{10}ORuPd]^{2+}$ requires 549.1127. **UV-vis** (MeCN) λmax/nm (ε, 10^3 $M^{-1}cm^{-1}$): 222 (102.6), 263 (107.8), 428 (18.7), 448 (20.7).

$[Ru(phen)_2(Pd\{5.10 - H\}Cl)][PF_6]_2$

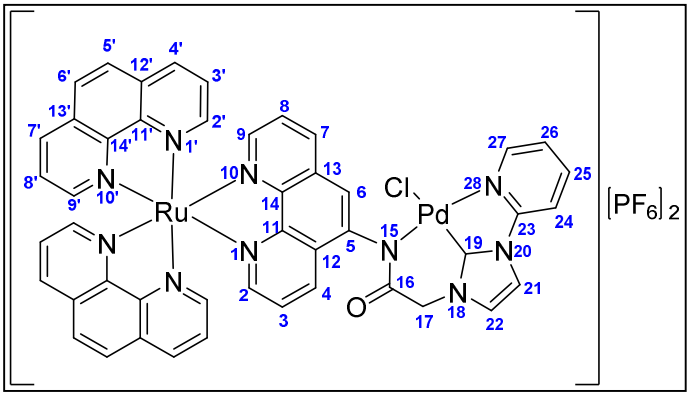

A Schlenk tube was charged with $[Ru(phen)_2$(**5.10.H**)$]Cl_3$ (0.0483 g, 0.0509 mmol) and an equivalent of Ag_2O (0.0117 g, 0.0505 mmol) and the flask sparged with nitrogen. Dry DMSO (3 mL) was added and the mixture stirred at room temperature in the absence of light for 20 hours. A solution containing an equivalent of $Pd(MeCN)_2Cl_2$ (0.0133 g, 0.0513 mmol) in DMSO (1.5 mL) was added to the deep red solution by syringe and rinsed through with additional DMSO (0.5 mL). Stirring was continued for 24 hours before pouring onto water (25 mL) and filtering through celite, rinsing the plug with additional water. The aqueous filtrate was loaded onto a short plug of sephadex-C25 ion exchange resin and rinsed thoroughly with water before elution of the red band with 0.5 M NaCl solution. Adequately pure product was obtained from the eluent by precipitating as a PF_6 salt and collecting the solid by filtration. After drying in a vacuum desiccator the material was purified by bulk slow vapour diffusion of diisopropyl-ether into a MeCN solution and collection of the crystalline material. Yield 0.0336 g (51%). Complex $[Ru(phen)_2(Pd\{$**5.10 - H**$\}Cl)][PF_6]_2$ is a mixture of atropisomeric diastereomers in a 2:1 ratio and for this reason the NMR spectra were too difficult to assign. **MP:** decomposition onset at 289 °C. **^{1}H NMR** (600 MHz, CD_3CN): δ 8.93 (1H, d, J = 5.3 Hz), 8.86 – 8.79 (1.5H, m), 8.76 (0.5H, d J = 8.3 Hz), 8.67 – 8.61 (1.5H, m), 8.61 – 8.53 (4.5H, m), 8.46 (1.5H, m), 8.42 (1H, d, J = 8.1 Hz), 8.31 (0.5H, d, J = 4.9 Hz), 8.30 – 8.16 (7.5H, m), 8.06 (1H, d, 4.9 Hz), 8.04 – 7.97 (3.5H, m), 7.93 (1H, d, J = 2.0 Hz), 7.91 (0.5H, d, J = 2.0 Hz), 7.87 (1H, d, J = 4.7 Hz), 7.83 (1H, t, J = 5.3 Hz), 7.82 – 7.67 (5.5H, m), 7.65 – 7.54 (5.5H, m), 7.54 – 7.45 (3H, m), 7.44 – 7.35 (2H, m), 5.12 (3H, m). **^{13}C NMR**

(150 MHz, CD_3CN): δ 167.92, 167.80, 157.79, 157.44, 154.43, 154.27, 154.21, 154.09, 153.83, 153.37, 153.01, 152.83, 152.77, 152.32, 152.29, 151.77, 151.72, 150.67, 149.39, 149.20, 149.15, 149.05, 149.03, 148.99, 148.97, 148.94, 147.10, 146.99, 143.89, 143.80, 137.70, 137.69, 137.64, 136.77, 134.99, 134.92, 132.25, 132.15, 132.08, 132.06, 132.01, 131.97, 131.95, 131.93, 131.91, 131.81, 131.78, 129.09, 129.07, 129.05, 129.04, 129.01, 126.98, 126.91, 126.90, 126.85, 126.83, 126.77, 126.66, 126.51, 126.44, 125.98, 125.93, 124.82, 124.48, 124.39, 123.01, 122.95, 117.99, 117.95, 113.09, 113.01, 54.18, 54.14. **FT-IR** ν/cm^{-1} (intensity)**:** 1623 (w), 1584 (w), 1563 (w), 1511 (w), 1481 (w), 1458 (w), 1423 (w), 1361 (w), 1306 (w), 1143 (w), 1121 (w), 1094 (w), 824 (s), 719 (s), 657 (m). **ESI-MS**: Found $[M - Cl + CN]^{2+}$ 486.5405. $[C_{47}H_{31}N_{11}OPdRu]^{2+}$ requires 486.5396. **UV-vis** (MeCN) λmax/nm (ε, 10^3 $M^{-1}cm^{-1}$): 221 (81.0), 263 (94.4), 428 (15.5), 447 (17.1).

$[Ru(phen)_2(Pd\{5.12\}Cl_2)][PF_6]_2$ and **$[Ru(phen)_2(Pd\{5.12 - H\}Cl)][PF_6]_2$**

Prepared by the same method as $[Ru(phen)_2(Pd\{$**5.10 - H**$\}Cl)][PF_6]_2$ using $[Ru(phen)_2($**5.12.H**$)]Cl_3$ (0.0463 g, 0.050 mmol) and a slightly different work-up. After pouring the reaction mixture onto water and filtering through celite, the aqueous filtrate was loaded onto a short plug of sephadex-C25 ion exchange resin and rinsed thoroughly with water before gradient elution with NaCl solution (0 – 0.1 M NaCl). The desired product was obtained from the appropriate fractions by addition of excess KPF_6 solution and extraction of the turbid suspension into DCM (3 x 20 mL). Drying of the organic extract over $MgSO_4$ followed by removal of the solvent provided pure $[Ru(phen)_2(Pd\{$**5.12**$\}Cl_2)][PF_6]_2$ as a fine red powder. Yield 0.0233 g (36%). Workup of other fractions provided additional material (0.0368 g) comprised of $[Ru(phen)_2(Pd\{$**5.12**$\}Cl_2)][PF_6]_2$ and $[Ru(phen)_2(Pd\{$**5.12 - H**$\}Cl)][PF_6]_2$. Further purification of this was not attempted and $[Ru(phen)_2(Pd\{$**5.12 - H**$\}Cl)][PF_6]_2$ was not fully characterised.

[Ru(phen)$_2$(Pd{5.12}Cl$_2$)][PF$_6$]$_2$

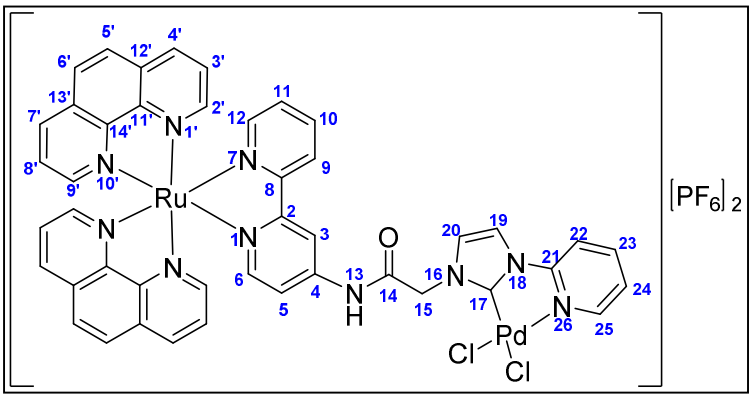

MP: decomposition onset at 284 °C. **^{1}H NMR** (400 MHz, CD_3CN): δ 9.82 (1H, br.s, H13), 9.24 (1H, d, J = 5.5 Hz, H25), 8.83 (1H, s, H3), 8.65 (2H, d, J = 8.2 Hz, H4'), 8.53 (2H, d, J = 8.2 Hz, H7'), 8.42 (1H, d, J = 8.2 Hz, H9), 8.33 (1H, d, J = 5.1 Hz, H2'), 8.29 – 8.16 (6H, m, H23, H2', H5', H6'), 7.99 (1H, t, J = 7.8 Hz, H10), 7.92 – 7.72 (6H, m, H19, H22, H3', H9'), 7.66 (1H, d, J = 5.5 Hz, H12), 7.54 (2H, dd, J = 3 Hz, 5.1 Hz, H8'), 7.50 – 7.40 (3H, m, H5, H6, H24), 7.25 (2H, m, H11, H20), 5.74 (2H, s, H15). **^{13}C NMR** (100 MHz, CD_3CN): δ 168.34 (C14), 159.22 (C8), 158.51 (C2), 158.62 (C4), 157.75 (C17), 154.44 (C2'), 154.17 (C2'), 154.08 (C9'), 153.99 (C9'), 153.83 (C6), 153.61 (C12), 153.26 (C21), 151.23 (C25), 149.28 (C11'/C14'), 148.12 (C11'/C14'), 144.04 (C23), 139.09 (C10), 138.08 (C4'/C7'), 137.94 (C4'/C7'), 132.39 (C12'/C13'), 132.33 (C12'/C13'), 132.32 (C12'/C13'), 129.43 (C5'/C6'), 129.37 (C5'/C6'), 128.77 (C11), 127.38 (C3'), 127.21 (C8'), 127.19 (C8'), 127.12 (C20), 125.54 (C9), 124.59 (C24), 117.73 (C19), 117.49 (C5), 114.53 (C3), 113.60 (C22), 54.76 (C15). **FT-IR** ν/cm^{-1} (intensity)**:** 1687 (w), 1598 (w), 1526 (w), 1490 (w), 1427 (w), 1412 (w), 1331 (w), 1271 (w), 1235 (w), 1205 (w), 1145 (w), 831 (s), 776 (m), 740 (w), 720 (m). **ESI-MS**: Found [M – Cl + CN]$^{2+}$ 474.5393. [$C_{45}H_{31}N_{11}ORuPd$]$^{2+}$ requires 474.5399. **UV-vis** (MeCN) λmax/nm (ε, 10^3 M^{-1}cm^{-1}): 226 (69.6), 263 (86.5), 286 (42.5), 428 (14.5), 451 (16.7).

Appendix

crystallography tables

Table A0.1: *Crystallographic data for compounds* ***2.1***, ***2.9.2HBr***, ***2.12.2HBr*** *and Pd(****2.4 - H****)(O,O'-acac).*

Thesis code	**2.1**	**2.9.2HBr**	**2.12.2HBr**	Pd(**2.4 - H**)(*O,O'*-acac)
Collection identification code	5wrk38	5wrk13a	5wrk37	5wrk16_twin1_hklf4
Empirical formula	$C_{12}H_{20}ClNO$	$C_{32}H_{58}Br_4N_6O_2$	$C_{32}H_{58}Br_4N_6O_{0.5}$	$C_{32}H_{45}N_3O_3Pd$
Formula weight	229.74	878.48	854.47	626.11
Temperature (K)	120.0(1)	120.0(1)	120.0(1)	120.0(1)
Crystal system	orthorhombic	monoclinic	orthorhombic	monoclinic
Space group	$P2_12_12_1$	$P2_1$	$P2_12_12$	$P2_1$
a (Å)	9.7003(2)	11.5248(2)	22.9490(3)	15.0671(2)
b (Å)	10.6340(2)	10.8474(2)	15.1385(2)	12.5634(2)
c (Å)	24.0173(6)	15.4425(4)	10.7544(2)	16.2805(2)
α (°)	90	90	90	90
β (°)	90	94.361(2)	90	102.972(2)
γ (°)	90	90	90	90
Volume (Å^3)	2477.47(9)	1924.94(7)	3736.22(11)	3003.13(7)
Z	8	2	4	4
Density (calculated) (Mg/m^3)	1.232	1.516	1.519	1.385
Absorption coefficient (mm^{-1})	0.284	4.217	5.492	5.266
F(000)	992	896	1736.4	1312
Crystal size (mm)	0.707 × 0.603 × 0.484	0.127 × 0.079 × 0.021	0.216 × 0.049 × 0.028	0.15 × 0.136 × 0.136
Radiation	MoKα (λ = 0.71073)	MoKα (λ = 0.71073)	Cu Kα (λ = 1.54184)	CuKα (λ = 1.54184)
2Θ range for data collection (°)	6.79 to 75.78	4.59 to 60.00	7 to 134.98	5.57 to 153.6
Reflections collected	35603	29741	26081	21927
Independent reflections [R(int)]	12738 [R_{int} = 0.0290]	10736 [R_{int} = 0.0370]	6739 [R_{int} = 0.0433]	21927 [R_{int} = ?]
Data / restraints / parameters	12738/0/277	10736/19/511	6739/0/391	21927/1/723
Goodness-of-fit on F^2	1.035	1.022	1.026	1.067
Final R indexes R_1 [I>2σ (I)]	R_1 = 0.0453, wR_2 = 0.1074	R_1 = 0.0356, wR_2 = 0.0745	R_1 = 0.0468, wR_2 = 0.1241	R_1 = 0.0340, wR_2 = 0.0954
Final R indexes (all data) wR_2	R_1 = 0.0594, wR_2 = 0.1188	R_1 = 0.0482, wR_2 = 0.0795	R_1 = 0.0502, wR_2 = 0.1273	R_1 = 0.0343, wR_2 = 0.0956
Flack Parameter	0.007(15)	0.000(7)	-0.05(2)	-0.005(3)

Table A0.2: *Crystallographic data for compounds Pt(**2.4 - H**)*(O,O'-acac), *Pd(**2.5**)Cl_2 and [Ru(**2.2**)*(p-cymene)Cl][PF_6].*

Thesis code	Pt(**2.4 - H**)(*O,O'*-acac)	Pd(**2.5**)Cl_2	[Ru(**2.2**)(*p*-cymene)Cl][PF_6]
Collection identification code	5wrk20a	wk4-137-1	5wrk29cu
Empirical formula	$C_{32}H_{45}N_3O_3Pt$	$C_{27}H_{34}Cl_2N_4OPd$	$C_{111}H_{164}Cl_{28}F_{24}N_{13}O_4P_4Ru_4$
Formula weight	714.80	607.88	3721.18
Temperature (K)	120.0(0)	293(2)	120.0(1)
Crystal system	monoclinic	orthorhombic	triclinic
Space group	$P2_1$	$P2_12_12_1$	P1
a (Å)	14.9618(2)	9.070(2)	12.3867(2)
b (Å)	12.5534(2)	17.570(4)	12.4102(2)
c (Å)	16.3368(2)	34.810(7)	27.9156(4)
α (°)	90	90	90.025(2)
β (°)	102.932(1)	90	90.025(2)
γ (°)	90	90	118.026(2)
Volume ($Å^3$)	2990.58(7)	5547.3(2)	3788.0(2)
Z	4	8	1
Density (calculated) (Mg/m^3)	1.588	1.456	1.631
Absorption coefficient (mm^{-1})	4.729	0.888	8.81
F(000)	1440	2496	1881
Crystal size (mm)	0.158 × 0.128 × 0.047	0.465 × 0.055 × 0.039	0.37 × 0.14 × 0.02
Radiation	MoKα (λ = 0.71073)	MoKα (λ = 0.71073)	CuKα (λ = 1.54184)
2Θ range for data collection (°)	5.25 to 75.68	2.60 to 55.77	8.07 to 154.01
Reflections collected	85024	137857	83724
Independent reflections [R(int)]	30492 [R_{int} = 0.0371]	13104 [R_{int} = 0.0606]	28795 [R_{int} = 0.0515]
Data / restraints / parameters	30492/1/721	13104/46/590	28795/15/1765
Goodness-of-fit on F^2	1.068	1.067	1.03
Final R indexes R_1 [I>2σ (I)]	R_1 = 0.0368, wR_2 = 0.0852	R_1 = 0.0452, wR_2 = 0.1097	R_1 = 0.0498, wR_2 = 0.1347
Final R indexes (all data) wR_2	R_1 = 0.0460, wR_2 = 0.0911	R_1 = 0.0482, wR_2 = 0.1115	R_1 = 0.0520, wR_2 = 0.1374
Flack Parameter	-0.011(3)	0.007(6)	-0.024(7)

Table A0.3: *Crystallographic data for compounds Pd(**3.3 - H**)*(O,O'*-acac), Pt(**3.3 - H**)*(O,O'*-acac) and Pd(**3.3**)*Cl_2.

Thesis code	Pd(**3.3 - H**)(*O,O'*-acac)	Pt(**3.3 - H**)(*O,O'*-acac)	Pd(**3.3**)(allyl)Cl
Collection identification code	5wrk22.a	5wrk23.a	5wrk28a
Empirical formula	$C_{28}H_{39}N_3O_3Pd$	$C_{28}H_{39}N_3O_3Pt$	$C_{26}H_{37}ClN_3OPd$
Formula weight	572.02	660.71	549.43
Temperature (K)	120.0(1)	120.0(1)	285.2(1)
Crystal system	monoclinic	monoclinic	monoclinic
Space group	$P2_1/c$	$P2_1/c$	$P2_1/c$
a (Å)	10.5941(3)	10.5909(3)	10.2536(4)
b (Å)	15.3153(4)	15.3547(5)	26.4965(10)
c (Å)	16.9971(6)	16.9427(5)	9.8590(3)
α (°)	90	90	90
β (°)	98.116(3)	98.372(3)	91.690(3)
γ (°)	90	90	90
Volume ($Å^3$)	2730.2(2)	2725.9(2)	2677.4(2)
Z	4	4	4
Density (calculated) (Mg/m^3)	1.392	1.61	1.363
Absorption coefficient (mm^{-1})	0.712	5.18	6.667
F(000)	1192	1320	1140
Crystal size (mm)	0.18 × 0.116 × 0.051	0.222 × 0.158 × 0.064	0.21 × 0.098 × 0.035
Radiation	MoKα (λ = 0.71073)	MoKα (λ = 0.71073)	CuKα (λ = 1.54184)
2Θ range for data collection (°)	3.60 to 62.80	4.706 to 66.182	6.67 to 154.90
Reflections collected	23960	18726	24066
Independent reflections [R(int)]	7869 [R_{int} = 0.0557]	9125 [R_{int} = 0.0389]	5611 [R_{int} = 0.0508]
Data / restraints / parameters	7869/0/322	9125/0/322	5611/6/302
Goodness-of-fit on F^2	1.016	1.032	1.05
Final R indexes R_1 [I>2σ (I)]	R_1 = 0.0428, wR_2 = 0.0868	R_1 = 0.0358, wR_2 = 0.0619	R_1 = 0.0469, wR_2 = 0.1250
Final R indexes (all data) wR_2	R_1 = 0.0702, wR_2 = 0.0989	R_1 = 0.0545, wR_2 = 0.0693	R_1 = 0.0559, wR_2 = 0.1343
Flack Parameter	-	-	-

Table A0.4: *Crystallographic data for compounds* ***4.6.HPF$_6$, 4.11.HI,*** *[Ru(bipy)$_2$(**4.2**)][PF$_6$]$_2$.*

Thesis code	**4.6.HPF$_6$**	**4.11.HI**	[Ru(bipy)$_2$(**4.2**)][PF$_6$]$_2$
Collection identification code	5wrk1a	5wrk30b	5wrk2a
Empirical formula	$C_{27}H_{21}F_6N_4P$	$C_{23}H_{21}N_4I$	$C_{40}H_{30}F_{12}N_8P_2Ru$
Formula weight	546.45	480.34	1013.73
Temperature (K)	120.0(1)	120.0(1)	120.0(1)
Crystal system	monoclinic	Triclinic	monoclinic
Space group	$P2_1/c$	P-1	$P2_1/c$
a (Å)	11.9184(5)	11.3337(4)	11.7918(2)
b (Å)	13.5720(4)	13.6113(6)	13.7398(2)
c (Å)	15.0568(6)	15.6739(6)	33.1338(5)
α (°)	90	100.595(4)	90
β (°)	108.105(4)	105.368(3)	94.064(2)
γ (°)	90	112.324(4)	90
Volume (Å^3)	2314.9(2)	2044.1(2)	5354.7(2)
Z	4	4	4
Density (calculated) (Mg/m^3)	1.568	1.561	1.257
Absorption coefficient (mm^{-1})	1.728	1.582	3.603
F(000)	1120	960	2032
Crystal size (mm)	0.3248 × 0.175 × 0.1114	0.409 × 0.185 × 0.059	0.213 × 0.124 × 0.08
Radiation	CuKα (λ = 1.54184)	MoKα (λ = 0.71073)	CuKα (λ = 1.54184)
2Θ range for data collection (°)	7.804 to 147.85	4.026 to 55.00	6.97 to 134.99
Reflections collected	8577	20955	26849
Independent reflections [R(int)]	4524 [R_{int} = 0.0315]	9394 [R_{int} = 0.0350]	9650 [R_{int} = 0.0305]
Data / restraints / parameters	4524/0/343	9394/0/507	9650/0/568
Goodness-of-fit on F^2	1.044	1.037	1.065
Final R indexes R_1 [I>2σ (I)]	R_1 = 0.0883, wR_2 = 0.2362	R_1 = 0.0339, wR_2 = 0.0733	R_1 = 0.0354, wR_2 = 0.0933
Final R indexes (all data) wR_2	R_1 = 0.1122, wR_2 = 0.2634	R_1 = 0.0462, wR_2 = 0.0804	R_1 = 0.0405, wR_2 = 0.0959
Flack Parameter	-	-	-

Table A0.5: *Crystallographic data for compounds [Ru(bipy)$_2$(**4.3**)][PF$_6$]$_2$ and [Ru(bipy)$_2$(**4.9.H**)][PF$_6$]$_3$.*

Thesis code	[Ru(bipy)$_2$(**4.3**)][PF$_6$]$_2$	[Ru(bipy)$_2$(**4.9.H**)][PF$_6$]$_3$
Collection identification code	5wrk3a	5wrk33b
Empirical formula	$C_{49}H_{47}F_{12}N_{11}OP_2Ru$	$C_{42}H_{34}F_{18}N_9P_3Ru$
Formula weight	1196.98	1200.76
Temperature (K)	120.0(1)	120.0(1)
Crystal system	Triclinic	monoclinic
Space group	P-1	$P2_1/c$
a (Å)	13.5205(3)	18.0604(2)
b (Å)	13.8672(3)	11.9307(2)
c (Å)	15.8109(3)	21.5060(2)
α (°)	108.098(2)	90
β (°)	95.841(2)	91.702(1)
γ (°)	111.463(2)	90
Volume (Å^3)	2543.4(1)	4631.93(9)
Z	2	4
Density (calculated) (Mg/m^3)	1.563	1.722
Absorption coefficient (mm^{-1})	0.465	4.789
F(000)	1216	2400
Crystal size (mm)	0.326 × 0.263 × 0.165	0.218 × 0.187 × 0.041
Radiation	MoKα (λ = 0.71073)	CuKα (λ = 1.54184)
2Θ range for data collection (°)	4.85 to 64.49	4.90 to 135.0
Reflections collected	31744	69032
Independent reflections [R(int)]	15775 [R_{int} = 0.0259]	8338 [R_{int} = 0.0344]
Data / restraints / parameters	15775/0/690	8338/0/663
Goodness-of-fit on F^2	1.03	1.04
Final R indexes R_1 [I>2σ (I)]	R_1 = 0.0438, wR_2 = 0.1105	R_1 = 0.0302, wR_2 = 0.0811
Final R indexes (all data) wR_2	R_1 = 0.0523, wR_2 = 0.1168	R_1 = 0.0327, wR_2 = 0.0832
Flack Parameter	-	-

Table A0.6: *Crystallographic data for compounds* ***5.2.HPF$_6$****,* *[Ru(bipy)$_2$(**5.2.H**)][PF$_6$]$_3$, [Ru(bipy)$_2$(**5.3**)][PF$_6$]$_2$ and* ***5.7.HPF$_6$****.*

Thesis code	**5.2.HPF$_6$**	[Ru(bipy)$_2$(**5.2.H**)][PF$_6$]$_3$	[Ru(bipy)$_2$(**5.3**)][PF$_6$]$_2$	**5.7.HPF$_6$**
Collection identification code	5wrk6a	5wrk5a_twin1_hklf4	5wrk27a	5wrk8a
Empirical formula	$C_{16}H_{13}F_6N_4P$	$C_{36}H_{29}F_{18}N_8P_3Ru$	$C_{40}H_{34}F_{12}N_6O_2P_2Ru$	$C_{90}H_{95}F_{24}N_{25}O_4P_4$
Formula weight	406.27	1109.65	1021.74	2170.78
Temperature (K)	120.0(1)	120.0(1)	285.2(1)	120.0(1)
Crystal system	monoclinic	monoclinic	triclinic	monoclinic
Space group	$P2_1/c$	$P2_1/c$	P-1	$P2_1/n$
a (Å)	12.8656(2)	14.7162(3)	11.8816(3)	28.011(2)
b (Å)	16.7917(3)	18.7579(2)	13.1625(5)	11.2189(3)
c (Å)	7.7312(1)	15.0007(3)	13.5986(4)	31.849(2)
α (°)	90	90	95.004(3)	90
β (°)	98.943(2)	107.590(2)	96.348(2)	91.559(4)
γ (°)	90	90	107.386(3)	90
Volume (Å^3)	1649.91(5)	3947.3(2)	2000.8(2)	10005.1(7)
Z	4	4	2	4
Density (calculated) (Mg/m^3)	1.636	1.867	1.696	1.441
Absorption coefficient (mm^{-1})	2.184	5.547	4.848	1.646
F(000)	824	2208	1028	4472
Crystal size (mm)	0.313 × 0.079 × 0.045	0.207 × 0.096 × 0.067	0.316 × 0.224 × 0.127	0.787 × 0.044 × 0.03
Radiation	CuKα (λ = 1.54184)	CuKα (λ = 1.54184)	CuKα (λ = 1.54184)	CuKα (λ = 1.54184)
2Θ range for data collection (°)	6.96 to 148.65	6.30 to 148.76	6.59 to 154.26	5.55 to 153.55
Reflections collected	16332	36450	16979	52714
Independent reflections [R(int)]	3329 [R_{int} = 0.0267]	7906 [R_{int} = 0.0552]	8150 [R_{int} = 0.0523]	20621 [R_{int} = 0.1147]
Data / restraints / parameters	3329/30/311	7906/0/596	8150/0/570	20621/13/1356
Goodness-of-fit on F^2	1.041	0.983	1.096	0.996
Final R indexes R_1 [I>2σ (I)]	R_1 = 0.0425, wR_2 = 0.1050	R_1 = 0.0387, wR_2 = 0.0961	R_1 = 0.0507, wR_2 = 0.1382	R_1 = 0.0715, wR_2 = 0.1632
Final R indexes (all data) wR_2	R_1 = 0.0464, wR_2 = 0.1081	R_1 = 0.0472, wR_2 = 0.0995	R_1 = 0.0555, wR_2 = 0.1456	R_1 = 0.1440, wR_2 = 0.2136
Flack Parameter	-	-	-	-

Table A0.7: *Crystallographic data for compounds* ***5.8.HPF$_6$****, [Ru(phen)$_2$(Pd{**5.9 - H**}{allyl}Cl)][PF$_6$]$_2$, [Ru(phen)$_2$(Pd{**5.10 - H**}Cl)][PF$_6$]$_2$ and [Ru(phen)$_2$(Pd{**5.12 - H**}Cl)][PF$_6$]$_2$.*

Thesis code	**5.8.HPF$_6$**	[Ru(phen)$_2$(Pd{**5.9 - H**}{allyl})][PF$_6$]$_2$	[Ru(phen)$_2$(Pd{**5.10 - H**}Cl)][PF$_6$]$_2$	[Ru(phen)$_2$(Pd{**5.12 - H**}Cl)][PF$_6$]$_2$
Collection identification code	5wrk9a	WK5-41-3	5wrk25	5wrk34a
Empirical formula	$C_{23}H_{20}F_6N_5O_2P$	$C_{59.5}H_{50.5}F_{12}N_9O_4P_2PdRu$	$C_{52}H_{32.5}ClF_{12}N_{13}OP_2PdRu$	$C_{50}H_{35.5}ClF_{12}N_{13}OP_2PdRu$
Formula weight	543.41	1452.32	1388.27	1383.22
Temperature (K)	120.0(1)	293(2)	284.9(1)	120.0(1)
Crystal system	orthorhombic	monoclinic	triclinic	monoclinic
Space group	Pbca	P2/c	P-1	I2/a
a (Å)	9.9233(7)	17.438(4)	15.7816(5)	27.235(1)
b (Å)	12.9691(8)	16.695(3)	18.0559(3)	18.5139(5)
c (Å)	35.856(3)	21.723(4)	21.6397(4)	23.746(1)
α (°)	90	90	90.724(2)	90
β (°)	90	91.90(3)	107.681(2)	97.203(4)
γ (°)	90	90	94.721(2)	90
Volume (Å^3)	4614.5(6)	6321(2)	5850.5(2)	11879.2(7)
Z	8	4	4	8
Density (calculated) (Mg/m^3)	1.564	1.526	1.576	1.547
Absorption coefficient (mm^{-1})	1.807	0.662	6.285	6.811
F(000)	2224	2921	2754	5480
Crystal size (mm)	0.211 × 0.091 × 0.066	0.15 × 0.1 × 0.01	0.439 × 0.346 × 0.054	0.213 × 0.075 × 0.043
Radiation	CuKα (λ = 1.54184)	MoKα (λ = 0.71073)	CuKα (λ = 1.54184)	CuKα (λ = 1.54184)
2Θ range for data collection (°)	10.19 to 153.18	2.34 to 51.49	6.65 to 150.00	5.786 to 134.998
Reflections collected	12310	82287	106656	32959
Independent reflections [R(int)]	4577 [R_{int} = 0.0837]	11772 [R_{int} = 0.1401]	24063 [R_{int} = 0.1835]	10690 [R_{int} = 0.0663]
Data / restraints / parameters	4577/0/337	11772/72/826	24063/10/1531	10690/0/752
Goodness-of-fit on F^2	1.003	1.038	1.039	0.979
Final R indexes R_1 [I>2σ (I)]	R_1 = 0.0632, wR_2 = 0.1417	R_1 = 0.0791, wR_2 = 0.1908	R_1 = 0.1260, wR_2 = 0.3084	R_1 = 0.0743, wR_2 = 0.1980
Final R indexes (all data) wR_2	R_1 = 0.1237, wR_2 = 0.1821	R_1 = 0.1203, wR_2 = 0.2185	R_1 = 0.1523, wR_2 = 0.3309	R_1 = 0.1085, wR_2 = 0.2325
Flack Parameter	-	-	-	-

References

1. R. S. Atkinson, *Stereoselective synthesis*, Wiley & Sons, New York;Chichester [England];, 1995.

2. G. Subramanian, *Chiral separation techniques: a practical approach*, John Wiley & Sons, 2008.

3. V. Prelog and G. Helmchen, *Angew. Chem. Int. Ed. Engl.*, 1982, **21**, 567-583.

4. D. Nasipuri, *Stereochemistry of organic compounds: principles and applications*, New Age International, 1994.

5. C. Wolf, *Dynamic stereochemistry of chiral compounds: principles and applications*, Royal Society of Chemistry, 2008.

6. M. Rickhaus, M. Mayor and M. Juríček, *Chem. Soc. Rev.*, 2016.

7. T. N. Tozer and M. Rowland, *Introduction to pharmacokinetics and pharmacodynamics: the quantitative basis of drug therapy*, Lippincott Williams & Wilkins, 2006.

8. B. S. Sekhon, *Journal of Modern Medicinal Chemistry*, 2013, **1**, 10-36.

9. G.-Q. Lin, Q.-D. You and J.-F. Cheng, *Chiral drugs: chemistry and biological action*, John Wiley & Sons, 2011.

10. W. A. Nugent, T. V. RajanBabu and M. J. Burk, *Science*, 1993, **259**, 479-479.

11. H. Lorenz and A. Seidel-Morgenstern, *Angew. Chem. Int. Ed.*, 2014, **53**, 1218-1250.

12. D. Ager, *Handbook of chiral chemicals*, CRC Press, 2005.

13. M. Tokunaga, J. F. Larrow, F. Kakiuchi and E. N. Jacobsen, *Science*, 1997, **277**, 936-938.

14. A. M. Dyas, M. L. Robinson and A. F. Fell, *Analytical Proceedings*, 1989, **26**, 346-348.

15. X. Hua and A. von Zelewsky, *Inorg. Chem.*, 1995, **34**, 5791-5797.

16. R. W. W. Hooft, L. H. Straver and A. L. Spek, *J. Appl. Crystallogr.*, 2008, **41**, 96-103.

17. H. D. Flack and G. Bernardinelli, *Chirality*, 2008, **20**, 681-690.

18. O. McConnell, A. Bach, C. Balibar, N. Byrne, Y. Cai, G. Carter, M. Chlenov, L. Di, K. Fan, I. Goljer, Y. He, D. Herold, M. Kagan, E. Kerns, F. Koehn, C. Kraml, V. Marathias, B. Marquez, L. McDonald, L. Nogle, C. Petucci, G. Schlingmann, G.

Tawa, M. Tischler, R. T. Williamson, A. Sutherland, W. Watts, M. Young, M.-Y. Zhang, Y. Zhang, D. Zhou and D. Ho, *Chirality*, 2007, **19**, 658-682.

19. L. M. Sweeting, D. C. Crans and G. M. Whitesides, *J. Org. Chem*, 1987, **52**, 2273-2276.

20. H. L. Goering, J. N. Eikenberry and G. S. Koermer, *J. Am. Chem. Soc.*, 1971, **93**, 5913-5914.

21. D. Parker, *Chem. Rev.*, 1991, **91**, 1441-1457.

22. A. Zimmermann and M. Oestreich, *Synthesis*, 2007, **2007**, 957-957.

23. W. Oppolzer, *Tetrahedron*, 1987, **43**, 1969-2004.

24. M. P. Bonner and E. R. Thornton, *J. Am. Chem. Soc.*, 1991, **113**, 1299-1308.

25. S. J. Miller, *Nature Chemistry*, 2012, **4**, 344-345.

26. L. Haughton and J. M. Williams, *J. Chem. Soc., Perkin Trans. 1*, 1999, 2645-2658.

27. C. E. Housecroft and A. G. Sharpe, *Inorganic Chemistry*, Pearson Education Limited, 2008.

28. R. Bates, *Organic synthesis using transition metals*, John Wiley & Sons, 2012.

29. C. C. Johansson Seechurn, M. O. Kitching, T. J. Colacot and V. Snieckus, *Angew. Chem. Int. Ed.*, 2012, **51**, 5062-5085.

30. N. T. Phan, M. Van Der Sluys and C. W. Jones, *Adv. Synth. Catal.*, 2006, **348**, 609-679.

31. J. P. Wolfe, S. Wagaw and S. L. Buchwald, *J. Am. Chem. Soc.*, 1996, **118**, 7215-7216.

32. N. Miyaura and A. Suzuki, *Chem. Rev.*, 1995, **95**, 2457-2483.

33. D. G. Hall, *Structure, properties, and preparation of boronic acid derivatives. Overview of their reactions and applications*, John Wiley & Sons: Weinheim, Germany, 2006.

34. A. J. Lennox and G. C. Lloyd-Jones, *Chem. Soc. Rev.*, 2014, **43**, 412-443.

35. I. Cepanec, *Synthesis of biaryls*, Elsevier, 2010.

36. M. Moreno-Mañas, M. Pérez and R. Pleixats, *J. Org. Chem*, 1996, **61**, 2346-2351.

37. N. Marion, O. Navarro, J. Mei, E. D. Stevens, N. M. Scott and S. P. Nolan, *J. Am. Chem. Soc.*, 2006, **128**, 4101-4111.

38. O. Navarro, N. Marion, N. M. Scott, J. González, D. Amoroso, A. Bell and S. P. Nolan, *Tetrahedron*, 2005, **61**, 9716-9722.

39. G. C. Fortman and S. P. Nolan, *Chem. Soc. Rev.,*, 2011, **40**, 5151-5169.

40. P. J. Walsh and M. C. Kozlowski, *Fundamentals of asymmetric catalysis*, University Science Books, 2009.

41. T. P. Yoon and E. N. Jacobsen, *Science*, 2003, **299**, 1691-1693.

42. W. S. Knowles, *Acc. Chem. Res.*, 1983, **16**, 106-112.

43. B. D. Vineyard, W. S. Knowles, M. J. Sabacky, G. L. Bachman and D. J. Weinkauff, *J. Am. Chem. Soc.*, 1977, **99**, 5946-5952.

44. L. S. Liebeskind, M. E. Welker and R. W. Fengl, *J. Am. Chem. Soc.*, 1986, **108**, 6328-6343.

45. U. Knof and A. von Zelewsky, *Angew. Chem. Int. Ed.*, 1999, **38**, 302-322.

46. R. L. Halterman, *Chem. Rev.*, 1992, **92**, 965-994.

47. K. Kromm, P. L. Osburn and J. Gladysz, *Organometallics*, 2002, **21**, 4275-4280.

48. T. Hayashi, M. Konishi, H. Ito and M. Kumada, *J. Am. Chem. Soc.*, 1982, **104**, 4962-4963.

49. L.-A. Chen, W. Xu, B. Huang, J. Ma, L. Wang, J. Xi, K. Harms, L. Gong and E. Meggers, *J. Am. Chem. Soc.*, 2013, **135**, 10598-10601.

50. E. B. Bauer, *Chem. Soc. Rev.*, 2012, **41**, 3153-3167.

51. Z.-Y. Cao, W. D. G. Brittain, J. S. Fossey and F. Zhou, *Catalysis Science & Technology*, 2015, **5**, 3441-3451.

52. I. Sato, K. Kadowaki, Y. Ohgo, K. Soai and H. Ogino, *Chem. Commun.*, 2001, 1022-1023.

53. G. Bertrand, *Carbene chemistry: from fleeting intermediates to powerful reagents*, CRC Press, 2002.

54. A. J. Arduengo, R. L. Harlow and M. Kline, *J. Am. Chem. Soc.*, 1991, **113**, 361-363.

55. H. Jacobsen, A. Correa, A. Poater, C. Costabile and L. Cavallo, *Coord. Chem. Rev.*, 2009, **253**, 687-703.

56. T. M. Trnka and R. H. Grubbs, *Acc. Chem. Res.*, 2000, **34**, 18-29.

57. X. Bugaut and F. Glorius, *Chem. Soc. Rev.,*, 2012, **41**, 3511–3522.

58. F. E. Hahn and M. C. Jahnke, *Angew. Chem. Int. Ed.*, 2008, **47**, 3122-3172.

59. C. Radloff, F. E. Hahn, T. Pape and R. Frohlich, *Dalton Trans.*, 2009, **0**, 7215-7222.

60. C. I. Ezugwu, N. A. Kabir, M. Yusubov and F. Verpoort, *Coord. Chem. Rev.*, 2016, **307, Part 2**, 188-210.

61. P. Pinter, H. Mangold, I. Stengel, I. Münster and T. Strassner, *Organometallics*, 2016, **35**, 673-680.

62. M. Tenne, S. Metz, G. Wagenblast, I. Münster and T. Strassner, *Organometallics*, 2015, DOI: 10.1021/acs.organomet.5b00136.

63. V. J. Catalano and M. A. Malwitz, *Inorg. Chem.*, 2003, **42**, 5483-5485.

64. L. Mercs and M. Albrecht, *Chem. Soc. Rev.*, 2010, **39**, 1903-1912.

65. S. P. Nolan, ed., *N-Heterocyclic Carbenes in Synthesis*, Wiley-VHC, 2006.

66. E. O. Fischer and A. Maasböl, *Angew. Chem. Int. Ed. Engl.*, 1964, **3**, 580-581.

67. H. W. Wanzlick, *Angew. Chem. Int. Edit.,*, 1962, **1**, 75-80.

68. H. W. Wanzlick and H. J. Schönherr, *Angew. Chem. Int. Ed. Engl.*, 1968, **7**, 141-142.

69. J. DePasquale, M. Kumar, M. Zeller and E. T. Papish, *Organometallics*, 2013, **32**, 966-979.

70. H. D. Velazquez and F. Verpoort, *Chem. Soc. Rev.,*, 2012, **41**, 7032-7060.

71. N. B. Jokić, C. S. Straubinger, S. Li Min Goh, E. Herdtweck, W. A. Herrmann and F. E. Kühn, *Inorg. Chim. Acta*, 2010, **363**, 4181-4188.

72. R. Dorta, E. D. Stevens, N. M. Scott, C. Costabile, L. Cavallo, C. D. Hoff and S. P. Nolan, *J. Am. Chem. Soc.*, 2005, **127**, 2485-2495.

73. H. Clavier and S. P. Nolan, *Chem. Commun.*, 2010, **46**, 841-861.

74. L. Cavallo, A. Correa, C. Costabile and H. Jacobsen, *J. Organomet. Chem.*, 2005, **690**, 5407-5413.

75. F. Wang, L.-j. Liu, W. Wang, S. Li and M. Shi, *Coord. Chem. Rev.*, 2012, **256**, 804-853.

76. R. H. Grubbs, *Angew. Chem. Int. Ed.*, 2006, **45**, 3760-3765.

77. *Angew. Chem. Int. Ed.*, 2005, **44**, 6982-6982.

78. Y. Chauvin, *Angew. Chem. Int. Ed.*, 2006, **45**, 3740-3747.

79. R. R. Schrock, *Angew. Chem. Int. Ed.*, 2006, **45**, 3748-3759.

80. G. C. Vougioukalakis and R. H. Grubbs, *Chem. Rev.*, 2009, **110**, 1746-1787.

81. T. J. Seiders, D. W. Ward and R. H. Grubbs, *Org. Lett.*, 2001, **3**, 3225-3228.

82. Cesati, J. de Armas and A. H. Hoveyda, *J. Am. Chem. Soc.*, 2003, **126**, 96-101.

83. K. Selvakumar, A. Zapf and M. Beller, *Org. Lett.*, 2002, **4**, 3031-3033.

84. K. Matsubara, S. Miyazaki, Y. Koga, Y. Nibu, T. Hashimura and T. Matsumoto, *Organometallics*, 2008, **27**, 6020-6024.

85. M. S. Viciu, R. F. Germaneau and S. P. Nolan, *Org. Lett.*, 2002, **4**, 4053-4056.

86. V. Khlebnikov, A. Meduri, H. Mueller-Bunz, T. Montini, P. Fornasiero, E. Zangrando, B. Milani and M. Albrecht, *Organometallics*, 2012, **31**, 976-986.

87. C. J. O'Brien, E. A. B. Kantchev, C. Valente, N. Hadei, G. A. Chass, A. Lough, A. C. Hopkinson and M. G. Organ, *Chem. Eur. J.*, 2006, **12**, 4743-4748.

88. M. G. Organ, S. Avola, I. Dubovyk, N. Hadei, E. A. B. Kantchev, C. J. O'Brien and C. Valente, *Chem. Eur. J.*, 2006, **12**, 4749-4755.

89. M. G. Organ, S. Çalimsiz, M. Sayah, K. H. Hoi and A. J. Lough, *Angew. Chem.*, 2009, **121**, 2419-2423.

90. V. Cesar, S. Bellemin-Laponnaz and L. H. Gade, *Chem. Soc. Rev.*, 2004, **33**, 619-636.

91. L. Benhamou, C. l. Besnard and E. P. Kündig, *Organometallics*, 2013, **33**, 260-266.

92. D. Zhang and Q. Wang, *Coord. Chem. Rev.*, 2015, **286**, 1-16.

93. L. Benhamou, E. Chardon, G. Lavigne, S. Bellemin-Laponnaz and V. César, *Chem. Rev.*, 2011, **111**, 2705-2733.

94. W. A. Herrmann and C. Koecher, *Angew. Chem. Int. Ed. Engl.*, 1997, **36**, 2162-2187.

95. A. J. Arduengo Iii, R. Krafczyk, R. Schmutzler, H. A. Craig, J. R. Goerlich, W. J. Marshall and M. Unverzagt, *Tetrahedron*, 1999, **55**, 14523-14534.

96. D. Tapu, C. Owens, D. VanDerveer and K. Gwaltney, *Organometallics*, 2008, **28**, 270-276.

97. K. Hirano, S. Urban, C. Wang and F. Glorius, *Org. Lett.*, 2009, **11**, 1019-1022.

98. F. Glorius, G. Altenhoff, R. Goddard and C. Lehmann, *Chem. Commun.*, 2002, 2704-2705.

99. E. Peris, in *N-Heterocyclic Carbenes in Transition Metal Catalysis*, Springer, 2006, pp. 83-116.

100. I. J. B. Lin and C. S. Vasam, *Coord. Chem. Rev.*, 2007, **251**, 642-670.

101. B. Liu, S. Pan, B. Liu and W. Chen, *Inorg. Chem.*, 2014, **53**, 10485-10497.

102. Q.-X. Liu, H.-L. Li, X.-J. Zhao, S.-S. Ge, M.-C. Shi, G. Shen, Y. Zang and X.-G. Wang, *Inorg. Chim. Acta*, 2011, **376**, 437-445.

103. S. Gründemann, A. Kovacevic, M. Albrecht, J. W. F. Robert and H. Crabtree, *Chem. Commun.*, 2001, 2274-2275.

104. S. Budagumpi and S. Endud, *Organometallics*, 2013, **32**, 1537-1562.

105. Y. Unger and T. Strassner, *J. Organomet. Chem.*, 2012, **713**, 203-208.

106. I. J. B. Lin and C. S. Vasam, *Coord. Chem. Rev.*, 2007, **251**, 642-670.

107. G. W. Nyce, S. Csihony, R. M. Waymouth and J. L. Hedrick, *Chem. Eur. J.,*, 2004, **10**, 4073-4079.

108. D. Enders, K. Breuer, G. Raabe, J. Runsink, J. H. Teles, J. P. Melder, K. Ebel and S. Brode, *Angew. Chem. Int. Ed. Engl.*, 1995, **34**, 1021-1023.

109. A. Tudose, A. Demonceau and L. Delaude, *J. Organomet. Chem.*, 2006, **691**, 5356-5365.

110. M. C. Perry, X. Cui and K. Burgess, *Tetrahedron: Asymmetry*, 2002, **13**, 1969-1972.

111. P. L. Arnold, S. A. Mungur, A. J. Blake and C. Wilson, *Angew. Chem. Int. Ed.*, 2003, **42**, 5981-5984.

112. S. Kumar, A. Narayanan, M. N. Rao, M. M. Shaikh and P. Ghosh, *J. Organomet. Chem.*, 2012, **696**, 4159-4165.

113. M. N. Rao, M. Haridas, M. K. Gangwar, P. Rajakannu, A. C. Kalita and P. Ghosh, *Eur. J. Inorg. Chem.*, 2015, **2015**, 1604-1615.

114. S. Kumar, A. Narayanan, M. N. Rao, M. M. Shaikh and P. Ghosh, *J. Chem. Sci. (Bangalore, India)*, 2011, **123**, 791-798,S791/791-S791/726.

115. M. Yoshimura, R. Kamisue and S. Sakaguchi, *J. Organomet. Chem.*, 2013, **740**, 26-32.

116. M. K. Samantaray, K. Pang, M. M. Shaikh and P. Ghosh, *Inorg. Chem.*, 2008, **47**, 4153-4165.

117. S. Sakaguchi, M. Kawakami, J. O'Neill, K. S. Yoo and K. W. Jung, *J. Organomet. Chem.*, 2010, **695**, 195-200.

118. C.-Y. Liao, K.-T. Chan, J.-Y. Zeng, C.-H. Hu, C.-Y. Tu and H. M. Lee, *Organometallics*, 2007, **26**, 1692-1702.

119. A. John and P. Ghosh, *Dalton Trans.*, 2010, **39**, 7183-7206.

120. M.-H. Sie, Y.-H. Hsieh, Y.-H. Tsai, J.-R. Wu, S.-J. Chen, P. V. Kumar, J.-H. Lii and H. M. Lee, *Organometallics*, 2010, **29**, 6473-6481.

121. J.-Y. Lee, P.-Y. Cheng, Y.-H. Tsai, G.-R. Lin, S.-P. Liu, M.-H. Sie and H. M. Lee, *Organometallics*, 2010, **29**, 3901-3911.

122. M. R. Kumar, K. Park and S. Lee, *Adv. Synth. Catal.*, 2010, **352**, 3255-3266.

123. K. Kalyanasundaram, *Coord. Chem. Rev.*, 1982, **46**, 159-244.

124. M. D. Kärkäs, O. Verho, E. V. Johnston and B. Åkermark, *Chem. Rev.*, 2014, **114**, 11863-12001.

125. E. Levin, E. Ivry, C. E. Diesendruck and N. G. Lemcoff, *Chem. Rev.*, 2015, DOI: 10.1021/cr400640e.

126. V. Balzani and A. Juris, *Coord. Chem. Rev.*, 2001, **211**, 97-115.

127. E. Breitmaier, *Terpenes: flavors, fragrances, pharmaca, pheromones*, John Wiley & Sons, 2006.

128. J. M. Finefield, D. H. Sherman, M. Kreitman and R. M. Williams, *Angew. Chem. Int. Ed.*, 2012, **51**, 4802-4836.

129. T. Money, *Natural Product Reports*, 1985, **2**, 253-289.

130. R. E. Gawley and P. Zhang, *J. Org. Chem.*, 1996, **61**, 8103-8112.

131. G. Chelucci, *Chem. Soc. Rev.*, 2006, **35**, 1230-1243.

132. J. Tydlitát, F. Bureš, J. Kulhánek, G. Mlostoń and A. Růžička, *Tetrahedron: Asymmetry*, 2012, **23**, 1010-1018.

133. K. Tomioka, *Synthesis*, 1990, **1990**, 541-549.

134. K. Narasaka, *Synthesis*, 1991, **1991**, 1-11.

135. Y. Zhou, J. Dong, F. Zhang and Y. Gong, *J. Org. Chem.*, 2011, **76**, 588-600.

136. Q. Li, W.-Y. Wong, W.-H. Chan and A. W. M. Lee, *Adv. Synth. Catal.*, 2010, **352**, 2142-2146.

137. Y. Langlois and C. Kouklovsky, *Synlett*, 2009, **2009**, 3065-3081.

138. D. R. Magar, C. Chang, Y.-F. Ting and K. Chen, *Eur. J. Org. Chem.*, 2010, **2010**, 2062-2066.

139. J. H. Hutchinson and T. Money, *Can. J. Chem.*, 1987, **65**, 1-6.

140. S. Lee and J. F. Hartwig, *J. Org. Chem*, 2001, **66**, 3402-3415.

141. M. B. Herbert, B. A. Suslick, P. Liu, L. Zou, P. K. Dornan, K. N. Houk and R. H. Grubbs, *Organometallics*, 2015, **34**, 2858-2869.

142. R. M. Thomas, B. K. Keitz, T. M. Champagne and R. H. Grubbs, *J. Am. Chem. Soc.*, 2011, **133**, 7490-7496.

143. D. Stepanovs, D. Posevins and M. Turks, *Acta Crystallographica Section E: Crystallographic Communications*, 2015, **71**, 1117-1120.

144. A. L. Thompson and D. J. Watkin, *Tetrahedron: Asymmetry*, 2009, **20**, 712-717.

145. W. E. Stewart and T. H. Siddall, *Chem. Rev.*, 1970, **70**, 517-551.

146. M. Avalos, R. Babiano, J. L. Barneto, J. L. Bravo, P. Cintas, J. L. Jiménez and J. C. Palacios, *J. Org. Chem*, 2001, **66**, 7275-7282.

147. J. Leonard, B. Lygo and G. Procter, *Advanced Practical Organic Chemistry*, Taylor and Francis Group, Florida, USA, third edn., 2013.

148. N. Ikota, H. Sakai, H. Shibata and K. Koga, *CHEMICAL & PHARMACEUTICAL BULLETIN*, 1986, **34**, 1050-1055.

149. Y. K. Chen, S.-J. Jeon, P. J. Walsh and W. A. Nugent, *Org. Synth.*, 2005, **82**, 87-92.

150. M. J. Bosiak, M. P. Krzemiński, P. Jaisankar and M. Zaidlewicz, *Tetrahedron: Asymmetry*, 2008, **19**, 956-963.

151. R. Boobalan, C. Chen and G.-H. Lee, *Org. Biomol. Chem.*, 2012, **10**, 1625-1638.

152. M. Periasamy, N. Sanjeevakumar and P. O. Reddy, *Synthesis*, 2012, **44**, 3185-3190.

153. C. Xie, L. M. Tang, C. Y. Pan and L. P. Guan, *Drug Res. (Stuttgart, Ger.)*, 2013, **63**, 607-613.

154. H. V. Huynh and R. Jothibasu, *J. Organomet. Chem.*, 2011, **696**, 3369-3375.

155. R. Houriet, H. Ruefenacht, P. A. Carrupt, P. Vogel and M. Tichy, *J. Am. Chem. Soc.*, 1983, **105**, 3417-3422.

156. A. Hassner, W. Wentworth and I. Pomerantz, *J. Org. Chem*, 1963, **28**, 304-306.

157. W. Hertler and E. Corey, *J. Org. Chem*, 1959, **24**, 572-573.

158. V. Leigh, D. J. Carleton, J. Olguin, H. Mueller-Bunz, L. J. Wright and M. Albrecht, *Inorg. Chem.*, 2014, **53**, 8054-8060.

159. S. Meiries, K. Speck, D. B. Cordes, A. M. Z. Slawin and S. P. Nolan, *Organometallics*, 2013, **32**, 330-339.

160. N. Marion, P. de Frémont, I. M. Puijk, E. C. Ecarnot, D. Amoroso, A. Bell and S. P. Nolan, *Adv. Synth. Catal.*, 2007, **349**, 2380-2384.

161. O. H. Winkelmann, A. Riekstins, S. P. Nolan and O. Navarro, *Organometallics*, 2009, **28**, 5809-5813.

162. N. Marion, E. C. Ecarnot, O. Navarro, D. Amoroso, A. Bell and S. P. Nolan, *J. Org. Chem*, 2006, **71**, 3816-3821.

163. S. W. Reilly, C. E. Webster, T. K. Hollis and H. U. Valle, *Dalton Trans.*, 2016, **45**, 2823-2828.

164. Z. Sun, Y. Liu, J. Chen, C. Huang and T. Tu, *ACS Catalysis*, 2015, **5**, 6573-6578.

165. US20150129840A1, 2015.

166. E. A. B. Kantchev and J. Y. Ying, *Organometallics*, 2009, **28**, 289-299.

167. U. Radius and F. M. Bickelhaupt, *Coord. Chem. Rev.*, 2009, **253**, 678-686.

168. K. V. Tan, J. L. Dutton, B. W. Skelton, D. J. D. Wilson and P. J. Barnard, *Organometallics*, 2013, **32**, 1913-1923.

169. X. Tian, R. Goddard and K.-R. Pörschke, *Organometallics*, 2006, **25**, 5854-5862.

170. S. A. De Pascali, P. Papadia, A. Ciccarese, C. Pacifico and F. P. Fanizzi, *Eur. J. Inorg. Chem.*, 2005, **2005**, 788-796.

171. S. A. De Pascali, P. Papadia, S. Capoccia, L. Marchiò, M. Lanfranchi, A. Ciccarese and F. P. Fanizzi, *Dalton Trans.*, 2009, 7786-7795.

172. S. Kawaguchi, *Coord. Chem. Rev.*, 1986, **70**, 51-84.

173. M. Horike, Y. Kai, N. Yasuoka and N. Kasa, *J. Organomet. Chem.*, 1974, **72**, 441-451.

174. Á. González-de-Castro, H. Broughton, J. A. Martínez-Pérez and J. F. Espinosa, *J. Org. Chem*, 2015, **80**, 3914-3920.

175. Y. Otani, O. Nagae, Y. Naruse, S. Inagaki, M. Ohno, K. Yamaguchi, G. Yamamoto, M. Uchiyama and T. Ohwada, *J. Am. Chem. Soc.*, 2003, **125**, 15191-15199.

176. H. Shanan-Atidi and K. H. Bar-Eli, *J. Phys. Chem. A*, 1970, **74**, 961-963.

177. C. C. Forbes, A. M. Beatty and B. D. Smith, *Org. Lett.*, 2001, **3**, 3595-3598.

178. R. R. Gardner, S. L. McKay and S. H. Gellman, *Org. Lett.*, 2000, **2**, 2335-2338.

179. G. Fischer, *Chem. Soc. Rev.*, 2000, **29**, 119-127.

180. S. R. LaPlante, P. Forgione, C. Boucher, R. Coulombe, J. Gillard, O. Hucke, A. Jakalian, M.-A. Joly, G. Kukolj, C. Lemke, R. McCollum, S. Titolo, P. L. Beaulieu and T. Stammers, *J. Med. Chem.*, 2014, **57**, 1944-1951.

181. T. Lanyon-Hogg, M. Ritzefeld, N. Masumoto, A. I. Magee, H. S. Rzepa and E. W. Tate, *J. Org. Chem*, 2015, **80**, 4370-4377.

182. H. M. J. Wang and I. J. B. Lin, *Organometallics*, 1998, **17**, 972-975.

183. L. Jackman, *Dynamic nuclear magnetic resonance spectroscopy*, Elsevier, 2012.

184. M. S. Viciu, R. F. Germaneau, O. Navarro-Fernandez, E. D. Stevens and S. P. Nolan, *Organometallics*, 2002, **21**, 5470-5472.

185. M. S. Viciu, F. K. Zinn, E. D. Stevens and S. P. Nolan, *Organometallics*, 2003, **22**, 3175-3177.

186. L. Canovese, F. Visentin, C. Levi, C. Santo and V. Bertolasi, *J. Organomet. Chem.*, 2013, **732**, 27-39.

187. J. Herrmann, P. S. Pregosin, R. Salzmann and A. Albinati, *Organometallics*, 1995, **14**, 3311-3318.

188. Félix A. Jalón, Blanca R. Manzano and B. Moreno-Lara, *Eur. J. Inorg. Chem.*, 2005, **2005**, 100-109.

189. M. C. Carrión, A. Díaz, A. Guerrero, F. A. Jalón, B. R. Manzano, A. Rodríguez, R. L. Paul and J. C. Jeffery, *J. Organomet. Chem.*, 2002, **650**, 210-222.

190. A. Gogoll, J. Oernebro, H. Grennberg and J.-E. Baeckvall, *J. Am. Chem. Soc.*, 1994, **116**, 3631-3632.

191. H. Friebolin and J. K. Becconsall, *Basic one-and two-dimensional NMR spectroscopy*, VCH Weinheim, 1993.

192. C. Elschenbroic and A. Salzer, *Organometallics A Concise Introduction*, Wiley VCH; 2nd Edition, 1992.

193. S. Filipuzzi, P. S. Pregosin, A. Albinati and S. Rizzato, *Organometallics*, 2008, **27**, 437-444.

194. P. S. Pregosin and R. Salzmann, *Coord. Chem. Rev.*, 1996, **155**, 35-68.

195. A. R. Chianese, P. T. Bremer, C. Wong and R. J. Reynes, *Organometallics*, 2009, **28**, 5244-5252.

196. V. J. Catalano and A. O. Etogo, *Inorg. Chem.*, 2007, **46**, 5608-5615.

197. M. R. Chapman, B. R. M. Lake, C. M. Pask, B. N. Nguyen and C. E. Willans, *Dalton Trans.*, 2015, **44**, 15938-15948.

198. A. A. Danopoulos, A. A. Tulloch, S. Winston, G. Eastham and M. B. Hursthouse, *Dalton Trans.*, 2003, 1009-1015.

199. T. Samanta, S. K. Seth, S. K. Chattopadhyay, P. Mitra, V. Kushwah and J. Dinda, *Inorg. Chim. Acta*, 2014, **411**, 165-171.

200. S. Díez-González, N. Marion and S. P. Nolan, *Chem. Rev.*, 2009, **109**, 3612-3676.

201. V. Dragutan, I. Dragutan, L. Delaude and A. Demonceau, *Coord. Chem. Rev.*, 2007, **251**, 765-794.

202. A. Tudose, A. Demonceau and L. Delaude, *J. Organomet. Chem.,*, 2006, **619**, 5356-5365.

203. W. Baratta, W. A. Herrmann, P. Rigo and J. Schwarz, *J. Organomet. Chem.*, 2000, **593–594**, 489-493.

204. H. Kücükbay, B. Cetinkaya, S. Guesmi and P. H. Dixneuf, *Organometallics*, 1996, **15**, 2434-2439.

205. M. Poyatos, A. Maisse-François, S. Bellemin-Laponnaz, E. Peris and L. H. Gade, *J. Organomet. Chem.*, 2006, **691**, 2713-2720.

206. M. Bennett, T. N. Huang, T. Matheson, A. Smith, S. Ittel and W. Nickerson, *Inorganic Syntheses, Volume 21*, 2007, 74-78.

207. L. Bernet, R. Lalrempuia, W. Ghattas, H. Mueller-Bunz, L. Vigara, A. Llobet and M. Albrecht, *Chem. Commun.*, 2011, **47**, 8058-8060.

208. H. Ohara, W. W. N. O, A. J. Lough and R. H. Morris, *Dalton Trans.*, 2012, **41**, 8797-8808.

209. WO2011000945A2, 2011.

210. 1003-5214, 2007.

211. W. C. Neikam and B. P. Dailey, *J. Chem. Phys*, 1963, **38**, 445-447.

212. M. S. Viciu, O. Navarro, R. F. Germaneau, R. A. Kelly, W. Sommer, N. Marion, E. D. Stevens, L. Cavallo and S. P. Nolan, *Organometallics*, 2004, **23**, 1629-1635.

213. H.-J. Park and Y. K. Chung, *Inorg. Chim. Acta*, 2012, **391**, 105-113.

214. H.-J. Park, K. Kim and Y. K. Chung, *Inorg. Chim. Acta*, 2014, **410**, 214-220.

215. K. Peuntinger, T. D. Pilz, R. Staehle, M. Schaub, S. Kaufhold, L. Petermann, M. Wunderlin, H. Gorls, F. W. Heinemann, J. Li, T. Drewello, J. G. Vos, D. M. Guldi and S. Rau, *Dalton Trans.*, 2014, **43**, 13683-13695.

216. A. A. Webster, S. K. K. Prasad, J. M. Hodgkiss and J. O. Hoberg, *Dalton Trans.*, 2015, **44**, 3728-3736.

217. J. Ettedgui and R. Neumann, *J. Am. Chem. Soc.*, 2008, **131**, 4-5.

218. B. Jing, T. Wu, C. Tian, M. Zhang and T. Shen, *Bull. Chem. Soc. Jpn.*, 2000, **73**, 1749-1755.

219. Z.-L. Xu, H.-X. Li, Z.-G. Ren, W.-Y. Du, W.-C. Xu and J.-P. Lang, *Tetrahedron*, 2011, **67**, 5282-5288.

220. C. Jin, J. Liu, Y. Chen, G. Li, R. Guan, P. Zhang, L. Ji and H. Chao, *Dalton Trans.*, 2015, **44**, 7538-7547.

221. A. R. Katritzky and J. M. Lagowski, *Heterocyclic Chemistry*, Methuen and Co LTD, London, 1960.

222. S.-W. Tong, W.-D. Song, D.-L. Miao and J.-B. An, *Acta Crystallographica Section E*, 2012, **68**, o1448.

223. E. G. Hohenstein and C. D. Sherrill, *The Journal of Physical Chemistry A*, 2009, **113**, 878-886.

224. Z.-Q. Zhu, S. Xiang, Q.-Y. Chen, C. Chen, Z. Zeng, Y.-P. Cui and J.-C. Xiao, *Chem. Commun.*, 2008, DOI: 10.1039/B810671A, 5016-5018.

225. T. Lv, Z. Wang, J. You, J. Lan and G. Gao, *J. Org. Chem.*, 2013, **78**, 5723-5730.

226. S. Li, F. Yang, T. Lv, J. Lan, G. Gao and J. You, *Chem. Commun.*, 2014, **50**, 3941-3943.

227. B. J. Coe, J. A. Harris, I. Asselberghs, K. Wostyn, K. Clays, A. Persoons, B. S. Brunschwig, S. J. Coles, T. Gelbrich, M. E. Light, M. B. Hursthouse and K. Nakatani, *Adv. Funct. Mater.*, 2003, **13**, 347-357.

228. B. Jdrzejewska, J. Kabatc, M. Pietrzak and J. Pączkowski, *Dyes and Pigments*, 2003, **58**, 47-58.

229. S. R. Marder, J. W. Perry and C. P. Yakymyshyn, *Chem. Mater.*, 1994, **6**, 1137-1147.

230. U. Narang, C. F. Zhao, J. D. Bhawalkar, F. V. Bright and P. N. Prasad, *J. Phys. Chem. A*, 1996, **100**, 4521-4525.

231. C.-X. Yuan, X.-T. Tao, Y. Ren, Y. Li, J.-X. Yang, W.-T. Yu, L. Wang and M.-H. Jiang, *The Journal of Physical Chemistry C*, 2007, **111**, 12811-12816.

232. H.-J. Park, W. Kim, W. Choi and Y. K. Chung, *New J. Chem.*, 2013, **37**, 3174-3182.

233. A. Juris, V. Balzani, F. Barigelletti, S. Campagna, P. Belser and A. von Zelewsky, *Coord. Chem. Rev.*, 1988, **84**, 85-277.

234. N. H. Damrauer, G. Cerullo, A. Yeh, T. R. Boussie, C. V. Shank and J. K. McCusker, *Science*, 1997, **275**, 54-57.

235. A. Quaranta, F. Lachaud, C. Herrero, R. Guillot, M.-F. Charlot, W. Leibl and A. Aukauloo, *Chem. Eur. J.*, 2007, **13**, 8201-8211.

236. S.-H. Fan, A.-G. Zhang, C.-C. Ju, L.-H. Gao and K.-Z. Wang, *Inorg. Chem.*, 2010, **49**, 3752-3763.

237. X. He, L. Zeng, G. Yang, L. Xie, X. Sun and L. Tan, *Inorg. Chim. Acta*, 2013, **408**, 9-17.

238. B. Jing, M. Zhang and T. Shen, *Spectrochimica Acta Part A: Molecular and Biomolecular Spectroscopy*, 2004, **60**, 2635-2641.

239. H. Xu, K.-C. Zheng, H. Deng, L.-J. Lin, Q.-L. Zhang and L.-N. Ji, *New J. Chem.*, 2003, **27**, 1255-1263.

240. D. P. Rillema, G. Allen, T. J. Meyer and D. Conrad, *Inorg. Chem.*, 1983, **22**, 1617-1622.

241. L. Wang, W. You, W. Huang, C. Wang and X.-Z. You, *Inorg. Chem.*, 2009, **48**, 4295-4305.

242. Y. Saitoh, T.-a. Koizumi, K. Osakada and T. Yamamoto, *Can. J. Chem.*, 1997, **75**, 1336-1339.

243. D. Tzalis, Y. Tor, F. Salvatorre and S. Jay Siegel, *Tetrahedron Lett.*, 1995, **36**, 3489-3490.

244. J. Clayden;, N. Greeves;, S. Warren; and P. Wothers;, in *Organic Chemistry*, Oxford University Press, 2001, ch. 43, pp. 1147-1183.

245. CN105175412A, 2015.

246. M. J. Cook, A. R. Katritzky and S. Nadji, *J. Chem. Soc., Perkin Trans. 2*, 1978, 1215-1222.

247. M. C. Nielsen, J. Borch and T. Ulven, *Bioorg. Med. Chem.*, 2009, **17**, 8241-8246.

248. S. Bodige and F. M. MacDonnell, *Tetrahedron Lett.*, 1997, **38**, 8159-8160.

249. C. Xu, *Monatsh. Chem.*, 2010, **141**, 631-635.

250. G. F. Smith and F. W. Cagle, *J. Org. Chem*, 1947, **12**, 781-784.

251. T. Gunnlaugsson, J. P. Leonard, K. Sénéchal and A. J. Harte, *J. Am. Chem. Soc.*, 2003, **125**, 12062-12063.

252. E. Belhadj, A. El-Ghayoury, T. Cauchy, M. Allain, M. Mazari and M. Sallé, *Eur. J. Inorg. Chem.*, 2014, **2014**, 3912-3919.

253. W. P. Griffith, *Quarterly Reviews, Chemical Society*, 1962, **16**, 188-207.

254. E. R. Talaty, S. Raja, V. J. Storhaug, A. Dölle and W. R. Carper, *The Journal of Physical Chemistry B*, 2004, **108**, 13177-13184.

255. N. M. Logacheva, V. E. Baulin, A. Y. Tsivadze, E. N. Pyatova, I. S. Ivanova, Y. A. Velikodny and V. V. Chernyshev, *Dalton Trans.*, 2009, DOI: 10.1039/B819805E, 2482-2489.

256. AU2011265513A1, 2013.

257. R. A. Jones, B. D. Roney, W. H. F. Sasse and K. O. Wade, *Journal of the Chemical Society B: Physical Organic*, 1967, **0**, 106-111.

258. F. W. J. Demnitz and M. B. D'Heni, *Org. Prep. Proced. Int.*, 1998, **30**, 467-469.

259. D. Wenkert and R. B. Woodward, *J. Org. Chem*, 1983, **48**, 283-289.

260. M. Sprecher, R. Breslow, O. Uziel and T. M. Link, *Org. Prep. Proced. Int.*, 1994, **26**, 696-701.

261. P. G. Baraldi, D. Preti, M. A. Tabrizi, F. Fruttarolo, G. Saponaro, S. Baraldi, R. Romagnoli, A. R. Moorman, S. Gessi, K. Varani and P. A. Borea, *Biorg. Med. Chem.*, 2007, **15**, 2514-2527.

262. H. Xie, D. Ng, S. N. Savinov, B. Dey, P. D. Kwong, R. Wyatt, A. B. Smith and W. A. Hendrickson, *J. Med. Chem.*, 2007, **50**, 4898-4908.

263. J. Coates, *Encyclopedia of analytical chemistry*, 2000.

264. F. R. Keene, *Chem. Soc. Rev.*, 1998, **27**, 185-194.

265. C. Fu, M. Wenzel, E. Treutlein, K. Harms and E. Meggers, *Inorg. Chem.*, 2012, **51**, 10004-10011.

266. J. L. Morgan, C. B. Spillane, J. A. Smith, D. P. Buck, J. G. Collins and F. R. Keene, *Dalton Trans.*, 2007, DOI: 10.1039/b706747j, 4333-4342.

267. B. T. Patterson and F. R. Keene, *Inorg. Chem.*, 1998, **37**, 645-650.

268. T. J. Rutherford, P. A. Pellegrini, J. Aldrich-Wright, P. C. Junk and F. R. Keene, *Eur. J. Inorg. Chem.*, 1998, **1998**, 1677-1688.

269. B. Bosnich and F. Dwyer, *Aust. J. Chem.*, 1966, **19**, 2229-2233.

270. U. McDonnell, J. M. C. A. Kerchoffs, R. P. M. Castineiras, M. R. Hicks, A. C. G. Hotze, M. J. Hannon and A. Rodger, *Dalton Trans.*, 2008, DOI: 10.1039/B711080D, 667-675.

271. B. Bosnich, *Inorg. Chem.*, 1968, **7**, 178-180.

272. A. Fedorova and M. Y. Ogawa, *Bioconjugate Chem.*, 2001, **13**, 150-154.

273. M. N. Hopkinson, C. Richter, M. Schedler and F. Glorius, *Nature*, 2014, **510**, 485-496.

274. G. Bringmann, A. J. Price Mortimer, P. A. Keller, M. J. Gresser, J. Garner and M. Breuning, *Angew. Chem. Int. Ed.*, 2005, **44**, 5384-5427.

275. J. Yin and S. L. Buchwald, *J. Am. Chem. Soc.*, 2000, **122**, 12051-12052.

276. A. N. Cammidge and K. V. L. Crepy, *Chem. Commun.*, 2000, DOI: 10.1039/B004513F, 1723-1724.

277. X. Shen, G. O. Jones, D. A. Watson, B. Bhayana and S. L. Buchwald, *J. Am. Chem. Soc.*, 2010, **132**, 11278-11287.

278. J. A. Love, J. P. Morgan, T. M. Trnka and R. H. Grubbs, *Angew. Chem. Int. Ed.*, 2002, **41**, 4035-4037.

279. L. Jafarpour, E. D. Stevens and S. P. Nolan, *J. Organomet. Chem.*, 2000, **606**, 49-54.

280. V. Lavallo, Y. Canac, C. Präsang, B. Donnadieu and G. Bertrand, *Angew. Chem. Int. Ed.*, 2005, **44**, 5705-5709.

281. P. L. Arnold and I. J. Casely, *Chem. Rev.*, 2009, **109**, 3599-3611.

282. O. V. Starikova, G. V. Dolgushin, L. I. Larina, P. E. Ushakov, T. N. Komarova and V. A. Lopyrev, *Russ. J. Org. Chem.*, 2003, **39**, 1467-1470.

283. J. Liu, J. Chen, J. Zhao, Y. Zhao, L. Li and H. Zhang, *Synthesis*, 2003, DOI: 10.1055/s-2003-42444, 2661-2666.

284. L. Zhu, P. Guo, G. Li, J. Lan, R. Xie and J. You, *J. Org. Chem*, 2007, **72**, 8535-8538.

285. L. Alakonda and M. Periasamy, *Synthesis*, 2012, **44**, 1063-1068.

286. Y. Nakabayashi, Y. Watanabe, T. Nakao and O. Yamauchi, *Inorg. Chim. Acta*, 2004, **357**, 2553-2560.